Development of methods for sample preparation using thin layer chromatography (TLC), preparative TLC and matrix-assisted laser desorption ionisation time of flight mass spectrometry (MALDI ToF MS) in support of understanding lipids detection in clinical samples.

Method validation was applied by implementing comparable sample groups from healthy, obese, and gestational diabetes mellitus human placentas and blood plasma.

Edyta Carrion Paczkowska BSc (Hons) MSc

Thesis Submitted to Swansea University in fulfilment
of the requirements for
the Degree of Doctor of Philosophy (PhD)

Date submitted: 31 January 2024,

Defence PhD Viva voce: 23 April 2024

Post Viva minor correction submitted 20 September 2024

Received minor corrections approval 25 November 2024

Final Thesis submission to Library January 2025

Edyta Carrion Paczkowska

"In the journey of life, the health of two becomes the strength of three.
Embracing a healthy BMI in pregnancy, we nurture new well-being and its vitality."(1-3)

Type text here

Declarations

This work has not previously been accepted in substance for any degree and is not being concurrently submitted in candidature for any degree.

Signed *Edyta Carrion Paczkowska*

Date 15/01/2025

This thesis is the result of my own investigations, except where otherwise stated. Other sources are acknowledged by footnotes giving explicit references. A bibliography is appended.

Signed *Edyta Carrion Paczkowska*

Date 15/01/2025

I hereby give my consent for my work, if relevant and accepted, to be available for photocopying and for inter-library loans **after expiry of a bar on access approved by the University.**

Signed *Edyta Carrion Paczkowska*

Date 15/01/2025

The University's ethical procedures have been followed and, where appropriate, that ethical approval has been granted.

Signed *Edyta Carrion Paczkowska*

Date 15/01/2025

Student ID: [redacted], Email: [redacted]

Dedication note

For my dearest Grandmother, whom I lost during the COVID-19 February 2020,

I want to dedicate this thesis work equally to my PhD supervisor, Professor Cathy Thornton and my loving, little grandmother, Wladyslawa Bilecka, age 92, whom I lost on 26th February 2022, during the last months of my PhD laboratory work. I dedicate all my life's hard work and education to my grandmother for her diligent life, for taking care of others before herself with all her heart and asking for nothing back. My loving grandmother, I miss you so much, and I vow to visit your grave soon when I finish my PhD studies. For you, my beautiful grandma, your hardworking ethics and caring heart will remain within my soul forever till we meet again. I also dedicate this to my whole family: my parents, brother, sisters, cousins, uncles and aunties, who also knew and loved my grandmother for her loving, kind and long life's hard work tyranny. May God Bless you all.

Polish translation of Dedication (Tlumaczenie) "Dla Babci Wladzi Bielickiej zyla lat 92, zmarla 26/02/2022 pandemia Korona Virus Covid-19."

Kochana babciu moja, dziekuje Ci za Twoje zycie i Twoja ciezka prace co wlozylas w nas wszystkich w rodzinie calej i w nasze wychowanie od dziecka. Swoja ciezka praca nauczylas nasz szcunku do ciezkiej pracy, do ludzi i do ciezkiego zycia. Twoje cieple serce I Twoja troska o innych nauczyla mnie skromnosci i opieki nad innymi ludzmi zanim pomyslalas o samej sobie. Pomagalas i dawalas ludziom wszystko ostatnia kromke chleba zeby mieli dobrze. Twoja dobroc nauczyla mnie skromnosci i wrazliwosci dla tych co potrzebua ciepla bardziej duzo wiecj niz ja. Kocham Cie bardzo i ofiaruje Ci zpalate poprzez swoje poswiecenie do pracy naukowej, to jest za cale Twoje zycie babciu. Twoja na zawsze w sercu wnuczka *Edyta Carrion Paczkowska.* Rowniez ten doktorat dedykuje swoim rodzicom i ich rodzicom a moim dziadkom, bratu, siostrom, kuzynom, w Polsce i za granicom i tym ktorzy odeszli z tej ziemi za ich dobre slowa, za ich wiare we mnie i za ich serca ktore mi okazali ze wlzami. Pan Bog z Wami.

Acknowledgements

First and foremost, I want to honour my supervisor, Professor Cathy Thornton. She kindly supervised me and allowed me to learn biochemistry, a small amount of immunology and placenta biology. Without this opportunity to study in Prof Thornton's group, I would not be doing this PhD study, so I am grateful forever. Special thanks to Dr Angelini and his collaborator, Dr Lopalco, who came from the University of Bari, Italy. They taught me lipid extraction, TLC, and MALDI ToF MS technique, and Dr Angelini's expertise in tissue imaging gave me a chance to learn about tissue preparation for imaging.

The learned appreciation of these methods prove invaluable in the workplace in the future. With these skills embedded in me for life, I want to practice them and treat them with the highest degree of accuracy and respect. Thank you to all the other supervisors and funders who have helped me with the PhD process. That includes all student members since I joined the CT group. It also includes Professor Martin Clift, Dr James Cronin and my second supervisor, Dr Ed Dudley. Professor Cathy Thornton, my doctoral supervisor, is the most caring, understanding, and supportive person I have ever met. This PhD thesis is completed thanks to Professor Cathy Thornton's support, checking on corrections and ensuring mental focus and well-being were on track. Due to this reason and many more, with humble gratitude and appreciation from the bottom of my heart, I thank you for the opportunity to work in Professor Cathy Thornton's group at the Institute of Life Sciences (ILS1). This thesis work is equally dedicated to Professor Cathy Thornton and my deep appreciation for the NMSF facility research scientists and technicians who have helped during my sample running and dealing with MALDI TOF MS calibration, especially Dr Ann Hunter, Dr Rhodri Owen, and Professor Gareth Brenton and Dr Angelini. Without their help and equal access to the mass spectrometry facility, I would not have been able to run samples correctly. I am humbly grateful for their expertise. Last, I thank all my friends and loved ones in Poland, abroad, and especially in the UK. They supported my thoughts and checked in with me during personal struggles with self-isolation and writing discipline. I thank you for all your messages.

Abstract

A placenta's lipid content and lipid intermediates are referred to in biology as lipid mediators, which act as cellular messengers established during pregnancy in the mother's cells. The outer and inner sites of the cell membrane rely on lipids' structural fluidity, permeability, and transport. Phospholipids in cell membranes are amphiphiles that affect cellular and metabolic pathways and the balance between pro- and anti-inflammatory responses. Pregnancy perturbations might be influenced by fluctuations between phospholipids and insulin in the body. This project aims to learn about and identify total lipid species from the human placenta and maternal plasma. A potential global marker of obesity and gestational diabetes mellitus (GDM) pregnancy as a pro-inflammatory biomarker can also be determined by measuring phosphatidylcholine (PC) versus lysophosphatidylcholine (LPC). Our work aims to develop extraction and bioanalytical TLC addition confirmation for MALDI TOF MS mass spectrometry to understand lipid biologics better. Also, learn and understand the placenta lipidome in obese and GDM placentas. MALDI TOF MS mass spectrometry is used to gain a broad understanding of lipid composition using thin-layer chromatography (TLC) and preparative TLC. Using MALDI ToF MS confirms total lipid species, including phospholipid species. As a potential biomarker that disrupts the balance between pro-inflammatory and anti-inflammatory responses, hydrolysed lysophosphatidylcholine LPC and native phosphatidylcholine PC can trigger pro-inflammatory responses. Placentas and plasmas of healthy controls and obese and GDM patients were compared for body mass index BMI. Using a total lipid extract and adapted chromatography, lipid extraction and separation could be performed to gain insights into what is inside the placenta regarding lipids. The experimental bioanalysis using TLC and MALDI ToF MS provided a good basis for observing and identifying the mass-to-charge ratios of lipid species and collaborative confirmation of the method's ability to be applied to further advanced chromatography techniques.

List of Tables

List of Figures

Abbreviations

2-AG 2-arachidonoylglycerol

AA Arachidonic acid

AEA Anandamide

APCI Atmospheric Pressure Chemical Ionization

ATGL Adipose triglyceride lipase

CE Cholesteryl ester

Cer ceramide

CT Cytotrophoblast

DAG Diacylglycerol

DAGL Diacylglycerol lipase

DE Delayed Extraction

DG Diglyceride

DHB 2,5-Dihydroxybenzoic Acid

EI Electron Impact

EL Endothelial lipase

ESI Electrospray Ionisation

FAAH Fatty acid amide hydrolase

FGF Fibroblast Growth Factor

GDM Gestational diabetes mellitus

HBC Hofbauer cell

hCG human chorionic gonadotropin

HDL High-density lipoprotein

HPLC High-Performance Liquid Chromatography

HSL Hormone-sensitive lipase

IL-1 Interleukin-1 : IL-1 alpha (IL-1α) and IL-1 beta (IL-1β)

IGF insulin-like growth factor

IR Infrared

IUGR intrauterine growth restriction

LAL Lysosomal acid lipase

LIF Leukaemia Inhibitory Factor

LPC Lyso-Phosphatidylcholine

LPL Lipoprotein lipase

m/z mass to charge ratio

MALDI Matrix-Assisted Laser Desorption and Ionization

MG Monoglyceride

MGL Monoacylglycerol lipase

MS Mass Spectrometry

MS mass spectrometry

MS/MS tandem mass spectrometry

MTBE tert-butyl methyl ether

NEFA non-esterified fatty acid

PC Phosphatidylcholine

PE Phosphatidylethanolamine

PE Pre-eclampsia

PG Phosphatidylglycerol

20

PI Phosphatidylinositol

PL phospholipid

PLA2 Phospholipase A2

PNA Para-Nitroaniline

PO Palmitoyl-oleoyl-

PS Phosphatidylserine

PSD Post Source Decay

PUFA polyunsaturated fatty acid

rpm rotations per minute

S/N Signal to Noise

SM Sphingomyelin

SM sphingomyelin TAG triacylglycerol-density lipoprotein

sn Stereospecific Numbering

ST Syncytiotrophoblast

TFA Trifluoroacetic Acid

TG Triglyceride

THC Tetrahydrocannabinol

TLC Thin-Layer Chromatography

TOF Time-of-Flight detector

UV Ultraviolet

VLDL Very low-density lipoprotein

Contents

T

Chapter: 1 Introduction

1.1 Overview

This introduction gives the reason for this work and describes already-known insights about human placental lipid composition, the cellular function of lipids, and approaches to lipid analysis. Work explains particularly phospholipids, thin layer chromatography (TLC), high-performance preparative thin layer chromatography (HP-TLC) separation of the placenta and plasma lipids, and analysis by matrix-assisted laser desorption ionisation-time of flight mass spectrometry (MALDI ToF MS. This work aims to understand the placenta's lipid content and identify the molecular masses of lipids to measure any differences in healthy compared to diseased samples. Disease samples include obesity based on body mass index (BMI) and gestational diabetes mellitus (GDM) based on clinical ascertainment. The aim is to provide biological insights by identifying placental lipids, particularly phospholipids, towards measuring inflammation to improve understanding of disease and as a potential biomarker. Limited literature exists on human placental lipids and their functions as cellular signalling molecules. However, this work focuses on setting up placental and plasma lipid chromatographic separation and analysis methods to facilitate the study of these.

One key focus is analysing phosphatidylcholine (PC) and lysophosphatidylcholine (LPC) to measure the relative ratio of these in placentas and plasma from women who are obese or have GDM compared to healthy gestation age-matched controls. The goal is a reliable method for lipid extraction and identification from the human placenta and blood plasma. The approach includes identification by TLC as a bridging opportunity to bioanalytical high-resolution mass spectrometry with collaborators in-house and externally. Further, this work also explains the initial stages of setting up methods for sample preparation and running MALDI Imaging. The MALDI Imaging work was an essential part of this research, and working efforts can help future research in lipid imaging in placental tissue.

1.1.1 Study Aims

This research study has investigated placental tissue and plasma lipids. Lipids, in general, are naturally occurring biochemical molecules alongside proteins and carbohydrates. Critical roles for lipids in biology include energy storage, cell membrane composition and metabolic breakdown pathways to cellular signalling via the intermediates of fatty acids, known as lipid mediators. The research objectives are methodology, protocol setup, and validation towards future research to enable the identification of lipids in biological environments. It includes placenta, blood plasma, or other human tissue samples that use lipids as ways of tracing, for example, the cancer microenvironment or inflammation-related disorders. The purpose of this research is to establish methods and find out differences or similarities in placenta lipids, having validated methods optimised on human tissue placenta and blood plasma approach with bioanalytical semiquantitative data acquisition and analysis using phosphatidylcholine with the hydrolysed lysophosphatidylcholine as a relative percentage ratio comparison between placenta BMI group and plasma. The aim of measuring total lipids in placenta tissue and blood plasma is to use this approach in identifying limits for lipid biomarkers in pregnancy obesity and gestational diabetes, which is essential and highly relevant to other diseases such as cancer, inflammation, and hypertension in obstetrics during adverse pregnancy. We aim to identify possible inflammatory biomarkers and, later, consider them as cellular signalling molecules through additional studies of fatty acids with future collaborations. The extraction methods and analysis of the total lipid extract by TLC and further isolation of the total lipid into separate lipid bands described in this thesis work as a methodical narrative setup and investigation by ionisation methods in MALDI ToF MS MS mass spectrometry with the reported relative ratio of the placenta extract and plasma total lipids evaluated as relative ratio PC/LPC plotted using GraphPad to observe differences and similarities in healthy control pregnancies versus obesity and gestational diabetes mellitus GDM.

1.2 Pregnancy Overview

Pregnancy affects hormone levels and weight gain and causes biophysical and emotional changes. Pregnancy lasts around 40 weeks, divided into three trimesters

(1). The start of pregnancy is considered the first day of the last menstrual period. In the first trimester, a fertilised egg implants into the uterus, the placenta forms, and major organs, such as the baby's heart, develop by the end of the first trimester. Miscarriage risk decreases during the second trimester when the baby's organs continue to evolve, the mother's belly grows, and the mother starts to feel fetal movement. The third trimester begins at around week twenty-nine and lasts until delivery. Pregnancy starts with fertilisation, which happens when a sperm cell successfully penetrates and fuses with an egg (ovum, oocyte), resulting in a zygote that contains all the genetic information needed for development. Cell division leads to the development of the multicellular morula (Figure 1.1), which moves through the fallopian tube to the blastocyst stage, which settles and then penetrates the endometrium of the uterus. The endometrium undergoes a structural change called decidualisation, which involves a morphological change of the endometrium lining into the decidua lining *(2)*. The decidua provides temporary nutrition for the embryo until the yolk sac and the placenta properly develop. The decidual reaction begins during the menstrual cycle after ovulation, where elevated progesterone levels initiate the molecular changes leading to decidualisation. It is accompanied by an influx of white blood cells that will either support endometrium breakdown if pregnancy does not occur or implantation and placentation if pregnancy does occur *(3, 4)*.

The implantation process is summarised in (Figure 1.1) early fertilisation and implantation stages are in (Figure 1.2). A critical stage in embryonic development is the formation of morula during fertilisation. Cell-to-cell tight junctions are established during the morula stage, characterised by a compact sphere of cells*(5)*. A trophectoderm (TE) precursor emerges during this transition, contributing to placental development. Also, at the same time, cells constitute the inner cell mass (ICM), contributing to embryonic and extraembryonic development *(6)*. Forming a mature placenta begins when morula ball cells become trophoblasts *(7)*. As morula compaction and blastocyst formation proceed, ICM and trophoblasts differentiate *(8)*.

A blastocyst forms about five to six days after fertilisation, consisting of two main parts: the inner cell mass ICM, which has the most cells (which produces the embryo

developments) and the trophoblast (which makes extraembryonic tissues). These pluripotent cells can create all types of organs and tissues. The trophoblast is one of two types of cells that differentiate from the outer layer in the blastocyst *(9)*. All human cells originate in three primary germ layers: ectoderm, mesoderm, and endoderm. There are two primary kinds of cells in the trophectoderm on the surface of the blastocyst: trophectoderm forms placentas, amnions, and chorions, which are extraembryonic tissues *(9)*. During implantation, trophectoderm attaches the blastocyst to the uterine wall—mother and embryo exchange waste and nutrients through the placenta *(10, 11)*. Placentation and implantation are dependent on it. The placenta is nourished and supported by trophoblasts, which convert cells into extraembryonic tissues *(10)*. It is trophoblasts that make pregnancy possible*(9)*.

Differentiation leads to various structures, including the placenta, which exchanges nutrients and supports the embryo. Trophectoderm derivatives are called trophoblasts in placenta development, as trophectoderm comes from trophoblasts*(9)*. Tissue differentiation into trophoblastic cells occurs as trophectoderm cells divide. The trophoblastic cells create the placenta, interact with the uterine lining, and produce hormones like HCG in pregnancy *(12)*. In pregnancy, trophoblast cells differentiate into syncytiotrophoblast and cytotrophoblast. The blastocyst outer layer is covered and formed from the trophoblast *(9)*. These cells help the blastocyst attach to the uterine wall during implantation and go on to produce the placenta. The trophoblast makes amnion, chorion, and allantois, supporting embryonic development and growth *(9, 12)*.

1.3 Placenta embryology overview

The placenta grows parallel to the development of the uterus as a temporary organ whose genetic characteristics are identical to the developing fetus. The placenta comprises the parenchyma, chorion, amnion, and umbilical cord. It forms from the zygote, separates the fetus from the endometrium, and gets delivered after birth. The contact of the trophoblast with the endometrium causes the development of the syncytiotrophoblast and cytotrophoblast, which secrete enzymes that break down the bond between endometrial cells so the syncytiotrophoblast can invade the endometrial wall. These cells are part of the chorion, which develops into the

placenta. The decidua connective tissue develops into decidua cells as progesterone increases, and the decidua capsularis villi degenerate and disappear as they fuse with the decidua parietalis. The monochorionic membrane then ruptures during labour. The monochorionic membrane with the fetal vessels makes up the chorionic plate, which is attached to the endometrium by the fetal chorionic sac. Fetal blood vessels are bathing in maternal blood, but there is usually no mixing between maternal and fetal red blood cells.

The placenta is an immune and endocrine organ that produces hormones and growth factors in autocrine and paracrine modalities. It can make its glycogen and cholesterol from maternal glucose and fatty acids, synthesising human chorionic gonadotropin and human lactogen. Several molecules interact with the placenta, including leptin, insulin, many growth factors, human chorionic gonadotropin, steroids, and hypoxia. The placenta is the means of communication between mother and fetus and is essential for transferring gases, electrolytes, hormones, maternal antibodies, fetal waste, and nutrition. The placenta uses channels for ion transport, facilitated diffusion for glucose using carrier proteins, and active transport for several solutes.

The placenta can grow through the total thickness of the myometrium and reach the serosa of the uterus, which can cause bleeding during pregnancy and bleeding complications postpartum. The umbilical cord can also have multiple arteries, veins, and cysts. The placenta can have a velamentous insertion or a marginal insertion. A velamentous insertion is dangerous because the vessels are exposed and not protected by Wharton's jelly. The placenta may be stored in a refrigerator or fixative for further examination after parturition. Placental detachment is a hazardous circumstance and may be due to hypertension, diabetes, or drug use. The placenta is a vital fetal organ necessary for a healthy pregnancy for both mother and fetus *(13-19)*.

1.3.1 Placenta stages

An effective pregnancy depends on the development of the placenta. Structures develop in the fetal and maternal environments to support the growing fetus. The

following are the main components and stages in placental development: During fertilisation, sperm cells fertilise eggs, forming zygotes—a ball of cells morula, forms in the zygote after several divisions. The morula divides into a blastocyst composed of two main parts: the trophoblast and the inner cell mass. An outer layer of cells in a blastocyst is known as the trophoblast. It undergoes differentiation and plays a vital role in implantation. The blastocyst connects to the uterine wall (endometrium) approximately six days after fertilisation. This attachment establishes pregnancy.

Following implantation, trophoblast cells differentiate and produce various fetal structures, including the amnion and chorion. The chorion at the fetal side surrounds the embryo. Endometrium changes on the maternal side to form the decidua, which consists of three parts: decidua basalis (deeply located at the implantation site), decidua capsularis (covering the implantation site), and decidua parietalis (surrounding the rest of the uterine cavity). The placenta gradually grows in complexity through the first trimester and beyond. It exchanges nutrients, oxygen, and waste products in circulation. The placenta interacts with the maternal environment during pregnancy, regulating hormone production, immune responses, and nutrition transfer. During pregnancy, the placenta transforms into a temporary organ, sharing the genetic characteristics of the fetus. A healthy pregnancy depends on the placenta's development. Complications or abnormalities in placental development can affect both mother and baby. A crucial part of prenatal care is monitoring the placenta's health *(13-19)*.

1.3.2 Early stage

The early stages of pregnancy highlight the remarkable journey from fertilisation to establishing a functional placenta. Following fertilisation, the zygote divides several times to form a morula, eventually developing into a blastocyst. There is an inner cell mass (the future embryo) and an outer layer called a trophoblast (the future placenta). Following fertilisation, the blastocyst implants into the uterus and differentiates into trophoblasts. A trophoblast differentiates into a syncytiotrophoblast that invades the endometrium and secretes hCG. In addition, these cells become cytotrophoblasts, which secrete enzymes that facilitate invasion.

The chorion, the basis of the placenta, evolves through the interaction between trophoblasts and extraembryonic mesoderm. In primary chorionic villi, the cytotrophoblast develops into the syncytiotrophoblast. The villi develop into secondary and tertiary villi to exchange between maternal and fetal circulation. A modified decidua endometrial lining and the amniotic sac surrounding the embryo develop simultaneously. As the decidua capsularis and parietalis merge, it provides stability. The placental cotyledon forms at the fetomaternal junction, where the chorionic villi anchor the fetus to the uterus. Each cotyledon is bathed in maternal blood via uterine spiral arteries, exchanging nutrients and gas without mixing maternal and fetal blood. The two arteries, one vein, connect the fetus with the placenta via the umbilical cord by supplying oxygenated blood and nutrients *(13-19)*.

1.3.3 Endocrine function

The multifunctional nature of the placenta, encompassing both protective and supportive roles, highlights its complexity and importance in human reproduction. The placenta is a complex organ with critical cellular structures and functions. These include immune and endocrine cellular tasks that protect the fetus from harmful substances and infections. They also produce hormones and growth factors critical for a healthy pregnancy. ATP-binding cassette (ABC) is a superfamily of protein transporters' biochemical structures. There are different ABC superfamily members which transport many substances found in the placenta. For example, multidrug resistance protein type 1 (MDR1), breast cancer resistance protein (BCRP), and multidrug resistance-like proteins (MRP2 and MRP5) are the most important proteins. They support the placenta by removing harmful substances from the placental and fetal circulation. These proteins protect the development of the fetus. The placenta provides an immune interface between the mother and fetus. It protects the fetus from infectious agents, while the mother's immune system suppresses to avoid rejecting the fetus. Placenta-derived immune cells and immune-modulating molecules facilitate the placenta's immunological function. A placenta is an endocrine organ that secretes hormones and growth factors essential for maintaining pregnancy and fetal development. It consists of the uterine lining maintained by progesterone, human chorionic gonadotropin (hCG, which signals the corpus luteum

to continue producing progesterone) and human placental lactogen (hPL, which is essential for maternal metabolism and fetal growth). The two types of cells secrete corticotropin-releasing hormone (CRH) and fibroblast growth factor (FGF), which function both during fetal development and pregnancy *(13-19)*.

1.3.4 Biochemical function

The placenta's biochemical functions convert maternal glucose into glycogen, which the fetus uses for energy. Progesterone and estrogen maintain pregnancy and prepare the mother for childbirth. Produced from maternal fatty acids, which are crucial for hormone production. The development and maturation of fetal lungs require glucocorticoids. In alveoli, surfactants are produced by glucocorticoids, which reduce surface tension by stimulating surfactant production *(20)*. It has been reported that it increases phosphatidylcholine activity and increases the production of surfactant proteins *(21)*. In fetuses and embryos, placental enzymes partially inactivate glucocorticoids. Glucocorticoids play a vital role in cell type differentiation and tissue maturation, especially in the lungs. That is, as the hypothalamus, pituitary, and adrenal systems mature. Glucocorticoids promote structural maturation by stimulating cell maturation and differentiation *(22)*.

Consequently, they alter interstitial DNA synthesis and alveolar development. That hormone helps the lungs absorb lung fluid when the fetal stage transitions to the neonatal stage. In the developing lungs, glucocorticoids act through enzymes like catalase, glutathione peroxidase, and superoxide dismutase to protect them from oxidative stress. The effects of glucocorticoids on lung function and development can be attributed to gene expression. The glucocorticoids that trigger lung maturation cause specific proteins to be synthesized. The activation of enzymes by glucocorticoids enhances surfactant production. The glucocorticoids also interact with transcription factors such as nuclear factor kappa-B and activated protein-1 to regulate inflammation *(22, 23)*.

Several peptide hormones engage in placental fetal development; for example, hCG boosts progesterone in the corpus luteum in pregnancy. For instance, hPL regulates maternal metabolism and fetal growth. Fetus growth is affected by Growth Hormone

(GH). Angiogenesis and vascular development depend on Vascular Endothelial Growth Factor (VEGF). The hypothalamic-pituitary-adrenal (HPA) axis function is regulated by corticotropin-releasing hormones (CRH). Prenatal growth depends on insulin-like Growth Factor (IGF). The placental growth factor (PlGF) promotes placental development. Cytokines stimulate immune responses *(13-19)*.

1.3.4.1 Hormonal interphase

Placental interactions during fetal development use leptin, a homeostatic agent that promotes proliferation, protein synthesis, and anti-apoptotic activity. Insulin, growth factors, hCG, steroids, and hypoxia affect regulation. Different substances, including growth factors, hormones, and oxygen, regulate placenta function and health. As an active endocrine organ, the placenta regulates fetal development and maternal physiology during pregnancy and provides nutrient and gas exchange. The interplay between hormones and molecular factors ensures healthy fetal development, demonstrating the profound complexity of pregnancy at a molecular and biochemical level. The placenta controls the HPA axis and parturition (childbirth) timing. The fetal HPA axis is a significant component of the neuroendocrine system, and the HPA axis regulates digestion, the immune system, mood and emotions, sexuality, and energy storage and expenditure in response to stress. The HPA axis influences lung development and maturation in the fetus *(13-19)*.

Like the brain's hypothalamus, the placenta produces CRH (Corticotropin-Releasing Hormone). Placental CRH stimulates ACTH (Adrenocorticotropic Hormone) secreted by the pituitary gland, stimulating cortisol production by the adrenal glands. Cortisol is especially crucial for fetal organ development, which produces surfactants that facilitate breathing after birth. Unlike adults, the fetal HPA axis does not have a fully developed feedback inhibition mechanism. High cortisol levels do not significantly inhibit CRH and ACTH production as they do in the adult HPA axis. Preparing the fetus for birth and initiating labour is a crucial function of the placental HPA axis. A complex interplay of hormones exists between the fetus, the placenta, and the mother. One of the critical events triggering labour is the activation of the fetal HPA axis, leading to an increase in cortisol production. In the uterus and placenta, cortisol from the fetus stimulates prostaglandin production, which initiates

labour. As labour approaches, the placental CRH increases. Increasing uterine contractility and influencing other labour hormones play a role in parturition timing. Placental hormones and fetal cortisol interact with maternal hormones, preparing the body for birth. They increase uterine sensitivity to contraction-inducing agents by converting maternal progesterone to estrogen. Parturition timing is also affected by mechanical factors (such as stretching of the uterus and cervix) (8-9).

1.3.4.2 Efficacy

Placental efficiency in nutrient and gas exchange can be affected by maternal health, blood flow, and substances or conditions (e.g., hypoxia leading to fetal growth restriction). Fetal development and the mother's well-being depend on the placenta's exchange of nutrients, gases, and wastes. The functions are as follows: oxygen and carbon dioxide exchange between mother and fetus through the placenta. Maternal blood oxygenates fetal blood, while fetal blood carbon dioxide is passed to maternal blood. Due to their lipophilic nature, these gases are highly permeable across placental tissues, facilitating fetal respiration. Mother and fetus share nutrients through the placenta. Nutrients include water, amino acids, glucose, vitamins, and free fatty acids. During this nutrient transfer, the bulk flow of water carries nutrients across the placental membrane through solvent drag. Maintaining a healthy fetal environment requires the removal of waste from the fetal system. The placenta transfers fetal waste products like urea, uric acid, and bilirubin to the mother's blood.

Placentas exchange hormones that maintain pregnancy and prepare the mother's body for childbirth and lactation. The placenta transfers maternal antibodies to the developing fetus, providing passive immunity. Alpha-fetoprotein and other essential molecules are exchanged through the placental barrier, affecting fetal development and maternal health. Placentas transfer beneficial substances, but they also function as selective barriers. Placental transport mechanisms include simple diffusion for gases, facilitated diffusion (such as carrier proteins for glucose), active transport for specific solutes, and ion channels to balance electrolytes (10-14).

In general, the placental barrier is effective but not impenetrable. Gaseous diffusion, glucose diffusion, active transport, and ion channels contribute to placental transport

(24). The placental barrier prevents harmful substances from reaching the fetus, but it is fallible. The congenital infections (**To**xoplasma gondii, **R**ubella virus, **C**ytomegalovirus, and **H**erpes virus) best known by the acronym TORCH pose a significant threat to reproductive health by potentially infecting fetuses and resulting in severe fetal outcomes *(25, 26) (27, 28) (29, 30) (31)*. It has been shown that these viral pathogens can bypass placental defences and cause intrauterine infections, which can lead to congenital disorders such as microcephaly, neurological damage, and hearing loss in infants *(29)*. A compromised fetoplacental barrier and potential harm caused by viral effects may manifest with placental insufficiency in women with TORCH infections *(27)*. Researchers need to understand the interaction of TORCH pathogens with the placenta to monitor and diagnose perinatal infections in at-risk newborns *(25, 32, 33)*. Infections of the TORCH type can lead to severe congenital anomalies during pregnancy*(31) (34)*. Some infections can cross the placental barrier, leading to infant death and lifelong morbidity in neonates *(26)* and mortality. Maternal TORCH serology screens for suspected fetal infection *(30)* are crucial for understanding their pathogenesis and defence mechanisms.

Environmental pollutants and nanoparticles have also been reported to cross the placental barrier through fetal exposure *(35, 36)*. In addition, research has been conducted on factors influencing placental barrier permeability. For example, a reduction in placental volume and surface area is associated with intrauterine growth restriction (IUGR) *(37)*. Placental proteins, transporters, and enzymes contribute to the placenta's drug permeability *(38)*. Researchers have developed placenta-on-a-chip models to study placenta biology and assess barrier permeability. These models provide insight into how substances are transported across the placental barrier *(39, 40)*. Studies using trophoblast stem cells have also contributed to developing novel human placental barrier models, allowing the investigation of substance exchange and fetus harm *(41)*.

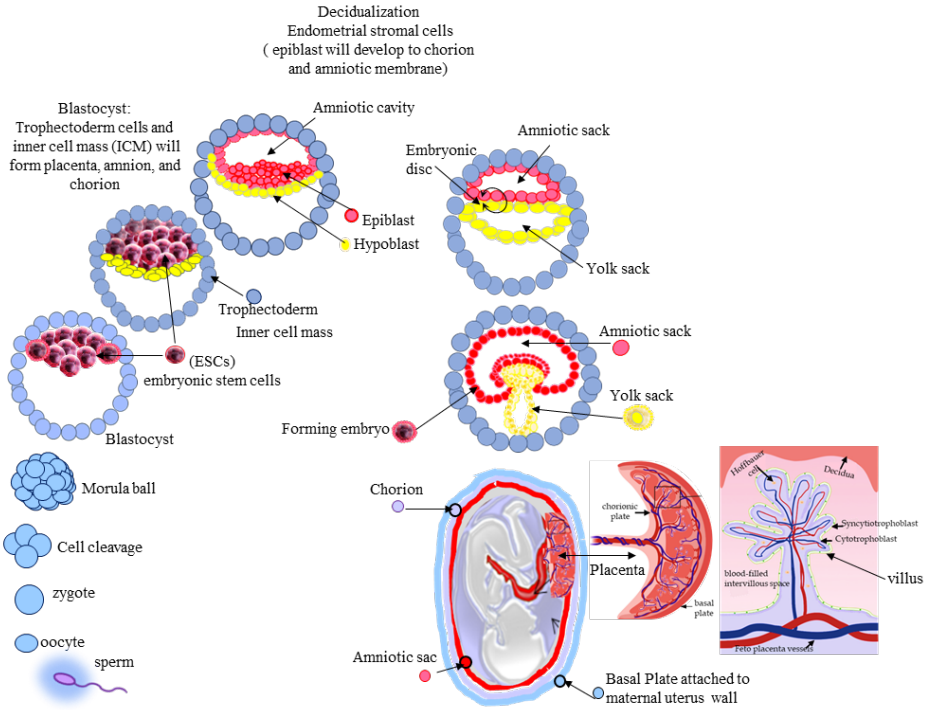

Figure 1:1 Diagram shows the early stages of fertilisation. The early fertilisation stages comprise morula ball forming, leading to embryonic endometrial stromal cells (ESCs). An embryonic blastocyst inner cell mass (ICM) is a cluster of cells within the early stages of development. I-pen drawings have been created in PowerPoint and saved as jpegs.

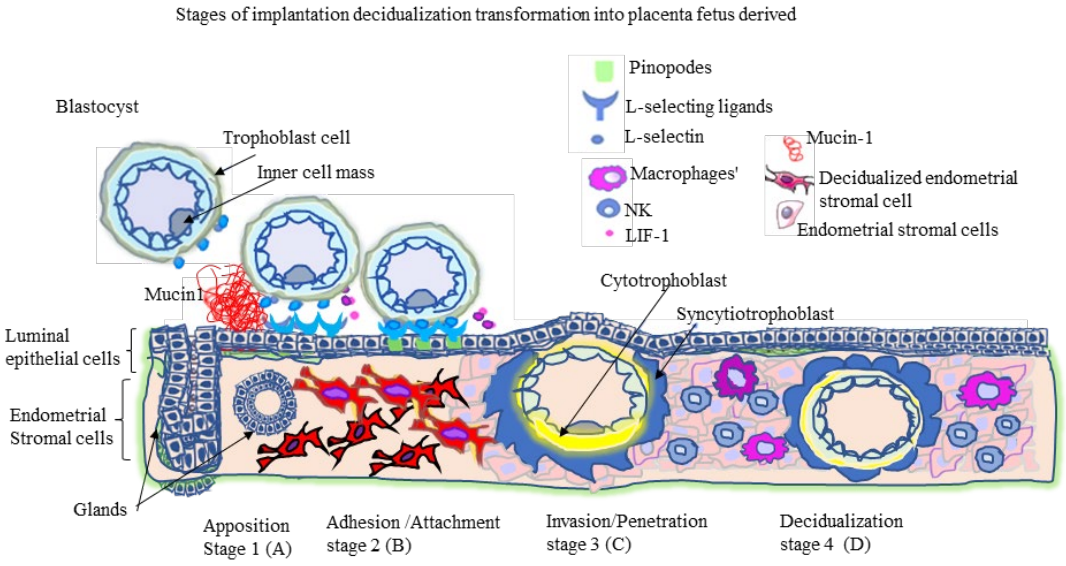

Figure 1:2 The stages of human implantation: apposition, adhesion, invasion, penetration, and decidualisation. The illustration has been hand drawn using an i-pen in PowerPoint and saved as a picture idea adapted from *(2)*

1.3.4.3 Trophoblast

Attachment of the blastocyst to the endometrium depends on integrins, selectins, and cell adhesion molecules. As the blastocyst implants, the embryo, yolk sac and placenta emerge as separate structures. The internal cellular mass evolves and develops into the fetus, and the external embryonic cells differentiate into the trophectoderm, which converts and expands into the mature placenta. Trophoblast cells from the trophectoderm invade the endometrium, where they remodel the local tissue, including the maternal vasculature, to eventually establish the fully functioning placenta that supports fetal development for the remainder of the pregnancy. During implantation, placental trophoblast cells release signalling molecules that control the embryo and the endometrium. There are two main types of trophoblast cells: cytotrophoblast and syncytiotrophoblast. Cytotrophoblasts differentiate from blastocysts and invade the endometrium through signalling molecules and proteolytic enzymes such as matrix metalloproteinases (MMPs). Hormones, growth factors, cytokines, and other mediators support communication between the embryo and endometrium to support the establishment of the placenta. Examples include human chorionic gonadotropin (hCG), leukaemia inhibitory factor (LIF), interleukin-1 (IL-1), insulin-like growth factor (IGF), fibroblast growth factor (FGF), and interferons.

1.4 The placenta

The placenta is genetically identical to the fetus. Placental development in humans brings the maternal and fetal circulations close together to enable gas exchange and nutrient delivery *(42)*. The placenta's job is to deliver oxygen, nutrients, and growth factors to the fetus, protect it against external toxins and pathogens, and remove waste and carbon dioxide. Once the folk sac disintegrates, all necessary nutrients must come from the maternal circulation via blood vessels in the placenta, umbilical cord, and fetus *(42)*. During placental development, the two blood circulations are only separated by the epithelial cell line layer called syncytiotrophoblast, the stromal layer comprising fibroblast blasts and macrophages, and the endothelial cells lining the fetal capillaries. The syncytiotrophoblast cells – derived by syncytialisation of cytotrophoblasts - of the syncytial epithelium are the critical transporters between

the fetal and maternal sides, being fundamental for solute transfer, diffusion, active transport, and endocytosis. The transport of nutrients from the mother to the placenta operates by the mother's ability to provide nutrients in response to the demands of the fetus. Therefore, the placenta's ability to deliver nutrients changes in response to maternal and fetal signalling demands. Any adverse changes in placental function can contribute directly to abnormal structural or physiological fetal growth. Therefore, understanding placenta function and maternal-fetal communication via the placenta is essential to understanding and preventing pregnancy abnormalities and developing new interventions or diagnostic strategies.

1.4.1 Structure

By full term, or from the 37th week of gestation, the placenta weighs 500-1500 grams, is about 2.5 cm thick at its thickest part and is 20-22 cm in circumference. The placenta has two surfaces. On the fetal side is a chorionic plate connecting with the umbilical cord, and the basal plate is attached to the uterus wall. Between the chorionic and basal plates, the intermediate layer of the placenta fills with a heavily branched, tree-like villous structure as the placenta develops and grows. Villous length, diameter, and structure change and expand during pregnancy. The branched villous tree originates from the villous stem cells attached to the chorionic plate that differentiate and branch off sequentially to populate a series of globular lobules approximately 3 cm in diameter. These lobules spread over the maternal spiral arteries (see Figure 1.3), enabling blood to flush over the basal plate, where nutrients, gases, and other molecules exchange before maternal blood drains to the uterine veins and maternal circulation. Exchange between the maternal and fetal circulation happens independently in each lobule. The branches of villous trees are final and terminal villi composed of large networks of fetal vascular capillaries spread in a sinusoidal wave-like shape to keep the fetal endothelium close to the trophoblast layer to optimise diffusion distance from maternal to fetal circulation. The villous tree coating is by epithelial syncytiotrophoblast cells. These are multinucleated syncytium and are unique to this area only. They specialise in forming a solid layer with no gaps that not only supports exchange between mother and fetus but also limits the passage of pathogens and harmful substances from mother to fetus *(43)*. A

diagram of the placental structure, including a cross-section of chorionic villi in the first and third trimesters, is shown in (Figure 1.3).

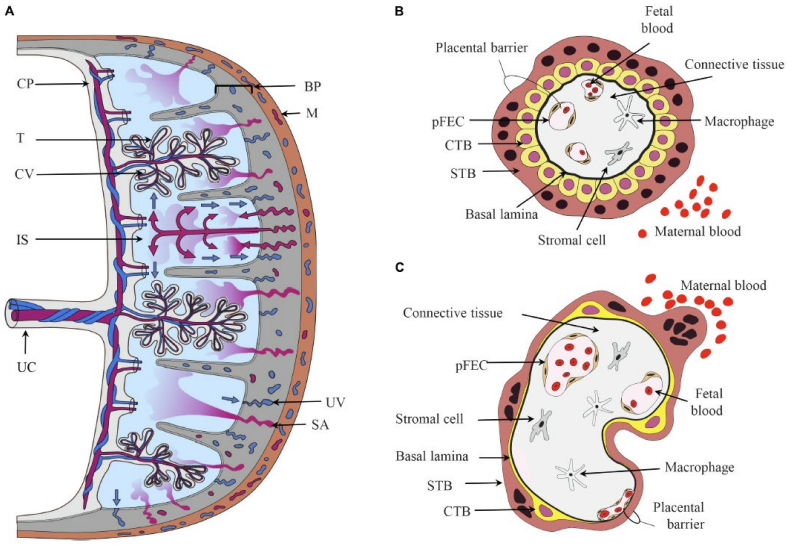

Figure 1:3 Structure of the placenta. Top images A, B, C

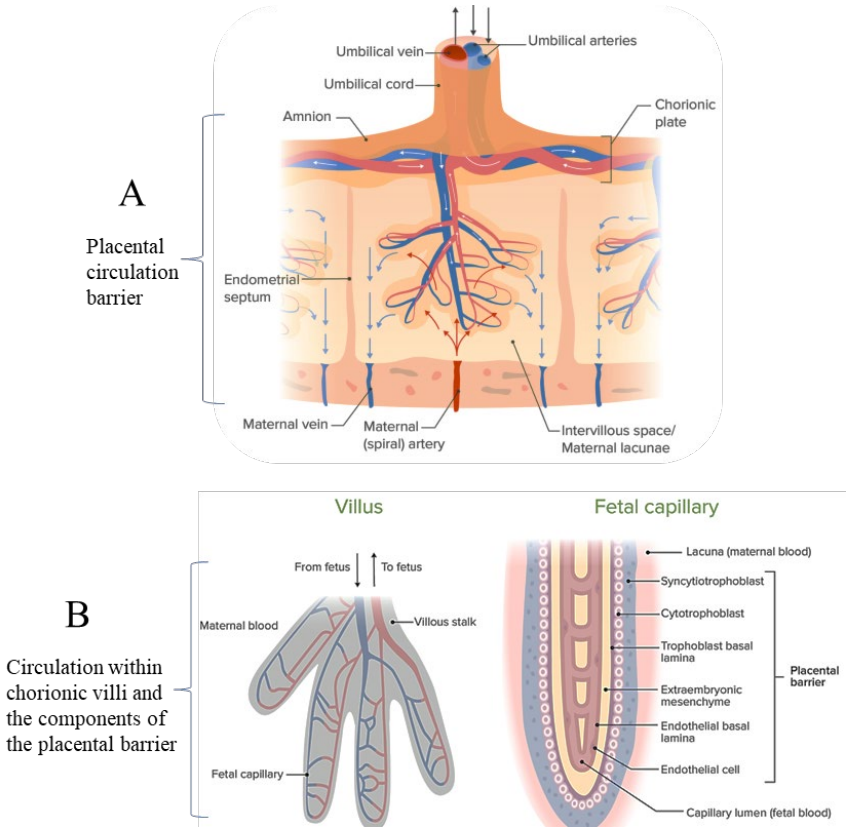

Figure 1:3 continued placenta circulation barrier. Top images A, B, C shows the cross-section of the placenta (A) with a cross-section of chorionic villi in the (B) first and (C) third trimester: chorionic plate(CP), umbilical cord (UC), chorionic villi (CV), intervillous space(IS), spiral arteries (SA), uterine veins (UV), villous

trophoblasts (T), basal plate (BP) contains extra villous trophoblasts and decidual cells, cytotrophoblasts (CTB), placental-fetal-endothelial-cells (pFEC), syncytiotrophoblast (STB). (Authors permission to reuse as a reference) *(44)*. Lower image A shows placental blood flow, and B blood circulation within the chorionic villi and components of the placental barrier.

Placental function depends heavily on the syncytiotrophoblast layer throughout pregnancy *(45)*. The location of the syncytiotrophoblast supports essential functions in the placenta, such as ion and nutrient exchange and the synthesis and secretion of steroids and peptide hormones *(45)*. Syncytiotrophoblast forms by the differentiation and fusion of mononuclear cytotrophoblasts *(45)*, and as pregnancy progresses, the syncytiotrophoblast layer gradually thins out, and the cytotrophoblast layer disperses *(46)*. Another crucial step in placental development is the establishment of maternal-fetal circulation. Under the syncytiotrophoblast, capillaries form, reducing the distance between placental pigs' maternal and fetal circulatory systems *(47)*. The mother and fetus exchange nutrients and waste products, and changes in this network affect placental development and fetal growth. Placenta studies use animal models, such as mice and swine, to study uterine structure and function *(48)*. As a result, these models provide valuable insights into how placentas develop. Human stem cells and microfluidics are future placenta developments *(47)*.

1.4.1.1 Placental blood supply

The chorionic villi regulate the amount of oxygen and carbon dioxide in the fetal bloodstream. Two arteries deliver deoxygenated blood and waste from the fetus to the placenta, while oxygen-rich blood travels directly to the fetus via the umbilical vein (Figure 1.3A). Maternal blood enters the uterus via spiral arteries remodelled during implantation and early placental development and leaves through uterine veins. The spiral arteries and uterine veins are specialised to provide access to the uterus and placenta for maternal blood. Villous trophoblast cells meet maternal blood in the intervillous space, where oxygen and nutrients transfer from maternal to fetal blood. Syncytiotrophoblast cells form the outermost layer of the placenta that contacts the mother's blood. It is a multinucleated layer without cell boundaries created by the fusion of cytotrophoblast located beneath the syncytiotrophoblast and forms the villous tree's outer epithelial covering. Connective tissue (stroma) is underneath the trophoblast layers, and there is a layer of connective tissue within the

chorionic villi that contains fibroblasts and macrophages, including Hofbauer cells, a specialist macrophage of the placenta. Endothelial cells of the fetal capillary blood vessels are the innermost cells in the chorionic villi. Fetal blood is brought close to maternal blood without mixing (Figure 1.3B). The thin walls of the capillaries enable the exchange of substances in the bloodstream. During pregnancy, this barrier narrows as the cytotrophoblast layer regresses and ensures an efficient exchange of gases and nutrients as the baby grows. While the placental barrier physically separates the fetal and maternal blood supplies, certain substances can cross this barrier, including nutrients like glucose and oxygen, waste products, and some drugs and viruses. However, the placental barrier provides some level of immunological protection to the fetus from pathogens in the maternal blood. It is critical to note that while there are these layers, they do not form a continuous "cell layer" barrier; instead, the placental barrier is a gradient allowing for selective exchange. The blood itself never mixes due to the tight control of the barrier. However, bi-directional cell transfer occurs in human and animal pregnancies across the placental barrier, creating fetal-maternal micro chimerism wherein a small number of cells originating from the fetus live within the mother and vice versa, the mother's cells that reside within the fetus.

1.4.1.2 Placental transport

The development of the placenta is crucial to the growth of the fetus and the outcome of the pregnancy. Villous cytotrophoblast and syncytiotrophoblast cells exchange gases and nutrients between the mother and fetus *(49)*. The properties of the vascular-syncytial exchange surface influence the placental transfer of oxygen and carbon dioxide through simple diffusion. The placenta uses transcellular and paracellular pathways to transport energy to the fetus – namely glucose proteins and lipids, examples of trans-placental transfer. Several factors influence the placental transfer of these and other substrates, including substance size, polarity, degree of binding, concentration gradient, presence of transporters, and enzyme activity *(50)*. Specific transporters expressed and distributed between placental cell types and subcellular membrane fractions affect the maternal-fetal transport kinetics of molecules.

Placental exchange factors and glucose metabolism balance are crucial for optimal fetal development *(51)*. For transporting glucose, the placenta engages the primary glucose transporter GLUT1 *(50)*, but other molecules, including iron, drugs, and hormones, can affect glucose transfer by competition for the transporter *(50)*. Maternal diabetes affects placental glucose transporters, such as GLUT1, affecting glucose delivery to the fetus *(52)*. Factors, including glucose concentrations, hormones, and metabolic status, can influence the maternal-fetal glucose gradient. The placenta's structure and flow area via syncytial exchange determine glucose transfer rate availability and utilisation *(51)*. For example, fetal insulin can lower fetal glucose levels and promote maternal-fetal glucose transfer, and insulin-like growth factors (IGF-1) might positively regulate fetal development and sugar metabolism *(53)*.

Fetal plasma amino acid concentrations are significantly higher than maternal plasma due to active transport across the placenta *(54)*. Impaired placental amino acid transport can reduce birth weight *(55)*, and, in turn, fetal growth restriction reduces amino acid uptake, emphasizing the importance of amino acid transport to normal fetal development *(56)*. During amino acid transport in the human placenta, the rapamycin (mTOR) signalling pathway senses nutrients and regulates the placental L-type amino acid transporter system (serine/threonine) kinase *(57)*. Abnormal mTOR pathways might contribute to preeclampsia, intrauterine growth restriction (IUGR), and gestational diabetes *(57)*.

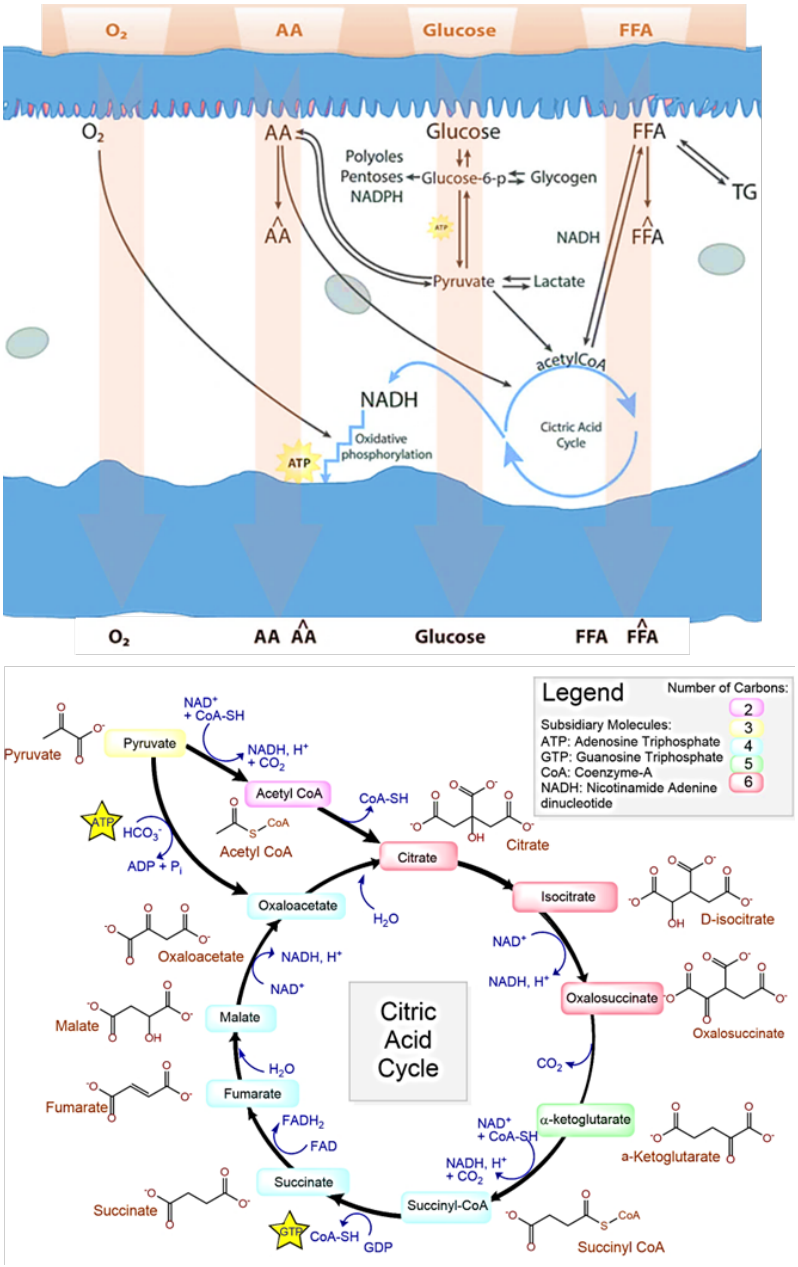

Figure 1:4 Placental metabolism and interconversion into the tricarboxylic acid cycle (also known as citric acid cycle) of substrates, top diagram simplified overview over possible pathways. Diagrams were handmade using ChemDraw and PowerPoint I-Pen and saved as images in a jpeg.

Glucose that is not transferred to the fetus may be directed into glycolysis to produce pyruvate, fermentation to lactate or the pentose phosphate or polyol pathways, both of which are important in the production of precursors of nucleotides for DNA and RNA synthesis. Glucose may also be stored as glycogen. Amino acids can be converted to and exchanged for other amino acids, used as building blocks for protein synthesis, or as fuel for the citric acid cycle. Free fatty acids can be used as fuel via

beta-oxidation to produce NADH and acetyl-CoA, stored as triglycerides, or they may be converted to other free fatty acids before being transported to the fetus. The relative importance of these pathways in the human placenta depends on oxygen and substrate availability and is yet to be determined. AA: amino acids, FFA: free fatty acids, TG: triglycerides, NADH: nicotinamide adenine dinucleotide, ATP: adenosine triphosphate.

Lipoprotein lipases produce free fatty acids and triglycerides for hormone synthesis, and these bind transmembrane proteins sitting on the cell surface, such as a cluster of differentiation 36 (CD36) that binds to fatty acids and helps their transport through the membrane bilayer in the placenta *(54)*. The regulation of placental lipid transport metabolism involves various other proteins and factors, including fatty acid transport protein (FATP) 2 and fatty acid binding proteins (FABPs) *(58)*. Providing enough lipids to the fetus through these proteins contributes to fetal growth and development *(59)*. FATP2 plays a role in transporting fatty acids across membranes, and placental cells transport fatty acids from the maternal circulation using FATP2. Various FABP isoforms exist in the placenta, and they facilitate the movement of fatty acids within the placental cells, directing them to appropriate metabolic pathways for energy production or membrane synthesis *(60)*.

Regulation of placental lipid metabolism by hypoxia-inducible factors (HIFs) is vital to help cells adapt to low oxygen levels (hypoxia). HIFs regulate lipid metabolism in the placenta based on oxygen levels, stabilising and activating lipid metabolism genes during low oxygen. HIFs also increase lipid storage and modify fatty acid oxidation during distorted glucose metabolism *(61)*. A sufficient supply of fatty acids during maternal obesity is essential for developing neurons in the fetus *(62)*; as a result of proteins such as HIFs, FATP2, and FABPs, the developing fetus normally receives enough lipids to grow and develop. The disruption or dysregulation of these proteins can have implications, including IUGR *(63)*. Placenta cells also require cholesterol for structure and function *(64)*. Cholesterol must be transferred from the maternal to the fetal compartment during fetal development. Placental cholesterol uptake occurs through low-density lipoprotein (LDL) using LDL scavenger receptors.

The classical LDL receptor pathway regulates LDL uptake to prevent cholesterol overload. Maternal blood sugar, triglyceride, and placental function influence fetal growth. Fetal hormones also regulate maternal metabolism, showing bidirectional communication between the fetus and the mother for nutrition allocation *(65)*. Complications can develop if supply is disturbed by maternal obesity, diabetes or undernutrition that causes constant or chronic pulsative maternal hyperglycaemia cells *(66, 67)*. As a result, complications like preeclampsia and fetal macrosomia can arise with both immediate and long-term effects on the health of the mother and child *(68)*.

1.5 Lipids in Biology

Understanding lipid expression and metabolism is essential to understanding normal and adverse placental function. What is a lipid? Lipids are molecules that are insoluble in water but soluble in organic solvents. The natural lipid group consists of fatty acids, waxes, eicosanoids, monoglycerides, diglycerides, triglycerides, phospholipids, sphingolipids, sterols, terpenes, phenols, and fat-based vitamins (like vitamins A, D, E, and K). Other major biological molecules, namely nucleic acids, amino acids, and carbohydrates, are not lipid-soluble. A lipid serves as a signalling molecule, energy storage molecule, and cell membrane structural component. Lipids are hydrophobic or amphipathic small molecules originating from carbanion-based condensations of thioesters and carbanion-based condensations of isoprenes. Lipids can be classified into distinct categories and perform different roles within and between cells. Lipids include six main categories: fatty acyls, glycerolipids, glycerophospholipids, sphingolipids, sacharolipids, and polyketides, sterols, steroids, and bile acids, which are the result of the fermentation/condensation of ketoacyl subunits. Lipids are insoluble in water but highly soluble in polar solvents like alcohols, ethers, chloroform, and benzene. Many studies describe lipid profiles and metabolism in cells, tissue and biological systems and predict approximate concentrations from milligrams per mol (mg/mol) to nanograms per mol (ng/mol) *(69)*.

Lipids not only have a role as an energy source, as noted above, but they exist in cell membranes and internal organelles where triglycerides, glycerolipids, and cholesterol contribute to the structural rigidity of cell membranes *(70)*. Lipids also

regulate biological processes in physiology, pathology, and disease, including cancer, inflammation, hypertension, and diabetes, through cellular signalling *(71)*. Evidence shows that ceramides derived from sphingosine can contribute to inflammation, particularly in obesity-linked conditions *(72)*. Several studies have identified ceramide-1-phosphate (C1P) as an anti-inflammatory, promoting glucose release from cells and producing Omega 6 arachidonic acid and prostaglandins *(73)*. Khanapure et al., 2007 show that eicosanoid mediators are released from phospholipid reservoirs and regulate inflammation, tumour proliferation, and diabetes *(74)*. Eicosanoids such as prostaglandin E2 (PGE2), prostaglandin D2 (PGD2), and hydroxy eicosatetraenoic acids (HETE) regulate immune responses and blood pressure *(75)*. Hait & Maiti, 2017 have well-documented the role of sphingosine-1-phosphate (S1P) and ceramide-1-phosphate (C1P) in inflammation and cancer *(73)*. Simanshu et al., 2013 reported phosphorylated sphingolipids, including ceramide-1-phosphate C1P and sphingosine-1-phosphate S1P, as critical cell growth, survival, migration, and inflammation regulators*(76)*. Sphingolipids are also integral components of cell membranes and regulate vital cell functions *(77)*. Several eicosanoids, including prostaglandins and leukotrienes, engage in inflammation. Numerous inflammatory diseases are linked to them *(78)*. Watrous et al., 2019 found that eicosanoids are associated with inflammation markers and clinical characteristics related to inflammation *(79)*. Shekhar et al., 2019 found that 20-HETE is essential in causing hypertension and stroke, with specific CYP4F2 and CYP4A11 gene polymorphisms involved *(80)*. The 20-HETE is also known to cause hypertension by regulating renin-angiotensin-aldosterone and causing renal fibrosis *(81)*. Sphingosine-based ceramides, C1P, and eicosanoids are crucial to inflammation, offering therapeutic possibilities.

A crucial role of lipids in reproductive physiology during pregnancy is their ability to synthesise hormones like progesterone and estrogen. Progesterone and estrogen influence placental health, maternal physiological adaptation to pregnancy, and fetal development. Lipids like cholesterol are precursors to steroid hormones like progesterone and estrogen. Conversion of cholesterol into pregnenolone leads to the synthesis of progesterone and other steroid hormones. It occurs primarily in the adrenal glands and gonads. In addition to maintaining pregnancy, it regulates various physiological processes during pregnancy. The production of progesterone and

estrogen depends on lipid metabolism and the availability of lipid precursors during pregnancy reproductive physiology. They are essential for establishing and maintaining a pregnancy in terms of placental function and maternal adaptation. Progesterone is produced in the ovary for early pregnancy. It encourages decidualisation of the endometrium, prepares it for embryo implantation, and supports placenta development. Progesterone also regulates specific genes and proteins crucial for pregnancy maintenance. The hormone estrogen also regulates many physiological processes during pregnancy. They include placenta growth and development, fetal organogenesis, and uterine function. It helps the uterus for embryo implantation and supports placentation by promoting endometrial cell proliferation and differentiation. The combined effects of progesterone and estrogen ensure a conducive implantation and growth environment for embryos. Napso et al., 2018 contend that hCG maintains the corpus luteum during early pregnancy, allowing the ovary to continue secreting progesterone and estrogen until the fetal-placental unit can compensate for maternal ovarian function *(82)*.

The progesterone and estrogen receptors -1 are critical mediators, including embryo implantation, placental development, and breast cancer *(83)*. These nuclear receptors are key in eliciting signalling pathways essential for early pregnancy success *(83)*. There is also a possibility that progesterone and estrogen may act through membrane receptors *(84)*. Competition between PGR and ESR1 might also contribute to progesterone attenuation of estrogen responses *(85)*. Recent studies have shown that nuclear receptor coactivator 6 maintains the appropriate level and activity of uterine ESR1 for successful embryo implantation *(86)*. ESR1 is more highly expressed in the endometrium than ESR2, emphasizing its primary role in estrogenic action *(87)*. ESR1 and PGR expression may be affected by genetic polymorphisms, which may affect their expression in breast tumours *(88)*. It has been shown that nuclear estrogen and progesterone receptors are present in osteoclasts, suggesting their potential role in bone physiology *(89)*. ESR1 and PGR expressions were evaluated with placental development during early pregnancy, revealing their patterns in utero-placental compartments *(90)*. Estrogen (E2) and progesterone (P4) are required for the proliferation and differentiation of stromal cells around the embryo during implantation *(91)* through nuclear estrogen (ER) and progesterone (PR) receptors. Embryo implantation requires estrogen, progesterone, and locally produced

signalling molecules *(86)*. Estrogen and progesterone are the dominant hormones during embryo implantation *(92)*. They are associated with an increase in transcript levels and secretion of human chorionic gonadotropin (hCG), human placental lactogen (hPL), placental growth hormone (PGH) and leptin *(93)*. Human placental lactogen (hPL), also known as human chorionic somatomammotropin (HCS), is a polypeptide hormone secreted from the syncytiotrophoblast of the placenta *(94)*.

1.5.1 Energy and metabolism

Fatty acids are transported via acyl-carnitines, and degradation occurs through beta-oxidation in mitochondria. This pathway sequentially removes two-carbon units from the fatty acid chain, producing acetyl-CoA molecules that enter the tetracarboxylic acid cycle to give ATP, the energy currency of our body, carbon dioxide (CO_2), and water (H_2O) *(71)*.

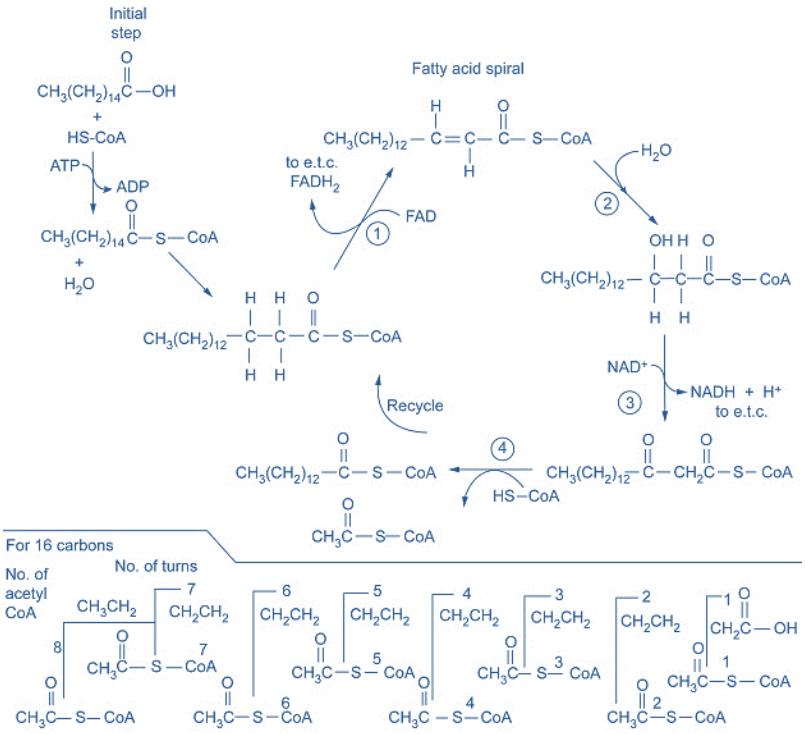

Figure 1:5 The β-oxidation of fatty acids occurring in the mitochondrion. In Figure 1:6, The β-oxidation of fatty acids occurring in the mitochondrion, the two carbons degrade the fatty acid at a time to form acetyl-CoA, and the steps are repeated until the entire fatty acid is converted to the acetyl-CoA two-carbon fragments. The acetyl-CoA produced can enter the citric acid cycle for conversion to ATP. ATP, Adenosine triphosphate; CoA, coenzyme A. Schematics idea came from literature with authors' permission adapted *(95)*.

The breakdown of fatty acids to acetyl-CoA molecules occurs in multiple steps involving the oxidation of fatty acids and the subsequent cleavage of the carbon chain. For example, during the breakdown of a 16-carbon fatty acid, the pathway proceeds through seven rounds of beta-oxidation, producing eight acetyl-CoA molecules, each of which can enter the citric acid cycle. Fatty acid biosynthesis, or lipogenesis, occurs in the cytoplasm. It uses acetyl-CoA derived from carbohydrates, amino acids, or other fatty acids as a precursor *(95)*. These triacylglycerols (converted fatty acids by lipogenesis) load onto lipoproteins, particularly very low-density lipoproteins (VLDLs), secreted from the liver. The storage and metabolism of energy-rich molecules such as triacylglycerols are crucial to maintaining energy balance and supporting various physiological functions. Other lipids include fat-soluble vitamins E, A, K, and D_3, which are only soluble in fat and are isoprene-based lipids essential for cell physiological functions. They are "fat-soluble" and can only be digested in the liver and further located for storage in adipose tissues. Each of these vitamins has separate roles in the body. For example, Vitamin D supports bones and immune function and controls calcium and phosphorous levels, and Vitamin K is an antioxidant essential for bone health and blood clots, which undergoes beta-oxidation into the mitochondria, generating energy.

Fatty acid synthesis in the cytoplasm pathway involves the stepwise addition of two-carbon units to a growing fatty acid chain, utilising acetyl-CoA and malonyl-CoA as building blocks, and these steps use the beta-oxidation pathway and the fatty acids synthesis pathway *(96)*. The second example of fatty acid synthesis is an anabolic pathway that allows our body to synthesise fatty acids for various purposes, such as production and hormone synthesis in the cell membrane. This pathway involves the stepwise addition of two-carbon units to a growing heavy acid chain. One of the critical enzymes involved in this process is fatty acid synthase. This enzyme catalyses the condensation of acetyl-CoA and malonyl-CoA to form a four-carbon intermediate. This intermediate is then further elongated through subsequent reactions. For instance, palmitic acid, a 16-carbon fatty acid, requires seven iterations of the fatty acid synthesis pathway. Animals use triglycerides for energy storage due to their high caloric content.

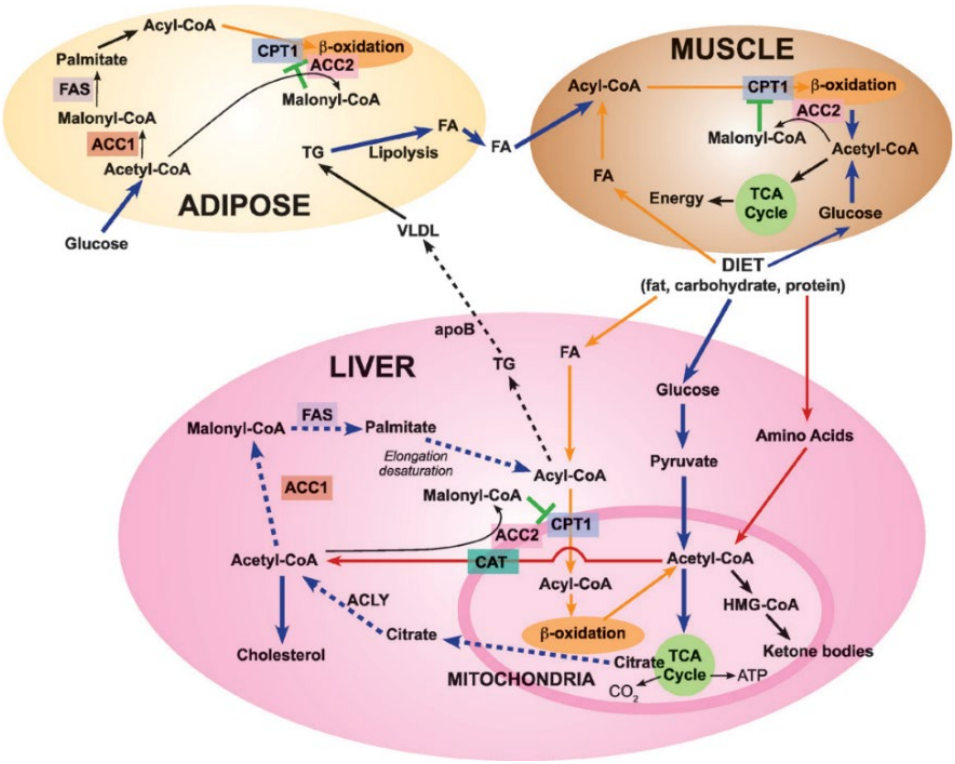

Figure 1:7 As part of the lipid metabolism in animal tissues, acetyl-coenzyme A carboxylase 1 (ACC1) differs from (ACC2). In the diet, fatty acids (FAs), glucose, and amino acids are transported to the liver, adipose tissue, and muscle tissue. In the liver, acetate is converted into acyl-CoA via glycolysis of glucose, which produces pyruvate, which is then oxidized by mitochondria via pyruvate dehydrogenase. As well as acetyl-CoA, amino acids produce adenosine. B-oxidation occurs in mitochondria when acyl-CoA is transferred to carnitine/palmitoyl-transferase 1. A citric acid cycle occurs when acetyl-CoA oxidizes to produce energy, water, and carbon dioxide, or it is converted to (1) citrate, which enters the cytosol and is converted to acetyl-CoA by ATP citrate lyase (ACLY), (2) ketone bodies by hydroxymethylglutaryl-CoA (HMG-CoA), or (3) carnitine/acetyl-CoA (CAT), which leaves the mitochondria. Carboxylation of acetyl-CoA by ACC1 produces malonyl-CoA, which is then converted into palmitate by fatty acid synthase (FAS), which produces triglycerides and VLDL. As acetyl-CoA passes through the mitochondrial membrane, it is carbonylated by ACC2 to form malonyl-CoA. That inhibits CPT1 and reduces the transfer of acyl-CoA. Similar reactions are occurring in adipose tissue and muscle tissue, although with appropriate modifications. Figure adapted from literature (Wakil, S. J., (**2009**) *(97)*

1.5.2 Lipids in cell and cell membrane overview

The active lipid constituents of cell membranes comprise biochemical and structural components that can spontaneously align themselves in an aqueous solution (Figure 1.5). The membrane fills with three main groups: phospholipids, sphingomyelins, and cholesterol. The distribution of phospholipids within the plasma membrane is

asymmetrical. The sphingomyelin (SM) and phosphatidylcholine (PC) are enriched in the outer membrane. The interior membrane facing the cytoplasm holds the amino-based phospholipids phosphatidylserine (PS), phosphatidylinositol (PI), and phosphatidylethanolamine (PE) *(98, 99)*. Cholesterol sits in the membrane interior, drives membrane distribution, and provides structural support *(69, 70)*. The phospholipid bilayer is selectively permeable and serves as a gate controlling incoming and outgoing macromolecules. Lipid bilayers contain microdomains of phospholipids, cholesterol, and sphingomyelin *(100)* that disappear after cholesterol reduction *(101-104)* and are critical to cell signalling as lipid rafts.

Glycerophospholipids are components of biological cell membranes embedded with sphingophospholipids and cholesterol to give structural support, hydration, and fluidity. These phospholipids contain a tail made up of an acyl chain, which consists of two fatty acids connected by glycerol, three carbon groups, and ester. Different head groups distinguish the six main classes: PC, PE, PS, PG, PI, and PA. Phosphatidic acid (PA) is an intermediate in lipid biosynthesis synthesised from glycerol kinase and serves as a precursor for synthesising other membrane lipids. The cytidine diphosphate diacylglycerol (CDP) diacylglycerol (CDP-DAG) plays a crucial role in lipid metabolism and synthesising various lipids, including phospholipids and glycerophospholipids. PE is a significant cell membrane component synthesised by enzymatic transfer of an ethanolamine group to CDP-DAG. PC is another abundant phospholipid in cell membrane synthesised from PE through a series of enzymatic reactions involving choline phosphotransferase.

In mammalian tissues and cell membranes, the PC headgroup functions with sphingolipid and sphingomyelin-forming ceramides *(105)*. PC is part of unsaturated hydrocarbon chains in tissues or organelles and a significant component of pulmonary surfactants, which are complex mixtures of lipids and proteins produced by type II alveolar cells such as dipalmitoyl phosphatidylcholine (DPPC) *(106)*.

Cardiolipins (Figure)are part of phospholipids located in the inner mitochondrial membrane, making up twenty per cent *(107)* constructed of four acyl units and three glycerol units where they activate enzymes involved in oxidative phosphorylation *(108)*, an essential process in mitochondrial energy production.

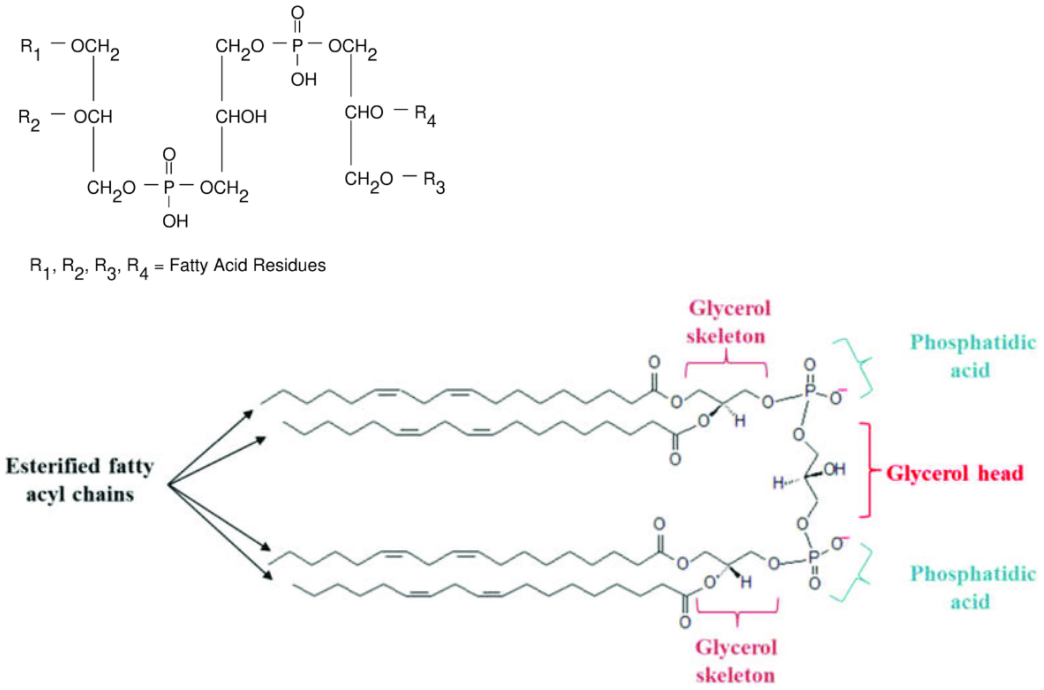

Figure 1:8 Cardiolipin top structure adapted from Merck-SigmaAldrich, the below structure of cardiolipin (CL) constricts of a glycerol head group bound to two phosphatidyl moieties, forming an anionic polar head group. The presence of four esterified fatty acyl chains bound to the glycerol head group forms a cone-shaped structure. Diagram adapted from literature with author's permission to reuse. *(109)*

Phosphatidylinositol (PI) is a minor but essential phospholipid in the cell membrane synthesised through a series of enzymatic reactions. Cholesterol is critical in cell membranes, contributing to their stability and fluidity. Cholesterol esters are found in the lipid droplets and lipoprotein particles. Cholesterol is also a precursor for synthesising essential molecules, including steroid hormones (such as cortisol, estrogen, and testosterone), bile acids, and the 7-dehydrocholesterol is the precursor of vitamin D. Cholesterol synthesis is only one aspect of cholesterol metabolism. The body also obtains cholesterol from the diet, primarily from animal-based foods. Cholesterol transport within the body is through low-density lipoprotein (LDL) and high-density lipoprotein (HDL). These lipoproteins are crucial in transporting cholesterol to various tissues and organs. Cholesterol synthesis is shown in (Figure 1:9) as a diagram, and it begins with the formation of acetyl-CoA, derived from multiple sources, including carbohydrates, fatty acids, and amino acids. In the cytoplasm, two acetyl-CoA molecules condense to form acetoacetyl-CoA. Then, a third acetyl-CoA molecule is reduced with acetoacetyl-CoA to produce 3-hydroxy-3-methylglutaryl-coenzyme A (HMG-CoA) using the enzyme thiolase in the

reaction. In the biosynthesis of cholesterol, HMG-CoA plays a central role. It serves as a precursor for synthesising steroid hormones and bile acids and is essential for the structure of cell membranes. HMG-CoA is then converted into mevalonate by HMG-CoA reductase. Mevalonate is a critical intermediate in cholesterol biosynthesis; HMG-CoA conversion to mevalonate is the committed step in cholesterol synthesis. Mevalonate is then phosphorylated by the enzyme mevalonate kinase, followed by a second phosphorylation catalysed by phosphomevalonate kinase. These reactions convert mevalonate to mevalonate 5-phosphate and then mevalonate-5-pyrophosphate. Mevalonate 5-pyrophosphate decarboxylation produces the five-carbon building blocks of isoprenoids and isopentenyl-5-pyrophosphate (IPP). The isopentenyl pyrophosphate IPP converts to geranyl pyrophosphate (GPP) by the enzyme geranyl pyrophosphate synthase. The geranyl pyrophosphate GPP undergoes another condensation reaction with isopentenyl pyrophosphate IPP, catalysed by farnesyl pyrophosphate synthase, to produce farnesyl pyrophosphate (FPP). Finally, two molecules of farnesyl pyrophosphate FPP combine to form squalene, a linear 30-carbon molecule. That is a reaction catalysed by squalene synthase. Squalene-to-cholesterol conversion involves complex reactions within the endoplasmic reticulum. Squalene is first converted to 2,3-oxidosqualene by the enzyme squalene epoxidase. Next, a series of enzyme-catalysed reactions, collectively known as cyclisation, convert 2,3-oxidosqualene to lanosterol. Lanosterol is then further modified through a series of responses, including removing three methyl groups, reducing a double bond, migrating another double bond, and changing a side chain. Various enzymes, including cytochrome P450 enzymes, catalyse these reactions.

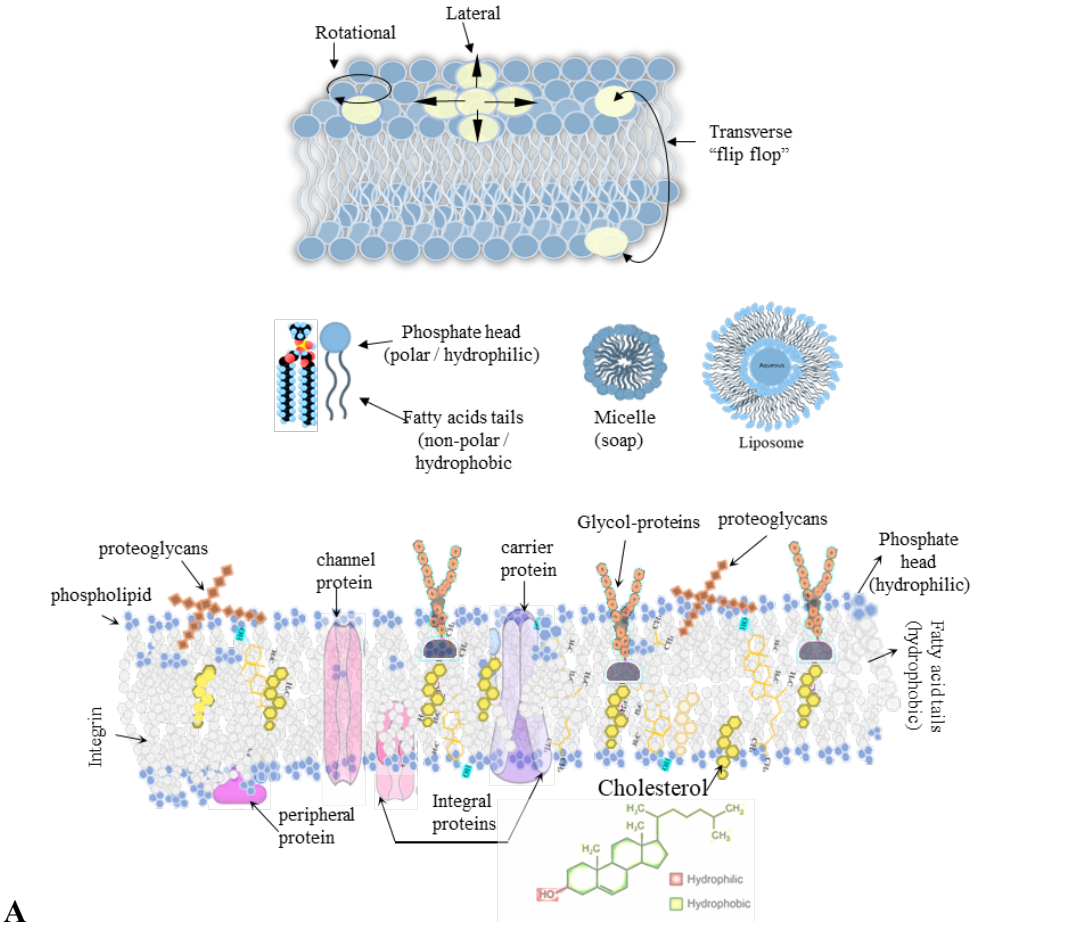

A

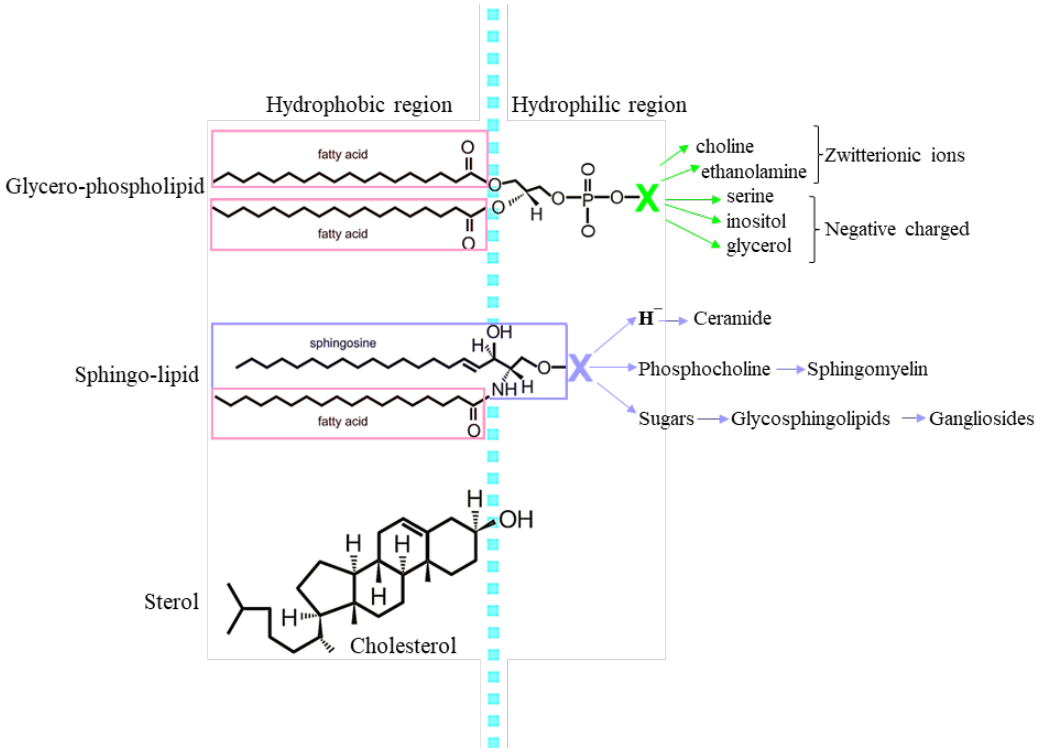

B

Figure 1:10 Lipids layout in cell membrane (A, B)

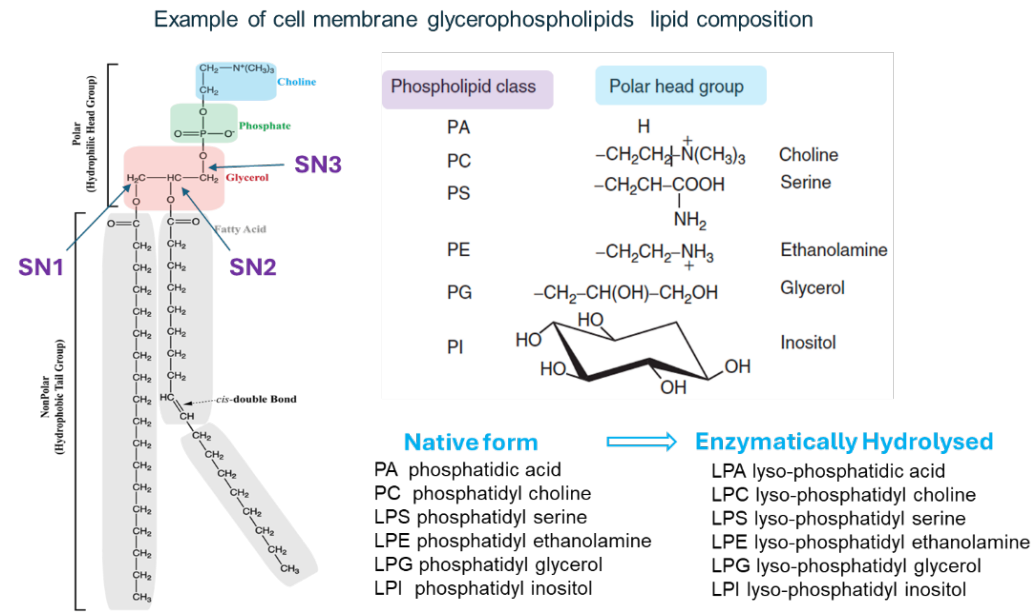

C

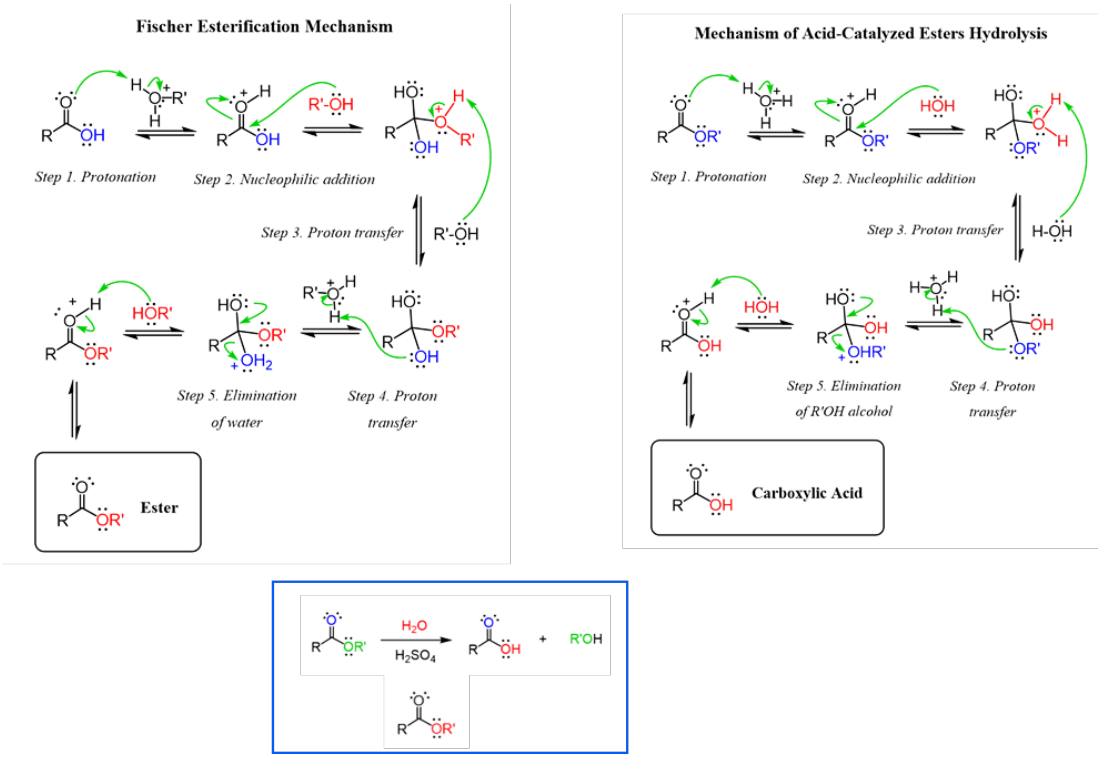

D

Figure 1:11 Lipids layout in cell membrane (C and D) hydrolysis reaction mechanism.

Figure 1:12 Lipids layout in cell membrane (C and D) hydrolysis reaction mechanism. All drawings are handmade in ChemDraw and PowerPoint using i-pen and saved as JPEGs. As shown in the above A-D diagrams, lipids layout in the cell membrane layout of glycerophospholipids, sphingolipids and sterols, carbohydrates cyclic chains and facing the outer cell membrane of the aqueous environment, the hydrophilic head groups, which are the most reactive Glycerophospholipids, sphingolipids and sterols -cholesterol. The membrane bilayer (Figure 1.10) is filled with saturated carbon chains and has sphingosine bases in the backbone of sphingomyelins in the ceramides. Hydrogen bonds between sterol cholesterol and ceramides add strength to the lateral packing between the sterol ring of the cholesterol and the sphingomyelin. ATP- the energy carrier connects with the family group called 'ABC protein transporters,' which utilises the ATP transport from the hydrophilic to the lipophilic phase of the cell membrane. Lipoproteins help to provide easier passage by diffusing lipid headgroups and activating translocators to maintain the lipid asymmetry and drive active translocation. The lipoproteins use ATP to help transport amino phospholipids such as phosphatidylethanolamine amine and phosphatidylserine by the ABC translocase protein group *(99, 104, 110) (111, 112)*.

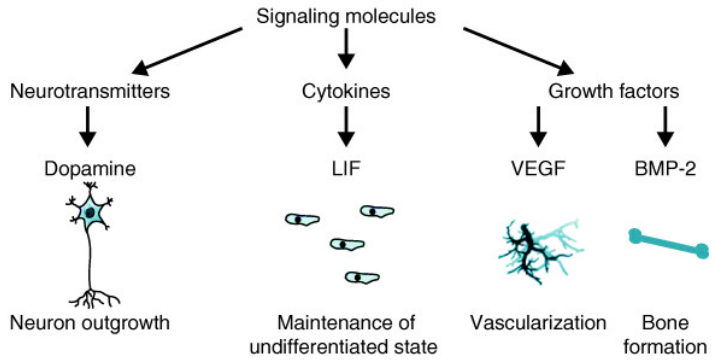

Figure 1:13 Cellular communication Cellular communication and signalling molecules

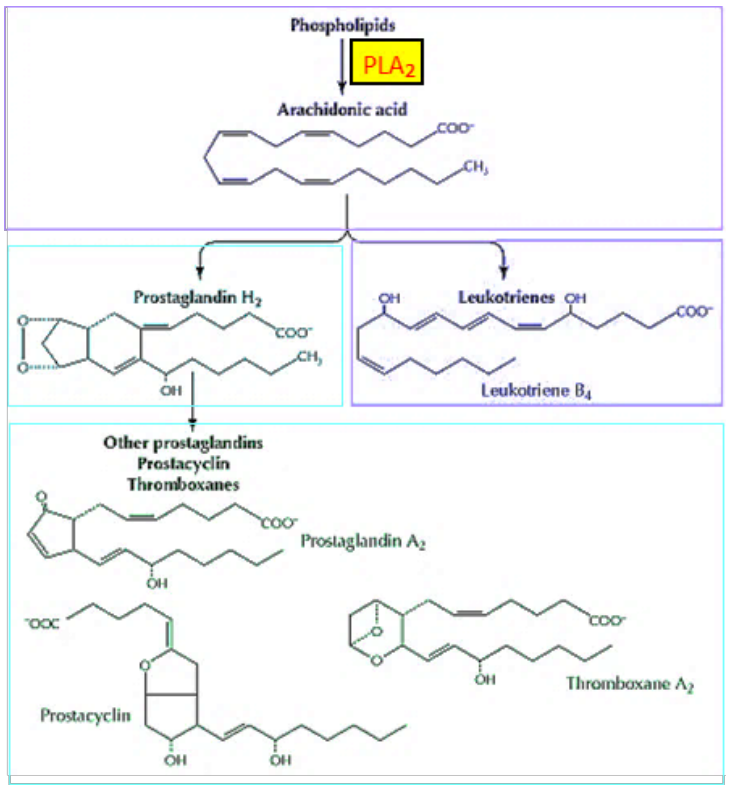

Figure 1:14 Cellular communication and signalling molecules phospholipase PLA2 hydrolyses phospholipids to release arachidonic acid, which is then converted to prostaglandins and leukotrienes, essential in cellular signalling. The idea was adapted from literature (118), reconstructed by hand in PowerPoint and saved as a jpeg.

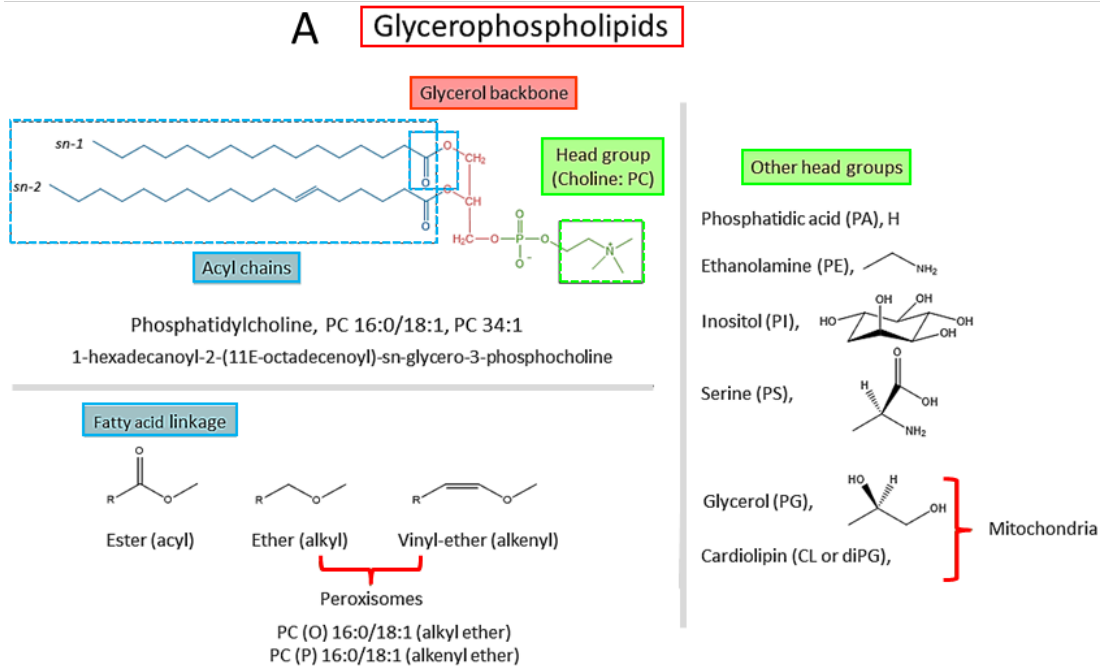

Figure 1:15 Structure schematics of (A) glycerophospholipids

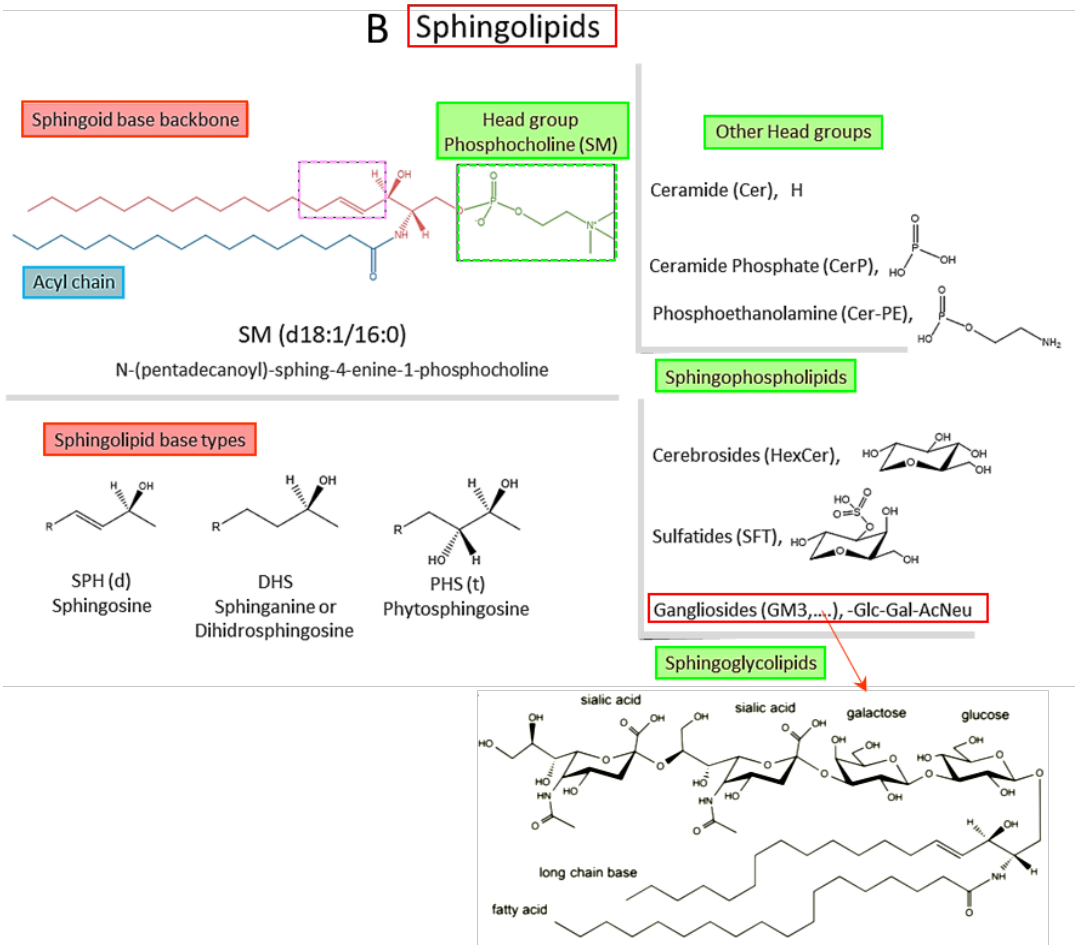

Figure 1:16 Structure schematics of (B) sphingolipids and gangliosides.

Figure 1:17 represents the cellular membrane and the representative structure schematics of (A) glycerophospholipids and (B) sphingolipids and gangliosides. Gangliosides are complex lipids that may contain a variable number of glucose units. Gangliosides make an extensive and heterogeneous family of glycosphingolipids. They are amphiphilic molecules composed of a hydrophobic ceramide moiety on which a hydrophilic oligosaccharides chain branched GD3 saccharide sequence: (Glc-Gal-AcNeu); (Glc)-glucose; (Gal)-galactose; (AcNeu)-n-acetylneuraminic acid in (Fig.1BGM3) next to sphingolipids. The chain's one or more sialic acids are a distinctive feature of gangliosides (GGs). For a detailed explanation of the structure of branched gangliosides, original reference (117) drawings are handmade, using an i-pen in PowerPoint, and saved as a jpeg.

Cellular communication (in Figure 1.11) is called cellular signalling and involves the molecules of the central nervous system's neurotransmitters and cells' cytokines in response to inflammation and hormone growth factors. These factors are centralised via the vascular system and osteoclast formation. Cellular signals can be transmitted by direct cell-to-cell contact or by secreted molecules. Endocrine signalling transports hormones to distant target cells through the circulatory system. The paracrine signalling system involves the release of a molecule from one cell that affects nearby target cells. Autocrine signalling means that cells produce signal molecules and respond to them. Lipid-mediated signalling is crucial for maintaining cellular homeostasis, regulating physiological processes, and responding to external stimuli. A sphingolipid derived from ceramide, such as sphingosine-1-phosphate (S1P), participates in cell processes, including calcium mobilisation, cell growth, and apoptosis (programmed cell death). S1P interacts with specific receptors, called S1P receptors, to transmit its signalling effects. Signalling regulates inflammation, immune response, cell proliferation, migration, and vascular development pathways. DAG and phosphatidylinositol phosphates (PIPs) participate in the calcium-mediated activation of protein kinase C (PKC), an essential enzyme in signal transduction pathways. PKC activation regulates various cellular processes and functions.

Fatty acid metabolites prostaglandins (Figure 1:12) in cellular communication and signalling are molecules which enzyme phospholipase PLA2 hydrolyses phospholipids to release arachidonic acid, which is then converted to prostaglandins and leukotrienes, derived from arachidonic acid, a polyunsaturated fatty acid, and mediate the body's response to injury or infection and regulate various immune and inflammatory processes. Different mechanisms can trigger inflammation through plasma membrane lipids. Among the most crucial aspects of resolving inflammation is the role of specialised pro-resolving mediators (SPMs). Several SPMs derive from membrane lipids, including resolvins, protectins, and maresins *(113)*. Biologically, these SPMs bind and enhance the killing and clearance of microbes and have organ-protective properties *(113)*, and they are crucial in regulating the resolution of inflammation and preventing chronic inflammation *(113)*. Steroid hormones derived from cholesterol include estrogen, testosterone, and cortisol. These hormones function as signalling molecules and regulate various bodily functions, such as

reproduction, metabolism, immune response, and blood pressure. They interact with specific nuclear receptors, modulating gene expression and cellular responses. Oxysterols are oxidised cholesterol derivatives, for example, 25-hydroxycholesterol, which serve as agonists for liver X receptors (LXRs), nuclear receptors regulating cholesterol metabolism and homeostasis. G-protein-coupled receptors (GPCRs) and nuclear receptors are common mechanisms through which lipid molecules signal. Sensory signals, hormones, neurotransmitters, and hormone-coupled receptors (GPCRs) mediate placental physiological processes *(114)*. Plasma lipids are essential in helping to distribute fatty acids to all tissues. PC is a critical component of cell membranes and the dominant phospholipid in most major organs, including the heart, lung, liver, and brain. PC is the most abundant phospholipid in circulation, forming part of plasma lipoproteins such as high-density lipoproteins (HDL) that facilitate its transport in circulation.

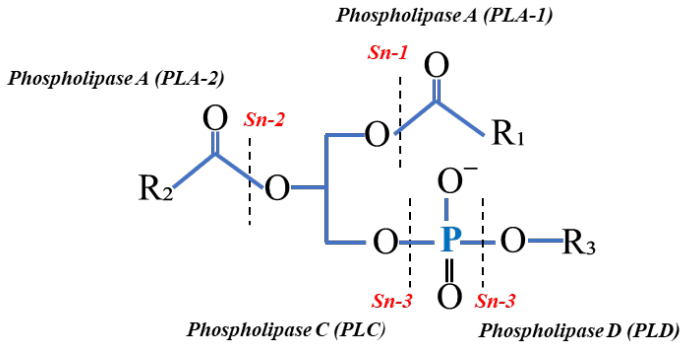

Figure 1:18 Membrane phospholipids hydrolyzing proteins enzymes on the Glycerophospholipids backbone structure: cleaving enzymes PLA1, PLA2, PLC, and PLD handmade schematics in PowerPoint and saved as picture jpeg.

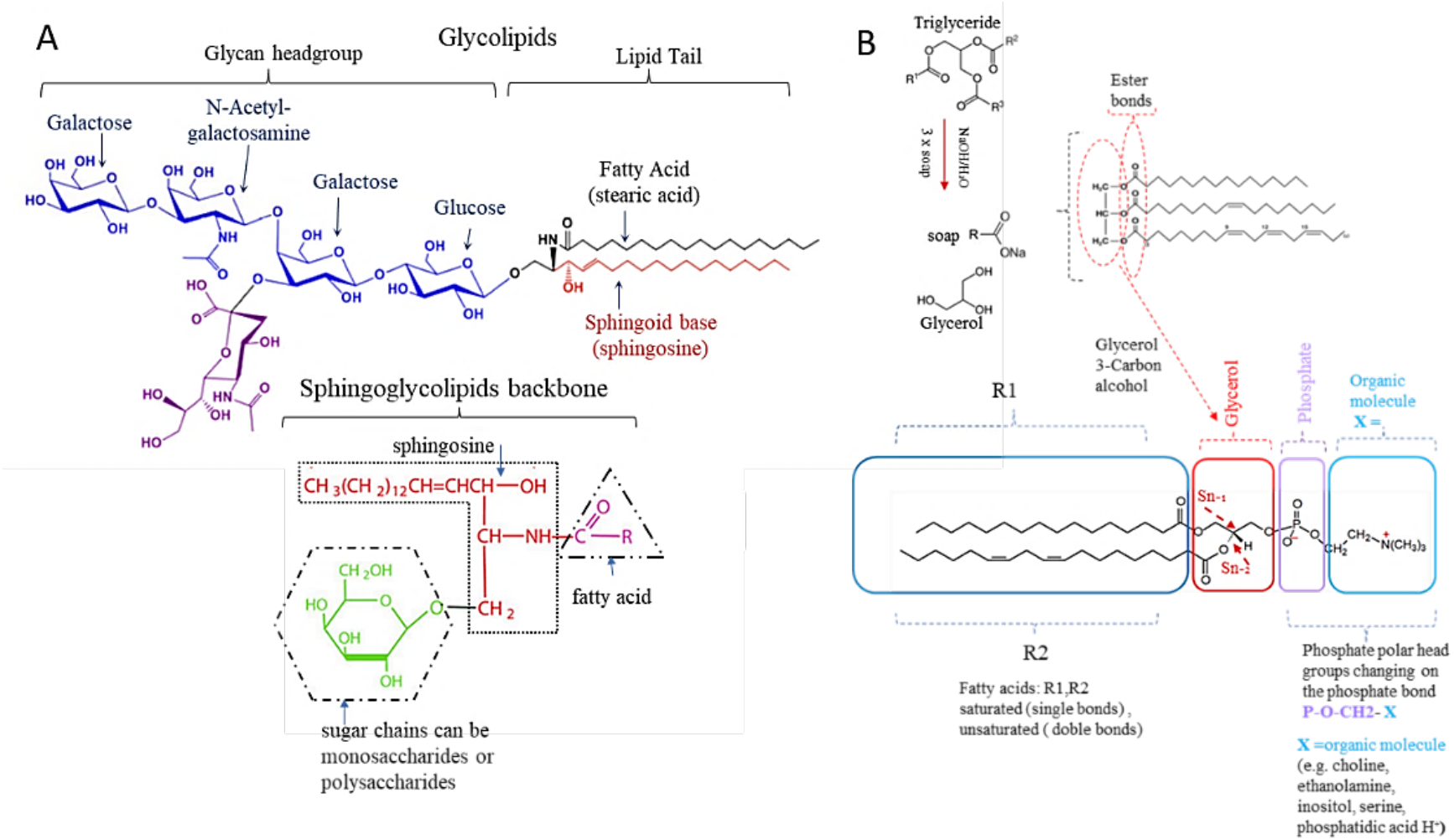

Figure 1:19 Chemical structures diagram A) glycolipids sphingoid base backbone B) glycerol backbone phospholipids, diagrams were handmade in PowerPoint, and Perking Elmer ChemDraw saved as a picture jpeg.

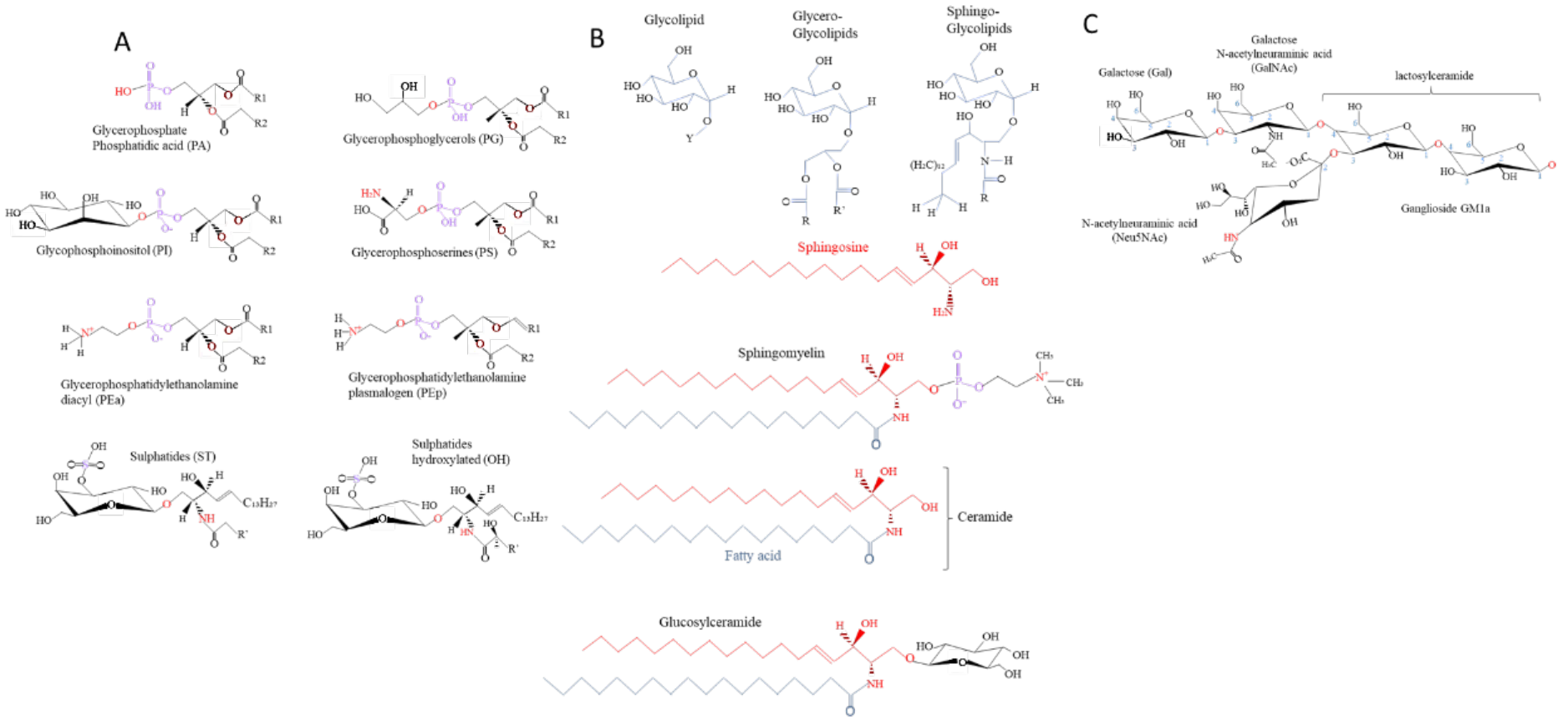

Figure 1:20 Chemical structures A) Glycerophospholipids, Sulfatides, B) Sphingolipids, Glyceroglycolipids, Sphingoglycolipids, ceramide, glucosylceramide and C) Gangliosides, GM1, significant ganglioside components of the human brain, diagrams were handmade in PowerPoint, and Perking Elmer ChemDraw saved as a picture jpeg.

1.5.3 Phosphatidylcholine (PC) and Lysophosphatidylcholine (LPC)

PC and LPC are a focus here due to interest in these research groups as broad inflammation markers *(115)*. The main pathway of PC synthesis in mammals is the cytidine diphosphate (CDP) choline pathway shown below *(Figure 1:12)*. When choline is ingested and absorbed from foods, it is subject to degradation by the enzyme choline kinase (CK), which phosphorylates choline in the cell cytoplasm and produces phosphocholine *(116)*. Phosphocholine reacts with cytidine triphosphate (CTP) via the enzyme CTP: phosphocholine cytidyltransferase (CCT) to form CDP-choline *(117)*. CCT is a rate-limiting step in synthesising PC and lipids derived from PC. It occurs as two isoforms, alpha (α) and beta (β); CCTα is in the nucleus and the endoplasmic reticulum, whereas CCTβ localises to the endoplasmic reticulum. PC can also come from PE via the methylation pathway (PEMT) that uses the methyl donor S-adenosylmethionine (SAM) for transfer of three methyl groups to PE catalysed by PE-N-methyltransferase *(Figure 1.7)*. Diacylation-re-acylation changes the fatty acid component of PC. Phospholipases (lipolytic enzymes) hydrolyse PC and other glycerophospholipids into lysophospholipids and free fatty acids. Both lysophospholipids and free fatty acids are essential for cell communication and can make membranes unstable. Excessive amounts of lysophospholipids can damage cells and cause inflammation. Maintaining a balanced production and breakdown of lysophospholipids is necessary for optimal cell function and health.

Phospholipases occur as different isoforms specific to each human phospholipid class. For example, phospholipase C produces diacylglycerol and phosphocholine by hydrolysis of the phosphodiester bond of PC, leading to phosphoinositide metabolism. Phospholipase C activates sphingomyelin synthesis and eliminates both fatty acids to produce glycerophosphocholine. Lysophosphatidylcholine (LPC) is the product of hydrolysis of PC by phospholipase A2 (PLA2). When phosphatidylcholine is cleaved, lysophosphatidylcholine and free fatty acids are released. While the breakdown of diacylglycerol leads to 2-arachidonoylglycerol, other phospholipases can produce degradation products such as lysophosphatidic acid and glycerophosphocholine. PLA2 is found primarily in neutrophilic granulocytes and plays a role in inflammation. LPC levels increase due to reactive

oxygen species generated by activated neutrophils. LPC plays a vital role in cardiovascular and neurodegenerative processes with pro-inflammatory properties. LPC is one of the significant components in the blood that causes an inflammatory state in arteries associated with atherosclerosis and might function as a plasma biomarker of the oxidation of lipoproteins in atherosclerotic lesions produced by overexpression of PLA2. LPC is the precursor of lysophosphatidic acid, an essential lipid mediator.

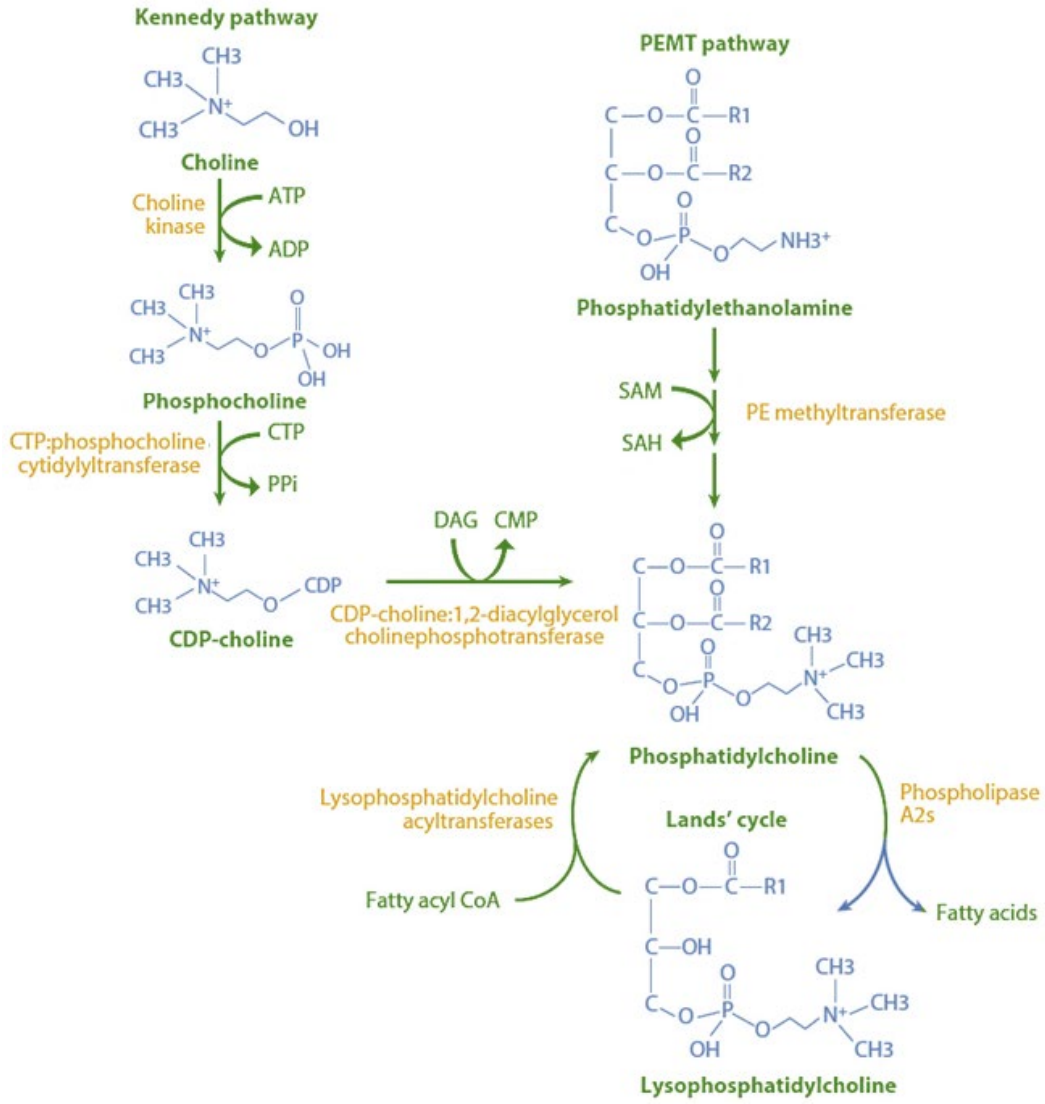

Figure 1:21 Phosphatidylcholine synthesis by the cytidine diphosphate (CDP)-choline (Kennedy) and phosphatidylethanolamine methylation (PEMT) pathways. Legend to (Figure1.7) was handmade in PowerPoint and saved as a picture jpeg. Adapted from (Wang, B. & Tontonoz, P. 2019) *(118)*.

1.5.4 Gestational diabetes mellitus (GDM) and obesity

The prevalence of gestational diabetes has risen in recent years due to increasing obesity and sedentary lifestyles. Obesity can lead to insulin resistance, a hallmark of GDM. The altered lipid profile of an obese pregnant woman puts her at a higher risk of not only GDM but also preeclampsia *(119)*. Among women with GDM, high blood sugar during pregnancy levels increases pregnancy complications, such as preeclampsia and caesarean delivery *(120)*. The mother and her child are at greater risk of developing type 2 diabetes *(119)*. Maternal glucose resistance allows accumulated carbohydrates to promote the rapid development of the fetus by switching from carbohydrate to fat utilization, promoting lipids as a maternal energy source *(121) (122)*. The underlying relationship between maternal obesity and GDM and fetal macrosomia (a condition where a newborn is significantly larger than average) is complex. It involves multiple pathways, including changes to lipid metabolism and other lipid-related mechanisms that might be affected, such as triglycerides, free fatty acids (FFA), cholesterol, lipoproteins: low-density lipoproteins (LDL) and very low-density lipoproteins (VLDL), adipose tissue hormones (adipokines: leptin, adiponectin, resistin, and visfatin), phospholipids, enzymes phospholipases, eicosanoids, ketone bodies, and insulin resistance and other endocrine glands and mediators (liver, kidney, pancreas, intestines and bile acids and salts).

The health of a mother and her unborn child is negatively affected by maternal pre-gestational obesity and excessive pregnancy weight gain *(123)*. A higher risk of overgrowth in newborns is associated with these conditions *(124)*. Globally, obesity prevalence among women of reproductive age has increased *(125)*. As a result of this increase in obesity rates among women of reproductive age, an intergenerational cycle of detrimental metabolic health effects in medical obstetrics and human health contributes to economic burden*(125-127)*. Maternal BMI is associated with pregnancy complications such as preeclampsia, GDM and caesarean delivery *(128)*. Pregnancy-related changes in lipid metabolism affect a mother's plasma lipid levels *(129)*. Lipid levels gradually change during pregnancy. Abnormal lipid levels in early pregnancy are associated with preterm birth, GDM, and small for gestational-

age babies *(122)*. Preferably, lipid levels must be monitored and managed during pregnancy to optimise maternal and fetal health. Evidence of altered lipid metabolism is also present in preeclampsia and hypertriglyceridemia during pregnancy *(130)*.

During pregnancy, insulin sensitivity fluctuates, with placental hormones such as hPL and progesterone increasing insulin deficiency in the second and third trimesters. This normal physiological reaction ensures enough glucose and other nutrients are available to the growing fetus. Typically, insulin sensitivity is unchanged or enhanced during early pregnancy, and glucose tolerance is standard or slightly improved. As fetal growth increases during late gestation, diabetogenic hormone levels rise, and insulin resistance develops *(131)*. The maternal pancreas makes more insulin as compensation in response to insulin resistance, but if this is insufficient, GDM develops. Through structural changes such as increased size and altered blood flow, insulin resistance in GDM affects the placenta's function and expression of glucose transporters, affecting the supply of glucose to the fetus. As a result, the fetus receives higher glucose levels, causing hyperinsulinemia and macrosomia (a larger-than-normal fetus) and complicating delivery. Hyperglycaemia impairs glucose transporter trafficking by downregulating AMPK in women with GDM *(132)*, disturbing mitochondria function and cellular metabolism *(133)*. In obese placentas, a lipotoxic environment is characterised by increased placental lipid content and reduced AMPK. Chronic low-grade inflammation associated with the obese placenta further impairs insulin signalling *(134)*. In GDM placentas, insulin resistance alters peptide metabolism and inflammation, impairing insulin receptor signal transduction *(135, 136)*.

Insulin sensitivity is also affected by hormones secreted by adipose tissue. So-called adipokines - leptin, adiponectin, resistin, and visfatin - contribute to insulin sensitivity, secretion, and inflammation, influencing placental nutrient transfer and fetal growth *(137)*. Adipose tissue produces pro-inflammatory cytokines when insulin resistance increases in obese individuals. Adipokines are altered with pregnancy, and the placenta releases adipokines into the maternal and fetal circulations during pregnancy *(138) (139) (140-142)*. These can be further

dysregulated, possibly contributing to obstetric and perinatal complications in pathological pregnancy *(143)*. Adipokines are associated with insulin resistance markers in GDM, further emphasizing insulin resistance and metabolic disorders during pregnancy. The adipokines visfatin and resistin are dysregulated during the second and third trimesters in GDM *(144-146)*. Leptin and adiponectin levels are also dysregulated in pathological conditions such as GDM, preeclampsia and IUGR *(147) (141, 148) (141, 142, 149-152)*.

High blood sugar levels are indicative of gestational diabetes during pregnancy. It is associated with various factors, including insulin resistance, hormonal changes, genetic predisposition, and obesity. Women with gestational diabetes may exhibit higher maternal triglyceride levels and HbA1c levels in the second trimester. Triglycerides are fats found in the blood. The medical test uses haemoglobin A1c (HbA1c) to measure the average blood glucose level over three months as a percentage. Insulin resistance, a key factor in gestational diabetes, is when cells do not respond to insulin efficacy, resulting in higher insulin production in the pancreas. Insulin controls lipid metabolism, which results in elevated triglyceride levels in the blood. Increased estrogen and progesterone concentrations during pregnancy affect insulin sensitivity, causing increased hunger and calorie consumption. It raises blood sugar protein (HbA1c) levels, which cannot be managed through diet. Genetic factors also play a role in gestational diabetes. Obese women are at higher risk due to higher triglyceride and HbA1c levels.

Furthermore, the placenta produces hormones that interfere with insulin action, potentially worsening insulin resistance as pregnancy progresses. It leads to higher triglyceride and HbA1c levels. Proper management of gestational diabetes is crucial, and it includes dietary modifications, physical activity, and lifestyle, with medication or insulin therapy may help. However, regular monitoring of HbA1c levels is essential for assessing long-term glycemic control in women with gestational diabetes. A decrease in HbA1c levels indicates better glucose control. Maintaining better blood sugar control reduces related difficulties and heart or kidney diseases with nerve damage. Researchers found that gestational diabetes significantly increases maternal triglycerides and HbA1c levels during the second trimester.

During gestational diabetes, Siminova-Krstevska et al. (2014) found elevated triglycerides and high HbA1c levels *(153)*.

Some insights into gastrointestinal diabetes (GDM) related to insulin and metabolic triglycerides increase obesity risk. In Olmos et al. 2014 study, maternal triglyceride levels contributed to large-for-gestational-age infants in obese and overweight mothers with gestational diabetes *(154)*. Recent studies have demonstrated that elevated triglycerides lead to impaired glucose metabolism during pregnancy, reinforcing the association between triglycerides and gestational diabetes *(155)*. Hormonal changes, genetic predisposition, and obesity can all contribute to gestational diabetes *(156)*. Gestational diabetes causes insulin resistance, which affects lipid metabolism and raises blood triglycerides *(155)*. As estrogen and progesterone rise during pregnancy, blood sugar and HbA1c levels rise *(156)*. A high triglyceride and HbA1c level in obese women increases gestational diabetes risk *(157)*. As pregnancy advances, placental hormones disrupt insulin action, increasing triglyceride and HbA1c levels *(156)*. Diet, exercise, and lifestyle changes are recommended to manage gestational diabetes *(158)*. By monitoring HbA1c levels regularly, diabetes-related complications can be reduced *(159)*. Maternal lipids influence the pregnancy environment and fetal growth *(156)*.

A hormone called Insulin-like Growth Factor-1 (IGF-1) plays a critical role in growth and development, both before and after birth. It is produced in response to the pituitary gland's release of growth hormone (GH) *(160)*. IGF-1 promotes cell growth and division, contributing significantly to fetal development. IGF-1 levels in maternal-fetal blood contribute to gestational diabetes-induced hypertrophy in the fetus *(160)*. Also, maternal serum triglyceride levels affect neonatal birth weight *(161)*. Gestational diabetes management requires addressing various factors, including insulin resistance, hormonal changes, and genetic predisposition. HbA1c levels and maternal triglycerides should be monitored regularly. The focus is on lifestyle changes and, if needed, insulin therapy. Factors like altered metabolism, maternal dietary patterns, and intrauterine growth restriction can explain lipid group differences in pregnancy. Prenatal health management depends on understanding these variations *(162)*.

Pregnant women with gestational diabetes have the highest triglycerides, followed by obese women. Healthy BMI pregnancies have lower cholesterol and LDL levels than obese and GDM pregnancies. The pattern may change in GDM pregnancies, with more apparent dyslipidemia, resulting in increased lipolysis and higher free fatty acids. With GDM and obesity, LDL particles are more significant, dense, and atherogenic *(153, 158, 163-167)*. Various factors influence maternal lipid profiles during pregnancy, such as gestational diabetes and obesity. A woman with gestational diabetes mellitus may experience higher glucose levels during pregnancy, which is a precursor to type 2 diabetes in the future*(168)*. A maternal dietary pattern during pregnancy was also associated with lower cardiometabolic markers like cholesterol and triglycerides *(169)*.

Additionally, pregnant women with gestational diabetes had higher maternal triglyceride and HbA1c levels in the second trimester compared to healthy pregnancies *(153)*. Also, intrauterine growth restriction has been associated with changes in the mother's lipoprotein composition and placental lipoprotein receptors *(165)*. Normal pregnancies had significantly higher maternal plasma LDL cholesterol levels than intrauterine growth-restricted pregnancies. During pregnancy, it has been suggested that increased triglyceride synthesis causes elevated serum triglycerides *(167)*. Compared to a healthy pregnancy, pregnancies with obesity and pregnancies with gestational diabetes mellitus, triglyceride, cholesterol, and LDL levels differ significantly.

1.5.5 Lipids in healthy and adverse pregnancy

Many essential changes in lipid metabolism occur during pregnancy to support fetal development and prepare for lactation. Pregnancy weight changes are affected by the mother's health, BMI, GDM, and other medical conditions. During pregnancy, women with a healthy BMI (less than ≤ 30 kg/m^2) naturally experience an increase in total cholesterol (TC), low-density lipoprotein cholesterol (LDL-C), and high-density lipoprotein cholesterol (HDL-C). The body's TG production increases during the second and third trimesters, and metabolism decreases with the rise in oestrogen and progesterone hormones. Adverse pregnancy environments such as obesity and

GDM are the focus here and have dramatic effects on lipid metabolism in pregnant women with detrimental effects on birth and child health outcomes. A woman with an obese BMI entering pregnancy has higher triglycerides, TC, LDL-C, and sometimes HDL-C levels than a woman with a healthy BMI. Obese pregnancies lead to inflammation and lipid changes. These women are at risk of hyperlipidaemia, which increases their risk of preeclampsia, pregnancy hypertension, and GDM. GDM symptoms include carbohydrate intolerance and insulin resistance. Pregnant women with GDM can have a similar lipid profile to a pregnant woman with type 2 diabetes, with higher triglycerides and lower HDL-C. GDM insulin resistance leads to pregnancy hyperlipidaemia, dyslipidaemia, and fetal macrosomia that cause complications during delivery and increase the risk of metabolic disorders later in life. Despite general trends, pregnancy lipid profiles differ from woman to woman.

Genetics, insulin resistance, diet, and metabolic changes can cause these changes. In the last trimester of pregnancy, long-chain polyunsaturated docosahexaenoic acid (DHA) with arachidonic acid (AA) is crucial in fetal development *(124, 170)*. Several studies have shown that these fatty acids are critical to proper neural and visual development *(124, 170)*. In maternal obesity, higher levels of DHA and arachidonic acid AA suggest an association of neuroprostanes derived from docosahexaenoic acid DHA and isoprostane derived from arachidonic acid AA, which might impact placental function *(171)*. Maternal obesity can significantly affect placental signalling *(172) (173)*; as a result, the placental level of interleukin-6 (IL-6), a pro-inflammatory cytokine, decreases *(174)*. Inflammation levels in the placental environment can be affected by changes in their levels and impact fetal development during pregnancy *(175)*. Hormones influence fetal growth and development, including leptin, which regulates energy balance, and human chorionic gonadotropin (HCG). Maternal obesity impacts placental function, including cytokine and hormone secretion, immune cell content, morphology, nutrient transporter expression, and vessel density. Inflammation in the mother has been linked to fetal inflammation, leading to changes in cytokine secretion and placental inflammatory status in the fetus *(176)*. Cetin et al. (2012) link maternal obesity to changes in placental lipid turnover, which impact hormone release and the placental lipid environment *(62)*. Musa et al., 2023 suggest that pregnancy-related low-grade

chronic inflammation may influence immune cells in the placenta, influencing their composition and function *(176)*. As a result, maternal obesity affects hormone secretion, gene expression in the placenta, and DNA methylation *(172)*. Maternal obesity affects nutrient transporter expression and placental fatty acid transport *(62)*. Diet-induced obesity decreases placental vascularity, compromising vessel density and impairing blood flow and nutrient exchange *(177)*.

1.5.6 Triglycerides

Triglycerides are part of the physiological support for fetal growth and development and contribute to metabolism and energy storage. During maternal adaptation to pregnancy, lipid synthesis and storage in adipose tissue are critical responses in the earlier phase of pregnancy. Then maternal metabolism slows down and increases triglyceride levels in maternal blood due to hormonal changes, mainly elevated estrogen and progesterone levels, ensuring a nutrient supply to the fetus *(178)*. Progesterone and estrogen help suppress the maternal breakdown of fats (lipolysis) and promote the storage of fats in the first and early second trimester, which aids in preserving fat stores for the energy demands of late pregnancy and lactation *(179)*. As pregnancy progresses, the stored fat in triglycerides is mobilized from maternal adipose tissue to provide energy with hormones such as placental lactogen (hPL) controlling the release of free fatty acids (FFAs) from maternal metabolism available to the fetus. Triglycerides do not transfer directly across the placenta. Lipoprotein lipase (LPL) and intracellular FATPs and FABPs transport maternal plasma triglycerides to the fetus for hydrolysis into FFAs and glycerol. Once FFAs are available in fetal circulation, they can be used immediately for energy by beta-oxidation or re-esterified into triglycerides and stored in fetal adipose tissue. They can also be incorporated into phospholipids and other complex lipids necessary to develop fetal brain and neuronal cell membranes.

As pregnancy progresses, placental hormones contribute to mild insulin resistance in the mother, which helps to increase glucose availability for the fetus but also causes a rise in maternal lipids due to decreased lipid clearance, accumulating lipid droplets as pregnancy progresses. These are also an essential source of nutrients for the

developing fetus and a building block for the developing fetus. In obese and GDM placentas, there is an accumulation of large quantities of triglycerides, causing metabolic risk. Hypertension, IUGR, preterm birth, and fetal macrosomia all correlate with maternal triglyceride levels in early pregnancy*(121, 131) (120, 122)*. GDM also causes immunoendocrine dysregulation in the placenta, leading to stress-activated and inflammatory responses *(180, 181)*. Dysregulation of these pathways might further harm triglyceride metabolism. Lipid receptor transporters become more abundant in the placenta, resulting in higher lipid uptake, triglyceride levels, lipid accumulation, and placental dysfunction due to increased lipid storage. As a result of the elevated lipid environment, the placenta experiences metabolic stress, resulting in a higher synthesis of reactive oxygen species (ROS). The circulating hormone levels altered with obese pregnancies, including leptin, insulin, and adiponectin, can affect placental function. The placenta can be affected by GDM in ways such as obesity. There is a more significant disruption in the lipid storage and mobilisation balance, often leading to increased triglyceride accumulation. Insulin resistance may also impair lipid metabolism in GDM since insulin regulates critical enzymes that synthesise and break down lipids. Dysregulation of triglyceride metabolism leads to an oversupply of lipids in the fetus, which can lead to fetal obesity and metabolic diseases later in life in the child.

1.5.7 Cholesterol pathways

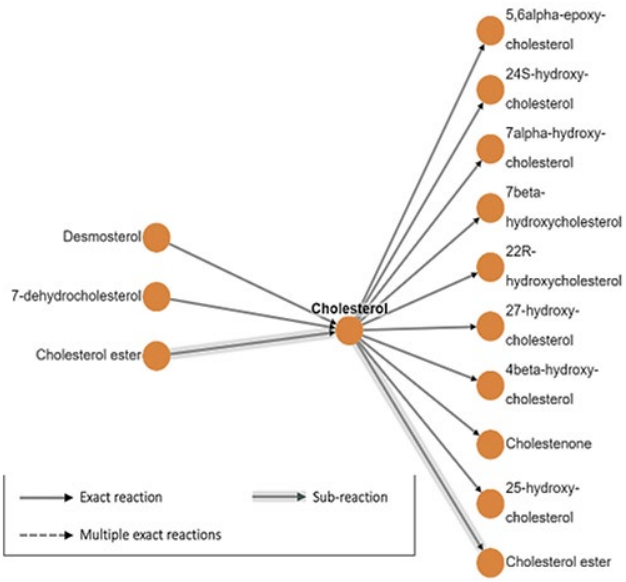

Figure 1:22 Cholesterol synthesis and its derivatives analogue are major parts of cell membrane providing major structural support as well as present in internal organs, liver, and adrenal glands where its metabolism and hydrolysis take place and travels to intestines via protein cargo using high-density lipid transporters and stores in low-density lipid transporters. The diagram was adapted using Lipid Maps, then ChemDraw, Bio Render, and PowerPoint to readapt and save as a jpeg.

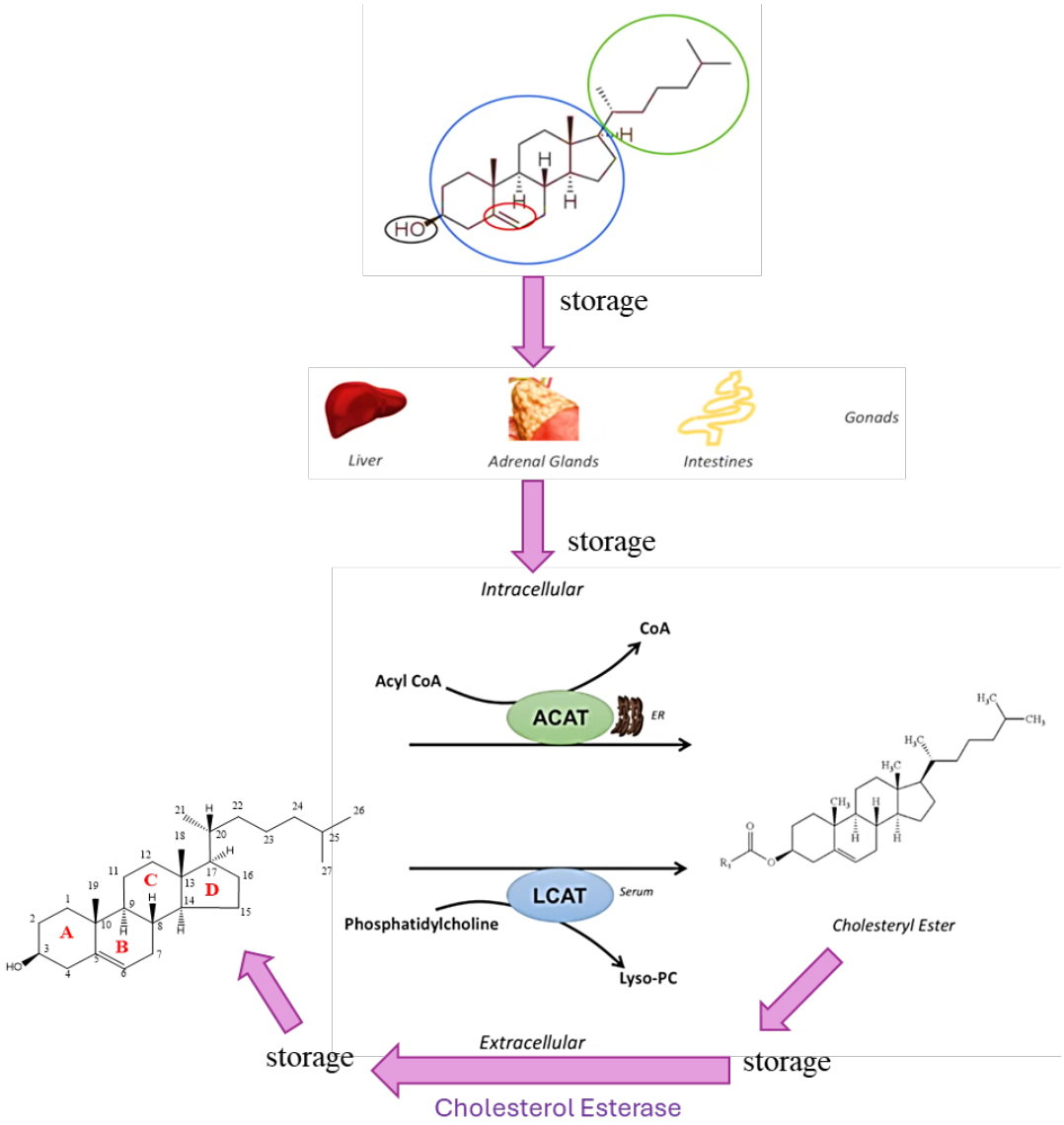

Figure 1:23 Cholesterol storage, used Biorender, PowerPoint, hand made saved as picture jpeg.

Cholesterol is essential for fetal development, but abnormal levels in the maternal circulation may influence fetal growth and development, causing hypercholesterolemia, changing fetal cholesterol metabolism, and contributing to macrosomia. Three types of total cholesterol (TC) participate in lipid metabolism

and regulation: low-density lipoproteins (LDL-C) and high-density lipoproteins (HDL-C). TC is the sum of all cholesterol types in the body, including LDL-C, HDL-C, and VLDL-C. The body requires cholesterol to synthesize hormones, maintain cellular structure, and the precursor 7-dehydrocholesterol to produce vitamin D. Placentas require cholesterol to produce progesterone and estrogen, fetal development hormones, and maintain pregnancy. While there is evidence of the transfer of maternal cholesterol to the fetus in early pregnancy, the baby relies on cholesterol, which synthesises itself from maternal LDL and HDL through a process mediated by placental lipase enzymes. Lipoprotein scavenger receptors and transporters class A (ApoA-1) and B type1 (SR-B1) control the transport of lipoprotein-bound cholesterol.

When pregnant, the body's demand for cholesterol increases, leading to an increase in LDL-C. In the placenta, receptor-mediated endocytosis takes up LDL-C through the LDL receptors that recognize apolipoprotein B100, the primary apolipoprotein on LDL particles. After uptake, LDL-C travels to lysosomes, where cholesterol is released and used by the placenta or transferred to fetal circulation. The placenta uses cholesterol to produce hormones and other essential molecules. As pregnancy progresses, HDL-C levels rise. The placenta uses HDL-C for transport, hormone production, cellular membrane synthesis, and overall growth and development. Maternal BMI status can influence the placental metabolism of TC, creating a lipotoxic environment characterised by increased placental lipid levels and CIDEA protein levels *(182)* and decreased AMP-activated protein kinase (AMPK) activation *(183)* in the obese placenta. These molecular changes suggest that obesity leads to dysregulation of TC metabolism in the placenta, contributing to the altered lipid profile. The plasma LPC species involved in lipid metabolism change in individuals with GDM *(184)*. As LPCs are involved in cholesterol transport and metabolism *(184)*, these changes could reflect dysregulated TC metabolism, which also occurs with GDM. Placental cholesterol transport in GDM placentas is affected by insulin treatment *(185)*.

Below Figure 1:24 Continuation to cholesterol, the systematic name is cholest-5-en-3β-ol, identification in lipid maps LMST01010001, C27H46O, the table containing exact masses in positive, negative and neutral exact mass 386.354865.

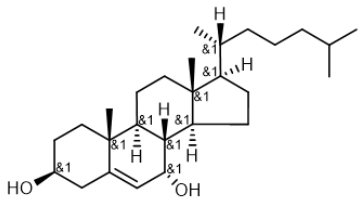

7alpha-hydroxy-cholesterol

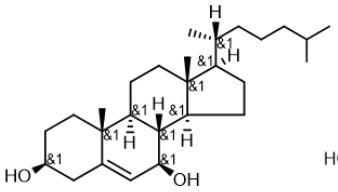

7beta-hydroxycholesterol

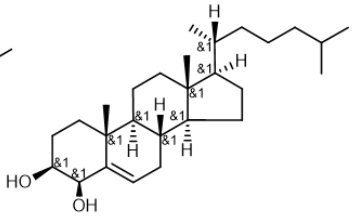

4beta-hydroxy-cholesterol

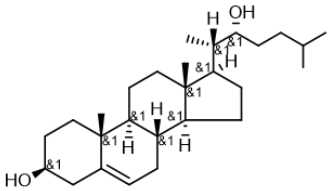

22R-hydroxycholesterol

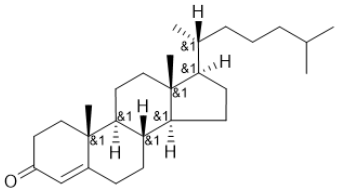

Cholestenone

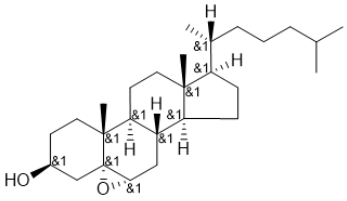

5,6alpha-epoxy-cholesterol

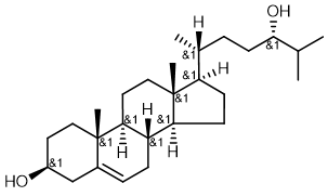

24S-hydroxy-cholesterol

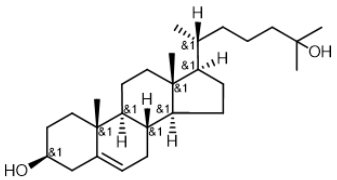

25-hydroxy-cholesterol

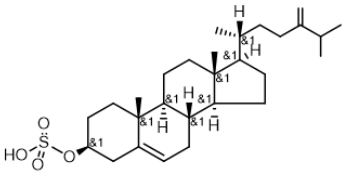

24-methylene-cholesterol sulfate

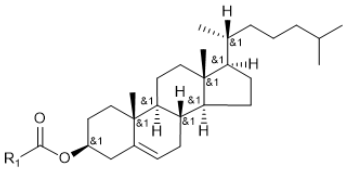

Cholesterol ester

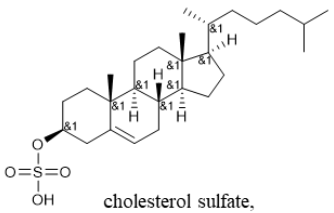

cholesterol sulfate,
cholest-5-en-3β-yl hydrogen sulfate

Cholesterol; cholest-5-en-3β-ol
LM ID: LMST01010001
Formula:C27H46O
Exact Mass:386.354865

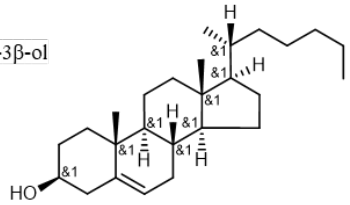

Neutral No adduct

Mass (offset 0.0000)	Δm	Lipid species	Lipid category	Lipid class	Sum formula
386.354866		Cholesterol	Sterol lipid	sterol	C27H46O

Positive ions

m/z (offset 0.0000)	Δm/z	Lipid species	Lipid category	Lipid class	Adduct	Charge	Sum formula
387.362143		Cholesterol	Sterol lipid	sterol	+H+	+1	C27H47O
409.344087		Cholesterol	Sterol lipid	sterol	+Na+	+1	C27H46ONa
404.388692		Cholesterol	Sterol lipid	sterol	+NH4+	+1	C27H50NO
369.351578		Cholesterol	Sterol lipid	sterol	+H+ -H2O	+1	C27H45O

Negative ions

m/z (offset 0.0000)	Δm/z	Lipid species	Lipid category	Lipid class	Adduct	Charge	Sum formula
385.34759		Cholesterol	Sterol lipid	sterol	-H+	-1	C27H45O
445.368719		Cholesterol	Sterol lipid	sterol	+CH3COO-	-1	C29H49O3
431.353069		Cholesterol	Sterol lipid	sterol	+HCOO-	-1	C28H47O3
465.304405		Cholesterol	Sterol lipid	sterol	-H+SO3-	-1	C27H45O4S

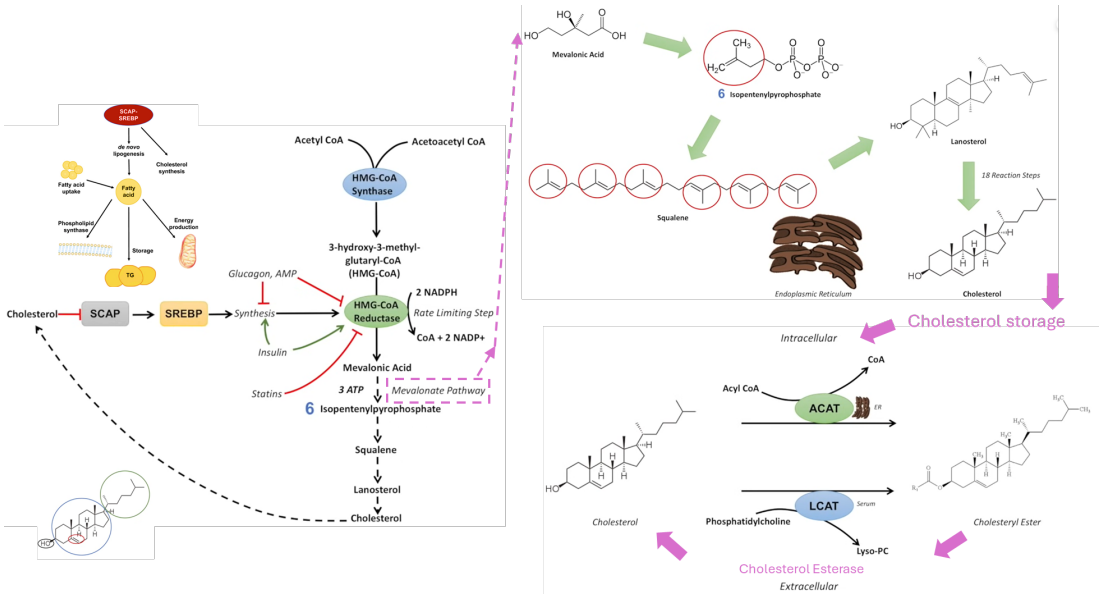

Figure 1:25 Schematical illustration of cholesterol synthesis metabolism.

A rate-limiting step (degradation and regulation) involves HMG-CoA reductase (HMGR), which slows down the enzyme catalytical process at the start of the pathway. That protein supports cholesterol homeostasis by activating HMG-CoA reductase HMGR. Firstly, cholesterol esterification by cholesterol acyltransferase (ACAT) is responsible for lipid droplet storage. Secondly, cholesterol is transported backwards via LDL receptors and HDL. Statins are HMG-CoA reductase HMGR inhibitors that lower (block) intracellular cholesterol synthesis to increase LDL uptake from extracellular sources. They regulate cholesterol synthesis and transporter efflux genes. In the cell, cholesterol homeostasis depends on the activity of 3-hydroxy-3-methylglutaryl-coenzyme A reductase(HMGR). The HMGR enzyme is the last enzyme in the mevalonate pathway to create cholesterol, ketones, polyols, prenylated proteins, dolichol, coenzyme Q, and the side chain of haemoglobin A. In cholesterol synthesis, mevalonic acid is synthesised from HMG-CoA by the enzyme. Hormones, proteins, and small molecules control the activity of the enzyme. All schematics were hand drawn in PowerPoint i-Pen and saved as jpeg images. The idea of the schematics comes from literature and student adaptation of originals *(44)*.

1.5.8 Free Fatty Acids (FFAs)

FFAs are essential to placenta metabolism and exert their effects by activating and binding to specific molecules. Peroxisome proliferator-activated receptors (PPARs) regulate energy balance by stimulating hormones and enzymes in lipid metabolism. In addition, they regulate fat storage and carbohydrate production. Albumin is a glycosylated protein that binds to FFA to support uptake and transport. Specific proteins in the syncytiotrophoblast such as fatty acid transport protein FAT/CD36 and plasma membrane-associated FATBPs, help transport FFAs into the placenta

and across to the fetus for energy and synthesis of structural lipids essential to fetal growth and development. In response to fetal metabolic signals, the placenta modulates FFA transfer and utilization through its enzymatic systems, such as elongases (enzymes that catalyses carbon chain extension, especially a fatty acid) and desaturases, which convert FFAs into long-chain polyunsaturated fatty acids (LCPUFAs), which are crucial for fetal development. Insulin is essential for transporting FFAs across the placenta, promoting uptake by regulating FATPs and FABPs. The lipotoxic environment of the obese placenta causes dysregulation of FFA metabolism. Increased levels of FFAs in maternal circulation can increase placental uptake of FFAs by upregulating FATPs and FABPs *(186)*. The hallmarks of insulin resistance in GDM are evident in the placenta and complicate FFA metabolism, decreasing the expression of FATPs and FABPs and reducing FFA uptake *(187, 188)*.

1.5.9 Lipoproteins

Lipoproteins carry cholesterol and triglycerides throughout the bloodstream in structures containing a lipid core surrounded by phospholipids, cholesterol, and proteins (apolipoproteins). As the fetus develops, hPL and progesterone mobilise fatty acids from maternal stores and alter lipoprotein lipase activity, hydrolysing triglycerides into lipoproteins. With a healthy maternal BMI, lipoprotein subfractions are stable and can meet the metabolic demands of the mother and fetus. Lipoprotein profiles related to a healthy BMI are favourable - higher HDL and lower LDL. HDL reduces inflammation and oxidative stress in the placenta. Placental enzymes and receptors that regulate lipid metabolism, including lipoprotein lipase (LPL), change due to maternal obesity, and lipoproteins accumulate in the placenta, causing cholesterol accumulation and impairing placental function. For example, lipoprotein transport is over-expressed in the first-trimester placenta of overweight or obese pregnant women *(189)*. The ensuing oxidative stress and inflammation within the placenta increase lipid deposits, potentially affecting fetal growth and health. Prenatal gestational weight impacts DNA methylation *(190)*, affecting lipoprotein metabolism *(190-192)*, and changes might impact lipoprotein metabolism in GDM placentas with affected placental trophoblast cells showing

mitochondrial dysfunction in the assembly and secretion of triacylglycerol-rich lipoproteins *(193)*.

1.6 Analysis of lipids

Determining how different lipid groups affect and are affected by maternal obesity and GDM is critical to the experimental models and interventional studies that can be used towards better strategies to mitigate the detrimental effects of these complex interactions. A better understanding of placental lipid changes can help us understand pregnancy-related complications. The literature presents mainly an analysis of animal tissues, especially from mice and rats, as models for studying lipids in biology. The most abundant bioactive lipids are within tissues such as the liver, heart, blood, and plasma. Adipose tissue is the leading site of lipid storage, which is equally important but in a different form as metabolites and intermediates. The most abundant lipid species in human and animal tissue and organs involve fatty acids *(194)*. The most abundant simple lipids are unesterified cholesterol, cholesterol esters and diglycerol. There is always the danger of hydrolysis, and artefacts can affect hydrolysis during sample preparation and analysis as they are related to the hydrolysis of fatty acids during extraction or storage *(195)*. During sample preparation of tissue extraction, a low temperature must be maintained to prevent this. Various methods can be used to provide insights into placental lipid composition, metabolism, and potential functions. The study of lipids in biological samples involves profiling and quantification with mass spectrometry for lipidomics analytics, which is the standard due to its sensitivity and specificity.

Lipid analysis usually involves chromatography, mass spectrometry, and spectroscopy, which can help identify changes in the lipid profiles during pregnancy. For example, it can enable us to understand better how lipid metabolism is affected by pregnancy and how it affects the fetus by determining the concentration of the lipid in the blood, such as lipoproteins, triglycerides, and cholesterol levels. As the most abundant sterol sulfate in human plasma, cholesterol sulfate overlaps with highly abundant dehydroepiandrosterone (DHEA) sulfate. Although these sulfolipids produce and disintegrate at similar rates, they come from distinct sources

and undergo different metabolic pathways. A regulatory molecule, cholesterol sulphate, serves a purpose that DHEA sulphate does not.

Among its functions, cholesterol sulphate protects erythrocytes from osmotic lysis and regulates sperm capacitation in cell membranes. It assists platelet adhesion in platelet membranes. In blood clotting, fibrinolysis, and epidermal cell adhesion, cholesterol sulphate regulates serine proteases. Signal transduction involves cholesterol sulphate because it regulates protein kinase C isoforms and modulates phosphatidylinositol 3-kinase activity. When cholesterol sulphate is present in the body, it induces genes that encode key factors in barrier development. By inducing genes that encode barrier components, cholesterol sulphate contributes to keratinocyte differentiation *(196)*. By measuring these lipids, it is possible to gain insight into changes during all stages of pregnancy *(197)*. Various techniques can be used to measure the concentration of different lipid species, including fatty acids, glycerolipids, glycerophospholipids, and sphingolipids and cholesterols in analytical biochemistry, which supports cell *(103)* biology of disease research, including obesity, diabetes, cardiovascular disease, neurodegeneration, and central nervous system and pulmonary pathways *(198-201)*.

The lipids are not soluble in water but are soluble in organic solvents, and lipid separation due to chemical differences in their matrices makes lipid analysis very complex *(202) (203)*. Choosing a lipid analysis method depends on the lipid of interest, the matrix complexity, the sensitivity, and the specificity required *(204, 205)*. A comprehensive profile of lipid composition uses a combination of hyphenated methods *(104, 206-211)*. Every method has its advantages and limitations. A lipid analysis method depends on the lipid class, the sample type, the sensitivity and specificity required, and the instrumentation available. The precision, speed, and breadth of lipid analysis improve with analytical techniques and instrumentation advances. Mass spectrometry has high sensitivity and specificity, making it ideal for lipidomics studies *(212-215)*. NMR provides structural information without destroying the sample, and thin-layer chromatography helps separate complex lipid mixtures *(216-221)*. In addition to exploring different lipid compositions and biological functions, each method offers advantages *(222, 223)*. It

is crucial to our understanding to identify lipid-related biomarkers, explore lipid-targeted therapies, and advance knowledge of lipid metabolism and their roles in disease development, metabolic processes, and overall physiological functions *(224)*.

1.6.1 Extraction

Most lipid analysis techniques, including TLC, GC, LC, MS, and NMR, require sample extraction before analysis. Therefore, lipid extraction is a standard starting point by isolating lipids from the sample matrix with a solvent like chloroform or methanol. Any impurities that are likely to interfere with analysis might need additional extraction. Standard lipid analysis methods from biological samples include extraction by the Folch method, which involves chloroform and methanol as solvents. The Bligh and Dyer *(225)* method uses chloroform, methanol, and water in different proportions than the Folch Stanley Sloan *(226)* method. The steps of extraction of the Bligh and Dyer method are fully presented in detail in Chapter 2.

1.6.2 Mass spectrometry

Lipid profiling methods often include mass spectrometry (MS), a powerful tool for identifying and quantifying lipids in various biofluids, including cells and tissues *(227)*. Researchers have used MS to investigate lipid profiles associated with cancer, cardiovascular diseases, diabetes, obesity, neurodegenerative diseases, and many others *(227)*. Due to its high sensitivity and ability to provide detailed structural information, MS is a powerful lipid analysis tool that can be coupled with chromatographic techniques like LC or GC. The mass-to-charge ratio (m/z) and fragmentation patterns can reveal individual lipid species, and double bond location can be determined. Multiple MS methods can be applied to the analysis of lipids: separation of fatty acid isomers uses supercritical fluid chromatography (SFC); electrospray ionisation spectrometry (ESI-MS) analyses complex lipid mixtures as does matrix-assisted laser desorption ionisation (MALDI-MS); double-bonded positions and configurations of fatty acid chains can be determined using tandem mass spectrometry (MS/MS). These single-stand or hyphenated techniques are

suitable for monitoring lipid changes in the placenta and plasma to provide insight into lipid metabolism and maternal health.

Several techniques can complement MS in lipidomics analysis, including mass spectrometry imaging, stable isotope labelling, and NMR spectrometry (see section 1.8.5). Different mass spectrometry methods are available for imaging tissue lipid distribution *(228)*. Mass spectrometry imaging can visualise a lipid map in cell tissue, including phospholipids and their oxides *(229)*, and provide a spatial mapping of lipid location in tissues, a feature typically lost when extracting lipids from tissues en masse. Studying lipid metabolism and turnover in lipidomics with stable isotope labelling is also possible *(230)*. The fate of lipid species can be tracked by incorporating stable isotopes into lipids to monitor the fate of specific lipid species and measure their turnover rates *(230)*. It offers high sensitivity, specificity, and versatility in lipid analysis *(231)* and is widely used in lipidomics research to investigate lipid profiles associated with various diseases and conditions *(232)*.

1.6.2.1 MALDI-ToF MS is an example.

Identification of lipid classes might benefit from MALDI-ToF MS, and an overview of the methodological approach is provided as an example of some of the critical considerations that need to be made when pursuing MS-based analysis ahead of applying this method in results chapters. MALDI ToF MS analysis involves peak picking, checking for Gaussian shape and centroid, and mass accuracy to four decimal places. It is necessary for lipid species identification and quantification, such as comparisons between samples or groups to identify changes in lipid content. Running each sample in triplicate is ideal for sample mass spectra repeatability, at least for its cumulative mass spectrum range. Any slight variations in instrumental parameters can be averaged by taking an average of three samples, reducing drift impact. As a final benefit, internal calibration ensures that the mass range remains constant, ensuring that the sample's identity does not change over time. It is critical to note that the specific details of sample preparation, matrix selection, and instrument parameters may vary depending on the research question and lipid classes

of interest when approaching testing. Optimising these parameters is necessary to achieve the most accurate results.

The following steps apply when measuring lipid content using MALDI-TOF mass spectrometry. Sample preparation begins with extracting lipids from tissue or biological fluid through appropriate extraction methods. Extracted lipids can then dissolve in a suitable solvent for MALDI-TOF analysis. Standard matrices for lipid analysis include 2,5-dihydroxybenzoic acid (DHB) or α-cyano-4-hydroxycinnamic acid (CHCA) *(208)*. The matrix solution typically dissolves the matrix in a solvent such as acetonitrile or methanol before spotting the sample mixed in the matrix onto the target using a pipette or an automated device. There are different methods and practices to apply the sample matrix to the target, depending on the protocol and user experience.

The sample is usually mixed with the matrix solution to target sample spots and left to dry. The matrix solution helps co-crystallise lipids and facilitates ionisation during the MALDI process. The working steps include loading the prepared target plate into the MALDI-ToF mass spectrometer, allowing time for the instrument to equilibrate, and setting the appropriate parameters for the analysis, including laser intensity, mass range, acquisition mode and vacuum voltage. Once all is working and the instrument system software changes the mode from docking to ready active, data acquisition begins by using the laser shots around the sample displayed in the viewing window, making sure there are crystals and accruing total accumulative mass spectra, starting with calibration with a known MALDI calibrant compound to ensure the mass range values of the calibrant are within an acceptable range. Data analysis of mass spectra uses appropriate software depending on the instrument provider. Most lipidomics use electrospray ionisation (ESI) *(233, 234)* rather than APCI *(235)*

1.6.2.2 TLC, MALDI ToF MS and MALDI imaging as an example

Several steps and considerations go into thin-layer chromatography (TLC) and matrix-assisted laser desorption/ionization time-of-flight mass spectrometry (MALDI-TOF MS).TLC analysis separates and identifies compounds in a mixture

using thin-layer chromatography. Lipid extracts from the placenta are prepared by homogenizing tissue and extracting lipids with organic solvents such as chloroform and methanol. The TLC experiment involves applying lipid extracts to a TLC plate coated with silica gel. With an appropriate solvent system, the lipids can separate by their polarity and affinity for the stationary phase. To detect sulphur-containing lipids such as cholesterol sulphate, the TLC plate is visualized using iodinated vapour or other staining methods. The MALDI-TOF technique is a tool for analysing complex mixtures. Its high sensitivity makes it ideal for analysing lipids such as cholesterol sulphate.

Cholesterol sulphate ionization depends on matrix selection. Sulphated lipids respond well to 9-aminoacridine. First, samples are co-crystallized with a matrix on a target plate for MALDI-TOF MS ionization and detection. Lasers ionize the sample, and then mass/charge ratios separate the ions. Detecting cholesterol sulphate as a deprotonated ion ([M-H]) in negative ion mode is suitable for sulphated compounds. Using mass spectra, we can determine lipid molecular weight and structure. A characteristic peak can be observed to identify and quantify cholesterol sulphate.

Here are some challenges and considerations when considering cholesterol and its derivatives that may show low ionization efficiency, which can be enhanced by derivatizing them or using specific matrices. It is critical to choose a matrix that minimizes interference with the analytes. Some studies have explored alternate ionization techniques to reduce matrix effects. There are key differences between TLC-MALDI-imaging and traditional lipid staining techniques in terms of sensitivity, specificity, and application. The system is capable of detecting and identifying a wide range of lipid species. The method is particularly useful for analyzing complex lipid mixtures since it allows the identification of individual lipid components that may be difficult to distinguish from traditional staining. In addition to providing spatially resolved data, TLC-MALDI-IMS offers a significant advantage for analyzing lipid distribution within a sample. Traditional staining techniques do not provide spatial context, only qualitative information. It can be used for both qualitative and quantitative analyses of lipids based on TLC-MALDI-IMS.

With traditional staining methods, it is often difficult to precisely quantify lipid species. These are the benefits of conventional staining, like Coomassie staining, which is generally less complex and requires less specialized equipment than TLC-MALDI-IMS. These methods are widely accessible in laboratories without advanced mass spectrometry facilities.

An analysis using staining techniques is primarily qualitative, providing a visual representation of lipids. However, they do not provide detailed structural information or precise lipid species quantification. Traditional staining is often more cost-effective than mass spectrometry. Because it is cheaper to implement and requires fewer resources, it is suitable for routine analysis. The combination of Thin-Layer Chromatography with Matrix-Assisted Laser Desorption/Ionization Imaging Mass Spectrometry (TLC-MALDI-IMS) offers several advantages over traditional staining techniques. A comparison of the two methods: Traditional staining methods, including primuline staining, detect fewer lipid classes. Specificity and resolution allow the identification of specific molecules within complex mixtures based on high-resolution images and detailed molecular information.

In contrast to molecular specificity, staining techniques are more qualitative and provide limited information about lipid structures. Despite not being inherently quantitative, TLC-MALDI-IMS provides relative concentration data that can be used to infer quantitative information. The traditional staining method provides qualitative information on lipid concentration rather than quantitative data. Combined separation and analysis in one workflow makes TLC-MALDI-IMS more efficient. While staining techniques are often simpler and faster to perform, they require additional steps for quantitative analysis and molecular identification. Specifically used for routine lipid separation and visualization, it is suitable for less complex lipidomics analysis of complex lipid mixtures. It is also ideal for lipid spatial distribution in tissues *(236-238)*.

1.6.2.3 ESI-MS as an example

By using Electrospray ionisation (ESI), which is an ionisation technique developed by Fenn and colleagues, polar compounds can be analysed. (Fenn et al., 1990, Fenn

Nobel 2003) *(239, 240)*, atmospheric pressure matrix-assisted laser desorption/ionisation (AP MALDI) (Creaser & Ratcliffe, 2006) *(235)*, and desorption electrospray ionisation (DESI) (Takats et al., 2004) *(241)* are among the many ionisation techniques. As ions are produced at higher pressures, narrow, conductance-limiting apertures must be used to separate differentially pumped vacuum chambers before reaching the mass analyser's high vacuum region to achieve maximum sensitivity. During these various vacuum stages, the ability to control ion motion really influences the mass spectrometer's ion transmission efficiency. When applying magnetic and electric fields, ions can be precisely manipulated even when no background gas molecules are present (e.g., in a low vacuum). Ion motion is influenced by collisions with gas molecules at higher pressures. It can also be transmitted in high vacuum at low pressures (10mTorr), where radio frequency (RF)-only multipoles enable efficient ion transmission (Thomson, 1998) *(242, 243)*. Great reviews of electrospray over the last thirty years by detailed literature of the specialists in the fields (Mann M. et al., 2019) and many electrospray developmental specialists *(244-247)*.

Electrospray ionisation ESI schematics as an example

There are many theories regarding how ions are produced, and many physical processes are described in detail. The figure diagrams below of the HPLC-ESI-MS show the working stages of the sample travelling via a capillary tube at a very slow rate flow of one to ten millilitres per minute (1–10 ml/min) and applied to a 106 V/m electric field potential difference of 3–6 kV under atmospheric pressure. Droplets of highly charged mobile phase spray from the capillary end when charges accumulate at the liquid surface. A coaxially flowing sheath gas limits the dispersion space and minimises the effects of mobile phase differences during ESI/MS. Ions are generated for MS analysis by passing droplets through heated inert gases (often nitrogen). A hundred years ago, Lord Rayleigh predicted that when droplets evaporate, Coulombic forces approach surface tension. The Rayleigh equation formula is represented by ($q2 = 8\pi2\varepsilon0\gamma D3$) where (q) represents charge, ($\varepsilon0$) is the permittivity of the environment, (γ) is the surface tension, and (D) is the diameter of a spherical droplet (Figure 1.11) and (Figure 1.12) When a droplet exceeds the Rayleigh

stability limit, it explodes, releasing many smaller ones. This results in successively smaller and smaller ruptures, followed by smaller and smaller droplets, such as "Columbic repulsion" explosions, as shown in the schematic diagram (Figure 1.12). A droplet is ionised after its solvent is sufficiently evaporated. The ESI method can also generate adduct ions for molecules that do not possess intrinsic ionising sites. If the conditions are right, small anions or cations can be ionised during ESI if there is enough dipole potential between the molecules. The nonpolar lipids, triacylglycerols (TAGs) containing long-chain fatty acids can be ionised and quantified with sensitivity to picomoles using noncovalently attached lithium ions to carbonyl molecules *(239, 240, 248-253)*.

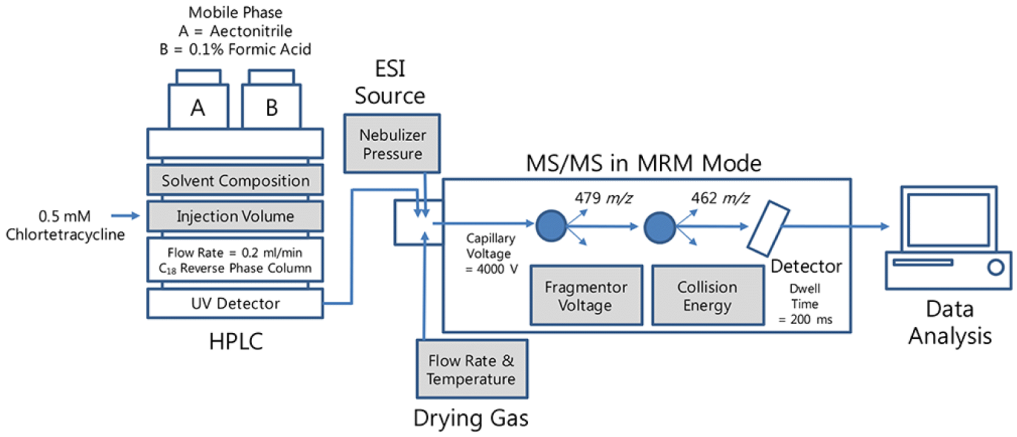

Figure 1:26 Schematics (HPLC-ESI-MS) analyses complex mixtures www.waters.com

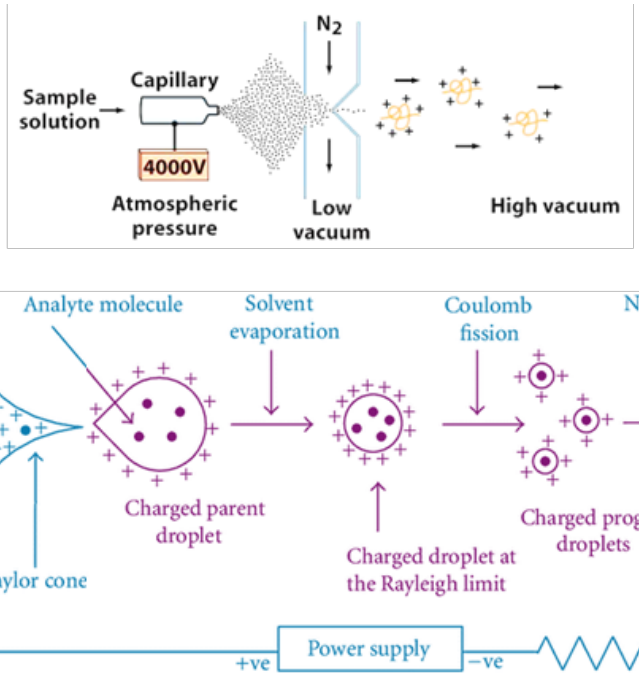

Figure 1:27 Schematics diagram of ESI and how it works. ESI droplets desorption ionization of a sample dissolved in an aqueous solution, for example, in methanol, which then produces multiply charged ions M+1, M+2, M+3. Generation of multivalent molecular ions and how solvent is removed. The figure was adapted from Waters.com, accessed on 30 May 2024, reconstructed in PowerPoint, and then saved as a picture.

1.6.2.4 APCI-MS as an example

As another example, atmospheric pressure-chemical ionisation mass spectrometry (APCI-MS) has emerged as an ideal technique for lipid analysis because it ionises large neutral molecules in a broad range of mobile phases. APCI-MS has been applied successfully to analyse triacylglycerols and their oxidation products, demonstrating its effectiveness *(254)*. Cellular lipids were analysed qualitatively and quantitatively by APCI-MS, showing potential for comprehensive lipid analysis and systems-level assessment *(255)*. A consistent sample is created by carefully preparing tissue samples, usually through homogenisation and extraction with chloroform and methanol. Samples are introduced in the liquid state and nebulised into delicate sprays in APCI ionisation by corona discharges or other sources. In the MS detector, the ionised molecule follows separated ion detection of mass-to-charge ratio *(m/z)*. Protons (H+) are added or removed from lipid molecules in APCI to form charged particles (ions). The conventional APCI-MS/MS technique has limited

sensitivity, especially in studies involving trace amounts of non-esterified bioactive lipids in cell culture systems *(256)*. As a result, it is crucial to examine APCI-MS limitations and potential advancements to make it more sensitive and applicable to analysing placenta lipids, cholesterol, and oxysterols. Identifying cholesterol and its oxidation products accurately and completing HPLC separations are essential when using HPLC-APCI-MS *(257)*, and this combination of HPLC and APCI-MS provides a powerful technique for analysing cholesterol and its oxides *(258)*.

1.6.2.5 Chromatography

Thin-layer chromatography (TLC) in lipid separation can only be used as a preliminary identification test for lipid groups and not individual lipid species. The detailed lipid identification and quantification can be made via liquid chromatography (LC), for example, high-performance liquid chromatography (HPLC), connected with Electrospray ionisation (ESI) and hyphenated with mass spectrometry detector (LC-MS) to support mass spectrometry comparative analysis. HPLC consists of different stationary stainless-steel columns packed with silica crystal granule phases to separate lipids based on their polarity, and quantifications of specific lipid classes are enabled by coupling LC with ultraviolet (UV) and fluorescence detectors. Using LC-based methods, researchers can determine lipid classes, subclasses, and individual species, allowing them to study lipid profiles and their relationship to physiological and pathological conditions. Liquid chromatography (LC) offers excellent separation and detection capabilities for lipids of different polarities and masses. Several LC techniques employ lipid analysis, including normal phase (NP), reverse phase (RP), and hydrophilic interaction liquid chromatography (HILIC). Bridging LC to mass spectrometry (LC-MS) makes lipid identification and quantification more specific. Lipid analysis in human biological samples can be improved significantly with high-performance liquid chromatography (HPLC) and ultra-performance liquid chromatography (UPLC), and these are commonly used variations of liquid chromatography with improved resolution. Different lipid classes, including cholesterol, phospholipids, and sphingolipids, are identified and quantified based on their polarity. Due to its high sensitivity and resolution, it is ideal for analysing complex lipid mixtures coupled

with UV, RI (Refractive Index), ELSD (Evaporative Light Scattering Detector), or MS (Mass Spectrometry). In GC, individual lipid molecules are separated depending on their volatility and affinity for the stationary phase. Analysis of fatty acids, triglycerides, and sterols is well suited to this technique. A helpful method for the study of fatty acid methyl esters (FAMEs) after derivatisation is gas chromatography (GC). Various downstream detectors can further analyse lipid composition, including flame ionisation (FID) and MS.

1.7 Introduction to MALDI ToF MS

An introduction to MALDI ToF MS, the results of which are presented later on in Chapter 4. Time of Flight mass spectrometry has been around since Stephens in 1946 *(259)* and Wiley and McLaren in 1955 *(260)* and has progressed into use in biological analyses. In 1985, German scientists Franz Hillenkamp and Michael Karas and co-workers *(261)* discovered the MALDI phenomenon using the amino acid alanine, which was not ionisable using a 266 nm UV laser pulse. However, adding another amino acid, tryptophan greatly increased alanine ionisation efficiency *(262-264)*. Moreover, they developed their discovery into the generalised MALDI ionisation method for mass spectrometry *(264, 265)*. In 1988, Koichi Tanaka observed a similar matrix effect using glycerol mixed with a metal powder and analysed polymers, proteins, and large molecules *(266)*. Hillenkamp and Karas analysed large proteins and used nicotinic acid as a solid organic matrix *(261)*. The discovery of adding an organic crystal structure that absorbs ultraviolet light helped charge polar biomolecules *(261)*. With that detection, the MALDI technique became popular in biomolecule analysis and led to the creation of the field of proteomics. Biomolecule analysis, including lipid analysis, using MALDI, has been growing but still needs development. With MALDI, it is now possible to routinely analyse proteins, peptides, polymers, and lipids *(69) (267)*. The significance of MALDI as an ionisation technique was recognised by the Nobel Prize in 2002/3. *(268)*

MALDI requires a suitable matrix mixed with the analyte. Usually, the matrix proportions are more than the sample depending on the species and are in molar ratios of (1:100, 1:500, or 1:1000). The correct ratio is a matter of trial and error to

find what gives a good signal for a given matrix and analyte. The characteristic matrix for MALDI experiments is a low molecular weight organic acid in a powder with high absorption for the UV laser wavelength. Upon irradiation, the matrix absorbs the laser energy, protecting the sample, which then desorbs from the surface, creating a plume of matrix and analyte molecules into the gas phase, during which the molecular ions gain charge – usually by protonation from the acidic matrix molecules - and the resulting ions carry that charge through the ion optics tube during the flight until they hit the detector plate.

After applying the matrix mixed with the sample to the target plate, the plate is attached to the target holder and sent via an airlock into the vacuum chamber. When the laser hits the target sample spots, the matrix mixed with the sample absorbs the laser energy, desorbs, vaporises the analyte, and travels away through the time-of-flight tube. The complete method of sample ionisation is still under vigorous debate in the literature, but the general mechanism involves the desorption of large clusters, which further dissociate into separate molecular ions with charged mass. Workable MALDI sample ionisation mechanism theories are in the MALDI section below *(269, 270)*. MALDI often couples with time-of-flight mass spectrometers but can also couple with other mass analysers like ion trap mass analysers and ion cyclotron resonance.

1.7.1 The Mechanism of MALDI

While the mechanism of MALDI is still under robust debate within the mass spectrometry literature, there is no doubt that it works, and several characteristics are apparent. MALDI requires a matrix to absorb the laser light, desorb the matrix/analyte crystals into the gas phase, and ionise the sample. During the MALDI experiment, the laser irradiates the matrix with short laser beam pulses of three to twenty nanoseconds (for UV lasers). *(271)* The adjusted and focused laser spot size is usually 50-200 nm. The laser fluence is laser power per area, a physical parameter in the window setting on the instrument control computer. The ideal initial value is a matter of experience. The applied laser pulses desorb the matrix/analyte crystals into the gas phase plume, where they undergo fission, resulting in free ions and a

substantial background of ionised matrix molecules. The mass spectrometer can detect these analytes if this matrix background is not in the same mass/charge ratio range as the analytes. MALDI can generate positive and negative ions via protonation or deprotonation. Radical cations or anions can also form with specific analytes, usually as a low-abundance component. When studying proteins and peptides, singly protonated species [M+H]+ and some dimers that carry double the mass $[2M+H]^+$ are usually seen. Multi–charged ions are sometimes generated, particularly with high molecular weight species *(272) (273)*.

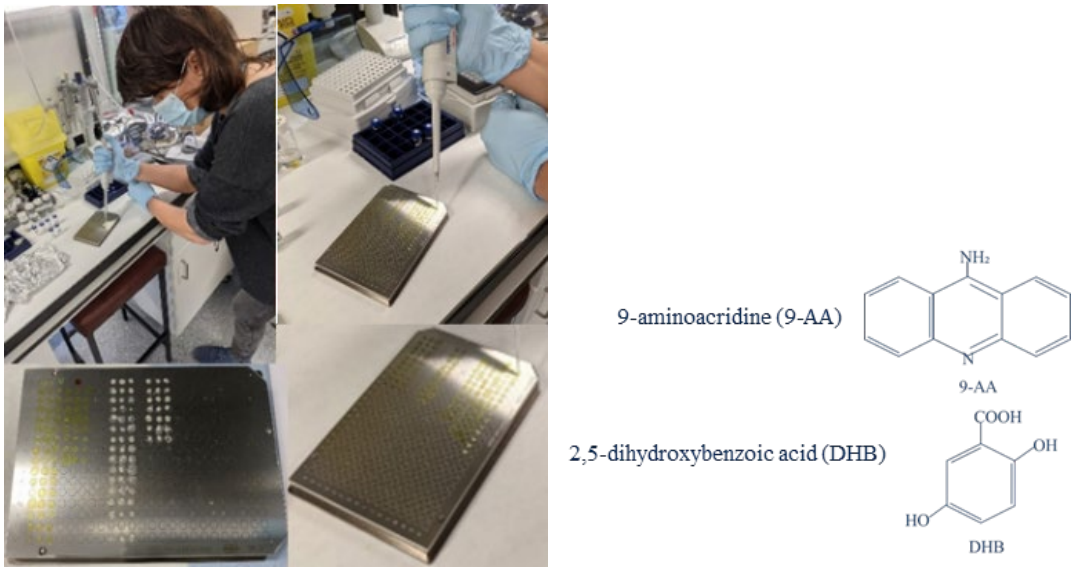

Figure 1:28 Chemical structure of Matric 9AA, DHB, and sample application to MALDI targets. Figure legend of (Figure 1:10): Two matrix molecules, 9-aminoacridine 9AA and 2,5-dihydroxybenzoic acid DHB, were used in this thesis's studies. The yellow spots are samples mixed with 0.5 M 9AA matrix dissolved in 3:2 isopropanol: acetonitrile (IPA/CAN v/v), and the white spots are lipid samples in 0.5 M DHB matrix dissolved in methanol. Each spot volume was 0.5 - 1 µl at 10 mg/ml, and the molecular structures of the two matrices are in the inset.

1.7.2 The desorption and Ion Formation mechanism

The desorption and photo-ionisation processes in MALDI are unclear, and the theory proposes thermodynamic processes that involve quasi-thermal evaporation due to increased molecular internal vibrational energy *(274) (275) (276)*. A suitable matrix

needs an excellent molar absorption coefficient to absorb the laser irradiation so that the matrix sublimes into the gas phase, where the sample competes for the charge.

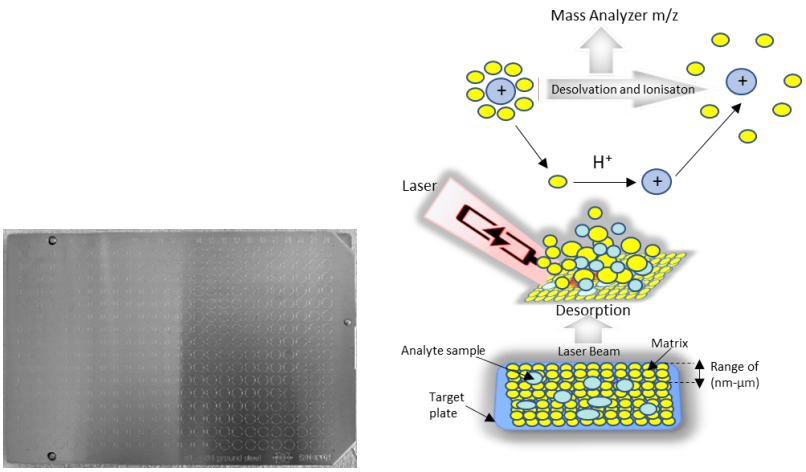

Figure 1:29 Figure MALDI target plate sample desorption. Figure legend of (Figure 1:14) One general hypothesis *(273, 276)* states that after sample desorption into the gas phase, it undergoes a proton transfer reaction from the excited matrix molecules that occurs during plume expansion. Agreeing with the Karas model, these excited matrix molecules must produce ionised gaseous analyte ions. Another hypothesis suggests that desorption into clusters is first, followed by desolvation like electrospray, where the hot matrix molecules effectively act as the solvent *(276)*. Time-of-flight mass analysis has the advantage of simplicity and speed and can cope with extremely high mass range and repetition rates *(276)*.

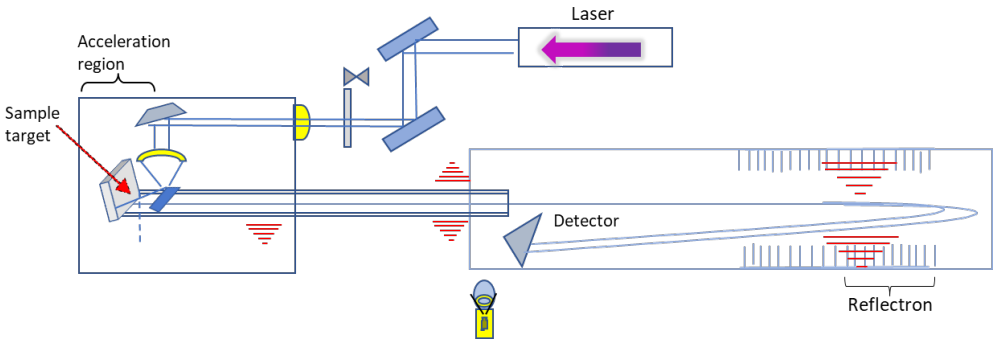

Figure 1:30 Figure Time of Flight Mass Analyser. Figure legend of (Figure1.15) Time of Flight Mass Analyser with pulsed laser ionisation, extracted ions accelerate through an electrical field (V) into a time-of-flight mass analyser tube for mass analysis.

1.7.3 MALDI ToF MS physics

Physicists define charge as a constant denoted by *(e) and as* the interaction between particles and electromagnetic fields. Charges can be positive or negative. Charges

that are similar repel each other, while charges that are opposite attract each other. Charge is measured in Coulombs (C), and it can be discrete (quantified) or continuous. The elementary charge is defined as the amount of charge on one electron or one proton. In general, protons carry a positive charge (approximately +1.6 x 10-19 C), electrons carry a negative charge (approximately -1.6 x 10-19 C), and neutrons have no charge. In an isolated system, the total electric charge remains constant over time according to charge conservation.

In the MALDI-ToF MS experiment, ions first need to gain charge, and they do that by accelerating the desorbed ions through an electric potential field as per (Eqn. 1).

$E_{pot} = zeV$ (Eqn. 1)

The ion's electric potential energy (E_{pot}) showing in (Eqn. 1) is the first energy of the ions found on the voltage plate where the ions gain charge (z), which is produced by the laser approximately 1.602 $x10^{-19}$ coluomb (C) and through the ion acceleration with the potential energy, it then produces ions with kinetic energy as per (Eqn. 2).

$E_{kin} = ½ mv^2$ (Eqn. 2)

When ions start leaving the ion source, they have velocity (v) and the accelerating ions through the source and the flight tube gain the ion's kinetic energy, which equals the potential energy (E_{pot}) as per (Eqn. 1) and when ions are in an isolated system, the total electric charge remains constant over time according to a charge conservation law.

$zeV = ½ mv^2$ (Eqn. 3)

The energy stays the same during ion acceleration and converts ions to kinetic energy. Thus, the kinetic energy equals the voltage (V) multiplied by the charge (z) and is scaled to the elemental charge (e-). Rearranging (Eqn. 3) to solve for velocity yields:

$\frac{2zeV}{m} = v^2$ (Eqn. 4)

or $\sqrt{\frac{2zeV}{m}} = v$ (Eqn. 5)

The time of flight equals the flight distance divided by the velocity.

$t = \frac{L}{v} = \frac{L}{\sqrt{\frac{2zeV}{m}}}$ (Eqn. 6)

or $t = L\sqrt{\frac{m}{2zeV}}$ (Eqn. 7)

The square root of (*m/ze*) is relative to the time of flight (Eqn.7) to or,

$t^2 = L^2\frac{m}{2zeV}$ (Eqn. 8)

or $\frac{2Vt^2}{L^2} = \frac{m}{ze}$ (Eqn. 9)

Introducing a constant calibration, A for the main terms,

$A = \frac{2V}{L^2}$ (Eqn. 10)

So, in charge units of e, (Eqn. 9) becomes:

$At^2 = m/z$ (Eqn. 11)

Furthermore, by adding constant B for drift delays and corrections, we achieve the time-of-flight calibration equation:

$At^2 + B = m/z$ (Eqn.12).

Variable definitions:

E_{pot} = potential energy

E_{kin} = kinetic energy

electron (e) number (1.602×10^{-19} C)

C = Coulomb C x V = Kg x $\frac{m^2}{s^2}$

mass conversion constant 1.66×10^{-26} kg/Da

V = electric field strength (Volts)

L = length of flight tube (m)

v = velocity

t = time seconds (s)

m = mass (kg)

z = ion charge

Assumptions: All ions have the same kinetic energy when entering the field-free region. The ion source region is much shorter than the free field path. Ions sit for a shorter time in the ion source than in the flight path. The ions' velocity stays constant in these equations. After laser desorption, the ion pulse travels down the flight tube and, at the detector, generates a pulse of ion current detection. Lighter mass to charge molecules arrive first at the analyser, followed by heavier mass to charge ions *m/z*. MALDI typically generates singly charged ions *(276, 277)*.

1.7.4 Pulsed Ion Extraction

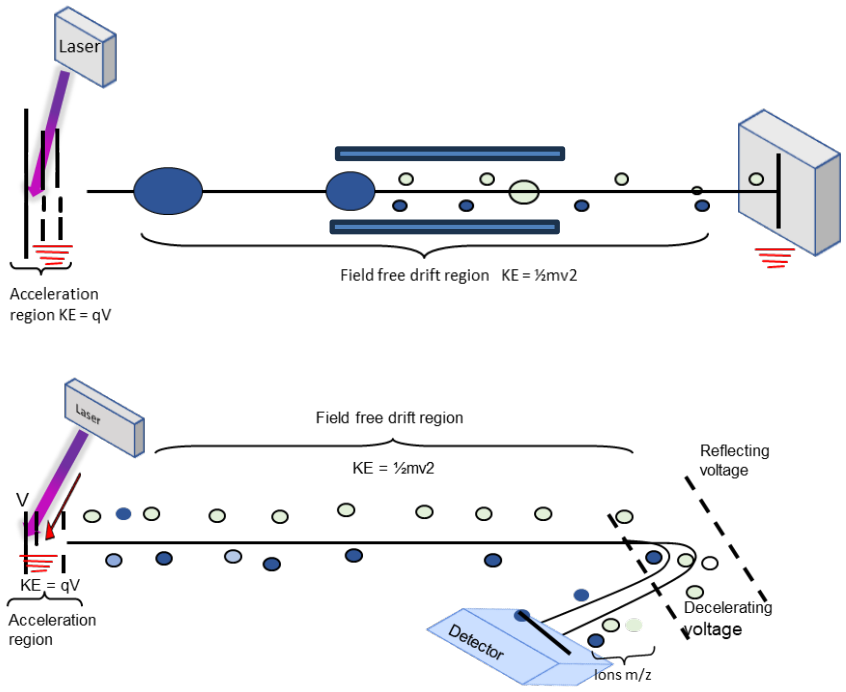

Figure 1:31 Figure The time-of-flight tube with the ion source in the top figure and reflectron time-of-flight tube lower drawing. Initially, upon desorption, the ions cloud expands slowly, and the matrix clusters disaggregate. Upon the molecular ions leaving the matrix cluster and leaving the ion source, the ions are accelerated further with a second voltage pulse. The second voltage timing pulse, typically less than a microsecond after the laser pulse, bunches the ions. This extra voltage pulse allows the slower ions which lagged in the ion source to catch up with the faster ions at a focal plane along the flight path, and with voltage tuning, that plane position can adjust to be at the detector to maximize resolution (459).

1.7.5 The Reflectron

When a pulse of ions arrives at the end of the flight tube, they are typically spread out over a flight arrival time distribution, redirecting the kinetic energy distribution. In the 1980s, Boris Mamyrin *(278)* developed the reflectron to reflect the ions to a second detector. In this manner, all ions turn around, and those with slightly higher kinetic energy experience slightly longer reflectron time delays, thus allowing ion kinetic energy distributions to be refocused at the detector plate and improve the mass resolution. *(279)*

1.7.6 Lipidomics

Recently, lipidomics has gained prominence alongside chromatography and spectroscopy-based methods. It is a rapidly growing field of biomedical research which studies lipids and their roles in health and disease *(227)*. It can be applied to the placenta and plasma. Lipidomics typically involves analyzing lipid profiles in biological samples with mass spectrometry and liquid chromatography *(280)*. It can provide incredible detail about the lipids present in a sample, but in the case of tissues, especially, all spatial information is lost during sample preparation. The development of MS-based lipidomics has revolutionised the field by providing comprehensive lipid profiles, structural characterisation of lipids, the discovery of lipid biomarkers, and the elucidation of lipid-related pathways with accompanying bioinformatics tools and databases essential to identifying and quantifying lipids. Shotgun lipidomics is a complementary approach that can even provide insight into lipid profiles with prior separation or extraction and is commonly used for the analysis of plasma. For example, in pregnancy, total lipid analysis methodologies offer insights into biological samples using shotgun lipidomics and lipid droplets,

giving a comprehensive, accurate, and practical analysis of placental lipids. The literature discusses strategies for enhancing shotgun lipidomics to analyse lipid species*(281)*. Considerations highlight the physiochemical properties of lipid groups and subclasses for shotgun lipidomics in biology and medicine to identify and quantify cellular lipidome *(282)*. Studies discuss developing a program for high-throughput lipid analysis using multidimensional mass spectrometry-based shotgun lipidomics, which could be relevant to placental lipid characterization *(283)*. The literature demonstrates the ability of shotgun lipidomics to resolve isobaric and isomeric species *(284)* and discusses using high-resolution shotgun lipidomics to quantify and analyze total lipids in uncharacterized biological membranes *(285)*.

1.7.6.1 Lipids Quantitation by Mass Spectrometry

The rationale behind why mass spectrometry is the ideal method for quantification is that it requires substantial method development for reliable results. The standard mass spectrometry method for quantitation, including lipids, involves single-reaction monitoring (SRM) or the multiplexed version known as multiple-reaction monitoring (MRM). SRM/MRM methods require LC-MS, typically using electrospray ionisation or atmospheric pressure chemical ionisation APCI with tandem mass spectrometry fragmentation using collision-induced dissociation (CID), so it is an LC-MS/MS method. The quantitative method setups require establishing a reliable quantitative calibration curve, using precise concentrations of internal standards either dosed into a matrix mimic or added quantitatively to a 'typical sample' matrix. A series of LC-MS/MS experiments are then run, in triplicate at least, at a series of concentration values spanning the concentration range of interest. In each SRM experiment, a specific precursor molecule is isolated and fragmented. Then, a selected ion chromatogram of a particular ion of a fragment is monitored (e.g. phosphate head groups, e.g. choline, ethanolamine, serine, inositol), and the peak of interest integrated to generate a value which is proportional to the original concentration of the precursor molecule in the matrix. With MRM methods, multiple precursors and- or multiple fragments monitoring by setting the instrument to 'hop' between precursors and fragments, and how many fragment pieces to monitor depends on the speed of instrument acquisition and the chromatographic separations'

average peak elution time profile. This approach is highly effective and routinely used throughout the clinical and pharmaceutical industries using shotgun lipidomics to acquire an estimated quantitative data of lipids groups as an overall but not individual molecules unless detailed molecular structure needs elucidation confirmation for the substrates position stereochemistry and cleavages of the substrates bonds. However, it requires that the separations be consistent and that there is no overlapping elution of the precursors and fragments – across the range of biological samples to be studied. MS/MS is usually the preferred method for quantitation rather than just monitoring the LC-MS peak profile of a precursor ion because the isolation event prior to the MS/MS fragmentation event provides selection and specificity to the experiment as it is far less likely to observe co-eluting peaks with the same (*m/z*) values which also have the same fragment ion masses.

Nevertheless, selected ion monitoring (SIM) from a specific peak elution profile in LC-MS mode can also be effective for simple mixtures or ions that are particularly abundant relative to other sample matrix molecules. Typically, setting up a new method for quantitative mass spectrometry clinical studies, such as for lipid profiling in pregnancy, requires about six months for an expert mass spectrometric because of the complexity of lipids within biological tissues, and using this method requires constant statistical evaluation and testing for new overlapping elution profiles in the LC-MS/MS experiment. Thus, in academia, accurate quantitative studies are usually not done except in cases where the research group focuses on a few specific molecules (e.g. cholesterol esters, fatty acids, sacharolipids, or lipoproteins carriers). Therefore, the time investment in setting up the method can pay off in the long run. For the experiments in this research, TLC followed by MALDI-TOF mass spectrometry was used to identify the lipid classes. However, as quantitative internal standards were not available, an attempt for accurate quantitation was not followed due to various reasons, from lack of expert knowledge support in instrumental methodology setups to instrumental optimisation and data acquisition and data analytics processing, which is something that could be expanded and worked on shortly perhaps.

Nevertheless, the MALDI-ToF peak intensities are proportional to the concentration in the sample (with different proportionality constants for each precursor ion class and with signal suppression events also modulating those constants), so the peak intensities only show as 'indicative trends' and not as an absolute value of relative ratios in the concentrations of various lipids, particularly within specific lipid classes as the most significant variance of the proportionality constants is between lipid classes. Therefore, in these experiments, we aim to identify relative concentration trends between sample types, which can, in the future, be followed up with the development of quantitative calibration methods using SRM/MRM approaches. Literature insights on quantitation by mass spectrometry approach can further expand using this research groundwork towards placenta total lipids quantitation. The human placenta's quantitative lipid composition depends on understanding its potential health significance. Using liquid chromatography and mass spectrometry for lipid profiling offers powerful advantages, and advances in quantification methods further enhance the accuracy of lipid analysis. Using these approaches is critical to understanding the placenta and plasma lipid content. Quantifying the lipid composition of the placenta is crucial for understanding its implications for health and disease. Most modern lipidomics studies use isotope-labelled standards. In lipid profiling and quantification, liquid chromatography and mass spectrometry are the standards for separating and detecting lipids based on their chemical behaviour *(286-288)*. Lam et al. (2011) have used this approach to characterise lipid profiles in various biological samples, including human meibum, where ageing impacts lipid composition *(289)*.

A thorough approach to lipid quantification, defined as the systematic investigation and analysis of lipids, is ideal for lipid profiling *(290)*. Toxicological evaluations and reproductive and developmental studies must understand the placenta's lipid composition. The human placenta is morphologically, physiologically, and toxicologically different from that of rats, emphasising the need to evaluate it in studies accurately *(291)*. Studies on lipid profiling use an expression of specific genes, such as CGB, LGALS13, and GH2, further supporting the importance of comprehensive lipid profiling *(292)*. The comparison of different quantification workflows shows improvements in accuracy, highlighting the importance of rigorous

quantification methods for lipid analysis *(293)*. Deuterium oxide labelling and carbon thirteen isotope (^{13}C) **l**ipidome **i**sotope-**l**abeling of **y**east (**LILY**)*(294)* lipids as internal standards have permitted compound-specific quantification of lipids in human plasma, highlighting the capability for precise quantification methods in lipidomics*(295)*. An example study by Watkins et al. 2019 used human villous placental explants from caesarean section pregnancies to investigate the processing of different stable isotope-labelled fatty acids (FAs) in these placental explants when incorporated into placental lipids *(296)*. It sheds light on the potential impact of maternal factors on placental lipid metabolism. It also discussed its relevance to fetal development and maternal metabolic health off fully quantitative analysis of placenta villi explants by treatment of three different stable isotope-labelled fatty acids: palmitic acid ((^{13}C -PA), oleic acid (^{13}C-OA) and docosahexaenoic acid (^{13}C-DHA) *(296)*Treatment durations are three, twenty-four and forty-eight hours. The study used liquid chromatography-mass spectrometry to quantify stable isotope-labelled lipids synthesised by placental explants*(296)*.

These lipids were phosphatidylcholines (PCs), triacylglycerols (TAGs), and phosphatidylethanolamines. The results showed that ^{13}C-PA was primarily directed into PC synthesis (74% of (^{13}C -PA–labelled lipids), while ^{13}C-oleic acid was directed almost equally into phosphatidylcholine PC and triacyl glycerides TAG synthesis (45%,53%, respectively, of ^{13}C-OA–labelled lipids) *(296)*. On the other hand, ^{13}C-docosahexaenoic acid DHA was only detectable in TAGs. Triacylglycerols (TAGs demonstrated the highest isotopic enrichment for all ^{13}C-FAs, with ^{13}C-OA–TAGs comprising over 50% of total OA-TAGs (labelled and unlabelled). It suggests that TAGs in the placenta act as accessible reservoirs for fatty acid storage. The study found that lipid incorporation variations into placental lipids correlate with maternal factors such as glycemia (blood glucose levels) and body mass index (BMI). It suggests maternal factors influence how the placenta metabolises and partitions fatty acids *(297)*. The study concluded that the metabolic partitioning of freshly imported fatty acids into labile and less labile lipid reservoirs in the placenta depends on the specific fatty acid. This process may play a role in the preferential transplacental transfer of specific fatty acids to the fetus. It may also be involved in the fetal-placental pathophysiology of maternal metabolic dysfunction

(297). Duttaroy, A.K. (2009) discusses long-chain fatty acids (LCFAs) uptake and translocation across the human placenta *(298)*. The passive diffusion of long-chain fatty acids into cells uses several proteins facilitating their transport because of their lipophilic nature. FAT/CD36 absorbs LCFAs. The LCFAs are actively bound and transported into cells through this channel. Membrane FABPs have a high affinity for the uptake of LCFAs captured from extracellular space and entering the cell membrane. Intracellular FABPs bind LCFAs once inside the cell. Fatty acids are transported intracellularly by these proteins to specific locations within the cell, such as the mitochondria for beta-oxidation or the endoplasmic reticulum for lipid synthesis. The placenta contains these transport and binding proteins, which ensure that essential fatty acids are efficiently transferred from the mother to the fetus during development, especially of the brain. By regulating LCFA uptake, these proteins help maintain a healthy fatty acid balance. These proteins also govern placental lipid metabolism, which is necessary for producing energy and synthesising essential lipid-based molecules *(298, 299)*. Dancy, B.C. (2015) used stable isotopes, specifically carbon-13 (^{13}C) and nitrogen-15 (^{15}N), to study the decay rate of individual fatty acids and intact phospholipids in lipid membranes *(300)*. ^{13}C and ^{15}N isotopes can quantify and trace specific molecules in biological systems. The isotopes are non-radioactive and safe for use in research. It is possible to detect and quantify these isotopes in fatty acids and phospholipids. It provides detailed insights into lipid metabolism. *(300)*. The mass spectrometry technique measures atoms' and molecules' mass and relative concentrations. This method enables precise quantitation of ^{13}C and ^{15}N labelled molecules, providing insights into lipid synthesis and conversions *(300)*. Keeping membranes fluid, functional, and intact depends on rapid phospholipid turnover. It allows cells to respond quickly to environmental changes, repair damage, and maintain essential processes like signalling. Data from this study indicate that phospholipid synthesis and recycling are highly active processes in cells. Keeping membrane integrity may also reflect cells' metabolic priorities. Phospholipid dynamics are important in neurodegenerative diseases, diabetes, and cancer, and they affect membrane composition and integrity. Development of targeted therapies that modulate lipid metabolism could use this knowledge. It highlights the metabolic roles and regulatory mechanisms governing phospholipids and neutral lipids (such as triglycerides and cholesterol esters).

Phospholipids structurally and functionally govern cells, while neutral lipids are energy storage *(300)*.

1.8 MALDI imaging mass spectrometry (IMS) is an example.

Mass spectrometry imaging is a rapidly expanding tool in mass spectrometry MS with pioneers in the field*(301-305)*. This method reveals molecular characteristics by measuring the 'mass-to-charge (m/z) ratio' of molecules in the sample. In addition to tissue localisation, MSI software can also produce images in 2D or 3D *(306, 307)*. Combining it with other imaging techniques can make it even more powerful. There is no need to label molecule-specific samples or to have prior knowledge of the tissue being analysed for imaging. Biological samples reveal peptides, proteins, oligonucleotides, lipids, sugars, and other small molecules *(308)*, making molecular mapping possible *(306)*.

In contrast to conventional MS, which loses spatial information after sample preparation, homogenisation, and extraction, MSI does not require extraction or separation, and it is possible to study a molecule's spatial distribution. Because MSI only determines m/z ratios and their distribution on the investigated sample or tissue, it provides no information about the molecule. As a result, it is unsuitable for biomolecule structural identification in complex biological or clinical tissues. It can, however, be overcome by combining it with different separation techniques, on-tissue enzyme digestion, and tandem MS. Mass spectrometry coupled with MALDI selects isolates and fragments precursor ions directly from tissue sections. A bottom-up proteomics workflow combined with MSI allows enzymatic digestion of tissue section proteins. As a result, MSI can be used to discover biomarkers under certain circumstances since it can be used with other fragmentation and molecule identification techniques to predict relative concentrations of molecules in tissues. There are several reasons for differences in intensities on different MSI images, e.g., differences in ionisation or matrix effects *(309)*. In addition to accumulating a biomarker in particular tissue fragments, we can also obtain its temporal characteristics. Expression of a specific molecule can be tracked across several time

points (e.g., during embryonic or tumour development) *(306, 307)*. The human body uses lipids for various functions.

Amphipathic phospholipids (PL) participate in cell membrane construction, while triacylglycerols (TAGs) are reserve nutrients. As components of cell membranes, glycerophospholipids possess a distinctive asymmetry between cell organelles (intra- and inter-cellular). A group of lipids known as sphingosines includes ceramides, gangliosides, and sphingomyelin *(310, 311)*. They are essential for apoptosis, cell growth, differentiation, and adhesion*(310)*. In addition to participating in endocytosis and exocytosis *(310, 312)*, these lipids also influence chemotaxis and cytokinesis. Physiologically, they also affect growth, synaptic signalling, and immune system monitoring *(310, 311)*. Lipids are biologically active because of fatty acids (FAs): TGs contain three fatty acids, whereas phospholipids have one or two. The carbon atoms in these (FAs) are usually even. Depending on how many double bonds there are in fatty acids, they can be classified as saturated or unsaturated. Saturated (FAs) increase cell membrane rigidity, while unsaturated fatty acids increase fluidity. Certain (FAs) participate in signalling, such as those with 20 carbon atoms. These (FAs) have oxygenated derivatives that promote platelet aggregation, cause inflammation, regulate immune responses, and stimulate smooth cell contraction, among placenta fatty acid transfer *(311, 313-315)*.

Using mass spectrometry imaging (MSI) technology in analytical biochemistry, it is possible to map the abundance of a particular compound in tissue slices pixel by pixel*(316)*. Compound distribution within tissue samples can be visualised via MSI, a novel analytical biochemistry technique *(317)*. The MSI generates compound-specific images, where each pixel represents the abundance of that compound *(317)*. Each pixel records mass spectra, allowing simultaneous compound analysis*(317)*. One limitation of MSI is that cholesterol and other neutral sterols often need to be better ionised by ionisation techniques *(317)*. MSI literature underrepresents cholesterol despite its abundance and biological significance in mammalian tissues. As Griffiths et al., 2023 pointed out, cholesterol ionisation has been a challenge in MSI; researchers explored ways to improve it and how MSI can be used to study cholesterol metabolism in animal models and human samples *(317)*. Different

disorders are related to cholesterol metabolism. Animal models and human biopsies can be examined with MSI to trace cholesterol-related metabolic disorders *(316-319)*.

1.9 MALDI imaging mass spectrometry of lipids

MALDI imaging mass spectrometry effectively visualises spatial lipid distribution in placenta tissue prepared from porcine gelatine. Biological tissues, including the placenta, use this technique due to its high-resolution and comprehensive profiling capability. Placental function and development can be better understood by understanding the differential impact of lipid aldehydes on lipid metabolism genes. Vidová et al. (2010) use matrix-assisted laser desorption/ionisation imaging and MALDI mass spectrometry to visualise lipid spatial distribution in porcine gelatine placenta tissue *(320)*. By combining this technique with high-resolution mass spectrometry, different biomolecules, including lipids, have been successfully studied in various tissues to reveal how they are organised spatially*(321)*. Several recent studies have demonstrated the importance of lipid analysis in placental tissue via the differential effect of lipid aldehydes on key lipid metabolism genes *(322)*. Integrating surface plasmon resonance imaging with MALDI imaging mass spectrometry enables quantitative and regioselective imaging of different proteins in placenta tissue prepared with porcine gelatine, demonstrating comprehensive lipid visualisation *(323)*. These results shed light on how oxidative stress, which causes lipid aldehydes to be produced, might affect placental function. A study of the effects of two lipid aldehydes on lipid metabolism in full-term human placentas, 4-hydroxynonenal (4-HNE) and 4-hydroxyhexenal (4-HHE), which are intermediates of AA arachidonic acid and DHA docosahexaenoic acid *(324)*. Normal fetal development and placental function require long-chain polyunsaturated fatty acids (LCPUFAs) like AA (omega-6) and DHA (omega-3). Preventing metabolic diseases later in life depends on providing the fetus with optimal LCPUFAs. It is not explicitly required for pregnant women to take n-3 LCPUFA supplements. Oxidative stress causes toxic compounds known as lipid aldehydes. A high level of these lipid aldehydes, specifically 4-HNE and 4-HHE, can negatively impact tissue function and cause inflammation. A full-term human placenta was treated with different

concentrations of 4-HNE and 4-HHE for the expression of 40 genes related to lipid metabolism. As a result, 4-HNE increased the expression of ACC, FASN, ACAT1, and FATP4 genes involved in lipogenesis and lipid uptake. The expression of LDLR, MFSD2a, and SCD1 was decreased by 4-HHE, while genes associated with lipogenesis and lipid uptake were increased. The results indicate that these two lipid aldehydes may alter the processing and utilisation of LCPUFAs within the placenta through differential effects on FA metabolism genes *(322)*. This study suggests that LCPUFA supplementation may have implications for oxidative stress's impact on placental lipid metabolism. According to the study, oxidative stress and specific lipid aldehydes can influence gene expression in placental lipid metabolism. That affects how essential LCPUFAs are used and potentially affects long-term metabolic health and fetal development *(325)*. A mass spectrometry imaging (MSI) method that enables the simultaneous acquisition of molecular information and the spatial distribution of analytes within a sample offers several advantages over traditional histochemical methods. Mass spectrometry imaging allows different structural modifications to be distinguished within a sample without labelling specific compounds. It can identify and map different molecules in tissue samples based on mass and molecular characteristics. High mass resolution is achieved with a resolution power (R) of 30,000. Molecules can be identified and characterised precisely, even with minute mass differences. Typically, the technique offers 5–10 micrometres of spatial resolution translated into cellular images. It provides detailed spatial information about molecular distributions. Matrix-assisted laser desorption/ionisation (MALDI) occurs at atmospheric pressure. Mass measurements are enhanced by an orbital trapping mass spectrometer coupled to this source. MSI has been successfully applied to various samples to image and analyse molecules, including phospholipids, peptides, drug compounds, and proteins. These samples include tissues, single cells, and human lung carcinoma tissue. Histological staining results from this MSI method are excellently correlated with traditional methods. It indicates that MSI provides the same molecular information as standard staining. The technique complements traditional histochemical protocols and reveals novel molecular processes. Biomedical research and pathology provide high-quality mass analysis and spatial resolution to single cells *(326)*. Some studies use matrix-assisted laser desorption/ionisation (MALDI) imaging and mass spectrometry to visualise

lipid distribution in biological tissues *(320, 327, 328)*. The technique provides high spatial resolution (x, y, z) and comprehensive lipid spatial distribution profiling *(325, 329)*. It has also been used to study how lipid distribution changes with age *(330)*. Researchers have explored the spatial distribution of proteins and small molecules in tissues using MALDI imaging mass spectrometry *(331, 332)*. By analysing tissues in situ, MALDI imaging mass spectrometry effectively examines the distribution of proteins and small molecules within biological systems *(332)*. Also, this technique has been applied to study glycerophospholipid spatial distribution in the ocular lens, demonstrating its potential to profile lipids over some time in complex biological structures *(320)*. Multiple relevant studies support the comprehensive profiling of the placental lipidome using matrix-assisted laser desorption/ionisation (MALDI) imaging mass spectrometry (IMS). MALDI-IMS has been demonstrated to analyse spatial distribution and relative abundance directly in situ, especially in tissue sections, without prior treatment *(333-335)*. A feasibility study explored the use of spatial lipidomics by MALDI-IMS for tissue differentiation based on content, suggesting the potential for comprehensive lipid visualisation in biological tissues *(336)*. A high-coverage pseudo-targeted lipidomics method has also been proposed for comprehensive studies *(326)*. Using high-resolution mass spectrometry lipidomics to characterise lipid species in placentas derived from pregnancies accompanied by gestational diabetes mellitus underscores the relevance of placental lipidomics *(337)*. A study has shown that MALDI-IMS provides spatial information about specific metabolites and lipid molecules across cells or tissues, which suggests its applicability to comprehensive lipid visualisation *(338)*. These references demonstrate that MALDI imaging mass spectrometry is useful for lipidomics in human tissues. They also demonstrate its potential for identifying and visualising lipid distributions and their relevance to cancer, neurodegenerative diseases, and drug localisation *(339, 340) (341)*.

1.9.1.1 Nuclear Magnetic Resonance (NMR) and other spectroscopy techniques

A valuable technique for lipid analysis is nuclear magnetic resonance (NMR). It provides information on structural dynamics with attached functional groups. In

NMR, fatty acid profiles and lipid interaction with other molecules can be used to study lipoproteins. NMR measures chemical shifts in magnetic interactions between nearby nuclei or chemical bonds to determine J-coupling constants measured in (Herts J=Hz). Organic molecules use a J-coupling constant between protons (hydrogen nuclei). NMR peak analysis of overlapping carbon-carbon (C-C) and or carbon-hydrogen (C-H) distance constrains coordination dynamics and can determine the exact molecular position with lipid chemical structures are primarily associated with spin-spin coupling, which is a result of the magnetic interactions between the nuclear spins of neighbouring atoms which can help when study lipid metabolic structures. It can also follow particular functional groups on the structure due to bile acids hydrolysis, bile salts, lipid-protein interactions, and lipid cleavage atomic order positions in lipids extracted from cells and tissues *(342)*. Using proton (1H) NMR, fatty acids can be classified based on their degree of unsaturation and type.

With carbon 13 isotopes (^{13}C), NMR provides structural information about the molecules. NMR provides accurate elucidation of lipid structure in two-dimensional (2D) but is more complex in three-dimensional (3D) *(220)*. NMR spectroscopy for lipid analysis is another non-destructive technique. Infrared spectroscopy helps determine certain functional groups in lipid molecules, like carbonyls (C=O), carbon-carbon (C=C), cyanide (C=N), and nitric oxides (N=O). Molecular bonds restrain vibrational information in lipid structure when applying Raman spectroscopy (vibrational light energy modes, stokes, and anti-stokes).

1.9.1.2 Enzyme and Other Assays

Enzyme assays measure specific lipid metabolites or enzymes involved in lipid metabolism. On the one hand, enzyme reactions measure lipid classes, such as cholesterol and triglycerides – the total or active component. On the other hand, antibodies detect and quantify lipid molecules and enzymes in immunoassays, such as enzyme-linked immunosorbent assays (ELISA). Enzymatic assays quantify the presence of certain lipid classes using enzymes, for example, cholesterol oxidase for cholesterol measurement, and triglyceride detection uses enzymatic reaction with

glycerol phosphate oxidase. Fluorescent and other dyes for microscopic visualisation of lipids in cells or tissue sections include Oil Red O and Nile Red, Sudan III, and Sudan IV. In gravimetric analysis, lipid quantification compares the extracted lipid's weight with the total sample weight. Phospholipase-based assays study the function activity of different phospholipases. Calorimetric assays use sulfophosphovanillin (SpV) reactions for total lipid content in microorganisms, for example *(343)*. Fluorometric assays detect specific lipid classes using fluorescent dyes that bind to lipid molecules.

When using a fluorometric assay to determine lipid droplets in the placenta, selecting fluorescent dyes that bind specifically to lipid molecules is crucial. A fluorometric assay with Nile red and BODIPY dyes has previously stained cellular lipid droplets. Phospholipids can also be quantified by enzyme fluorometry in cells and intracellular organelles, which may apply to placental tissues. Particularly in pregnancy, studies have highlighted the importance of lipid metabolism and toxicity in the placenta. These enzymatic fluorometric assays for measuring all major phospholipid classes may apply to tissues, fluids, lipoproteins, extracellular vesicles, and intracellular organelles of many organisms. Literature insights of fluorescent dyes assay in cells and tissue assays to detect specific lipid classes using fluorescent dyes that bind to particular lipid molecules for cellular or tissue lipids (Sudan III, IV, black, Oil red O) are in-depth in the following papers *(344-350)*. These assays can assess multiple diseases, such as dyslipidaemia, cardiovascular disease, and metabolic disorders. They can be complemented by mass spectrometry by microscopy using white light or fluorescent microscopy or imaging (MSI) to visualise lipid distribution in tissue sections and other techniques.

1.10 Lipids as biomarkers in pregnancy

Placental tissue is a valuable source for studying lipid biomarkers in various conditions. More and more studies are exploring lipid profiles in different situations in pregnancy, and there is immense interest in using high-throughput platforms for detailed lipidomic analysis of various mouse tissues and the human placenta *(351, 352) (353)*. However, plasma analysis is also pursued as the placenta is not readily

available until the baby is born after a healthy pregnancy or one afflicted by the disorder of interest. In pre-eclampsia, lipidomic analysis of plasma and placenta has been used to reveal alterations in patients with pre-eclampsia, showing increased levels of plasma glycerophosphoserines(PS), glycerophosphoethanolamines(PE), glycerophosphocholine (PC), and flavonoids (FLV) compared to controls *(354)*.

Additionally, markers of lipid peroxidation, such as F2-isoprostanes, nitrotyrosine, and 4-hydroxynonenal, were elevated in preeclamptic placentas *(355)*. The placenta shows altered fatty acid metabolites in pre-eclampsia due to responding to inflammation caused by oxidative stress with placental function affected by vasoconstriction and pro-inflammatory metabolites such as hydroxy eicosatetraenoic acids (HETEs) and F2-isoprostanes. Lipid analysis helps establish trimester-specific reference intervals for serum lipids and evaluates their associations with pregnancy complications and undesirable perinatal outcomes *(356)*. Lipid analysis in adverse pregnancy focuses on understanding the association between lipid metabolism and gestational diabetes, pregnancy-induced hypertension, and high birth weight, which are associated with fetal blood lipid concentrations *(357)* observed in mouse models of gestational diabetes mellitus (GDM) *(353)*. Maternal intrahepatic cholestasis during pregnancy has been shown to program genetic disease in offspring, with an accumulation of lipids in the fetoplacental unit *(358)*. During pregnancy and GDM, changes in lipid metabolism are due to increased cortisol and insulin, which regulate lipid metabolism. Placenta-derived extracellular vesicles (EVs) have also come under scrutiny. Analysis of the lipidome of EVs from primary placental explants cultured for 72 hours revealed that placentas from healthy women's placentas can incorporate glucose into lipids, reduce fatty acid oxidation, and increase triglyceride accumulation in the placenta under high glucose conditions *(359)*. This model is intended to replicate GDM *in vitro.* By analysing the concentration of lipid species through lipidomic and metabolomic approaches, researchers have sought to gain insight into metabolic changes during maternal adaptation to pregnancy that might lead to cardiometabolic risk in women in later life *(197)*. The study showed that the concentration of specific lipid species was higher during pregnancy, indicating that lipid metabolism had shifted. This shift in lipid metabolism was then linked to

changes in mothers' cardiometabolic risk profiles, demonstrating that lipid analysis can be a powerful tool for understanding metabolic changes during pregnancy.

APCI-MS has also been used to study placental lipid and metabolite changes in fetal development, pregnancy complications (such as preeclampsia), and different maternal nutritional and environmental exposures *(254, 360, 361)*. To understand the metabolic reprogramming associated with IUGR, APCI-MS has been used for targeted metabolomics study of the placenta by analysing crude extracts of biological cellular lipidomes*(234)*. It has shown not only the versatility of this approach for profiling *(362)* but by analysing triacylglycerols and their oxidation products enabled an understanding of products formed by triacylglycerol oxidation by APCI-MS characterised lipid metabolite changes in placental function and pregnancy complications *(363)*.

Proton magnetic resonance spectroscopy (1H MRS) has also been used to assess placental metabolism, with reductions in N-acetyl aspartate (NAA) / choline ratio and detection of lactate methyl emerging as potential biomarkers of impaired neuronal metabolism and fetal hypoxia in placental compromise *(364) (351, 353, 365)*. Nuclear magnetic resonance spectroscopy (NMR) analyses placental lipid composition and structure. The method identifies and quantifies different lipid species based on proton NMR chemical shifts and spin coupling pattern analysis for intra-uterine growth restriction IUGR *(366)*. A powerful tool for analysing lipid composition and structure in various biological samples is nuclear magnetic resonance (NMR). Spin-spin coupling (J-coupling constraints distance hydrogen to hydrogen H-H, hydrogen to carbon H-C) analysis of proton and carbon NMR chemical shifts identifies and quantifies lipid species *(367)*. There are several relevant references supporting proton NMR studies in placenta lipidomics. For example, Pinto et al. (2015) examined maternal plasma and lipid extracts for pre- and post-diagnosis GDM metabolic biomarkers and examined how NMR can be used to identify lipid metabolism biomarkers *(368)*. Denison et al. (2012) demonstrated that NMR can detect biomarkers associated with impaired placental function by reducing the choline/lipid ratio in IUGR placentae as a novel biomarker of reduced cell turnover *(369)*. Wang et al. (2020) used NMR to identify and quantify

lipid species in biological matrices and provide atomic resolution structural information *(370)*. A study by Oostendorp et al. (2006) demonstrated the potential of NMR spectroscopy for lipid analysis as it simultaneously detected and measured patients' blood to monitor different inborn errors in lipid metabolism *(371)*. Himmelreich et al. (2003) also applied NMR spectroscopy to characterize metabolite profiles versus lipid species identification *(372)*. Medina et al.(1995) used the technique to study lipid modifications during industrial processes, such as tuna canning *(373)*. Kostara et al. (2010) demonstrate NMR-based lipidomics' potential for biomarker discovery and disease research, in addition to studying lipid species in physiological processes and diseases *(374)*. These and other analysis approaches can be complemented by placenta immunohistochemistry and the like to provide depth to lipid profiling. Specific antibodies can stain placental tissue sections and assess the distribution and co-location of, for example, oxidative stress maternal placental interactions in pre-eclampsia *(375, 376)*. Overall, these findings highlight the importance of lipid biomarkers in understanding placental physiology and pathologies *(377-379) (380) (381) (382) (383, 384)*, but in the setting of GDM, primarily, even within obesity, changes are not fully understood.

1.11 Hypothesis and Objectives

1.11.1 Hypothesis

Do PC and LPC have potential as global biomarkers for predicting adverse pregnancy outcomes? What do we learn from the analysis of experimental studies?

1.11.2 Objectives

Establish methods of extraction and analysis towards further detailed approaches to the placenta and plasma lipidome and gain biological insights so that this research work can be expanded further and collaborated with other specialists in lipidomics research.

Establishing method protocol for human placenta/ and blood plasma preparation for total lipid extract analysis by TLC ,

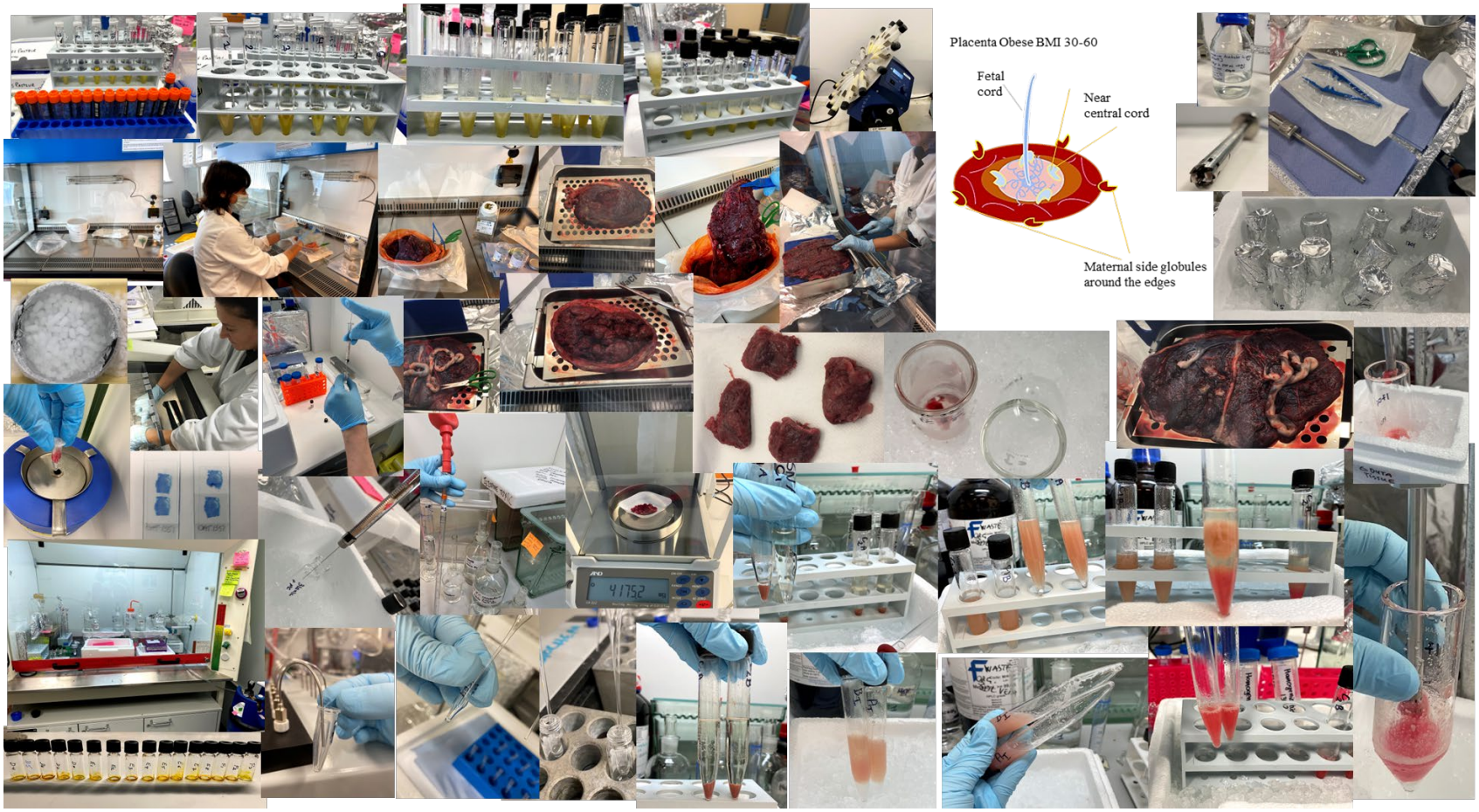

Chapter: 2 Thin Layer Chromatography

2.1 Introduction

Historically, partition chromatography was pioneered by Martin and Synge in 1941, and Consden et al. developed paper chromatography in 1944, extending partition chromatography *(385)*. These methods were rapidly adopted after developing paper chromatography and related techniques. Compared to earlier separation methods, they offered small sample sizes, excellent resolution, and quick analysis. Chromatography on paper has several advantages, making it highly attractive for various applications. Small sample volumes and fast results contributed to excellent amino acid and hydrophilic compound separation. Paper chromatography and related methods were not effective in separating lipophilic compounds (or hydrophobic compounds). The problems of lipophilic compounds could not be fully addressed by reversed-phase paper chromatography. It was Mikhail Semyonovich Tswett, a Russian botanist, who first described chromatography in 1906 when he separated colour-coding plant pigments into coloured bands within a column *(386)* (Figure 2.1) *(387)*. The technique worked well for lipophilic materials and represented an early separation solution. Tswett was working on separating plant pigments, and he developed adsorption chromatography based on a column of calcium carbonate, sucrose, and alumina. He used petroleum ether/ethanol as an eluent to pass the leaf extract through the column *(388)*. The adsorption chromatography of liquids in Tswett's research is considered the scientific foundation of chromatography *(389)*. As well as separating mixtures by passing them through towers or columns of powdered adsorbents, Tswett's chromatographic adsorption method, which originated in 1942, could also detect inorganic and organic substances *(390)*.

2.2 Historical routes of chromatography

With a technique involving a glass column filled with powdered limestone calcium carbonate ($CaCO_3$), Tswett separated various plant cellular physiology pigments, such as chlorophyll, from plants much earlier in 1896 *(391)*, then followed with chlorophyll (alpha and beta), xanthophylls, and carotenoids. Leaf pigments were extracted with ethanol (EtOH) and flushed down the column using EtOH. As a result, different pigments in the original plant extract formed a series of coloured bands. As a result of its ability to separate solution components by colour, Tswett called this method "chromatography" (Figure 2.1). As a result of his liquid chromatography technique, chromatographic methods such as paper chromatography, thin-layer chromatography (TLC), high-pressure liquid chromatography (HPLC), ion chromatography, and gas chromatography (GC) have since evolved. As a pivotal aspect of chromatography, Mikhail Tswett observed that chlorophyll pigments have "insolubility" in petrol ether and ligroin (petroleum naphtha), in contrast to their "solubility" in ethanol. He also proposed that this behaviour arose from molecular forces interfering in the tissue, causing adsorption. Several years after Tswett's experiments, adsorption chromatography was developed. The techniques were also the basis for chromatography, as published in "The Discovery of Chromatography: Early Work 1899-1903"*(392)*. Chromatography was revolutionised and laid the groundwork for a broad range of analytical chemistry applications, including scientific and industrial, and it has been profoundly influenced by it in the modern age. An understanding of Mikhail Tswett's adsorption chromatography, published in 1906 by Nobel laureates Martin and Synge, was revealed by reconstructing Tswett's chromatography from his observatory experiments *(393)*. It elucidates utilising a natural process for a meaningful purpose and developing a systematic laboratory separation method. The article explains and corrects the factual historical background of the Nobel Prize in Chemistry awarded to Martin and Synge in 1952 for partition chromatography and honouring Tswett's resemblance chromatography in 1906 and its impact on scientific and industrial applications *(393)*.

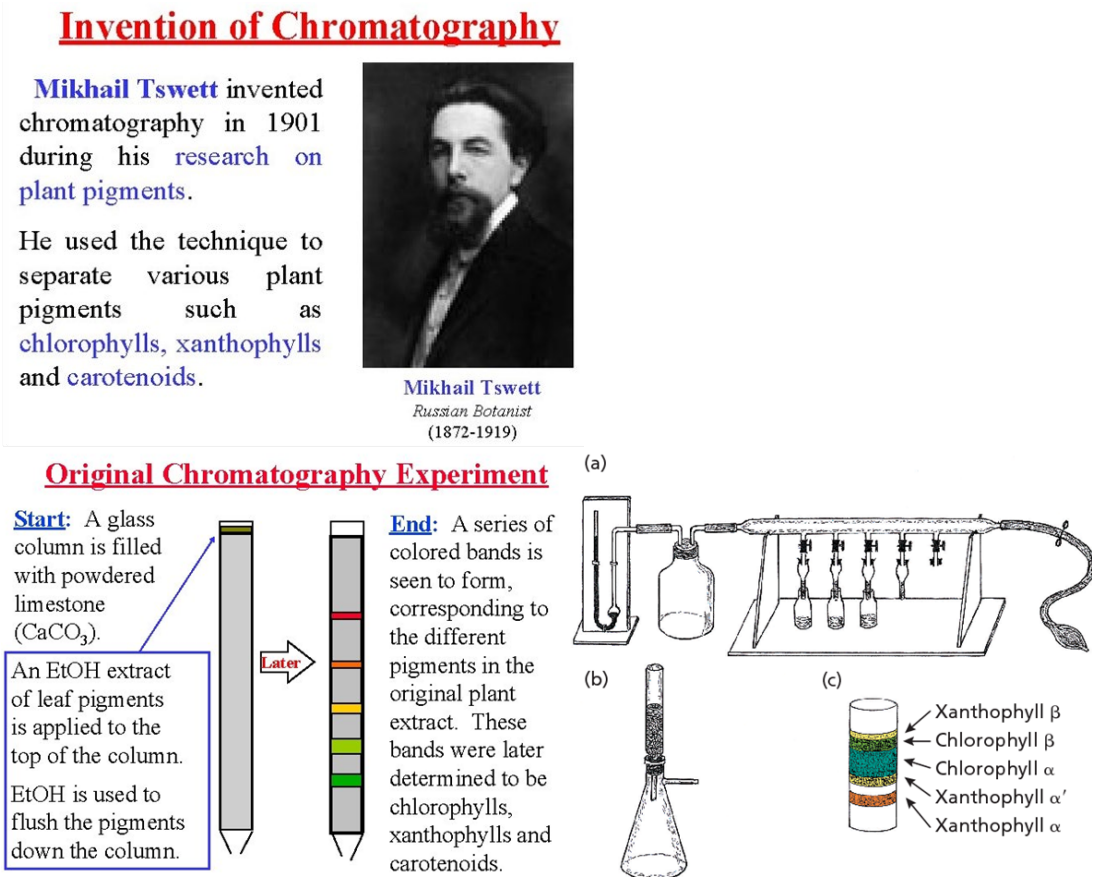

Figure 2:1 Schematics annotations using the illustration from Tswett's experiments on chlorophyll, xanthophylls, and carotenoid adsorption were published in 1906.

Legend of an illustration of apparatus and methodology used in chromatographic separation along with the description of the stationary phase (calcium carbonate, $CaCO_3$) and eluent (disulfates, $S_2O_5^{-2}$), as a result of his observations and experiments, we now understand the fundamentals of chromatography, including the dissolving power of ligroin and the interaction of similar molecular forces in tissues plant pigments Xanthophyl (beta,) chlorophyll (beta), chlorophyll (alpha), Xanthophyl (alpha prime), and Xanthophyl (alpha). Apparatus (a) for the simultaneous use of as many as five columns. The lower part of the small funnel-like glass pieces (2-3mm density and 20-30 mm length) served as the packed column. Apparatus (b) for larger samples (1-3cm in density packing, length 5-9cm) Chromatographic separation (c) of plant tissue pigments as drawn by Tswett. Stationary phase: calcium carbonate ion ($CaCO_3$), eluent disulfates ion, ($S_2O_5^{-2}$) known as (metabisulfite or pyrosulfates) provides an excellent foundation for understanding early chromatography technique (272, 279-281). Tswett's 1906 original paper in German, "Berichte der Deutscher Botanischen Gesellschaft 1906", excerpted in Henry M. Leicester, Source Book in Chemistry 1900-1950 and translated into English "Reports of the German Botanical Society 24, 316-23 (1906)" (276, 278-280) Tswett chromatography archives' Phenomenex UK Accessed 16 January 2024

2.2.1 TLC in lipid analysis

Lipid analysis techniques often rely on chromatography, which separates lipids based on their chemical properties, such as polarity or size *(394)*. TLC is a commonly used technique for simple lipid isolation, while preparative TLC allows for the large-scale isolation of specific lipid classes *(394)* from complex mixtures for further analysis to understand the composition of lipids in biological processes *(395)*. Research studies have highlighted that pregnancy complications such as preeclampsia and GDM are associated with changes to lipid metabolism and alter the function of the placenta in these disorders. While early studies centred on TLC, including somewhere GC accompanied TLC, mass spectrometry and lipidomics have become more common. Different methods can be used to prepare human placenta lipid extracts for analysis. For example, matrix solid-phase dispersion of short-chain chlorinated paraffin has been used for the study of the human placenta *(396, 397)*. Rotor-stator homogenization and wet weight normalization have been the most suitable techniques for quantitatively analysing lipids in placental blood vessels *(397)*.

The placenta can be processed by crushing, extracting with organic reagents, and fractionating with sodium chloride solution *(397)*. The isolation of lipid droplets from the human placenta has been developed by modifying existing methods for other tissues *(397)*. Klingler's studies developed a technique for measuring fatty acid concentrations in placental tissue involving lipid extraction with chloroform/methanol and isolating different lipid fractions *(398)*. These methods provide the foundations for valuable insights into the lipid composition of the placenta and its role in fetal nutrition and pregnancy disorders.

TLC has already been used to provide information about the composition of placental lipids, including the total lipid content of the placenta *(399, 400)*. In the human placenta, phospholipids comprise 75% of essential lipids, while neutral fats comprise 25% *(394, 401-405)*. Given the size of the placenta, it is necessary to note that fatty acid composition varies across different sites in the placenta *(406)*, so a consistent sampling strategy is essential for comparisons between different study groups *(407-409)*. A study comparing lipid profiles between preeclampsia-affected and healthy

placentas found that preeclampsia-pregnancy placentas contained higher lipids, storage cholesterol, ester, polyunsaturated fatty acids and triglycerides *(399)*. Fatty acids in the placenta have numerous roles, discussed in Chapter 1, just as in other tissues. However, in the placenta, linoleic, linolenic, and arachidonic acids, for example, are readily detectable. In gestational diabetes mellitus (GDM), Yang et al. (2021) have demonstrated the significance of long-chain fatty acid (LFA) as a potential biomarker *(410)*. Linolenic acid has been associated with a lower prevalence of hypertension, indicating it may benefit cardiovascular health *(411)*. The placenta synthesises polyunsaturated fatty acids (PUFAs) during pregnancy, supplying these essential nutrients to fetal cells *(412)*. Phospholipids, necessary for various placental functions, are hydrolysed, absorbed, and synthesised in the placenta *(413)*. The phospholipid composition of preeclampsia is altered, including elevated levels of phosphatidylcholine (PC), phosphatidylserine (PS), phosphatidylinositol (PI), and phosphatidylethanolamine (PE), indicating dyslipidemia can harm placental health *(414)*. In the placenta, lipid storage droplets are found, demonstrating their role in fat metabolism and storage *(415)*.

The phospholipids in cell membranes are vital to cellular processes. The precursors PA, PS, PE, PC, PG, cardiolipin (CL), and PI are phosphorylated to form other phosphoinositides. As phospholipid levels and composition change, so do diseases. Among the essential lipids in the placenta, sphingomyelin, PC, PS, and PI comprise a significant portion *(416, 417)*. Placental phospholipids undergo hydrolysis, uptake, and resynthesis *(418)*. Diabetes mellitus also affects the placenta, accumulating fats and lipids *(410, 419)*. Literature findings highlight GDM's significant influence on pregnancy outcomes *(420)*. A type of diabetes mellitus that affects pregnancy and the placenta is gestational diabetes mellitus (GDM). As a result of GDM, human placentas undergo functional and structural changes, including increased placental weight and a higher incidence of placental lesions, such as villous maturational defects and fibrinoid necrosis*(420, 421)*. Placental mitochondrial dysfunction is associated with the progression of GDM *(422, 423)*. Type 2 diabetes mellitus enhances lipid accumulation in non-adipose tissue, particularly in skeletal muscle and liver *(424, 425)*. There is also evidence that GDM affects the placenta by showing only a few differentially expressed genes in placentas complicated by type

2 and type 1. In contrast, the effects of preeclampsia and GDM were not identified in a specific cohort *(426)*. There is a higher risk for pregnancies with GDM. Depending on gestational age, these include placental abruption, placenta previa, and placenta *per Creta (427)*.

The composition of sphingomyelin and PC in human-term placentas has also been altered under pathological maternal malperfusion conditions, which refers to a condition where there is insufficient blood flow or circulation to a specific organ or tissue *(407, 408)*. Placental phospholipid levels are elevated in preeclampsia *(414)*. In pregnant women, high-fat diets can contribute to lipid deposition in the placenta, affecting placental health and fetal development *(428)*. There are also changes in glycosphingolipid composition in rat placentas during pregnancy, indicating dynamic lipid changes *(428, 429)*. Since altered phospholipids are implicated in many diseases, detecting and quantifying specific phospholipids must be quick and easy. A thin-layer chromatogram was first discovered in 1938 by Izmailov and Shreiber and described in Perry in 1973 *(385) (430) (431)*. Perry et al., 1973 described the first method as spotting plant extracts onto microscope slides covered in adsorbent layers.

The components are applied to a thin layer of stationary phase and then separated by a mobile phase interaction with the stationary phase (phase separation). Eventually, in 1944, Consden et al. introduced paper chromatography. Efforts were made in the 1950s to extend the technique to lipophilic solutes. It was not until 1956 that Stahl recognized that TLC needed standardized procedures, adsorbents, and equipment. In 1958, commercial TLC equipment, including coating apparatus, glass carrier plates, developing tanks, and adsorbents, became available. There are over 1000 publications per year using TLC in fields like biochemistry, pharmaceuticals, synthetic organic chemistry, and industrial organic analysis since 1960. TLC was initially used to separate qualitatively, but recent developments have improved reproducibility and quantitative analysis. Specific separation mechanisms may vary, but the techniques and apparatus are applicable. Separation using TLC is simple, rapid, and cost-effective. This technique is beneficial when analysing samples that can be separated easily.

In comparison with high-efficiency columns, they tend to offer lower efficiency. A thin layer of stationary phase coats the bottom of a plate with diluted solutions. A stationary phase layer is typically 100mm - 300mm thick *(385)*. Firstly, there is a stationary phase, most commonly silica gel, with particle size ranging from 10nm to 50nm for standard TLC and a 5nm particle size for high-performance TLC (HP-TLC). Secondly, there is a mobile phase, a combination of organic solvents. The composition varies between different protocols.

In preeclampsia (PET), high blood pressure and increased protein are found in the urine. The percentage of pregnancies affected by morbidity and mortality is 2% to 10%. Various clinical presentations are described in PET *(399)*. It is caused by an atypical maternal vascular response and a defect in the invasion of trophoblast cells (cells that form the placenta) *(432-434)*. A maternal obesity risk factor is associated with PET. It suggests a link between metabolic health and disease development. Mothers' metabolism of lipids changes during pregnancy. Pregnancy hormones increase insulin resistance and adipose tissue storage of fatty acids *(435-439)*. The fetus receives energy and essential lipids for development from these processes *(440-443)*. Evidence shows that PET decreases adipose tissue expansion and increases insulin-resistant adipocytes. As a result, the liver produces more very low-density lipoprotein (VLDL), resulting in gestational hypertriglyceridemia *(121, 444-446)*. Poor handling of fatty acids during pregnancy can result in vascular dysfunction *(438, 447, 448)*, insulin resistance *(449)*, and difficulty mobilizing long-chain PUFAs. Poor handling of long-chain polyunsaturated fatty acids PUFAs during pregnancy leads to liver dysfunction, coagulation dysfunction, and insulin resistance *(450-452)*.

Stress during pregnancy can affect the immune system, leading to vascular dysfunction and immune-mediated diseases, such as cardiovascular disease *(453)*. Poor maternal nutrition, for example, can alter the development of the metabolic, endocrine, and cardiovascular systems during pregnancy, increasing the risk of visceral obesity and insulin resistance post-partum *(454)*. Lactating women transfer long-chain PUFAs across the placenta to the fetus *(455)*. Changes in maternal fatty acid and oxylipin levels have been observed during pregnancy, indicating that

maternal fatty acid metabolism is critical for fetal development *(456)*. The link between maternal consumption of oily fish, containing long-chain omega-3 PUFAs, and reduced aortic stiffness in offspring emphasizes the vital role fatty acids play in vascular health *(456, 457)*. Hypertensive disorders can impair uteroplacental blood flow and lead to poor pregnancy outcomes *(458, 459)*. Insulin resistance during pregnancy may also be associated with increased fatty acid oxidation, reducing glucose utilization in oxidative muscles *(460)*. In addition, ectopic fat accumulation, such as in the liver, can result in lipotoxicity *(378, 444, 445)*. Haematoxylin staining of the rat's placenta revealed lipid storage droplets in preeclampsia *(428)*.

There is also a difference in lipid content between placentae from healthy pregnancies and those affected by preeclampsia. Literature offers lipid analysis *(449)*, including insights on PET and intrauterine growth restriction (IUGR) lipid content in placental tissue, showing that women with preeclampsia had higher phospholipid (PL) and cholesterol *(461, 462)*. Differences in lipid mass spectral ion intensity exist between healthy pregnancies and those affected by preeclampsia *(463)*. No detailed information in the literature includes quantitative data regarding neutral lipid storage in the human placenta. These are triglycerides and cholesterol esters that are neutral lipids and would be detected as intermediate or derivatives from free cholesterol molecules in the forms of bile acids salts and sterols, a specialist area belonging to the metabolomics field and would require a special method of fractional collection separation and use or specialist method to run on mass spectrometry instrument and tracing the hydroxide (OH-) isotopically labelled groups or other specialist method that research group has validated previously.

The placental lipid profiles of women who were lean versus those who were obese versus those with GDM were found to be very similar, and it was only the subsets with obesity and GDM that showed any difference, having significantly higher triglyceride levels than the healthy BMI placental group *(464)*. Studies by Hirschmugl et al. (2016-2021) were conducted on the modulation of intracellular lipid turnover in the placenta of pregnant women in the context of maternal obesity. They found that triglyceride content was increased in the placental tissue of women with obesity versus those with normal weight *(465-469)*. Accompanying analysis of

proteins that might regulate lipid metabolism identified that expression of CGI-58, a primary regulator of triglyceride hydrolysis, was doubled in the placentas of obese women. Navarro et al. (2010) explored the increase in placental apolipoprotein D as an adaptation to GDM that might provide a placental defence mechanism against oxidative stress related to lipid metabolism *(470)*. It highlights that once differences in lipid content are revealed, studies of why this occurs are important to understanding the contribution to pregnancy disorder *(471)*.

Plasma has also been the focus of analysis, including maternal peripheral and umbilical venous plasma from healthy and GDM pregnancies, where TLC analysis revealed alterations in high-density lipoprotein (HDL) composition in neonates of women with GDM *(472)*. In maternal peripheral or umbilical venous plasma from GDM pregnancies, a low-density lipoprotein (LDL) composition has been observed *(473)*. Women with GDM cannot control blood sugar during the second or third trimester *(474)*. A study by Ryckman et al. (2015) found that dyslipidemia during pregnancy is a potential indicator of preexisting insulin resistance in women with GDM *(475)*. A woman's serum triglyceride levels during mid-pregnancy may help identify women who give birth to large-for-gestational-age (LGA) babies *(476)*. In addition, maternal lipid profiles have been studied extensively in women with and without GDM, with inconsistent results reported in the literature *(477)*. Increasing lipoprotein receptors and reducing protein transporters class ABC in GDM explain reduced total cholesterol, low-density lipoprotein, high-density lipoprotein, LDL, HDL, apoA1, and apoB100 levels in maternal circulation *(478)*. Women undergoing assisted reproductive treatment have a higher risk of developing GDM than women conceiving naturally *(479)*. The mother's triglycerides and free fatty acid levels also affect fetal growth in GDM *(480)*. Although previous studies have yielded inconsistent results, aberrant lipid metabolism is also suspected to be a factor in GDM. *(481)* Lipid metabolism, GDM, and fetal outcome interact complexly, as highlighted in the literature, and further research continues to elucidate the underlying mechanisms.

2.2.2 TLC in pregnancy studies for lipid detection

The TLC separation of human placental lipids can be optimised by considering many factors demonstrating lipid separation efficiency using commercial TLC plates with minimal post-separation processing requirements *(482)*. Burdge et al. (2000) also demonstrated a rapid and efficient alternative to TLC for isolating lipid classes from plasma *(483)*. Klingler et al. (2003) emphasised that further research on fatty acid content in human placentas is needed *(195)*. Rejšek et al. (2016) found desorption atmospheric pressure photo ionisation -mass spectrometry effective for detecting TLC-identified lipids *(484)*. To achieve high-sensitivity detection, Chai et al. (2002) emphasised the need to precondition TLC plates by reducing chemical background noise, which is crucial for accurate lipid separation *(485)*. Using these references, TLC can be optimised for separating and detecting human placental lipids, highlighting the potential for efficient and rapid techniques. Another important factor in TLC lipid separation is the combination of mobile phase solvents. In this research study, we followed Bligh-Dyer's 1959 *(225)* method of methanol with chloroform and a fraction of aqueous ammonium acetate, 155 millimolar. Placenta total lipids can be separated using different mobile phases in chromatography. As a mobile phase, Pojjanapornpun et al. (2021) demonstrated that ethyl acetate/isooctane with 0.1% acetic acid is promising for the simultaneous separation of neutral lipids *(486)*. Dassou et al. (2010) also highlighted the importance of acidic additives in the mobile phase for basic drug enantiomers resolving by separation *(487)*. Depending on the additive (basic or acidic) in the mobile phase, Gogaladze et al. (2015) observed opposite elution orders for enantiomers *(488)*. The mobile phase composition is crucial to achieving effective lipid separation. Jiskra et al. (2003) also separated strongly, moderately, and weakly basic, acidic, and neutral solutes containing n-hexylamine as a comprising base in a single run *(489)*. The choice of a mobile phase may affect the separation of different compounds simultaneously. Wan et al. (2016) found that silicon oxynitride stationary phases were hydrophilic when combined with reversed-phase mobile phases, showing that stationary and mobile phase properties are critical for effective separation *(490)*.

2.2.3 Lipid detection

There is well-documented evidence of a neutral lipid increase in preeclampsia, suggesting lipid metabolism may be associated with its pathogenesis. During preeclampsia pregnancy, researchers conducted a lipidomic analysis of the placenta, which showed higher neutral lipid content than healthy placentae, with 40% more triacylglycerol and 33% more cholesteryl ester in preeclampsia, independent of maternal gestation *(415)*. There were also higher neutral lipid contents in placental lipid profiles from PET pregnancies, with increases in triacylglycerol, cholesteryl ester, and high phosphatidylcholine (PC) lipids *(464)*. These findings suggest that placental-neutral lipids consistently elevate in preeclampsia. An increase in small and large-dense low-density lipoproteins (LDL) was observed in preeclampsia, suggesting an alteration in lipid composition within the maternal vascular system *(491)*. Lipidomic analysis of plasma and placenta was conducted in women with preeclampsia early in pregnancy; PS and macrolides/polyketides-PK04 levels were higher in patients with preeclampsia than in a control group *(354)*. The study also showed that preeclampsia increased total cholesterol, triglycerides, and low-density lipoprotein-cholesterol (LDL-C), suggesting estrogen stimulation and insulin resistance may contribute to an altered lipid profile in preeclampsia *(492)*. Preeclampsia placentas contain increased levels of glycerophosphocholine, further indicating disturbed lipid metabolism *(493)*. The evidence from the selected references suggests the presence of neutral lipids in preeclampsia, highlighting the role of altered lipid metabolism in disease progression.

Recent research has focused on the direct coupling of TLC and mass spectrometry (MS). By coupling TLC and electrospray MS, direct analysis of compounds separated by TLC was demonstrated in many world-class bioanalytical research groups, Costello C, *(494-496)* Clench M, *(497)* Fuchs B, Schiller. J, *(218)*, Sherma J *(498)* and many more *(103, 209, 217, 218, 253, 401, 482, 496, 499-515)*. This approach offers low detection levels and molecular identification. Using liquid chromatography-electrospray with MS fragmentation LC/ESI-MS/MS, the precise elucidation of structures from ganglioside and sulfatide fragmentation patterns was demonstrated *(516)*. The literature is replete with examples of mass spectrometry used to analyse fractions separated on TLC plates by the offline method of "scrape

and elute." There have been many attempts to combine TLC and MS, all failing directly. Matrix-assisted laser desorption/ionisation (MALDI) and electrospray (ES) have been discussed in the literature for TLC/MS coupling. TLC/MS, MALDI-MS has had recent success, but it has limitations, such as extensive post-separation TLC plate preparation and low-mass spectral noise. In contrast, ES offers an atmospheric pressure inlet/ionisation system alternative for TLC/MS coupling without many of the limitations of MALDI-MS. Rationale

The overarching goal of this research study was to learn about placental and plasma lipids and, if possible, identify lipid biomarkers for obesity/GDM in pregnancy by knowing what to expect and what is different. This chapter aimed to create a library of information about the total lipids present and observed in the placenta and plasma. As a result, further studies could assess lipid profiles in more detail guided by this baseline information. TLC was chosen for this first step as a broad mapping approach. This project analysed placental and plasma lipids to determine the total lipid content using TLC ahead of further work where TLC-separated lipid bands would be isolated (high performance-TLC abbreviated to HP-TLC) and mass spectrometry matrix-assisted laser desorption ionisation and time of flight mass spectrometry detection (MALDI ToF MS). TLC was also able to be pursued during COVID-19 lockdowns/working from home by UK/Welsh government recommendations. While laboratories in the Institute of Life Science 1 (ILS1) at Swansea University Medical School were re-opened in July 2020 after extensive risk assessment, there were limitations to the number of users who could be present in general laboratories at any one time and access to specialist laboratory facilities such as MS was very limited.

2.3 Methodology

2.3.1 Samples and ethics

Placentas were collected from healthy term pregnancies less than thirty-seven weeks of gestation, and all of them were delivered by elective caesarean section at Singleton Hospital, Swansea, UK. Placentas were processed within two hours of delivery with agreed written consent from study participants and ethical approval from Wales Research Ethics Committee 6 (REC No. 11/WA/0040). Blood was collected from

full-term (≥ 37 weeks of gestation) pregnant women during caesarean pre-operative appointments in Singleton Hospital, Swansea. A maximum of 35ml of blood could be obtained from pregnant women. Non-pregnant women aged 18–40 years were drawn from Swansea University staff and students; up to 120 ml of blood could be collected from this group of participants. Blood was collected in BD Vacutainer heparin blood collection tubes (Greiner Bio-one, Frickenhausen, Germany) to prevent coagulation. Ethical approval was given by a Health Research Authority (HRA) Research Ethics Committee (13/WA/0190 – healthy volunteers; 11/WA/0040 – full-term pregnant women). All tissue and blood donations were voluntary, and donors had the right to withdraw consent at any point. Personal information was confidential, and informed written consent was obtained from all donors. Samples were collected from healthy non-pregnant women, healthy normal/overweight pregnant women (BMI 18.5 – 29.9 kg/m^2), obese pregnant women (BMI >30 kg/m^2), and pregnant women with a diagnosis of GDM. Due to the COVID-19 pandemic, before 23 March 2020, GDM was diagnosed via glucose tolerance testing (GTT), but from the first lockdown that started 23rd March 2020 until July 2022, it was diagnosed by measurement of HbA1c.

2.3.2 Placenta preparation

The placenta was received in the laboratory within 2 hours of delivery and transferred to a biological safety level (BSL) 2 cabinet for all handling. All instruments, such as tweezers, scissors, and sample containers, were sterile, single-use, and freshly opened from the packaging. The maternal decidua was removed from the maternal side of the placenta, and pieces of villous tissue of around 1 cm^3 were removed and placed into phosphate buffered (PBS pH 7.4; Gibco UK) and rinsed with PBS to remove as much blood as possible. Placental tissue was put into a pre-weighed glass tube containing freshly prepared ammonium acetate 155 mM in HLPC analytical grade deionized water (Fisher Scientific, Germany Darmstadt, Sigma-Aldrich UK). The tissue was homogenised after re-weighing to provide the total tissue weight (PowerGen 125 Homogenizer Probe, 5mm blade; Fisher Scientific UK). The tissue was gently homogenised for two minutes on ice, stopping every thirty seconds to

prevent the tissue from warming up. Occasionally, prepared placental biopsies were wrapped in aluminium foil, snap-frozen on liquid nitrogen, placed into a labelled container and then stored at (-80°C) until needed.

2.3.3 Plasma preparation

Peripheral blood from pregnant women collected into heparinised vacutainers was centrifuged at 1811 x g for 10 minutes. All plasma was removed with a sterile disposable single-use pipette in a BSL2 cabinet with 4 ml of plasma retained and stored at -80°C until downstream processing.

2.3.4 Lipid extraction

Some lipid extraction methods are available. Bligh & Dyer's method *(225)* uses a solvent system chloroform : methanol: water in volumetric ratio 1: 1: 0.9 (v/v/v) to extract a small amount of biological samples. After phase separation, total lipids are present in the chloroform phase. It is a well-established and widely used method. Disadvantages include using hazardous chloroform and collecting chloroform extract from the bottom layer (which may cause water-soluble impurities to carry over), as well as difficulty with automation. Folch method *(226)* uses a solvent system chloroform/methanol (2:1,v/v) to extract biological tissue, then add water or 0.9% NaCl to wash the solvent extract. Like the modified Bligh & Dyer method, it has advantages and disadvantages. MTBE method (Methyl, Tetryl Butyl Ether) is the Matyash method *(517)*, which uses the solvent system (methyl-tertiary-butyl ether (MTBE)/methanol/water) (5:1.5:1.45, v/v/v). The method resolves some of the disadvantages of chloroform-based methods because MTBE is present in the top layer after phase separation and, therefore, is more feasible for high throughput and automation. The disadvantage of the MTBE phase is that it contains significant aqueous components that may carry water-soluble contaminants. Relevant literature discussed the optimisation of the three methods *(518)*. One-phase extraction in 1 ml polypropylene tubes containing ceramic beads for the initial homogenization is performed using butanol and methanol (BUME). The BUME method uses the solvent system butanol/methanol (BUME, 3:1, v/v) to a small aqueous phase volume of three parts heptane with three parts ethyl with one part acetate (3:1, v/v) and 1%

acetic acid (v/v) to induce phase separation *(519)*. The BUME method compensates for the MTBE method with fewer water-soluble contaminants carried over into the organic phase. Its difficulty is in evaporating butanol components in the organic phase *(519, 520)*.

This research study follows Bligh and Dyer's method with modifications. Tissue 1000 mg is placed into a thick glass specifically designed for homogenisation, and then 5 ml of freshly prepared [155 mM] ammonium acetate is added. Homogenisation was performed on ice using a stainless steel electrical, mechanical probe hand-held blender with removal probe length 10 cm with tip engraved blade diameter 5 mm research for tough human tissue Fisher Scientific for 2 minutes with stopping every 30 seconds to prevent sample heating. Once the 5 ml of placenta tissue stock is homogenised, 1.6 ml of the sample is added to each glass tube A and B to process duplicate samples. For plasma, 1.6 ml is processed without this step, directly taking 1.6 ml and going to solvent extraction in a single tube as there is not enough plasma to use as double repeats as per placental case homogenates tube A 1.6ml and tube B 1.6ml. Plasma is just one tube A containing a standard lone volume of 1.6 ml. In the future, this should be run in doubles like placenta. The extraction process is detailed in (Figure 2.3, Figure 2.4, and Figure 2.5). Details of all placental and plasma sample weights, concentrations, and percentage recovery (%) are provided in the table of this chapter.

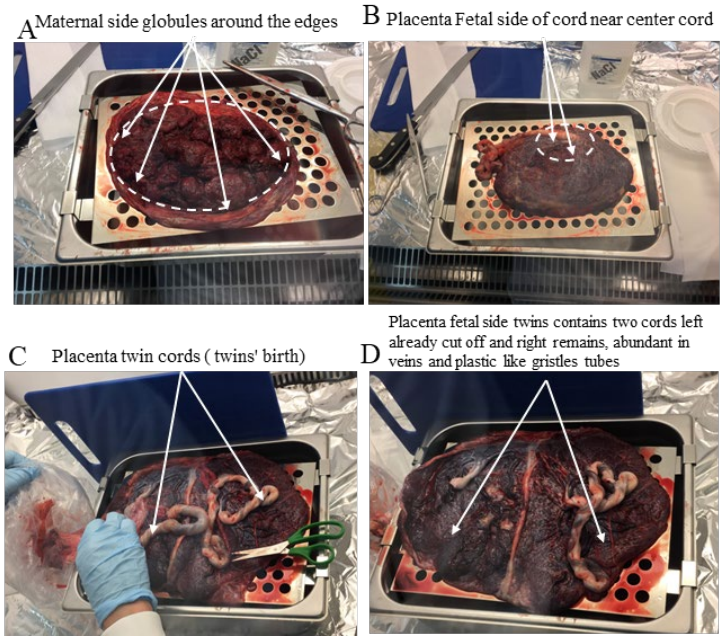

Figure 2:2: Experimental Images of Placenta sides. Legend to (Figure 2.2): Placenta edges and central near cord (A) Maternal side globules around the edges, (B) Placenta Fetal side of cord near the centre, (C) Placenta wins' birth contains two cords, (D) Placenta fetal side twins contain two cords left already cut off, and right remains, abundant in veins and plastic like gristles tubes.

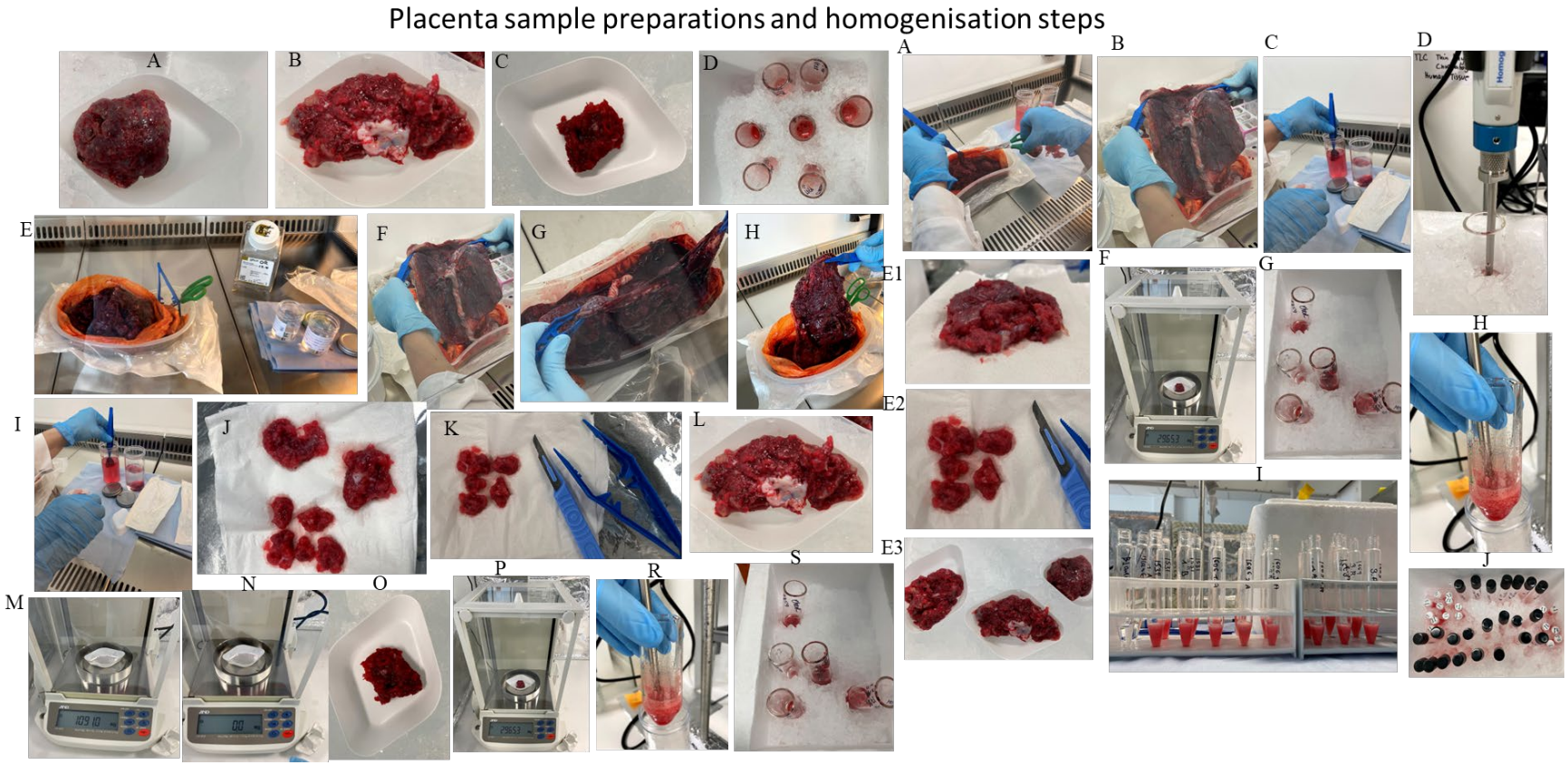

Figure 2:3: Photographic images of placenta preparation and homogenisation All placenta and plasma samples used in the Phd research study are included in the three tables and organised into groups: healthy, obese, and GDM. Concentration tables 1A,1B, and 1C for all placenta and plasma sample weights.

Table 1A: Contains all control placentas with healthy BMI (blue color)

From September 2020 untill March 2022	Samples comencing 08/09/2020, 15/09/2020, 10-17/10/2020, 28-11-2021, 7-24/12/2021,	Date weighed Homogenise the tissue and dried lipid extracts	Sample ID: CRF Plasma ; CAT a) placenta edges globules; b) placenta near cord centre; c) placenta random cuts	Body Mass Index BMI	Placenta Pathology Healthy BMI = Control vs. Diseased = Obese, Diabetic GDM	Wet placenta weight (mg) before freezing or Plasma volume (1.6ml)	Homogen.Sample Volume 1.6mL	Before weight of empty vial in (mg) accuracy (0.01mg)	After N_2 dried weight in (mg) containing lipid extract accuracy (0.01mg)	Calculated dried lipid extract minus empty vial (mg)	Total vial v=1500 µL, thus $CHCL_3$ added to dried extract in (µL)	Concentration based on dried lipid exctract [mg/mL]	Dilution of concentrated samples aliquotes (µl) c1v1=c2v2	added chloroform (µl) volume stock [10 mg/ml]	all lipid exctracts standardise to [10mg/ml]	Placenta Recovery dried weigh/wet weight x100% = placenta total lipid percent weight per weight (% w/w)
1	placenta	07/09 - 30/09/2020	CAT 1342	30.1	control- healthy	925.1	2 x (1.6ml)	2793.9	2798.8	4.9	490	10 [mg/mL]	no dilute	no dilute	10 [mg/mL]	0.5
2	placenta	07/09 - 30/09/2020	CAT 1491	29	control- healthy	1020.3	2 x (1.6ml)	2763.4	2776.7	13.3	1330	10 [mg/mL]	no dilute	no dilute	10 [mg/mL]	1.3
3	placenta	07/09 - 30/09/2020	CAT 1495	23.4	control- healthy	974.9	2 x (1.6ml)	2725.7	2738.9	13.2	1320	10 [mg/mL]	no dilution	no dilution	10 [mg/mL]	1.4
4	placenta	07/09 - 30/09/2020	CAT 1501	25.3	control- healthy	1751.5	2 x (1.6ml)	2757.1	2788.3	31.2	1560	25 [mg/mL]	624	376	10 [mg/mL]	1.8
5	placenta	07/09 - 30/09/2020	CAT 1502	27.5	control- healthy	1053.9	2 x (1.6ml)	2805.9	2832.2	26.3	1315	20 [mg/mL]	657	343	10 [mg/mL]	2.5
6	placenta	07/09 - 30/09/2020	CAT 1509	27.7	control- healthy	1799.6	2 x (1.6ml)	2769.5	2785.8	16.3	815	20 [mg/mL]	408	592	10 [mg/mL]	0.9
7	placenta	07/09 - 30/09/2020	CAT 1515	25.5	control- healthy	995.4	2 x (1.6ml)	2680.9	2697.7	16.8	840	20 [mg/mL]	420	580	10 [mg/mL]	1.7
8	placenta	07/09 - 30/09/2020	CAT 1516	28.5	control- healthy	1016.9	2 x (1.6ml)	2681.4	2714.7	33.3	1110	30 [mg/mL]	370	630	10 [mg/mL]	3.3
9	placenta	07/09 - 30/09/2020	CAT 1518	25.7	control- healthy	1172.1	2 x (1.6ml)	2700.3	2735.5	35.2	1173	30 [mg/mL]	391	609	10 [mg/mL]	3.0
10	placenta	07/09 - 30/09/2020	CAT 1531	28.7	control- healthy	1020.8	2 x (1.6ml)	2739.7	2749.1	9.4	940	10 [mg/mL]	no dilution	no dilution	10 [mg/mL]	0.9
11	placenta	07/09 - 30/09/2020	CAT 1565	22	control- healthy	1424.3	2 x (1.6ml)	2770.8	2777.6	6.8	680	10 [mg/mL]	no dilution	no dilution	10 [mg/mL]	0.5
12	placenta	28/11/ - 24/12/2021	CAT 1534-a	25.9	control- healthy	614.7	2 x(1.6ml)	2280	2286.6	6.6	660	10 [mg/mL]	no dilute	no dilute	10 [mg/mL]	1.1
13	placenta	28/11/ - 24/12/2021	CAT 1688	26	control- healthy	592.3	2x (1.6ml)	2653.5	2659.4	5.9	590	10 [mg/mL]	no dilute	no dilute	10 [mg/mL]	1.0
14	placenta	28/11/ - 24/12/2021	CAT 1678	26.3	control- healthy	712.7	2x (1.6ml)	2633.9	2638.3	4.4	440	10 [mg/mL]	no dilute	no dilute	10 [mg/mL]	0.6
15	placenta	28/11/ - 24/12/2021	CAT 1676	28.4	control- healthy	773.3	2x (1.6ml)	2688.9	2694.5	5.6	560	10 [mg/mL]	no dilute	no dilute	10 [mg/mL]	0.7
16	placenta	28/11/ - 24/12/2021	CAT 1702	20.5	control- healthy	691.7	2x (1.6ml)	2746.9	2754.1	7.2	720	10 [mg/mL]	no dilute	no dilute	10 [mg/mL]	1.0
17	placenta	28/11/ - 24/12/2021	CAT 1679	26.3	control- healthy	725.3	2x (1.6ml)	2664.1	2672	7.9	790	10 [mg/mL]	no dilute	no dilute	10 [mg/mL]	1.1
18	placenta	28/11/ - 24/12/2021	CAT 1684	22.1	control- healthy	765.7	2x (1.6ml)	2640.1	2646.4	6.3	630	10 [mg/mL]	no dilute	no dilute	10 [mg/mL]	0.8
19	placenta	28/11/ - 24/12/2021	CAT 1681	26.3	control- healthy	696.1	2x (1.6ml)	2682.2	2688.6	6.4	640	10 [mg/mL]	no dilute	no dilute	10 [mg/mL]	0.9
20	placenta	28/11/ - 24/12/2021	CAT 1531	28.7	control- healthy	670.9	2x (1.6ml)	2700.8	2707.9	7.1	710	10 [mg/mL]	no dilute	no dilute	10 [mg/mL]	1.1
21	placenta	28/11/ - 24/12/2021	CAT 1653	26.4	control- healthy	724.0	2x (1.6ml)	2654	2657.1	3.1	310	10 [mg/mL]	no dilute	no dilute	10 [mg/mL]	0.4
22	placenta	28/11/ - 24/12/2021	CAT 1701	24.1	control- healthy	636.2	2x (1.6ml)	2396.4	2399.8	3.4	340	10 [mg/mL]	no dilute	no dilute	10 [mg/mL]	0.5
23	placenta	28/11/ - 24/12/2021	CAT 1706	22.7	control- healthy	679.4	2x (1.6ml)	2377.1	2381.8	4.7	470	10 [mg/mL]	no dilute	no dilute	10 [mg/mL]	0.7
24	placenta	28/11/ - 24/12/2021	CAT 1707	27.1	control- healthy	782.1	2x (1.6ml)	2368.6	2374.5	5.9	590	10 [mg/mL]	no dilute	no dilute	10 [mg/mL]	0.8
25	placenta	28/11/ - 24/12/2021	CAT 1708	26.1	control- healthy	694.2	2x (1.6ml)	2378.3	2385.2	6.9	690	10 [mg/mL]	no dilute	no dilute	10 [mg/mL]	1.0
26	placenta	28/11/ - 24/12/2021	CAT 1715	21	control- healthy	671.6	2x (1.6ml)	2358.8	2366.6	7.8	780	10 [mg/mL]	no dilute	no dilute	10 [mg/mL]	1.2
27	placenta	28/11/ - 24/12/2021	CAT 1705	22.7	control- healthy	741.1	2x (1.6ml)	2410.4	2416.2	5.8	580	10 [mg/mL]	no dilute	no dilute	10 [mg/mL]	0.8
28	placenta	28/11/ - 24/12/2021	CAT 1694	25	control- healthy	796.2	2x (1.6ml)	2358.8	2363.3	4.5	450	10 [mg/mL]	no dilute	no dilute	10 [mg/mL]	0.6
29	placenta	28/11/ - 24/12/2021	CAT 1695	24.7	control- healthy	802.6	2x (1.6ml)	2395.8	2401.9	6.1	610	10 [mg/mL]	no dilute	no dilute	10 [mg/mL]	0.8
30	placenta	28/11/ - 24/12/2021	CAT 1685	22	control- healthy	775.9	2x (1.6ml)	2358.8	2363.4	4.6	460	10 [mg/mL]	no dilute	no dilute	10 [mg/mL]	0.6
32	placenta	28/11/ - 24/12/2021	CAT 1734	21.7	control- healthy	493.7	2x (1.6ml)	2411.7	2419.5	7.8	780	10 [mg/mL]	no dilute	no dilute	10 [mg/mL]	1.6
33	placenta	09/02/ - 30/03/2022	CAT 1681-c	23.4	control- healthy	970.2	2 x (1.6ml)	2395.1	2398.5	3.40	340	10 [mg/mL]	no dilute	no dilute	10 [mg/mL]	0.4
34	placenta	09/02/ - 30/03/2022	CAT 1687-c	22.5	control- healthy	860.5	2 x (1.6ml)	2344.7	2347.4	2.70	270	10 [mg/mL]	no dilute	no dilute	10 [mg/mL]	0.3
35	placenta	09/02/ - 30/03/2022	CAT 1701-c	24.5	control- healthy	623.7	2 x (1.6ml)	2319.7	2324.4	4.70	470	10 [mg/mL]	no dilute	no dilute	10 [mg/mL]	0.8
36	placenta	09/02/ - 30/03/2022	CAT 1653-a	26.4	control- healthy	563.2	2 x (1.6ml)	2362.1	2368.5	6.40	640	10 [mg/mL]	no dilute	no dilute	10 [mg/mL]	1.1
37	placenta	09/02/ - 30/03/2022	CAT 1708-c	26.1	control- healthy	598.9	2 x (1.6ml)	2378.3	2383.5	5.20	520	10 [mg/mL]	no dilute	no dilute	10 [mg/mL]	0.9
38	placenta	09/02/ - 30/03/2022	CAT 1760-a	21.9	control- healthy	541.5	2 x (1.6ml)	2369.4	2376.3	6.90	690	10 [mg/mL]	no dilute	no dilute	10 [mg/mL]	1.3
39	placenta	09/02/ - 30/03/2022	CAT 1676-c	28.4	control- healthy	647.1	2 x (1.6ml)	2390.6	2395.4	4.80	480	10 [mg/mL]	no dilute	no dilute	10 [mg/mL]	0.7
40	placenta	09/02/ - 30/03/2022	CAT 1645-c	22.9	control- healthy	761.1	2 x (1.6ml)	2380.1	2385.3	5.20	520	10 [mg/mL]	no dilute	no dilute	10 [mg/mL]	0.7
41	placenta	09/02/ - 30/03/2022	CAT 1679-c	25.5	control- healthy	985.2	2 x (1.6ml)	2334.7	2338.4	3.70	370	10 [mg/mL]	no dilute	no dilute	10 [mg/mL]	0.4
42	placenta	09/02/ - 30/03/2022	CAT 1702-c	20.5	control- healthy	672.1	2 x (1.6ml)	2374.3	2378.5	4.20	420	10 [mg/mL]	no dilute	no dilute	10 [mg/mL]	0.6
43	placenta	09/02/ - 30/03/2022	CAT 1621-c	40.4	control- healthy	543.2	2 x (1.6ml)	2374.7	2377.9	3.20	320	10 [mg/mL]	no dilute	no dilute	10 [mg/mL]	0.6
44	placenta	09/02/ - 30/03/2022	CAT 1706-a	22.7	control- healthy	565.3	2 x (1.6ml)	2377	2384.4	7.40	740	10 [mg/mL]	no dilute	no dilute	10 [mg/mL]	1.3
45	placenta	09/02/ - 30/03/2022	CAT 1574-c	22.7	control- healthy	457.2	2 x (1.6ml)	2355.5	2361.8	6.30	630	10 [mg/mL]	no dilute	no dilute	10 [mg/mL]	1.4
46	placenta	09/02/ - 30/03/2022	CAT 1763-a	23.5	control- healthy	733.5	2 x (1.6ml)	2388.5	2397.1	8.60	860	10 [mg/mL]	no dilute	no dilute	10 [mg/mL]	1.2

Table 2.1 Tables containing samples of placenta recovery percentage weight from 0.5-1.5% w/w in control (healthy BMI Placentas n=46) Concentration tables 1A,1B, and 1C for all placenta and plasma sample weights.

Table 1 B: Contains placentas with obese BMI (purple color) and placentas with GDM (red color)

From September 2020 untill March 2022	Sample: week comencing 08/09/2020 , 15/09/2020 , 10-17/10/2020 , 28-11-2021, 7-24/12/2021,	Date weighed Homogenise the tissue and dried lipid extracts	Sample ID: CRF Plasma ; CAT a) placenta edges globules; b) placenta near cord centre; c) placenta random cuts	Body Mass Index BMI	Placenta Pathology Healthy BMI = Control vs. Diseased = Obese, Diabetic GDM	Wet placenta weight (mg) before freezing or Plasma volume (1.6ml)	Homogen.Sample Volume 1.6mL	Before weight of empty vial in (mg) accuracy (0.01mg)	After N_2 dried weight in (mg) containing lipid extract accuracy (0.01mg)	Calculated dried lipid extract minus empty vial (mg)	Total vial v=1500 µL, thus $CHCL_3$ added to dried extract in (µL)	Concentration based on dried lipid exctract [mg/mL]	Dilution of concentrated samples aliquotes (µl) c1v1=c2v2	added chloroform (µl) volume stock [10 mg/ml]	all lipid exctracts standardise to [10mg/ml]	Placenta Recovery dried weigh/wet weight x100% = placenta total lipid percent weight per weight (% w/w)
1	placenta	09/02/ - 30/03/2022	CAT 1514-c	31.5	obese	459.7	2 x (1.6ml)	2372.7	2378.73	6.03	603	10 [mg/mL]	no dilute	no dilute	10 [mg/mL]	1.3
2	placenta	09/02/ - 30/03/2022	CAT 1550-c	41.8	obese	541.6	2 x (1.6ml)	2391.8	2397.25	5.45	545	10 [mg/mL]	no dilute	no dilute	10 [mg/mL]	1.0
3	placenta	09/02/ - 30/03/2022	CAT 1489-c	33.7	obese	494.2	2 x (1.6ml)	2381.7	2386.37	4.67	467	10 [mg/mL]	no dilute	no dilute	10 [mg/mL]	0.9
4	placenta	09/02/ - 30/03/2022	CAT 1670-c	49.5	obese	589.8	2 x (1.6ml)	2397.4	2401.71	4.31	431	10 [mg/mL]	no dilute	no dilute	10 [mg/mL]	0.7
5	placenta	09/02/ - 30/03/2022	CAT 1656-b	50	obese	596.6	2 x (1.6ml)	2353.7	2357.43	3.73	373	10 [mg/mL]	no dilute	no dilute	10 [mg/mL]	0.6
6	placenta	09/02/ - 30/03/2022	CAT 1505-a	32	obese	568.9	2 x (1.6ml)	2365.3	2374.94	9.64	964	10 [mg/mL]	no dilute	no dilute	10 [mg/mL]	1.7
7	placenta	09/02/ - 30/03/2022	CAT 1759-c	34.2	obese	619.7	2 x (1.6ml)	2346.7	2351.18	4.48	448	10 [mg/mL]	no dilute	no dilute	10 [mg/mL]	0.7
8	placenta	09/02/ - 30/03/2022	CAT 1655-c	36.1	obese	583.7	2 x (1.6ml)	2375.4	2380.35	4.95	495	10 [mg/mL]	no dilute	no dilute	10 [mg/mL]	0.8
9	placenta	09/02/ - 30/03/2022	CAT 1539-c	31.2	obese	595.2	2 x (1.6ml)	2400.8	2407.76	6.96	696	10 [mg/mL]	no dilute	no dilute	10 [mg/mL]	1.2
10	placenta	09/02/ - 30/03/2022	CAT 1492-c	39	obese	596.3	2 x (1.6ml)	2383.6	2388.59	4.99	499	10 [mg/mL]	no dilute	no dilute	10 [mg/mL]	0.8
11	placenta	09/02/ - 30/03/2022	CAT 1606-c	41	obese	597.1	2 x (1.6ml)	2365.3	2371.29	5.99	599	10 [mg/mL]	no dilute	no dilute	10 [mg/mL]	1.0
12	placenta	09/02/ - 30/03/2022	CAT 1499-c	30.5	obese	597.2	2 x (1.6ml)	2363	2367.64	4.64	464	10 [mg/mL]	no dilute	no dilute	10 [mg/mL]	0.8
13	placenta	09/02/ - 30/03/2022	CAT 1614-a	32.4	obese	597.6	2 x (1.6ml)	2375.8	2383.24	7.44	744	10 [mg/mL]	no dilute	no dilute	10 [mg/mL]	1.2
14	placenta	09/02/ - 30/03/2022	CAT 1680-c	30.4	obese	568.1	2 x (1.6ml)	2362.2	2367.89	5.69	569	10 [mg/mL]	no dilute	no dilute	10 [mg/mL]	1.0
15	placenta	09/02/ - 30/03/2022	CAT 1771-c	58.3	obese	565.4	2 x (1.6ml)	2348.8	2354.99	6.19	619	10 [mg/mL]	no dilute	no dilute	10 [mg/mL]	1.1
16	placenta	09/02/ - 30/03/2022	CAT 1644-c	40.8	obese	541.7	2 x (1.6ml)	2371.8	2376.93	5.13	513	10 [mg/mL]	no dilute	no dilute	10 [mg/mL]	0.9
17	placenta	09/02/ - 30/03/2022	CAT 1686-c	30.9	obese	604.6	2 x (1.6ml)	2356.3	2361.98	5.68	568	10 [mg/mL]	no dilute	no dilute	10 [mg/mL]	0.9
18	placenta	07/09 - 30/09/2020	CAT 1487	39.4	obese	1263.5	2 x (1.6ml)	2781.3	2795.9	14.6	730	20 [mg/mL]	365	635	10 [mg/mL]	1.2
19	placenta	07/09 - 30/09/2020	CAT 1489	33.7	obese	1026.9	2 x (1.6ml)	2793.2	2827.1	33.9	1130	30 [mg/mL]	377	623	10 [mg/mL]	3.3
20	placenta	07/09 - 30/09/2020	CAT 1492	39	obese	1076.1	2 x (1.6ml)	2802.8	2827.4	24.6	1230	20 [mg/mL]	615	385	10 [mg/mL]	2.3
21	placenta	07/09 - 30/09/2020	CAT 1499	30.5	obese	1967.7	2 x (1.6ml)	2677.6	2688	10.4	1040	10 [mg/mL]	no dilution	no dilution	10 [mg/mL]	0.5
22	placenta	07/09 - 30/09/2020	CAT 1500	49.8	obese	1341.7	2 x (1.6ml)	2692.9	2710.9	18	900	30 [mg/mL]	300	700	10 [mg/mL]	1.3
23	placenta	07/09 - 30/09/2020	CAT 1514	31.5	obese	1119.7	2 x (1.6ml)	2763.7	2779.4	15.7	785	20 [mg/mL]	393	607	10 [mg/mL]	1.4
24	placenta	07/09 - 30/09/2020	CAT 1539	31.2	obese	1225.4	2 x (1.6ml)	2779.7	2811.9	32.2	1073	30 [mg/mL]	537	463	10 [mg/mL]	2.6
25	placenta	07/09 - 30/09/2020	CAT 1622	48.4	obese	1935.4	2 x (1.6ml)	2797.8	2831.5	33.7	1123	30 [mg/mL]	374	626	10 [mg/mL]	1.7
26	placenta	28/11/ - 24/12/2021	CAT 1550-a	45	Obese	568.5	2x (1.6ml)	2286	2292.2	6.2	620	10 [mg/mL]	no dilute	no dilute	10 [mg/mL]	1.1
1	placenta	07/09 - 30/09/2020	CAT 1494	48.8	GDM/obese	1057.5	2 x (1.6ml)	2679.6	2710	30.4	1013	40 [mg/mL]	253	747	10 [mg/mL]	2.9
2	placenta	07/09 - 30/09/2020	CAT 1496	41.6	GDM/obese	1057.5	2 x (1.6ml)	2694.6	2720.4	25.8	1290	20 [mg/mL]	645	355	10 [mg/mL]	2.4
3	placenta	07/09 - 30/09/2020	CAT 1512	27.5	GDM	1670.5	2 x (1.6ml)	2775.6	2803.1	27.5	1375	20 [mg/mL]	688	313	10 [mg/mL]	1.6
4	placenta	07/09 - 30/09/2020	CAT 1513	18.5	GDM	1736.9	2 x (1.6ml)	2781.6	2806.1	24.5	1225	20 [mg/mL]	613	388	10 [mg/mL]	1.4
5	placenta	07/09 - 30/09/2020	CAT 1545	22.7	GDM	1559.7	2 x (1.6ml)	2777.8	2816.9	39.1	1303	40 [mg/mL]	326	674	10 [mg/mL]	2.5
6	placenta	07/09 - 30/09/2020	CAT 1564	57.3	GDM/obese	1424.3	2 x (1.6ml)	2760.8	2818.1	57.3	1146	50 [mg/mL]	229	771	10 [mg/mL]	4.0
7	placenta	07/09 - 30/09/2020	CAT 1578	38.7	GDM/obese	1218.1	2 x (1.6ml)	2773.3	2812.3	39	975	40 [mg/mL]	244	756	10 [mg/mL]	3.2
8	placenta	28/11/ - 24/12/2021	CAT 1669-a	32.8	GDM	509.6	2x (1.6ml)	2285.7	2291.9	6.2	620	10 [mg/mL]	no dilute	no dilute	10 [mg/mL]	1.2
9	placenta	10/01/ - 30/01/2022	CAT 1651-c	29.3	GDM	834.6	2 x (1.6ml)	2068.7	2076.4	7.70	770	10 [mg/mL]	no dilute	no dilute	10 [mg/mL]	0.9
10	placenta	10/01/ - 30/01/2022	CAT 1785-c	44	GDM	663.9	2 x (1.6ml)	2099.7	2104.1	4.40	440	10 [mg/mL]	no dilute	no dilute	10 [mg/mL]	0.7
11	placenta	10/01/ - 30/01/2022	CAT 1574-b	22.7	GDM	575.5	2 x (1.6ml)	2173.9	2175.6	1.70	170	10 [mg/mL]	no dilute	no dilute	10 [mg/mL]	0.3
12	placenta	10/01/ - 30/01/2022	CAT 1677-c	44.6	GDM	515.3	2 x (1.6ml)	2073.7	2077.6	3.90	390	10 [mg/mL]	no dilute	no dilute	10 [mg/mL]	0.8
13	placenta	10/01/ - 30/01/2022	CAT 1699-c	42.2	GDM	580.1	2 x (1.6ml)	2078.8	2082.5	3.70	370	10 [mg/mL]	no dilute	no dilute	10 [mg/mL]	0.6
14	placenta	10/01/ - 30/01/2022	CAT 1568-c	26.1	GDM	528.6	2 x (1.6ml)	2073.5	2078.3	4.80	480	10 [mg/mL]	no dilute	no dilute	10 [mg/mL]	0.9
15	placenta	10/01/ - 30/01/2022	CAT 1719-c	42.6	GDM	635.1	2 x (1.6ml)	2093.1	2097.8	4.70	470	10 [mg/mL]	no dilute	no dilute	10 [mg/mL]	0.7
16	placenta	10/01/ - 30/01/2022	CAT 1577	46.5	GDM	703.8	2 x (1.6ml)	2101.6	2105	3.40	340	10 [mg/mL]	no dilute	no dilute	10 [mg/mL]	0.5

Table 2.2 Tables containing placenta group obese BMI n=26, and placenta group gestational diabetes GDM n=16 all samples recovery percentage weight from (0.6 -2.6 % w/w) in (obese BMI Placentas n=26) and (0.5- 4% w/w) in (GDM Placentas n=1 Concentration tables 1A,1B, and 1C for all placenta and plasma sample weights.

Table 1 C: Contains all pregnant plasmas with healthy BMI,(blue color) with obese BMI (purple color) with GDM (red color) and non pregnant plasmas (green color)

September 2020 March 2022	Sample: week comencing 08/09/2020, 15/09/2020, 10-17/10/2020, 28-11-2021, 7-24/12/2021,	Date weighed Homogenise the tissue and dried lipid extracts	Sample ID: CRF Plasma, CAT a) placenta edges globules; b) placenta near cord centre; c) placenta random cuts	Body Mass Index BMI	Plasma Pathology Healthy BMI = Control vs. Diseased = Obese, Diabetic GDM	Wet placenta weight (mg) before freezing or Plasma volume (1.6ml)	Homogen.Sample Volume (1.6mL)	Before weight of empty vial in (mg) accuracy (0.01mg)	After N_2 dried weight in (mg) containing lipid extract accuracy (0.01mg)	Calculated dried lipid extract minus empty vial (mg)	Total vial v=1500 µL, thus $CHCl_3$ added to dried extract in (µL)	Concentration based on dried lipid exctract [mg/mL]	Dilution of concentrated samples aliquotes (µl) c1v1=c2v2	added chloroform (µl) volume stock [10 mg/ml]	all lipid exctracts standardise to [10mg/ml]	Plasma Recovery dried lipid extract weight / fresh plasma volume = weigh per volume (w/v)
1	plasma	07/09 - 30/09/2020	CAT 1530	34.7	pregnant-GDM/obese	1.6	1 x(1.6ml)	2752.1	2776.2	24.1	1205	20 [mg/mL]	602	398	10 [mg/mL]	15.1
2	plasma	07/09 - 30/09/2020	CAT 1545	22.7	pregnant-GDM	1.6	1 x(1.6ml)	2803.5	2834.6	31.1	1037	30 [mg/mL]	346	654	10 [mg/mL]	19.4
3	plasma	07/09 - 30/09/2020	CAT 1558	27.3	pregnant-GDM	1.6	1 x(1.6ml)	2819.4	2844.6	25.2	1260	20 [mg/mL]	630	370	10 [mg/mL]	15.7
4	plasma	07/09 - 30/09/2020	CAT 1564	57.3	pregnant-GDM/obese	1.6	1 x(1.6ml)	2776.7	2784.2	7.5	750	10 [mg/mL]	no dilution		10 [mg/mL]	4.7
4	plasma	07/09 - 30/09/2020	CAT 1568	26.1	pregnant-GDM	1.6	1 x(1.6ml)	2782.6	2796.2	6.8	340	20 [mg/mL]	170	830	10 [mg/mL]	4.3
6	plasma	07/09 - 30/09/2020	CAT 1574	22.7	pregnant-GDM	1.6	1 x(1.6ml)	2787.5	2798.8	5.65	283	20 [mg/mL]	141	859	10 [mg/mL]	3.5
7	plasma	07/09 - 30/09/2020	CAT 1577	46.5	pregnant-GDM/obese	1.6	1 x(1.6ml)	2817.7	2845.3	27.6	760	10 [mg/mL]	no dilution	no dilution	10 [mg/mL]	14.8
8	plasma	07/09 - 30/09/2020	CAT 1578	38.7	pregnant-GDM/obese	1.6	1 x(1.6ml)	2816.6	2841.7	25.1	1255	20 [mg/mL]	627	373	10 [mg/mL]	15.7
1	plasma	07/09 - 30/09/2020	CAT 1557	46.1	pregnant-obese	1.6	1 x(1.6ml)	2771.8	2785	13.2	1320	10 [mg/mL]	no dilution	no dilution	10 [mg/mL]	8.2
2	plasma	07/09 - 30/09/2020	CAT 1593	31.6	pregnant-obese	1.6	1 x(1.6ml)	2761.8	2786.8	25	1250	20 [mg/mL]	625	375	10 [mg/mL]	15.6
3	plasma	07/09 - 30/09/2020	CAT 1606	41	pregnant-obese	1.6	1 x(1.6ml)	2767.3	2778.7	11.4	570	20 [mg/mL]	285	715	10 [mg/mL]	7.1
4	plasma	07/09 - 30/09/2020	CAT 1613	41.3	pregnant-obese	1.6	1 x(1.6ml)	2781.4	2804.7	23.3	1165	20 [mg/mL]	582	418	10 [mg/mL]	14.6
5	plasma	07/09 - 30/09/2020	CAT 1614	32.4	pregnant-obese	1.6	1 x(1.6ml)	2700.3	2735.5	35.2	1173	30 [mg/mL]	391	609	10 [mg/mL]	22.0
6	plasma	02/10 -16/10/2020	CAT 1636	31.8	pregnant-obese	1.6	1 x(1.6ml)	2681.08	2710.18	29.1	970	30 [mg/mL]	323	677	10 [mg/mL]	18.2
1	plasma	07/09 - 30/09/2020	CAT 1515	25.5	pregnant- healthy	1.6	1 x(1.6ml)	2649.4	2653.6	4.2	420	10 [mg/mL]	no dilution	no dilution	10 [mg/mL]	2.6
2	plasma	07/09 - 30/09/2020	CAT 1531	28.7	pregnant- healthy	1.6	1 x(1.6ml)	2637.5	2655.8	18.3	915	20 [mg/mL]	458	542	10 [mg/mL]	11.4
3	plasma	07/09 - 30/09/2020	CAT 1532	18.7	pregnant- healthy	1.6	1 x(1.6ml)	2741.7	2745.1	3.4	170	20 [mg/mL]	85	915	10 [mg/mL]	2.1
4	plasma	07/09 - 30/09/2020	CAT 1543	26	pregnant- healthy	1.6	1 x(1.6ml)	2799.7	2809.9	10.2	1020	10 [mg/mL]	no dilution	no dilution	10 [mg/mL]	6.4
5	plasma	07/09 - 30/09/2020	CAT 1549	27	pregnant- healthy	1.6	1 x(1.6ml)	2769.3	2791.5	22.2	2220	10 [mg/mL]	no dilution	no dilution	10 [mg/mL]	13.9
6	plasma	07/09 - 30/09/2020	CAT 1565	22	pregnant- healthy	1.6	1 x(1.6ml)	2772.9	2789.3	8.2	410	20 [mg/mL]	205	795	10 [mg/mL]	5.1
7	plasma	02/10 -16/10/2020	CAT 1639	20	pregnant- healthy	1.6	1 x(1.6ml)	2668.48	2674.88	6.4	640	10 [mg/mL]	no dilute	no dilute	10 [mg/mL]	4.0
8	plasma	02/10 -16/10/2020	CAT 1642	25.3	pregnant- healthy	1.6	1 x(1.6ml)	2662.74	2671.92	9.18	918	10 [mg/mL]	no dilute	no dilute	10 [mg/mL]	5.7
9	plasma	02/10 -16/10/2020	CAT 1643	25.4	pregnant- healthy	1.6	1 x(1.6ml)	2682.92	2689.2	6.28	628	10 [mg/mL]	no dilute	no dilute	10 [mg/mL]	3.9
1	NP plasma	02/10 -16/10/2020	CRF 424	27.5	Non-pregnant plasma	1.6	1 x(1.6ml)	2769.8	2774.9	5.1	510	10 [mg/mL]	no dilute	no dilute	10 [mg/mL]	3.2
2	NP plasma	02/10 -16/10/2020	CRF 453	25.1	Non-pregnant plasma	1.6	1 x(1.6ml)	2765.8	2767.9	2.1	210	10 [mg/mL]	no dilute	no dilute	11 [mg/mL]	1.3
3	NP plasma	02/10 -16/10/2020	CRF 458	29	Non-pregnant plasma	1.6	1 x(1.6ml)	2764.2	2773.7	9.5	950	10 [mg/mL]	no dilute	no dilute	10 [mg/mL]	5.9
4	NP plasma	02/10 -16/10/2020	CRF 474	23.8	Non-pregnant plasma	1.6	1 x(1.6ml)	2795	2802.3	7.3	730	10 [mg/mL]	no dilute	no dilute	10 [mg/mL]	4.6
5	NP plasma	02/10 -16/10/2020	CRF 318	25.8	Non-pregnant plasma	1.6	1 x(1.6ml)	2763.2	2769.6	6.4	640	10 [mg/mL]	no dilute	no dilute	10 [mg/mL]	4.0
6	NP plasma	02/10 -16/10/2020	CRF 384	32.8	Non-pregnant plasma	1.6	1 x(1.6ml)	2796.7	2801.7	5	500	10 [mg/mL]	no dilute	no dilute	10 [mg/mL]	3.1
7	NP plasma	02/10 -16/10/2020	CRF 480	24.6	Non-pregnant plasma	1.6	1 x(1.6ml)	2784.3	2791.7	7.4	740	10 [mg/mL]	no dilute	no dilute	10 [mg/mL]	4.6
8	NP plasma	02/10 -16/10/2020	CRF 513	na	Non-pregnant plasma	1.6	1 x(1.6ml)	2784.7	2791.2	6.5	650	10 [mg/mL]	no dilute	no dilute	10 [mg/mL]	4.1
9	NP plasma	02/10 -16/10/2020	CRF 518	na	Non-pregnant plasma	1.6	1 x(1.6ml)	2682.3	2684.2	1.9	190	10 [mg/mL]	no dilute	no dilute	10 [mg/mL]	1.2

Table Legend:		
Plasma	**Placenta**	**Placenta chunks**
Healthy	Healthy	a- placenta edges globules
Obese	Obese	b- placenta near cord centre
GDM	GDM	c- random cuts given by students
NP non pregnant		

Table 2.3 Tables containing all plasma samples from non-pregnant to healthy BMI, obese BMI, and GDM samples. Concentration tables 1A,1B, and 1C for all placenta and plasma recovery percentage weight per volume (1.6ml plasma per each sample subjected to lipid extraction gives different approximations in ratio recovered of total dried lipid extract weight group red (GDM/obes w/v 3.5-19.4%,) purple (obese BMI w/v 7.1-22%), blue (healthy BMI w/v 2.6-%13.9) and green non-pregnant patients (man/woman w/v 1.3-4.6%

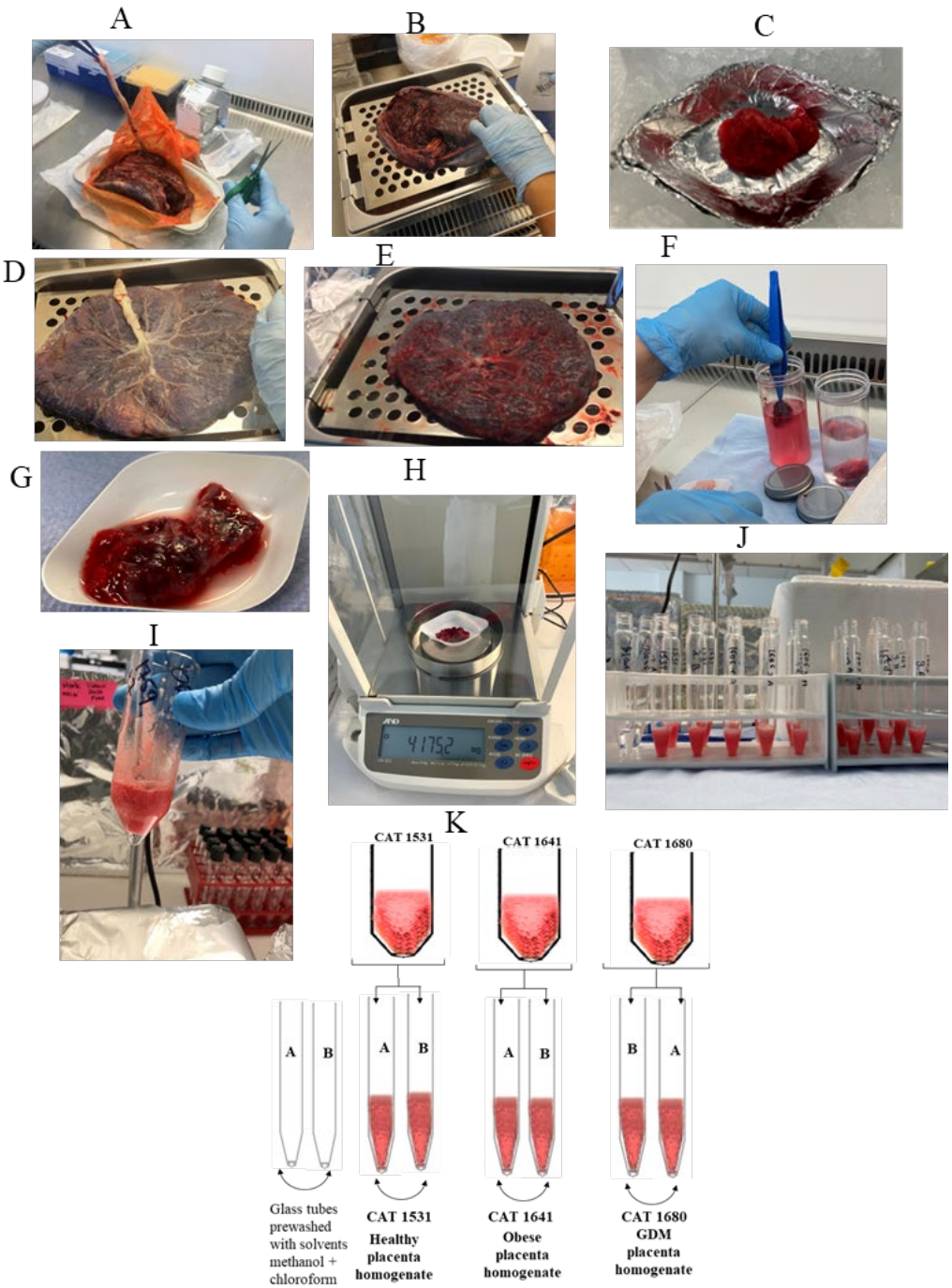

Figure 2:4 Photographic images during the placenta tissue handling experiment, which involves systematic steps, washing, cutting, and weighing followed by placenta homogenisation and the homogenate aliquots in duplicates 1.6ml per tube A and per tube B used per each placement for lipid extraction and combine into one tube at the end during solvent nitrogen drying.

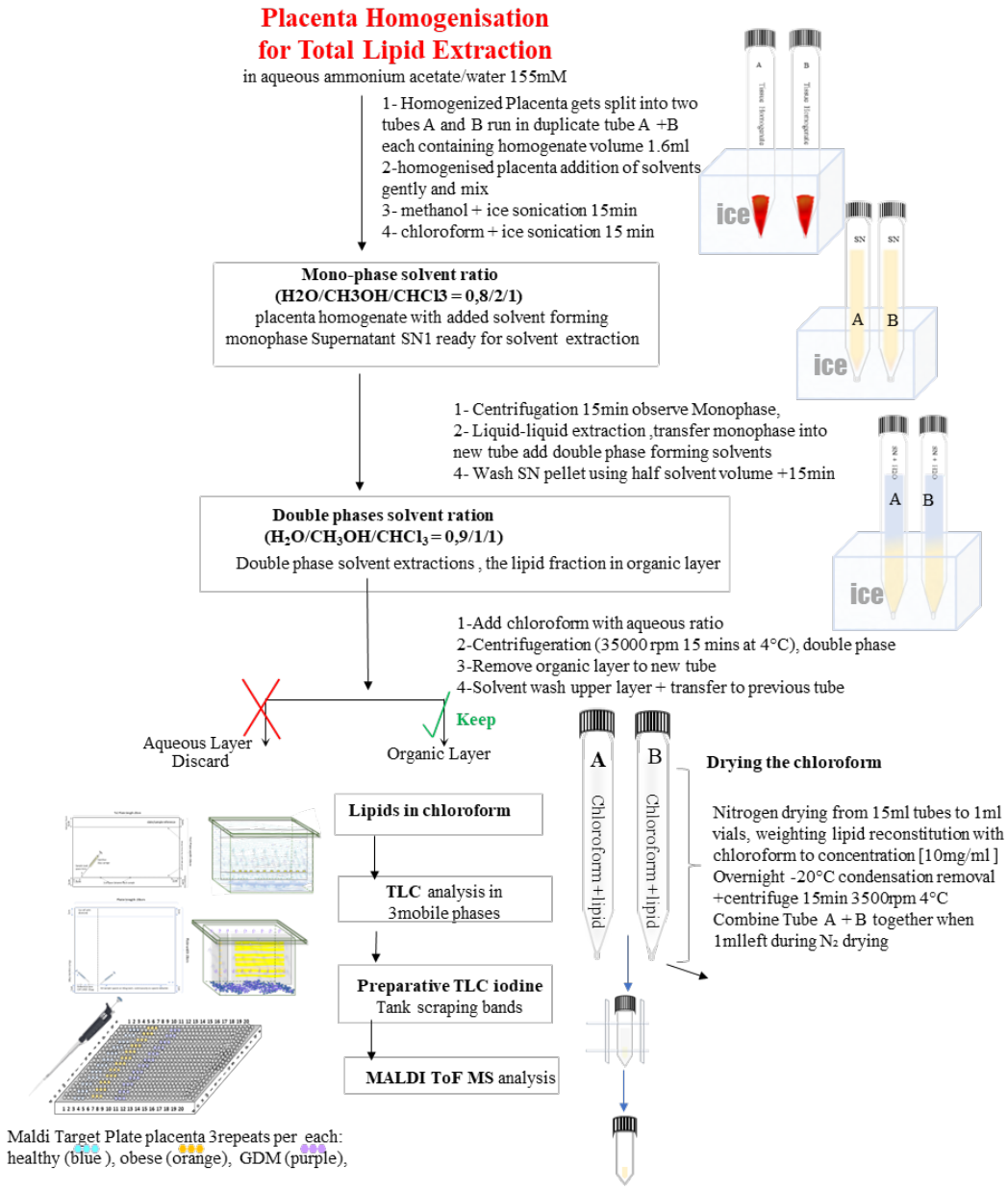

Figure 2:5 The pictorial overview of Bligh& Dyer: lipid extraction from homogenisation to target for MALDI ToF MS. Below in (Figure 2.12) a detailed overview of the Swansea adaptation of Dr Lapalco's method protocol in detailed steps of each stage learnt from Dr Lopalco lipid extraction from microalgae and adapted and modified to placenta organ tissue, and blood plasma.

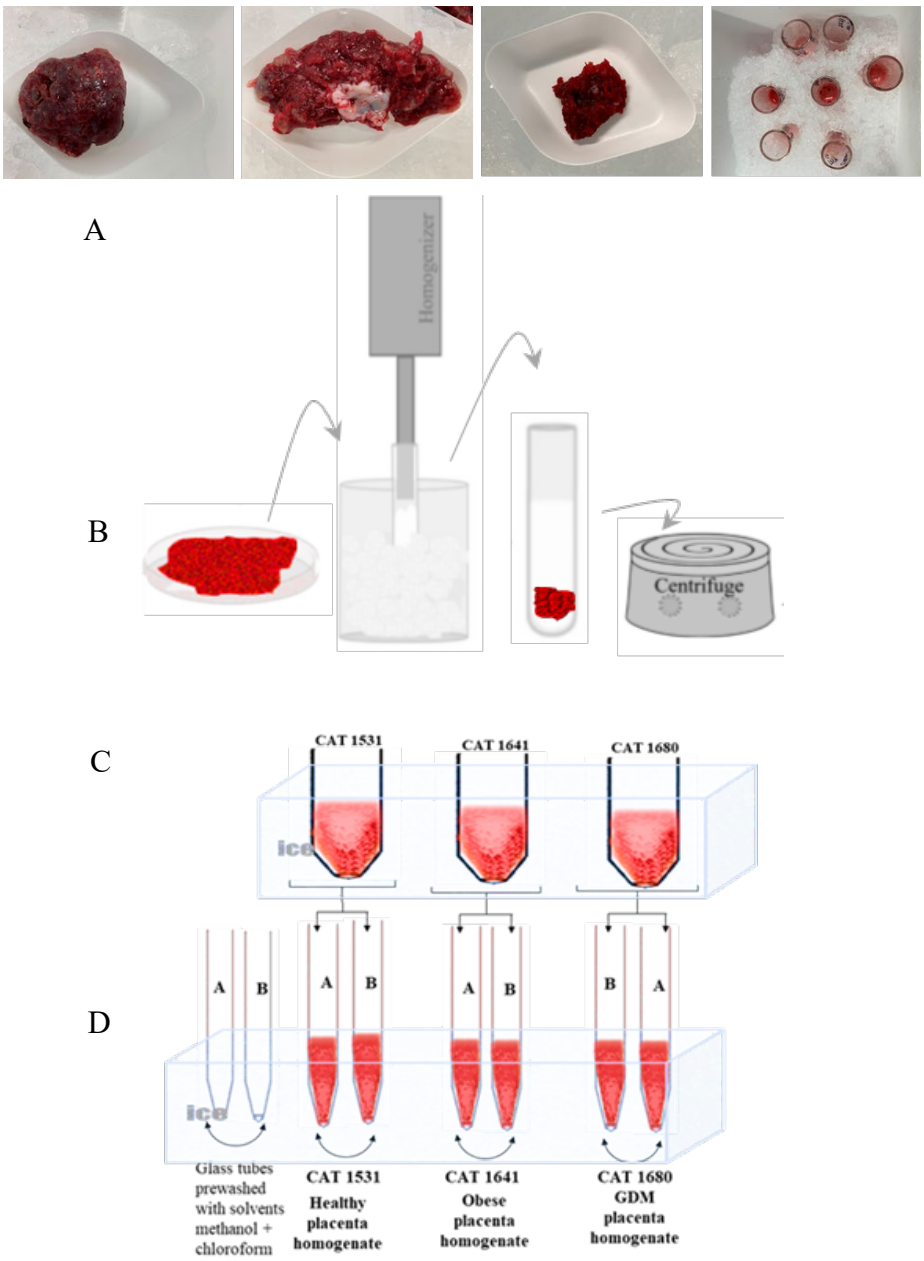

Figure 2:6 Placental homogenisation total and aliquoted duplicate portions of 1.6ml to tubes A and B counted as one sample.

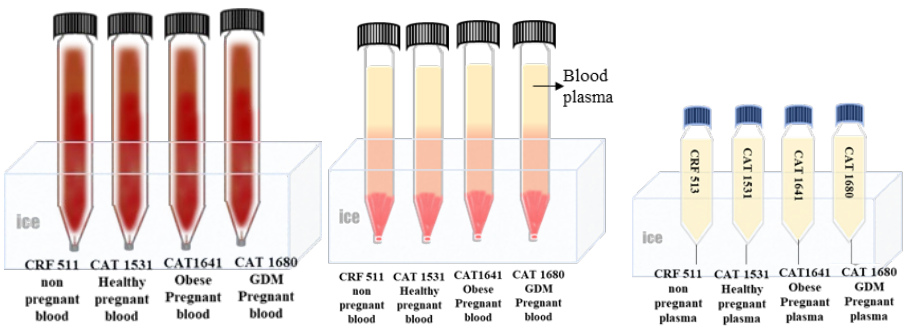

Figure 2:7 Blood separation to prepare blood plasma for lipid extraction.

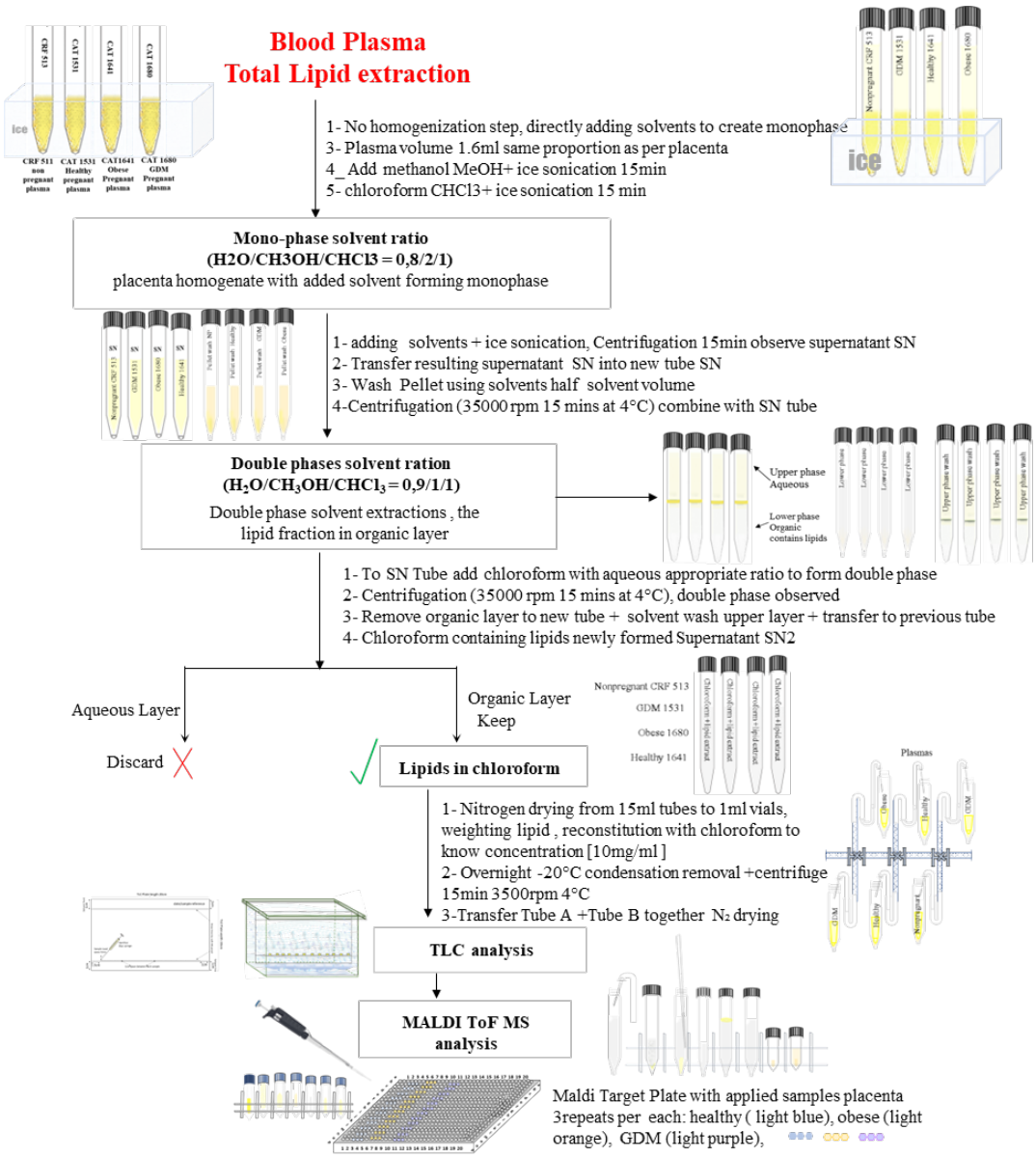

Figure 2:8 All-in-one diagram overview of plasma lipid extraction.

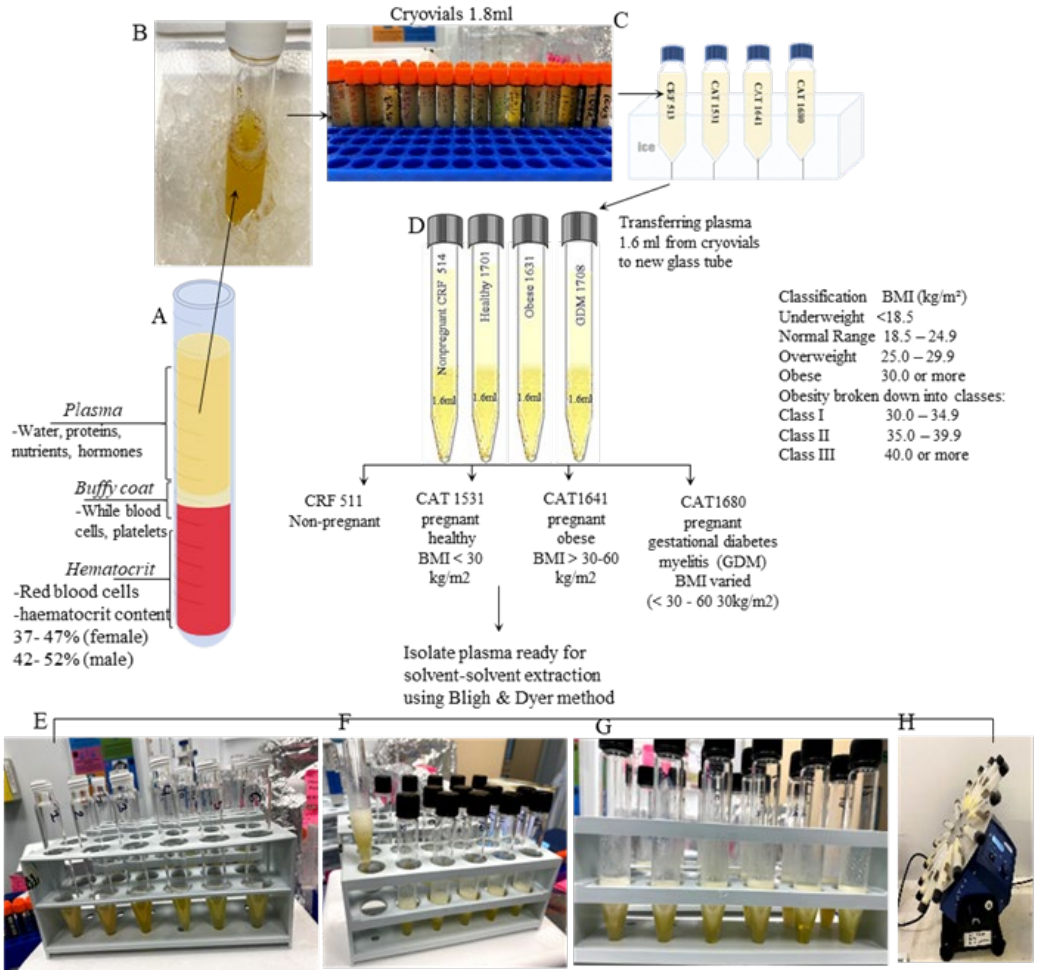

Figure 2:9 The separation of plasma from the full blood volume was received at 1.8 ml and used for extraction at 1.6 ml. Legend to (Figure 2.9): Placenta sample reference CAT1680 pregnant gestational diabetes myelitis (GDM) BMI varied 30 - 60 kg/m2 CAT1641 Pregnant obese BMI > 30-60 kg/m2, CRF 511 Nonpregnant BMI not relevant, CAT 1531 Pregnant healthy BMI < 30 kg/m2. As per classification, BMI (kg/m²): Underweight <18.5 BMI (kg/m²): Normal Range 18.5 – 24.9 BMI (kg/m²): Overweight 25.0 – 29.9 BMI (kg/m²): Obese 30.0 or more BMI (kg/m²): Obesity broken down into classes: Class I 30.0 – 34.9 BMI (kg/m²): Class II 35.0 – 39.9 BMI (kg/m²): Class III 40.0 or more BMI (kg/m²):

The schematic and images below follow the steps of plasma preparation and, when isolated from blood, are subjected to solvent addition, mixing, centrifugation and extraction using the Bligh & Dyer method protocol of the solvent methanol to chloroform ratio. Blood composition is a mix of cellular and liquid elements *(521)*. During centrifugation, we observe red blood cells called erythrocytes, the heaviest cells carrying heme complexes *(224)*. Hence, they sink to the bottom because their standard volume is plus or minus 45% of the total blood volume. Another part of blood is white blood cells, leukocytes, and platelets in the middle of the blood tube

(522), and studies on mononuclear cells use that system *(523)*. Most of the blood in the top yellow layer is water, which floats *(524)*; therefore, 90% of the blood is water. Plasma is mostly water, 90% and contains gases, hormones, waste products, and ions. Blood proteins comprise 7-7% of albumin protein blood carriers composed of immunoglobulins and fibrinogen, a clotting protein, Na+, K+, Ca2+, Mg2+, Cl, and HCO3-. After coagulation, the fluid is serum, a noncellular blood component. The serum is plasma without clotting factors. Erythrocytes transport oxygen throughout the body. Granulocytes and leukocytes contain polymorphonuclear cytoplasmic granules. Approximately 60% of neutrophils fight bacteria and some cancers; 3% fight parasites and allergic reactions; 0.5% fight basophilic infections and allergic reactions. There are 5% of leukocytes in the body, and since leukocytes are constantly replenishing resident macrophages and dendritic cells *(525)*. Under normal conditions, 30% of lymphocytes are rare circulating and are responsible for the innate immune system (T-cells, B-cells, NK-cells). The T-lymphocytes mediate cellular immune responses, while the B-lymphocytes produce antibodies to fight infection—platelets from fragmented megakaryocytes clot *(248, 524, 526-530)*.

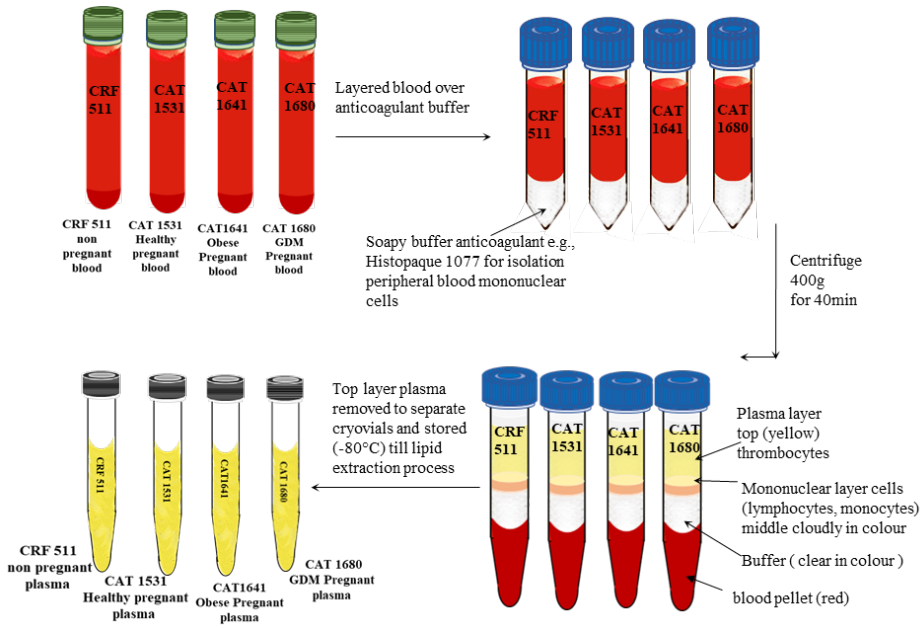

Figure 2:10 Figure Representative diagram of plasma family Legend to (Figure 2.10): Plasma comprises four groups, which include non-pregnant patients' blood, pregnant with healthy BMI blood, pregnant with obese BMI blood, and gestational diabetes GDM blood with variable BMIs, it could be with healthy or obese BMI.

Figure 2:11 Photographic images overview of placenta homogenates,

Legend to (Figure 2.11): Images (A-P) show photographic steps starting from cutting placenta chunks to weighing them. After that, lipid extraction in methanol chloroform was dried under nitrogen gas, and then the dried lipid extract was reconstituted and ready for TLC and MALDI ToF MS analysis. Placenta Homogenisation throughout adding solvents during the extraction process, till nitrogen drying the chloroform containing total lipids until fully dried total lipid extract in the vial showing darker yellow colour (L), then weighing the dried extract and re-constituting back with chloroform accordingly to the measured weight and record concentration which is always constant at 10[mg/ml].

2.3.5 Monophase solvent system

The mono-phase solvent system consists of water, methanol, and chloroform [$H_2O/CH_3OH/CHCl_3$] in ratios of (0.8/2/1), respectively. A 1.6ml aliquot of homogenised placental tissue or plasma was placed into glass tubes. Solvents were then added sequentially – 4 ml methanol and 2 ml chloroform - to tubes placed in the ice bath sonicate for 15 gentle sonication with the addition of each solvent. Once both solvents had been added and gently mixed, samples were centrifuged at 2,800

x g for 15 min at 4°C. The supernatant layer was gently removed into a new 15 ml glass tube, and the pellet was washed again with 2 ml methanol and 1 ml chloroform by centrifugation. The supernatant from the second centrifugation was added to that from the first. This solvent mixture homogenises to create a single mixed-solvent phase, called the “monophase system.” The next step involves changing the solvent ratio to create a “double phase system, " forming an organic phase, mostly chloroform, on the bottom layer and an ‘aqueous phase’ layer, mostly methanol, on the top. The lipids are mostly confined to the bottom ‘organic phase,’ so they are extracted from the lower chloroform layer.

2.3.6 Double-phase solvent system

The supernatant from the above is then further extracted using $H_2O/CH_3OH/CHCl_3$ at a ratio of 0.9/1/1 by adding 1.7 ml aqueous 155 mM ammonium acetate (this is your water) and 2 ml chloroform $CHCl_3$. After gentle mixing, centrifuge at 2,800 x g for 15 minutes at 4°C. The double layer that results consists of a top layer of aqueous methanol/water and a bottom layer of organic chloroform containing lipids. Using a long glass Pasteur pipette, the organic chloroform containing lipid layer is removed and transferred to a new pre-weighed glass vial. The methanol-water layer is washed again with half volume of extracting solvents with 0.85 ml of aqueous 155 mM ammonium acetate and 1 ml chloroform. After centrifugation, as before, the lower chloroform layer is removed and added to that collected after the first centrifugation. The lipid-rich chloroform is then dried gently under nitrogen. Once completely dry, the glass vial is re-weighed to calculate the total lipid extract before reconstituting with pure chloroform to 10 mg/ml and then stored at -20 °C until analysis.

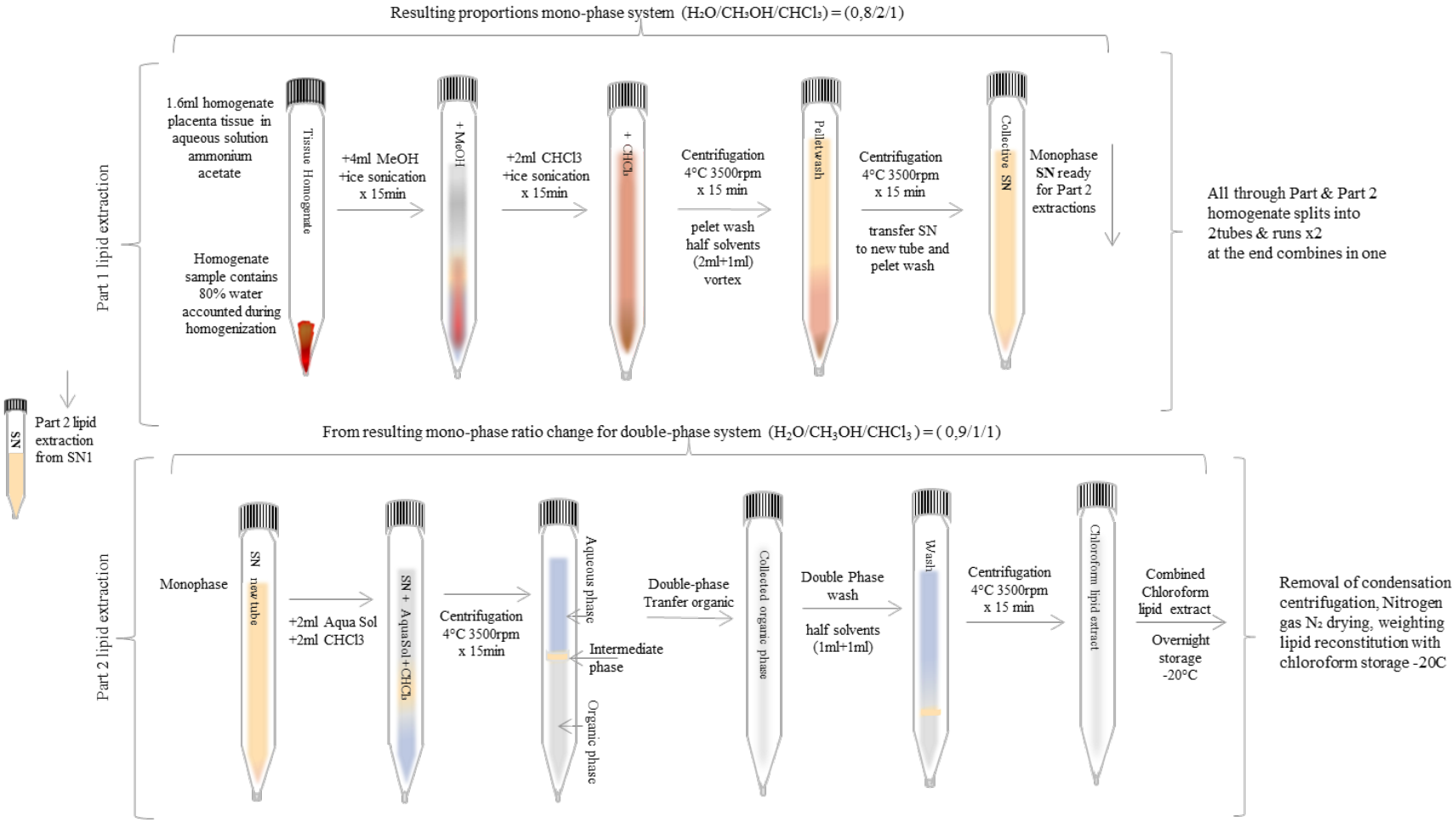

Figure 2:12 Legend to (Figure 2.12): Placenta lipid extraction starts with Part 1 of lipid extraction H2O/CH3OH/CHCl3 (0.8/2/1), then creating double phase for extraction H2O/CH3OH/CHCl3 (0.9/1/1) (Bligh and Dyer 1956) (225). All schematics are hand-made in PowerPoint using i-pen and saved as jpeg.

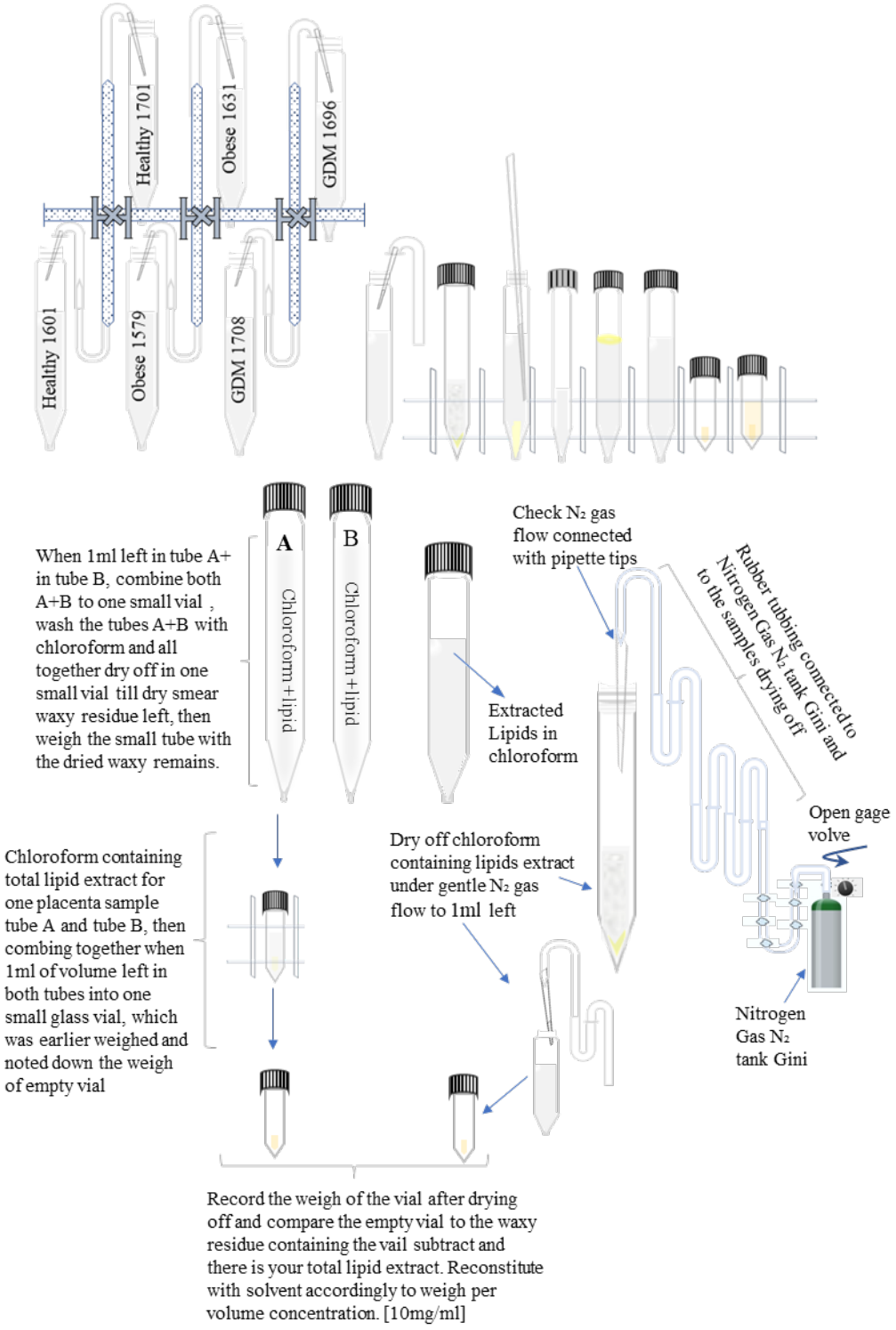

Figure 2:13 Overview method protocol of placenta lipid extraction solvent drying off using nitrogen gas and transferring it from large tubes into small vials and weighing the dried residue before reconstituting in solvent chloroform as weigh per volume concentration to [10mg/ml].

2.3.7 Thin Layer Chromatography

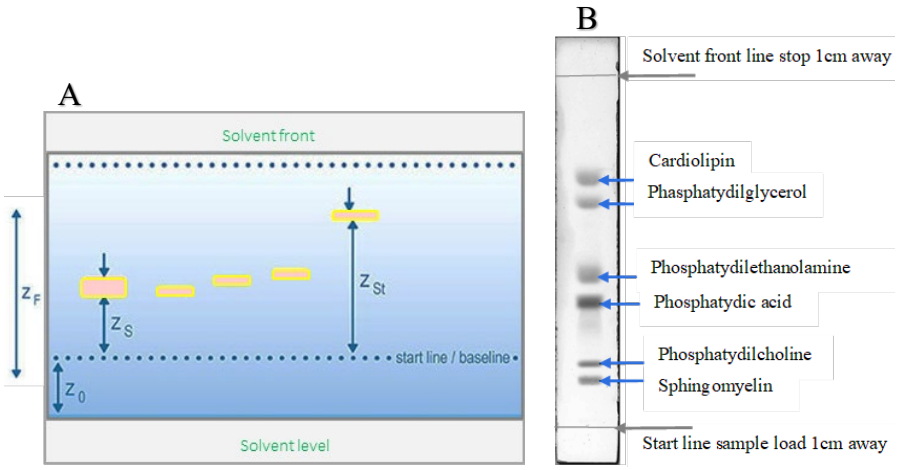

Figure 2:14 The thin-layer chromatogram (A) shows the migration behaviour of separated substances.

As a result of migration distances of separated substances behaviour in the TLC experiment shown in (Figure 2.13 A and B), it estimates the retardation factor (RF), which is the measure of the distance travelled by the sample against the distance travelled of the solvent front top line. Identity confirmation uses Rf values compared to corresponding standards run under identical conditions. (RF) means the retardation factor and is equal to Zs / Zf – Z0; the distance (Zs) between the substance zone and the starting line (mm); the distance (Zf) between the solvent front and the solvent liquid level (mm) and (Z0) indicates how far the solvent liquid level is from the starting line (mm)—image (A) diagram of TLC plate showing solvent level, separation bands and solvent from distances. Image (B) is an example of a TLC plate strip cut off the preparative TLC used to analyse biological phospholipids. It demonstrates the lipid band's neat separation of phospholipids in the TLC results. The black and white TLC strip adapted from literature modified with annotation additions to the original *(253)*. They used electrospray (ESI) mass spectrometry and prior thin-layer chromatography to separate phospholipids—retardation factor (Rf) on TLC elution order. Rf is calculated by dividing the distance moved by the sample species from the baseline to the top line of the solvent front by the distance moved by the lipid reference standards. It gives the difference of the moved sample. Theoretically, this equation applies if the solvent mobile phase and extraction steps are the same. Because species share complex molecular similarities, a millimetre measurement is not always an exact measurement as the physical parameter. As an

example of the elution of lipid species, Rf distances in millimetres were originally conducted by Lerey et al. (1987) *(531)*.

Rf mm Compound (lipid species)	**Assignment**
0.08 mm Lysophosphatidylcholine (LPS)	Band 1/ Band 2
0.11mm Sphingomyelin (SM)	Band 1/ Band 2
0.21mm Lysophosphatidylcholine (LPC) 0.21mm Phosphatidylcholine (PC)	Band 1/ Band 2 Band 3
0.22 mm Cerebroside type I	Band 1/ Band 2
0.25mm Cerebroside type II	Band 1/ Band 2
0.26 mm Phosphatidylinositol (PI)	Band 1/ Band 2
0.32mm Sulfatides	Band 1/ Band 2
0.32mm Lysophosphatidylethanolamine (LPE) 0.32 mm Phosphatidylcholine (PC)	Band 2 Band 3
0.38mm Phosphatidylserine (PS)	Band 2
0.47 mm Phosphatidylglycerol (PG)	Band 2
0.51mm Phosphatidylethanolamine (PE)	Band 4
0.58 mm Phosphatidic acid (PA)	Band 4
0.68 mm Cardiolipin (CL)	Band 5
0.70 mm Ceramide (CER) Sphingosine Fatty acids esters	Band 5
0.74 mm Free fatty acids	Band 6
0.81mm N-acyl phosphatidylethanolamine	Band 6
0.96mm Cholesterol	Band 6/ Band 7
0.98mm Mono, di and triacylglycerols	Band 6/ Band 7

Table 2.4 As an example of the elution of lipid species Rf distances in millimeters conducted originally by Lerey et al. 1987. It confirms theoretical distance elution with the Avanti lipids reference table of standards. The bands were assigned by the student based on the original estimated measurements by hand using a soft ruler. They were compared to visual observations of lipid standards and eluted distances. Based on the ruler's estimated measurements, this study confirmed distance elution with lipid maps. Solvent Systems Lipid Migration: Charts are included below. Lipids standards Avanti Polar USA date of access 30 March 2020, linked verified last accessed 26 January 2024. https://avantilipids.com/wpcontent/uploads/2015/11/SolventSystemsChart.pdf.

2.3.8 Stationary phase

TLC uses glass or aluminium plates coated with silica gel, allowing the samples to adhere and partition during migration as the mobile phase solvent rises through the plate. This study used 20cm x 10cm glass plates coated in silica gel (HPTLC Silica gel 60 RP-18). Preparing the plate for sample loading involves line drawing with a soft pencil, plate washing and oven activation at 180°C. Preheat oven temperature to 185°C for one hour. Draw the lines 1.5 cm from the top and 1.5 cm from the bottom, with sample wells of 5mm starting 1.5 cm from the left spaced every 1cm across the

plate, stopping 1cm from the right-hand side (Figure 2.6). Washing TLC plates requires 50:50 % v/v methanol: chloroform (MeOH: $CHCl_3$ 50:50 v/v). The first wash uses 50 ml, and the second uses 30 ml. The plate is allowed to dry at room temperature for one hour before oven activation for 2 hrs at 180°C.

2.3.9 Sample loading

Plate layout accommodates 6 samples and 6 lipid standards or 8 samples and 4 standards, depending on the experiment. Typically, the reference samples are loaded, followed by the experimental samples and the standards. Cholesterol, TAG, DAG, and MAG mix (all Avanti Polar, Alabama, USA) were standard. Placental and plasma lipid samples were loaded as 10µL of 8 µg/µl, and standards were loaded as 10µL of 5 µg/µl using Hamilton glass syringes. When all samples and standards are loaded onto the TLC plate, the plate is placed into the glass tank, gently resting the bottom of the plate on the gridded lines in the tank and the top of the plate is leaning against the tank wall so that the plate is at an angle.

2.3.10 Materials, solvents, and standards are included in all TLC experiments.

2.3.11 Lipid standards

All lipid standards are purchased from Avanti Polar, Alabama, USA. The original samples contain a *"stock concentration"* of 10 mg/ml. Once opened, sets of aliquots were distributed into two vials and kept at -20 °C. The aliquoted portion of stock standards was diluted accordingly with pure chloroform to make a *"working standards concentration"* of 1 mg/ml, which was used throughout this research study in all TLC samples and all MALDI ToF MS as well as with the University of Warwick collaborator from the first day of opening.

- Brain PS contains chloroform L-α-phosphatidylserine (Brain, Porcine) sodium salts reference code:840032C-10MG-B827; [MW 824.966 g/mol], stock 1x10 mg (1mL); concentration [10mg/ml]; made aliquots 2 x (500ml).
- Soy PI contains chloroform, L-α-phosphatidylinositol (Soy) sodium salt, reference code: 840044C-10MG-D-179 [MW 866.647 g/mol], 1 x 10 mg (1mL) [10 mg/ml], (5 x 200ml).

- Egg SM contains chloroform, Sphingomyelin (Egg, Chicken), reference code: 860061C-25MG-A-116 [MW 710.965 g/mol], 1 x 25 mg (2.5 mL) [10 mg/ml] (3x 500ml 5x 200ml).
- 18:1 LysoPE contains chloroform, 1-oleoyl-2hydroxy-sn-glycerol-3-phosphoethanolamine, reference code:846725C-25MG-A-056, [MW 479.588 g/mol], 1 x 25 mg (2.5 mL) [10 mg/ml] (3 x 500ml, 5 x 200ml).
- 18:1 LysoPC contains chloroform, 1-oleoyl-2hydroxy-sn-glycerol-3-phosphocholine, reference code: 845875C-25MG-A-072 [MW 521.667 g/mol], 1 x 25 mg (2.5 mL) [10 mg/ml], (3 x 500ml, 5x 200ml).
- 16:1 (Δ9-Cis) PC, contains chloroform, 1,2-dipalmitoyl-sn-glycerol-3-phosphocholine, reference code: 850358C-25MG-B-046 [MW 730.007 g/mol], 1 x 25 mg (2.5 mL) [10 mg/ml], (3x 500ml, 5x 200ml).
- 18:1 Cardiolipin contains reference code: 710335C-25MG-B-056 [MW 1501.959 g/mol], 1 x 25 mg (2.5 mL) [10 mg/ml] (3x 500ml, 5x 200ml).
- 15:0 Cholesteryl-d7ester, cholesteryl-d7 pentadecanoate, reference code: 700144p-10MG-A-011 [MW 618.095 g/mol], 1x10 mg powder [10 mg/ml] (2x 500ml)
- Cholesteryl Sulphate 700016P-25MG-E-013 [MW 488.699 g/mol], 1 x 25 mg powder [10 mg/ml] (5x 500ml); Mix standard concentration [1mg/ml] prepared by Dr Lopalco during her visit and included (monoglycerides, diglycerides, triglycerides)
- TLC plates (10x10cm, 10x20cm) silica gel coated Merck (Merck TLC Silica gel 60, Glass plates). Acetonitrile, ACS reagent, ≥99.5%.
- Flex Analysis version 3.3 MALDI-TOF MS MicroFlex LRF. MALDI Matrix: 9 Aminoacridine (9-AA) hemihydrate - Acros Organics (Morris Plains, NJ) 98%; 2,5-dihydroxybenzoic acid (DHB)-Fluka Germany.
- Lipid standards Avanti Polar Lipids, (Inc. USA). Glass ampules content from (1 ml) to (2.5 ml) stocks at concentration [10 mg/ml].
- Working standards diluted with pure chloroform $CHCL_3$ [1mg /ml].
- Chloroform 34854 2.5l Sigma-Aldrich UK with amylene stabiliser Chloroform 650471 1L purity 99.9% for residue analysis 0.5-1% with ethanol stabiliser.
- Methanol 34885 2.5L 99.9% HPLC-MS Grade Sigma-Aldrich UK.
- Nitrogen Genie British GAS BOC 1066, compressed G20EC 231-783-9, 300 15°C.
- Pyrex glass tubes 15ml disposable cap GPI 15-415 Corning Life Science Mexico.
- Analytical Balance AND-Medical accuracy 0.01mg. (Japan).

Glass Vials (1.5ml) Fisher Scientific HPLC certified 1343-9748 blue inserts tops. Hamilton glass syringes 5µL, 10µL, 50µL, 100µL Cole Palmer UK. Pork skin gelatine powder Sigma Aldrich Merck Life Science UK Limited CAS RN: 9000-70-8 Synonyms: Gelatine, Teleostean gelatine (G7765 and G7741). All detailed materials in the Appendix.

2.3.12 All samples and Body Mass Index BMI (kg/m2)

Placenta Plasma extracted all samples run on TLC Plates and then MALDI ToF MS

Sample ID	BMI
1614	32.4
1615	20.9
1616	28.7
1617	25.2
1618	23.4
1619	36.7
1620	23.8
1621	24.7
1622	40.4
1623	27.1
1624	22
1625	25.2
1626	29.3
1627	22
1628	45.3
1629	23.8
1630	24.7
1631	30.5
1632	23.9
1633	29.6
1634	35.3
1635	21.3
1636	31.8
1637	53.4
1638	20.8
1639	20
1640	31.9
1641	22.9
1642	25.3
1643	25.4
1708	26.1

Sample ID	BMI
1709	44.9
1710	23.8
1711	32.7
1712	29.8
1713	38
1714	20.3
1715	21
1716	26.1
1717	28.7
1718	33.7
1719	42.6
1720	29.8
1721	22.5
1722	21.5
1723	36.8
1724	38.5
1725	22.3
1726	27
1727	25.7
1728	26.8
1729	40.4
1730	30.1
1731	26.7
1732	43.4
1733	31.4
1734	21.7
1735	26.3
1736	28.8
1737	31.5
1738	20.8
1739	24.4

Sample ID	BMI
1740	32.4
1741	31.6
1742	42
1743	29.7
1744	33.1
1745	-
1746	31.2
1747	27.8
1748	23.9
1749	26.8
1750	33.9
1751	26.3
1752	50.6
1753	23.9
1754	17.1
1755	24.6
1756	20.3
1757	20.8
1758	26.8
1759	34.2
1760	21.9
1761	41.6
1762	31.2
1763	23.5
1764	29.1
1765	-
1766	33.3
1767	23.3
1768	22.9
1769	20.2
1770	36.1
1771	58.3
1772	22.5
1773	32.5

Sample ID	BMI
1774	20.3
1775	30.1
1776	27.7
1777	23
1778	25.8
1779	23.1
1780	22.5
1781	42.2
1782	29.2
1783	34.5
1784	25.3
1785	44
1786	29.8
1787	22.9
1788	36.9
1789	42.9
1790	47.3
1791	25.5
1792	23
1793	31.6
1794	21.8
1795	40.5
1796	31.5
1797	31.9
1798	33.3
1799	22.8
1800	35.1
1801	35
1802	35.7

Sample ID	DATE	BMI	GDM
1643	26/05/2021	25.4	
1644	01/06/2021	40.8	
1645	03/06/2021	22.9	
1646	03/06/2021	21.5	
1647	04/06/2021	24.8	
1648	04/06/2021	25	
1649	07/06/2021	24.5	
1650	07/06/2021	32.4	
1651	09/06/2021	29.3	YES
1652	09/06/2021	19.4	
1653	10/06/2021	26.4	
1654	11/06/2021	40.5	
1655	14/06/2021	36.1	
1656	15/06/2021	50	
1657	15/06/2021	21.3	
1658	21/06/2021	26.3	
1659	21/06/2021	29.1	
1660	21/06/2021	25.3	
1661	25/06/2021	47.7	YES
1662	28/06/2021	27.3	
1663	28/06/2021	22.5	
1664	01/07/2021	40.6	
1665	01/07/2021	27.7	
1666	02/07/2021	29.3	
1667	02/07/2021	25.8	
1668	05/07/2021	28	
1669	05/07/2021	32.8	YES
1670	06/07/2021	49.5	
1671	06/07/2021	36	
1672	07/07/2021	34.4	
1673	07/07/2021	25.9	
1674	09/07/2021	34.5	

Sample ID	DATE	BMI	GDM
1675	09/07/2021	34.4	
1676	12/07/2021	28.4	
1677	12/07/2021	44.6	YES
1678	13/07/2021	26.3	
1679	15/07/2021	25.5	
1680	15/07/2021	30.4	
1681	15/07/2021	23.4	
1682	19/07/2021	34	
1683	19/07/2021	25.2	
1684	20/07/2021	22.1	
1685	20/07/2021	22	
1686	21/07/2021	30.9	
1687	22/07/2021	22.5	
1688	22/07/2021	26	
1689	22/07/2021	34.1	
1690	23/07/2021	45	
1691	23/07/2021	36	
1692	27/07/2021	35.3	
1693	27/07/2021	28.3	
1694	02/08/2021	25	
1695	02/08/2021	24.7	
1696	02/08/2021	32.9	
1697	03/08/2021	31.6	
1698	03/08/2021	42.5	
1699	04/08/2021	42.2	YES
1700	06/08/2021	36.4	
1701	09/08/2021	24.5	
1702	09/08/2021	20.5	
1703	10/08/2021	34.5	
1704	10/08/2021	39.8	
1705	16/08/2021	27.3	
1706	17/08/2021	22.7	
1707	17/08/2021	27.1	
1708	23/08/2021	26.1	

Table 2.5 Placenta or plasma content of all samples extracted and run on bioanalytical TLC and then MALDI ToF MS body mass index BMI measure kg/m^2 is used to determine types of pregnancies BMI in National Health Service Wales NHS Wales is divided by pregnancies BMI: Very Healthy (up to 25 BMI), Normal Healthy UK (25-30 BMI), Obese (30-60) gestational diabetes Mellitus GDM 30-60 BMI.

2.3.13 All samples of TLC layouts plan

Placenta Plasma TLC Layout of all samples run on TLC Plates and then MALDI ToF MS

Study 1 Placenta
A 1351 1351 PI SM LPE LPC PC PG Chol PE5µg PE10µg
B 1351 1351 PI SM LPE LPC PC PG Chol PE5µg PE10µg
Study 2 Placenta
QC1 1351 1342 1342 1342 1342 Chol PE PG PC SM PI LPE
QC2 1351 1342 1342 1342 1342 Chol PE PG PC SM PI LPE
QC3 1351 1342 1342 1342 1342 Chol PE PG PC SM PI LPC
QC4 1351 1342 1342 1342 1342 Chol PE PG PC SM PI LPC
Study 3 Placenta /Plasma
A1 1351 1342 1487 1489 1492 1491 1500 1495 1499 1494 1496 1502 Chol.Sulf
A2 1351 1342 1487 1489 1492 1491 1500 1495 1499 1494 1496 1502 Chol.Sulf.
A3 1342 1487 1489 1492 1491 1500 1495 1499 1502 1494 PE LPE
B1 513 515 009 458 359 474 518 424 1511 1515 Chol Sulf.
B2 513 515 009 458 359 474 518 424 1511 1515 Chol Sulf.
B3 009 359 513 515 458 474 518 424 1511 1515 PE LPE
Study 4 Placenta /Plasma
A 1487 1489 1491 1492 1494 1496 1495 LPC SM LPE PC PE
B 1499 1500 1501 1502 1509 1512 1514 PI PC PG PE Mix: MAG DAG TAG
C 1515_1 1515_2 1516 1518 11 12 424 LPC SM LPE PC PE
D 458 474 513 515 518 359 009 PI PC PG PE Mix:MAG DAG TAG
Study 5 Plasma
A 424 458 497 384 474 480 LPC SM LPE PC PE CL18:1
B 513 515 518 1531 1532 1543 LPC SM LPE PC PE CL18:1
C 1549 1639 1642 1544 1643 1557 1565 LPC SM PC PE CL18:1

Study 5 Placenta
D 1509 1487 1489 1495 1502 1512 LPC SM LPE PC PE CL18:1
E 1534 1491 1516 1342 1492 1500 LPC SM LPE PC PE CL18:1
F 1534 1491 1516 1342 1492 1500 LPC SM LPE PC PE CL18:1
Study 6 Non-pregnant plasma
A 424 518 458 497 384 474 480 515 PI SM LPE PC
B 458 497 384 474 480 513 515 518 LPC SM LPE PC
Study 6 Pregnant plasma healthy obese GDM
C 1501 1502 1509 1515 1516 1518 1531 1534 LPC SM PC PE
D 1531 1532 1543 1544 1549 1593 1557 1606 LPC LPE PC PE
E 1530 1545 1578 1558 1564 1565 1568 1574 LPC LPE PC PE
Study 7 all plasmas in neutral solvent
A 1531 1532 1543 1549 1639 1642 1643 1565 1564 1544 Chol Mix
B 1558 518 424 458 497 384 474 420 513 515 Mix Chol
C 1613 1614 1639 1593 1606 1557 1531 1532 009 359 Mix Chol
D 1530 1545 1568 1574 1564 1578 1565 1515 1557 1577 Mix Chol
Study 8 all placenta in neutral solvent
A 1509 1487 1489 1495 1502 1512 1534 1491 1516 1342 Mix Chol
B 1492 1500 1501 1531 1499 1578 1505 15111557 Mix Chol
C 1494 1496 1512 1513 1530 1545 1564 1565 1539 1538 Mix Chol
D 1574 1577 1514 1613 1644 1622 1515 1545 1564 1568 Mix Chol
E 1501 1502 1509 1515 1516 1518 1531 1534 1491 1495 Chol Mix Trgs
F 1494 1496 1512 1593 1530 1564 1565 1578 1545 1502 Chol Mix Trgs

Placenta Plasma TLC Layout of all samples run on TLC Plates and then MALDI ToF MS

Study 9a September 2021 Six months of method improvement after overcoming contamination
A 1531 1532 1543 1544 1549 1557 1593 1606 LPC LPE PC PE
B 1613 1614 1636 1636 1642 1643 LPC LPE PC PG PE Chol
C 1530 1545 1558 1564 1565 1568 LPC LPE PC PG PE Chol
D 1530 1545 1558 1564 1565 1568 LPC LPE PC PG PE Chol
E 480 497 513 515 LPC PI PE SM LPE PC PG Chol
F 518 1574 1577 1578 LPC PI PE SM LPE PC PG Chol
G 1531 1532 1543 1549 LPC PI LPE SM PC PG PE Chol
H 1639 1642 1643 1564 LPC PI LPE SM PC PG PE Chol
Study 9b October 2021
A 1501 1509 1534 1531 1491 1495 1516 1518 1515 1502 LPC PC
B 1487 1489 1492 1499 1500 1514 1539 1505 1622 1342 LPC PC
C 1494 1512 1513 1530 1564 1565 1578 1496 1545 LPC PI PC
Study 9b November 2021
D 1531 1534 1606 1550 1622 1669 1578 1545 Blank PI LPC PC
E 1531 1534 1606 1550 1622 1669 1578 1545 Blank PI LPC PC
F 1531a 1531b 1531c 1669a 1669b 1669c 1606a 1606b 1606c LPC LPE PC PE
Study 9c December 2021
A 1568 1699 1494 1545 1677 1574 blank 1487 1759 1499 1492 1514
B 1622 1655 1606 1500 1656 1670 1686 1505 1539 1489 LPC PC
C LPC PC
Study 9c January 2021
D 1542 1516 1491 1551 1543 1552 1514 1515 1518 1545 LPC PC
E 1547 1534 1495 1537 1501 1509 1502 1549 1546 1548 LPC PC
F 1681 1688 1678 1676 1702 1679 1684 1681 1653 1531 LPC PC
Study 9c March 2022 last New homogenization all healthy placentas only March 2022
G 1688 1676 1621 1645 1706 1679 1707 1702 PI LPC LPE CL18:1
H 1621 1678 1706 1574 1763 1687 1534 1687 LPC PI LPE PC

Study 10 Comparative study 3 solvents 12 heathy 12 obese 12 gdm
Study 10 Acidic solvent mobile phase
A1 1708 1574 1645 1500 1670 1759 1677 1578 1661 PI LPC PC
B1 1688 1702 1707 1644 Blank 1771 1564 1719 1651 PI LPC PC
C1 1706 1679 1687 1606 1550 1655 1496 1785 1574 PI LPC PC
D1 1701 1763 1621 1680 1622 1656 1699 1545 1577 PI LPC PC
Study 10 Basic solvent mobile phase
A2 1708 1574 1645 1500 1670 1759 1677 1578 1661 CL18:1 PC PE
B2 1688 1702 1707 1644 1614 Blank 1564 1719 1651 LPC PC PE
C2 1706 1679 1687 1606 1550 1655 1496 1785 1574 LPC PC PI
D2 1701 1763 1621 1680 1622 1656 1699 1545 1577 LPC PC CL18:1
Study 10 Neutral solvent mobile phase
A3 1708 1574 1645 1500 1670 1759 1677 1578 1661 Mix:TAG,DAG,MAG
B3 1688 1702 1707 1644 1614 1771 1564 1719 1651 Chol.Est. Mix:TAG,DAG,MAG
C3 1706 1679 1687 1606 1550 1655 1496 1785 1574 Chol.Est. Mix:TAG,DAG,MAG
D3 1701 1763 1621 1680 1622 1656 1699 1545 1577 Chol.Est. Mix:TAG,DAG,MAG

Table 2.6 All TLC experiment layouts from Study 1 to Study 10

2.4 Experiment TLC Results Setting up quality control (QC)

The first step was to ensure good quality lipid extraction and TLC by repeatedly extracting and processing from the same placenta of a normal-weight woman and running in parallel with samples prepared by Dr Lopalco, who taught this technique. The purpose is to establish a baseline of the sample homogenisation and solvent extraction with bioanalytical checking using TLC to a reasonable qualitative level. Extractions and analysis of samples from one placenta on four different days across two months showed good reproducibility (Figure 2.9).

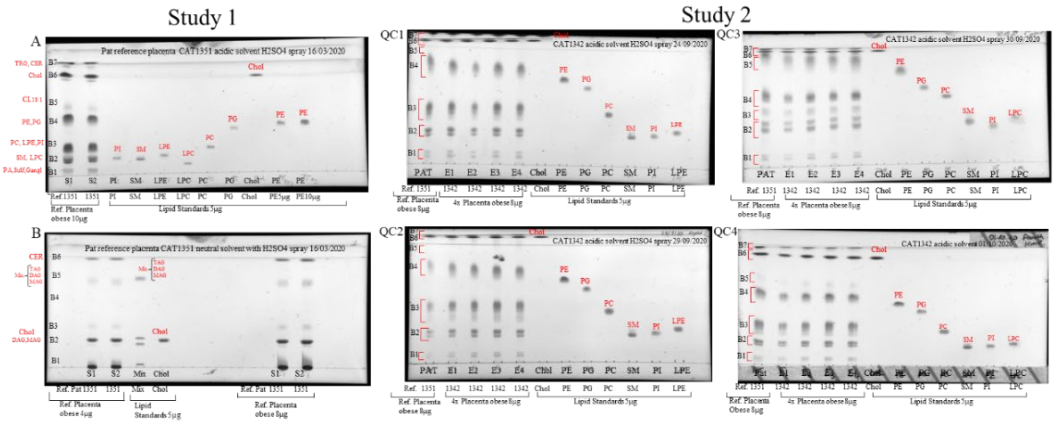

Figure 2:15 Quality control and reproducibility. Samples were extracted and run in acid solvent on silica TLC plates. Plates were imaged using Bio-Rad Chem Station white light scanner images saved in .tiff format using a calorimetric set filter white light format resolution of 600 pixels.

2.4.1 Optimization of mobile phases and visualisation methods

A series of placental samples from normal-weight, obese, and women with GDM and plasma samples from non-pregnant women were run in various mobilisation solvents and visualised with multiple stains (Figure 2.10). In image A1, the total lipids of the placentas run in acidic solvent and stained with sulphuric acid show much darker or denser spots of the lipid groups in bands 2 to 6 and 7. In contrast, the B1 plasma of eight non-pregnant women and two healthy pregnant placentas shows apparent gaps in bands 1 and 4 to 5. Bands six and seven have much thinner lines than the pregnant placentas extract in A1. The identical A2 lipid extracts, according

to the A1 TLC plate, only show the six and seven bands, which are the most lipophilic lipid groups such as sterols, triglycerides, and cholesterol at the top line, but the mobile phase has overrun. B2, on the other hand, the non-pregnant plasma sample and two placentas lipid extracts show bands 2 and 3 with bands 6 and 7. It could mean that those lipids contain phosphate groups. A3 TLC placentas lipids, according to plate A1, were incubated in the mobile phase with a neutral solvent and sprayed with ninhydrin to determine amino acids, with the lipid standards used in this case being PE and LPE. It shows lipid band 2 with darker and denser lipid spots in placentas samples, while B3 TLC, with non-pregnant plasma and two placenta samples, shows much lighter lipid spots in band 2. It demonstrates the start of observing and understanding the elution and separation of similar lipid molecules to properly separate and visualise lipid classes within the placenta and plasma.

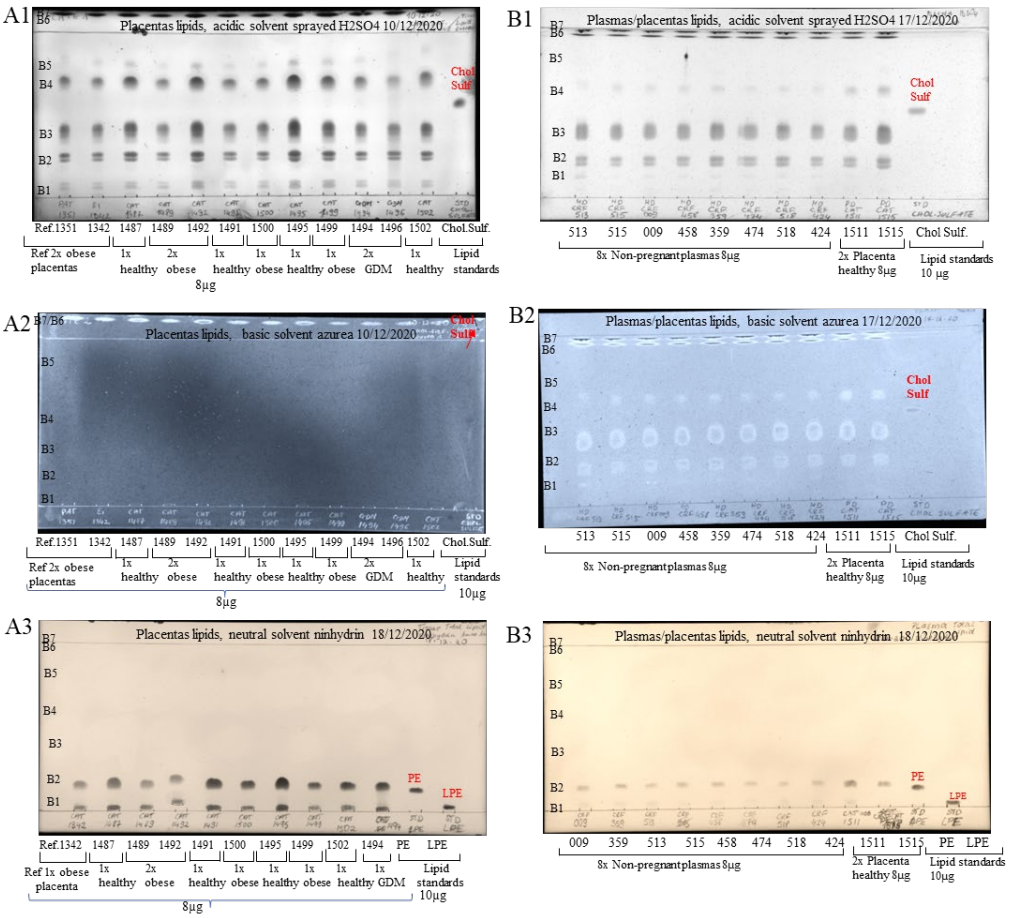

Figure 2:16 Comparison of different mobile phase solvents and visualisation methods of placental and plasma lipid extracts. Lipids extracted from (A) placenta and (B) plasma were separated and visualise using (1) acidic mobile phase and sulphuric acid, (2) basic mobile phase and Azure A, and (3) neutral mobile phase and ninhydrin. Each TLC has 12 spots and contains the following placental - healthy n=4; obese n=6; GDM n=2 – or plasma samples from 8 non-pregnant women, and the last spot is lipid standard cholesterol sulphate (Chol Sulf) for acidic and basic solvent or last two spots PE and LPE for neutral solvent. Plates were imaged using Bio-Rad ChemStation white light scanner images saved in tiff format using a calorimetric set filter white light format resolution of 600 pixels.

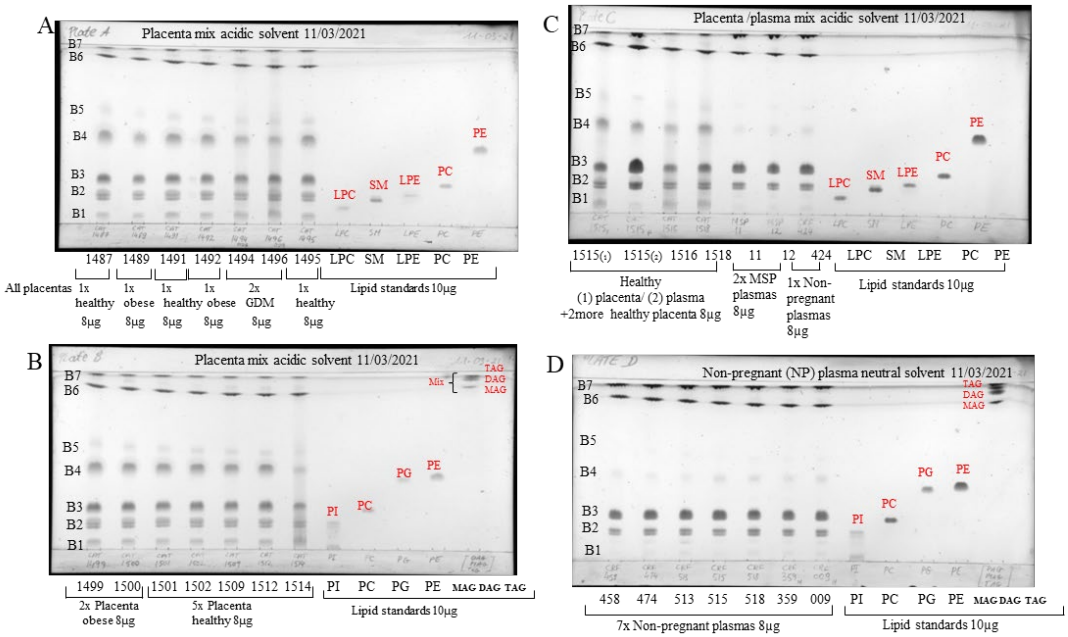

Figure 2:17 Analysis of placenta and plasma samples using acid and neutral solvents visualise using sulphuric acid. The sample type in each well is labelled in the figure. Lipid standards vary on the plate, such as LPC, SM, LPE, PC, or PE. PI, PC, PG, PE, and a mix containing mono, di, triglycerides. Plates were imaged using Bio-Rad ChemStation white light scanner images saved in .tiff format using a calorimetric set filter white light format resolution of 600 pixels.

2.4.2 Continuity of sample extraction and observing how and what to improve

Each time a new placenta or plasma sample came to the laboratory, they were subjected to sample handling and preparation for storage at -80 °C until they were ready for homogenisation and total lipid extraction, followed by TLC quality and precision assurance. In Figure 2.17, plates A, B and C were a mixture of different placentas and plasma total lipid extracts, all incubated in the acidic mobile phase, then air-dried and sprayed with 5 % (v/v) sulfuric acid (90% pure) fixing agent, then a hot air-dried before putting them in the oven at 180 °C for ten minutes to see the change of the lipid spots. Plate D was run in a neutral mobile phase and contained non-pregnant plasma samples with lipid standards (Figure 2.17). The four plates have similarities in TLC plate A and TLC plate B, which include healthy, obese GDM placenta with clear separation of lipids from band 1 to band 7.

2.4.3 Identification of lipid bands

A comparison of TLC lipid bands with lipid standards, literature, and the elution table for lipid maps could indicate what to expect. Lipid band 1 spreading to band 2 includes LPS, SM, LPC, cerebrosides, phosphatidylinositol (Cer-PI), and sulfatides—lipid band 2 LPE, PS, and LPE. Lipid band 3 includes PC, SM, and sphingosine-based choline headgroups. Lipid band 4 includes PG, PE, and phosphatidic acid PA. Lipid band 5 includes CL 18:2, ceramide (CER), sphingosine, fatty acid esters, and squalene. Lipid band 6 / band 7 include the following: squalene, FFAs, N-acyl phosphatidylethanolamine, total cholesterol, cholesterol esters, and triglycerides (monoglyceride, diglyceride and triacylglycerols). The placentas of healthy, obese, and GDM women show all lipid groups, and when compared to the standards on the right side, we can see that the total lipid extract of the placentas contains these species. Some spots are darker or more intense than others in placental lipid extracts, which could mean more lipid species and subspecies are in those bands. Plate C contains a mixture of plasmas and placenta, and contrast is more visible, especially in lipid band 2, showing darker spots in plasma but lighter spots in bands 1 to 5. It could mean fewer hydrolysed lipids in plasma or samples that are not clean enough. The last TLC plate D contains all non-pregnant plasma samples run in a neutral solvent mobile phase, and it clearly shows distinct lipid bands 2 and 3 with upper bands 6 and 7. It shows darker spots of triglycerides, sterols, and cholesterol in non-pregnant samples with high PI, PC and PG. Thus, the main difference is the mobile phase, from acidic to neutral, which distinguishes the apparent differences in lipid species that we can observe.

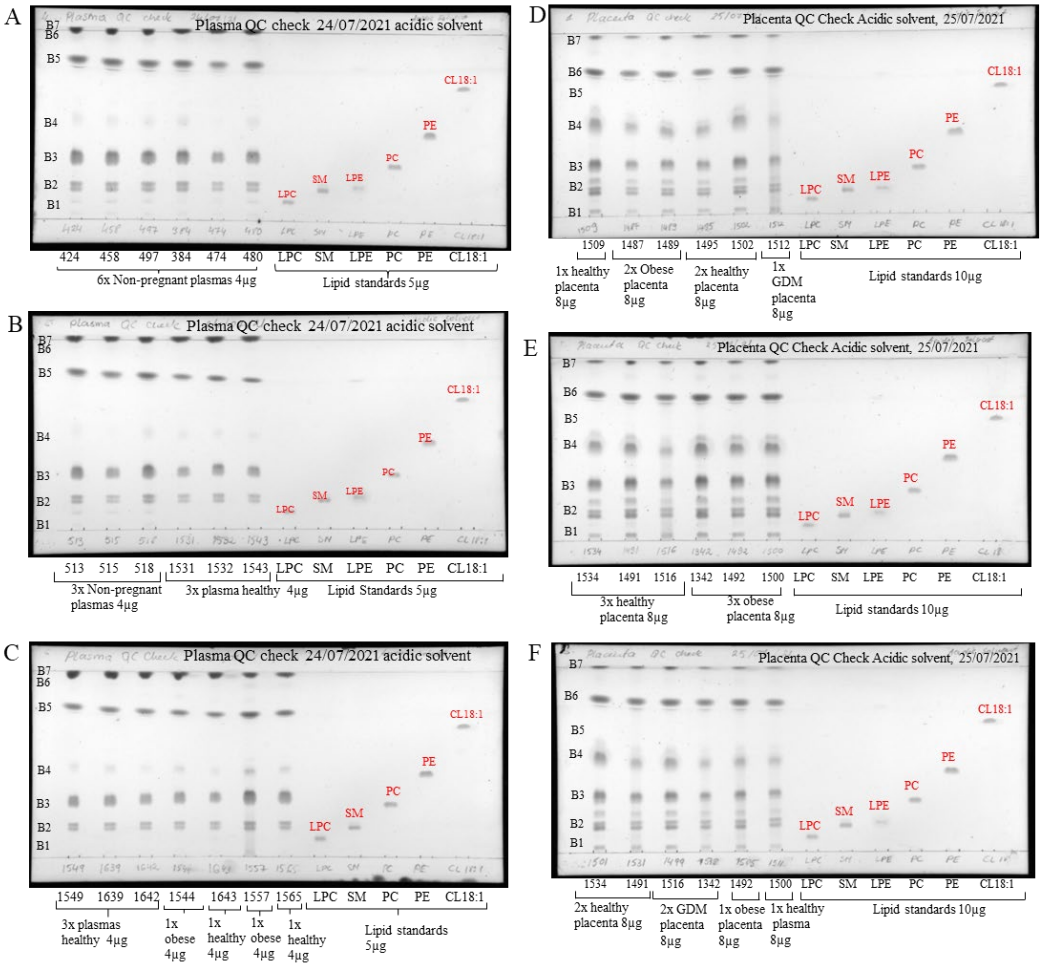

Figure 2:18 Analysis of placenta and plasma samples using acid and neutral solvents visualise using sulphuric acid. The sample type in each well is labelled on the figure, and six lipid standards, LPC, SM, LPE, PC, PE CL18: 1, were included. Plates were imaged using Bio-Rad ChemStation white light scanner images saved in .tiff format using a calorimetric set filter white light format resolution of 600 pixels.

2.4.4 Analysis of plasma lipids with acidic mobile phase

Plates A, B, and C in Figure 2.18 show the initial quality control experiment results of extracted plasma samples from non-pregnant and pregnant women, all incubated and developed with sulphuric acid and charring. Plasma samples in plates A, B, and C show similarities in lipid band 2, lipid band 3, and lipid bands 6 and 7—the presumptive identification of observed lipids in band 2 includes LPE, PS, and LPE. Lipid band 3 includes PC, SM, and Sphingosine-based choline headgroups. Lipid band 4 includes PG, PE, and PA. Lipid band 5 includes CL 18:2, CER, sphingosine, fatty acid esters, and squalene. Lipid band 6 / band 7 include the following: squalene, FFAs, N-acyl phosphatidylethanolamine, total cholesterol, cholesterol esters, and

triglycerides (mono, di and triacylglycerols). The eluting lipid species in plasma samples are sphingomyelin belonging to sphingolipids, shown on the image as SM, then PC and lighter spots in PE and darker spots in the top of bands 6 and 7, which belong to cholesterol, sterol, triglycerides, and ceramides.

2.4.5 Comparison of plasma samples from non-pregnant and pregnant women

A comparison included lean versus obese pregnant women and women with GDM (n = 8/group; Figure 2.18). In the acidic mobile phase, all plasma samples seem the same. Some spots appear more intense and prominent, while others are more defined. However, all non-pregnant patients show similar bands with darker spots for PC. In contrast, bands 6 and 7 are much darker in healthy BMI plasma, indicating they belong to cholesterol and triglycerides. It appears consistent with pregnancy literature that accumulated sugar is energy stored and converted to fats. The band 1 lipid groups are not displayed in obese and GDM plasma. It suggests that the gangliosides are not visible in acidic plasma since they normally have negative charges and would be more visible in basic plasma. Also, non-pregnant women have a much lower amount of PE compared to healthy, obese GDM patients, which might be due to the amino acids, which are also present in amino acids, and this makes sense and confirms that higher levels of PE occur during pregnancy due to higher levels of protein production and amino acids are the fundamental constituents of protein synthesis, especially in pregnancy.

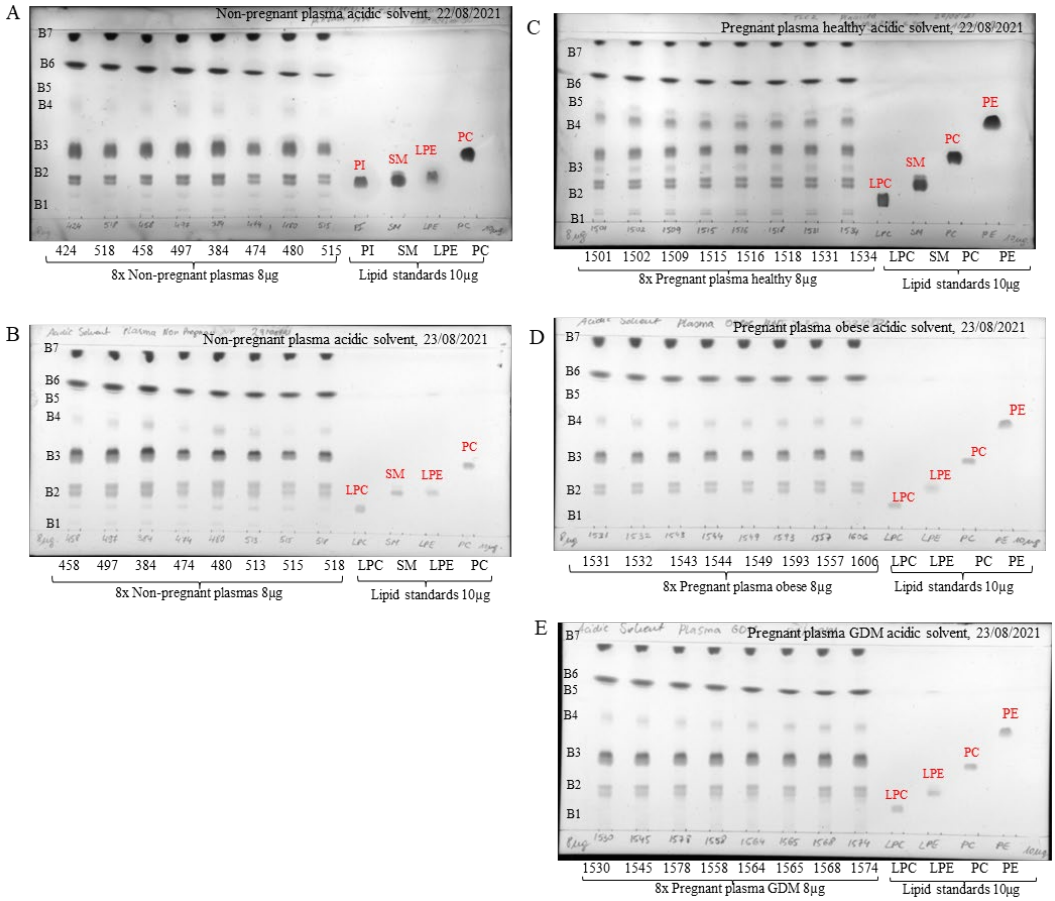

Figure 2:19 shows that plasma samples (A, B, Non-pregnant) exhibit much darker lipid spots than PC, PI, SM, and LPE tissues.

The plate is still dark because it was too long in the oven. Due to this, the scan looks much darker than it should. Similar to Plate C, Plate C appears much darker due to oven overstay and later dark scans. Comparing groups on the same plate rather than separately emphasizes the importance of doing so. Comparing groups should also be done using densitometry or another semi-quantitative method. As seen on Plate C, total lipid extracts are separated, all with healthy body mass indexes. There are no lipid spots on plate D with obese BMI plasma samples, but there are lighter spots in bands 2, 3 and 4. It suggests no hydrolyzed polar groups but more sphingoid lipids such as sphingosine PC, PE gangliosides, and ceramides. In the acidic mobile phase, plates (C, D, E healthy, obese, GDM pregnant plasma) were visualized with sulphuric acid. On each plate, the sample type is labelled and includes samples from non-pregnant women, obese pregnant women, and pregnant women with GDM (n = 8 / group). The lipid standards included in each plate are LPC, LPE, PC, and PE. Images were captured using a Bio-Rad ChemStation white light scanner and saved as .tiff files. Calorimetric image filters with 600-pixel resolution were used to capture images.

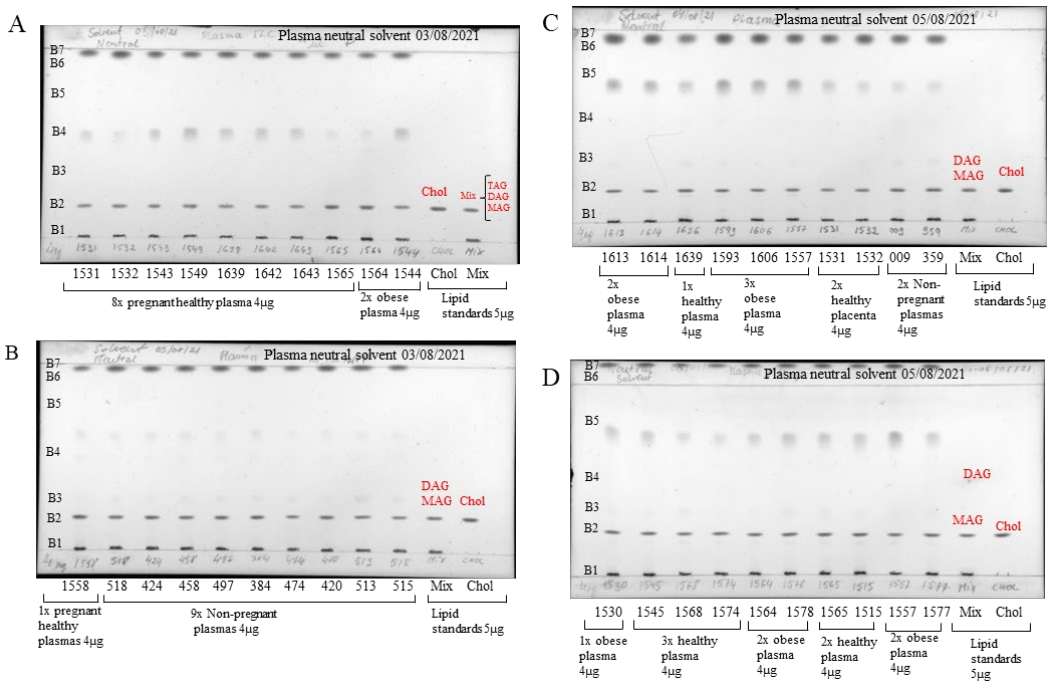

Figure 2:20 Analysis of plasma samples using neutral mobile phase and visualise using sulphuric acid. Sample type in each well is labelled on the figure and includes samples from non-pregnant women, normal-weight pregnant women, pregnant women with obesity and pregnant women with GDM (n = 8 /group); lipid standards were cholesterol and MAG/DAG/TAG mix and were included on every plate. Plates were imaged using Bio-Rad ChemStation white light scanner images saved in tiff format using a calorimetric set filter white light.

2.4.6 Analysis of plasma lipids with neutral mobile phase

The same plasma samples used in Figure 2.20 were separated with a neutral mobile phase for comparison. In all four plates from plate A to plate D, we can see that plasma total lipid extract contains lipids in band 2, which contains cholesterol and triglycerides, and top band 6/7 shows intense dark spots that belong to higher neutral charge lipids and steroids.

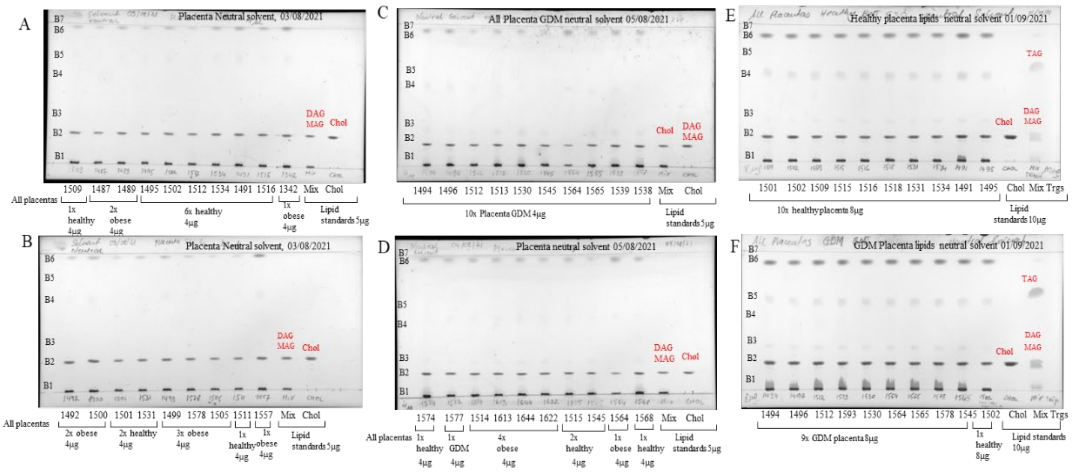

Figure 2:21 Analysis of placenta sample plates TLC-A, TLC-B, TLC-C, TLC-D, TLC-E, and TLC-F using neutral mobile phase and visualise using sulphuric acid. Sample type in each well is labelled on the figure and includes samples from non-pregnant women, normal-weight pregnant women, pregnant women with obesity, and pregnant women with GDM (n=8/group); lipid standards were cholesterol and MAG/DAG/TAG mix and were included on every plate. Plates were imaged using Bio-Rad ChemStation white light scanner images saved in tiff format using a calorimetric filter white light format resolution of 600 pixels.

2.4.7 Analysis of placental lipids with a neutral mobile phase

Plates (A-C) in Figure 2.21 contain sample loading at a half concentration of 4µg, whereas TLC plates (E-F) contain 8µg sample loading to compare the elution of lipid when halved concentration in case there was smearing. It shows that the last two plates (E-F) have darker lipid spots, suggesting more lipids present as expected with double the amount loaded. However, with the samples from the placenta of lean women, there is no smearing, whereas smearing is seen with the GDM placentas. It could be because of poor separation from some unknown methodological reason or some other species trying to separate first, such as glycolipids having additional mono and polysaccharides moieties such as saccharose, pentose, mannose, hexose sugar rings, and alcohols. That would suggest that the GDM placenta contains a high abundance of glycolipids mono and polysaccharides, which would elute first in band 1, leaving the smearing suggesting a richer content of triglyceride storage lipids that are resistant to accumulating saccharides, which correlates with altered carbohydrate metabolism with GDM. Smearing has also occurred in other samples, so contamination of the samples was considered.

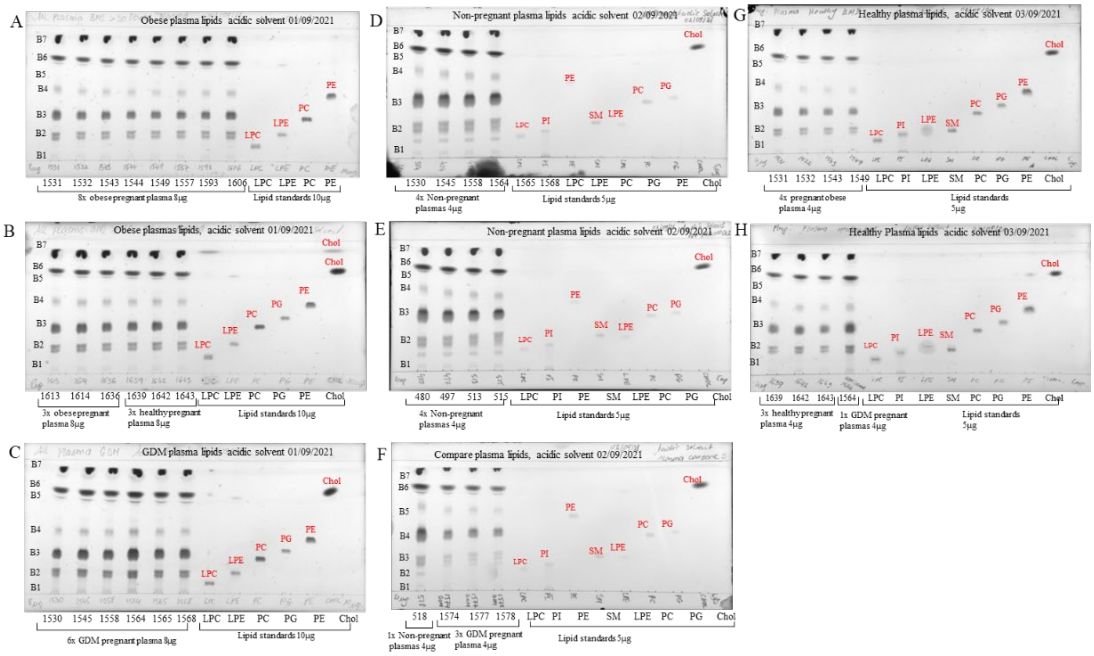

Figure 2:22 Trying 4µg and 8µg concentrations to observe for smearing new homogenization of frozen older chunks healthy obese GDM Centre, random. Analysis of freshly extracted plasma samples using acidic mobile phase and visualisation using sulphuric acid. Sample type in each well is labelled on the figure and includes samples from non-pregnant women, normal-weight pregnant women, pregnant women with obesity, and pregnant women with GDM (n = 8 /group); eight lipid standards LPC, PI, LPE, SM, PC, PG, PE and cholesterol were included on every plate. Plates were imaged using Bio-Rad ChemStation white light scanner images saved in .tiff format using a calorimetric set filter white light format resolution of 600 pixels. It needs changing letters and wrong names.

2.4.8 Re-analysis of plasma lipids with acidic mobile phase

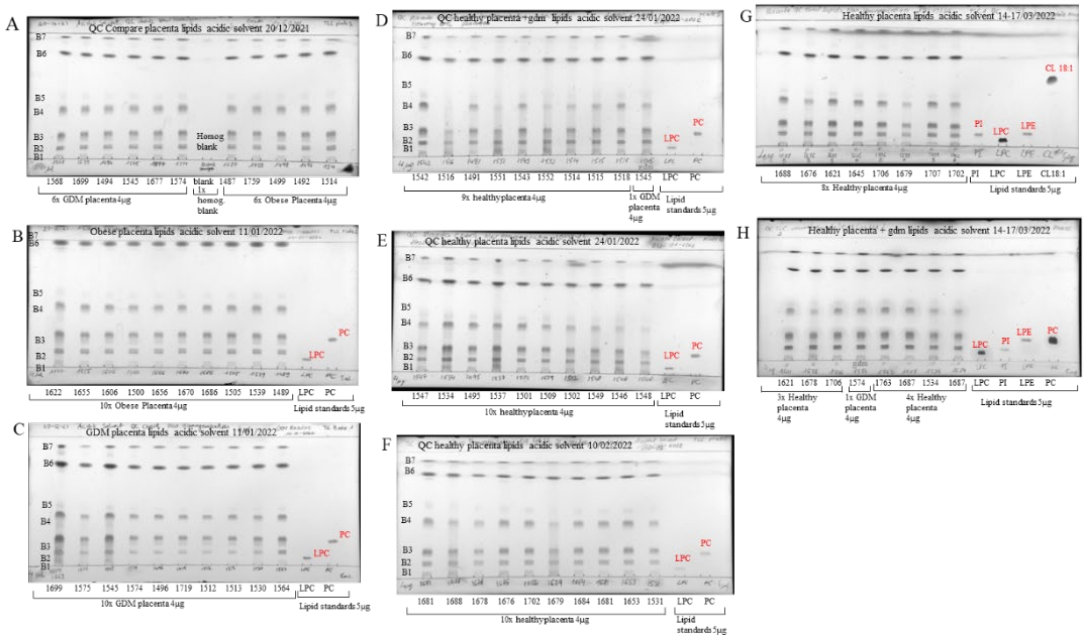

Figure 2:23 Further analysis of plasma samples was made with a more extensive array of standards for better presumptive identification of bands.TLC Plates A, B, C, D, E, and F show the analysis of freshly extracted placental samples using acidic mobile phase and visualised using sulphuric acid. The sample type in each well is labelled on the figure and includes samples from normal-weight pregnant women (n =8/group healthy); lipid standards of LPC and PC +/- PI were included on every plate. Plates were imaged using BioRad ChemStation white light scanner images saved in .tiff format using a calorimetric set filter white light format resolution of 600 pixels.

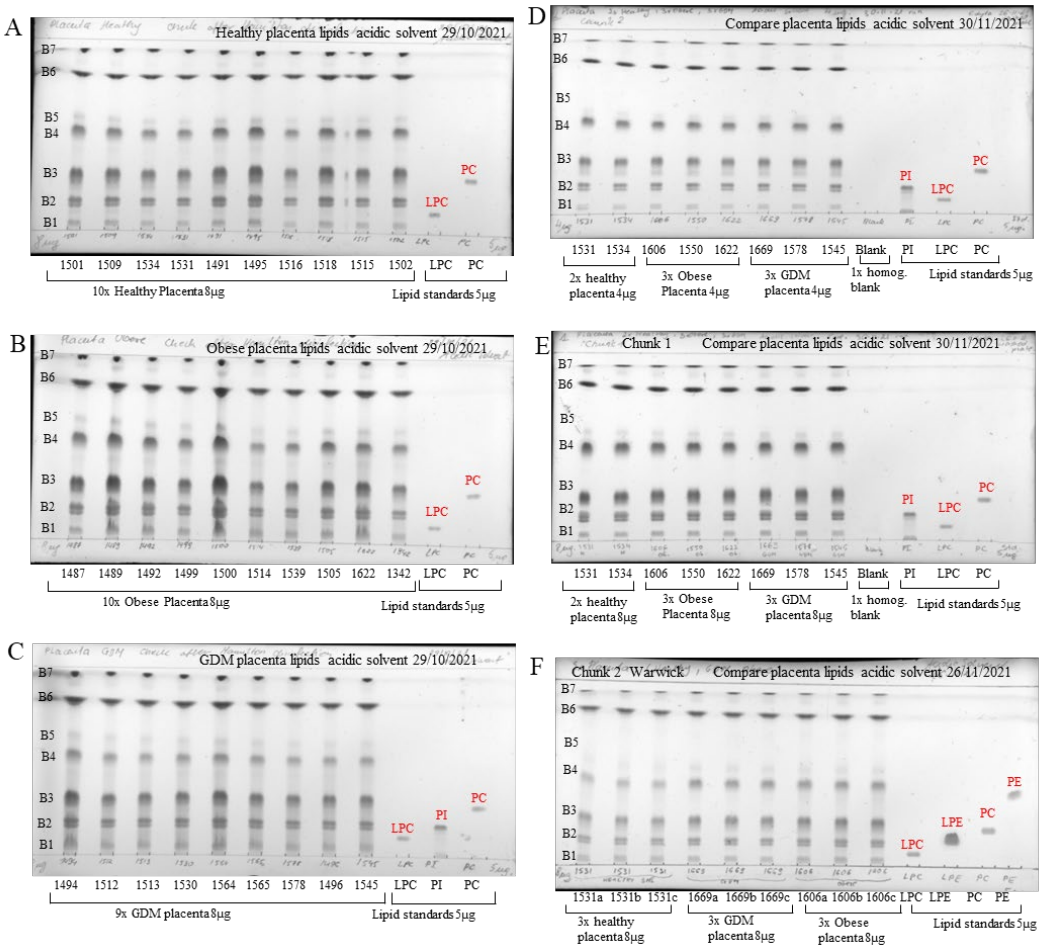

Figure 2:23 Analysis of freshly extracted placental samples using acidic mobile phase and visualised using sulphuric acid. Sample type in each well is labelled on the figure and includes samples from non-pregnant women, normal-weight pregnant women, pregnant women with obesity, and pregnant women with GDM (n = 8 /group); lipid standards of LPC and PC +/- PI were included on every plate. Plates were imaged using BioRad ChemStation white light scanner images saved in .tiff format using a calorimetric set filter white light format resolution of 600 pixels.

2.4.9 Re-analysis of placental lipids with acidic mobile phase

After recognising hints of contamination, an extensive deep cleaning of all components was performed on the homogeniser and tanks. Deep cleaning of the Hamilton syringes - hot water sonication bath, followed by methanol wash and drying in a fume hood under a protected glass chamber - was introduced as standard practice and seemed to resolve this issue. Repeated runs of freshly extracted samples over several months (Figure 2.24) revealed that the contaminated issue was resolved.

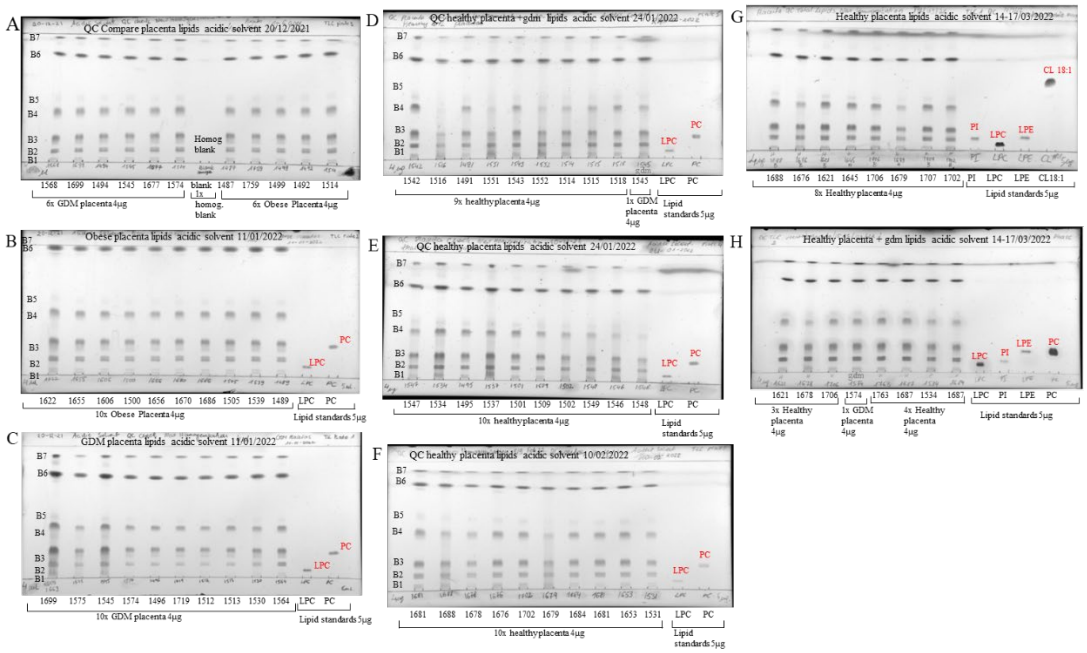

Figure 2:24 Analysis of freshly extracted placental samples using acidic mobile phase and visualise using sulphuric acid. Sample type in each well is labelled on the figure and includes samples from non-pregnant women, normal-weight pregnant women, pregnant women with obesity, and pregnant women with GDM (n =8/group); lipid standards of LPC and PC +/- PI were included on every plate. Plates were imaged using Bio-Rad ChemStation white light scanner images saved in .tiff format using a calorimetric set filter white light format resolution of 600 pixels.

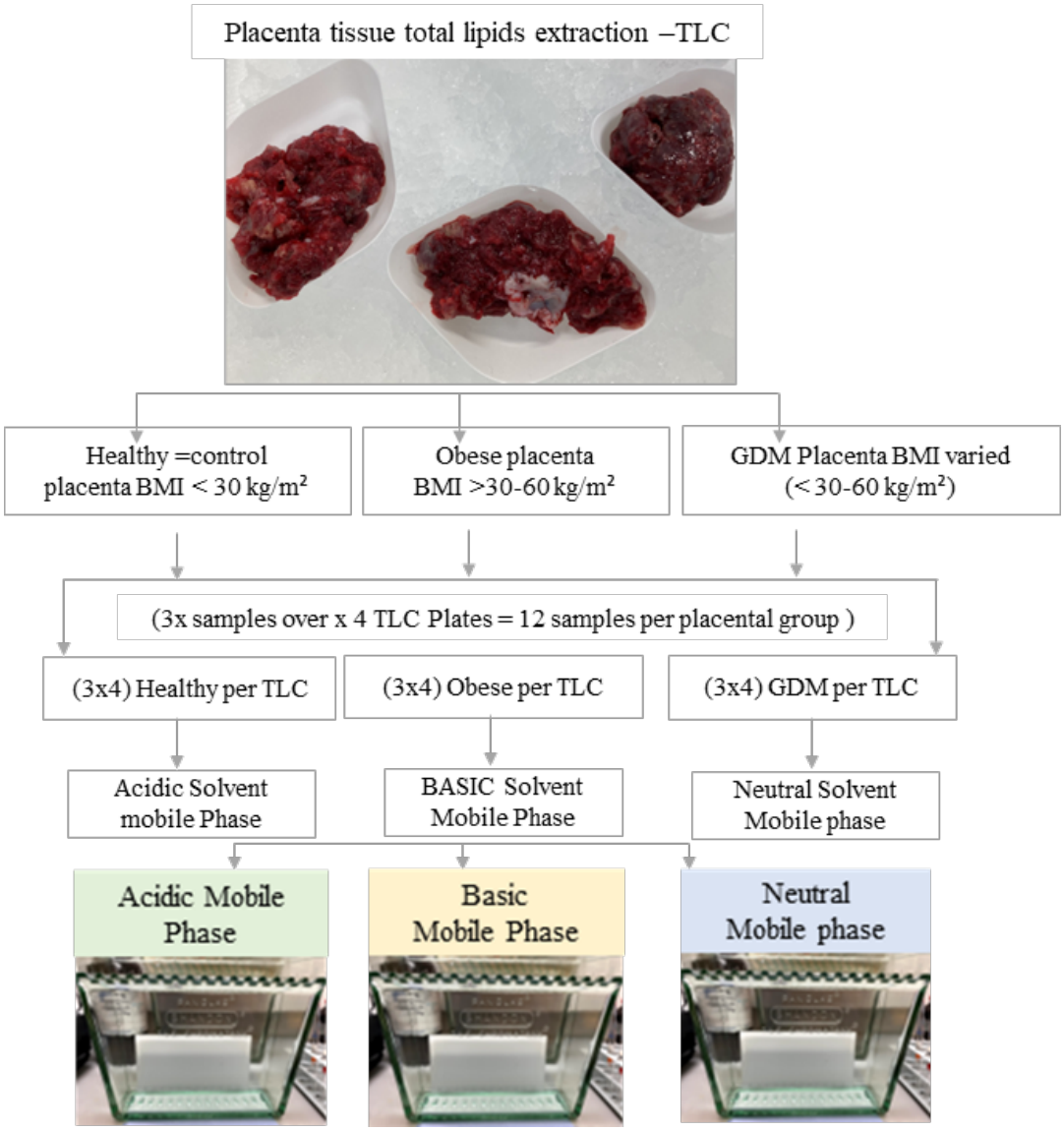

Figure 2:25 Summarizes a three-phase mobile comparison of placental lipid extracts from women who are normal/overweight or obese or have GDM in the acidic, basic, and neutral mobile phases.

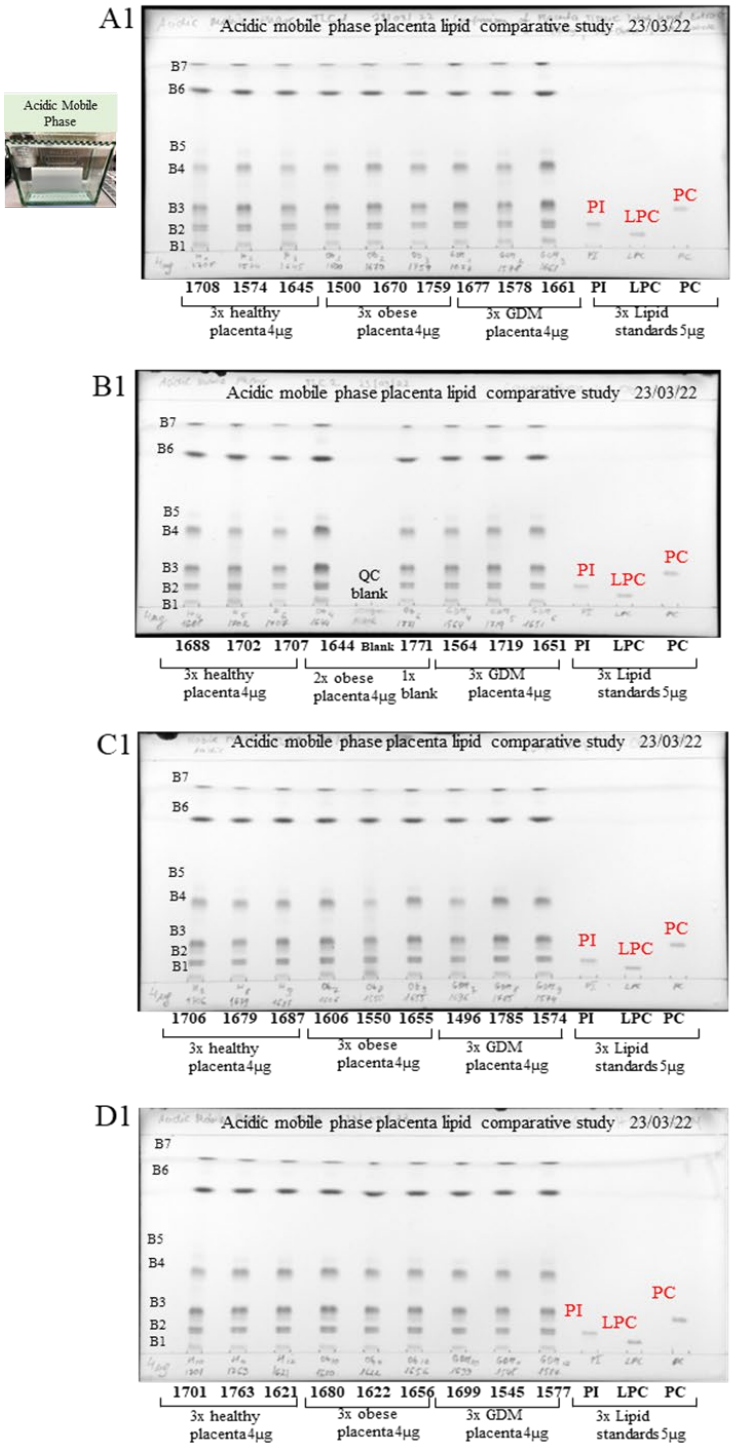

Figure 2:26 Analysis of freshly extracted placental samples using acidic, mobile phase and visualise using sulphuric acid. Sample type in each well is labelled on the figure and includes samples from non-pregnant women, normal-weight pregnant women, pregnant women with obesity, and pregnant women with GDM (n = 12 /group); lipid standards of cholesterols and MAG/DAG/TAG were included on every plate. Plates were imaged using Bio-Rad ChemStation white light scanner images saved in .tiff format using a calorimetric set filter white light format resolution of 600 pixels.

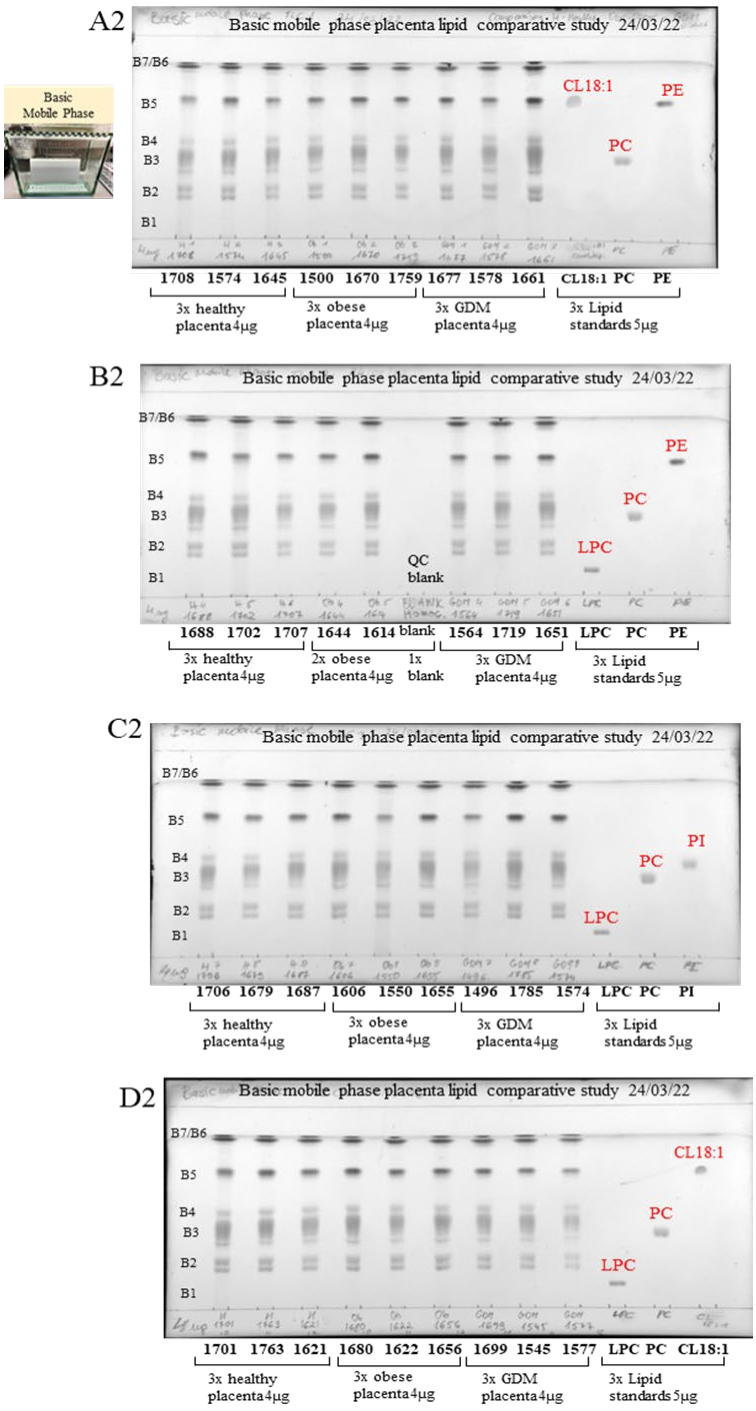

Figure 2:27 Analysis of freshly extracted placental samples using basic mobile phase and visualise using sulphuric acid. Sample type in each well is labelled on the figure and includes samples from non-pregnant women, normal-weight pregnant women, pregnant women with obesity, and pregnant women with GDM (n =12 /group); lipid standards of cholesterols and MAG/DAG/TAG were included on every plate. Plates were imaged using Bio-Rad ChemStation white light scanner images saved in .tiff format using a calorimetric set filter white light resolution of 600 pixels.

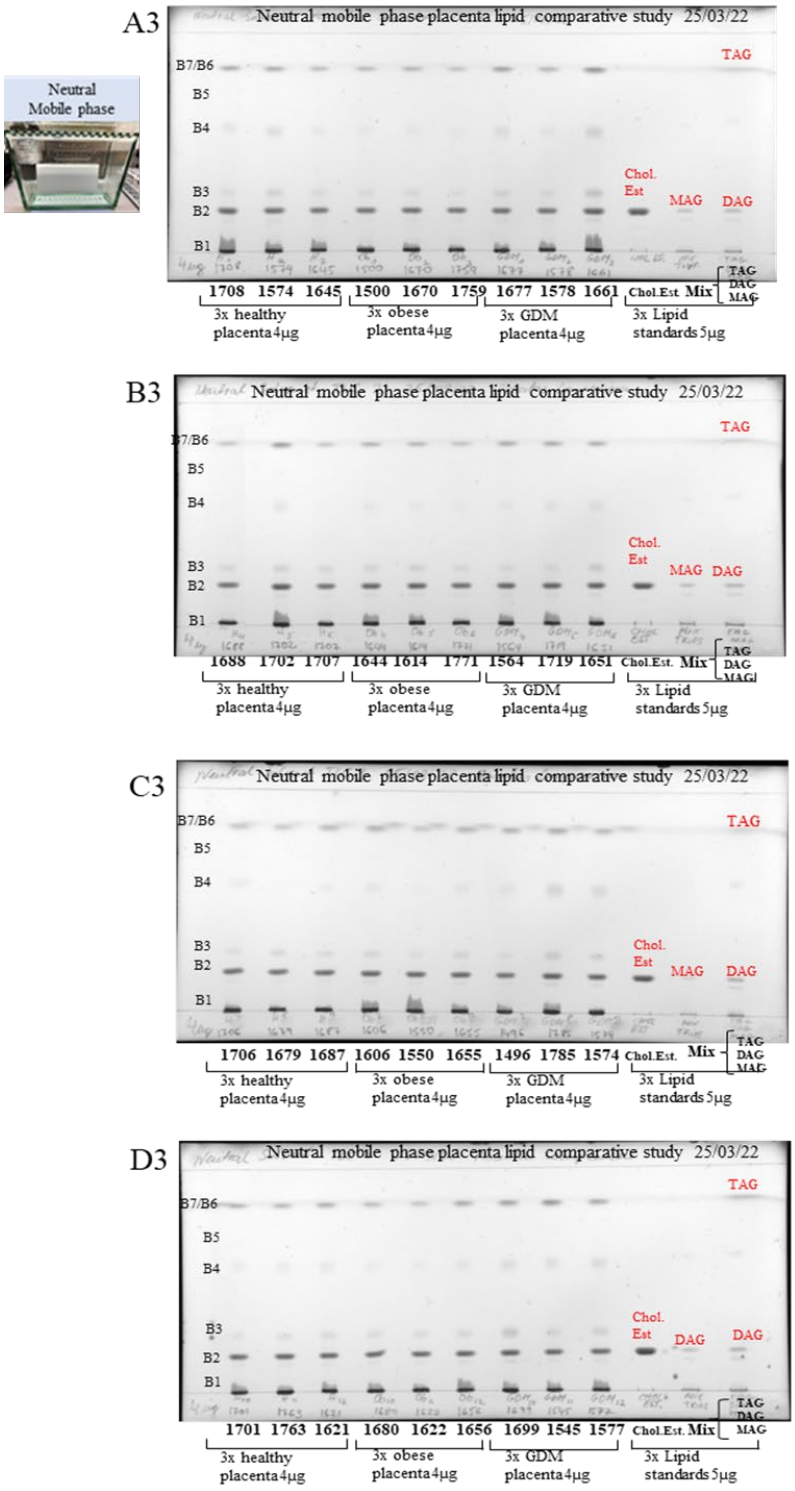

Figure 2:28 Analysis of freshly extracted placental samples using neutral mobile phase and visualise using sulphuric acid. Sample type in each well is labelled on the figure and includes samples from non-pregnant women, normal-weight pregnant women, pregnant women with obesity, and pregnant women with GDM (n = 12 /group); lipid standards of cholesterols and MAG/DAG/TAG were included on every plate. Plates were imaged using Bio-Rad ChemStation white light scanner images saved in .tiff format using a calorimetric set filter white light format resolution of 600 pixels.

2.5 Analysis of comparative placental groups study.

Having optimised the TLC analysis, including addressing contamination issues, the final step was to compare lipid extracts from placental samples from the three study groups separated using each mobile phase, as summarised in (Figures 2.27 - 2.29). The mobile phase separation of the acidic solvent total lipid extract revealed all the lipid bands from bands 1 to 7 amongst all the three groups of placentas with no specific visual difference between them (Figure 2.27 A1 – D1). Basic solvent mobile phase separation of the total lipid extract shows different spread elution visible to the naked eye and not showing lipid band 1 in all samples with clear distinction of high abundance in PC, PE, and visible cardiolipin 18:1 in Plate A2 and plate D2 luting in lipid band 5 but with no observable differences in the groups (Figure 2.28 A2 – D2). Neutral solvent mobile phase separation of the total lipid extract shows visible cholesterol high abundance elution in band 2 in all plates A3-D3 and the mix of monoglycerides, diglycerides and triglycerides but with no observable differences in the groups (Figure 2.29 A3 – D3).

2.6 Discussion

2.6.1 TLC observed results

The primary purpose of the TLC approach here was to identify lipid species groups visible to the human eye and compare their distribution and abundance in placentas from lean and obese women and women with GDM, as well as plasma from the same groups of women alongside plasma from non-pregnant women. Total lipids can be separated using placental tissue and plasma. A system of acidic solvents, a system of basic solvents, and a system of neutral solvents were used to separate and elute lipids.

There was a clear separation of lipid species groups with a positive or negative charge on the head groups in acidic and basic solvents. Our observations in the neutral mobile phase included lipid species with no charge and cholesterol and triglyceride mixes composed of mono glycerol, diacylglycerol, and triacylglycerol. However, we cannot confirm which of the mixed glycerides are present, and additional analysis using gas chromatography separation would be required in future work studies. Other observations include healthy pregnancies in plasma or placentas or non-pregnancies. They differ in the context of darker or larger spots, but not much

else is different. TLC spots are larger in obese and GDM placenta and plasma samples but separate in healthy and non-pregnant samples. TLC analysis involves many steps of preparation and a careful and clean approach to avoid disturbing the previously prepared, washed, and activated TLC plate.

Lipids are a diverse class of biomolecules insoluble in water but soluble in organic solvents. Organic solvents play a crucial role in lipid analysis. These solvents are essential for extracting, separating, and identifying lipids from various biological samples. Notably, the choice of organic solvents in lipid analysis depends on the specific lipid classes of interest. Proper solvent selection and optimisation ensure accurate and reliable lipid analysis results. Here, acidic, basic, and neutral mobile phases are used. The chloroform-methanol-acetic acid (CMA) method is commonly used to extract and analyse phospholipids with positively charged headgroups such as PC and PE *(532, 533)*. An acidic environment facilitates their separation and quantification. Although relatively rare, these positively charged lipid groups are critical for cell signalling and membrane structural support, so they are expected to be relatively abundant in tissues, cells and biological fluids *(532, 533)*.

At lower pH levels, the choline head group of PC is positively polar and interacts with other polar molecules to modulate cellular processes *(532)*. It can also be used for separating and analysing negatively charged lipids, including phospholipids with anionic phosphate groups *(532)*. The cationic lipids SM and sphingosine-1-phosphate (S1P) are found in human tissues and are essential for cell signalling, proliferation, migration, and immunity *(532)*. These cationic lipids are less prevalent than neutral or negatively charged lipids in the placenta and plasma *(533)*. Cell membranes contain a variety of cationic lipid molecules, including PS and PI. They contribute to membrane stability, protein localization, and cellular processes *(532)*. These anionic lipids maintain signal transduction pathways, membrane fusion events, membrane stability, and protein localization *(533)*. A phospholipid's hydrophilic head, such as PS, contains negatively charged oxygen atoms. These oxygen atoms are essential to forming and stabilizing cell membranes and improving hydrophilicity *(533)*. Ions are transported into and out of cells by lipid rafts, which are enriched with anionic phosphate groups. To modulate cellular processes, they interact with positively charged groups *(533)*. Compared to neutral lipids, such as

triglycerides, waxes, cholesterol, and squalene, anionic and cationic lipids are essential for energy storage, insulation, and membrane structure.

In contrast to neutral lipids, anionic and cationic lipids are soluble in nonpolar organic solvents such as chloroform and dichloromethane and are insoluble in polar solvents, for example, water or methanol *(533)*. Studies have shown that peptides selectively bind to anionic lipids and disorder them in mixed membranes *(534)*, indicating the specificity of the interactions. Developing a non-ionic phospholipid fluorescent sensor demonstrates the importance of understanding how anionic lipids act in biological systems *(535)*. Anionic lipids in membrane biology have been highlighted by stabilising transmembrane protein complexes by annular anionic lipids *(536)*.

Negatively charged lipids enhance protein binding to lipid bilayers, affecting their orientation relative to the membrane *(537)*. At low concentrations of peptide/lipid, positively polarized lipids can also bind to membranes, causing phase boundary defects *(538)*. Proton exchange membrane fuel cells may also benefit from composite membranes containing strongly reactive components. Adding negatively charged components can improve membrane performance and stability, making them potential fuel-cell materials *(539-541)*. Negatively charged lipid molecules in cell membranes are critical for biological processes and hold significant technological potential, particularly for fuel cell membrane development.

When separating negatively charged lipids, such as phospholipids, from negatively phosphorylated groups, it is crucial to choose an organic solvent. Several studies provide valuable insights into organic solvent choice. Chloroform/methanol is used for phase separation of charged and neutral lipids, lipids, and cholesterol dissolving *(542)*. It highlights the potential of chloroform/methanol (2:1) as a solvent for dissolving and separating lipids. A three-gradient solvent system that combines lipid hydrophilic interaction and liquid chromatography (HILIC) was used to separate yeast lipids, suggesting the effectiveness of this method *(543)*. Ultrahigh-performance capillary liquid chromatography improves lipidome coverage and separates isomeric and isobaric species *(544)*. Vacher et al. (1989) discussed lipid extraction and separation due to the similarities in solubility between charged lipids

and proteolipids *(545)*. Comprehensive lipid analysis is also characterized by the need for different chromatographic separations to provide optimal separation of polar (or ionic) and nonpolar lipid classes *(546)*. Selecting organic solvents for chromatography separation of negatively charged lipids is critical for accurate and comprehensive analyses. These studies' insights provide effective lipid separation and analysis using specific solvent systems, such as chloroform/methanol and HILIC.

An analysis of the specific extraction and separation requirements can determine the correct solvent system for separating glycolipids from lipids in TLC. It is critical to select a correct solvent system to ensure that the lipids in the sample are effectively extracted and not contaminated by non-lipid components *(547)*. It is difficult to isolate pure lipids in TLC without the sugar moieties, as other more advanced techniques, such as HPLC, also have those problems *(548)*. Literature also highlighted the difficulty of quantitative analysis with HPLC due to glycolipid separation challenges*(548)*. The study by Huang et al. (2020) separated glycerophospholipids from sphingolipids and glycolipids in aprotic solvents, which may provide insights into selecting suitable solvent systems *(549)*. Wojcik et al. (2017) explored using placenta and blood in obese pregnancies by applying an advanced technique called ultra-high-resolution ion mobility spectrometry separations for lipid and glycolipid isomer analyses, indicating their potential as advanced separation techniques *(550)*. Therefore, when choosing the most appropriate solvent system for separating glycolipids from lipids in TLC, lipid extraction effectiveness, glycolipid separation challenges, and advanced separation techniques should be considered.

Polar and neutral glycolipids have been separated using butanol for organic phase extraction, showing their potential for glycolipid isolation from lipid extracts *(551)*. Extracting and analysing glycolipids from placental tissue lipid extracts can be easier using this solvent. A volumetric ratio one-to-one (1:1,v/v) solution containing methanol to chloroform extracts fatty acids and lipids from placental tissue lipid extracts *(552)*. This solvent composition can also extract and separate fatty acids and neutral lipids. To separate and analyse cholesterol, fatty acids, neutral lipids, and

glycolipids in placental tissue lipid extracts, a chloroform/methanol (2:1) solvent system, butanol solvent, or methanol/chloroform solvent is recommended.

Anionic lipid dysregulation and associated processes can adversely affect placental tissues. Biological membranes, including those in the placenta, are maintained by anionic lipids, such as PS. GDM and maternal obesity are associated with dysregulation of lipid metabolism in the placenta *(553, 554)*. Placental expression and activity of lipoprotein lipase (LPL) are dysregulated in women with pregnancy complications like obesity and GDM *(553)*. As a result of oxidative stress-induced damage to lipids, proteins, and DNA in the placental tissue, adverse pregnancy outcomes have been observed *(554)*. Dysregulation of lipid hydrolysis contributes to fetal hepatic lipid accumulation and possibly overgrowth *(555)*. Furthermore, lipid aldehydes, such as 4-hydroxynonenal and 4-hydroxyhexenal, affect lipogenic pathways in the placenta, leading to inflammation and perhaps affecting tissue function *(556)*.

GDM is associated with dysregulation of placental endothelial lipase in obese women, highlighting the importance of lipid regulation for placental function *(557)*. Dysregulation of lipid metabolism in the placenta has been linked to altered maternal-fetal transfer, impaired mitochondrial function, and increased oxidative stress *(558)*. There is an association between these metabolic changes and elevated placental lipid accumulation*(558)*. Anionic lipid dysregulation and associated processes can impact pregnancy outcomes and maternal health.

Neutral lipids are stored primarily in lipid droplets (LD) *(559)*. Placental lipid droplet fractions can be enriched for neutral lipids using this information for neutral lipid extraction and isolation. The Kennedy pathway regulates the balance between mouse placenta phospholipids and neutral lipid profiles *(560)*. Placental lipid synthesis and accumulation can be understood by understanding the regulatory pathways involved in lipid metabolism. Additionally, neutral lipids can be detected in frozen tissue sections through staining techniques such as “Oil Red O” (ORO) staining *(561)*. This method allows neutral lipids within the placenta to be visualized and localized.

2.6.2 Conclusions

A range of mobile phases, including acidic, basic, and neutral, are useful for separating plasma and placental lipids. The results of the TLC analysis showed differences between placenta and plasma, as expected, but only slight differences between the study groups. It is possible to answer that question by doing an image densitometry analysis, but it cannot be verified as it only gives preliminary identification. We must comprehensively analyse each lipid group to get a more detailed answer on lipids in particular groups. Its goal is to establish a lipid map of observable lipids in the placenta and plasma. In the next steps of this project, quantitative analyses can be conducted to gather more details. The research focus can be narrowed down to specific areas of inquiry. Still, it is the primary method of assessing total lipid quality, providing the basis for preparative TLC and MALDI ToF MS mass spectrometry, which are the focus of Chapter 3. The next chapter explains the mechanism of preparative TLC, its use, and what was learned from it.

Chapter: 3 Preparative TLC

3.1 Introduction

Preparative thin-layer chromatography (TLC), or high-performance thin-layer chromatography (HP-TLC), was used in this study as a complementary follow-up technique to study the individual six to seven lipid bands of the total lipid extract previously observed in chapter two. HP-TLC is a chromatographic technique that separates and isolates large quantities of compounds from a mixture. Purifying organic compounds, natural products, and other substances is essential in research and analytical laboratories. Preparative TLC operates on the same principles as analytical TLC but scales to manage larger sample quantities. The basic idea is to separate a mixture of compounds based on their differential migration on a TLC plate. That is due to differences in their affinity for the stationary phase (typically silica gel or other suitable adsorbents) and the mobile phase (solvent).

This chapter explains the principles of the technique and reasons for applying it as a purification step of each separate lipid band. Two approaches were taken: extraction of the lipid band for further separation on another TLC plate exposed to a mobile phase and extraction of the parent/further separated lipid bands for MALDI ToF MS mass spectrometry. The preparative TLC or HP-TLC is similar to traditional analytical TLC with additional steps, such as the development of the separated total lipid extract in the mobile phase as per Chapter 2, which is then subjected to a further development stage using a separate glass tank filled with solid iodine granules which saturate the tank with the oxidising fumes. When the plate develops in the iodine granules, fumes react with the lipid bands in the stationary phase silica, oxidating the lipids and changing their colour to a light brown. This change of colour is visible to the naked eye, and spots for analysis can be highlighted with a soft pencil as soon as possible, as the iodine reaction process is reversible. The silica spot is then scraped gently and transferred into individual 15ml glass tubes for solvent extraction and bioanalytical TLC alongside lipid standards ahead of MALDI to check individual lipid bands.

3.2 Material and apparatus use.

3.2.1 Use of preparative TLC literature synopsis

These studies demonstrate the utility of preparative TLC in analysing lipid extracts, especially phospholipids and glycerolipids. Topics include metabolomic analysis of phospholipids, lipid metabolism in the fetal-placenta unit, lipidomic assessment of plasma and placenta in preeclampsia, and animal models for pregnancy research [342]. The second conceptual model is based on metabolic analysis of molecular phospholipids changes during normal and preeclamptic placentas, which are explored using preparative TLC [163, 343-346] [308, 347-350] [300]. Using *Arabidopsis thaliana* as a model, glycerolipids profiles related to plant development, physiology, and genetics have been studied using polar lipid extracts and preparative TLC analysis and GC [351] [352]. Selective binding between phospholipids and silica gel was investigated using thin-layer chromatography combined with MALDI-TOF-MS and 31P-NMR [353]. TLC and Coomassie staining were used to prepare lipidomics samples quickly and efficiently [354]. The first step was to prepare TLC extracts for LC-MS analysis [355]. Combining TLC with nano MALDI MS with ionic liquid stabilisation allowed efficient separation, detection, and identification of oligosaccharides [356]. TLC was also used to separate neutral oligosaccharides, highlighting its utility in separating complex carbohydrate mixtures [357]. Also, the power of TLC in carbohydrate analysis has been demonstrated by coupling it to matrix-free MALDI MS [358]. Together, these studies demonstrate the diverse applications of preparative TLC in carbohydrate analysis, including acidic carbohydrates.

Many publications provide deeper insights into lipid separation using preparative TLC [342, 359-364]. Two examples of eliminating the scraped silica from lipid extracts are using a chromatographic short column packed with long-chain carbohydrates reverse phase (C18-Sep-Pak) cartridges [342] or using anhydrous sodium sulphate [360] as a drying agent. These approaches commonly purify lipids using preparative TLC and eliminate silica contamination from scraped samples. Scraped silica gel is usually used to extract gangliosides using chloroform-methanol. Methanol concentrations in the extraction solvent are favourable for higher ganglioside recovery. As a result, gangliosides are contaminated with more silica gel

when methanol is used as a solvent. This dilemma limits ganglioside purification with preparative TLC. With a short reverse-phase column and C18 Sep-Pak cartridge, salts and other nonlipid contaminants can be removed from gangliosides. Protein contaminants can be removed using liquid-liquid extraction. The TAG fraction can be separated from these contaminants using preparative TLC. Fresh anhydrous sodium sulphate is added at all filtering stages to eliminate silica, but it can affect lipid weight accuracy [342]. A preparative TLC method has been used to analyse integumentary lipids in mammals with hexane, ether, and acetic acid as the mobile phase. The TLC plate can be resolved into four distinct bands: sterols, free fatty acids, trans fatty acids, and sterol esters/wax esters/squalene, although this is not always possible as sterols and waxy esters are not always separated. However, these bands can be separated using a different mobile phase (isooctane: ethyl ether). A poor TLC separation can be caused by chamber conditions, seal quality, equilibration time, and chamber cleanliness. These factors must be controlled for consistent and high-quality TLC separations and data.

3.2.1.1 Rationale

This study quantitatively uses high-performance (HP) preparative TLC to separate individual lipid bands. Separating placental and plasma total lipid extracts is to observe a more detailed lipid profile. This study aims to map the lipid composition of the placenta and link it to potential biomarkers of placental inflammation and, similarly, analyse plasma. As in Chapter 2, the COVID-19 pandemic impacted experimental planning, focusing on TLC overcoming laboratory access limitations.

3.3 Materials and Methods

3.3.1 Reagents, materials and equipment

All reagents, materials and equipment used for the work described in this chapter are summarised in Table 3.1

3.3.1.1 Samples and Ethics

All sample and ethical approval as described in Chapter 2, section 2.3.1

3.3.2 Tissue/blood processing and lipid extraction

Lipid extraction by Bligh and Dyer methods is summarised in Chapter 2.

3.3.3 Preparative TLC Experiment run

3.3.3.1 Preparative TLC plate preparation experiment

The total dry mass of lipids in each run of preparative TLC is equivalent to 12-14 mg. Once the plate is ready, the total lipid extract is applied. The first step in preparing a plate is drawing its lines, twice washing it, and oven activation at 180 °C. Plate line drawings show solvent front lines at the bottom and top of the plate. In the preparative HP-TLC at the start baseline, thirty-five millimetres wide markings are spaced one by one continuously. With a soft pencil and a micro ruler, draw 30 strips of 5 mm depth. Once all line drawings are done, the plate is ready for a solvent wash in the tall glass tank with a glass lid using a 50 ml (50:50 v/v) ratio of methanol and chloroform as wash solvent. Once the plate has dried off in the fume hood, a minimum of two hours at 180 °C is required for activation. Plates can remain at 50 °C until use. Standards are applied 5-8 ug per 5 mm allocated space, and for samples, 40 ug per 5 mm allocated slot, continuously applying small volumes up to thirty times/space. Preparative TLC uses the sample glass plate coated with silica stationary phase as the typical TLC Plate, but they are twice the size. It separates lipid bands during the mobile phase run liquid phase separation and offers each band scraping analysis after comparison to the reference classic TLC strip of total lipids.

Bio-Rad Scanner white calorimetric filter resolution 600 pixels black and white image ready for publication saved as jpeg/tiff on the computer file folder. The TLC silica gel-coated glass plates contain a fluorine metal (F254) binder purchased from Merk UK. The preparative TLC plate size is 20 cm x 20 cm. A total of 1200 ug/ul for all samples in this study, making a 10 mg/ml concentration. The 12 mg of dried lipid extract reconstitutes into 1200 µl of chloroform) and distributes across the plate in a continuous line, covering 30 slot spaces as shown in the diagram below (Figure 3.1). The plate runs first in the acidic mobile phase for 3 hours until the solvent front reaches the plate line's top. The total lipid sample is 1200 µL application dropwise per loading capacity of 40µg. These 30 wells at 40 µg/well of the same sample form into one long lipid lane, which separates into 7 bands as described in Chapter 2. Once

the run is complete, the plate is placed into an iodine-deep glass tank for the iodine vapours to work. Once the sublimation of the iodine fumes develops a deep yellow colour on the large plate, the plate is removed. With soft pencil circle markings, each lipid band as the iodine staining is reversible, and the yellow colours disappear once they are out of the iodine tanks.

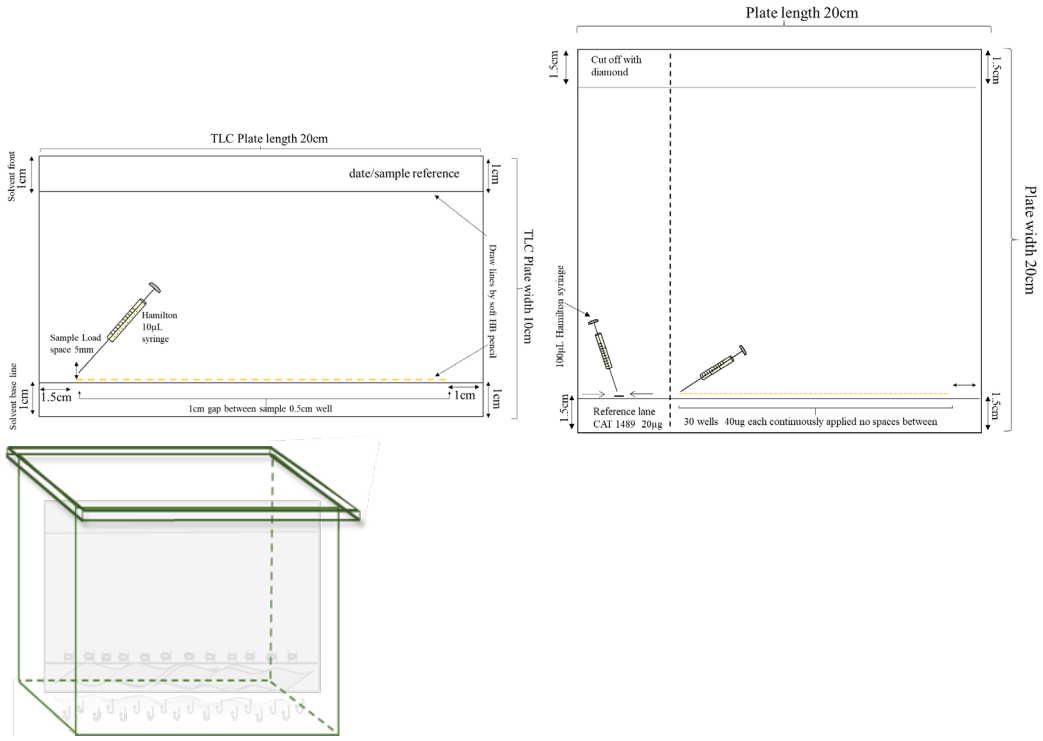

Figure 3:1 Images hand-made starting from the left-hand side smaller size 10x10cm TLC plate line drawing, the middle is the large plate of 20x20cm for preparative high-performance HP-TLC for iodine staining and silica scraping for individual bands, and last is the incubation tank with solvent and TLC Plate in it during development and saturate fumes fill up the tanks.

3.3.3.2 Lipid band collection and extraction

Iodine granules are used to saturate the glass tank with iodine fumes to enable the reaction and colour change of the separated lipid species. Iodine vapours are highly reactive to organic compounds that contain saturated single carbon-hydrogen (C─H) bonds and unsaturated carbon-hydrogen double (C=C) bonds in fatty acids chains of hydrocarbons and molecules such as polysaccharide glycans or glycolipids. The TLC plate remains inside the iodine tank and waits until the colour changes and the bands appear. The plate is carefully removed with gloved hands and gently placed onto a clean bench when the colour changes. The lipid bands are gently circled with a soft

pencil. A scalpel blade is used to scrape each band from silica off the plate into the silver foil, which is then gently transferred to a glass tube with a glass funnel to avoid silica powder overflow. The scraped silica is then washed with a polar solvent of 1 ml of methanol, ready for extraction. After scraping from the large preparative TLC plate, the single band samples named band one (b1), band two (b2), band three (b3), band four (b4), band five (b5), band six (b6), and band seven (b7) were stored at -20 °C in 1 ml of methanol for up to 7 months during the COVID-19 lockdowns. Samples were then re-extracted using the Bligh and Dyer method for this extraction process, as described in Chapter 2.

3.3.4 Bioanalytical TLC

3.3.4.1 Preparations of the matrix for MALDI ToF MS

All extracted lipids were resuspended at 10 mg/ml in chloroform and were applied to the MALDI Target (MTP 384 target plate non-polished steel BC 828078, MTP target frame III 8074115 Brucker UK Limited, UK). Two different matrix preparations - 9AA and 2.5 DHB- were used.

3.3.4.2 Materials, solvents, standards

- Preparative TLC plates 10x20cm Merck UK TLC Silica gel 60, Glass plates. Isopropanol, Acetonitrile, ACS reagent, ≥99.5%, Sigma Aldrich MSD UK.
- MALDI Matrix: 9 Aminoacridine (9-AA) hemihydrate - Acros Organics (Morris Plains, NJ) 98%, 2,5-dihydroxybenzoic acid (DHB)- Fluka Germany.
- Lipid standards Avanti Polar Lipids, (Inc. USA) 1 ml to 2.5 ml stocks at concentration [10 mg/ml]-then working standards diluted with pure chloroform $CHCL_3$ [1mg /ml].
- Chloroform 34854 2.5l Sigma-Aldrich UK with ethanol stabilizer amylene 99.9%. Chloroform 650471 1L purity 99.9% for residue analysis 0.5-1% ethanol stabilizers. Methanol 34885 2.5L 99.9% HPLC-MS Grade Sigma-Aldrich UK. Nitrogen Genie
- British GAS BOC unit 1066, compressed gas, G20ec 231-783-9, 300 15°C. Glass Vials (1.5ml) Fisher Scientific
- HPLC-certified 1343-9748 blue inserts tops.
- Special Hamilton glass syringes (5µL, 10µL, 50µL, 100µL) purchase Cole Palmer UK

3.3.4.3 Lipid identification

Different lipid species were first identified by observing TLC relative retention volumes, and the MALDI-ToF results were searched against the lipid maps database for molecular weight masses in positive and negative ions to assign the chemical structure. The negative and positive ion spectra were then compared to the results from an in-depth literature search study, including published supplementary data results, to build the mass assignment tables.

3.3.4.4 Data analysis

Statistical analysis was done with one-way ANOVA, Kruskal-Wallis and Dunns non-parametric pairwise multiple comparisons. Data plots presented in this work were plotted using GraphPad Prism version 10.1.2 (324).

3.4 Results of Preparative TLC Lipid Bands

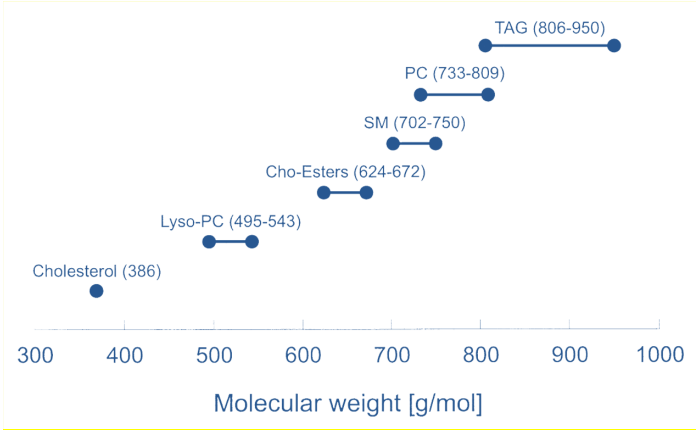

Figure 3:2 Figure: Literature example of lipid bands molar concentration [g/mol] elution using high-performance liquid chromatography with mass spectrometry, LC-MS, electrospray ESI mass spectrometry and MALDI imaging mass spectrometry. The order of elution of lipid groups as molar mass distribution of compounds was extracted from lipoproteins with apolar (non-polar) solvents. The ranges of molar masses are caused by a different fatty acid composition (ranging from palmitic acid 16:0 up to arachidonic acid 20:4). The lysophosphatidylcholine Lyso-PC, triacylglycerides TAG, cholesteryl esters, only a few studies have been done in which DHB was used as MALDI matrix (Leopold et al. 2018). In another study, apolar lipid constituents like diacylglycerol (DAG), Triacylglycerol (TAG), sterols, and cholesteryl esters were determined by MALDI-TOF MS (Holcapek et al. 2015). A study by Zaima et al. showed that cholesterol linoleate and cholesterol oleate in human and mouse lipid-rich regions were determined by imaging mass spectrometry using DHB as a matrix (Zaima et al. 2011).

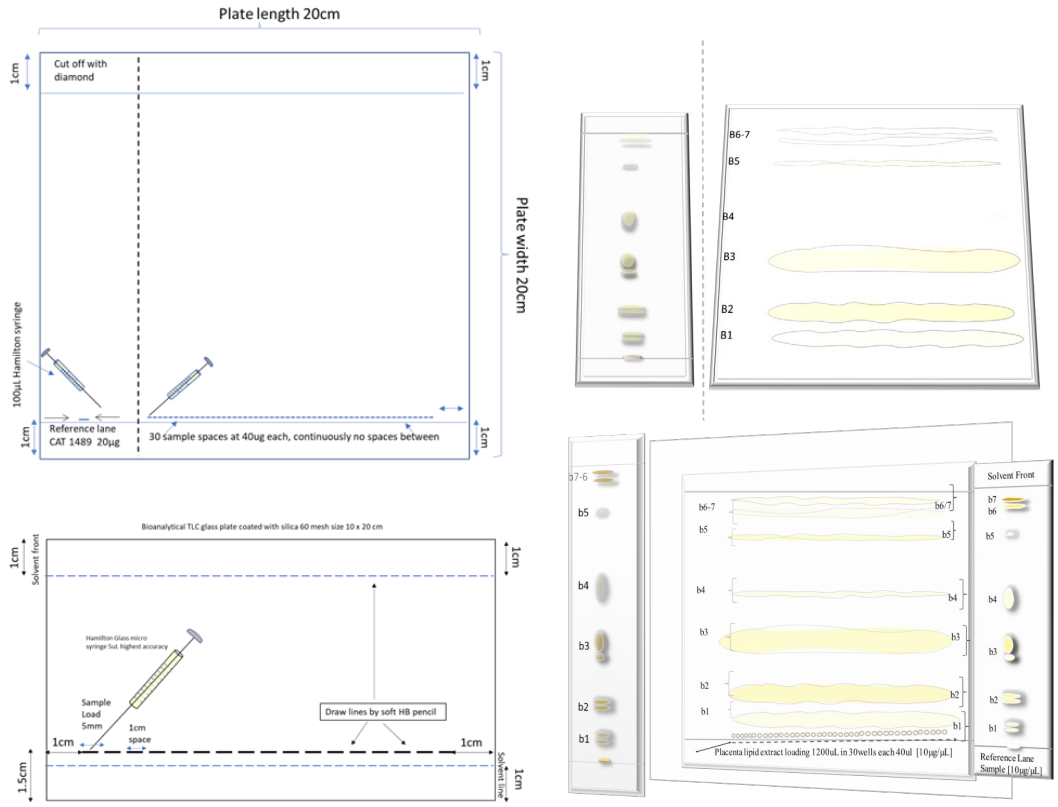

Figure 3:3: Schematic of preparative TLC using a larger plate (top left) with pencilled-in yellow lipid bands after iodine granules development (top right) that are then scraped off, solvent extracted, dried and run on the bioanalytical TLC plate alongside quality control samples (smaller bottom plate).

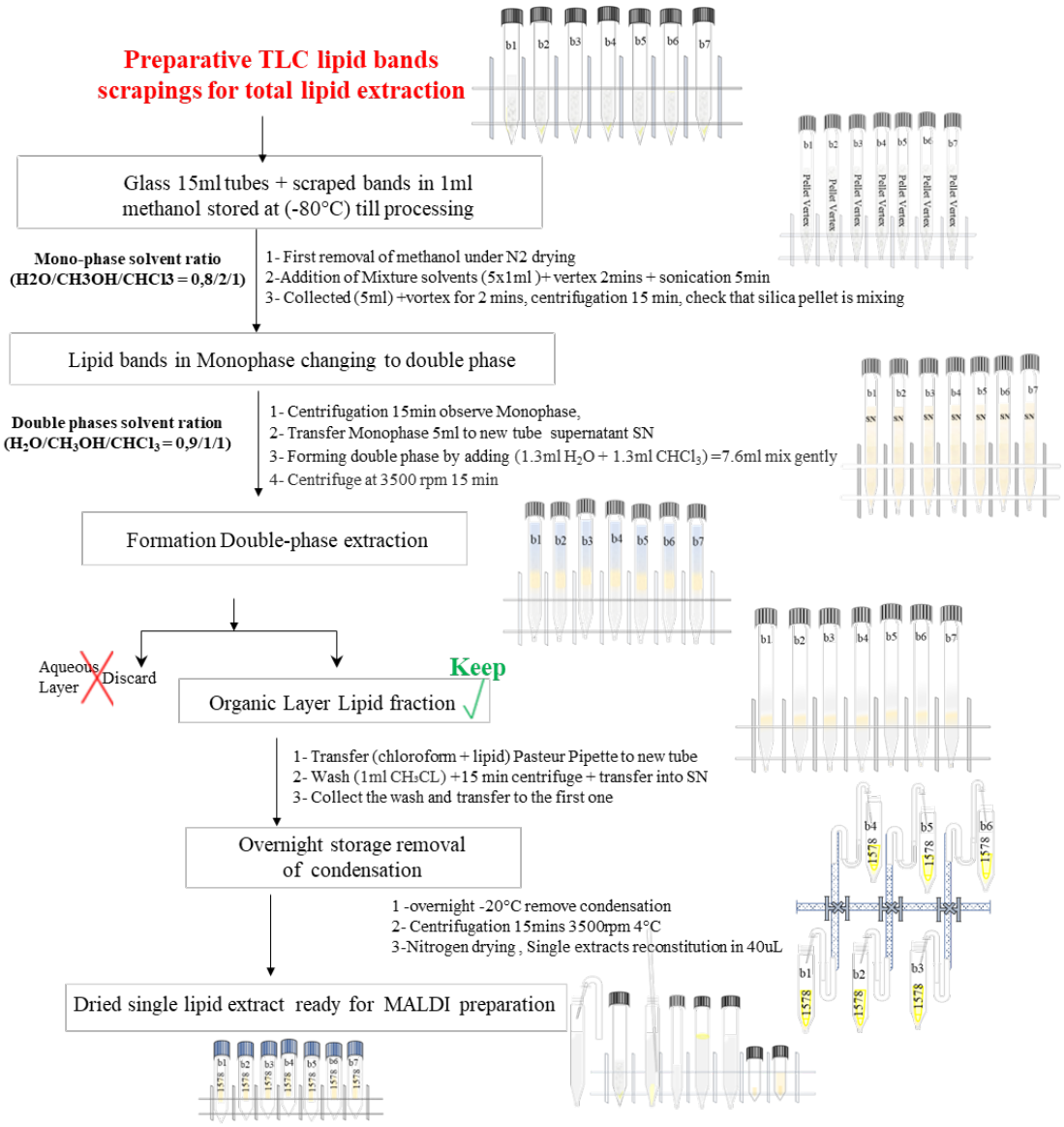

Figure 3:4: Overview of lipid extraction of silica scrapings.

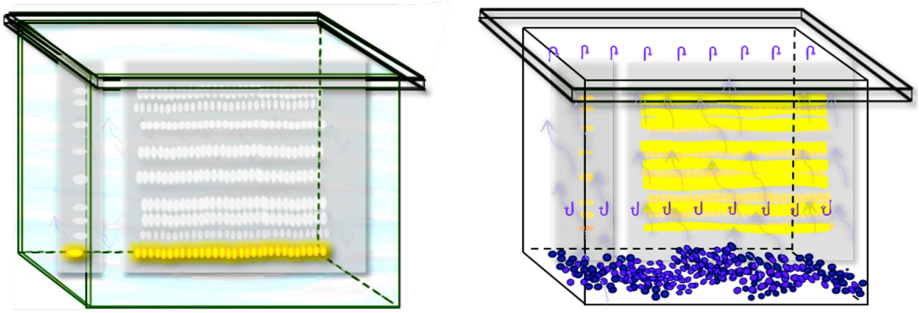

Figure 3:5: Preparative TLC plate with applied total lipid extract in the acidic mobile phase (left tank). Then, after drying, the TLC plate is placed into the iodine tank (right tank) for the iodine vapours to saturate the lipid bands and observed change of colour to yellow/light brown, enabling each lipid band to be marked by soft pencil to identify an area for scraping.

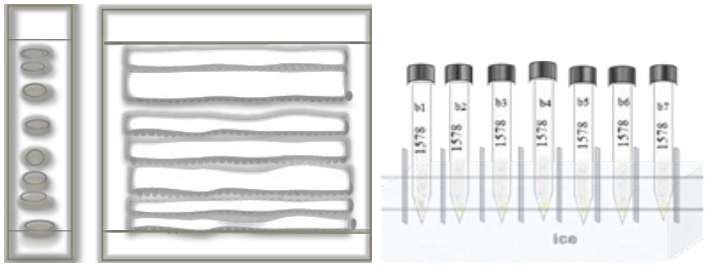

Figure 3:6: Schematics of preparative TLC after developing lipid bands with iodine vapour marking each band region with a soft pencil, the scraped silica from each band is transferred to separate glass tubes and stored in 1 ml methanol at -20°C to preserve lipid integrity until ready for lipid extraction. Each tube is labelled with the sample number (e.g. 1578) and corresponding band number (b1 – b7).

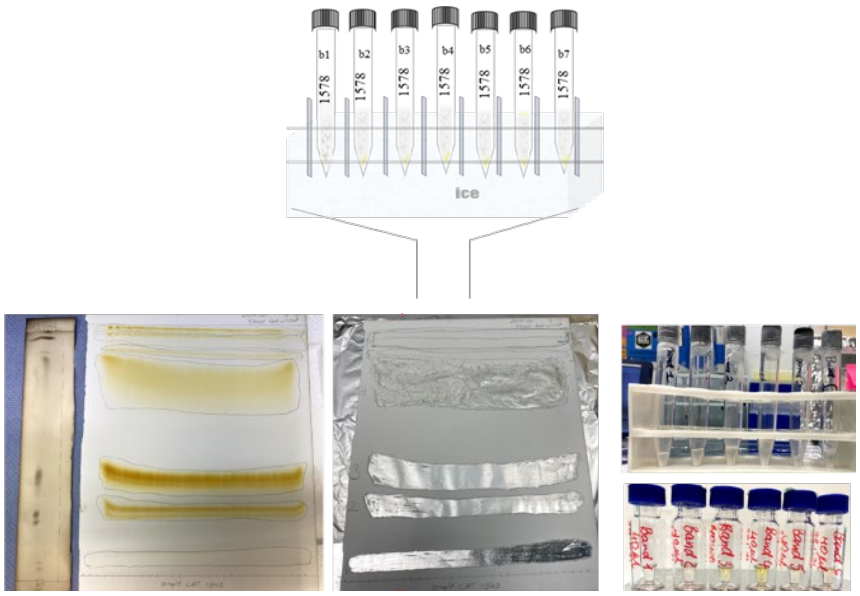

Figure 3:7: Example of preparative TLC – staining and scraping of discrete lipid bands into glass tubes and then preserved overnight in 1 ml methanol at -20°C, ready for further processing the next day.

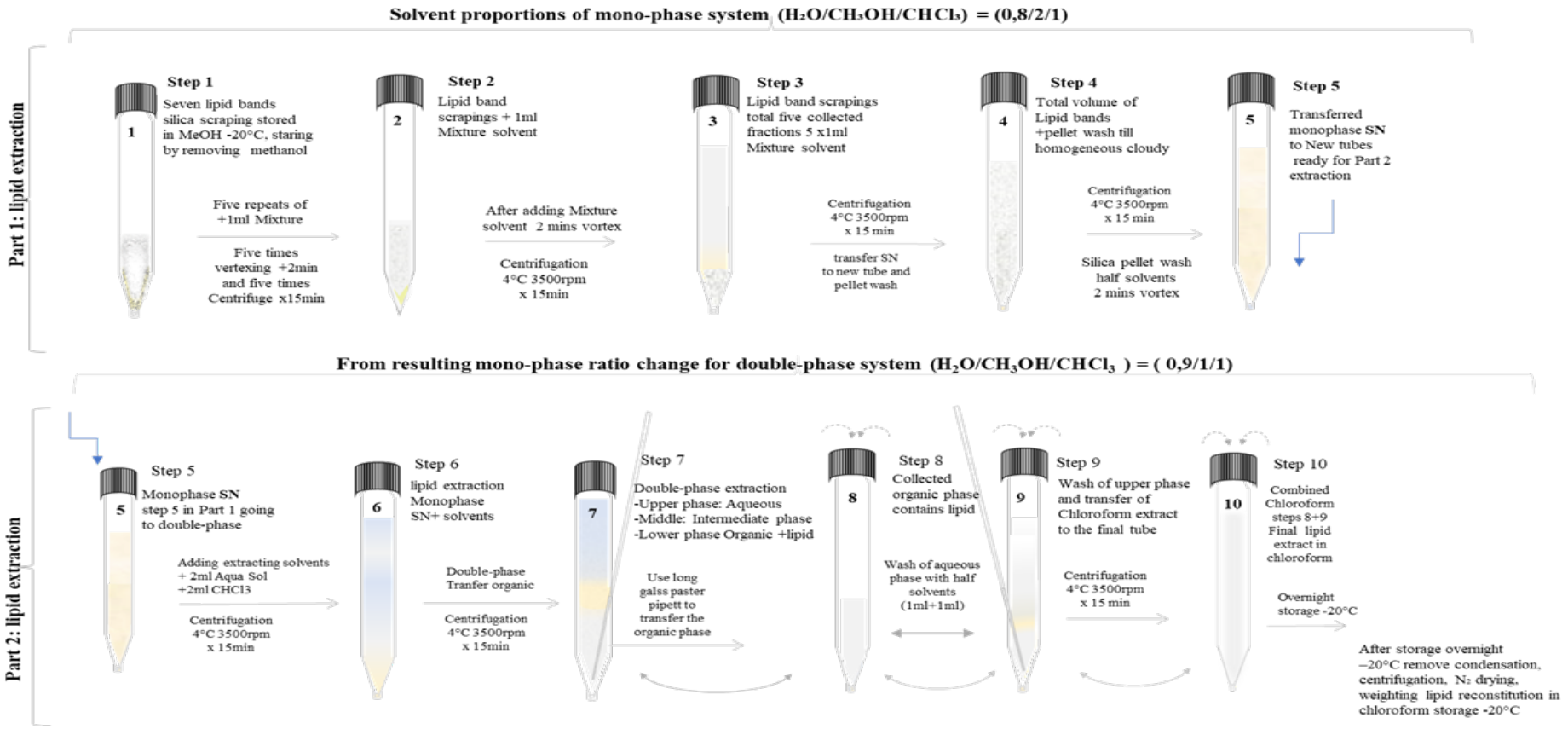

Figure 3:8: Schematic of lipid extraction from scraped silica lipid bands. After evaporating the initial methanol stored scraping using nitrogen, samples were extracted repeatedly per the Bligh & Dyer method, as summarised in this figure.

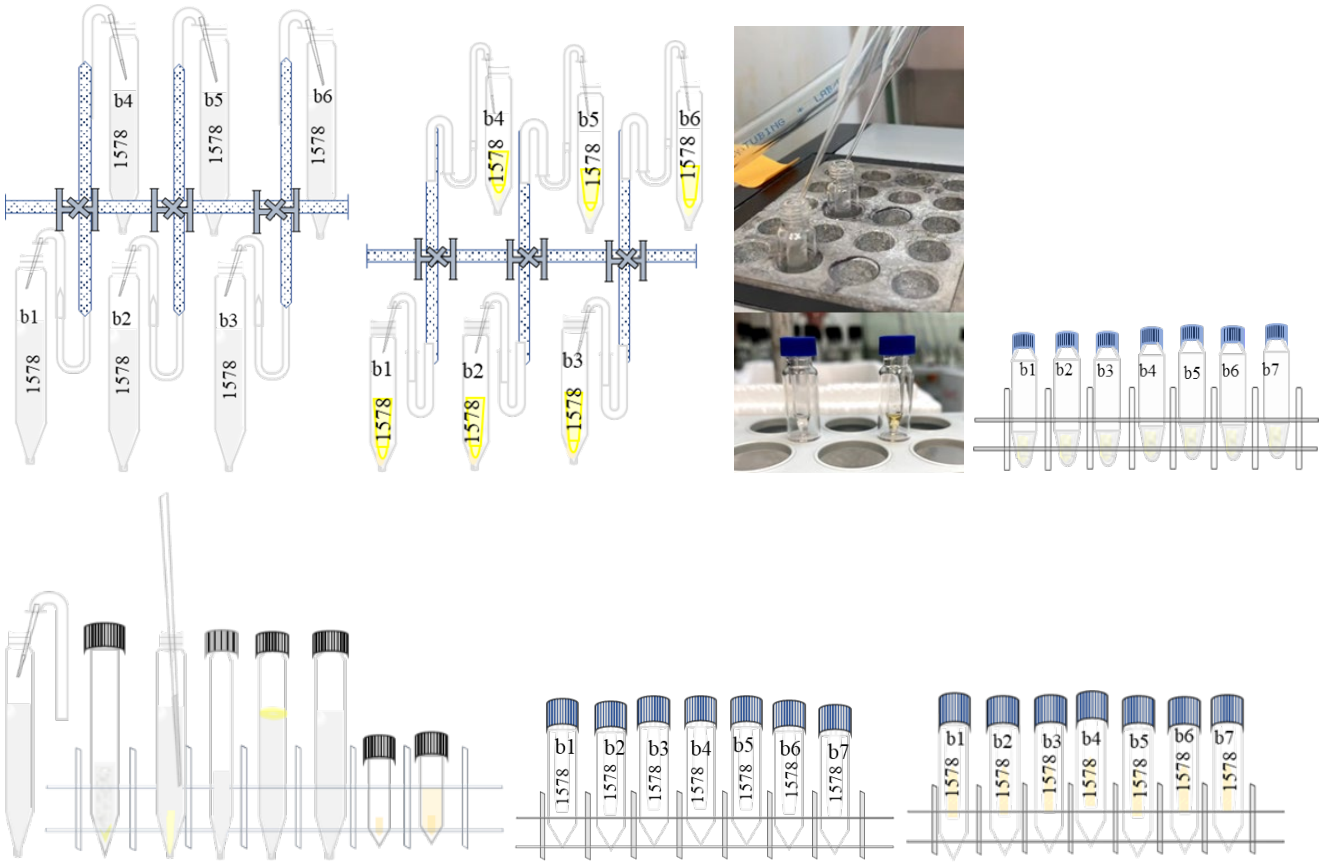

Figure 3:9: Sample drying using a gentle stream of nitrogen gas initially from a large 15ml glass that held scraping/methanol through to smaller vials used for lipid extraction by the Bligh & Dyer method. The weight of the small vials is recorded before and after each extraction/reconstitution step. The final lipid extract is dried with nitrogen, weighed in a pre-weighed final glass vial, and reconstituted to 10mg/ml concentration with pure chloroform ready for analytical TLC and MALDI TOF MS analysis.

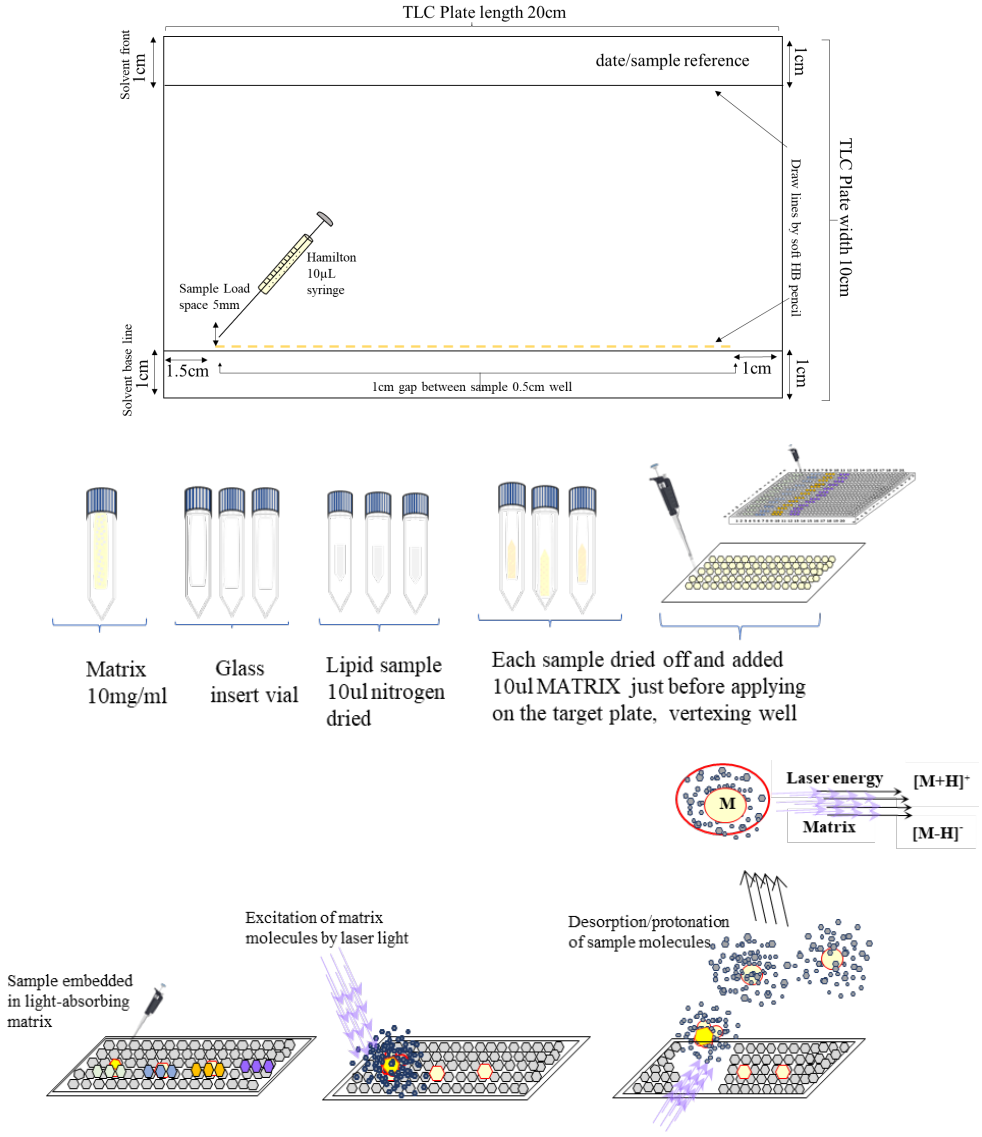

Figure 3:9: Bioanalytical TLC quality control of the preparative TLC lipid bands before MALDI ToF MS Once the quality of the sample is confirmed, the lipoid extract is dried and resuspended in the matrix. After thoroughly resuspending, the sample in the matrix is applied to the target for mass spectrometry.

3.4.1 Results from Preparative TLC

After Dr Lopalco taught the basic principles and procedures of preparative TLC (Figure 3.15), the next step was to optimise this approach further. It included reproducibility of the 7 bands in repeated samples (Figure 3.16 C and F) and tentative confirmation of the lipid type represented by various bands (Figure 3.16 D and E). Having established the principle of preparative TLC for placental lipid extracts, further band characterisation was optimised using different mobile phases (Figures 3.17, 3.18 and 3.19).

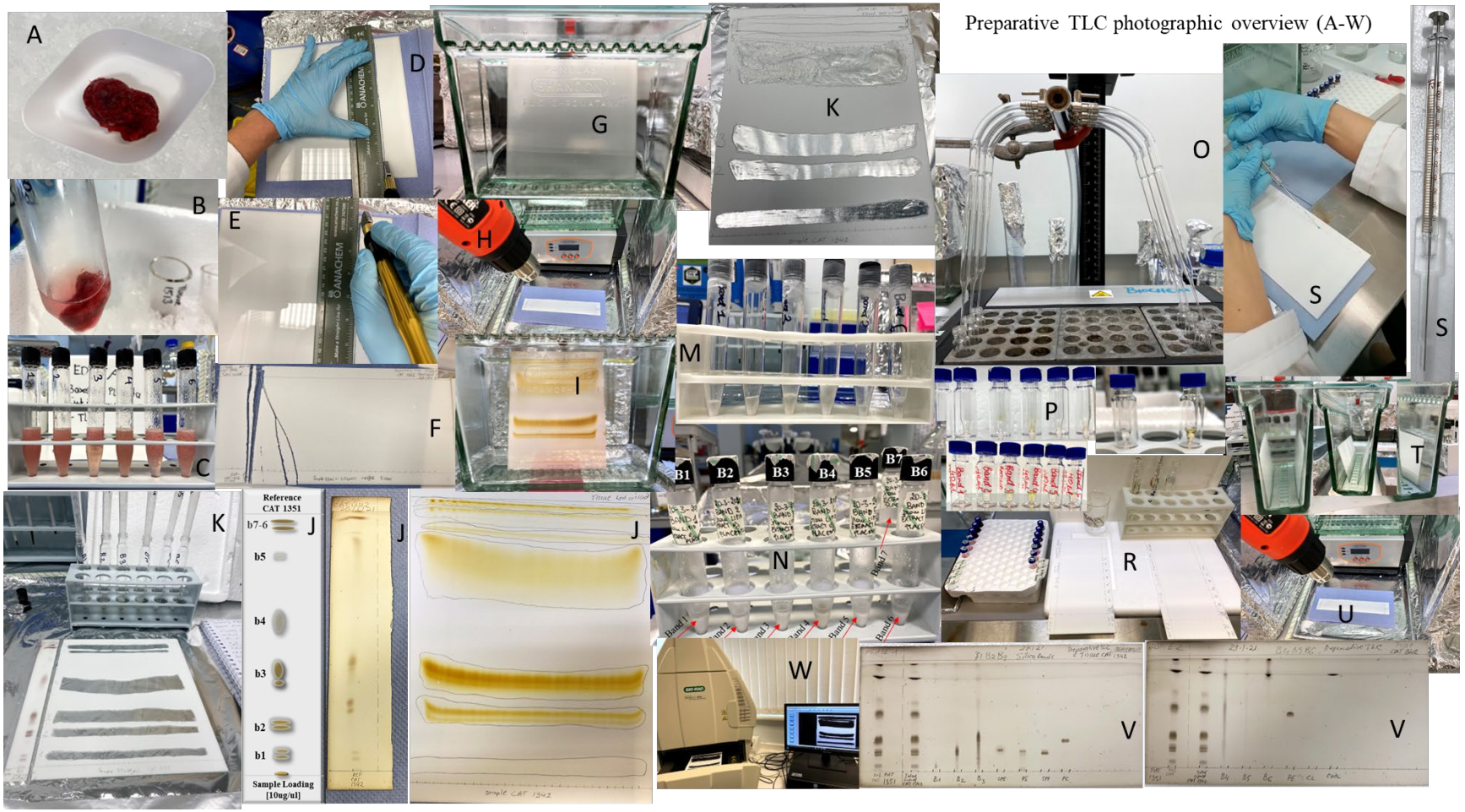

Figure 3:10: Photographic overview of laboratory experimental work of silica scraping in preparative TLC. Results from Preparative TLC

3.4.2 Results from Preparative TLC

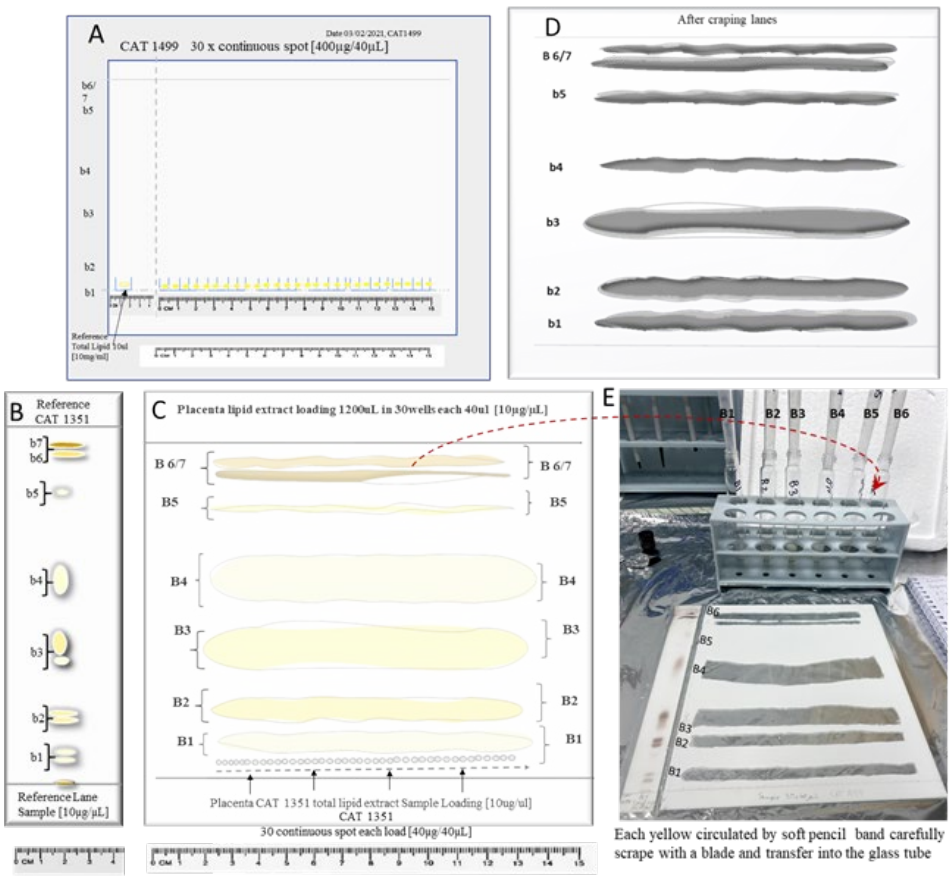

Figure 3:11: Illustrations of preparative TLC drawing the line with sample wells (A). After iodine incubation, each lipid band changes colour to yellow (reference lane B, iodine stains yellow makes circulated with soft pencil C), scraped yellow bands black and white plate scanned using Bio-Rad scanner (D) transferred each scraped band into glass tube (E) all hand made.

3.4.3 Results from Preparative TLC

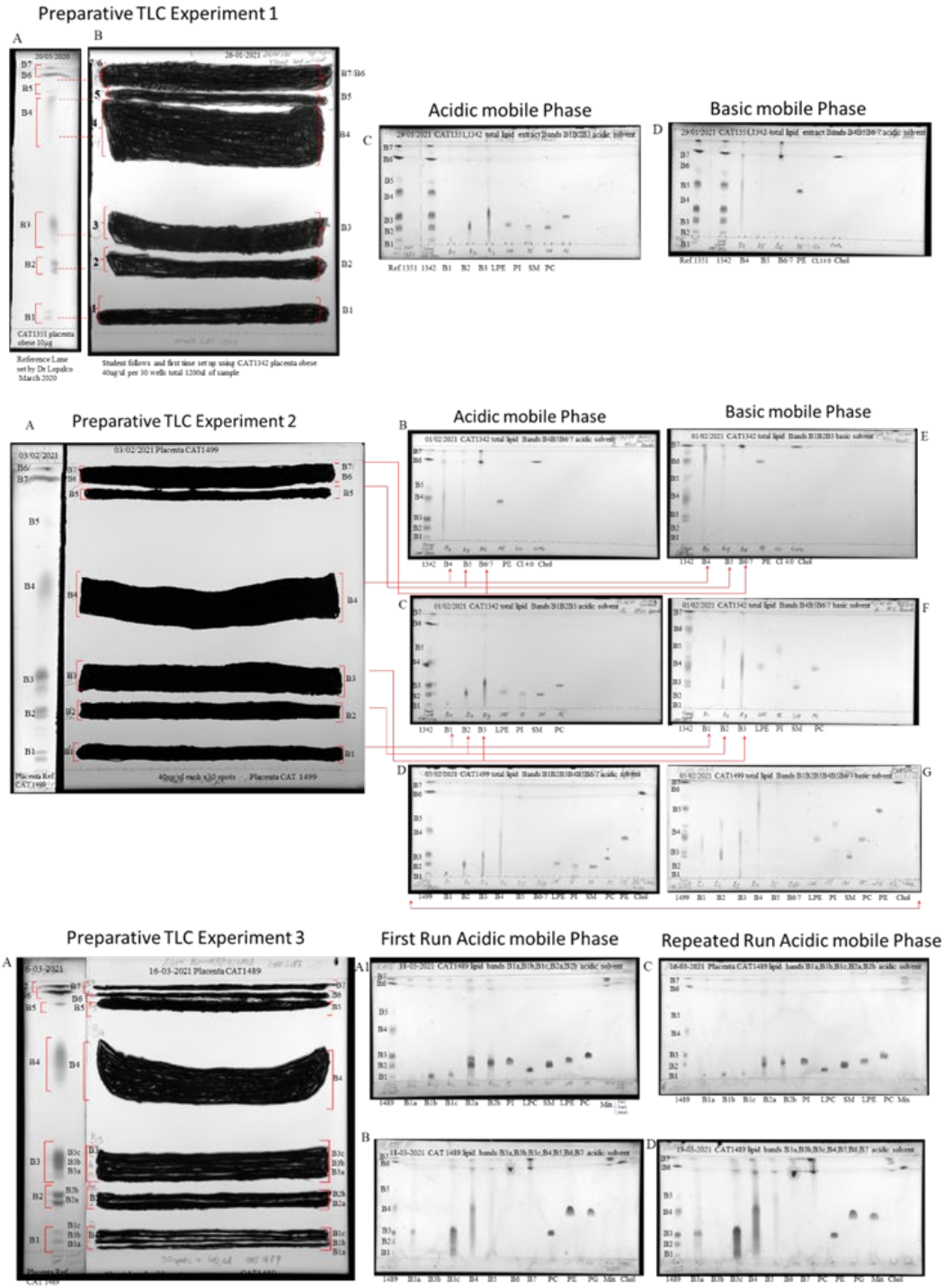

Figure 3:12: Silica scraping of total lipid bands using large plate 20x20cm preparative TLC, then each scraped lane was solvent extracted as per Bligh Dyer Method described previously in Chapter 2. Each separated band was run on analytical TLC using acidic and neutral solvents over three experiment sets, as shown in experiment1, 2, and 3

3.4.4 Results from Preparative TLC

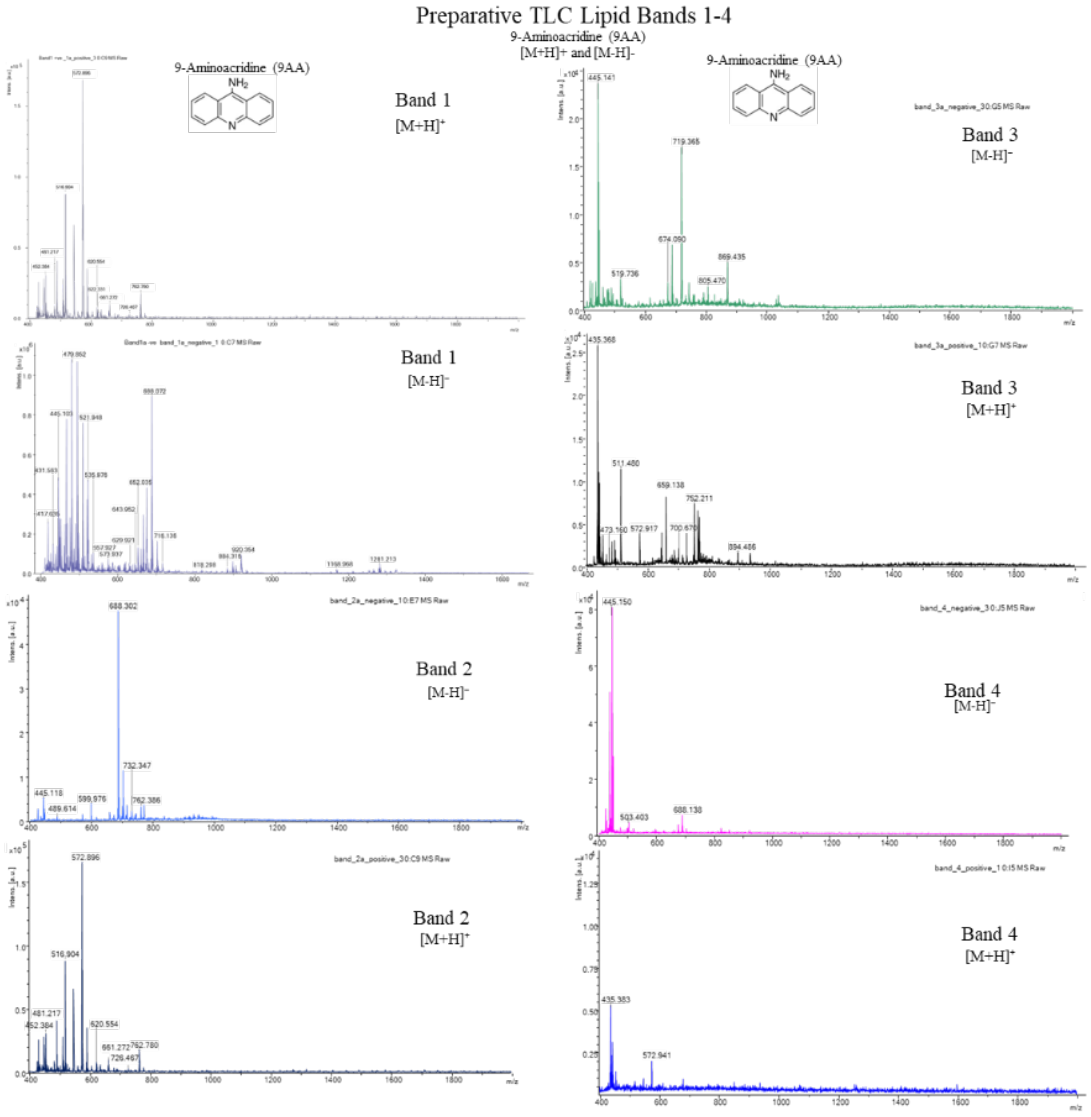

Figure 3:13: Preparative TLC Lipid Band 1-4 of the 3 experiments continuing below in Figure 3.14 Preparative TLC Lipid Band 5-7run in positive +ve and negative -ve ion mode on MALDI ToF MS in 9AA matrix.

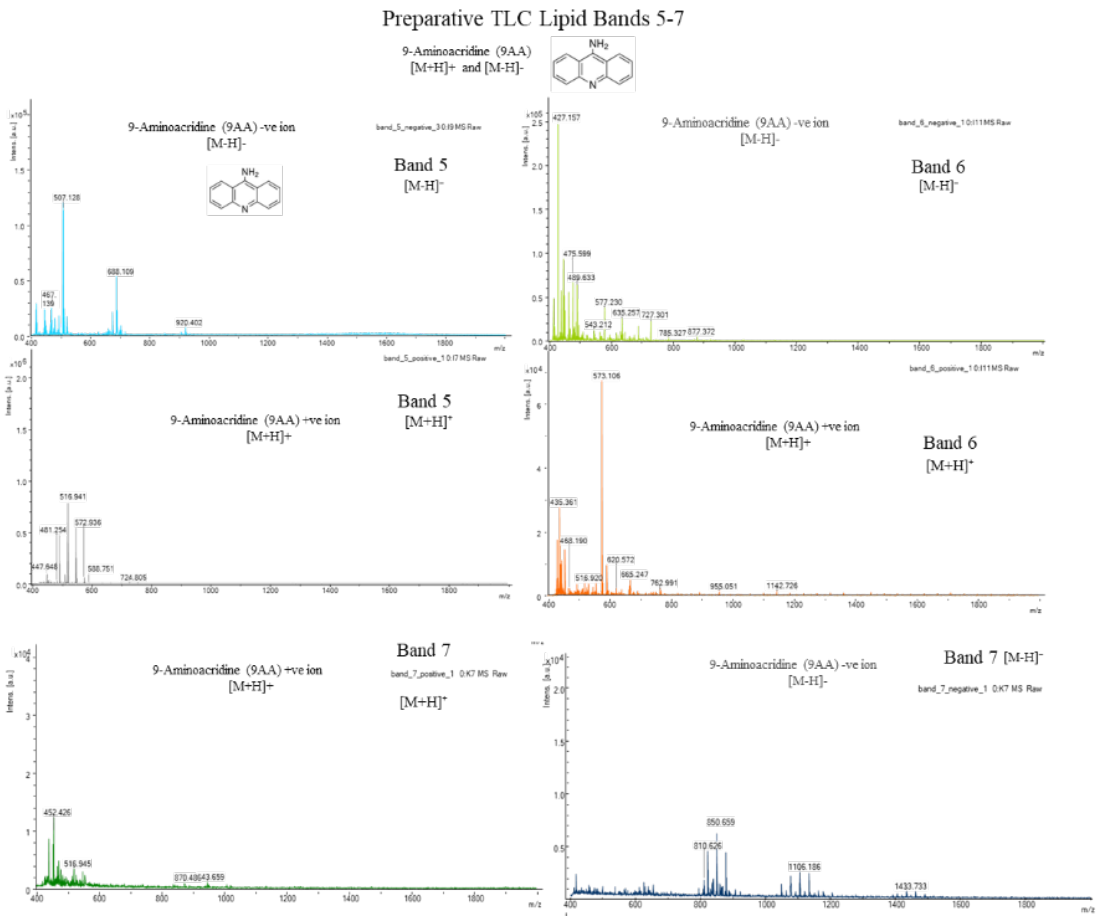

Figure 3:14 Preparative TLC Lipid Bands 5-7 of the 3 experiments continuing from the previous page, figure 3.13: band 5 and 6/7 run in positive +ve and negative -ve ion mode on MALDI ToF MS in 9AA matrix.

The general observations of preparative TLC purification of lipid bands assignment are based on visualisation during analytical TLC and further purity by preparative TLC. The MALDI observations allow the assignment of lipid species based on mass-to-charge ratio, *m/z,* as qualitative results. The prominent peaks take the hydrolysed state's ratio to the native state of lipid as PC only to observe differences in healthy versus diseased samples in blood plasma and placenta tissue.

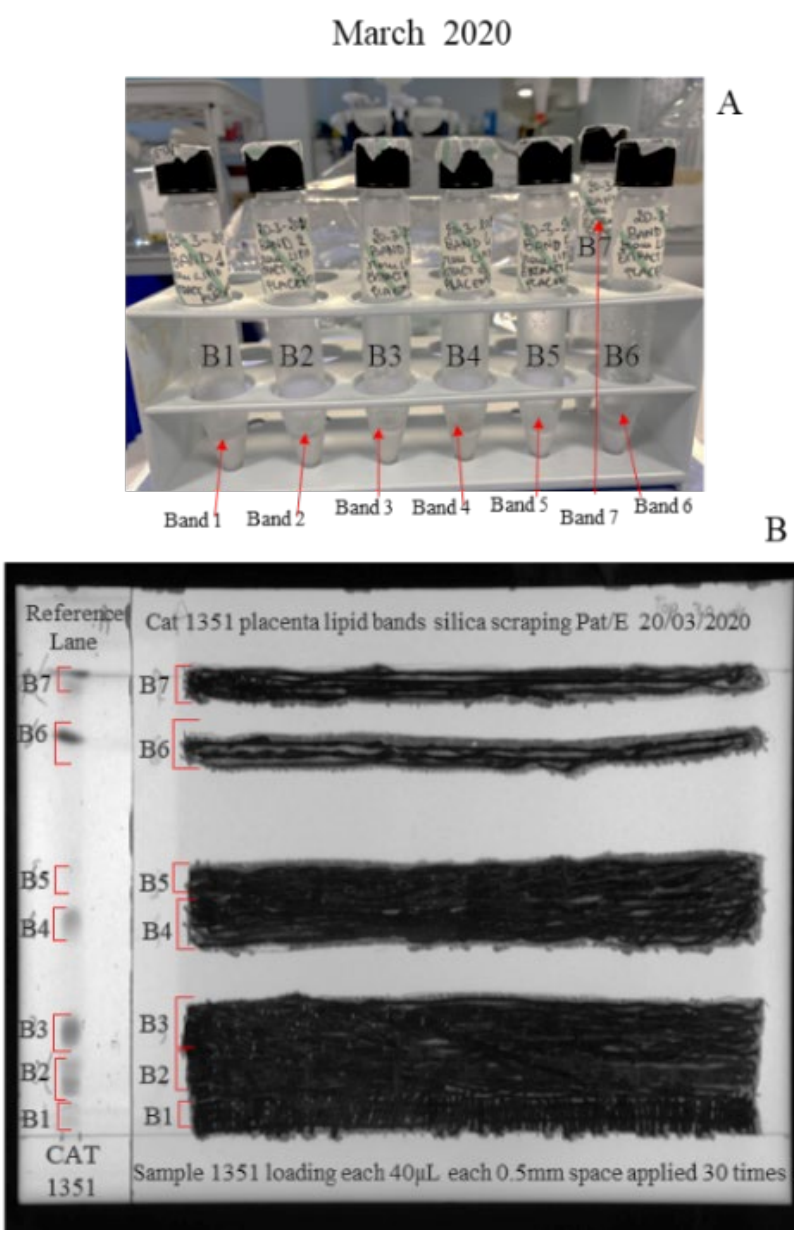

Figure 3:15: (A) Scraped silica bands during the first teaching of the method, prepared in methanol and stored at -80C. TLC based on Dr Loplaco TLC B, All placenta and plasma sample concentrations are the same throughout this research: 10mg/ml with 4ul or 8ul applied to TLC, followed by lipid standards at the same working concentration [1mg/ml] with aliquots 5ul PI, SM, LPE, LPC, PC, PG, Chol and PE, mono-, di-, triglycerides, all run in acidic mobile phase.

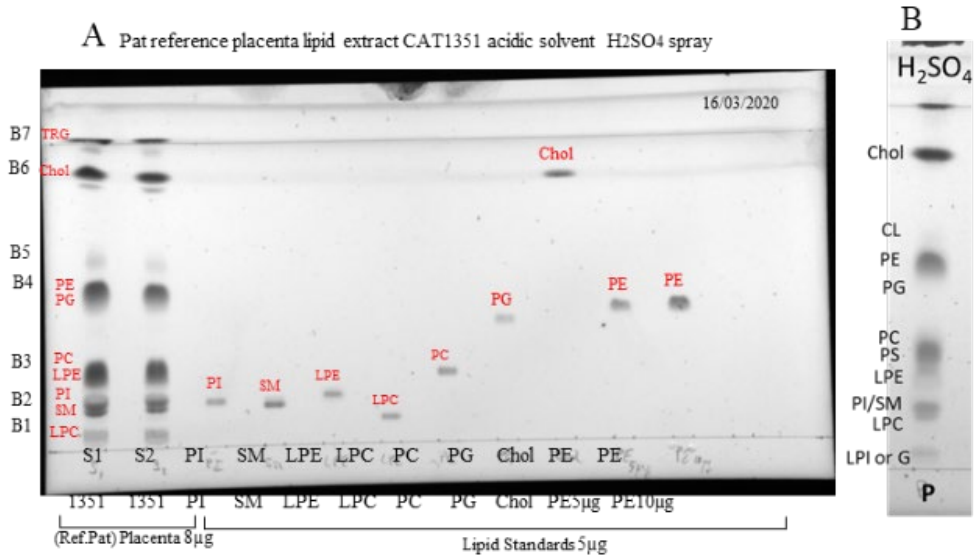

D B1 [M-H]- Lyso PI + Gangliosides
B1 [M+H]+ LPC,LPE MAG,DAG,TGR
B2 [M-H]- Sphingomyelin + LysoPE, +PI+ PS B2 [M+H]+ Sphingomyelin + LysoPC
B3 [M-H]- None
B3 [M+H]+ PC
B4 [M-H]- None
B4 [M+H]+ PE
B5 [M+H]+ micelles soap
B5 [M-H]- Cardiolipin CL 18:1
B6 [M+H]+ Cholesterol
B6/B7 [M-H]- Squalene , Cholesterol + TAG (triacyl glycerides)

Figure 3:16 A, B Dr Lopalco's TLC results in data during her teaching visit to Swansea. The A B shows two repeats of the same placental Cat1351 obese BMI samples S1, S2 followed by lipids standards at 1mg/ml 5ul. (B) Dr Lapalco's visit and teaching are included as a TLC reference guide during the original training process. (D). The student annotated lipid bands with lipid standards to show how they are obtained by cutting off the rest of the plate. Blue oval shapes are used to indicate band spreading. Dr Lopalco ran Swansea placenta samples (P) is the loaded placenta total lipid extract at the start line, G: Gangliosides, LPI: Lysophosphatidylinositol, LPC: Lysophosphatidylcholine, PI: Phosphatidylinositol, SM: Sphingomyelin, LPE: Lysophosphatidylethanolamine, PS: Phosphatidylserine, PC: Phosphatidylcholine, PG: phosphatidylglycerol, PE: Phosphatidylethanolamine, CL: Cardiolipin, Chol: Cholesterol.

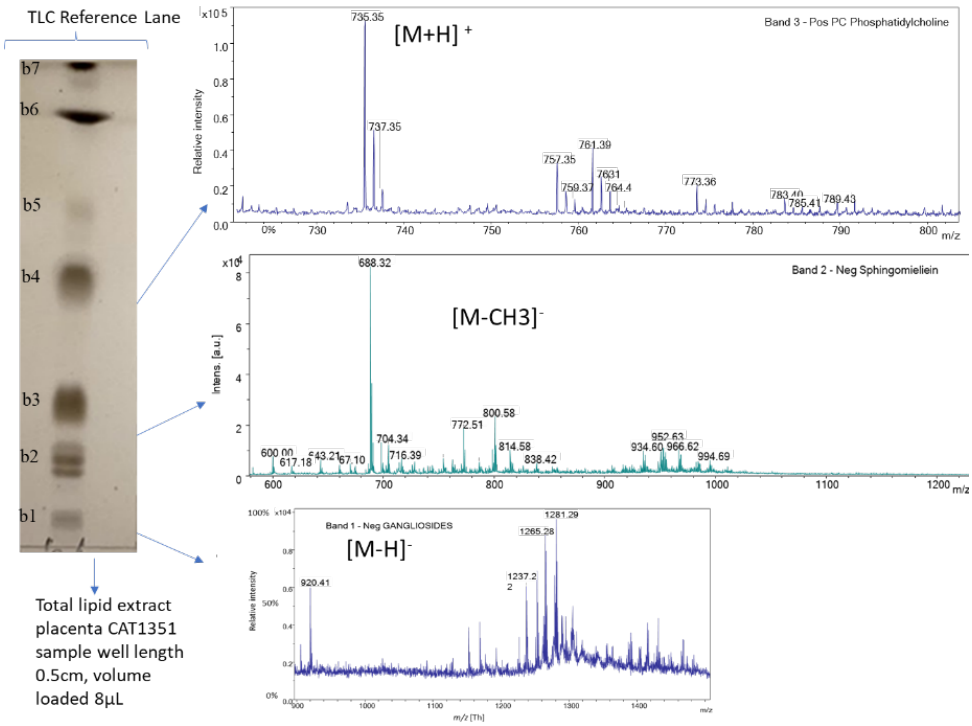

Figure 3:17 First result of Preparative TLC band3, band 2, band 1

3.4.5 MALDI TOF MS analysis of lipids separated with preparative TLC.

Having confirmed that preparative TLC consistently yielded 7 bands that had a putative assignment of various lipid families – lysophospholipids LPC, LPI, LPE, LSM, SM, and PS, the next step was to provide more information about each of these lipid families using MALDI TOF MS. Initial analysis (Figure 3.20) was made with samples sent to Dr Lopalco at University of Barri as the MS facility there re-opened after first COVID-19 lockdown sooner than the local Swansea University facility and this work was in collaboration with them. Further analysis was in Swansea. MALDI TOF MS analysis of bands 1, 2, and 3 was run in an acidic mobile phase on the analytical TLC and then on positive and negative ion mode MALDI matrix 9AA. The lower bands display ganglioside and polar hydrolysed lipid headgroups, moving up to observable lipids SM, PI, PS, LPC, PC, and PE, then in neutral mobile phase observable cholesterol and triglycerides. The scraped silica bands were not clean enough and contained smearing, and masses were different in MALDI due to unresolved lipid separation and would need additional separation; however, when lipid extracts from healthy placentas were sent to Italy, the total lipid extract well, as

comparative approaches to check Swansa samples run by the student. The preparative gave some clean separations but with smearing tailing for each band, indicating silica contamination and requiring additional clean sample separation.

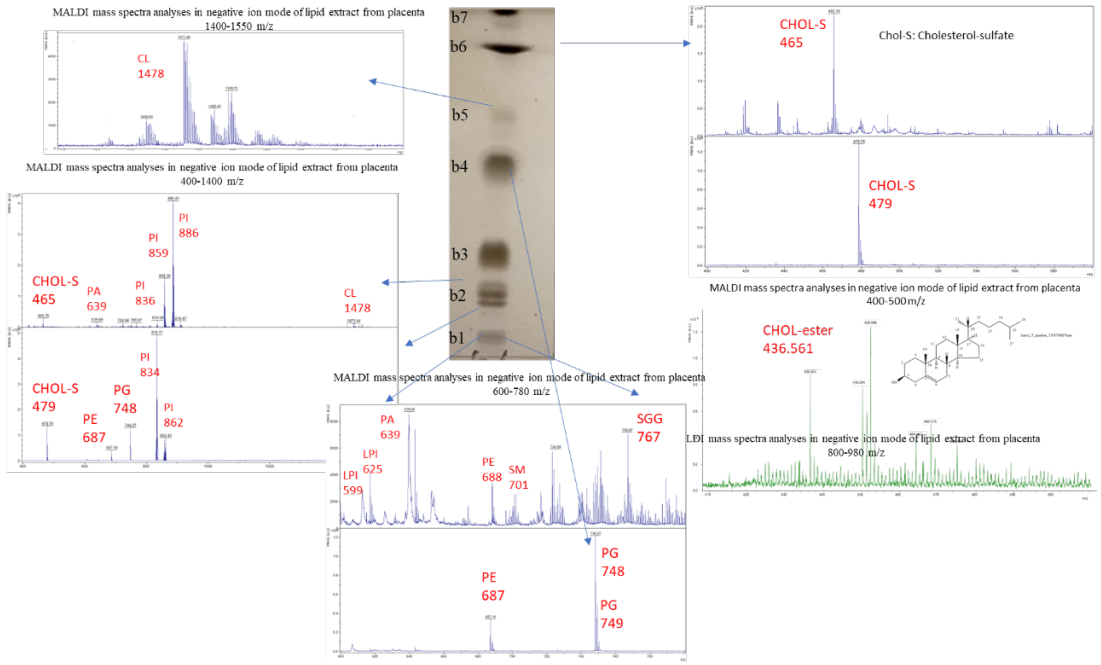

Figure 3:18 This is the first identification of lipid bands from preparative TLC and MALDI ToF MS results. Samples were sent to Dr Lopalco laboratory in Italy for an initial run of the total lipid extract from the placenta. Dr Lopalco analyses them as an introductory identification and guideline towards Swansea data compassion. The data in this figure contains data images sent from Dr Lopalco to use as a guide towards the data acquisition expected at Swansea Labs. Dr Lapalco's data figure for MALDI ToF mass spectra represents the following: In the middle of the figure, there is a preparative TLC strip as a guide for each lipid band eluted, and each lipid band scraped from the preparative TLC plates was extracted and run on MALDI ToF MS. Beginning from the bottom of the TLC plate strip showing lipid band 1 in negative ion mode noted as [M-H]- in DHB matrix Dr Loplaco identified as gangliosides, observable in MALDI ToF MS. In Band 2, Dr Loplaco identified lipid groups as sphingolipids and phosphatidylinositol PI dominating the mass spectra. It is consistent with lipid groups phosphatidylglycerol PG and phosphatidylethanolamine PE in lipid band 4 in negative ions. The lipid band 3 was run in positive ion mode noted as [M+H]+ Dr Lopalco interpreted it as phosphatidylcholine PC, Sphingomyelin SM, Ceramides, which construct a choline headgroup. Cardiolipin CL18:2 1478 m/z, possibly band 5 or 6, very visible, cholesterol esters 436.561 m/z, cholesterol sulphate 465.76 m/z and other cholesterol derivatives. These derivatives would require further analysis to confirm accuracy using electrospray ionisation and mass spectrometry.

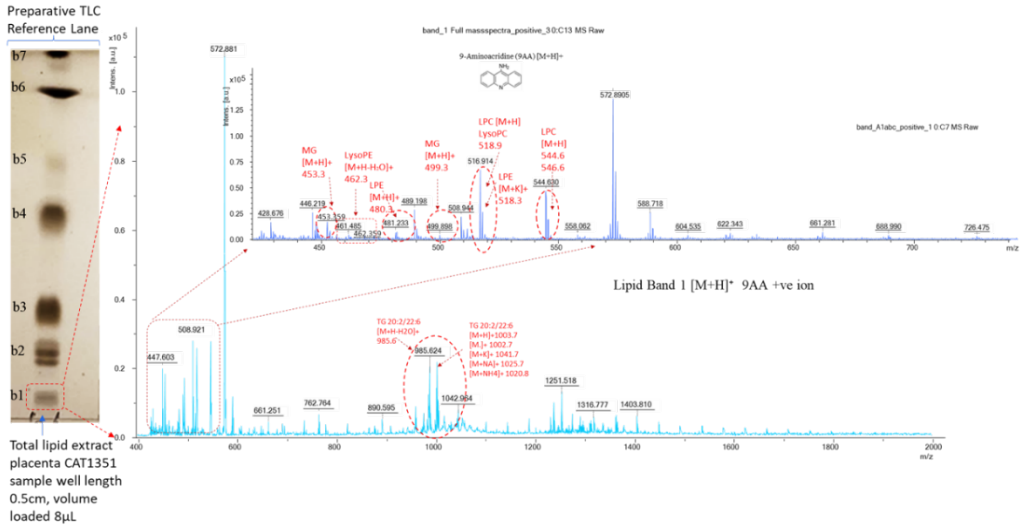

Figure 3:20 shows an example of Preparative TLC Lipid band 1. Figure 3:19 shows preparative TLC lipid band 1 specifically showed that better spectra were obtained from normal plasma lipid extracts than pre-emptive. As a result, I used normal MALDI and full mass spectra of band 1 from placental (left) and plasma (right) lipid extracts in negative ion mode with 9AA as a matrix. A pregnant woman with obesity provided both samples, zoomed in to the region 417-716 m/z (top left) of the wider placental 1220-1320 m/z (bottom right), 1225-1450 m/z plasma BMI Obese-9AA, and glycolipids (sphingolipid bases, saccharolipids, galactosidase, gangliosides, ceramides, glucosides). This figure shows the complete mass spectra of band 1 obtained using an acidic mobile phase during preparative TLC. Using the 9AA matrix, MALDI ToF MS was performed in positive ion mode. The top right spectra are zoomed in at 400-750 m/z 9AA+ve from the bottom right spectrum. The spectra of the silica scrapings from lipid Cath 1351 band 1 are not very clear; they are noisy at the lower end, so the purple colour of the top spectra illustrates that the spectra from ordinary lipid extraction are better and cleaner than those from preparative TLC scraping. A circular peak at 995-1000 indicates triglyceride hydrolysis. I used that purposely to show how I can better identify the total lipid extract from normal extraction instead of Preparative TLC without further cleanup.

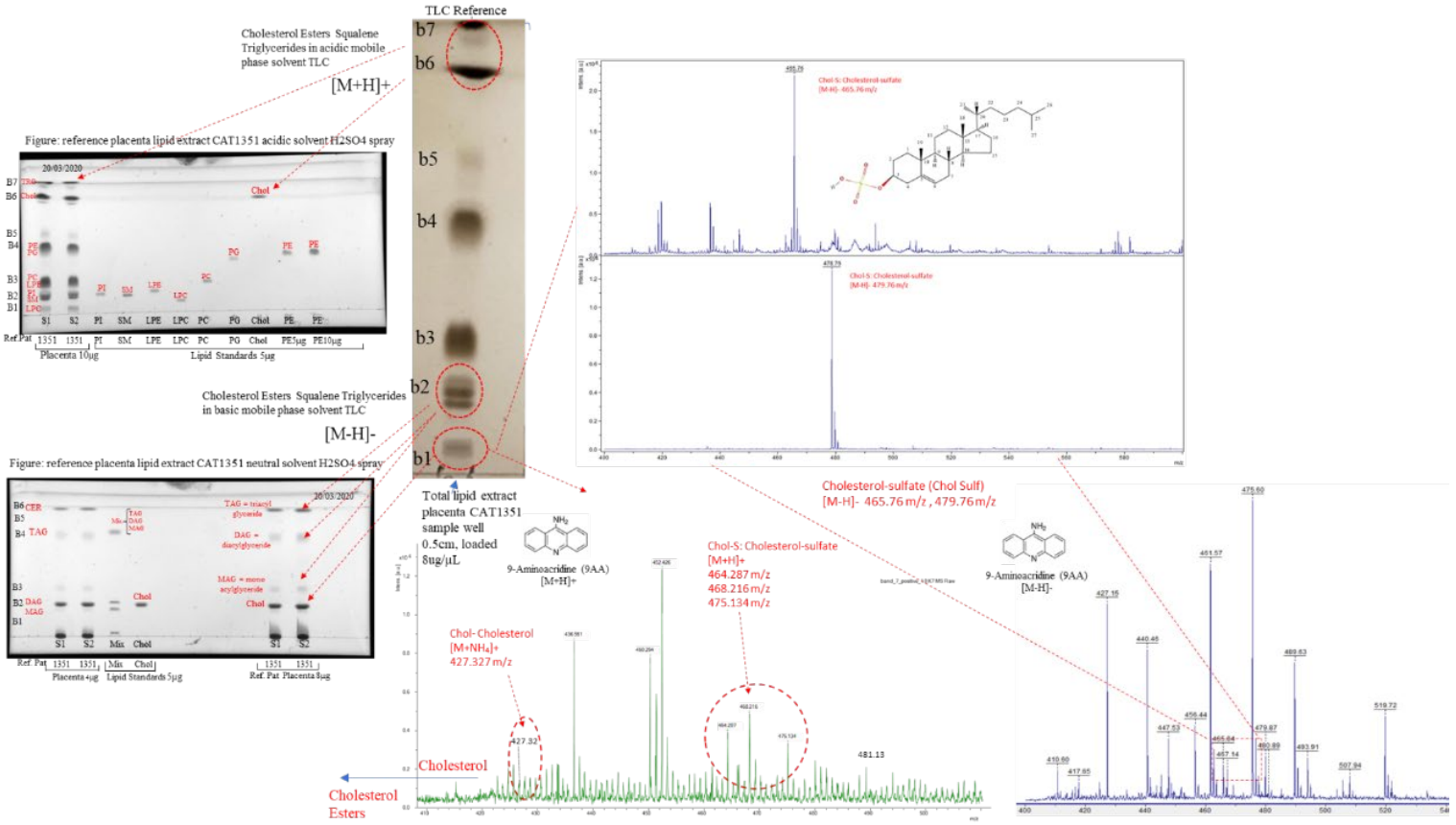

Figure 3:21 Preparative TLC identification of lipid band 1, band 2 and band 6/7 Figure 3:21 shows MALDI spectra run at Swansea Labs identified lipid bands 1 and top right MALDI mass spectra run and identified by Dr Lopalco Laboroarory in Italy identified as cholesterol sulphate run in negative ion [M-H]- and in positive ion mode [M+H]+ identified as 24-methylene-cholesterol sulfate, which also has been observed in Swansea labs from placenta and plasma samples run at Swansea on MALDI ToF MS.

Common Name:	Systematic Name:	Synonyms:	Lipid Maps ID:	Formula:	M (neutral)	Exact Mass Calculated m/z	Positive ion $[M+H]^+$	Formula:	Negative ion $[M-H+e^-]^-$	Formula:	Negative ion $[M-H-H_20+e]^-$	Negative ion $[M-CH3+e]^-$
Cholesterol	cholest-5-en-3β-ol	(3beta)-Cholest-5-en-3-ol,	LMST01010001	(C27H46O)	386.3549	386.354865	387.3621	(C27H47O)	383.3319	(C27H47O)	367.3365	371.3319
Desmosterol	cholest-5,24-dien-3β-ol	none	LMST01010016	(C27H44O)	384.3392	384.339215	385.3465	(C27H45O)	383.3319	(C27H43O)	365.3208	369.3163
7-dehydrocholesterol	cholesta-5,7-dien-3β-ol	7-DHC	LMST01010069	C27H44O	384.3392	384.339215	385.3465	(C27H45O)	383.3319	(C27H43O)	365.3208	369.3163
Cholesterol ester example: 5,6alpha-epoxy-cholesterol	5α,6α-epoxy-5α-cholestan-3β-ol	5,6alpha-epoxy-cholestanol	LMST01010011	C27H46O2	402.3498	402.34978	403.3571	(C27H47O2)	401.3425	(C27H45O2)	383.3314	387.3269
24S-hydroxy-cholesterol	cholest-5-en-3β,24S-diol	none	LMST01010019	C27H46O2	402.3498	402.34978	403.3571	(C27H47O2)	401.3425	(C27H45O2)	383.3314	387.3269
7alpha-hydroxy-cholesterol	cholest-5-en-3β,7α-diol	none	LMST01010013	C27H46O2	402.3498	402.34978	403.3571	(C27H47O2)	401.3425	C27H46O2	383.3314	387.3269
7beta-hydroxycholesterol	5-cholestene-3β,7β-diol	none	LMST01010047	C27H46O2	402.3498	402.34978	403.3571	(C27H47O2)	401.3425	(C27H45O2)	383.3314	387.3269
22R-hydroxycholesterol	cholest-5-en-3β,22R-diol	none	LMST01010086	C27H46O2	402.3498	402.34978	403.3571	(C27H47O2)	401.3425	(C27H45O2)	383.3314	387.3269
27-hydroxy-cholesterol	cholest-5-en-3β,26-diol	26-hydroxy-cholesterol	LMST01010057	C27H46O2	402.3498	402.34978	403.3571	(C27H47O2)	401.3425	(C27H45O2)	383.3314	387.3269
4beta-hydroxy-cholesterol	cholest-5-en-3β,4β-diol	none	LMST01010014	C27H46O2	402.3498	402.34978	403.3571	(C27H47O2)	401.3425	(C27H45O2)	383.3314	387.3269
Cholestenone	cholest-4-en-3-one	Cholestenone (delta 4)	LMST01010015	C27H44O	384.3392	384.339215	385.3465	(C27H45O)	383.3319	(C27H43O)	365.3208	369.3163
25-hydroxy-cholesterol	cholest-5-en-3β,25-diol	25-OHC	LMST01010018	C27H46O2	402.3498	402.34978	403.3571	(C27H47O2)	401.3425	(C27H45O2)	383.3314	387.3269
24-methylene-cholesterol sulfate	24-methylene-cholest-5-en-3β-ol-3-sulfate	none	LMST05020012	C28H46O4S	478.3117	478.311682	479.3190	(C28H47O4S)	477.3044	(C28H45O4S)	459.2933	463.2888
cholesterol sulfate	cholest-5-en-3β-yl hydrogen sulfate	cholesteryl sulfate	LMST05020016	C27H46O4S	466.3117	466.311682	467.319	(C27H47O4S)	465.3044	(C27H45O4S)	447.2933	451.2888

Input Mass	Matched Mass	DELTA	Name	Formula	Ion	LMSD	LM_ID	Common Name	Systematic Name	Main class	Sub class	Mass	Formula
465.303892	465.3044	0.0005	ST 27:1;O;S	C27H46O4S	[M-H]-	e.g.	LMST05020016	cholesterol sulfate	cholest-5-en-3beta-yl hydrogen sulfate	Steroid conjugates [ST05]	Sulfates [ST0502]	466.31	C27H46O4S
465.303892	465.2987	0.0052	LPA 20:0	C23H47O7P	[M-H]-	e.g.	LMGP10050018	PA(20:0/0:0)	1-eicosanoyl-glycero-3-phosphate	Glycerophosphates [GP10]	Monoacylglycerophosphates [GP1005]	466.31	C23H47O7P
465.303892	465.3222	0.0183	ST 27:1;O6	C27H46O6	[M-H]-								
465.303892	465.3374	0.0335	ST 31:5;O3	C31H46O3	[M-H]-								
465.303892	465.2647	0.0392	ST 29:7;O5	C29H38O5	[M-H]-								

Figure 3:20 Cholesterol derivatives conjugate Cholesterol sulphate or glycerophosphatydic acid 465 regarding calculations explained later on in the MALDI results section

Common Name:	Systematic Name:	Lipid Maps ID:	Formula:	M (neutral)	Exact Mass Calc m/z	Positive ion $[M+H]^+$	Formula:	Negative ion [M-H]+e- (e)= 0.00054858	Formula:
Cholesterol	cholest-5-en-3β-ol	LMST01010001	(C27H46O)	386.3549	386.354865	387.3621	(C27H47O)	383.3319	(C27H47O)
Desmosterol	cholest-5,24-dien-3β-ol	LMST01010016	(C27H44O)	384.3392	384.339215	385.3465	(C27H45O)	383.3319	(C27H43O)
7-dehydrocholesterol	cholesta-5,7-dien-3β-ol	LMST01010069	C27H44O	384.3392	384.339215	385.3465	(C27H45O)	383.3319	(C27H43O)
5,6alpha-epoxy-cholesterol	5α,6α-epoxy-5α-cholestan-3β-ol	LMST01010011	C27H46O2	402.3498	402.34978	403.3571	(C27H47O2)	401.3425	(C27H45O2)
24S-hydroxy-cholesterol	cholest-5-en-3β,24S-diol	LMST01010019	C27H46O2	402.3498	402.34978	403.3571	(C27H47O2)	401.3425	(C27H45O2)
7alpha-hydroxy-cholesterol	cholest-5-en-3β,7α-diol	LMST01010013	C27H46O2	402.3498	402.34978	403.3571	(C27H47O2)	401.3425	(C27H46O2)
7beta-hydroxycholesterol	5-cholestene-3β,7β-diol	LMST01010047	C27H46O2	402.3498	402.34978	403.3571	(C27H47O2)	401.3425	(C27H45O2)
22R-hydroxycholesterol	cholest-5-en-3β,22R-diol	LMST01010086	C27H46O2	402.3498	402.34978	403.3571	(C27H47O2)	401.3425	(C27H45O2)
27-hydroxy-cholesterol	cholest-5-en-3β,26-diol	LMST01010057	C27H46O2	402.3498	402.34978	403.3571	(C27H47O2)	401.3425	(C27H45O2)
4beta-hydroxy-cholesterol	cholest-5-en-3β,4β-diol	LMST01010014	C27H46O2	402.3498	402.34978	403.3571	(C27H47O2)	401.3425	(C27H45O2)
Cholestenone	cholest-4-en-3-one	LMST01010015	C27H44O	384.3392	384.339215	385.3465	(C27H45O)	383.3319	(C27H43O)
25-hydroxy-cholesterol	cholest-5-en-3β,25-diol	LMST01010018	C27H46O2	402.3498	402.34978	403.3571	(C27H47O2)	401.3425	(C27H45O2)
24-methylene-cholesterol sulfate	24-methylene-cholest-5-en-3β-ol-3-sulfate	LMST05020012	C28H46O4S	478.3117	478.311682	479.3190	(C28H47O4S)	477.3044	(C28H45O4S)
cholesterol sulfate	cholest-5-en-3β-yl hydrogen sulfate	LMST05020016	C27H46O4S	466.3117	466.311682	467.319	(C27H47O4S)	465.3044	(C27H45O4S)
Cholesterol Ester 18:2	cholest-5-en-3β-yl (9Z,12Z-octadecadienoate)	LMST01020008	C45H76O2	648.5845	648.58453	649.5918	(C45H77O2)	647.5773	(C45H75O2)

Name	Symbol average mass	Relative Atomic Mass	Abund.
Carbon	C (12)	12.000000	98.9
Hydrogen	H (1)	1.007825	99.99
Nitrogen	N (14)	14.003074	99.63
Oxygen	O (16)	15.994915	99.76
Phosphorus	P (31)	30.973763	100
Sulfur	S (32)	31.972072	95.02
Sodium	Na (23)	22.989770	100
Potassium	K (39)	38.963708	93.2
atomic mass unit (amu) of electron	(e)-	0.000549	
Acetate ion OAc (C2H3O2-)	(C2H3O2-)	59.012756	
Methyl group	CH3	15.023475	
water	(H2O)	18.010564	
CH2 methyl ketone group	CH2	13.007825	
OH Hydoxide group	OH	17.002739	
SO_4H Sulphate Hydroxide	SO_4H	96.959552	
Cholesterol	(C27H46O)	386.354865	
SO_4H+ cholesterol= cholesteryl sulfate	C27H46O4S	483.314452	
cholesterol sulfate (-H2O)	C27H46O4S - (H2O)	18.010564	
Cholesterol sulfate negative ion [M-H]-	(C27H46O4S)	465.303892	
24-methylene-cholesterol sulfate	(C28H46O4S)	496.322247	
24-methylene-cholesterol sulfate - H2O	(C28H46O4S) - (H2O)	478.311683.	

Figure 3:21 Cholesterol derivatives conjugate Cholesterol sulphate or glycerophosphatydic acid 465 regarding calculationsThe theoretical calculations were done using Excel, and lipid maps were matched. The calculation table for cholesterol sulphate and derivatives is below.

As cholesterol elutes with triglycerides first during neutral mobile phase TLC, it ranks lowest on the plate. Acidic mobile phase TLC elutes cholesterol last on the spot 6/7. MALDI detects cholesterol only as cholesterol esters, sulphates in negative ion mode or cholesterol esters since cholesterol does not ionise well. Cholesterol sulphate in acidic solvent elutes band 6/7 and cholesterol and triglycerides. Cholesterol elutes in the neutral mobile phase in band 2, showing MALDI Mass spectrum of attentive assignment (See table below) of phosphatidic acid PA, 465.303 m/z and or a cholesterol sulphate 465.642 m/z, 468.216 m/z, 475.134 m/z, 479.76 24-methylene-cholesterol sulphate m/z, cholesterol with ammonium ion (NH4+) 427.327 m/z, with TLC plates placenta total lipid extract samples showing the presence of cholesterol standard and mix of triglycerides (monoglyceride, diglyceride and triglycerides) standard.

The theoretical calculations were done using Excel, and using lipid maps were matched. The calculation table for cholesterol sulphate and derivatives is below.

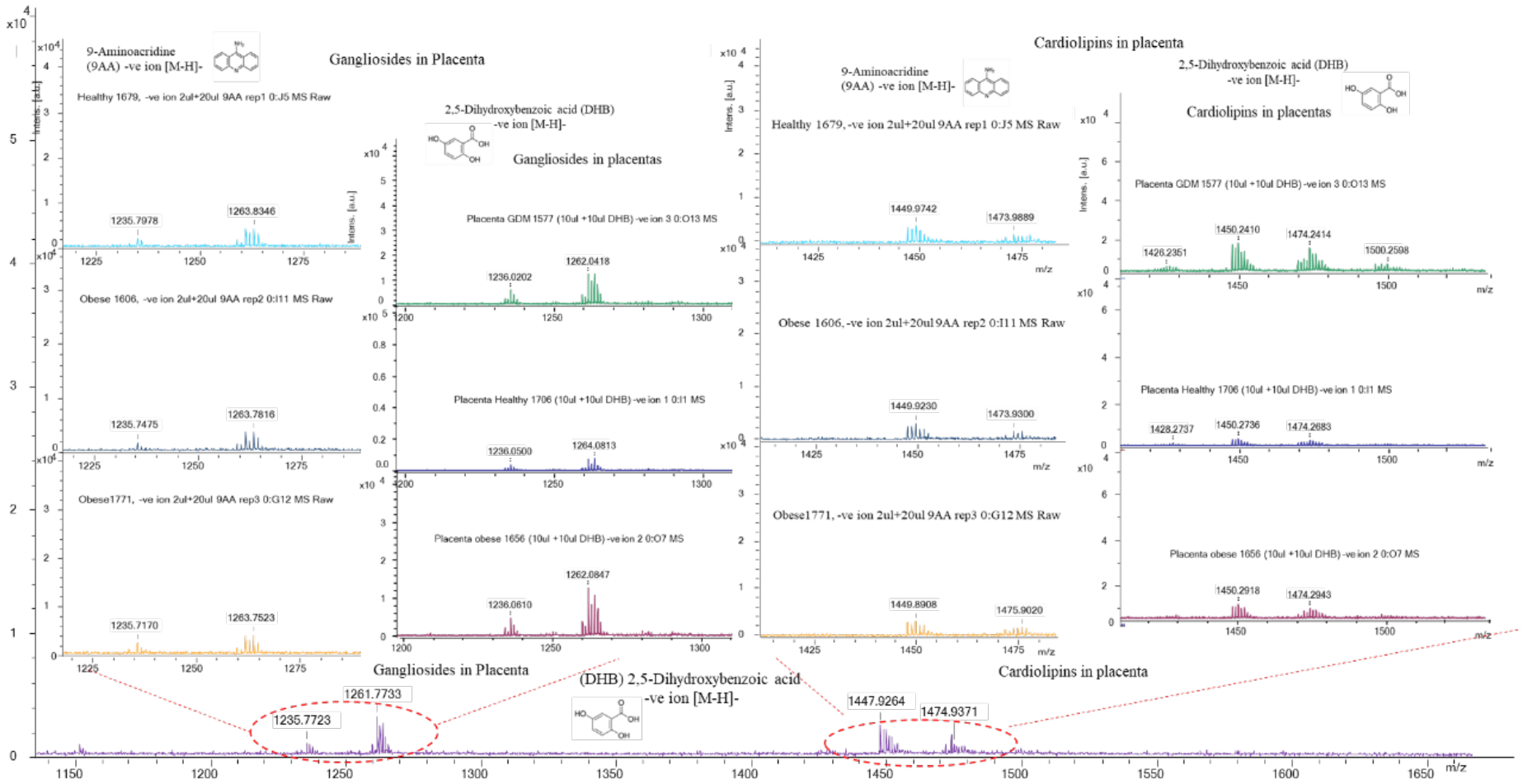

Figure 3:22 Gangliosides and cardiolipins in placental lipid extracts samples GDM/Obese 1614, -ve ion 2ul+20ul 9AA rep1 0:K10 MS Ganglioside and Cardiolipins in the placenta in negative ion 9AA, DHB

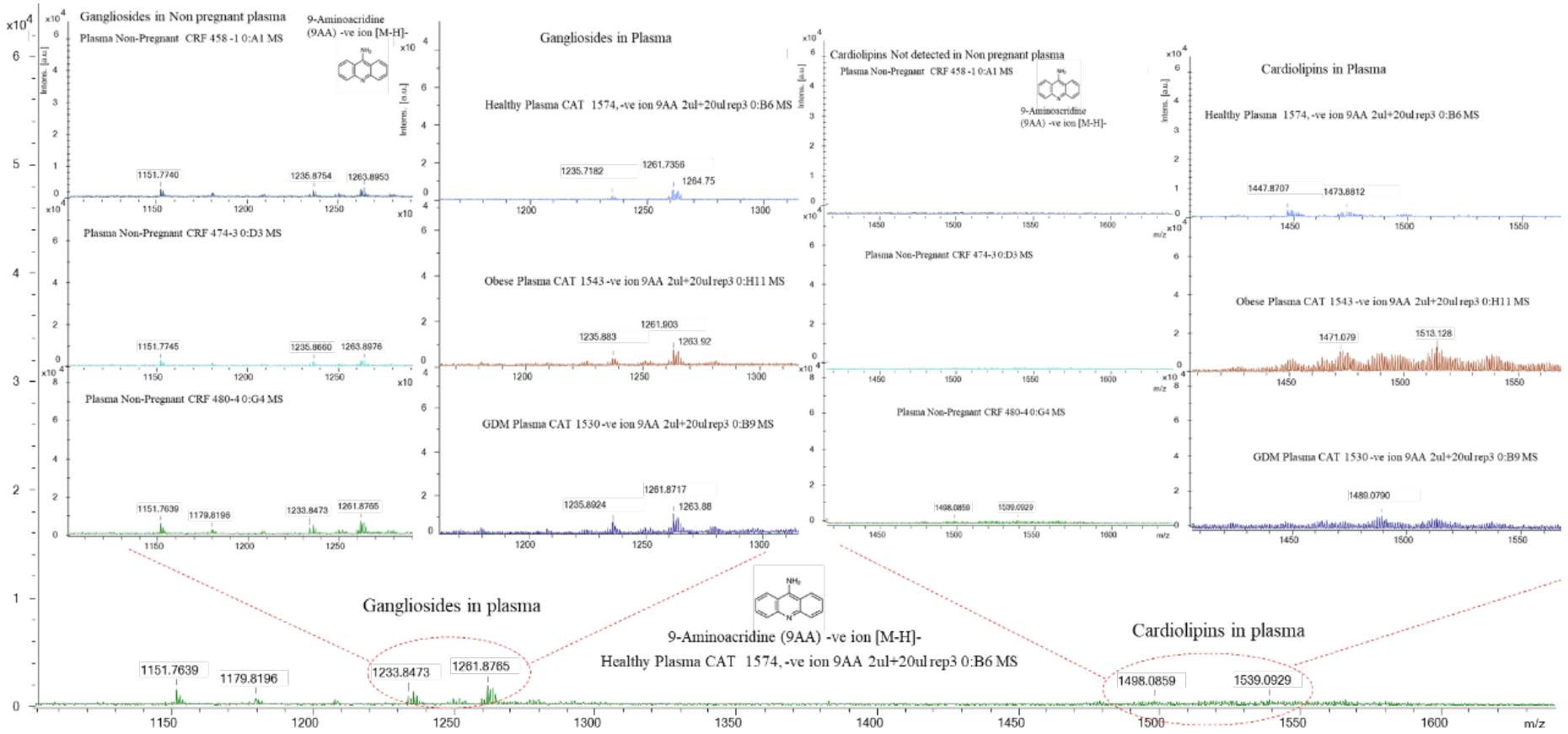

Figure 3:23 Gangliosides and cardiolipins in plasma lipid extracts analyses in negative ion mode with -ve 9AA matrix. Non-pregnant plasma (n = 3) versus pregnant plasma (n = 3 – one each of healthy weight, obese and GDM).

3.4.6 LPC and PC analysis in plasma and placental total lipid extracts.

As expected, there are big differences in the total lipid extract of placental tissue versus plasma. Plasma is rich in low-density lipoproteins, and tissue contains less depending on the patient's BMI. Plasma contains cholesterol and lipoproteins, so the dried lipid extract was always much bigger than from the placenta. There were purity challenges with smearing on TLC and noisy MALDI spectra.

As MALDI TOF MS clearly showed several different species of PC and LPC in the biological samples of interest, and there was wider interest in the research group in using this ratio to reveal overall inflammation status, further analysis of this using total lipid extracts was made. All mass spectral data, focusing on calculating the PC/LPC ratios, are included in the Excel tables attached in the appendices. Smaller tables represent the plotted graphs of the PC/LPC *m/z* intensities values and the average of each total lipid extra placenta or plasma of three repeats. Because of matrix ions, the MALDI ToF MS technique is known for its high chemical noise' in the mass spectra below 400 *m/z*. So, some low molecular weight dissociating fragments of phospholipids that occur during the in-source ionisation could not be identified. Still, we can observe some useful peaks in the low mass range, which are identified and compared through the literature in the negative ion Excel table in the MALDI result chapter and observable peaks in negative ion [M-H]- are highlighted in the green column in the excel table presented in the MALDI result chapter.

3.4.7 Lipid bands identification on MALDI

Calculations used in this study of total lipid extract used to calculate the relative percentage ratio using hydrolysed lysophosphatidylcholine LPC to native form phosphatidylcholine PC was adapted from literature by Angelini R. et al., 2014 and it using “intact horse serum for the determination of the PC/LPC by MALDI-TOF MS as “an easy-to-follow lipid biomarker of inflammation” *(562-564)* In addition the publication by Lopalco P. at al. 2016 *(565)*, Lopalco P. et al. 2019 *(566)*, Lopalco P. et al. 2019 *(567)*, Eibisch M. et al., 2011,*(223)* Le Bon A et al.,2018,*(568)*

3.4.8 Explaining calculation steps include tables with annotations

The theoretical calculations were done using Excel, and using lipid maps were matched. The calculation table for cholesterol sulphate and derivatives is below.

Using each element's atomic masses, then showing how the PC LPC theoretical literature masses versus observed in experiments study then calculated for positive ion mode using Lipid Mass Tables check and excel individual input as lipid maps do not include mass of the electron (e^-) in the negative ion mode [M-H]-, In mass spectrometry measurements, the notation of mass accuracy error is denoted as parts-per-million (ppm, 10−6), parts-per-billion (ppb, 10−9), parts-per-trillion (ppt, 10−12) and parts-per-quadrillion (ppq, 10−15)

Agelini 2014 Theoretical Mass - from lipid Maps		Edyta Actual MALDI Observed mass m/z [M+H]+ in Healthy_Placenta_	Standard deviation of 3 reps of each sample	lipid maps	Positive ion mode with added aducts hydrogen and sodoim				Calculated relaive mass acucracy parts per million (ppm) (Mm-Mt) / (Mt x10^{-6})	
PC/LPC	[M+H]+	Experimental m/z [M+H]+	Experiemntal SD error	Matched Mass	Lipid maps relative error	Name	Formula	Positive ion $[M+H]^+$	Scienetific notation	numeral notation
LPC 16:0 (+H+)	496.3398	496.3800	0.04	496.3398	0	LPC 16:0	C24H50NO7P	[M+H]+	8.09E-11	(+/-) 8.1 ppt
LPC 16:0 (+Na+)	518.3241	518.4305	0.16	518.3217	0.0024	LPC 16:0	C24H50NO7PNa	[M+Na]+	2.10E-10	(+/-) 2.1 ppb
LPC 18:2 (+H+)	520.2905	520.3860	0.05	520.3398	0.0493	LPC 18:2	C26H50NO7P	[M+H]+	8.88E-11	(+/-) 9 ppt
LPC 18:1 (+H+)	522.1672	522.4241	0.08	522.3554	0.0362	LPC 18:1	C26H52NO7P	[M+H]+	1.32E-10	(+/-) 1.3 ppb
LPC 18:0 (+H+)	524.2854	524.4047	0.03	524.3135	0.0281	LPC 20:5	C28H48NO7P	[M+H-H2O]+	1.74E-10	(+/-) 2 ppb
LPC 18:2 (+Na+)	542.3241	not observed	N/A	542.3241	0	LPC 20:5	C28H48NO7P	[M+H]+	N/A	N/A
LPC 18:1 (+Na+)	544.2672	544.3913	0.05	544.3164	0.0492	LPC O-18:2	C26H52NO6PK	[M+K]+	1.38E-10	(+/-) 1.4 ppb
LPC 18:0 (+Na+)	546.3554	546.3840	0.02	546.3530	0.0024	LPC 18:0	C26H54NO7PNa	[M+Na]+	5.67E-11	(+/-) 6 ppt
PC 16:0/18:2 (+H+)	758.5694	758.6673	0.12	758.5694	0	PC 34:2	C42H80NO8P	[M+H]+	1.29E-10	(+/-) 1.3 ppb
PC 16:0/18:1 (+H+)	760.5851	760.5850	0.15	760.5851	0	PC 34:1	C42H82NO8P	[M+H]+	-1.72E-13	(+/-) 2 ppt
PC 16:0/18:2 (+Na+)	780.5538	780.6207	0.06	780.5514	0.0024	PC 34:2	C42H80NO8PNa	[M+Na]+	8.88E-11	(+/-) 9 ppt
PC 16:0/18:1 (+Na+) and PC 16:0/20:4 (+H+)	782.5694	782.6326	0.06	782.5670	0.0024	PC 34:1	C42H82NO8PNa	[M+Na]+	8.38E-11	(+/-) 9 ppt
PC 18:0/18:3 (+H+)	784.5851	784.6526	0.07	784.5851	0	PC 36:3	C44H82NO8P	[M+H]+	8.61E-11	(+/-) 9 ppt
PC 18:0/18:2 (+H+)	786.6454	786.5303	0.28	786.6007	0.0447	PC 36:2	C44H84NO8P	[M+H]+	-8.95E-11	(+/-) 9 ppt
PC 16:0/20:4 (+Na+)	804.5749	804.6244	0.08	804.5514	0.0235	PC 36:4	C44H80NO8PNa	[M+Na]+	9.07E-11	(+/-) 9 ppt
PC 18:0/18:3 (+Na+)	806.5694	806.6303	0.06	806.5670	0.0024	PC 36:3	C44H82NO8PNa	[M+Na]+	7.85E-11	(+/-) 8 ppt
PC 18:0/18:2 (+Na+)	808.5851	808.5834	0.22	808.5827	0.0024	PC 36:2	C44H84NO8PNa	[M+Na]+	8.70E-13	(+/-) 9 ppt

Figure 3:24 Peaks list adapted from literature by Angelini 2014 theoretical mass m/z Spectrum: E:\Edyta Placenta flex analysis all data 22 04 2021\Positive ion mode 1mgml\CAT1315[10mg-ml]

Sample ID	Observed m/z	Intens.	S/N set to 9	Sample ID	Observed m/z	Intens.	S/N set to 9	Sample ID	Observed m/z	Intens.	S/N set to 9
CAT 1315 - 1st rep	496.3458259	124346	33.72302933	CAT 1315 - 2nd rep	496.4157953	99018	32.56718082	CAT 1315 - 3rd rep	496.4260453	89273	32.30956681
	518.4447797	144043	38.38645235		518.504833	289057	99.51168153		518.5104347	374103	140.7706944
	524.3846068	54754	13.54751328		524.455741	91504	30.55715802		524.4646696	86971	31.68918633
	758.5348193	70576	18.33304141		758.609914	44198	15.84675108		758.6214921	76751	32.35866334
	760.5565502	73689	19.29504323		760.6227814	50089	18.25636366		760.634539	43026	17.20714171
	780.5278378	30795	6.050805606		782.6113365	46923	17.00050467		780.5974413	36134	13.76007554
	782.5404357	83966	23.51700769		784.6252659	31350	10.47010682		782.622494	36186	14.07244039
	784.5525036	55515	14.26512351		786.6449423	26559	8.461043948		784.5820945	30138	11.24903581
	786.360054	37298	8.34119908		808.6290446	20973	6.228147739		786.650872	35793	13.88897511
	804.5285507	30289	6.233222843						804.6245588	19018	6.161309706
	806.5491321	38687	9.041291154						806.6223239	20093	6.671725299
	808.5556786	35553	7.993364733						808.6290446		

Figure 3:25 Showing 3 repeats, then put each intensity versus sample identity in GraphPad using sample identification type and maldi calculate the average intensity of the repeats to plot for each

Graph Pad Prism Group comparison Kruskal –Wallis's test descriptive statistics Anova results					
Plasma Groups BMI	Samples	Std. Deviation	Std. Error Mean	Lower 95% CI	Upper 95% CI
Control (Non-Pregnant)	n=7	2.357	0.891	0.1984	4.559
Healthy BMI	n=10	1.411	0.4463	3.443	5.462
Obese BMI	n=10	1.824	0.5767	2.047	3.618
GDM BMI	n=10	2.377	0.7518	5.462	7.019

Figure 3:26 In Graph pad, when you do the plots, then use one-way non-parametric test Kruskall Wallis One way Anova to compare between each group and eal liner parallel, and gives you an idea of standard error as per table.

Placenta Plasma 10 [mg/mL] MALDI ToF MS	Peak intensities 3 repeats per sample	LPC 16:0 (+H+) 496.3398 m/z	LPC 16:0 (+Na+) 518.3241 m/z	LPC 18:0 (+H+) 524.2854 m/z	LPC 18:0 (+Na+) 546.3554	PC 16:0/18:2 (+H+) 758.5694 m/z	PC 16:0/18:1 (+H+) 760.5851 m/z	PC 16:0/18:2 (+Na+) 780.5538 m/z	PC 16:0/18:1 (+Na+); PC 16:0/20:4 (+H+) 782.5694 m/z	PC 18:0/18:3 (+H+) 784.5851 m/z	PC 18:0/18:2 (+H+) 786.6454 m/z	PC 16:0/20:4 (+Na+) 804.5749 m/z	PC 18:0/18:3 (+Na+) 806.5694 m/z	PC 18:0/18:2 (+Na+) 808.5851 m/z	∑LPC	∑PC	∑PC/∑LPC	Average of 3 Replicat
Edyta Observed LPC ,PC m/z		496.3458	518.445	524.385	0	758.535	760.557	780.528	782.540	784.553	786.360	804.529	806.549	808.556				
Sample refernce	Intensity 3 reps	Intensity 3 reps	Intensity 3 reps	Intensity 3 reps	Intensity 3 reps	Intensity 3 reps	Intensity 3 reps	Intensity 3 reps	Intensity 3 reps	Intensity 3 reps	Intensity 3 reps	Intensity 3 reps	Intensity 3 reps	Intensity 3 reps				
CAT1315 tissue	1st repeat	56724.000	78882.000	26690.000	0	30404.000	30404.000	0	35993.000	23123.000	20321.000	23123.000	20321.000	0	162296.000	183689.000	1.131814709	
CAT1315 tissue	2nd repeat	119748.000	233643.000	66810.000	0	53608.000	53608.000	0	64682.000	0	38278.000	44770.000	0	0	420201.000	254946.000	0.606723925	
CAT1315 tissue	3rd repeat	124346.000	144043.000	54754.000	0	70576.000	73689.000	30795.000	83966.000	55515.000	45256.000	30289.000	38687.000	35553.000	323143.000	464326.000	1.436905642	1.0585
CAT 1487 tissue	1st repeat	38869.000	125406.000	33240.000	0	41448.000	40984.000	38880.000	57361.000	37114.000	42285.000	36260.000	41085.000	0	197515.000	335417.000	1.698184948	
CAT 1487 tissue	2nd repeat	40885.000	135198.000	33085.000	0	42307.000	46486.000	41093.000	62994.000	42997.000	47210.000	63405.000	42652.000	38543.000	209168.000	427687.000	2.044705691	
CAT 1487 tissue	3rd repeat	37614.000	82551.000	25422.000	0	46290.000	49174.000	45448.000	69266.000	46050.000	47697.000	68296.000	44974.000	37828.000	145587.000	455023.000	3.125437024	2.2894
CAT1489 tissue	1st repeat	55519.000	201886.000	50850.000	0	59941.000	59670.000	64685.000	84422.000	59596.000	63845.000	74687.000	60410.000	48863.000	308255.000	576119.000	1.868968873	
CAT1489 tissue	2nd repeat	40843.000	113665.000	36076.000	0	68062.000	59981.000	62598.000	92559.000	62004.000	62604.000	77243.000	68849.000	53076.000	190584.000	606976.000	3.184821391	
CAT1489 tissue	3rd repeat	37614.000	9300.000	0	0	0	0	3967.000	0	0	0	0	0	3875.000	46914.000	7842.000	0.167156925	1.7403
CAT1494 GDM tissue	1st repeat	65572.000	179767.000	42768.000	0	42813.000	39627.000	0	44020.000	35670.000	60656.000	34258.000	0	0	288107.000	257044.000	0.892182418	
CAT1494 GDM tissue	2nd repeat	56068.000	150021.000	35464.000	0	33654.000	33743.000	0	39585.000	28397.000	0	0	0	27866.000	241553.000	163245.000	0.675814418	
CAT1494 GDM tissue	3rd repeat	43424.000	66296.000	22144.000	0	32860.000	31125.000	0	37667.000	29876.000	24358.000	25956.000	22351.000	0	131864.000	204193.000	1.548512103	1.0388
CAT1496 GDM tissue	1st repeat	42548.000	0	0	0	0	0	0	0	0	0	28858.000	0	0	42548.000	28858.000	0.678245746	
CAT1496 GDM tissue	2nd repeat	13232.000	29145.000	0	0	0	12553.000	0	16253.000	0	12369.000	11680.000	0	0	42377.000	52855.000	1.247256767	
CAT1496 GDM tissue	3rd repeat	18984.000	52498.000	14548.000	0	0	18014.000	0	24546.000	16472.000	18084.000	19538.000	0	0	86030.000	96654.000	1.123491805	1.0163
CAT 1515 plasma	1st repeat	206092.000	88147.000	45080.000	0	563857.000	262922.000	59336.000	171545.000	135651.000	154860.000	20087.000	82301.000	42675.000	339319.000	1493234.000	4.400679007	
CAT 1515 plasma	2nd repeat	254982.000	78402.000	51267.000	0	59655.000	336607.000	77054.000	230273.000	172829.000	192736.000	24549.000	104023.000	59864.000	384651.000	1257590.000	3.269431251	
CAT 1515 plasma	3rd repeat	290603.000	56628.000	17263.000	0	67884.000	387732.000	90133.000	264363.000	191738.000	223664.000	28572.000	120243.000	69999.000	364494.000	1444328.000	3.962556311	3.8776
CRF424 NP plasma	1st repeat	220318.000	48130.000	67000.000	0	194734.000	143014.000	69771.000	91280.000	63961.000	101428.000	17251.000	66193.000	59397.000	335448.000	807029.000	2.40582445	
CRF424 NP plasma	2nd repeat	152572.000	28209.000	48304.000	0	116925.000	88675.000	55614.000	65623.000	44239.000	63728.000	0	43510.000	44785.000	229085.000	523099.000	2.283427549	
CRF424 NP plasma	3rd repeat	210147.000	33987.000	70493.000	0	17260.000	129919.000	69220.000	84821.000	63360.000	97561.000	0	60347.000	57026.000	314627.000	579514.000	1.841908037	2.1771
CRF458 NP plasma	1st repeat	176967.000	381973.000	100594.000	0	145017.000	93548.000	36517.000	69645.000	50678.000	62326.000	0	25114.000	25009.000	659534.000	507854.000	0.770019438	
CRF458 NP plasma	2nd repeat	173898.000	350136.000	91124.000	0	170385.000	109386.000	50390.000	91374.000	63797.000	75419.000	23043.000	34778.000	34723.000	615158.000	653295.000	1.061995455	
CRF458 NP plasma	3rd repeat	233821.000	356409.000	106710.000	0	23519.000	135219.000	62037.000	103921.000	75752.000	87035.000	25901.000	41557.000	41599.000	696940.000	596540.000	0.855941688	0.896

Figure 3:27Performing calculations in Excel for PC/LPCacquired spectrum: E:\Edyta placenta flex analysis all data 22 04 2021\Positive ion mode [10mgml] \CAT1315 in order to get the average of three replicas per each sample to have a data point to plan on GraphPad. Flex Analysis copied data to Excel Intensities 6x10-4 - 1x10-5. First, all sample intensities data, acquired at least three times signal to noise 3 S/N and already method preset to S/N=9, Observed Intensities 6x10-4 - 1x10-5 LPC and PC m/z in MALDI ToF MS. Fully annotated based on normal extraction rather than preparative TLC as the samples were smearing and gave unclean spectra. 9AA matrices are weak bases, while DHB matrices are weak acids well known in literature and mass spectrometry, providing a stronger enhancement signal. Several other matrices can be used. The matrix might help with ionisation but also depresses the signal by causing a matrix effect. See Figure 3.29 for the results of the placental work.

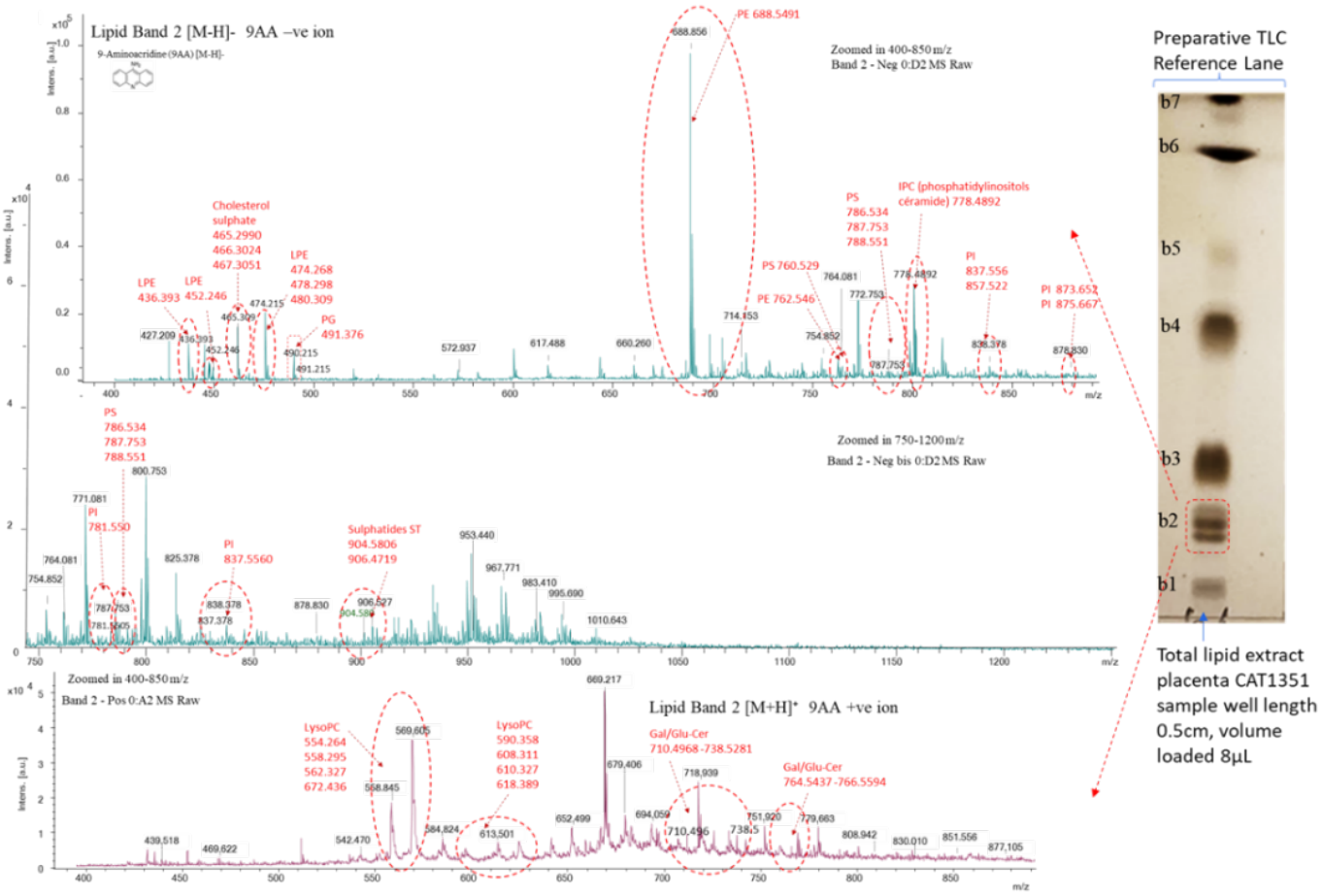

Figure 3:28 The full mass spectra of band 2 from preparative TLC were run using an acidic mobile phase. MALDI TOF -MS analysis was in negative and positive ion mode using a 9AA matrix. The top left negative ion mass spectra are zoomed in from the middle left negative ion mass spectra; positive mass spectra are shown at the bottom left.

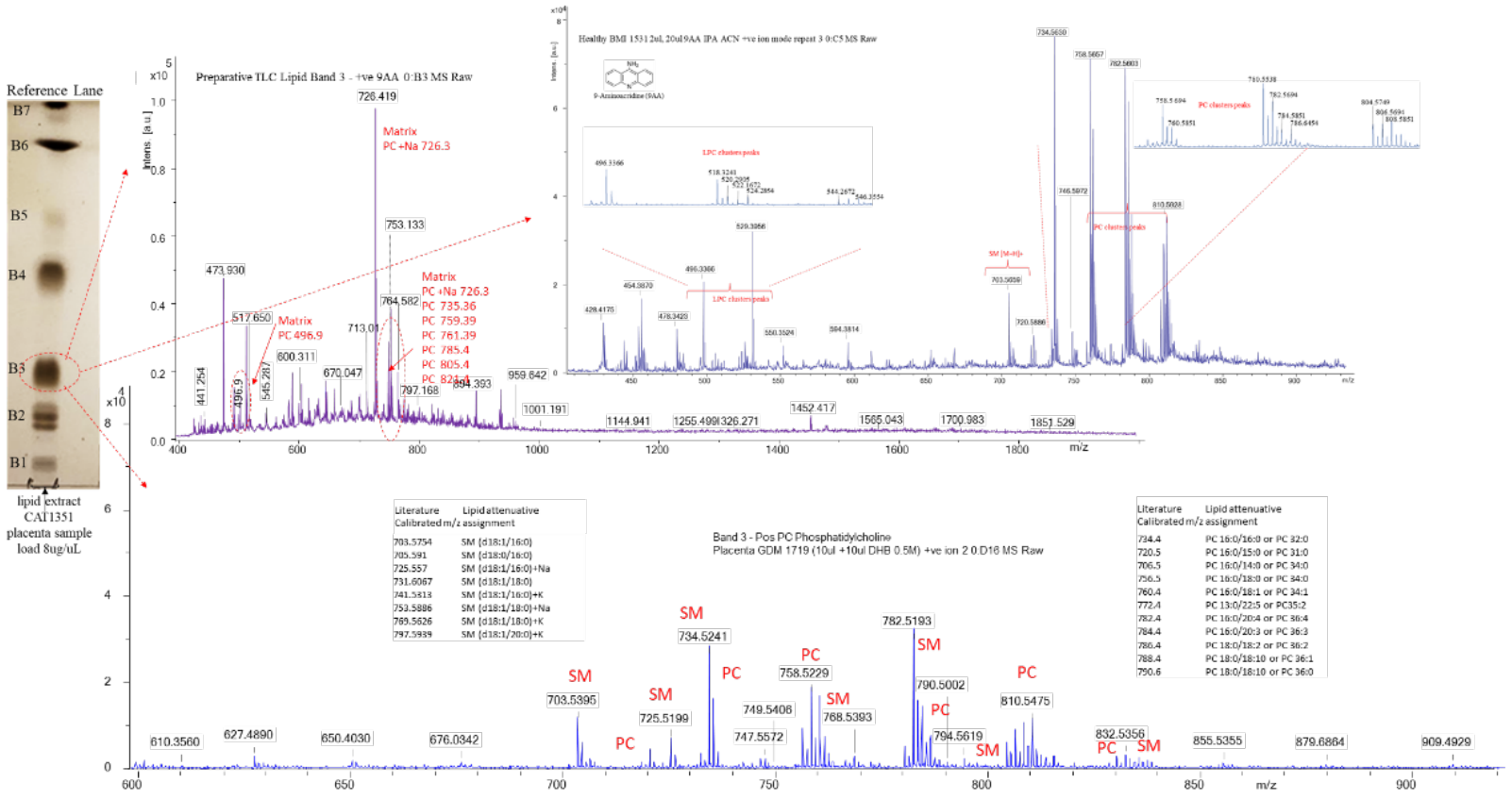

Figure 3:29 The full mass spectra of band 3 from preparative TLC were run using an acidic mobile phase. MALDI TOF MS analysis was in positive ion mode using 9AA or DHB matrix. All top right mass spectra are in positive ion mode with 9AA as the matrix; bottom right mass spectra are in positive ion mode with DHB as the matrix.

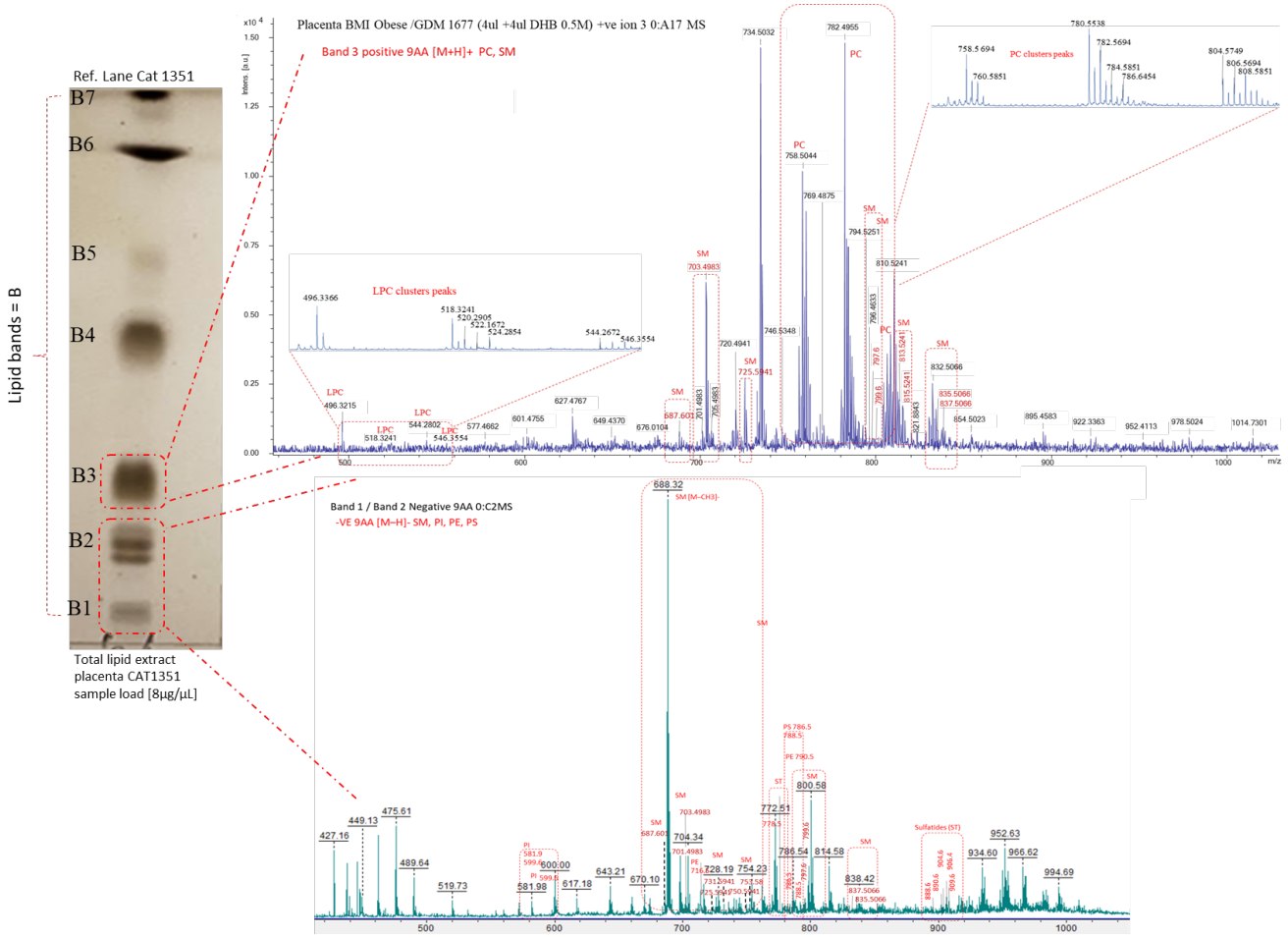

Figure 3:30 MALDI TOF MS analysis of lipid bands 1, 2 and 3 preparative TLC using acidic mobile phase, lipid bands 1, 2 shown are from negative ion mode with 9AA matrix confirmed the presence of PI, SM, PS, and sulphatides. Band 3 mass spectra are from positive ion mode with DHB matrix showing the LPC and PC peaks.

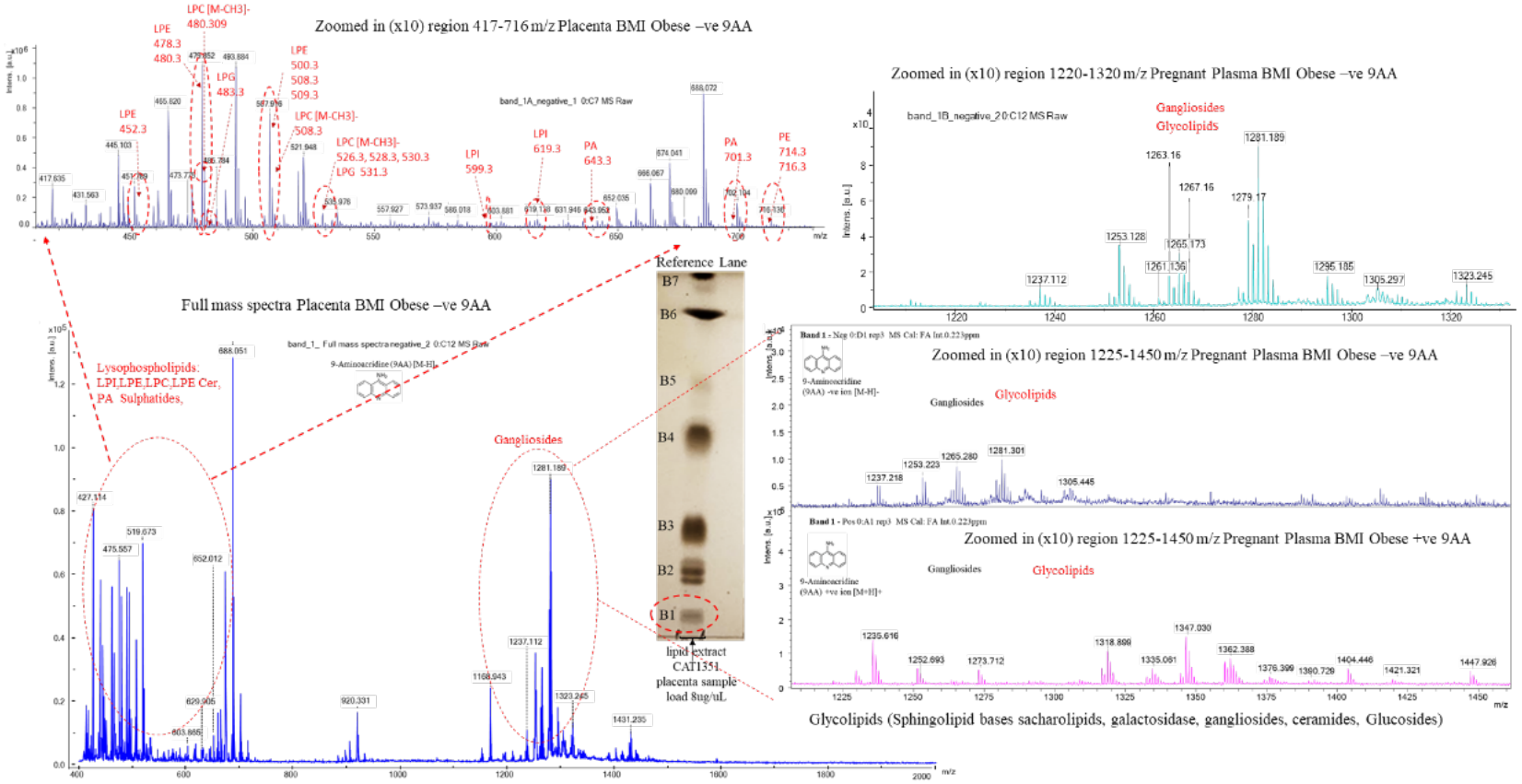

Figure 3:31 MALDI ToF MS analysis of lipid bands 1, obtained on preparative TLC using acidic mobile phase. Bands 1 and 2 mass spectra shown are from negative ion mode [M-H]- 9AA matrix and confirmed the presence of hydrolysed lipid groups LPI, LPE, LPC, PA, SM, ceramides, and glycolipids presence in obese and GDM plasma and placentas sample

3.4.9 Results Summary

This research focused on screening total lipids extracts total lipids from the human placenta and maternal plasma without specifically targeted aims to learn and investigate lipids as potential biomarkers, creating a whole lipid map of placenta lipid content to inform other tissue analysis, for example. The total lipids extract enables essential identification of the lipid group species with clear evidence of phospholipids subgroups, including the hydrolysed glycerophospholipids such as LPC, LPI, LPS, LPE PG, PA, as well as the native glycerophospholipids including phosphatidylcholine, phosphatidylethanolamine, sphingosine phospholipids such as sphingomyelin, gangliosides, ceramides, PS, PI, and neutral lipids cholesterol esters, cholesterol sulphates, and observable fragments of sulphatides, and the mixture of triglycerides, that are observable by TLC and assignable by MALDI ToF MS. It is a method of investigation for optimisation of detection of all lipids within placenta tissue towards further translational and clinical work.

The main point of this project was to establish a reliable lipid extraction methodology that can be adapted and easily understood. As many different lipids have significant structural complexity, the methodical and bioanalytical literature approaches explore more advanced techniques than those employed here. In the literature, for example, many lipid researchers use a mass spectrometry approach to use single-ion or multiple-ion monitoring of a specific species of interest. By applying advanced mass spectrometry, lipidome researchers can identify the observable lipid functional groups with specific diagnostic peaks for structural identification when searching the Lipid Maps database, the most respected current academic lipid database with an excellent reputation for critically perceived bioanalytical data sets *(206, 217, 335, 401, 405, 505, 511, 569-578)*.

This research analysed placental and plasma samples using Bligh and Dyer lipid extraction without additional derivatisation or lipid-protein digestion. The reasons for not doing that were a slow start on the student's part, lack of organisation and a methodical approach with insufficient lipid knowledge at the time, which put these techniques out of this research's scope. Nevertheless, accomplishing that in

subsequent studies would be helpful as we are likely missing much of the lipoprotein components.

In this research, we have specifically focused on relative PC/LPC ratios, as previous literature had suggested that PC/LPC ratios could be used as a simple biomarker of adverse events in pregnancy. These ratios were studied with two MALDI matrices with different ionisation effects, likely due to the polarity of the matrix molecules. The 9AA matrix is a mild base, and DHB is a weak acid known to influence how the sample gets ionised, and all ions start travelling simultaneously through the time-of-flight reflectron mode. DHB is an excellent matrix for positive ion mode as it produces low-fragmentation products in phospholipids and enhances detection.

Samples analysed here were placentas from healthy women, obese women, and women with GDM, as well as plasma from the same groups alongside plasma from non-pregnant women. PC and LPC measurements were taken in positive ion mode to calculate discrepancies, and in negative ion mode, PE, PI, PS, PA, SM, PG, and cardiolipin were measured. PE/LPE with PI/LPI were the most intense peaks for the calculation ratio in negative ion mode. Within lipid headgroup classes, the relative quantitation of ion abundance is correlated with concentration, but ionisation efficiencies vary highly between lipid classes, so relative quantitation is unreliable without quantitative internal standards. To be able to identify accurately the dissociation of the phosphate head group in the glycerophospholipids, a more sensitive mass spectrometry technique would be helpful with soft chemical ionisation such as atmospheric pressure chemical ionisation or electrospray ionisation to confirm the phosphate head group and any expected loss diagnostic ions.

When we compare the two matrices, 9AA is a base, and DHB is acidic, and as the matrix produces spectra with varying peak heights, which arises from the phospholipids ionising differently in each matrix, we cannot expect the same mass spectral intensities for the PC/LPC due to ionisation differences. In the 9AA matrix, lipids ionise with lower signal intensity, whereas in the DHB matrix, lipids ionise at much higher intensities. However, it does not mean more lipids are in the DHB matrix until we run a quantitative calibration curve to determine the ionisation

efficiencies of these species with these exact ionisation conditions. Nevertheless, since we were primarily interested in determining trends, the lack of absolute quantitation information is not a great hindrance.

Based on this investigation, both matrices are excellent for lipids analysis. A key result from these investigations is that negative ion mode for most lipid species is generally a very effective tool, apart from the positively charged quaternary ammonium ions on the choline and the sphingosine-based lipids. The remaining neutral and basic charged lipids, specifically cardiolipin, ethanolamine, inositol, serine, phosphatides, glycolipids, and gangliosides, are easily detectable in negative ion mode.

The placental and plasma studies focused on PC/LPC abundance ratios acquired from MALDI ToF MS. The PC/LPC of triplicate repeats were averaged to calculate the intensity amongst healthy versus diseased groups to observe for any differences or similarities. The peak cluster for each phospholipid subgroup in positive and negative ion modes is presented to point out that they can be seen in spectra, although they have yet to be fully quantified.

An example of the hydrolysed lipid is LPC and the free hydroxyl group on the glycerol's connection to the fatty acid in the sn-2 position makes the molecule prone to enzymatic cleavage. In MALDI ToF MS positive ion, the intensity for PC/LPC cluster peaks containing several isotopic peaks can be monitored. The most intense peak corresponds to PC (758.6, [M + H] +), (760.6, [M + H] +), (780.6, [M + H]+), (782.6, [M + H] +), and (810.6, [M + H] +). The sodium adducts PC 758.6 [M+Na] contribute to the peaks at 780.6 and 782.6. The polarity and charge state must play an important role. This lower sensitivity of MALDI-TOF toward detecting phospholipids of higher polarity could make the quantification of individual phospholipids in a phospholipid mixture difficult *(579) (580)*.

With a better visual understanding of lipid separation from the experimental results, the next step was to analyse the total lipid extract using MALDI ToF MS. The total lipid identification was conducted on normal TLC lipid extracts in negative ion mode for most neutral or ionic lipids. Positive ions were used for positively charged groups like phosphatidylcholine-based and sphingolipid-based ceramides. Although

preparative TLC separated all the bands into smaller bands in the initial and secondary observations, there is smearing likely due to silica contamination in the lipid extracts or samples containing similar species that were not separated. The scraped silica powder would need to be filtered out of the lipid extracts in additional extraction steps. As the results of the three independent experiments were similar, no further experiments were carried out. However, the next approach should include a cartridge solid phase extraction step, avoid preparative TLC, and use high-performance liquid chromatography HPLC to separate individual lipid bands. Due to overlapping lipid groups and clear non-discrimination between the lipid groups, the scraped lipid bands (1-6) could not provide sufficient lipid identification for the individual species.

3.4.10 Summarising Preparative TLC Results

Careful sample preparations are critical for preparative TLC and MALDI analysis. In the last ten years, lipid analysis of biological samples has advanced, and quantitative approaches are now possible. In this project, semi-quantitative analysis, which is still a reliable qualitative method for bioanalytical measurement, was performed. When developing and setting up novel methods for total lipid quantitative analysis, expert knowledge is a critical priority to have a reliable process and instrument, whether MALDI ToF MS or other LC-MS methods are employed. In our case, data was reliably acquired from 400 m/z to 2000 m/z, which enabled the semi-quantitative analysis of total lipids.

For full, reliable quantitation, an analytical method requires liquid chromatography and mass spectrometry using tandem mass spectrometry CID, which requires experience with mass spectrometry and understanding lipids. It must rely on knowledgeable expertise in preparing, running and analysing this set-up, and the LC-MS/MS methodology takes time to run or learn. For full quantitation, each lipid species needs selective internal standards for the individual lipid headgroups (isotopically labelled), which is costly and requires extensive optimisation to find the best parameter settings in data acquisition, avoiding the many potential mass overlaps that could distort the quantitation.

This research study employed MALDI Time-of-flight (ToF) Mass Spectrometry (MS) as the primary confirmative of the mass-to-charge ratio for the lipid species. Furthermore, with internal standards, a calibration curve should be created for each lipid head group. Running samples, with at least triplicate analysis, would take a long time to get a reliable and reproducible signal to construct a calibration curve that can be relied upon and trusted. There is no fast-paced process for accurate absolute quantitation in mass spectrometry. Instead, it is a laborious and time-consuming process, which can be inconvenient without enough time or access to the necessary equipment. Full quantitative mass spectrometry requires either developing the LC-MS/MS methods with dedicated instruments or sending the quantitation experiments to external laboratories. The experimental and instrumental time was cut short by lack of time and COVID lock.

Chapter: 4 (MALDI ToF MS)

Matrix-assisted laser desorption ionisation time of flight mass spectrometry

Figure 4:1 Pictorial overview sample crystallization in matrix applying to the target

4.1 Rationale in the pictorial overview

In this thesis, we used thin-layer chromatography (TLC) at the analytical and preparative scales to extract and separate the lipids from placental tissue and plasma. TLC bands can be partially assigned to specific lipid subclasses compared to the

literature elution order and profiles, but the more accurate assignment of the lipid classes and structures requires more information. MALDI-ToF mass spectrometry can provide additional information about the masses of the molecules desorbed from the TLC plate bands, and it can sometimes yield further information regarding the relative concentration of specific lipids and some fragment ions which helps to confirm the class of the lipids. This chapter explains the MALDI-ToF experiment, gives details of the sample preparation and acquisition methods, and highlights many of the lipid analyses revealed using MALDI-ToF, the TLC bands described in chapters 2 and 3.

4.2 Materials and Methods

All reagents, materials and equipment used for the work described in this chapter are summarised in Table 3.1., sample ethical approval as per Chapter 2, section 2.3.1

4.2.1 MALDI Sample Preparation

The sample mixes into the matrix, and tiny spots at an analyte concentration of 0.5 - 1 µg/µL were applied onto a MALDI target, as shown in the schematic diagram (Figure 4.1). Different methods are available for sample preparation, depending on the sample, solvent system, and matrix. Different matrices can be tried when unsure of what gives us the best signal. Popular peptide analysis requires sample evaporation that needs mixing with a matrix on the MALDI target, creating thin crystals, as per the literature. The sample spots holding the mixed analyte/matrix spots are dried and subjected to MALDI *(236, 237)*.

4.2.2 Choosing a Matrix

Experiments used 9-aminoacridine (9-AA) and 2,5-dihydroxybenzoic acid (DHB) as matrices. The matrix 9-AA molecular weight MW 194.23 g/mol was used at [0.5 M] dissolved in isopropanol with acetonitrile (IPA/ACN 3:2 v/v). DHB MW 154.12 g/mol was used at [0.5 M] dissolved in methanol *(236, 237, 270) (581)*. In negative mode, the 9AA works by deprotonation, whereas protonation in positive ion mode adds a hydrogen atom. Most matrices (e.g. Figure 4.2), like DHB, easily donate

protons, and 9AA readily accepts them, forming $[M-H]^-$ species *(223, 236, 237, 563, 582, 583)*.

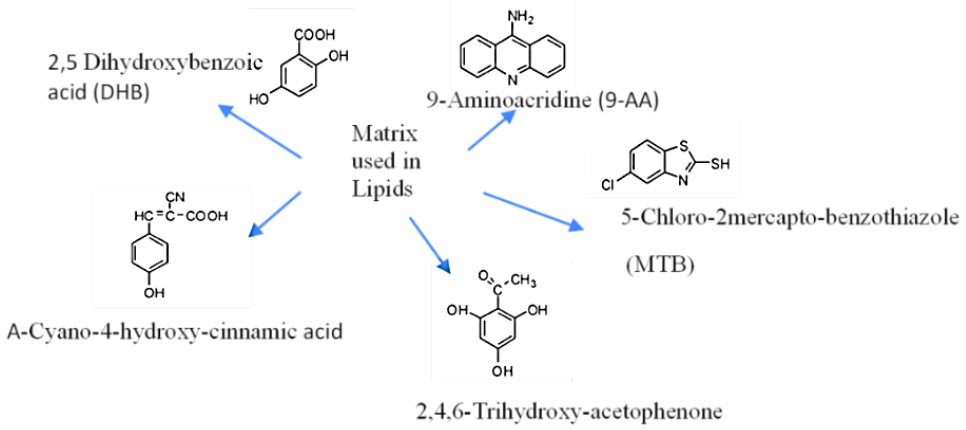

Figure 4:1 Some typical MALDI matrices. The choice of matrix is critical for successful MALDI analysis. The key in sample preparation is careful handling to prevent contamination of the lipid samples. Sample and matrix integrity depends on careful, homogeneous preparation and mixing, vortexing, and speedy spotting so that the sample and matrix mixture form large, flat crystals after evaporation of the solvent. These crystals absorb light and desorb molecules, and as the initial position of the desorption surface determines kinetic energy reproducibility, it is critical for spectral mass resolution. For experiments here, all samples were run in triplicate for comparability and reproducibility control during method validation *(236, 237)*.

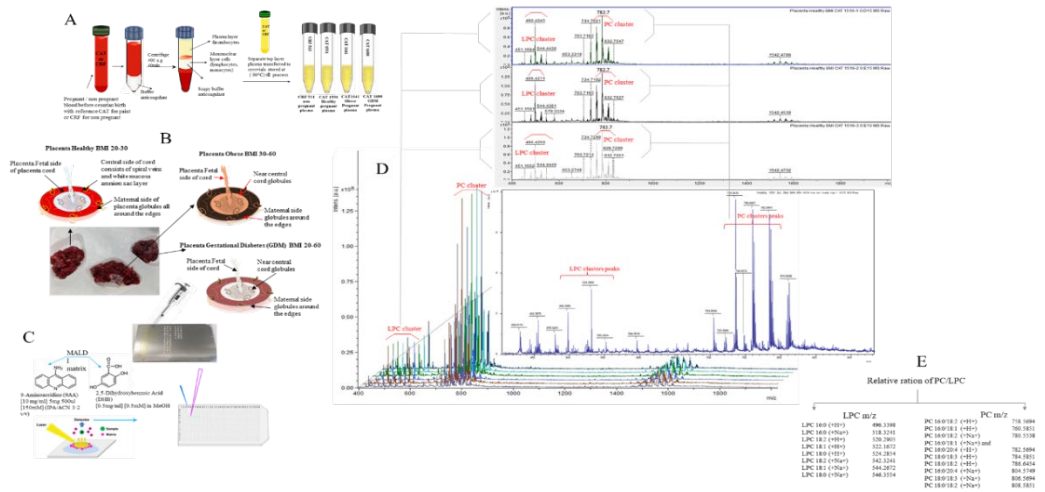

Figure 4:3 Visual diagrams of samples and the MALDI measurements. A) Plasma sample total lipid extracts, B) placenta chunks edges, near the centre from placenta groups based on BMI kg/m2 range where healthy range group is within 30 BMI, obese 30-60 BMI and GDM 20-60 BMI. Therefore, measured placenta groups in image (B) and plasma groups in image (A) were then applied to MALDI ToF MS analysis with Matrix 9AA, DHB, on the image (C) and followed by triplicate runs

per each lipid extract per group and using the clusters of phosphatidylcholine to lysophosphatidylcholine mass to charge ration m/z value on the image (D) base on the average ration of the three replicates calculation in excel tablet PC/LPC image (E).

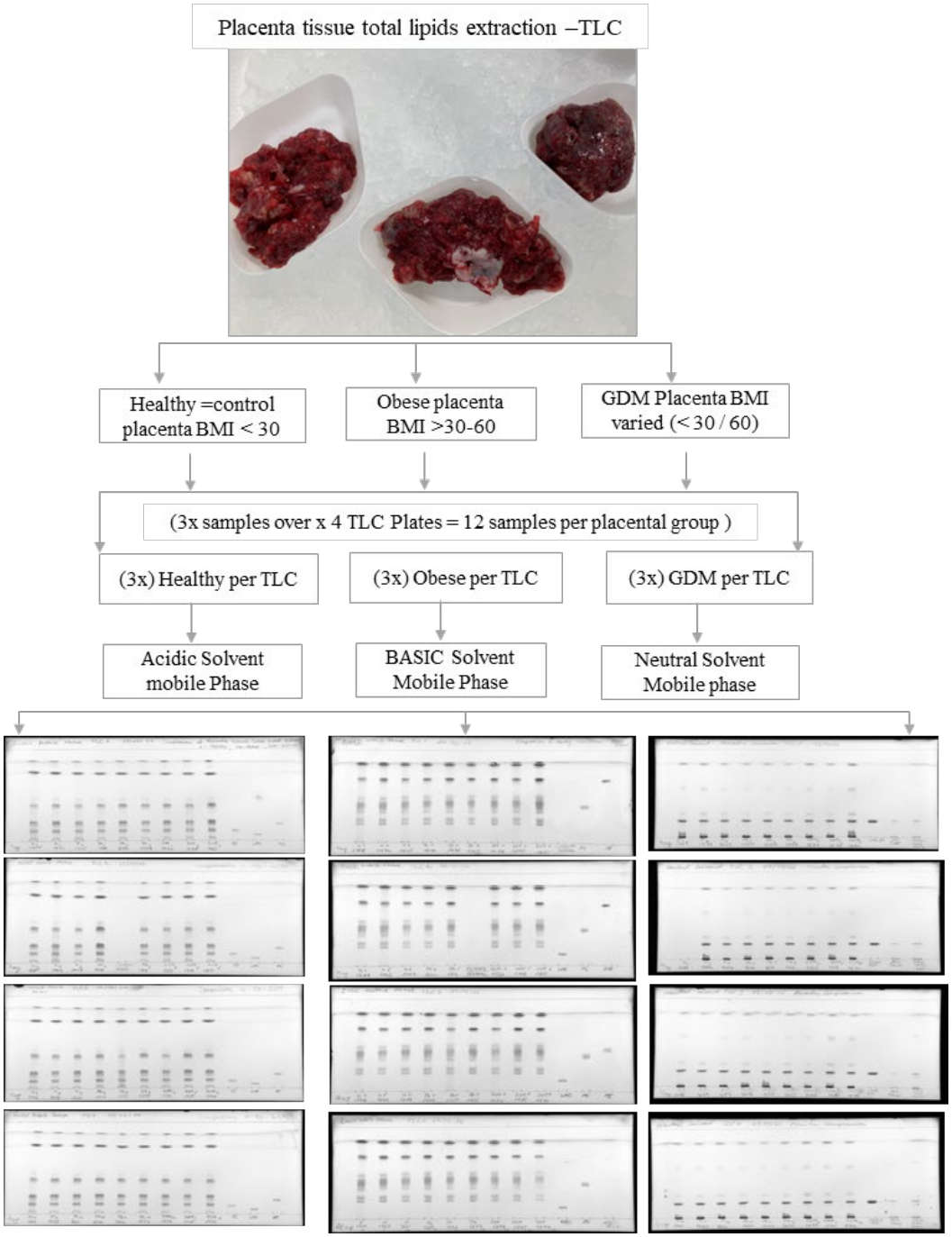

Figure 4:2 The three placenta groups, healthy, healthy and GDM, and the total lipid extract subjected to TLC analysis before MALDI as the first lipid separation and observation site

4.2.3 Standards:

All lipid standards were from Avanti Polar Lipids Inc. (Alabaster, AL). As purchased, the initial stock concentration of lipids standards was 20 mg/ml in chloroform. The 9AA and DHB matrices were purchased from Sigma/Merck (Germany).

4.2.4 Protocol for sample-to-matrix preparation for the MALDI target

The DHB matrix was weighed and diluted in HPLC-grade methanol to prepare a 0.5 molar solution. Lipid standard dilutions were made using 99.98% pure chloroform to a 10 mg/ml stock concentration and 1 mg/ml working concentration. All samples were prepared by weighing the total dried extract and reconstituting it with chloroform, homogenisation, extraction, and nitrogen drying. The weights of all placenta and plasma total lipid extracts are calculated on recovered weight (mg) and reconstituted in solvent volume (ml). Samples were reconstituted with chloroform and stored at -20 °C until analysis. Sample preparation consists of taking 10 µL from the sample vial using a Hamilton syringe and transferring this sample into the small glass insert vial. The nitrogen gas stream dries the 10 µL of the lipid extract until no more droplets are visible. Ten microliters of the prepared matrix (0.5 M 9AA or 0.5 M DHB) are then added to that dried lipid extract and placed on a small vial vortex.

Immediately after vortexing, 0.5 – 1 µL of the sample was gently applied onto the MALDI target and dried. Each sample was spotted three times. The facility manager presets instrument parameters and adds a caesium iodide calibrant mixture to a free sample spot to ensure instrument calibration is within 5 ppm or better. Internal calibration makes higher mass accuracy possible. The signal is acquired and signal-averaged for each spot for each MALDI mass spectrum until a sufficient signal-to-noise (S/N) level. S/N of 3 is a general guideline for a peak to be accepted, which usually requires approximately five to fifteen laser shots per target spot before moving on to the next sample. Each sample data is recorded with reference number, matrix, and positive or negative ion mode and saved to a flash drive to open and process on the laptop later using a naming convention of year /month /date/sample reference/matrix. From the estimated recovery weight of dried lipid extract from the placenta tissue, we estimate that total lipid recovery is plus or minus 0.3 – 1 % w/w

from a tissue sample and 2 – 4 % w/v from plasma samples. That number takes the original wet weight of tissue and compares it to the recovered total lipid extract.

4.2.5 The instrument

In this research work, an instrument by Bruker Daltonics Ultra-Flex MALDI ToF MS was used and applied to all data acquisition and data processing with the software Flex Analysis. The instrument uses a pulsed nitrogen laser, emitting at 337 nm. The stable base pressure of the instrument was 1 x 10-6 mbar, and the kinetic energy of the ion source was 20 keV. MALDI ToF MS detection was used in reflectron mode to enhance the spectral resolution over a flight path of two meters. Positive and negative mode ion calibration was performed using CsI clusters over an m/z range from 399 – 2000 m/z, and the six masses were selected as a minimum out of ten masses to calibrate the instrument for mass accuracy within 1 ppm. After the spectral acquisition, internal calibration was reapplied again by selecting the CsI peaks applied earlier. The calibration masses are shown in Table A and Table A1 below calibrant caesium iodine CsI, which is suitable and sufficient for sample mass calibration of the accurate mass of lipids of interest in positive and negative ion modes with good reproducibility using the DHB. The 9AA matrix gave moderate intensity but not as good as the DHB matrix. The laser power used during CsI calibration was ten per cent of the maximum available in the instrument. For lipid analysis, the laser was adjusted between 10% and 40% of the total laser power available using the instrument control parameters within the MALDI user view window. The table contains calibration masses in negative ion mode acquired on each running day located at Swansea University Mass Spectrometry Facility NMSF calibration masses of caesium iodine (CsI_3) used for instrument calibration to run lipids in positive and negative ion modes. The exact calibration was applied as internal calibration to improve the mass accuracy error to 5 parts per million (ppm). All acquired lipid mass spectra were recalibrated in positive [M+H]+ and negative [M-H]- ion modes at the acquisition and reapplying calibration to improve mass accuracy. Mass accuracy as calculated lipid species PC/LPC in all run batches was checked randomly across the whole spectra to obtain part per million relative error and standard deviation to justify the analysis accuracy amongst all samples.

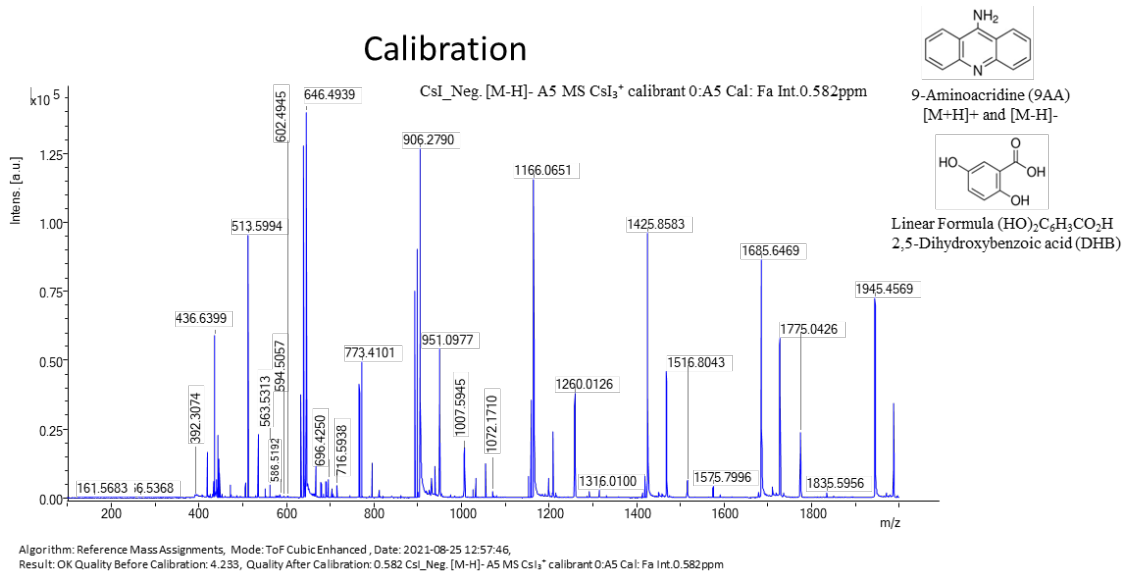

Algorithm: Reference Mass Assignment, Assigned Calibrants: 6	
Mode: ToF Cubic Enhanced, Mass Control List: CsI_Neg,	
Quality Before Calibration: 84.655, Quality After Calibration: 0.008	
Calibrant 1:	Calibrant 4:
Calibrant Name: [Cs2I3]	Calibrant Name: [Cs5I6]
Calibrant Mass: 646.525 Da	Calibrant Mass: 1425.955 Da
Mass Before Calibration: 646.562 Da	Mass Before Calibration: 1426.072 Da
Mass After Calibration: 646.525 Da	Mass After Calibration: 1425.955 Da
Mass Error: 0.001 ppm	Mass Error: 0.011 ppm
Calibrant 2:	Calibrant 5:
Calibrant Name: [Cs3I4]	Calibrant Name: [Cs6I7]
Calibrant Mass: 906.335 Da	Calibrant Mass: 1685.765 Da
Mass Before Calibration: 906.395 Da	Mass Before Calibration: 1685.911 Da
Mass After Calibration: 906.335 Da	Mass After Calibration: 1685.765 Da
Mass Error: 0.004 ppm	Mass Error: 0.007 ppm
Calibrant 3:	Calibrant 6:
Calibrant Name: [Cs4I5]	Calibrant Name: [Cs7I8]
Calibrant Mass: 1166.145 Da	Calibrant Mass: 1945.574 Da
Mass Before Calibration: 1166.233 Da	Mass Before Calibration: 1945.749 Da
Mass After Calibration: 1166.145 Da	Mass After Calibration: 1945.574 Da
Mass Error: 0.009 ppm	Mass Error: 0.002 ppm

Figure 4:3 Table A mass spectra of C Mass calibration Caesium Iodine MALDI

4.3 Results

This study involves a comparative analysis of total placenta lipids of 94 samples in triplicate MALDI-TOF spectra runs per placenta group in positive ion mode and negative ion mode in two matrices for a total of 2 x 282 =564 (in triplicate) mass spectra total of MALDI mass spectra 1692 acquired and analyzed. The two matrices used are 9AA and DHB in positive ion mode for the semi-quantitative analysis of LPC to PC relative ratio based on the representative cluster peaks mass to charge ratio values m/z for LPC experimentally observed in MALDI ToF MS mass spectra of placenta groups comprising of placentas- healthy, placentas-obese and placentas-GDM, as well as for plasma groups comprising of non-pregnant plasma group, healthy pregnancy plasma group, obese pregnant plasma group and GDM pregnant plasma group are shown in comparisons data used from MALDI ToF MS and generated plots using software Prism GraphPad starting from comparative placenta sides Centre versus edges as a representative in Table 4.1: GraphPad which is comparing the PC/LPC ratio at the edges versus the centre of the placenta. Continue explaining

Preparative TLC and analytical TLC analysed 94 combined samples (placentas, plasma), run in triplicate in MALDI-TOF mass spectrometry, and recorded by date, BMI, and GDM status. The table of these samples is in the Appendix, and all TLC and MALDI results are available separately. Representative MALDI mass spectra are included in this chapter for discussion. The many mass spectra were analysed by comparing the observed mass spectral peaks to the literature reports of lipid mass spectral peaks. Table 4.1, below, is typical. In this table, observed positive ion $[M+H]^+$ peaks are highlighted in yellow in the last column, and they are assigned due to their prior observation in the literature in the referenced papers. The peaks were counted as 'observed' in our spectra if detected in 9AA in DHB or. Table 4.2, below, also shows the observed mass spectral peaks in negative ion mode, using 9AA and DHB as the matrix. In the negative ion spectra, some fragments were also observed in the literature in the right column and our peaks (in green), but fragment ion masses from the literature marked in red in the right column were not observed in our spectra. Table 4.1 and Table 4.2 is shown below. The peak identification shown in Table 4.1 is of the positive ion mode $[M+H]^+$m/z 9AA, DHB matrix. By

reviewing supplementary data tables showing lipid mass to charge ratios (m/z) obtained from tissues, hearts, kidneys, lungs, and placenta with MALDI ToF MS Ultra Flex, Brucker observed peaks of positive ions $[M+H]^+$ in matrix 9AA, DHB based on the literature, using animal and human models and stem cells *(103, 503, 584) (562, 585) (303, 563, 565-567, 585, 586)* (Sarbu, M. 2022), *(587)* Sup Data +ve ion DHB $[M+H]^+$, $[M+Na]^+$, $[M+K]^+$ big tables all data for +ve ion and -ve ion saved in excel. Effect of MALDI matrices on lipid analyses of biological tissues using MALDI-2 post ionisation mass spectrometry. Journal of Mass Spectrometry (12). Generally, DHB yielded better spectra in positive and negative ion mode and showed almost twice as many assignable masses compared to the 9AA in positive ion 9AA and yielded better 9AA in negative ion mode, and the fragment ion masses visible in the negative ion mode were useful to confirm many of the assignments.

4.3.1 Explained the steps involved in each calculation

Starting from Excel, create tables in order to get the PC/LPC relative ratio for each sample of three repeats.

First, you acquire data in Maldi ToF Instruments and save it under your folder: day/month/year/ sample ID/matrix/ ion mode.

Then, after acquiring data, you copy the raw data file exported from the USB saved from Brucker Flex Analysis, so you can open it on your laptop using the FlexAanlysis software previously downloaded. Best use the external portable drive.

Then, for each sample (three repeats), you export excellent rad data from which you pick the intensity values of your LPC and PC as well as the actual mass-to-charge values for each LPC PC. Here is the example below:

Export raw data to Excel: Create a table with your PC/LPC actual experimental mass to charge ration m/z in the table highlighted read, measure PC LPC M/Z, and the top line is your literature peak mass values, and that helps you to work out SD for each sample.

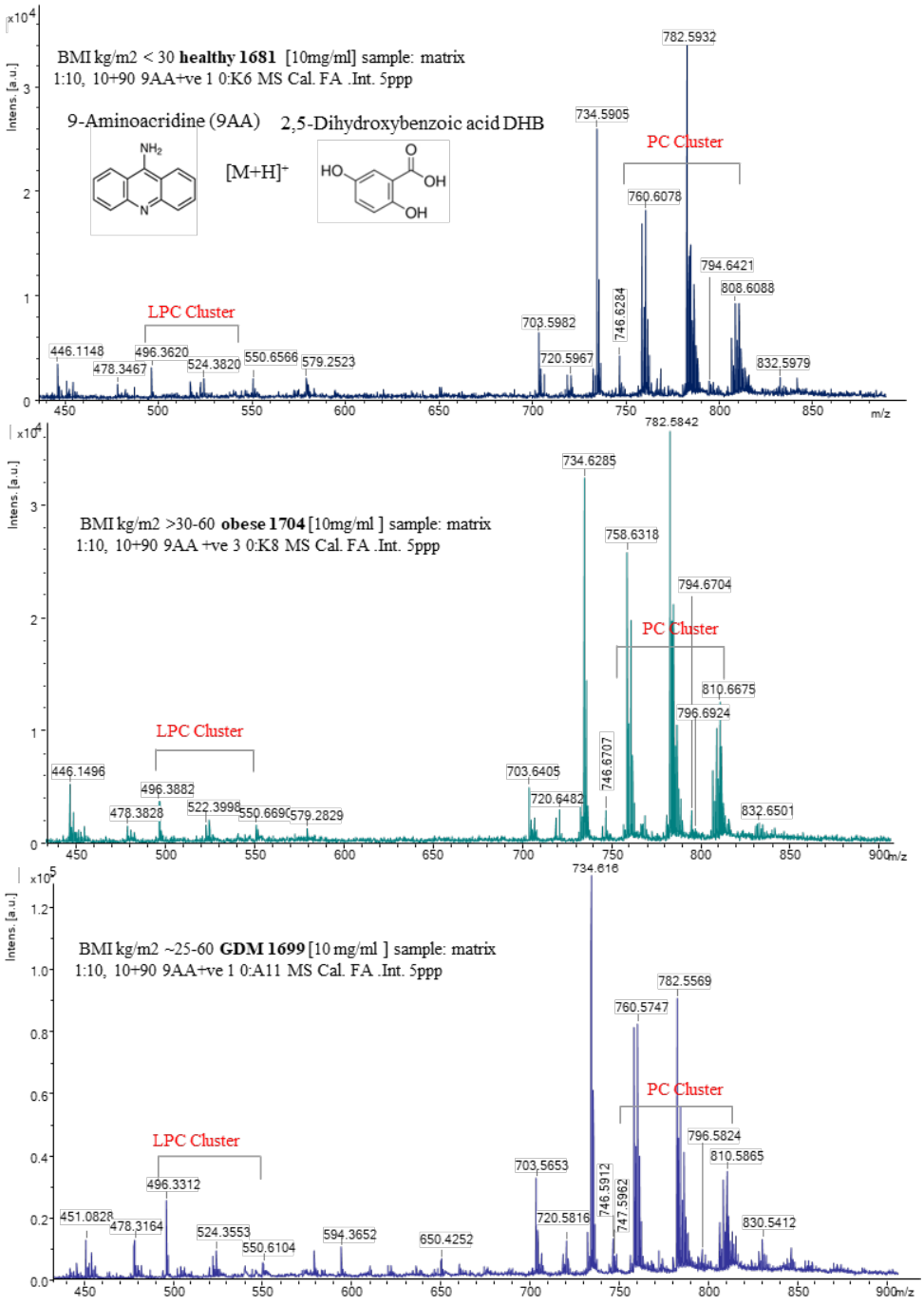

Figure 4:4 Analysis explanation working step 1 for cluster peaks PC/LPC on MALDI ToF MS showing three replicates per sample

Angelini 2014 Literature reference	
Positive ion mode [M+H]+ matix 9AA	m/z
LPC 16:0 (+H+)	496.3398
LPC 16:0 (+Na+)	518.3241
LPC 18:0 (+H+)	524.2854
LPC 18:2 (+Na+)	542.3241
LPC 18:1 (+Na+)	544.2672
LPC 18:0 (+Na+)	546.3554
PC 16:0/18:2 (+H+)	758.5694
PC 16:0/18:1 (+H+)	760.5851
PC 16:0/18:2 (+Na+)	780.5538
PC 16:0/18:1 (+Na+) and PC 16:0/20:4 (+H+)	782.5694
PC 18:0/18:3 (+H+)	784.5851
PC 18:0/18:2 (+H+)	786.6454
PC 16:0/20:4 (+Na+)	804.5749
PC 18:0/18:3 (+Na+)	806.5694
PC 18:0/18:2 (+Na+)	808.5851

Figure 4:5 Explanation working step 2 m/z peaks PC/LPC (Angelini et al. 2014)

CAT 1315- 1st repeat

m/z	Intensity	S/N 9
496.3458	124346.0	33.7
518.4448	144043.0	38.4
524.3846	54754.0	13.5
758.5348	70576.0	18.3
760.5566	73689.0	19.3
780.5278	30795.0	6.1
782.5404	83966.0	23.5
784.5525	55515.0	14.3
786.3601	37298.0	8.3
804.5286	30289.0	6.2
806.5491	38687.0	9.0
808.5557	35553.0	8.0

CAT 1315- 2nd repeat

m/z	Intensity	S/N 9
496.4158	99018.0	32.6
518.5048	289057.0	99.5
524.4557	91504.0	30.6
758.6099	44198.0	15.8
760.6228	50089.0	18.3
780.5278	not observed	
782.6113	46923.0	17.0
784.6253	31350.0	10.5
786.6449	26559.0	8.5
804.5286	not observed	
806.5491	not observed	
808.6290	20973.0	6.2

CAT 1315- 3rd repeat

m/z	Intensity	S/N 9
496.4260	89273.0	32.3
518.5104	374103.0	140.8
524.4647	86971.0	31.7
758.6215	76751.0	32.4
760.6345	43026.0	17.2
780.5974	36134.0	13.8
782.6225	36186.0	14.1
784.5821	30138.0	11.2
786.6509	35793.0	13.9
804.6246	19018.0	6.2
806.6223	20093.0	6.7
808.6290	not observed	

Figure 4:6 Explanation of working step on how to select mass values m/z versus intensities providing single-to-noise ratio is greater than 3 as a minimum for each of the three replicates.

All Nonpregnant plasma		All Healthy pregnant plasma		All Obese pregnant plasma		GDM pregnant plasma	
Experimental m/z	SD +/- (x3 reps)	Experimental m/z	SD +/- (x3 reps)	Experimental m/z	SD +/- (x3 reps)	Experimental m/z	SD +/- (x3 reps)
496.41082	0.03	496.4021	0.01	496.4044	0.00	496.4179	0.00
518.42334	0.007	518.3908	0.01	518.3937	0.01	518.4084	0.02
524.44421	0.04	524.4400	0.00	524.4399	0.00	524.4522	0.01
not observed	not observed	not observed	not observed	not observed	not observed	not observed	not observed
544.43433	0.04	544.4100	0.00	544.4109	0.01	not observed	not observed
not observed	not observed	546.4234	0.01	546.4269	0.01	not observed	not observed
758.67447	0.05	758.6655	0.00	758.6662	0.01	758.6849	0.01
760.63825	0.16	760.6821	0.00	760.6422	0.16	760.6597	0.17
780.65938	0.06	780.6530	0.01	780.7799	0.51	780.6723	0.01
782.67565	0.05	782.6706	0.00	782.6715	0.01	782.6890	0.01
784.69237	0.05	784.6870	0.01	784.6882	0.01	784.7053	0.01
786.70743	0.05	786.6712	0.13	786.7053	0.01	786.6493	0.20
804.70638	0.02	804.6541	0.01	804.6594	0.01	804.6877	0.01
806.68295	0.05	806.6739	0.00	806.6758	0.01	806.6941	0.01
808.69086	0.06	808.6908	0.01	808.6947	0.01	808.7088	0.01

Figure 4:7 Explanation of working step 4 calculation in excel using monoisotopic masses theoretical mass values for PC/LPC versus compared to Lipid Maps and the actual experimental values later on of three replicates per each sample

						Peaks list adapted from literaure by Angelini 2014 theoretical mass m/z												
Edyta Observed LPC PC m/z in MALDI ToF MS Intensities values 6x10-4 - 1x10-5 Placenta tissue or Plasma Concentr 10 [mg/mL]	Peak intensities 3 repeats per sample	LPC 16:0 (+H+) 496.3398 m/z	LPC 16:0 (+Na+) 518.3241 m/z	LPC 18:0 (+H+) 524.2854 m/z	LPC 18:0 (+Na+) 546.3554 m/z	PC 16:0/18:2 (+H+) 758.5694 m/z	PC 16:0/18:1 (+H+) 760.5851 m/z	PC 16:0/18:2 (+Na+) 780.5538 m/z	PC 16:0/18:1 (+Na+); PC 16:0/20:4 (+H+) 782.5694 m/z	PC 18:0/18:3 (+H+) 784.5851 m/z	PC 18:0/18:2 (+H+) 786.6454 m/z	PC 16:0/20:4 (+Na+) 804.5749 m/z	PC 18:0/18:3 (+Na+) 806.5694 m/z	PC 18:0/18:2 (+Na+) 808.5851 m/z	ΣLPC	ΣPC	ΣPC/ΣLPC	Intensity PC/LPC average of three replicates
Measured LPC and PC m/z		496.3458	518.445	524.385	0	758.535	760.557	780.528	782.540	784.553	786.360	804.529	806.549	808.556	1539.1752	7072.706	4.5951	4.5951
CAT1315 tissue	1st repeat	56724.000	78882.000	26690.000	0	30404.000	30404.000	0	35993.000	23123.000	20321.000	23123.000	20321.000	0	162296.0000	183689.000	1.1318	
CAT1315 tissue	2nd repeat	119748.000	233643.000	66810.000	0	53608.000	53608.000	0	64682.000	0	38278.000	44770.000	0	0	420201.0000	254946.000	0.6067	
CAT1315 tissue	3rd repeat	124346.000	144043.000	54754.000	0	70576.000	73689.000	30795.000	83966.000	55515.000	45256.000	30289.000	38687.000	35553.000	323143.0000	464326.000	1.4369	1.0585
CAT 1487 tissue	1st repeat	38869.000	125406.000	33240.000	0	41448.000	40984.000	38880.000	57361.000	37114.000	42285.000	36260.000	41085.000	0	197515.0000	335417.000	1.6982	
CAT 1487 tissue	2nd repeat	40885.000	135198.000	33085.000	0	42307.000	46486.000	41093.000	62994.000	42997.000	47210.000	63405.000	42652.000	38543.000	209168.0000	427687.000	2.0447	
CAT 1487 tissue	3rd repeat	37614.000	82551.000	25422.000	0	46290.000	49174.000	45448.000	69266.000	46050.000	47697.000	68296.000	44974.000	37828.000	145587.0000	455023.000	3.1254	2.2894
CAT1489 tissue	1st repeat	55519.000	201886.000	50850.000	0	59941.000	59670.000	64685.000	84422.000	59596.000	63845.000	74687.000	60410.000	48863.000	308255.0000	576119.000	1.8690	
CAT1489 tissue	2nd repeat	40843.000	113665.000	36076.000	0	68062.000	59981.000	62598.000	92559.000	62004.000	62604.000	77243.000	68849.000	53076.000	190584.0000	606976.000	3.1848	
CAT1489 tissue	3rd repeat	37614.000	9300.000	0	0	0	0	3967.000	0	0	0	0	0	3875.000	46914.0000	7842.000	0.1672	1.7403
CAT1494 GDM tissue	1st repeat	65572.000	179767.000	42768.000	0	42813.000	39627.000	0	44020.000	35670.000	60656.000	34258.000	0	0	288107.0000	257044.000	0.8922	
CAT1494 GDM tissue	2nd repeat	56068.000	150021.000	35464.000	0	33654.000	33743.000	0	39585.000	28397.000	0	0	0	27866.000	241553.0000	163245.000	0.6758	
CAT1494 GDM tissue	3rd repeat	43424.000	66296.000	22144.000	0	32860.000	31125.000	0	37667.000	29876.000	24358.000	25956.000	22351.000	0	131864.0000	204193.000	1.5485	1.0388
CAT1496 GDM tissue	1st repeat	42548.000	0	0	0	0	0	0	0	0	0	28858.000	0	0	42548.0000	28858.000	0.6782	
CAT1496 GDM tissue	2nd repeat	13232.000	29145.000	0	0	0	12553.000	0	16253.000	0	12369.000	11680.000	0	0	42377.0000	52855.000	1.2473	
CAT1496 GDM tissue	3rd repeat	18984.000	52498.000	14548.000	0	0	18014.000	0	24546.000	16472.000	18084.000	19538.000	0	0	86030.0000	96654.000	1.1235	1.0163
CAT 1515 plasma	1st repeat	206092.000	88147.000	45080.000	0	563857.000	262922.000	59336.000	171545.000	135651.000	154860.000	20087.000	82301.000	42675.000	339319.0000	1493234.000	4.4007	
CAT 1515 plasma	2nd repeat	254982.000	78402.000	51267.000	0	59655.000	336607.000	77054.000	230273.000	172829.000	192736.000	24549.000	104023.000	59864.000	384651.0000	1257590.000	3.2694	
CAT 1515 plasma	3rd repeat	290603.000	56628.000	17263.000	0	67884.000	387732.000	90133.000	264363.000	191738.000	223664.000	28572.000	120243.000	69999.000	364494.0000	1444328.000	3.9626	3.8776
CRF424 NP plasma	1st repeat	220318.000	48130.000	67000.000	0	194734.000	143014.000	69771.000	91280.000	63961.000	101428.000	17251.000	66193.000	59397.000	335448.0000	807029.000	2.4058	
CRF424 NP plasma	2nd repeat	152572.000	28209.000	48304.000	0	116925.000	88675.000	55614.000	65623.000	44239.000	63728.000	0	43510.000	44785.000	229085.0000	523099.000	2.2834	
CRF424 NP plasma	3rd repeat	210147.000	33987.000	70493.000	0	17260.000	129919.000	69220.000	84821.000	63360.000	97561.000	0	60347.000	57026.000	314627.0000	579514.000	1.8419	2.1771
CRF458 NP plasma	1st repeat	176967.000	381973.000	100594.000	0	145017.000	93548.000	36517.000	69645.000	50678.000	62326.000	0	25114.000	25009.000	659534.0000	507854.000	0.7700	
CRF458 NP plasma	2nd repeat	173898.000	350136.000	91124.000	0	170385.000	109386.000	50390.000	91374.000	63797.000	75419.000	23043.000	34778.000	34723.000	615158.0000	653295.000	1.0620	
CRF458 NP plasma	3rd repeat	233821.000	356409.000	106710.000	0	23519.000	135219.000	62037.000	103921.000	75752.000	87035.000	25901.000	41557.000	41599.000	696940.0000	596540.000	0.8559	0.8960

No.	Control	BMI healthy	average relative ratio of 3 repeats Maldi Intensities calculated m/z ∑PC / ∑LPC m/z
1	1501	25.3	3.3016
2	1502	27.5	2.5394
3	1509	27.7	3.1200
4	1515	25.5	4.1923
5	1516	28.5	2.6491
6	1518	25.7	1.9540
7	1531	28.7	1.7863
8	1534	25.9	2.0247
9	1491	29	2.2241
10	1495	23.4	2.0739
11	1543	26	3.0064
12	1487	29.4	2.6449

Figure 4:9 Explanation: working step 5 shows how it was created and calculated in Excel of three replicates per sample and then used the last column as an average of the three repeat values to plot on GraphPad. Figure 4:8 Explanation step 6 showing how to create a table and what to do from working step 5 in order to plot on GrapHad for every three replicates per each sample and used the average intensities calculated in the fourth column in the table following the formula sum of m/z pc intensities divided by sum of the LPC m/z intensities.

Additional extra information from researched literature peaks of gangliosides in negative ion mode with reference below. They play a dominant part in placenta and plasma and cannot be ignored. They are also observed in this research work.

Gangliosides	Negative Ions	Experimental Mass (m/z)	Theoretical Mass (m/z)	Error (m/z)
GM1/GD1-sialic acid (d18:1/18:(	M-H	1545.4	1544.9	0.5
GM1/GD1-sialic acid (20:1/18:0)	M-H	1573.5	1572.9	0.6
GD1 (18:1/18:0)	M+K-2H	1874.5	1874.1	0.4
GD1 (20:1/18:0)	M+Na-2H	1886.5	1886	0.5
GD1 (20:1/18:0)	M+K-2H	1902.3	1902.1	0.2
GM2 (18:0/18:0)	M-H	1385.4	1384.7	0.7
GM3 (18:0/20:1)	M-H	1208.3	1207.8	0.5
GM3 (18:1/24:0)	M-H	1264.1	1263.8	0.3
m/z (Monoisotopic)	Molecular Ion	Proposed Structure		
787.37	[M-H]−	LacCer(d18:1/11:2)		
834.26	[M-H]−	LacCer(d18:1/14:0)		
884.32	[M-H]−	LacCer(d18:1/18:2)		
891.06	[M-H]−	LacCer(d18:0/18:0)		
995.86	[M-H]−	GA2(d18:0/11:0)		
1041.1	[M-H]−	GM4(d18:1/20:2)		
1149.99	[M-H]−	GM3(d18:1/16:1)		
1151.98	[M-H]−	GM3(d18:1/16:0)		
1167.7	[M-H]−	GM3(t18:1/16:0)		
1177.96	[M-H]−	GM3(d18:1/18:1)		
1233.93	[M-H]−	GM3(d18:1/22:1)		
1259.9	[M-H]−	GM3(d18:1/24:2)		
1261.91	[M-H]−	GM3(d18:1/24:1)		
1275.82	[M-H]−	GM3(t18:1/24:2)		
1277.8	[M-H]−	GM3(t18:1/24:1)		
1437.65	[M-H]−	GM2(d18:1/22:1)		
1462.61	[M-H]−	GM2(d18:1/24:2)		
1489.55	[M-H]−	GD3(t18:0/18:0)		
1514.44	[M-H]−	GD3(d18:0/21:0) or O-Ac-GD3(d18:0/18:0)		
1542.41	[M-H]−	GM1(d18:1/18:1)		
1570.45	[M-H]−	GM1(d18:1/20:1)		
1598.4	[M-H]−	GM1(d18:1/22:1)		
1626.23	[M-H]−	GM1(d18:1/24:1) or GM1(d18:0/24:2)		
1628.22	[M-H]−	GM1(d18:1/24:0)		
1640.35	[M-H]−	GM1(d18:1/25:1)		
1644.31	[M-H]−	GM1(d18:0/25:0)		
1659.32	[M-H]−	GM1(t18:1/25:0)		
1792.69	[M-H]−	GD1(d18:1/15:1)		
1833.98	[M-H]−	GD1(d18:1/18:1)		
1861.95	[M-H]−	GD1(d18:0/20:1)		
1915.07	[M-H]−	GD1(t18:1/24:3)		
1916.92	[M-H]−	GD1(d18:1/24:2)		
1919.86	[M-H]−	GD1(d18:1/24:0) or GD1(t18:1/23:1)		

Figure 4:9: Table: An example of negative [M+H]+ and positive [M-H]- ions in the DHB matrix of ganglioside identification adapted from literature with permission of authors is given in table: Sarbu, M.; Ica, R.; Zamfir, A.D. Gangliosides as Biomarkers of Human Brain Diseases: Trends in Discovery and Characterization by High-Performance Mass Spectrometry. Int. J. Mol. Sci. 2022, 23, 693

Below three are two tables in positive ion mode represented by formula [M+H]+ where M=mass m/z, [H]+ / [H]- proton and in negative ion mode [M-H]-. The table contains this work experimentally observed mass-to-charge ratios m/z in positive ion mode [M+H] with researched literature supplementary data and then compared to actual observable m/z ions in this work run in MALDI ToF MS.

Observed in Placenta total lipids extract acquired on MALDI ToF MS Ultra Flex Brucker observed peakspositive ion [M+H]+ m/z in Matrix 9AA, DHB		
Literature Refernces:	Observed m/z [M+H]+	
Beate Fuchs 2008 Analysis of stem cell lipids by offline HPTLC-MALDI-TOF MS Authors: (B.Fuchs 2008), (M.Eibisch J. Schiller 2011), (R.Agelini 2012), (K.A. Zemski-Berry 2011), (P.Lopalco 2019), (Sarbu, M. 2022), (Sup Data J.C. McMillen, R. M. Caprioli 2020	Attentative assigment	Observed in MALDI [M+H]+ m/z
B.Fuchs 2008, M Petkovic 2009 , M.Eibisch J. Schiller 2011, R.Agelini 2012,McMillen, Caprioli 2020	LPC 16:0 (+H+)	496.3398
B.Fuchs 2008, M Petkovic 2009 , M.Eibisch J. Schiller 2011, R.Agelini 2012,McMillen, Caprioli 2020	LPC 16:0 (+Na+)	518.3241
B.Fuchs 2008, M Petkovic 2009 , M.Eibisch J. Schiller 2011, R.Agelini 2012,McMillen, Caprioli 2020	LPC 18:2 (+H+)	520.2905
B.Fuchs 2008, M Petkovic 2009 , M.Eibisch J. Schiller 2011, R.Agelini 2012,McMillen, Caprioli 2020	LPC 18:1 (+H+)	522.1672
B.Fuchs 2008, M Petkovic 2009 , M.Eibisch J. Schiller 2011, R.Agelini 2012,McMillen, Caprioli 2020	LPC 18:0 (+H+)	524.2854
B.Fuchs 2008, M Petkovic 2009 , M.Eibisch J. Schiller 2011, R.Agelini 2012,McMillen, Caprioli 2020	LPC 18:2 (+Na+)	542.3241
B.Fuchs 2008, M Petkovic 2009 , M.Eibisch J. Schiller 2011, R.Agelini 2012,McMillen, Caprioli 2020	LPC 18:1 (+Na+)	544.2672
B.Fuchs 2008, M Petkovic 2009 , M.Eibisch J. Schiller 2011, R.Agelini 2012,McMillen, Caprioli 2020	LPC 18:0 (+Na+)	546.3554
B.Fuchs 2008, M Petkovic 2009 , M.Eibisch J. Schiller 2011, R.Agelini 2012,McMillen, Caprioli 2020	PC 16:0/18:2 (+H+)	758.5694
B.Fuchs 2008, M Petkovic 2009 , M.Eibisch J. Schiller 2011, R.Agelini 2012,McMillen, Caprioli 2020	PC 16:0/18:1 (+H+)	760.5851
B.Fuchs 2008, M Petkovic 2009 , M.Eibisch J. Schiller 2011, R.Agelini 2012,McMillen, Caprioli 2020	PC 16:0/18:2 (+Na+)	780.5538
B.Fuchs 2008, M Petkovic 2009 , M.Eibisch J. Schiller 2011, R.Agelini 2012,McMillen, Caprioli 2020	PC 16:0/20:4 (+H+)	782.5694
B.Fuchs 2008, M Petkovic 2009 , M.Eibisch J. Schiller 2011, R.Agelini 2012,McMillen, Caprioli 2020	PC 16:0/20:4 (+H+)	782.5694
B.Fuchs 2008, M Petkovic 2009 , M.Eibisch J. Schiller 2011, R.Agelini 2012,McMillen, Caprioli 2020	PC 18:0/18:3 (+H+)	784.5851
B.Fuchs 2008, M Petkovic 2009 , M.Eibisch J. Schiller 2011, R.Agelini 2012,McMillen, Caprioli 2020	PC 18:0/18:2 (+H+)	786.6454
B.Fuchs 2008, M Petkovic 2009 , M.Eibisch J. Schiller 2011, R.Agelini 2012,McMillen, Caprioli 2020	PC 16:0/20:4 (+Na+)	804.5749
B.Fuchs 2008, M Petkovic 2009 , M.Eibisch J. Schiller 2011, R.Agelini 2012,McMillen, Caprioli 2020	PC 18:0/18:3 (+Na+)	806.5694
B.Fuchs 2008, M Petkovic 2009 , M.Eibisch J. Schiller 2011, R.Agelini 2012,McMillen, Caprioli 2020	PC 18:0/18:2 (+Na+)	808.5851
B.Fuchs 2008 ,M Petkovic 2009, M.Eibisch J. Schiller 2011, K.A. Zemski-Berry 2011, McMillen, Caprioli 2020	SM(d18:1/16:0)	703.4000
B.Fuchs 2008 ,M Petkovic 2009, M.Eibisch J. Schiller 2011, K.A. Zemski-Berry 2011, McMillen, Caprioli 2020	SM(d18:0/16:0)	705.4000
B.Fuchs 2008 ,M Petkovic 2009, M.Eibisch J. Schiller 2011, K.A. Zemski-Berry 2011, McMillen, Caprioli 2020	SM(d18:1/16:0)+Na	725.5000
B.Fuchs 2008 ,M Petkovic 2009, M.Eibisch J. Schiller 2011, K.A. Zemski-Berry 2011, McMillen, Caprioli 2020	SM(d18:1/18:0)	731.5000
B.Fuchs 2008 ,M Petkovic 2009, M.Eibisch J. Schiller 2011, K.A. Zemski-Berry 2011, McMillen, Caprioli 2020	SM(d18:1/16:0)+K	741.5000
B.Fuchs 2008, M Petkovic 2009 , M.Eibisch J. Schiller 2011, K.A. Zemski-Berry 2011, McMillen, Caprioli 2020	SM(d18:1/18:0)+Na	753.4000
B.Fuchs 2008, M Petkovic 2009, M.Eibisch J. Schiller 2011, K.A. Zemski-Berry 2011, P.Lopalco 2019, McMillen, Caprioli 2020	SM (d16:1–22:0)	759.6370
B.Fuchs 2008, M Petkovic 2009, M.Eibisch J. Schiller 2011, K.A. Zemski-Berry 2011, P.Lopalco 2019, McMillen, Caprioli 2020	SM(d18:1/18:0)+K	769.5000
B.Fuchs 2008, M Petkovic 2009, M.Eibisch J. Schiller 2011, K.A. Zemski-Berry 2011, P.Lopalco 2019, McMillen, Caprioli 2020	SM (d17:1–22:0)	773.6530
B.Fuchs 2008, M Petkovic 2009 , M.Eibisch J. Schiller 2011, K.A. Zemski-Berry 2011, P.Lopalco 2019, McMillen, Caprioli 2020	SM (d17:0–22:0)	775.6690
B.Fuchs 2008, M Petkovic 2009 , M.Eibisch J. Schiller 2011, K.A. Zemski-Berry 2011, P.Lopalco 2019, McMillen, Caprioli 2020	SM(d18:1/20:0)+K	797.5000
B.Fuchs 2008, M Petkovic 2009 , M.Eibisch J. Schiller 2011, K.A. Zemski-Berry 2011, P.Lopalco 2019, McMillen, Caprioli 2020	SM (d18:0–22:0)	789.6840
B.Fuchs 2008, M Petkovic 2009 , M.Eibisch J. Schiller 2011, K.A. Zemski-Berry 2011, P.Lopalco 2019, McMillen, Caprioli 2020	SM (d20:2–22:1)	811.6690
B.Fuchs 2008, M Petkovic 2009 , M.Eibisch J. Schiller 2011, K.A. Zemski-Berry 2011, P.Lopalco 2019, McMillen, Caprioli 2020	SM (+ Na^+) (d16:1–18:0)	725.5570
B.Fuchs 2008 , M Petkovic 2009 , M.Eibisch J. Schiller 2011, K.A. Zemski-Berry 2011,McMillen, Caprioli 2020	SM(d18:1/24:1)+Na	835.8000
B.Fuchs 2008 , M Petkovic 2009 , M.Eibisch J. Schiller 2011, K.A. Zemski-Berry 2011,McMillen, Caprioli 2020	SM(d18:1/24:0)+Na	837.5000
B.Fuchs 2008 , M Petkovic 2009, M.Eibisch J. Schiller 2011, K.A. Zemski-Berry 2011, P.Lopalco 2019 ,McMillen, Caprioli 2020	SM (+ Na^+) (d16:1–22:0)	781.6190
B.Fuchs 2008 , M Petkovic 2009, M.Eibisch J. Schiller 2011, K.A. Zemski-Berry 2011, P.Lopalco 2019 ,McMillen, Caprioli 2020	SM (+ Na^+) (d17:1–22:0)	795.6350
B.Fuchs 2008 , M Petkovic 2009, M.Eibisch J. Schiller 2011, K.A. Zemski-Berry 2011, P.Lopalco 2019 ,McMillen, Caprioli 2020	SM (+ Na^+) (d17:0–22:0)	797.6510
B.Fuchs 2008 , M Petkovic 2009, M.Eibisch J. Schiller 2011, K.A. Zemski-Berry 2011, P.Lopalco 2019 ,McMillen, Caprioli 2020	TAG (+Na^+) (48:1)	827.7200
B.Fuchs 2008 , M Petkovic 2009, M.Eibisch J. Schiller 2011, K.A. Zemski-Berry 2011, P.Lopalco 2019 ,McMillen, Caprioli 2020	TAG (+Na^+) (48:0)	829.7360
B.Fuchs 2008 , M Petkovic 2009, M.Eibisch J. Schiller 2011, K.A. Zemski-Berry 2011, P.Lopalco 2019 ,McMillen, Caprioli 2020	TAG (+Na^+) (52:4)	877.7360
B.Fuchs 2008 , M Petkovic 2009, M.Eibisch J. Schiller 2011, K.A. Zemski-Berry 2011, P.Lopalco 2019 ,McMillen, Caprioli 2020	TAG (+Na^+) (54:6)	901.7360
B.Fuchs 2008 , M Petkovic 2009, M.Eibisch J. Schiller 2011, K.A. Zemski-Berry 2011, P.Lopalco 2019 ,McMillen, Caprioli 2020	TAG (+Na^+) (54:5)	903.7520
B.Fuchs 2008 , M Petkovic 2009, M.Eibisch J. Schiller 2011, K.A. Zemski-Berry 2011, P.Lopalco 2019 ,McMillen, Caprioli 2020	TAG (+Na^+) (54:1)	911.8150
B.Fuchs 2008 , M Petkovic 2009, M.Eibisch J. Schiller 2011, K.A. Zemski-Berry 2011, P.Lopalco 2019 ,McMillen, Caprioli 2020	TAG (+Na^+) (54:0)	913.8300
B.Fuchs 2008 , M Petkovic 2009, M.Eibisch J. Schiller 2011, K.A. Zemski-Berry 2011, P.Lopalco 2019 ,McMillen, Caprioli 2020	DAG (+Na^+) 32:2	587.4750
B.Fuchs 2008 , M Petkovic 2009, M.Eibisch J. Schiller 2011, K.A. Zemski-Berry 2011, P.Lopalco 2019 ,McMillen, Caprioli 2020	DAG (+Na^+) 34:2	615.5070
B.Fuchs 2008 , M Petkovic 2009, M.Eibisch J. Schiller 2011, K.A. Zemski-Berry 2011, P.Lopalco 2019 ,McMillen, Caprioli 2020	DAG (+Na^+) 36:4	639.5070
B.Fuchs 2008 ,M Petkovic 2009 ,M.Eibisch J. Schiller 2011, K.A. Zemski-Berry 2011, P.Lopalco 2019 ,McMillen, Caprioli 2020	DAG (+Na^+) 36:3	641.5220
Sarbu, M. Sarbu, M.Ica, R. Zamfir, A.D. 2022	GM2 (18:0/18:0)	1385.4000
Sarbu, M. Sarbu, M.Ica, R. Zamfir, A.D. 2022	GM3 (18:0/20:1)	1208.3000
Sarbu, M. Sarbu, M.Ica, R. Zamfir, A.D. 2022	GM3 (18:1/24:0)	1264.1000
Literature Reference	DHB Matrix	[M+H]+ m/z
B.Fuchs 2008 , M Petkovic 2009 ,M.Eibisch J. Schiller 2011, K.A. Zemski-Berry 2011, P.Lopalco 2019 ,McMillen, Caprioli 2020	PC(16:0/OH)	496.9000
B.Fuchs 2008 , M Petkovic 2009 ,M.Eibisch J. Schiller 2011, K.A. Zemski-Berry 2011, P.Lopalco 2019 ,McMillen, Caprioli 2020	PC(34:1) +Na	726.3000
B.Fuchs 2008 , M Petkovic 2009 ,M.Eibisch J. Schiller 2011, K.A. Zemski-Berry 2011, P.Lopalco 2019 ,McMillen, Caprioli 2020	PC(32:0)	735.3600
B.Fuchs 2008 , M Petkovic 2009 ,M.Eibisch J. Schiller 2011, K.A. Zemski-Berry 2011, P.Lopalco 2019 ,McMillen, Caprioli 2020	PC(34:2)	759.3900
B.Fuchs 2008 , M Petkovic 2009 ,M.Eibisch J. Schiller 2011, K.A. Zemski-Berry 2011, P.Lopalco 2019 ,McMillen, Caprioli 2020	PC(34:1)	761.3900
B.Fuchs 2008 , M Petkovic 2009 ,M.Eibisch J. Schiller 2011, K.A. Zemski-Berry 2011, P.Lopalco 2019 ,McMillen, Caprioli 2020	PC(36:3)	785.4000
B.Fuchs 2008 , M Petkovic 2009 ,M.Eibisch J. Schiller 2011, K.A. Zemski-Berry 2011, P.Lopalco 2019 ,McMillen, Caprioli 2020	PC (36:4)	805.4000
B.Fuchs 2008 , M Petkovic 2009 ,M.Eibisch J. Schiller 2011, K.A. Zemski-Berry 2011, P.Lopalco 2019 ,McMillen, Caprioli 2020	PC (36:4)	821.4000

Figure 4:10: Positive ion mode observed mass spectral peaks and their assignments according to expected peaks from the literature (references in column 1). The peaks in the (yellow) column were included if they were observed in [M+H]+ m/z 9AA, DHB matrix. Literature reference for positive and negative ions (70, 103, 233, 253, 270, 335, 513, 582, 588-607).

Literature authors:(Han Gross 1996);(Brugger 1997); (Houjou 2004); (Han Gross 2004); (R.Murphy 2009); (K.Zemsky-Berry 2011); (R Caprioli 2009); (K .Burnum 2009); (B Fuchs 2009);(M.Petkovic 2009) (J Schiller 2009); (R.Angelini 2012); (D Anderson 2013); (RC.Baker 2014);(T Goto 2014) (R.Angelini 2014);(Zaczek 2016),(Messias 2018) (P. Lopalco 2019); (Han Gross 1996); (T Goto 2014); (RC.Baker 2014); (YuliaTyurina 2014) (Peggy Angel 2012); (Weingartner 2012); (Khalil 2017); (Wang& Han 2018) (Minkler & Hoppel 2020), Lipid Maps						Attentative assignment Lipid species [M-H]- Matrix 9AA ; DHB	Observed peaks [M-H]- m/z	MALDI ToF Ms negative ion Fragments: (I see) (I do not see)
					L. Maps neutral	Sterols ST 27:2;O3	415.3272	
					Messias 2018	PA 18:1	418	
						LPI	419.3655	415
						LPE 16:0	436.3938	418 436
				Khalil 2017	Lopalco 2019	LPE 16:0	452.246	418 ##
						PG 34:2	465.3756	
					L. Maps neutral	Chol. Sulph. CS	465.299	
					L. Maps neutral	Chol. Sulph. CS	466.3024	
					L. Maps neutral	Chol. Sulph. CS	467.3051	
					Lopalco 2019	LPE 18:3	474.268	
				Khalil 2017	Lopalco 2019	LPE 18:1	478.298	
			Han Gross 1996	Khalil 2017	Lopalco 2019	LPE 18:0	480.309	
					Khalil 2017	LPG(16:0)	483.2153	
						PG 34:1	491.3768	
				B Fuchs 2009	Lopalco 2019	Plsm-LPE 20:0	494.302	
					Khalil 2017	LPE (20:4)	500.3272	
					Khalil 2017	LPE (20:0)	508.3983	
					Khalil 2017	LPG (18:1)	509.3797	
					L. Maps neutral	LPI	535.1621	
					L. Maps neutral	LPI	571.3186	
					L. Maps neutral	PI 36:2	581.3417	
					L. Maps neutral	LPI	597.3291	
	Goto 2014	Khalil 2017	P Angel 2012	Burnum 2009	Murphy 2009	PI (18:0/OH)	599.3048	283 315 ## 535 571 577 597
				T Goto 2014	Brugger 1997	PA 30:0	619.3042	
			Khalil 2017	RC.Baker 2014	Brugger 1997	PA32:2	643.4995	
				Khalil 2017	T Goto 2014	PA	673.3273	spliting
			Houjou 2004 [M-(	Zaczek 2016[SM-C	Khalil 2017	Cer-PE (36:1)	687.546	
					Khalil 2017	PE (32:1)	688.5491	
					L. Maps neutral	PA 36:4	695.4731	splitin hump*
			Brugger 1997	T Goto 2014	P Angel 2012	PA	699.5029	
			Brugger 1997	Khalil 2017	Goto 2014	PA	701.5234	
					Brugger 1997	PA	703.3163	
				[M-H]- POPE	Lopalco 2019	PE 34:3	712.516	
	B Fuchs 2009	Khalil 2017	T Goto 2014	Burnum 2009	Murphy 2009	PE	716.5513	hump 255 ## 478 436 418 508
					Murphy 2009	PE 16:0/18:1	722.4837	
			Brugger 1997	[M-2H]-² 1447.958	Han Gross 2004	[CL M-2H]2-	723.5108	
					Murphy 2009	PE 18:1/18:2	726.5521	
					Murphy 2009	PE	728.5645	
					Lopalco 2019	PE 34:4	736.55	
				Khalil 2017	Lopalco 2019	PE 36:4	738.557	
				Khalil 2017	Lopalco 2019	PE 36:3	740.565	
	T Goto 2014	Khalil 2017	Lopalco 2019	Burnum 2009	Murphy 2009	PE 36:2	742.582	279 283 ## 480 478
		[PC 16:0/18:1 -CH	B Fuchs 2009	P Angel 2012	Murphy 2009	PE	744.565	
					Lopalco 2019	PG 34:2	745.563	465 483 ## 509
			P Angel 2012	Burnum 2009	Murphy 2009	PE	746.517	327 436 ##
			Houjou 2004 [M+	Burnum 2009	Murphy 2009	PG 34:1	747.521	281 255 ## 465 483 491
				PC -SM-Ceramide	P Angel 2012	PEp	748.5362	
			P Angel 2012	Burnum 2009	Murphy 2009	PE	750.549	331 436
					P Angel 2012	PS	760.5293	
			P Angel 2012	Lopalco 2019	Murphy 2009	PE 38:6	762.546	
					P Angel 2012	PS	762.5184	
			Lopalco 2019	Burnum 2009	Murphy 2009	PE 38:5	764.529	303 281 ##
			P Angel 2012	Lopalco 2019	Murphy2009[PC-C	PE 38:4	766.58	
					Lopalco 2019	PE 38:3	768.585	
			Lopalco 2019	Burnum 2009	Murphy 2009	PE 38:2	770.575	279 283 ## 460 508 307
					P.Angel 2012	PE	772.6451	
				P Angel 2012	Murphy 2009	PE	774.5061	
				Weingartner 2012	Murphy 2009	IPC d34:1	778.4892	
					Lopalco 2019	PS 36:5	780.609	701 419 ## 699 415
					P Angel 2012	PI	781.5505	
					Lopalco 2019	PS 36:4	782.628	
					Lopalco 2019	PS 36:3	784.643	
		P Angel 2012	Lopalco 2019	Burnum 2009	Murphy 2009	PS 36:2	786.534	699 419 ## 415 279
	P Angel 2012	Khalil 2017	Lopalco 2019	Burnum 2009	Murphy 2009	PS 36:1	788.551	701 419 ## 417 504
				P Angel 2012	Murphy 2009	PE	790.5038	hump*
					Murphy 2009	PI	794.483	
					P.Angel 2012	PI	795.5198	
				Khalil 2017	Goto 2014	PI (16:0/16:0)	809.5377	
			Khalil 2017	P.Angel 2012	Murphy 2009	PS (38:4)	810.4899	
					P Angel 2012	PS	812.5554	
				Weingartner 2012	Lopalco 2019	PI	831.612	
		Khalil 2017	T Goto 2014	Burnum 2009	Murphy 2009	PI (16:0/18:2)	833.523	553 391 ## 599 415 279
				Weingartner 2012	P Angel 2012	IPC d38:1	834.4865	
				Khalil 2017	T Goto 2014	PI(16:0/18:1)	835.5827	
					L. Maps neutral	PI	836.5882	
		Khalil 2017	T Goto 2014	Burnum 2009	Murphy 2009	PI (16:0/18:0)	837.556	531 419 ## 577 599 415 297
T Goto 2014	P Angel 2012	Khalil 2017	Lopalco 2019	Burnum 2009	Murphy 2009	PI (16:0/20:4)	857.522	553 391 ## 303 255 439 297
				T Goto 2014	Lopalco 2019	PI (16:0/20:3)	859.666	
	T Goto 2014	Khalil 2017	Lopalco 2019	Burnum 2009	Murphy 2009	PI (18:0/18:2)	861.534	581 419 ## 599 415 297
			D Anderson 2013	T Goto 2014	Murphy 2009	PI	862.5132	
					Petkovic 2009	Sulphatides Ceramide	862.6097	
			A Weingartner 20	Khalil 2017	T Goto 2014	IPC (18:0/18:1)	863.618	
					Lopalco 2019	Plsm-PI 38:3	873.652	
					Lopalco 2019	PI	875.667	
					Lopalco 2019	PI	877.673	
				Khalil 2017	P Angel 2012	PI (38:6)	881.5189	
					L. Maps neutral	PI	882.5216	
T Goto 2014	P Angel 2012	Khalil 2017	Lopalco 2019	Burnum 2009	Murphy 2009	PI (18:1/20:4)	883.541	579 417 ## 597 601 303 439
					L. Maps neutral	PI 38:4	884.5374	
	T Goto 2014	P Angel 2012	Lopalco 2019	Burnum 2009	Murphy 2009	PI (18:0/20:4)	885.553	581 419 ## 599 601 303 297 ##
					Murphy 2009	PI 38:2	886.5548	
					T Goto 2014	PI(18:0/20:3)	887.5642	
					M Petkovic 2009	Sulphatides Ceramide	888.5694	
				Khalil 2017	T Goto 2014	PI(18:0/20:2)	889.659	
					Lopalco 2019	Plsml-PI 40:4	899.666	
					Murphy 2009	ST	890.5387	hump*
					Lopalco 2019	Plsml-PI 40:3	901.685	
					Murphy 2009	ST	904.5806	hump*
				P Angel 2012	Murphy 2009	ST	906.4719	hump*
			T Goto 2014	Burnum 2009	Murphy 2009	PI (18:0/22:6)	909.556	581 419 ## 599 625 297
					L. Maps neutral	CL 18:1	1447.9582	
				Lopalco 2019	Angelini 2012	CL 18:1	1448.0333	see
					Angelini 2012	CL 18:1	1450.9671	see
					Angelini 2012	CL 18:1	1452.978	see
					Angelini 2012	CL18:1	1474.97	see
					Angelini 2012	CL 18:1	1476.988	see
					Angelini 2012	CL [M+Na-2H]-	1478.9957	see
						CL 18:1	1494.9819	
						CL 18:1	1496.0439	

Figure 4:13: The table contains this work experimentally observed peaks in Maldi in negative ion mode [M-H]- from literature supplementary tables compared to actual observable in this research work run in MALDI ToF MS with peaks in the (yellow) were included observed in either 9AA or DHB [M-H]- m/z.

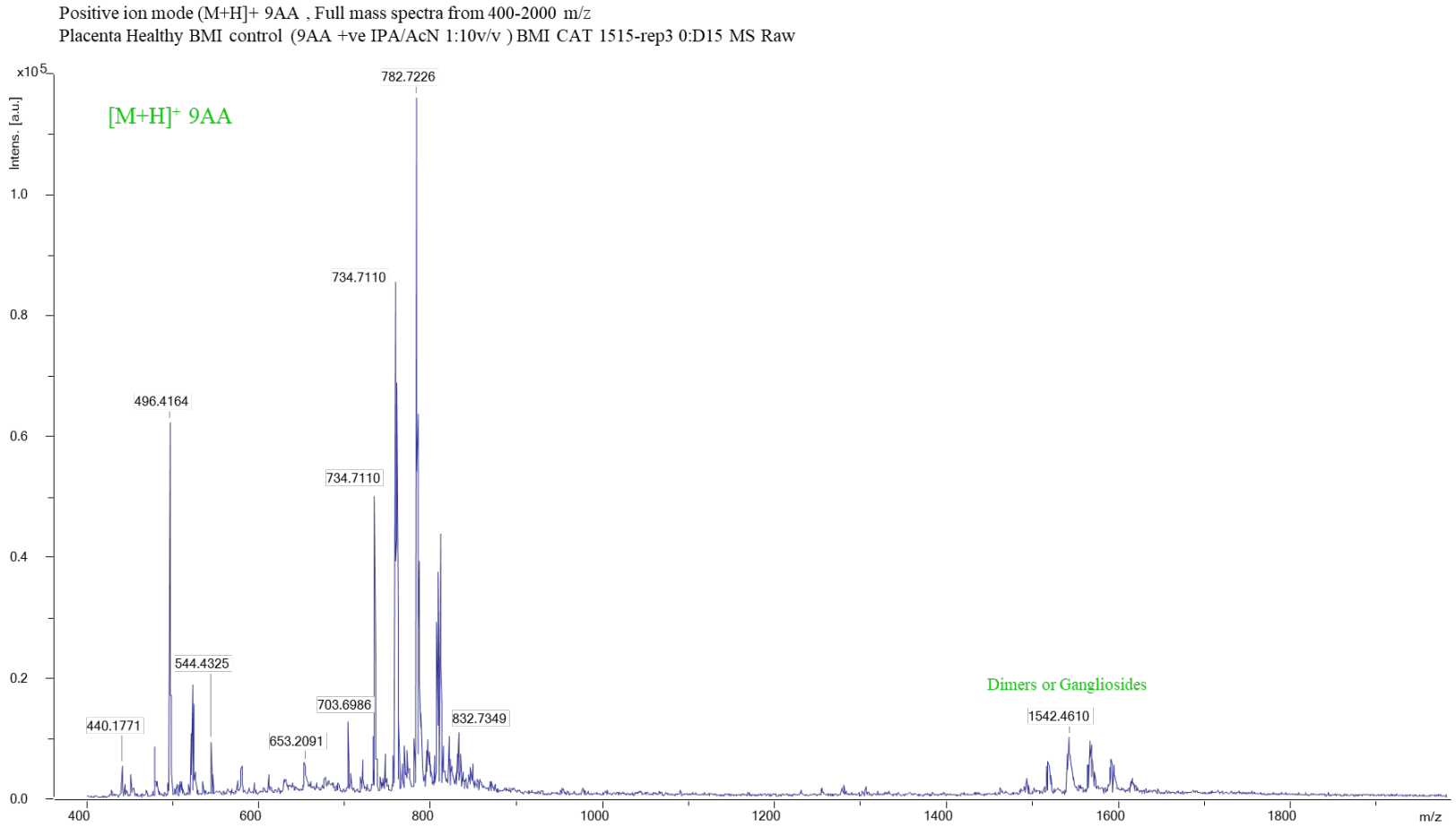

Figure 4:11: MALDI Full mass spectra 400-2000 m/z of the total lipid extracts from a healthy placenta in positive ion mode (M+H]+ in 9AA placenta CAT 1515 healthy BMI.

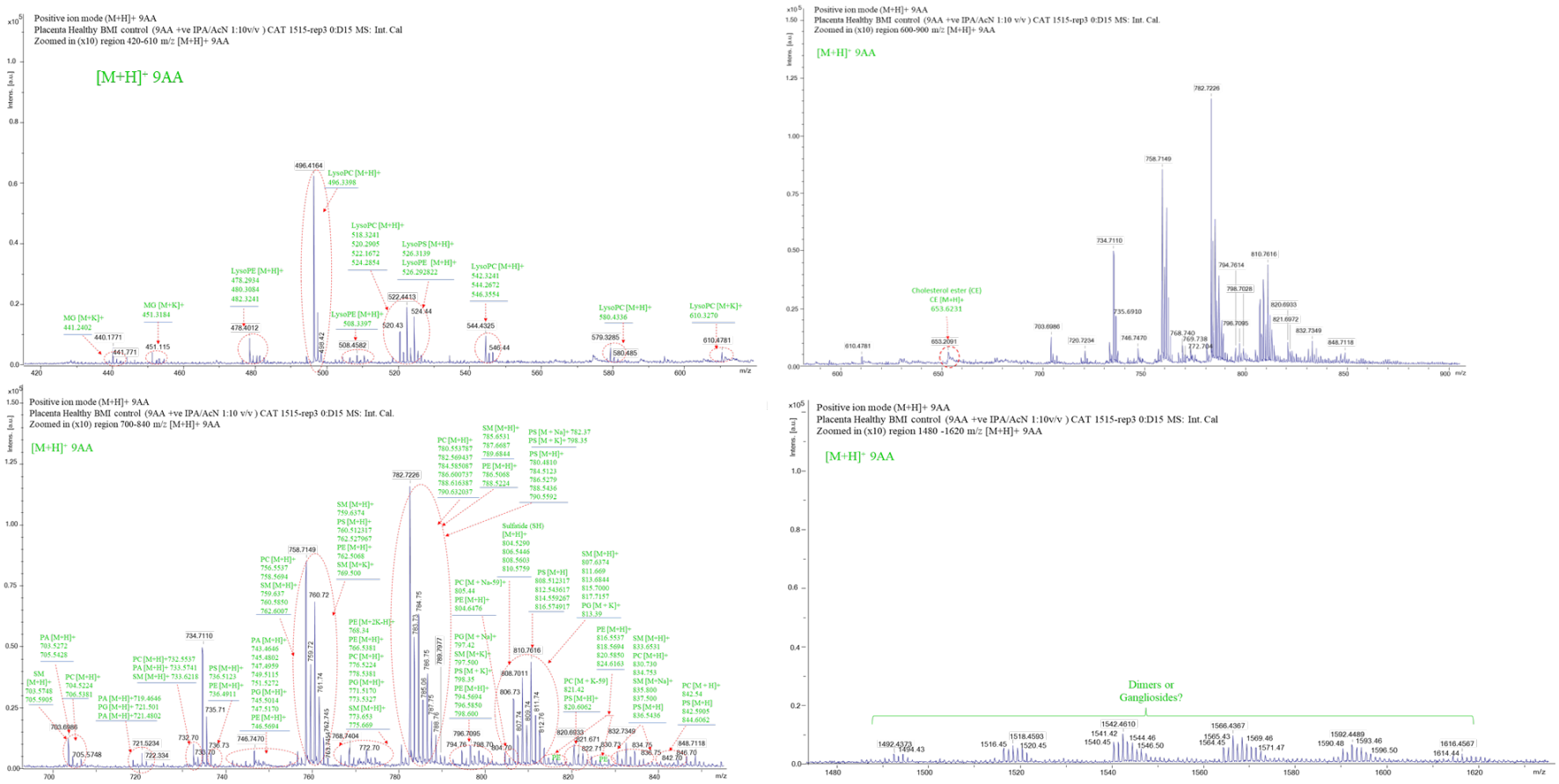

Figure 4:12 Positive ion mode (M+H]+ 9AA, Placenta Healthy BMI control (9AA +ve IPA/AcN 1:10v/v) CAT 1515-rep3 0:D15 MS: Int.Cal Zoomed in (x10) regions: 420-610 m/z, 700-840 m/z, 1480 -1620 m/z Figure: 4.35. Positive ion mode (M+H]+ DHB, The top plot is the full spectrum, and the four subplots below are the zoomed-in regions Zoomed in (x10) region 420 - 600 m/z, 580-725 m/z, 580-725 m/z, 720 – 840 m/z, 1440 – 1620 m/z of the same spectrum. Different assigned peaks are mostly labelled, including PC, LPC, SM, PI, sulfatides, CER, cholesterol and cholesterol esters, mono, di, triacyl glycerides, and PE. The assignments are from Table 4.21 literature.

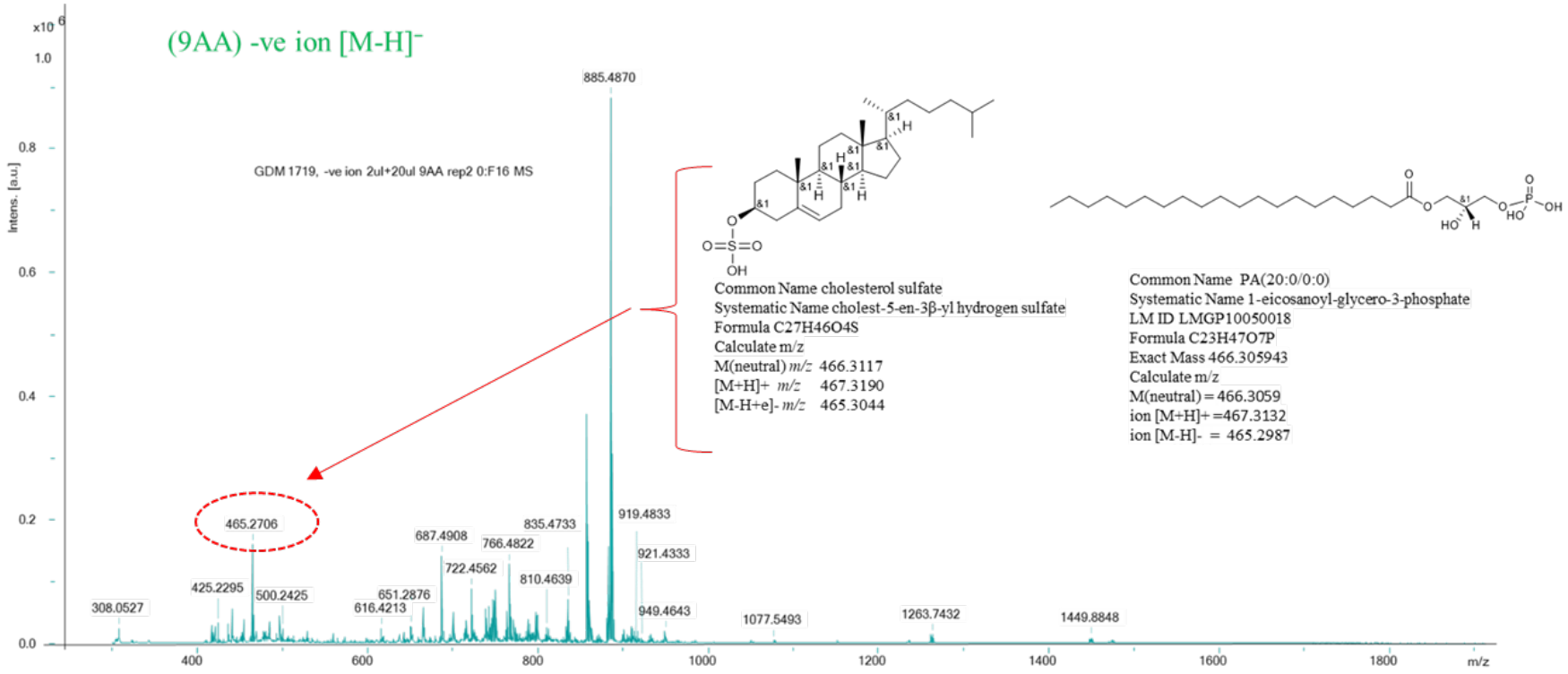

Figure 4:13: Full mass spectra obese BMI placenta CAT 1719 negative ion mode in 9AA matrix solvent isopropanol API /acetone nitrile CAN(3:2 v/v, sample: Matrix 1:10) peak 465.2706 m/z [M-H-H2O]- is either cholesterol sulphate or phosphatidic acid, showing similarities below table composed from checking with lipid maps using matched mass accuracy and calculation are explained as well using excel tables and then in text.

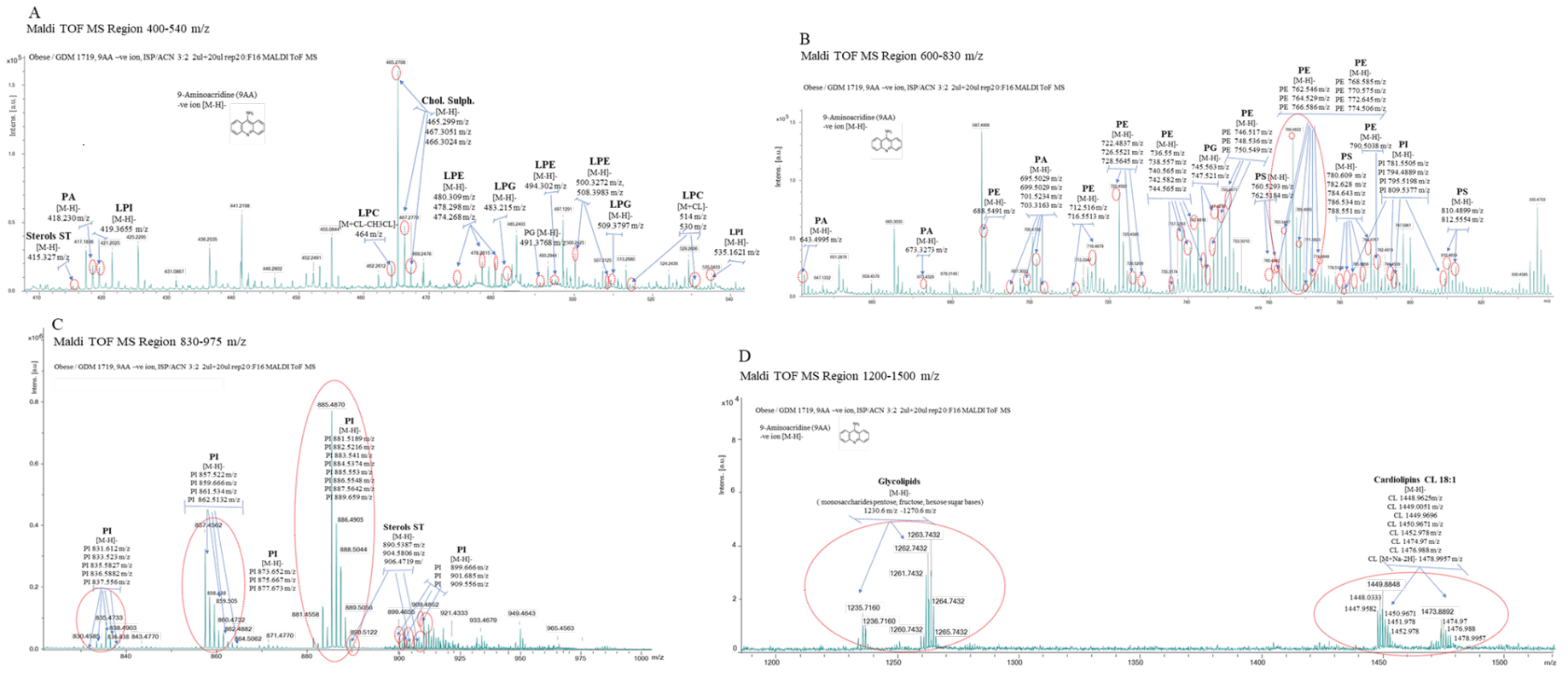

Figure 4:14: Full mass spectra showing zoomed in (x10) on each region A (400-500 m/z); B (600-830 m/z); C(830-975 m/z) ;D (1200-1500 m/z) comparing matrix 9AA in negative ion [M-H]- (IPA/ACN 3:2, 2ul+20ul) representative example of placenta obese/GDM CAT 1719

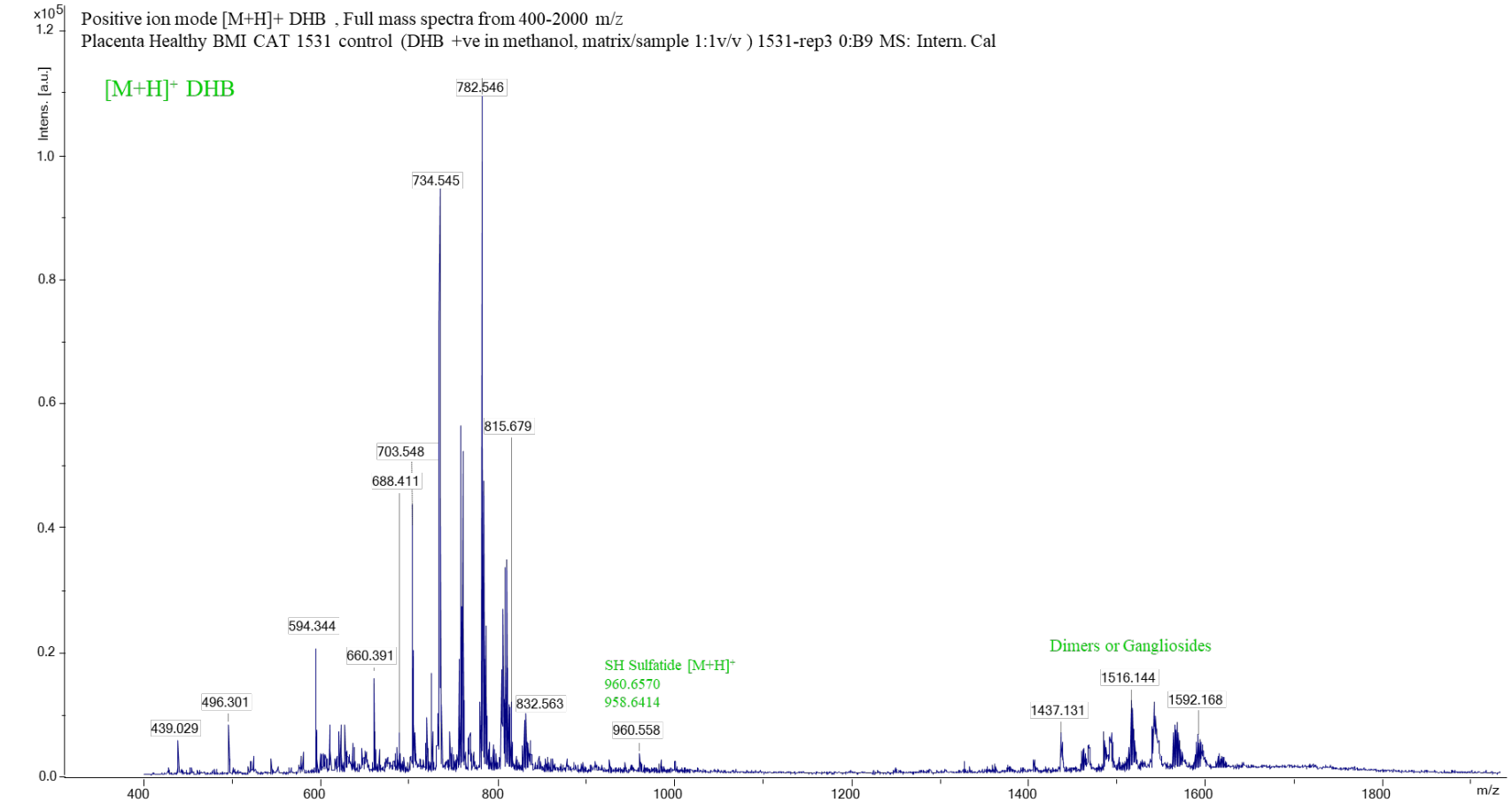

Figure 4:15: Positive ion mode (M+H]+ DHB, Full mass spectra from 400-2000 m/placenta healthy BMI CAT 1531 control (DHB +ve in methanol, matrix/sample 1:1v/v) 1531-rep3 0:B9 MS: Intern. Cal

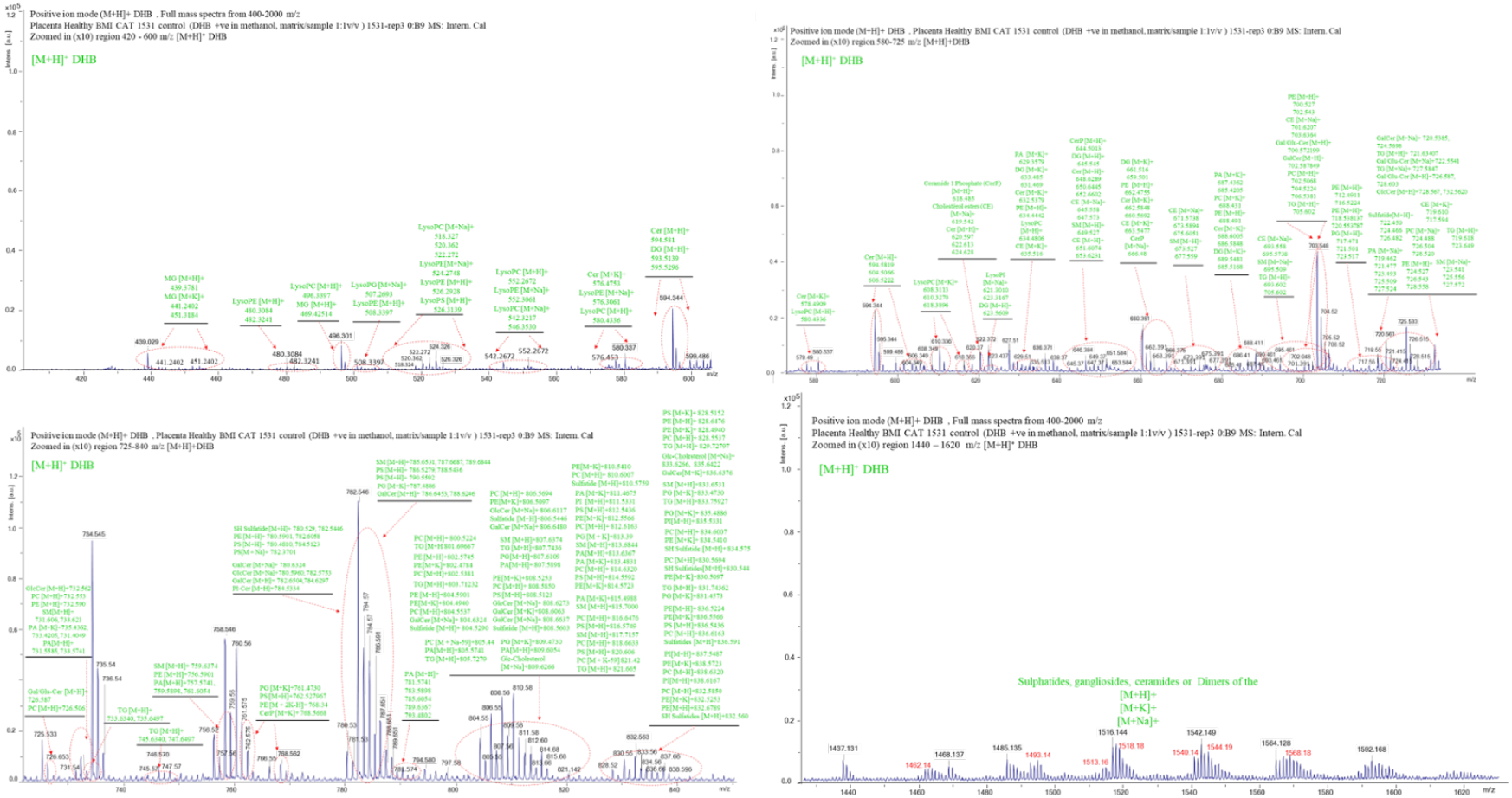

Figure 4:16 Positive ion mode (M+H]+ DHB, Full mass spectra from 400-2000 m/z, Placenta Healthy BMI CAT 1531 control (DHB +ve in methanol, matrix/sample 1:1v/v) 1531-rep3 0:B9 MS: Intern. Cal, Zoomed in (x10) regions 420 - 600 m/z , 580-725 m/z 720 – 840 m/z and 1440 – 1620 m/z

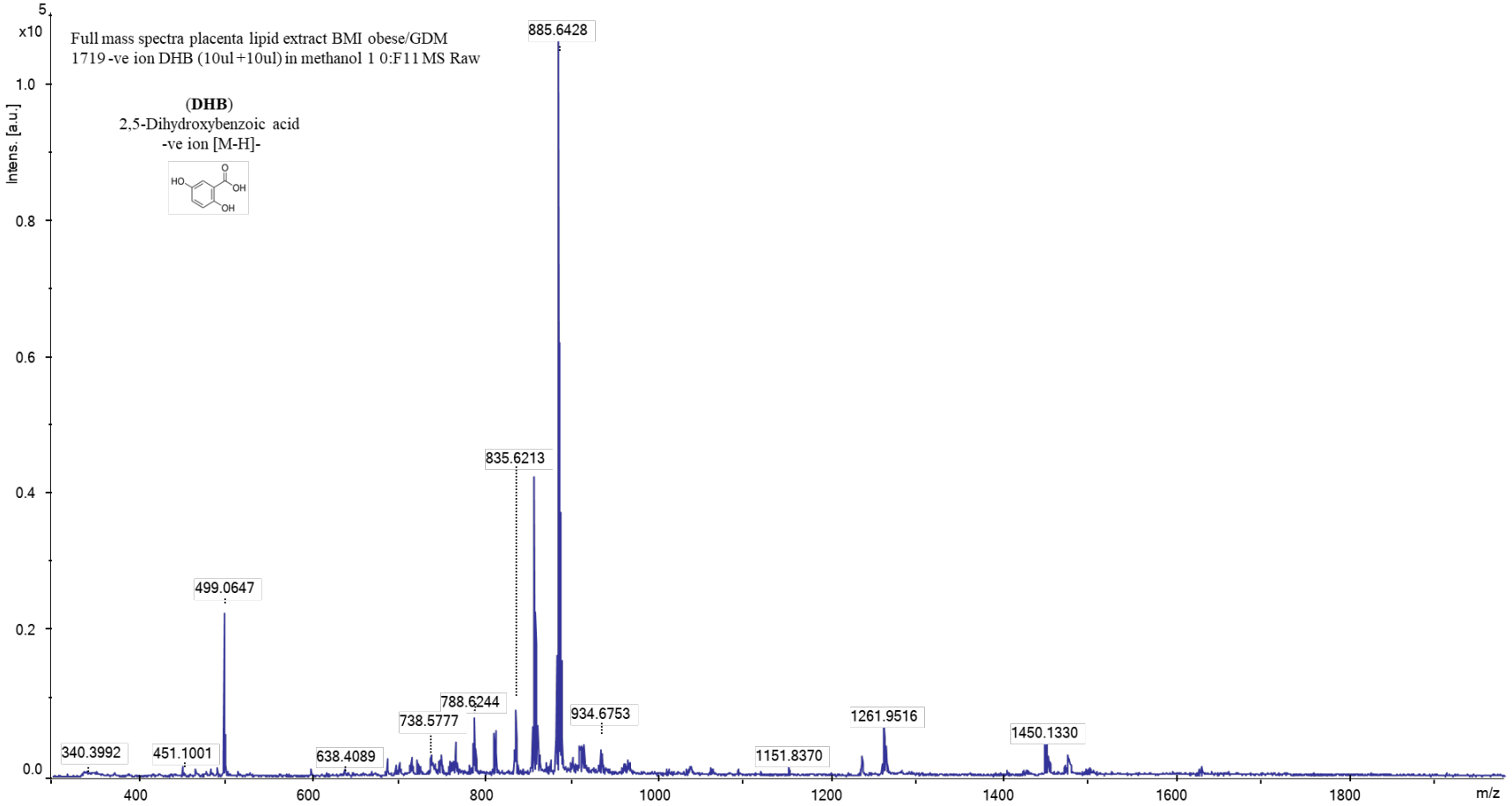

Figure 4:17: Whole mass spectra lipid extract BMI obese/GDM 1719 -ve ion DHB 2,5-Dihydroxybenzoic acid [M-H]- (10ul +10ul) in methanol 1 0:F11 MS Raw

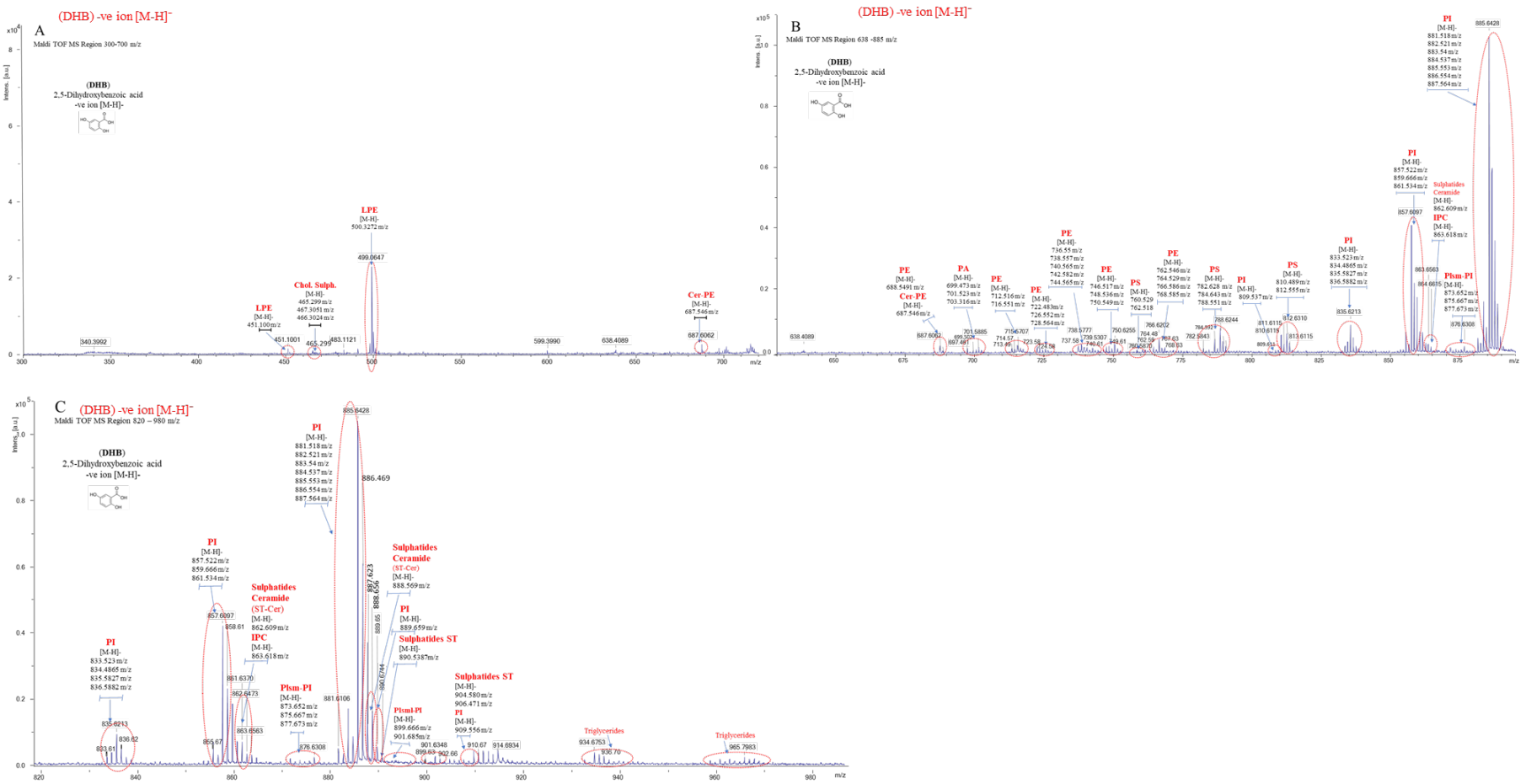

Figure 4:18: The full mass spectrum of the same sample (CAT 1719 total lipid extract from an obese patient placenta), DHB –ve mass spectra zoomed in (x10) on each region A (300 - 700 m/z); B (600-885 m/z); C (820 - 980 m/z) Sulphatides (ST) Ceramide (Cer) (ST-Ce

4.3.2 PC/LPC ratio analysis

The mass spectra of phospholipids in the negative-ion mode show heights lower than those in the positive-ion mode. It occurs because, in positive mode, molecules such as hydrogen, sodium, or potassium ions are present during ionisation, competing for an ionic charge. In the negative ion mode, the main characteristic of the molecular species is the loss of one hydrogen proton, which generates the negatively charged molecular ion [M-H]. The presence of negatively charged ions changes the molecular weight of phospholipids, which decreases by two mass units (also called Daltons, Da) compared to the same molecule observed in positive ion mode [M+H]+ versus negative ion mode [M-H]-. Below are sets of figures: Figure 4.12, Figure 4.13, and Figure 4.14 show representative MALDI mass spectra of the total lipid extracts from the placenta of healthy, obese, and GDM patients, respectively. The PC and LPC peaks are noted both on the spectra and insets, as these are important for further analysis and the discussion below. The project attempted to focus on PC and LPC lipids because there are many assignable lipids from TLC combined with MALDI-TOF mass spectral analysis. As the ratio of PC/LPC lipids was previously reported as a biomarker correlated with adverse pregnancy outcomes (April's paper), all 282 mass spectra were analyzed by summing the peak intensities of the PC and LPC peaks and calculating the ratio. The peak intensities from the mass spectra and these calculations are in the tables in the Appendix. The PC and LPC components were identified according to the m/z ratio of the peaks in the mass spectra, and the PC/LPC ratio comparisons between healthy controls, obese, and gestational diabetes mellitus (GDM) were plotted in the bar charts below. Healthy versus obese assignment is based on the mother's body mass index, with healthy patients having a BMI of less than 25 and obese with a 30-60 kg/m2 BMI. GDM was a clinical diagnosis, and patients have varying BMIs for this analysis.

4.3.3 Explanatory working steps showing the PC/LPC ratio

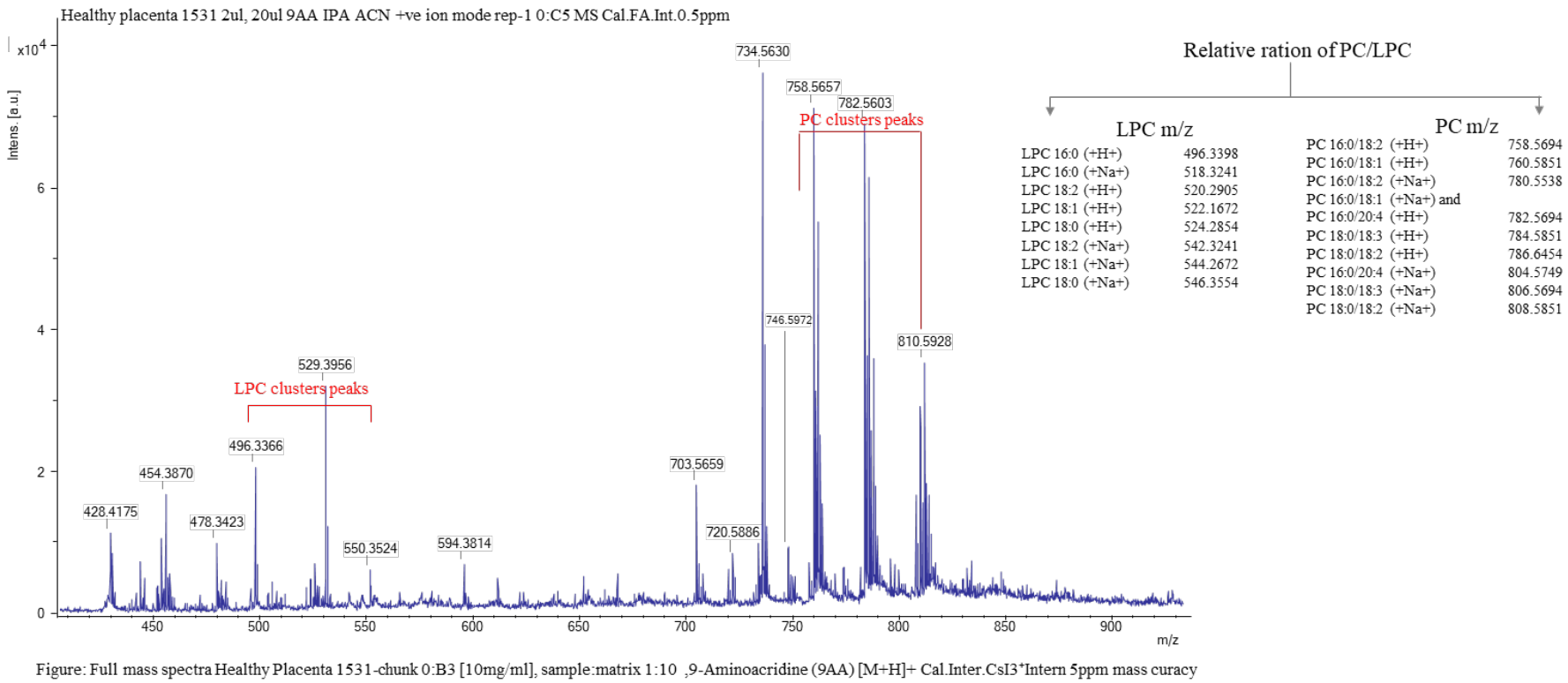

Figure 4:19 PC/LPC Peaks m/z MALDI mass spectrum of the placenta of a healthy patient. The masses of the observed PC and LPC lipids are shown in the inset and noted on the spectrum.

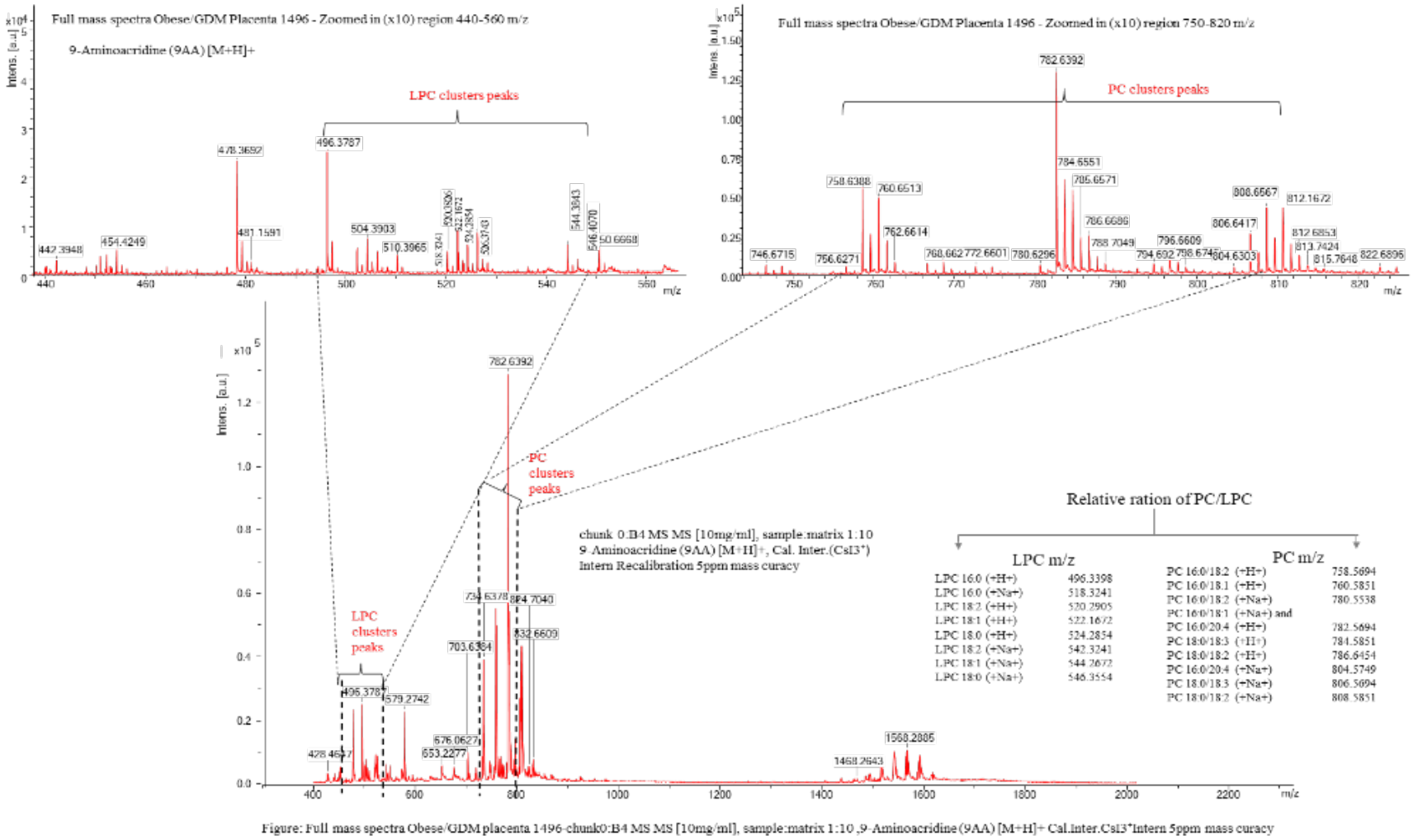

Figure: Full mass spectra Obese/GDM placenta 1496-chunk0:B4 MS MS [10mg/ml], sample:matrix 1:10 ,9-Aminoacridine (9AA) [M+H]+ Cal.inter.CsI3+Intern 5ppm mass curacy

Figure 4:20 Representative MALDI ToF MS of placental lipids from an obese patient.

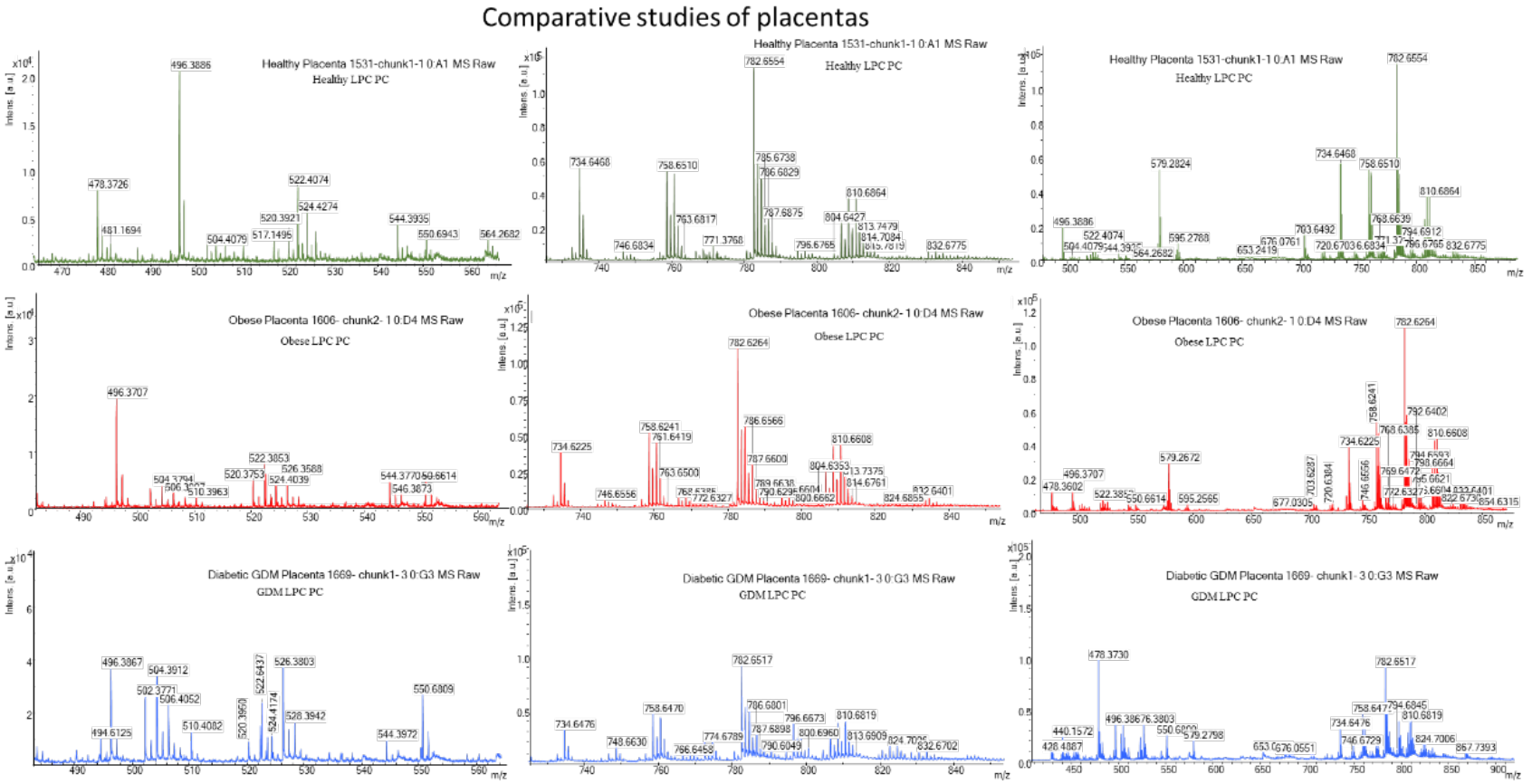

Figure 4:21 Placenta three groups comparative study top in green is healthy placentas, middle in red obese placentas and bottom in blue GDM placentas comparison of relative ration LPC/PC acquired on MALDI ToF MS showing total lipid extraction and the intensities from clusters peaks for PC/LPC are plotted in GraphPad. These spectral zooms indicate the 18 PC/LPC m/z peaks analyzed in all comparative studies. A healthy placenta total lipid extract is at the top (green), an obese placenta total lipid extract is in the middle (red), and a GDM placenta total lipid extract is at the bottom (blue).

4.3.4 Explanation - calculations for observed cholesterol sulphates

4.3.5 Plot Data of MALDI ToF MS Intensities

All data was calculated in order to show data representative plots for each placenta and plasm group acquired by MALDI ToF MS. Total of 94 samples, including placenta plasma, were run triplicate in this work in positive ion mode noted as [M+H]+ in both matrices +ve 9AA and +ve DHB matrix and all 94 samples resulted in generating a total of 20 GraphPad Plots covering all samples run in triplicate on MALDI ToF MS, and prior run on bioanalytical TLC. Each data plot 1-20 used LPC/PC ratios for a set of sample intensities acquired by MALDI-ToF MS using per each sample three repeats and taking an average of the three intensities of each cluster peaks for LPC and PC then added all together and calculated in excel by dividing sum of LPC intensity peaks by sum of PC intensities peaks per each placenta groups and plotting that number against each sample per group as a data point in the GraphPad representative for each group as the average of three replicas using ratio formula ∑LPC/∑PC and all sample calculation excel tables of each.

4.3.6 Steps: How to do it

Step 1 First, from Flex Analysis, import to Excel all sample intensities data, acquired at least three times signal to noise 3 S/N and already method preset to S/N=9 Spectrum: Exported data file to Excell Raw Data file from Flex Analysis: Spectrum: E:\Edyta Placenta flex analysis all data 22 04 2021\210422\Positive mode 22 04 2021\Positive ion mode 1mgml\CAT1315 1mg-ml POSITIVE 2\0_A1\1\1Ref.

Results Observed in Placenta total lipids extract acquired on MALDI ToF MS Ultra Flex Brucker observed positive ion [M+H]+ m/z in Matrix 9AA, DHB, followed by literature using supplementary data tables and mass spectra including Beate Fuchs 2008 Analysis of stem cell lipids by offline HPTLC-MALDI-TOF MS Authors: (Fuchs 2008), (M.Eibisch J. Schiller 2011), (Angelini 2012), (K.A. Zemski-Berry 2011), (Lopalco 2019), (Sarbu, M. 2022), (Sup Data J.C. McMillen, R. M. Caprioli 2020).

Results Observe in the negative ion Attenuative assignment Lipid species [M-H]- Matrix 9AA; DHB in-depth literature was used, searched and studies

supplementary data including the following Literature authors: *(107)*and Lipid Maps theoretical calculations and matches

Step 2 Use the monoisotopic molecular mass for each atomic element in the formula to calculate molecular atomic masses used from NIST.

Name	Symbol average mass	Relative Atomic Mass	Abund.
Carbon	C (12)	12.0000000	98.9
Hydrogen	H (1)	1.007825	99.99
Nitrogen	N (14)	14.003074	99.63
Oxygen	O (16)	15.994915	99.76
Phosphorus	P (31)	30.973763	100
Sulfur	S (32)	31.972072	95.02
Sulphurdihydrate ion SH_2	SH_2	33.987722	
Sodium	Na (23)	22.98977	100
Potassium	K (39)	38.963708	93.2
atomic mass unit (amu) of electron	(e)-	0.00054858	
Acetate ion OAc (C2H3O2-)	(C2H3O2-)	59.01275642	
Methyl group	CH3	15.023475	
Water	(H2O)	18.010564	
Methyl ketone group	CH2	13.007825	
Hydoxide group	OH	17.002739	
Sulphate Hydroxide	SO_4H	96.959552	
Cholesterol	(C27H46O)	386.354865	
Sulphate hydoxide + cholesterol = cholesteryl sulfate	C27H46O4S	483.314452	
cholesterol sulfate minus Water negative ion [M-H]-	C27H46O4S - (H2O)	465.303892	
24-methylene-cholesterol sulfate	(C28H46O4S)	496.322247	
24-methylene-cholesterol sulfate - H2O	(C28H46O4S) - (H2O)	478.311683.	
Cholesterol ester depending on Fatty Acyl =Fatty acids : Archchidonic, Palmitic, Oleic, etc			

https://physics.nist.gov/cgi-bin/Compositions/stand_alone.pl accessed January 2024. Figure 4:22 Step 2 Use the monoisotopic molecular mass

Step 3 checking for each type of place ta groups and plasma groups average accurate mess m/z observed in experimental MALDI ToF MS Calculated relative mass accuracy parts per million (ppm) (Mm-Mt) / (Mt x10^6): parts-per-million (ppm, 10^{-6}), parts-per-billion (ppb, 10^{-9}), parts-per-trillion (ppt, 10^{-12}) and parts-per-quadrillion (ppq, 10^{-15}).

Step 4 Check your literature peaks' mass values by using Excel calculations and lipid maps to double check the mass accuracy of the literature peaks versus your actual peaks observed in experimental data acquisition m/z and compare the error values as shown below using Literature reference Angelini et al.,2014 and then compare to your values observed in placenta and plasma groups for the PC/LPC m/z.

Agelini 2014 Theoretical Mass - from lipid Maps [M+H]+ PC/LPCm/z	Theoretical Reference m/z	Observed m/z in MALDI ToF MS + Int. Calibr Placenta_Healthy_BMI_CAT_1495-2	lipid maps MATCHED MASS	Lipid maps relative error SD	Name	Formula	Positive ion $[M+H]^+$	(Mm-Mt) / (Mt) x100 relative mass accuracy %
LPC 16:0 (+H+)	496.3398	496.441	496.3398	0.000	LPC 16:0	C24H50NO7P	[M+H]+	0.02
LPC 16:0 (+Na+)	518.3241	518.430	518.3217	0.002	LPC 16:0	C24H50NO7PNa	[M+Na]+	0.02
LPC 18:2 (+H+)	520.2905	520.443	520.3398	0.049	LPC 18:2	C26H50NO7P	[M+H]+	0.02
LPC 18:1 (+H+)	522.1672	522.461	522.3554	0.036	LPC 18:1	C26H52NO7P	[M+H]+	0.02
LPC 18:0 (+H+)	524.2854	524.409	524.3135	0.028	LPC 20:5	C28H48NO7P	[M+H-H2O]+	0.02
LPC 18:2 (+Na+)	542.3241	not observed / noise level	542.3241	0.000	LPC 20:5	C28H48NO7P	[M+H]+	not observed
LPC 18:1 (+Na+)	544.2672	544.452	544.3164	0.049	LPC O-18:2	C26H52NO6PK	[M+K]+	0.02
LPC 18:0 (+Na+)	546.3554	546.380	546.3530	0.002	LPC 18:0	C26H54NO7PNa	[M+Na]+	0.01
PC 16:0/18:2 (+H+)	758.5694	758.733	758.5694	0.000	PC 34:2	C42H80NO8P	[M+H]+	0.02
PC 16:0/18:1 (+H+)	760.5851	760.195	760.5851	0.000	PC 34:1	C42H82NO8P	[M+H]+	-0.05
PC 16:0/18:2 (+Na+)	780.5538	780.722	780.5514	0.002	PC 34:2	C42H80NO8PNa	[M+Na]+	0.02
PC 16:0/18:1 (+Na+) and PC 16:0/20:4 (+H+)	782.5694	782.742	782.5670	0.002	PC 34:1	C42H82NO8PNa	[M+Na]+	0.02
PC 18:0/18:3 (+H+)	784.5851	784.753	784.5851	0.000	PC 36:3	C44H82NO8P	[M+H]+	0.02
PC 18:0/18:2 (+H+)	786.6454	786.768	786.6007	0.045	PC 36:2	C44H84NO8P	[M+H]+	0.02
PC 16:0/20:4 (+Na+)	804.5749	804.727	804.5514	0.024	PC 36:4	C44H80NO8PNa	[M+Na]+	0.02
PC 18:0/18:3 (+Na+)	806.5694	806.746	806.5670	0.002	PC 36:3	C44H82NO8PNa	[M+Na]+	0.02
PC 18:0/18:2 (+Na+)	808.5851	808.764	808.5827	0.002	PC 36:2	C44H84NO8PNa	[M+Na]+	0.02

	Edyta Calculated					
	M+H]+	[M-H]-	H(1)-e-	CH3		LPC PC
Agelini et al 2014 Literature refence	PC/LPC	pc/lpc	1.00727642	15.023475	[M-CH3]-	Sum [M-CH3]-
LPC 16:0 (+H+)	496.3398	495.3325	1.0073	15.0235	480.3090	480.3085
LPC 16:0 (+Na+)	518.3241	517.3168	1.0073	15.0235	502.2933	480.3085
LPC 18:2 (+H+)	520.2905	519.2832	1.0073	15.0235	504.2597	504.3085
LPC 18:1 (+H+)	522.1672	521.1599	1.0073	15.0235	506.1364	506.3241
LPC 18:0 (+H+)	524.2854	523.2781	1.0073	15.0235	508.2546	526.2928
LPC 18:2 (+Na+)	542.3241	541.3168	1.0073	15.0235	526.2933	526.2928
LPC 18:1 (+Na+)	544.2672	543.2599	1.0073	15.0235	528.2364	490.3292
LPC 18:0 (+Na+)	546.3554	545.3481	1.0073	15.0235	530.3246	508.3398
PC 16:0/18:2 (+H+)	758.5694	757.5621	1.0073	15.0235	742.5386	742.5381
PC 16:0/18:1 (+H+)	760.5851	759.5778	1.0073	15.0235	744.5543	744.5538
PC 16:0/18:2 (+Na+)	780.5538	779.5465	1.0073	15.0235	764.5230	742.5381
PC 16:0/18:1 (+Na+) and PC 16:0/20:4 (+H+)	782.5694	781.5621	1.0073	15.0235	766.5386	744.5538
PC 18:0/18:3 (+H+)	784.5851	783.5778	1.0073	15.0235	768.5543	766.5381
PC 18:0/18:2 (+H+)	786.6454	785.6381	1.0073	15.0235	770.6146	768.5538
PC 16:0/20:4 (+Na+)	804.5749	803.5676	1.0073	15.0235	788.5441	770.5694
PC 18:0/18:3 (+Na+)	806.5694	805.5621	1.0073	15.0235	790.5386	766.5381
PC 18:0/18:2 (+Na+)	808.5851	807.5778	1.0073	15.0235	792.5543	768.5538

Figure 4:26 Checking mass to charge ration m/z values and mass accuracy error first Literature Angelini et al.,2014 compared to your observed PC/LPC m/z in placenta and plasma groups for the calculated table observed in the results from MALDI Tof Ms

Edyta Observed LPC PC m/z in MALDI ToF MS Intensities values 6x10-4 - 1x10-5 Placenta tissue or Plasma Concentre 10 [mg/mL]	Peak intensities 3 repeats per sample	LPC 16:0 (+H+) 496.3398 m/z	LPC 16:0 (+Na+) 518.3241 m/z	LPC 18:0 (+H+) 524.2854 m/z	LPC 18:0 (+Na+) 546.3554 m/z	PC 16:0/18:2 (+H+) 758.5694 m/z	PC 16:0/18:1 (+H+) 760.5851 m/z	PC 16:0/18:2 (+Na+) 780.5538 m/z	PC 16:0/18:1 (+Na+); PC 16:0/20:4 (+H+) 782.5694 m/z	PC 18:0/18:3 (+H+) 784.5851 m/z	PC 18:0/18:2 (+H+) 786.6454 m/z	PC 16:0/20:4 (+Na+) 804.5749 m/z	PC 18:0/18:3 (+Na+) 806.5694 m/z	PC 18:0/18:2 (+Na+) 808.5851 m/z	∑LPC	∑PC	∑PC/∑LPC	Intensity PC/LPC average of three replicates
Measured LPC and PC m/z		496.3458	518.445	524.385	0	758.535	760.557	780.528	782.540	784.553	786.360	804.529	806.549	808.556	1539.1752	7072.706	4.5951	4.5951
CAT1315 tissue	1st repeat	56724.000	78882.000	26690.000	0	30404.000	30404.000	0	35993.000	23123.000	20321.000	23123.000	20321.000	0	162296.0000	183689.000	1.1318	
CAT1315 tissue	2nd repeat	119748.000	233643.000	66810.000	0	53608.000	53608.000	0	64682.000	0	38278.000	44770.000	0	0	420201.0000	254946.000	0.6067	
CAT1315 tissue	3rd repeat	124346.000	144043.000	54754.000	0	70576.000	73689.000	30795.000	83966.000	55515.000	45256.000	30289.000	38687.000	35553.000	323143.0000	464326.000	1.4369	1.0585
CAT 1487 tissue	1st repeat	38869.000	125406.000	33240.000	0	41448.000	40984.000	38880.000	57361.000	37114.000	42285.000	36260.000	41085.000	0	197515.0000	335417.000	1.6982	
CAT 1487 tissue	2nd repeat	40885.000	135198.000	33085.000	0	42307.000	46486.000	41093.000	62994.000	42997.000	47210.000	63405.000	42652.000	38543.000	209168.0000	427687.000	2.0447	
CAT 1487 tissue	3rd repeat	37614.000	82551.000	25422.000	0	46290.000	49174.000	45448.000	69266.000	46050.000	47697.000	68296.000	44974.000	37828.000	145587.0000	455023.000	3.1254	2.2894
CAT1489 tissue	1st repeat	55519.000	201886.000	50850.000	0	59941.000	59670.000	64685.000	84422.000	59596.000	63845.000	74687.000	60410.000	48863.000	308255.0000	576119.000	1.8690	
CAT1489 tissue	2nd repeat	40843.000	113665.000	36076.000	0	68062.000	59981.000	62598.000	92559.000	62004.000	62604.000	77243.000	68849.000	53076.000	190584.0000	606976.000	3.1848	
CAT1489 tissue	3rd repeat	37614.000	9300.000	0	0	0	0	3967.000	0	0	0	0	0	3875.000	46914.0000	7842.000	0.1672	1.7403
CAT1494 GDM tissue	1st repeat	65572.000	179767.000	42768.000	0	42813.000	39627.000	0	44020.000	35670.000	60656.000	34258.000	0	0	288107.0000	257044.000	0.8922	
CAT1494 GDM tissue	2nd repeat	56068.000	150021.000	35464.000	0	33654.000	33743.000	0	39585.000	28397.000	0	0	0	27866.000	241553.0000	163245.000	0.6758	
CAT1494 GDM tissue	3rd repeat	43424.000	66296.000	22144.000	0	32860.000	31125.000	0	37667.000	29876.000	24358.000	25956.000	22351.000	0	131864.0000	204193.000	1.5485	1.0388
CAT1496 GDM tissue	1st repeat	42548.000	0	0	0	0	0	0	0	0	0	28858.000	0	0	42548.0000	28858.000	0.6782	
CAT1496 GDM tissue	2nd repeat	13232.000	29145.000	0	0	0	12553.000	0	16253.000	0	12369.000	11680.000	0	0	42377.0000	52855.000	1.2473	
CAT1496 GDM tissue	3rd repeat	18984.000	52498.000	14548.000	0	0	18014.000	0	24546.000	16472.000	18084.000	19538.000	0	0	86030.0000	96654.000	1.1235	1.0163
CAT 1515 plasma	1st repeat	206092.000	88147.000	45080.000	0	563857.000	262922.000	59336.000	171545.000	135651.000	154860.000	20087.000	82301.000	42675.000	339319.0000	1493234.000	4.4007	
CAT 1515 plasma	2nd repeat	254982.000	78402.000	51267.000	0	59655.000	336607.000	77054.000	230273.000	172829.000	192736.000	24549.000	104023.000	59864.000	384651.0000	1257590.000	3.2694	
CAT 1515 plasma	3rd repeat	290603.000	56628.000	17263.000	0	67884.000	387732.000	90133.000	264363.000	191738.000	223664.000	28572.000	120243.000	69999.000	364494.0000	1444328.000	3.9626	3.8776
CRF424 NP plasma	1st repeat	220318.000	48130.000	67000.000	0	194734.000	143014.000	69771.000	91280.000	63961.000	101428.000	17251.000	66193.000	59397.000	335448.0000	807029.000	2.4058	
CRF424 NP plasma	2nd repeat	152572.000	28209.000	48304.000	0	116925.000	88675.000	55614.000	65623.000	44239.000	63728.000	0	43510.000	44785.000	229085.0000	523099.000	2.2834	
CRF424 NP plasma	3rd repeat	210147.000	33987.000	70493.000	0	17260.000	129919.000	69220.000	84821.000	63360.000	97561.000	0	60347.000	57026.000	314627.0000	579514.000	1.8419	2.1771
CRF458 NP plasma	1st repeat	176967.000	381973.000	100594.000	0	145017.000	93548.000	36517.000	69645.000	50678.000	62326.000	0	25114.000	25009.000	659534.0000	507854.000	0.7700	
CRF458 NP plasma	2nd repeat	173898.000	350136.000	91124.000	0	170385.000	109386.000	50390.000	91374.000	63797.000	75419.000	23043.000	34778.000	34723.000	615158.0000	653295.000	1.0620	
CRF458 NP plasma	3rd repeat	233821.000	356409.000	106710.000	0	23519.000	135219.000	62037.000	103921.000	75752.000	87035.000	25901.000	41557.000	41599.000	696940.0000	596540.000	0.8559	0.8960

CAT 1315- 1st repeat

m/z	Intensity	S/N 9
496.3458	124346.0	33.7
518.4448	144043.0	38.4
524.3846	54754.0	13.5
758.5348	70576.0	18.3
760.5566	73689.0	19.3
780.5278	30795.0	6.1
782.5404	83966.0	23.5
784.5525	55515.0	14.3
786.3601	37298.0	8.3
804.5286	30289.0	6.2
806.5491	38687.0	9.0
808.5557	35553.0	8.0

CAT 1315- 2nd repeat

m/z	Intensity	S/N 9
496.4158	99018.0	32.6
518.5048	289057.0	99.5
524.4557	91504.0	30.6
758.6099	44198.0	15.8
760.6228	50089.0	18.3
780.5278	not observed	
782.6113	46923.0	17.0
784.6253	31350.0	10.5
786.6449	26559.0	8.5
804.5286	not observed	
806.5491	not observed	
808.6290	20973.0	6.2

CAT 1315- 3rd repeat

m/z	Intensity	S/N 9
496.4260	89273.0	32.3
518.5104	374103.0	140.8
524.4647	86971.0	31.7
758.6215	76751.0	32.4
760.6345	43026.0	17.2
780.5974	36134.0	13.8
782.6225	36186.0	14.1
784.5821	30138.0	11.2
786.6509	35793.0	13.9
804.6246	19018.0	6.2
806.6223	20093.0	6.7
808.6290	not observed	

Graph Pad Healthy Placentas +ve ion 9AA Matrix

No.	Cut Area chunk	CAT	BMI (body mass index)	PC/LPC Average 3replica
1	Near centre	1706	22.7	7.12
2	edges	1645	22.9	9.33
3	Random edge 1	1706	22.7	7.84
4	Random edge 2	1706	22.7	7.21
5	Left side edge 3	1706	22.7	6.92
6	Random edge	1679	25.5	11.42
7	Left side edge 1	1681	23.4	9.83
8	Random edge 2	1681	23.4	9.40
9	Random edge 3	1681	23.4	16.61
10	new homg. Ave 10 reps	1706	22.7	9.33

Figure 4:27 Your observed PC/LPC m/z average intensity Use for GraphPad Plots

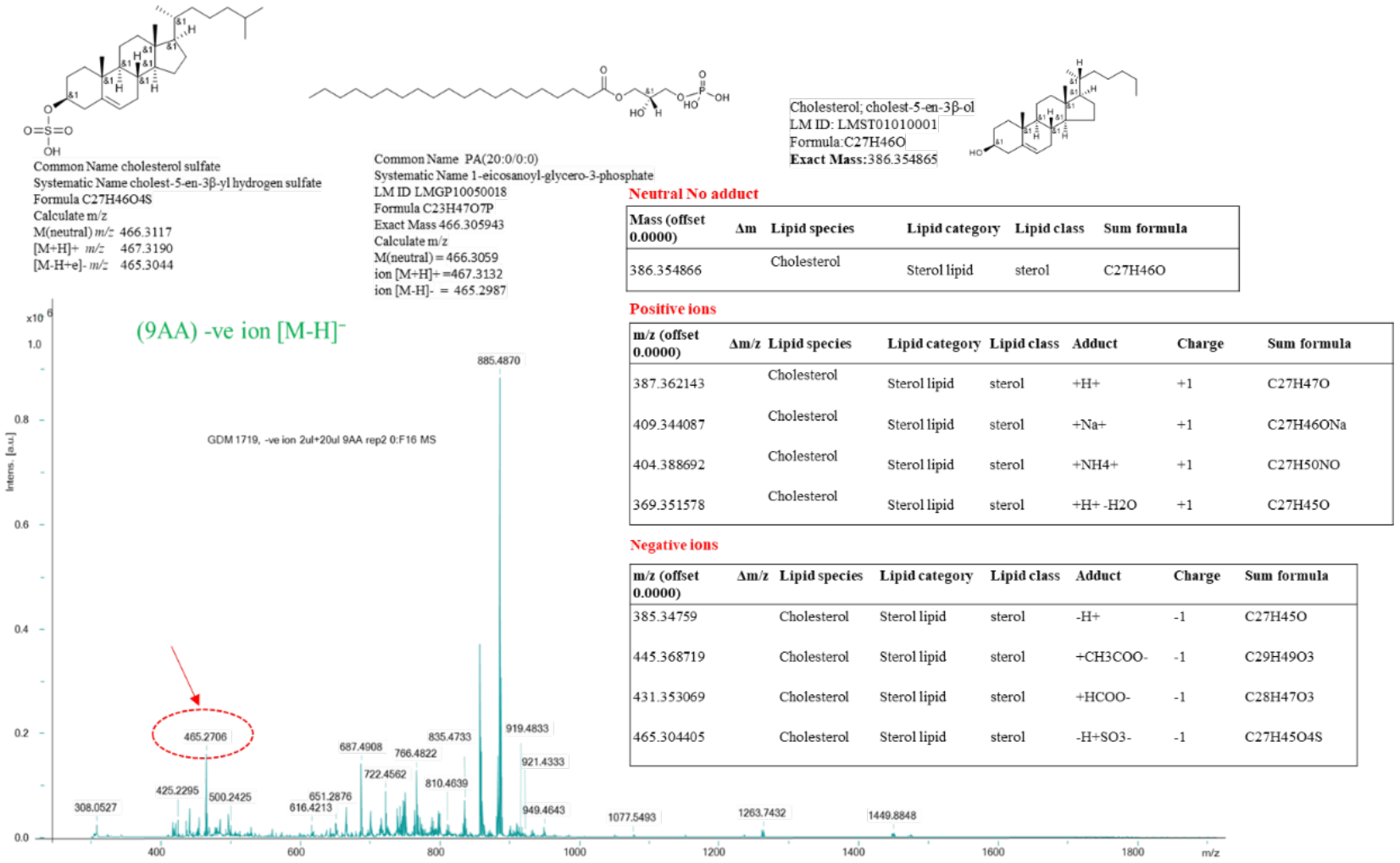

Neutral No adduct

Mass (offset 0.0000)	Δm	Lipid species	Lipid category	Lipid class	Sum formula
386.354866		Cholesterol	Sterol lipid	sterol	C27H46O

Positive ions

m/z (offset 0.0000)	Δm/z	Lipid species	Lipid category	Lipid class	Adduct	Charge	Sum formula
387.362143		Cholesterol	Sterol lipid	sterol	+H+	+1	C27H47O
409.344087		Cholesterol	Sterol lipid	sterol	+Na+	+1	C27H46ONa
404.388692		Cholesterol	Sterol lipid	sterol	+NH4+	+1	C27H50NO
369.351578		Cholesterol	Sterol lipid	sterol	+H+ -H2O	+1	C27H45O

Negative ions

m/z (offset 0.0000)	Δm/z	Lipid species	Lipid category	Lipid class	Adduct	Charge	Sum formula
385.34759		Cholesterol	Sterol lipid	sterol	-H+	-1	C27H45O
445.368719		Cholesterol	Sterol lipid	sterol	+CH3COO-	-1	C29H49O3
431.353069		Cholesterol	Sterol lipid	sterol	+HCOO-	-1	C28H47O3
465.304405		Cholesterol	Sterol lipid	sterol	-H+SO3-	-1	C27H45O4S

Figure 4:23 Explanation for cholesterol sulphate or phosphatidic acid: how did I get that

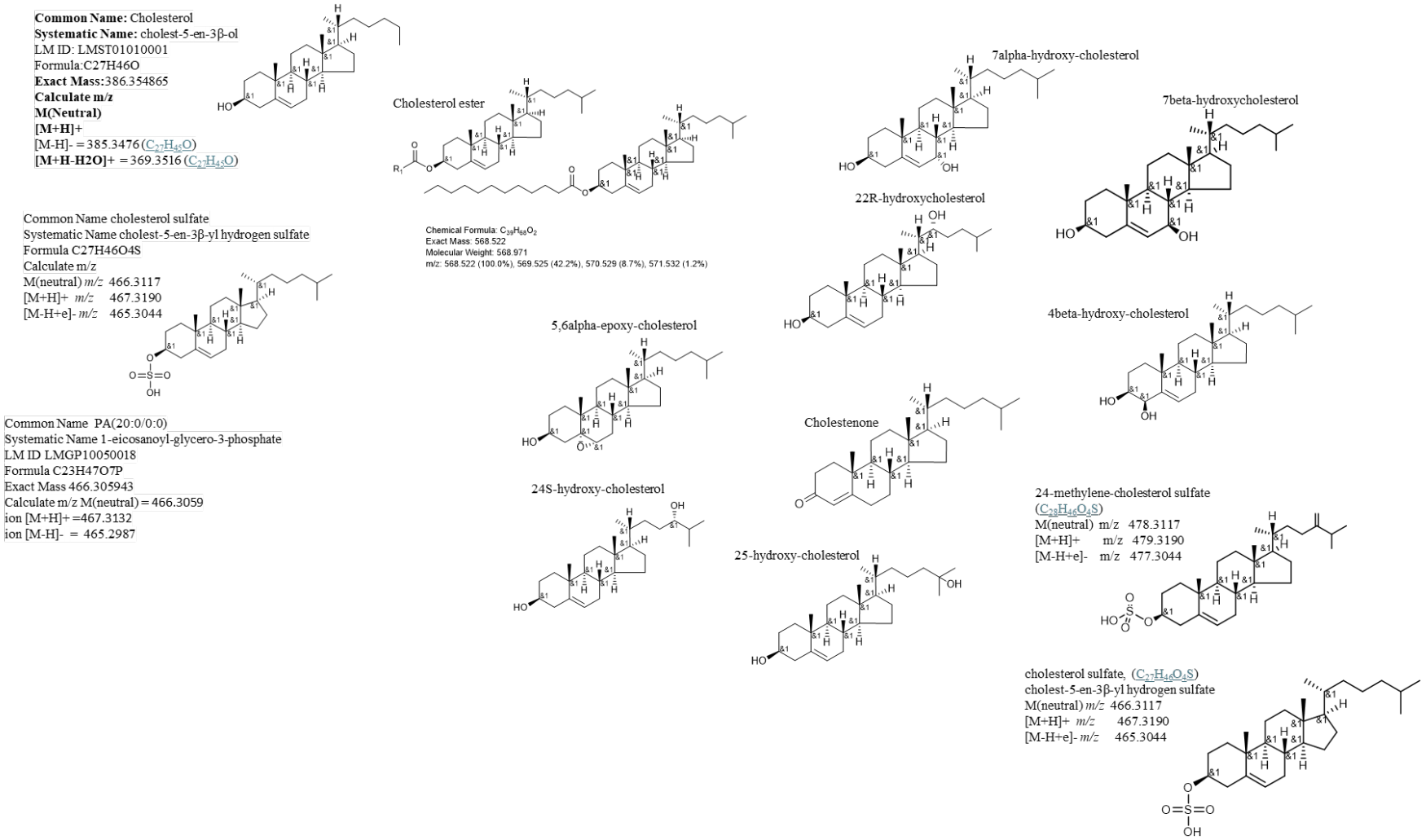

Figure4:28 Cholesterol structure Note: explain what was summed to give the ratio in words and calculations for cholesterol sulphates

Common Name:	Systematic Name:	Lipid Maps ID:	Formula:	M (neutral)	Exact Mass Calculated m/z	Positive ion $[M+H]^+$	Formula:	Negative ion $[M-H+ e^-]^-$	Formula:	Negative ion $[M-H- H_20+ e]^-$	Negative ion $[M-CH3+ e]^-$
Cholesterol	cholest-5-en-3β-ol	LMST01010001	(C27H46O)	386.3549	386.354865	387.3621	(C27H47O)	383.3319	(C27H47O)	367.3365	371.3319
Desmosterol	cholest-5,24-dien-3β-ol	LMST01010016	(C27H44O)	384.3392	384.339215	385.3465	(C27H45O)	383.3319	(C27H43O)	365.3208	369.3163
7-dehydrocholesterol	cholesta-5,7-dien-3β-ol	LMST01010069	C27H44O	384.3392	384.339215	385.3465	(C27H45O)	383.3319	(C27H43O)	365.3208	369.3163
Cholesterol ester example: 5,6alpha-epoxy-cholesterol	5α,6α-epoxy-5α-cholestan-3β-ol	LMST01010011	C27H46O2	402.3498	402.34978	403.3571	(C27H47O2)	401.3425	(C27H45O2)	383.3314	387.3269
24S-hydroxy-cholesterol	cholest-5-en-3β,24S-diol	LMST01010019	C27H46O2	402.3498	402.34978	403.3571	(C27H47O2)	401.3425	(C27H45O2)	383.3314	387.3269
7alpha-hydroxy-cholesterol	cholest-5-en-3β,7α-diol	LMST01010013	C27H46O2	402.3498	402.34978	403.3571	(C27H47O2)	401.3425	C27H46O2	383.3314	387.3269
7beta-hydroxycholesterol	5-cholestene-3β,7β-diol	LMST01010047	C27H46O2	402.3498	402.34978	403.3571	(C27H47O2)	401.3425	(C27H45O2)	383.3314	387.3269
22R-hydroxycholesterol	cholest-5-en-3β,22R-diol	LMST01010086	C27H46O2	402.3498	402.34978	403.3571	(C27H47O2)	401.3425	(C27H45O2)	383.3314	387.3269
27-hydroxy-cholesterol	cholest-5-en-3β,26-diol	LMST01010057	C27H46O2	402.3498	402.34978	403.3571	(C27H47O2)	401.3425	(C27H45O2)	383.3314	387.3269
4beta-hydroxy-cholesterol	cholest-5-en-3β,4β-diol	LMST01010014	C27H46O2	402.3498	402.34978	403.3571	(C27H47O2)	401.3425	(C27H45O2)	383.3314	387.3269
Cholestenone	cholest-4-en-3-one	LMST01010015	C27H44O	384.3392	384.339215	385.3465	(C27H45O)	383.3319	(C27H43O)	365.3208	369.3163
25-hydroxy-cholesterol	cholest-5-en-3β,25-diol	LMST01010018	C27H46O2	402.3498	402.34978	403.3571	(C27H47O2)	401.3425	(C27H45O2)	383.3314	387.3269
24-methylene-cholesterol sulfate	24-methylene-cholest-5-en-3β-ol-3-sulfate	LMST05020012	C28H46O4S	478.3117	478.311682	479.3190	(C28H47O4S)	477.3044	(C28H45O4S)	459.2933	463.2888
cholesterol sulfate	cholest-5-en-3β-yl hydrogen sulfate	LMST05020016	C27H46O4S	466.3117	466.311682	467.319	(C27H47O4S)	465.3044	(C27H45O4S)	447.2933	451.2888

Input Mass	Matched Mass	DELTA	Name	Formula	Ion	LMSD	LM_ID	Common Name	Systematic Name	Mass	Formula
465.303892	465.3044	0.0005	ST 27:1;O;S	C27H46O4S	[M-H]-	EXAMPLES	LMST05020016	cholesterol sulfate	cholest-5-en-3beta-yl hydrogen sulfate	466.31	C27H46O4S
465.303892	465.2987	0.0052	LPA 20:0	C23H47O7P	[M-H]-	EXAMPLES	LMGP10050018	PA(20:0/0:0)	1-eicosanoyl-glycero-3-phosphate	466.31	C23H47O7P
465.303892	465.3222	0.0183	ST 27:1;O6	C27H46O6	[M-H]-	EXAMPLES					
465.303892	465.3374	0.0335	ST 31:5;O3	C31H46O3	[M-H]-	EXAMPLES					
465.303892	465.2647	0.0392	ST 29:7;O5	C29H38O5	[M-H]-	EXAMPLES					

Hydrogen	H	1.007825
atomic mass unit (amu) of electron	(e)-	0.00054858
Hydroxide group	OH	17.002739
Sulphate Hydroxide	SO_4H	96.959552
Cholesterol	(C27H46O)	386.354865
Sulphate hydroxide + cholesterol = cholesteryl sulphate	C27H46O4S	483.314452
cholesterol sulphate -H20 in $[M-H]^-$ + $(e)^-$	C27H46O4S - H2O	465.303892
24-methylene-cholesterol sulphate	C28H46O4S)	496.322247
24-methylene-cholesterol sulphate – (H_2O)	C28H46O4S - (H2O)	478.311683

Figure 4:30 Explaining Cholesterol and cholesterol sulphate calculations the Sulphate hydroxide head group molecular mass SO_4H 96.959552 plus cholesterol (C27H46O) 386.354865 molecular mass sum equals to C27H46O4S 483.314452 molecular mass and in negative ion ionisation loss of hydroxide and loss of proton (minus water) plus electron negative mass value added equals to cholesterol sulphate minus water in negative ion $[M-H]^-$ + $(e)^-$ formula C27H46O4S - (H2O) = 465.303892.

All Placenta Observed / Measured in MALDI ToF MS Positive ion mode [M+H]+ 9AA, +DHB PC LPC m/z								
Measured All Healthy Placenta Experimental m/z	SD +/- (x3 reps)	(Mm-Mt) / (Mt) x100 relative mass accuracy %	Measured All Obese Placenta Experimental m/z	SD +/- (x3 reps)	(Mm-Mt) / (Mt) x100 relative mass accuracy %	Measured All GDM Placenta Experimental m/z	SD +/- (x3 reps)	(Mm-Mt) / (Mt) x100 relative mass accuracy %
496.3800	0.039	0.008	496.3969	0.036	0.012	496.4290	0.006	0.018
518.4305	0.033	0.021	518.4493	0.038	0.025	not observed	not observed	not observed
520.3860	0.047	0.009	520.4254	0.039	0.016	520.4432	0.000	0.020
522.4241	0.078	0.013	522.4734	0.102	0.023	522.5115	0.118	0.030
524.4053	0.033	0.018	524.4385	0.039	0.024	524.5070	0.102	0.037
not observed	not observed	not observed	not observed	not observed	not observed	not observed	not observed	not observed
544.4116	0.051	0.017	544.4020	0.041	0.016	not observed	not observed	not observed
546.3828	0.007	0.005	not observed	not observed	not observed	not observed	not observed	not observed
758.6673	0.119	0.013	758.6490	0.065	0.010	758.7000	0.017	0.017
760.5850	0.154	0.000	760.6671	0.066	0.011	760.7155	0.019	0.017
780.6207	0.061	0.009	780.6346	0.070	0.011	780.6346	0.070	0.011
782.6326	0.064	0.008	782.6928	0.113	0.016	782.6928	0.113	0.016
784.6638	0.070	0.010	784.6683	0.064	0.011	784.8907	1.047	0.039
786.5567	0.274	-0.006	786.6804	0.230	0.010	786.7268	0.008	0.016
804.6193	0.080	0.008	804.6404	0.069	0.011	804.6854	0.018	0.017
806.6303	0.063	0.008	806.6529	0.065	0.011	806.7072	0.020	0.017
808.5834	0.218	0.000	808.6712	0.068	0.011	808.6185	0.250	0.004

Angelini 2014 Literature reference		All Plasma Observed/Measured in MALDI ToF MS Positive ion mode [M+H]+ 9AA, +DHB PC LPC m/z										
Positive ion mode [M+H]+ matix 9AA	PC LPC	Measured All Non-pregnant plasma Experimental m/z	SD +/- (x3 reps)	(Mm-Mt) / (Mt) x100 relative mass accuracy %	Measured All Healthy pregnant plasma Experimental m/z	SD +/- (x3 reps)	(Mm-Mt) / (Mt) x100 relative mass accuracy %	Measured All Obese pregnant plasma Experimental m/z	SD +/- (x3 reps)	(Mm-Mt) / (Mt) x100 relative mass accuracy %	Measured All GDM pregnant plasma Experimental m/z	SD +/- (x3 reps)
LPC 16:0 (+H+)	496.3398	496.41082	0.03	0.014	496.4021	0.01	0.013	496.4044	0.00	0.013	496.4179	0.00
LPC 16:0 (+Na+)	518.3241	518.42334	0.007	0.020	518.3908	0.01	0.013	518.3937	0.01	0.014	518.4084	0.02
LPC 18:2 (+H+)	520.2905	not observed			not observed	not observed		not observed	not observed		not observed	not observed
LPC 18:1 (+H+)	522.1672	not observed			not observed	not observed		not observed	not observed		not observed	not observed
LPC 18:0 (+H+)	524.2854	524.44421	0.04	0.025	524.4400	0.00	0.024	524.4399	0.00	0.024	524.4522	0.01
LPC 18:2 (+Na+)	542.3241	544.43433	0.04	0.389	not observed	not observed		not observed	not observed		not observed	not observed
LPC 18:1 (+Na+)	544.2672	not observed	not observed		544.4100	0.00	0.017	544.4109	0.01	0.017	not observed	not observed
LPC 18:0 (+Na+)	546.3554	not observed	not observed		546.4234	0.01	0.013	546.4269	0.01	0.014	not observed	not observed
PC 16:0/18:2 (+H+)	758.5694	758.67447	0.05	0.014	758.6655	0.00	0.013	758.6662	0.01	0.013	758.6849	0.01
PC 16:0/18:1 (+H+)	760.5851	760.63825	0.16	0.007	760.6821	0.00	0.013	760.6422	0.16	0.008	760.6597	0.20
PC 16:0/18:2 (+Na+)	780.5538	780.65938	0.06	0.014	780.6530	0.01	0.013	780.7799	0.51	0.029	780.6723	0.01
PC 16:0/18:1 (+Na+) and PC 16:0/20:4 (+H+)	782.5694	782.67565	0.05	0.014	782.6706	0.00	0.013	782.6715	0.01	0.013	782.6890	0.01
PC 18:0/18:3 (+H+)	784.5851	784.69237	0.05	0.014	784.6870	0.01	0.013	784.6882	0.01	0.013	784.7053	0.01
PC 18:0/18:2 (+H+)	786.6454	786.70743	0.05	0.014	786.6712	0.13	0.009	786.7053	0.01	0.013	786.6493	0.20
PC 16:0/20:4 (+Na+)	804.5749	804.70638	0.02	0.019	804.6541	0.01	0.013	804.6594	0.01	0.013	804.6877	0.01
PC 18:0/18:3 (+Na+)	806.5694	806.68295	0.05	0.014	806.6739	0.00	0.013	806.6758	0.01	0.013	806.6941	0.01
PC 18:0/18:2 (+Na+)	808.5851	808.69086	0.06	0.013	808.6908	0.01	0.013	808.6947	0.01	0.014	808.7088	0.01

Figure 4:29Observed and measured PC/LPC per each placenta group and plasma standard error in mass accuracy: Mm = measured mass m/z; Mt = theoretical mass m/z; ppm= 1 part per million or in per cent % ; (Mm-Mt) / (Mt) x100 relative mass accuracy (%)

4.4 MALDI ToF MS Results GraphPad Plots for all studies

All data plots below are numbered starting from plot number 12, which compares placental sides centre from edges to illustrate place groups overview. Starting from Plot No.1, comparative study. Then, from No.2 till No.20, show MALDI-TOF peaks intensity, taking an average of three repeats per sample per each group of patient donors.

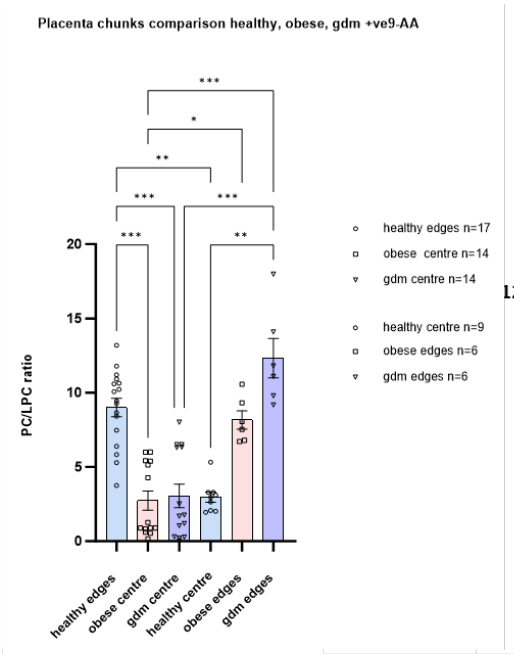

12

Placenta 3Groups (+DHB) PC/LPC MALDI data sets values			Placenta 3Groups (+DHB) PC/LPC MALDI data sets values		
healthy edges n17	obese centre n=14	gdm centre n=14	healthy centre n=9	obese edges n=6	gdm edges n=6
8.647	4.277	2.525	2.074	8.053	17.974
8.418	0.156	1.686	3.302	10.571	14.088
10.072	0.623	1.045	5.317	6.715	9.183
9.448	1.276	0.034	1.954	6.789	11.103
7.472	0.821	1.763	2.025	7.530	11.805
11.791	0.530	1.200	3.302	9.325	9.796
10.601	0.900	0.217	3.120		
10.928	0.900	0.282	2.649		
10.641	0.900	0.298	2.959		
11.205	5.139	8.019			
10.222	5.995	6.505			
13.199	5.389	6.505			
6.393	6.002	6.331			
3.753	5.413	6.305			
5.291					
9.284					
5.835					

Table:12 All combined					
Kruskal-Wallis test Anova Results	Placenta 3Groups (+DHB) PC/LPC Results				
Table Analyzed	Combined healthy (edges + centre)				
ANOVA					
Kruskal-Wallis test					
P value	<0.0001				
Exact or approximate P value?	Approximate				
P value summary	****				
Do the medians vary signif. (P < 0.05)?	Yes				
Number of groups	6				
Kruskal-Wallis statistic	43.65				
Kruskal-Wallis test Multiple comparisons					
Dunn's multiple comparisons test	Mean rank diff.	Significant?	Summary	Adjusted P Value	
healthy edges vs. obese centre	31.03	Yes	***	0.0001	A-B
healthy edges vs. gdm centre	28.75	Yes	***	0.0005	A-C
healthy edges vs. healthy centre	27.07	Yes	**	0.0094	A-D
healthy edges vs. obese edges	2.51	No	ns	>0.9999	A-E
healthy edges vs. gdm edges	-10.16	No	ns	>0.9999	A-F
obese centre vs. gdm centre	-2.286	No	ns	>0.9999	B-C
obese centre vs. healthy centre	-3.968	No	ns	>0.9999	B-D
obese centre vs. obese edges	-28.52	Yes	*	0.0349	B-E
obese centre vs. gdm edges	-41.19	Yes	***	0.0002	B-F
gdm centre vs. healthy centre	-1.683	No	ns	>0.9999	C-D
gdm centre vs. obese edges	-26.24	No	ns	0.0763	C-E
gdm centre vs. gdm edges	-38.9	Yes	***	0.0005	C-F
healthy centre vs. obese edges	-24.56	No	ns	0.2282	D-E
healthy centre vs. gdm edges	-37.22	Yes	**	0.0035	D-F
obese edges vs. gdm edges	-12.67	No	ns	>0.9999	E-F

Table 4.1: GraphPad Plot no.12 Comparing the PC/LPC ratio at the edges versus the centre of the placenta. Placenta samples from the edges of healthy (n = 17), obese (n = 6), and GDM (n = 6) placentas and the centre of health (n = 9), obese (n = 14), GDM (n = 14) were extracted and processed for in MALDI positive ion mode using

9AA matrix. Statistical Data Analysis for Each graph pad plot presented in the results:

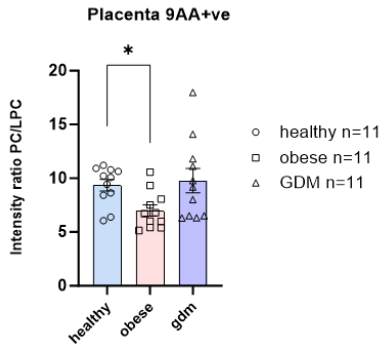

1 Comaparative study (3x n=11) Matirx 9AA +ve

Placenta 3 Groups (+9AA) PC/LPC MALDI data sets values

healthy n=11	obese n=11	gdm n=11
10.790	5.139	8.019
10.928	5.995	17.974
8.647	5.389	14.088
8.418	8.053	9.183
10.072	10.571	11.103
6.393	6.715	6.505
10.641	6.002	11.805
11.205	5.413	6.505
9.448	6.789	6.331
10.222	7.530	9.796
6.062	9.325	6.305

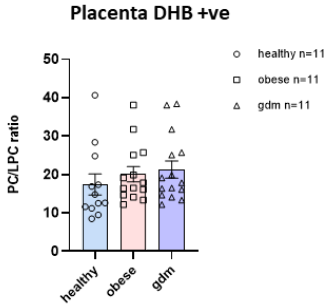

1 Comaparative study (3x n=11) Matirx DHB +ve

Placenta 3Groups (+DHB) PC/LPC MALDI data sets values

healthy n=12	obese n=12	gdm n=12
12.584	12.190	14.847
14.830	19.877	31.396
16.888	19.159	16.410
24.795	16.091	33.254
40.634	25.732	38.053
17.360	13.340	20.019
28.401	25.065	14.467
11.625	16.358	15.843
9.469	16.496	30.512
12.500	17.871	27.859
8.488	14.657	34.270
11.205	14.109	11.446

Table:1 Comaprative study 9AA +ve (3 greoup 3x n=11)

Date: 11-11-2022	Placenta 9AA+ve Healthy Obese GDM n=11				
Kruskal-Wallis test					
P value	0.022				
Exact or approximate P value?	Approximate				
P value summary	*				
Do the medians vary signif. (P < 0.05)?	Yes				
Number of groups	3				
Kruskal-Wallis statistic	7.631				
Number of comparisons per family	3				
Alpha	0.05				
Dunn's multiple comparisons test	Mean rank diff.	Significant?	Summary	Adjusted P Value	
healthy vs. obese	10.36	Yes	*	0.0359	A-B
healthy vs. gdm	1.091	No	ns	>0.9999	A-C
obese vs. gdm	-9.273	No	ns	0.0735	B-C
Test details	Mean rank 1	Mean rank 2	Mean rank diff.	n1	n2
healthy vs. obese	20.82	10.45	10.36	11	11
healthy vs. gdm	20.82	19.73	1.091	11	11
obese vs. gdm	10.45	19.73	-9.273	11	11

1 Comparative study (3x n=11) Matirx 9AA +ve

Placenta 3Groups (+DHB) PC/LPC MALDI data sets values

healthy n=11	obese n=11	gdm n=11
10.790	5.139	8.019
10.928	5.995	17.974
8.647	5.389	14.088
8.418	8.053	9.183
10.072	10.571	11.103
6.393	6.715	6.505
10.641	6.002	11.805
11.205	5.413	6.505
9.448	6.789	6.331
10.222	7.530	9.796
6.062	9.325	6.305

Table: 1 Comaparative study (3x n=11) Matirx DHB +ve

Date 18-07-2022:	Placenta DHB +ve Healthy Obes GDM n=12				
Kruskal-Wallis test					
P value	0.1027				
Exact or approximate P value?	Approximate				
P value summary	ns				
Do the medians vary signif. (P < 0.05)?	No				
Number of groups	3				
Kruskal-Wallis statistic	4.551				
Data summary					
Number of treatments (columns)	3				
Number of values (total)	36				
Number of comparisons per family	3				
Alpha	0.05				
Dunn's multiple comparisons test	Mean rank diff.	Significant?	Summary	Adjusted P Value	
healthy vs. obese	-3.417	No	ns	>0.9999	A-B
healthy vs. gdm	-9.083	No	ns	0.1041	A-C
obese vs. gdm	-5.667	No	ns	0.563	B-C
Test details	Mean rank 1	Mean rank 2	Mean rank diff.	n1	n2
healthy vs. obese	14.33	17.75	-3.417	12	12
healthy vs. gdm	14.33	23.42	-9.083	12	12
obese vs. gdm	17.75	23.42	-5.667	12	12

1 Comaparative study (3x n=11) Matirx DHB +ve

Placenta 3Groups (+DHB) PC/LPC MALDI data sets values

healthy n=12	obese n=12	gdm n=12
12.584	12.190	14.847
14.830	19.877	31.396
16.888	19.159	16.410
24.795	16.091	33.254
40.634	25.732	38.053
17.360	13.340	20.019
28.401	25.065	14.467
11.625	16.358	15.843
9.469	16.496	30.512
12.500	17.871	27.859
8.488	14.657	34.270
11.205	14.109	11.446

Table 4.2: GraphPad plots No.1 run +9AA,+DHB for PC/LPC ratio in the placenta groups with calculated statistical data Kruskal-Wallis test, Dunn's multiple comparisons tests; * < 0.05 for each placenta group of healthy, obese and GDM placentas (n=11/group).

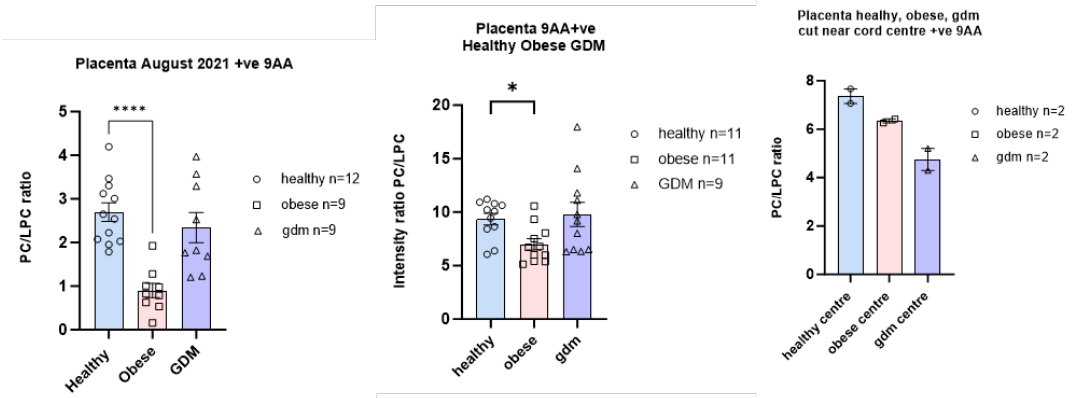

2 Placenta Groups (+9AA) PC/LPC MALDI data

A Healthy n=12	B Obese n=9	C GDM n=9
3.302	0.623	2.525
2.539	1.276	1.686
3.120	0.821	1.763
4.192	0.530	1.821
2.649	0.156	3.294
1.954	0.787	3.568
1.786	1.921	3.969
2.025	0.979	1.231
2.224	1.007	1.200
2.074		
3.006		
3.464		

3 Placenta Groups (+9AA) PC/LPC MALDI data

A Healthy n=11	B Obese n=11	C GDM n=9
10.790	5.139	8.019
10.928	5.995	17.974
8.647	5.389	14.088
8.418	8.053	9.183
10.072	10.571	11.103
6.393	6.715	6.505
10.641	6.002	11.805
11.205	5.413	6.505
9.448	6.789	6.331
10.222	7.530	9.796
6.062	9.325	6.305

4 Placenta 3Groups (+9AA) PC/LPC MALDI data sets

healthy centre n=2	obese centre n=2	gdm centre n=2
7.664	6.422	5.205
7.062	6.258	4.295

Table:2

06/09/2021	Placenta 3Groups (+9AA) PC/LPC Results				
Data sets values	A Healthy n=12	B Obese n=9	C GDM n=9		
Ordinary one-way ANOVA results					
P value	<0.0001				
P value summary	****				
Significant diff. among means (P < 0.05)?	Yes				
R squared	0.5154				
Kruskal-Wallis Test multiple comparison	A Healthy n=12	B Obese n=9	C GDM n=9		
Alpha	0.05				
Dunn's multiple comparisons test	Mean Diff.	Below threshold?	Summary	Adjusted P Value	A-Healthy
Healthy vs. Obese	1.795	Yes	****	<0.0001	B obese
Healthy vs. GDM	0.3549	No	ns	0.3136	C gdm
Test details	Mean 1	Mean 2	Mean Diff.	SE of diff.	
Healthy vs. Obese	2.695	0.9	1.795	0.3456	
Healthy vs. GDM	2.695	2.34	0.3549	0.3456	

2	Placenta 3Groups (+9AA) PC/LPC MALDI data sets values		
	A Healthy n=12	B Obese n=9	C GDM n=9
	3.302	0.623	2.525
	2.539	1.276	1.686
	3.120	0.821	1.763
	4.192	0.530	1.821
	2.649	0.156	3.294
	1.954	0.787	3.568
	1.786	1.921	3.969
	2.025	0.979	1.231
	2.224	1.007	1.200
	2.074		
	3.006		
	3.464		

Table:3

Table 11/11/2021	Placenta 3Groups (+9AA) PC/LPC Results				
Data sets analyzed	A Healthy n=11	B Obese n=11	C GDM n=9		
Ordinary one-way ANOVA results	11-11-2021 Placenta 9AA+ve Healthy Obese GDM n=11				
Kruskal-Wallis test Anova Results					
P value	0.022				
Exact or approximate P value?	Approximate				
P value summary	*				
Do the medians vary signif. (P < 0.05)?	Yes				
Number of groups	3				
Kruskal-Wallis statistic	7.631				
Alpha	0.05				
Dunn's multiple comparisons test	Mean rank diff.	Significant?	Summary	Adjusted P Value	
healthy vs. obese	10.36	Yes	*	0.0359	A-B
healthy vs. gdm	1.091	No	ns	>0.9999	A-C
obese vs. gdm	-9.273	No	ns	0.0735	B-C

3	Placenta 3Groups (+9AA) PC/LPC MALDI data sets values		
	A Healthy n=11	B Obese n=11	C GDM n=9
	10.790	5.139	8.019
	10.928	5.995	17.974
	8.647	5.389	14.088
	8.418	8.053	9.183
	10.072	10.571	11.103
	6.393	6.715	6.505
	10.641	6.002	11.805
	11.205	5.413	6.505
	9.448	6.789	6.331
	10.222	7.530	9.796
	6.062	9.325	6.305

Table:4

Table Analyzed	Placenta 3Groups (+9AA) PC/LPC Results		Number of families	1	
Kruskal-Wallis test			Number of compari	3	
P value	0.0667				
Exact or approximate P value?	Exact				
P value summary	ns				
Do the medians vary signif. (P < 0.05)?	No				
Number of groups	3				
Kruskal-Wallis statistic	4.571				
Alpha	0.05				
Dunn's multiple comparisons test	Mean rank diff.	Significant?	Summary	Adjusted P Value	
healthy centre vs. obese centre	2	No	ns	0.8551	A-B
healthy centre vs. gdm centre	4	No	ns	0.0975	A-C
obese centre vs. gdm centre	2	No	ns	0.8551	B-C
Test details	Mean rank 1	Mean rank 2	Mean rank diff.	n1	n2
healthy centre vs. obese centre	5.5	3.5	2	2	2
healthy centre vs. gdm centre	5.5	1.5	4	2	2
obese centre vs. gdm centre	3.5	1.5	2	2	2

4	Placenta 3Groups (+9AA) PC/LPC MALDI data sets values		
	healthy centre n=2	obese centre n=2	gdm centre n=2
	7.664	6.422	5.205
	7.062	6.258	4.295

Table 4.3: GraphPad Plots no.2, no.3, no.4, no.5, and no.6 MALDI-ToF MS analysis of PC/LPC ratios for a set of samples and Statistical Data Analysis for Each graph pad plot presented in the results:

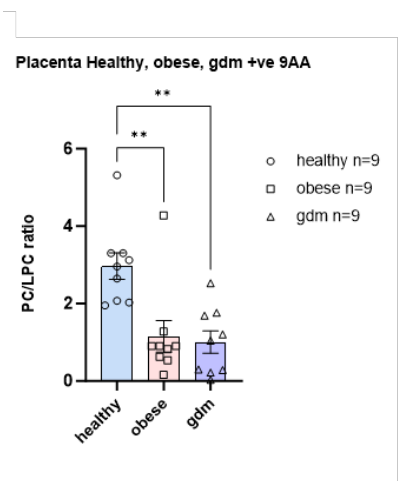

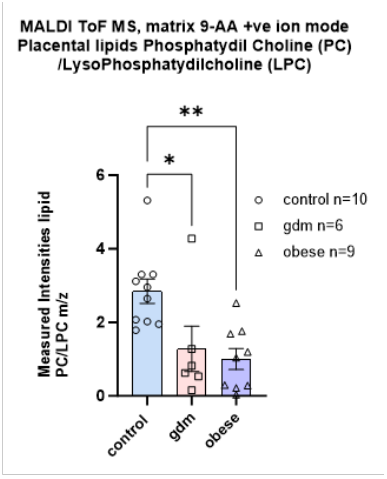

5 Placenta 3Groups (+9AA) PC/LPC MALDI data sets values

healthy n=9	obese n=9	gdm n=9
2.074	4.277	2.525
3.302	0.156	1.686
5.317	0.623	1.045
1.954	1.276	0.034
2.025	0.821	1.763
3.302	0.530	1.200
3.120	0.900	0.217
2.649	0.900	0.282
2.959	0.900	0.298

6 Placenta 3Groups (+9AA) PC/LPC MALDI data sets values

Healthy control n=10	gdm n=6	obese n=9
2.074	4.277	2.525
3.302	0.156	1.686
5.317	0.623	1.045
1.954	1.276	0.034
2.025	0.821	1.763
3.302	0.530	1.200
3.120		0.217
2.649		0.282
1.786		0.298
2.959		

Table:5	Placenta 3Groups (+9AA) PC/LPC Results				
Kruskal-Wallis Ordinary one-way ANOVA					
P value	0.0015				
Exact or approximate P value?	Approximate				
P value summary	**				
Do the medians vary signif. (P < 0.05)?	Yes				
Number of groups	3				
Kruskal-Wallis statistic	13				
Dunnett's multiple comparisons test	Mean rank diff.	Significant?	Summary	Adjusted P Value	
healthy vs. obese	11.44	Yes	**	0.0066	A-B
healthy vs. gdm	11.89	Yes	**	0.0044	A-C
obese vs. gdm	0.4444	No	ns	>0.9999	B-C
Dunnett's multiple comparisons test	Mean Diff.	95.00% CI of diff.	Below threshold?	Summary	Adjusted P Value
healthy vs. obese	1.813	0.1164 to 3.510	Yes	*	0.0379
healthy vs. gdm	1.961	0.7120 to 3.211	Yes	**	0.0055
Test details	Mean 1	Mean 2	Mean Diff.	SE of diff.	
healthy vs. obese	2.967	1.154	1.813	0.6348	
healthy vs. gdm	2.967	1.006	1.961	0.4674	

5	Placenta 3Groups (+9AA) PC/LPC MALDI data sets values		
	healthy n=9	obese n=9	gdm n=9
	2.074	4.277	2.525
	3.302	0.156	1.686
	5.317	0.623	1.045
	1.954	1.276	0.034
	2.025	0.821	1.763
	3.302	0.530	1.200
	3.120	0.900	0.217
	2.649	0.900	0.282
	2.959	0.900	0.298

Table:6	Placenta 3Groups (+9AA) PC/LPC Results				
Kruskal-Wallis test Anova Results					
P value	0.0025				
Exact or approximate P value?	Approximate				
P value summary	**				
Do the medians vary signif. (P < 0.05)?	Yes				
Number of groups	3				
Kruskal-Wallis statistic	11.95				
Dunn's multiple comparisons test	Mean rank diff.	Significant?	Summary	Adjusted P Value	
control vs. gdm	9.533	Yes	*	0.0363	A-B
control vs. obese	10.87	Yes	**	0.0039	A-C
gdm vs. obese	1.333	No	ns	>0.9999	B-C
Descriptive Statistics Kruskal-Wallis test	control	gdm	obese		
Number of values	10	6	9		
Minimum	1.786	0.1562	0.03437		
25% Percentile	2.007	0.4369	0.2495		
Median	2.804	0.722	1.045		
75% Percentile	3.302	2.026	1.724		
Maximum	5.317	4.277	2.525		
Mean	2.849	1.281	1.006		
Std. Deviation	1.046	1.513	0.8642		
Std. Error of Mean	0.3306	0.6178	0.2881		
Lower 95% CI	2.101	-0.3074	0.3413		
Upper 95% CI	3.597	2.869	1.67		

6	Placenta 3Groups (+9AA) PC/LPC MALDI data sets values		
	Healthy control n=10	gdm n=6	obese n=9
	2.074	4.277	2.525
	3.302	0.156	1.686
	5.317	0.623	1.045
	1.954	1.276	0.034
	2.025	0.821	1.763
	3.302	0.530	1.200
	3.120		0.217
	2.649		0.282
	1.786		0.298
	2.959		

Table 4.4: GraphPad Plots no.2, no.3, no.4, no.5, and no.6 MALDI-ToF MS analysis of PC/LPC ratios for a set of samples and Statistical Data Analysis for Each graph pad plot presented in the results:

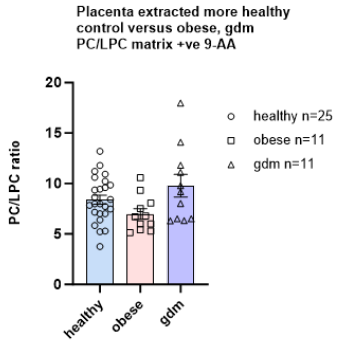

7 Placenta 3Groups (+9AA) PC/LPC
MALDI data sets values

healthy n=25	obese n=11	gdm n=11
3.753	5.139	6.305
5.223	5.284	6.331
5.291	5.413	6.505
5.835	5.995	6.505
6.393	6.002	8.019
7.151	6.715	9.183
7.472	6.789	9.796
7.843	7.530	11.103
7.998	8.053	11.805
8.418	9.325	14.088
8.647	10.571	17.974
9.448		
9.592		
9.836		
10.222		
10.601		
10.928		
11.205		
11.791		
13.199		
7.001		
7.011		
7.720		
7.998		
9.364		

Table:7	Placenta 3Groups (+9AA) PC/LPC Results				
13/05/2022					
ANOVA					
Kruskal-Wallis test Anova Results					
P value	0.0719				
Exact or approximate P value?	Approximate				
P value summary	ns				
Do the medians vary signif. (P < 0.05)?	No				
Number of groups	3				
Kruskal-Wallis statistic	5.265				
Dunnett's multiple comparisons test	Mean rank diff.	Significant?	Summary	Adjusted P Value	
healthy vs. obese	9.269	No	ns	0.1851	A-B
healthy vs. gdm	-3.458	No	ns	>0.9999	A-C
obese vs. gdm	-12.73	No	ns	0.0885	B-C

healthy n=25	obese n=11	gdm n=11
3.753	5.139	6.305
5.223	5.284	6.331
5.291	5.413	6.505
5.835	5.995	6.505
6.393	6.002	8.019
7.151	6.715	9.183
7.472	6.789	9.796
7.843	7.530	11.103
7.998	8.053	11.805
8.418	9.325	14.088
8.647	10.571	17.974
9.448		
9.592		
9.836		
10.222		
10.601		
10.928		
11.205		
11.791		
13.199		
7.001		
7.011		
7.720		
7.998		
9.364		

Table 4.5: GraphPad Plots no.7, no.8, no.9, and no.10 MALDI-ToF MS analysis of PC/LPC ratios for a set of samples and Statistical Data Analysis for Each graph pad plot presented in the results:

An explanatory note from the left-hand side begins with Plot 2 to Plot 6 and continues on the following pages. For example Table 2-Table 6 each contains the following: three groups of placenta samples per group healthy n= number of samples , obese n=number of sample, Gestational Diabetes GDM n=number of samples, which are run on MLADI in the positive ion and negative ion in two matrices 9AA matrix (IPA/CAN 3:2 v/v sample to Matrix 1:1 ration , applies spot to MALDI target 1ul) and DBH matrix (Methanol 1:1 matrix to sample, 1 ul spotted to MALDI plate) each sample run in triplicate then intensities of the cluster peaks mass to charge ration m/z for phosphatidyl choline PC native form to the hydrolysed degraded form Lyso phosphatidylcholine LPC using the 18 Peaks masses intensities showing in Figure 4.20, 4.21 and 4.22 in the mass spectra and each run in triplicate then the calculated average ration in the excel tables were taken and plotted on the GraphPad producing those column plots as comparison of how my of the native versus hydrolyses PC to

LPC is measurable by the intensities signal in each sample per each group , by taking to consideration the group BMI Healthy versus obese. So, the point is to determine if measuring the native state of PC to hydrolyses from LPC can be monitored amongst the groups and potentially used as a biomarker of obesity in complicated pregnancies as an indicator of lipid groups. By measuring large amounts of samples in human biological tissue, which is very heterogeneous, and that is the reason for using so many samples, we try to learn and build up a better understanding of how we can apply and follow this approach and further develop to monitor problematic pregnancies especially gestational diabetes and obesity as those pregnancies require all caesarean delivery because of the health risk and complications from obesity. The educational development towards better underacting and educational transparency amongst obstetricians and patients and family planning clinics is to educate and make all new and potential mothers aware of the health risks such as obesity and gestational diabetes. We aim to develop this further as group interest is in this particularly active topic of research and health and not easily or comfortably made aware to pregnant women. Ealy lipid measurement diagnostics could offer information if there were problems of miscarriage, hypertension, preeclampsia or other unsuccessful pregnancy outcomes. Plot 2 Placenta groups samples (healthy n=12, obese n=9, GDM n=9) 3*star rating showing significance in healthy and obese groups. Plot 3 Placenta group samples (healthy n=11, obese n=11, GDM n=9) 1*star rating showing only significance in healthy and obese groups. Plot 4 Placenta group samples(healthy n=9, obese n=9, GDM n=9) showed no significance in placenta chunks cut from the central part near the cord. Plot 5 Placenta group samples (healthy n=9, obese n=9, GDM n=9) 2*star rating showing significance in healthy and obese and 2*healthy with gestational diabetes GDM group. Plot 6 Placenta groups samples (healthy n=10, obese n=6, GDM n= 9) 2*star rating showing significance healthy and obese and 1*healthy with gestational diabetes GDM group

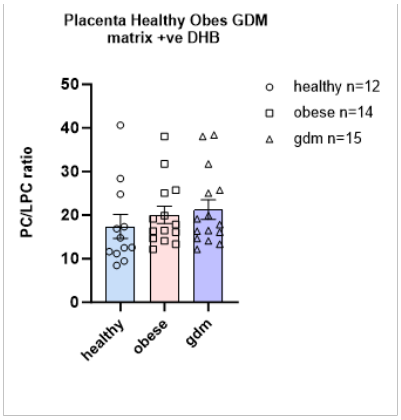

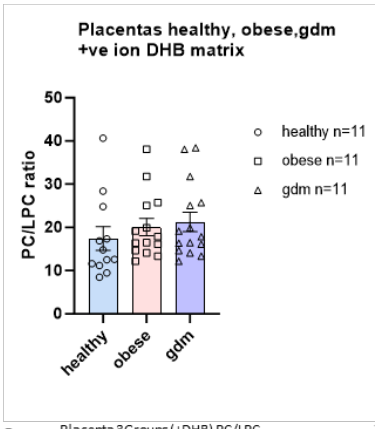

8

Placenta 3Groups (+DHB) PC/LPC MALDI data sets values		
healthy n=12	obese n=14	gdm n=15
12.584	12.190	12.190
14.830	19.877	19.877
16.888	19.159	19.159
24.795	16.091	16.091
40.634	25.732	25.732
17.360	31.779	31.779
28.401	13.340	38.384
11.625	38.078	13.340
9.469	25.065	38.078
12.500	16.358	25.065
8.488	16.496	16.358
11.205	17.871	16.496
	14.657	17.871
	14.109	14.657
		14.109

9

Placenta 3Groups (+DHB) PC/LPC MALDI data sets values		
healthy n=11	obese n=11	gdm n=11
12.584	12.190	12.190
14.830	19.877	19.877
16.888	19.159	19.159
24.795	16.091	16.091
40.634	25.732	25.732
17.360	31.779	31.779
28.401	13.340	38.384
11.625	38.078	13.340
9.469	25.065	38.078
12.500	16.358	25.065
8.488	16.496	16.358
11.205	17.871	16.496
	14.657	17.871
	14.109	14.657
		14.109

Table:8						**8**	Placenta 3Groups (+DHB) PC/LPC MALDI data sets values		
Date 18-07-2022:	Placenta 3Groups (+DHB) PC/LPC Results						healthy n=12	obese n=14	gdm n=15
ANOVA							12.584	12.190	12.190
Mixed-effects model (REML)	Matching: Across row						14.830	19.877	19.877
Assume sphericity?	No						16.888	19.159	19.159
Alpha	0.05						24.795	16.091	16.091
Fixed effect (type III)	P value	P value summary	Statistically significant (P < 0.05)?				40.634	25.732	25.732
Treatment (between columns)	0.395	ns	No				17.360	31.779	31.779
Random effects	SD	Variance					28.401	13.340	38.384
Individual (between rows)	3.319	11.01					11.625	38.078	13.340
Residual	7.872	61.96					9.469	25.065	38.078
Chi-square, df	0.7634, 1						12.500	16.358	25.065
P value	0.3823						8.488	16.496	16.358
P value summary	ns						11.205	17.871	16.496
Is there significant matching (P < 0.05)?	No							14.657	17.871
Kruskal-Wallis test Multiple comparisons								14.109	14.657
Dunnett's multiple comparisons test	Mean Diff.	95.00% CI of diff.	Below threshold?	Summary	Adjusted P Value				14.109
healthy vs. obese	-2.659	-11.35 to 6.028	No	ns	0.661				
healthy vs. gdm	-3.881	-11.65 to 3.891	No	ns	0.3716				
Descriptive Statistics Kruskal-Wallis test									
Number of values	12	14	15						
Number of missing values	3	1	0						
Minimum	8.488	12.19	12.19						
25% Percentile	11.31	14.52	14.66						
Median	13.71	17.18	17.87						
75% Percentile	22.94	25.23	25.73						
Maximum	40.63	38.08	38.38						
Mean	17.4	20.06	21.28						
Std. Deviation	9.456	7.538	8.669						
Std. Error of Mean	2.73	2.015	2.238						
Lower 95% CI	11.39	15.7	16.48						
Upper 95% CI	23.41	24.41	26.08						

Table:9						**9**	Placenta 3Groups (+DHB) PC/LPC MALDI data sets values		
Date 18-07-2022:	Placenta 3Groups (+DHB) PC/LPC Results						healthy n=11	obese n=11	gdm n=11
ANOVA							12.584	12.190	12.190
Kruskal-Wallis test Anova Results							14.830	19.877	19.877
P value	0.2093						16.888	19.159	19.159
Exact or approximate P value?	Approximate						24.795	16.091	16.091
P value summary	ns						40.634	25.732	25.732
Do the medians vary signif. (P < 0.05)?	No						17.360	31.779	31.779
Number of groups	3						28.401	13.340	38.384
Kruskal-Wallis statistic	3.128						11.625	38.078	13.340
Number of families	1						9.469	25.065	38.078
Number of comparisons per family	3						12.500	16.358	25.065
Alpha	0.05						8.488	16.496	16.358
Kruskal-Wallis test Multiple comparisons							11.205	17.871	16.496
Dunn's multiple comparisons test	Mean rank diff.	Significant?	Summary	Adjusted P Value				14.657	17.871
healthy vs. obese	-6.583	No	ns	0.4865	A-B			14.109	14.657
healthy vs. gdm	-7.75	No	ns	0.2839	A-C				14.109
obese vs. gdm	-1.167	No	ns	>0.9999	B-C				

Table 4.4: GraphPad Plots no.7, no.8, no.9, and no.10 MALDI-ToF MS analysis of PC/LPC ratios for a set of samples and Statistical Data Analysis for Each graph pad plot presented in the results:

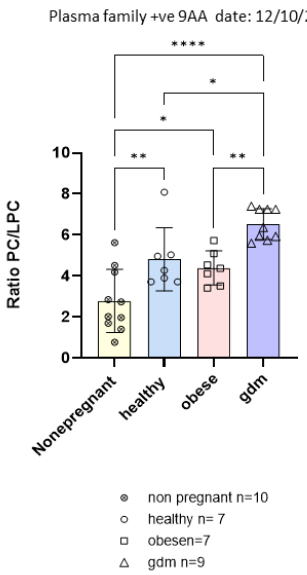

Non pregnant Plasmas +ve ion 9AA Matrix

No.	CAT	BMI	PC/LPC Average of 3 Maldi Intensities ∑PC / ∑LPC
1	CRF384	32.8	2.75
2	CRF424	27.5	4.19
3	CRF 453	25.1	1.71
4	CRF458	29	4.52
5	CRF474	23.8	1.41
6	CRF480	24.6	0.78
7	CRF497	24.5	2.86
8	CRF513*	NO BMI	2.03
9	CRF515*	NO BMI	1.98
10	CRF518*	NO BMI	5.63

Obese Plasmas +ve ion 9AA Matrix

No.	CAT	BMI	PC/LPC Average of 3 Maldi Intensities ∑PC / ∑LPC
1	CAT1544	44.6	5.1
2	CAT1557	46.1	3.5
3	CAT1593	48	4.4
4	CAT1606	41	4.1
5	CAT1613	41.3	5.7
6	CAT1614	32.4	4.5
7	CAT1636	31.8	3.4

Healthy Plasmas +ve ion 9AA Matrix

No.	CAT	BMI	PC/LPC Average of 3 Maldi Intensities ∑PC / ∑LPC
1	CAT1531	28.7	8.1
2	CAT1532	18.7	3.7
3	CAT1543	26	5.0
4	CAT1549	27	3.9
5	CAT1639	20	3.7
6	CAT1642	25.3	5.0
7	CAT1643	25.4	4.3

GDM Plasmas +ve ion 9AA Matrix

No.	CAT	BMI	PC/LPC Average of 3 Maldi Intensities ∑PC / ∑LPC
1	CAT1530	34.7	6.4
2	CAT1545	22.7	5.7
3	CAT1577*	46.5	7.4
4	CAT1558	27.3	1.9
5	CAT1564	57.3	5.9
6	CAT1565	22	5.6
7	CAT1568	26.1	7.3
8	CAT1574	22.7	7.3
9	CAT1578	38.7	7.3

Table: 10 All Plasma

						10 Placenta 3Groups (+9AA) PC/LPC MALDI data sets values			
Date:04-09-2022	Plasma 4Groups (+DHB) PC/LPC Results					Non pregnant N=10	healthy N=7	obese N=7	gdm N=9
ANOVA						2.748	8.085	5.097	6.370
Kruskal-Wallis test Anova Results						4.194	5.040	3.519	5.747
P value	0.0002					1.706	4.970	4.379	7.403
Exact or approximate P value?	Approximate					4.518	4.281	4.114	5.945
P value summary	***					1.410	3.906	5.727	5.937
Do the medians vary signif. (P < 0.05)?	Yes					0.779	3.725	4.544	5.605
Number of groups	4					2.856	3.720	3.417	7.251
Kruskal-Wallis statistic	19.63					2.033			7.251
Number of families	1					1.977			7.251
Number of comparisons per family	3					5.628			
Alpha	0.05								
Dunn's multiple comparisons test	Mean rank diff.	Significant?	Summary	Adjusted P Value	A-?				
Non pregnant vs. healthy	-8.943	No	ns	0.1814	B healthy				
Non pregnant vs. obese	-7.371	No	ns	0.3653	C obese				
Non pregnant vs. gdm	-19.58	Yes	****	<0.0001	D gdm				
Descriptive Statistics Kruskal-Wallis test	Non pregnant n=10	healthy n=7	obese n=7	gdm n=9					
Minimum	0.7792	3.72	3.417	5.605					
25% Percentile	1.632	3.725	3.519	5.842					
Median	2.39	4.281	4.379	6.37					
75% Percentile	4.275	5.04	5.097	7.251					
Maximum	5.628	8.085	5.727	7.403					
Mean	2.785	4.818	4.4	6.529					
Std. Deviation	1.541	1.542	0.8259	0.751					
Std. Error of Mean	0.4873	0.5829	0.3121	0.2503					
Lower 95% CI	1.682	3.392	3.636	5.952					
Upper 95% CI	3.887	6.244	5.163	7.106					

Table 4.6: GraphPad Plots no.7, no.8, no.9, and no.10 MALDI-ToF MS analysis of PC/LPC ratios for a set of samples and statistical analysis for each graph pad plot presented in the results:

An explanatory note from the left-hand side begins with table Plot 7 Placenta groups samples +ve 9AA matrix (healthy n=25, obese n=11, GDM n=11) showing NO significance amongst the three groups. Plot 8 Placenta group samples run in +ve DHB Matrix (healthy n=12, obese n=14, GDM n=15) showing NO significance amongst the three groups. Plot 9 Placenta groups samples run in +ve DHB Matrix (healthy n=9, obese n=9, GDM n=9) 2*star rating showing significance healthy and obese and 2*healthy with gestational diabetes GDM group. Plot 10 Plasma group samples run in +ve 9AA matrix (non-pregnant n=10 pregnant healthy n=7, pregnant obese n=7, pregnant GDM n= 9) showing 4* star rating highest significance amongst non-pregnant patients with gestational diabetes GDM patience difference in PC/LPC relative ratio.

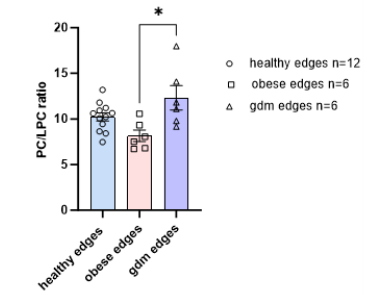

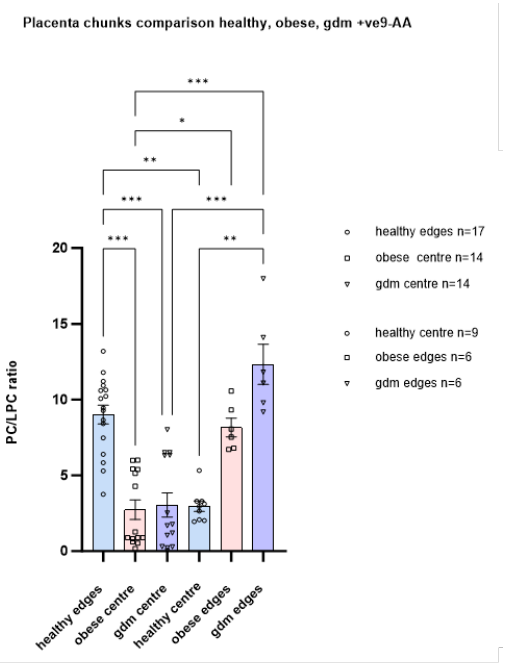

11 Placenta 3Groups (+DHB) PC/LPC MALDI data sets values

healthy edges	obese edges	gdm edges
10.601	8.053	17.974
10.928	10.571	14.088
10.641	6.715	9.183
11.205	6.789	11.103
10.222	7.530	11.805
13.199	9.325	9.796
8.647		
8.418		
10.072		
9.448		
7.472		
11.791		

12 Placenta 3Groups (+DHB) PC/LPC MALDI data sets values

healthy edges n17	obese centre n=14	gdm centre n=14	healthy centre n=9	obese edges n=6	gdm edges n=6
8.647	4.277	2.525	2.074	8.053	17.974
8.418	0.156	1.686	3.302	10.571	14.088
10.072	0.623	1.045	5.317	6.715	9.183
9.448	1.276	0.034	1.954	6.789	11.103
7.472	0.821	1.763	2.025	7.530	11.805
11.791	0.530	1.200	3.302	9.325	9.796
10.601	0.900	0.217	3.120		
10.928	0.900	0.282	2.649		
10.641	0.900	0.298	2.959		
11.205	5.139	8.019			
10.222	5.995	6.505			
13.199	5.389	6.505			
6.393	6.002	6.331			
3.753	5.413	6.305			
5.291					
9.284					
5.835					

Table:11	Placenta 3Groups (+DHB) PC/LPC Results				
Table Analyzed	Healhy centre vsobese , gdm				
Kruskal-Wallis test					
P value	0.0143				
Exact or approximate P value?	Approximate				
P value summary	*				
Do the medians vary signif. (P < 0.05)?	Yes				
Number of groups	3				
Kruskal-Wallis statistic	8.5				
Number of families	1				
Number of comparisons per family	3				
Alpha	0.05				
Dunn's multiple comparisons test	Mean rank diff.	Significant?	Summary	Adjusted P Value	
healthy edges vs. obese edges	7.5	No	ns	0.1017	A-B
healthy edges vs. gdm edges	-4.167	No	ns	0.7158	A-C
obese edges vs. gdm edges	-11.67	Yes	*	0.0128	B-C

Table:12 All combined					
Kruskal-Wallis test Anova Results	Placenta 3Groups (+DHB) PC/LPC Results				
Table Analyzed	Combined healthy (edges + centre)				
ANOVA					
Kruskal-Wallis test					
P value	<0.0001				
Exact or approximate P value?	Approximate				
P value summary	****				
Do the medians vary signif. (P < 0.05)?	Yes				
Number of groups	6				
Kruskal-Wallis statistic	43.65				
Kruskal-Wallis test Multiple comparisons					
Dunn's multiple comparisons test	Mean rank diff.	Significant?	Summary	Adjusted P Value	
healthy edges vs. obese centre	31.03	Yes	***	0.0001	A-B
healthy edges vs. gdm centre	28.75	Yes	***	0.0005	A-C
healthy edges vs. healthy centre	27.07	Yes	**	0.0094	A-D
healthy edges vs. obese edges	2.51	No	ns	>0.9999	A-E
healthy edges vs. gdm edges	-10.16	No	ns	>0.9999	A-F
obese centre vs. gdm centre	-2.286	No	ns	>0.9999	B-C
obese centre vs. healthy centre	-3.968	No	ns	>0.9999	B-D
obese centre vs. obese edges	-28.52	Yes	*	0.0349	B-E
obese centre vs. gdm edges	-41.19	Yes	***	0.0002	B-F
gdm centre vs. healthy centre	-1.683	No	ns	>0.9999	C-D
gdm centre vs. obese edges	-26.24	No	ns	0.0763	C-E
gdm centre vs. gdm edges	-38.9	Yes	***	0.0005	C-F
healthy centre vs. obese edges	-24.56	No	ns	0.2282	D-E
healthy centre vs. gdm edges	-37.22	Yes	**	0.0035	D-F
obese edges vs. gdm edges	-12.67	No	ns	>0.9999	E-F

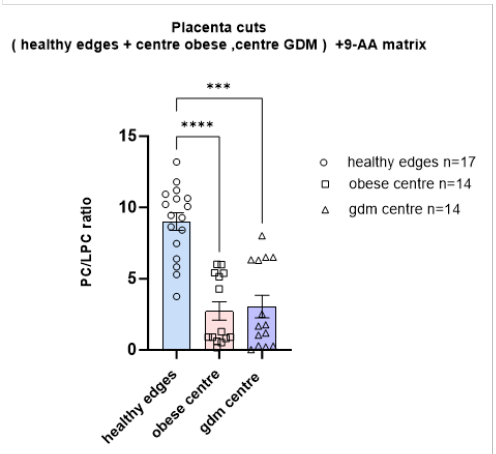

13 Placenta 3Groups (+DHB) PC/LPC MALDI data sets values

healthy edges n=17	obese centre n=14	gdm centre n=14
8.647	4.277	2.525
8.418	0.156	1.686
10.072	0.623	1.045
9.448	1.276	0.034
7.472	0.821	1.763
11.791	0.530	1.200
10.601	0.900	0.217
10.928	0.900	0.282
10.641	0.900	0.298
11.205	5.139	8.019
10.222	5.995	6.505
13.199	5.389	6.505
6.393	6.002	6.331
3.753	5.413	6.305
5.291		
9.284		
5.835		

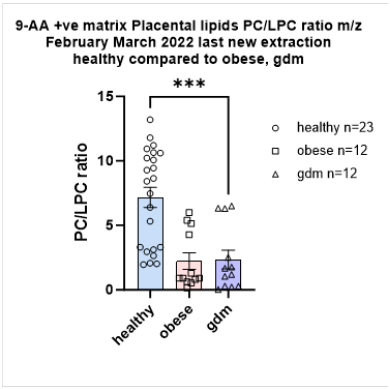

14 Placenta 3Groups (+DHB) PC/LPC MALDI data sets values

healthy n=23	obese n=9	gdm n=9
2.074	4.277	2.525
3.302	0.156	1.686
5.317	0.623	1.045
1.954	1.276	0.034
2.025	0.821	1.763
3.302	0.530	1.200
3.120	0.900	0.217
2.649	0.900	0.282
2.959	0.900	0.298
10.601		
10.928		
8.647		
8.418		
10.072		
6.393		
10.641		
11.205		
9.448		
10.222		
9.284		
7.472		
11.791		
13.199		

Table:13

Table Analyzed	Placenta 3Groups (+DHB) PC/LPC Results				
ANOVA					
Kruskal-Wallis test Anova Results					
P value	<0.0001				
Exact or approximate P value?	Approximate				
P value summary	****				
Do the medians vary signif. (P < 0.05)?	Yes				
Number of groups	3				
Kruskal-Wallis statistic	23.72				
Kruskal-Wallis test Multiple comparisons					
Dunn's multiple comparisons test	Mean rank diff.	Significant?	Summary	Adjusted P Value	
healthy edges vs. obese centre	20.75	Yes	****	<0.0001	A-B
healthy edges vs. gdm centre	18.39	Yes	***	0.0003	A-C
obese centre vs. gdm centre	-2.357	No	ns	>0.9999	B-C

13	Placenta 3Groups (+DHB) PC/LPC MALDI data sets values		
	healthy edges n=17	obese centre n=14	gdm centre n=14
	8.647	4.277	2.525
	8.418	0.156	1.686
	10.072	0.623	1.045
	9.448	1.276	0.034
	7.472	0.821	1.763
	11.791	0.530	1.200
	10.601	0.900	0.217
	10.928	0.900	0.282
	10.641	0.900	0.298
	11.205	5.139	8.019
	10.222	5.995	6.505
	13.199	5.389	6.505
	6.393	6.002	6.331
	3.753	5.413	6.305
	5.291		
	9.284		
	5.835		

Table:14

Date: 01-04-22	Placenta 3Groups (+DHB) PC/LPC Results				
ANOVA summary					
Kruskal-Wallis test Anova Results					
P value	<0.0001				
Exact or approximate P value?	Approximate				
P value summary	****				
Do the medians vary signif. (P < 0.05)?	Yes				
Number of groups	3				
Kruskal-Wallis statistic	26.53				
Kruskal-Wallis test Multiple comparisons					
Dunn's multiple comparisons test	Mean rank diff.	Significant?	Summary	Adjusted P Value	
healthy vs. obese	19.19	Yes	***	0.0001	A-B
healthy vs. gdm	19.63	Yes	****	<0.0001	A-C
obese vs. gdm	0.4444	No	ns	>0.9999	B-C

14	Placenta 3Groups (+DHB) PC/LPC MALDI data sets values		
	healthy n=23	obese n=9	gdm n=9
	2.074	4.277	2.525
	3.302	0.156	1.686
	5.317	0.623	1.045
	1.954	1.276	0.034
	2.025	0.821	1.763
	3.302	0.530	1.200
	3.120	0.900	0.217
	2.649	0.900	0.282
	2.959	0.900	0.298
	10.601		
	10.928		
	8.647		
	8.418		
	10.072		
	6.393		
	10.641		
	11.205		
	9.448		
	10.222		
	9.284		
	7.472		
	11.791		

Table 4.7: LPC/PC ratios for a set of samples Plots 11-14. GraphPad Plot no.11, Plot no.12, Plot no.13, and Plot no.14 peak intensities acquired by MALDI-ToF MS Statistical Data Analysis for Each graph pad plot presented in the results using per each sample three repeats and taking an average of the three intensities of each cluster peaks for LPC and PC and plotting as a data point in the GraphPad using ∑LPC/∑PC and all sample calculation excel tables of each

Plot 11 Placenta groups samples (healthy n=12, obese n=6, GDM n=6) 1*star rating showing significance of healthy and gestational diabetes GDM group. Plot 12 Placenta groups samples cut from near central cord versus edges as the comparison on one graph plot (Healthy edges n=17, obese centre n=14, GDM centre n=14), and healthy centre n=9, obese edges n=6 GDM edges n=6) 3*star, 2*, 1* rating showing the significance of among these three groups in placenta cuts from central cord versus placenta l edges, which suggested the wealthiest parts in nutrients are the placenta globules edges not the centre. Which is very fibrous and full of nodular capillaries, almost plastic straw-like connectors, and the edges are meatier and have more tissue present. Plot 13 Placenta groups samples(healthy edges n=17, obese centre n=14, GDM centre n= 14) 4*star and 3*star significance in placenta chunks cut from healthy edges globules compared to cuts from central parts near the cord of placentas cuts from obese and gestational diabetes GDM, which suggests that not only the parts of placenta are essential as well as the lipid accumulation contes prefers to be in the maternal side globules trophoblast more meaty parts rather then in plasticity side of cord closer to the fetal side. Plot 14 Placenta group samples (healthy n=23, obese n=9, GDM n= 9) 3*star rating showing the significance of more significant numbers of healthy placenta samples to the lower number of obese and GDM samples, specifically GDM and obese and 2*healthy with gestational diabetes GDM group. The research could suggest that the control healthy samples have less PC/LPC and need twice as many volume samples to observe significant differences amongst the group's PC/LPC reactivation.

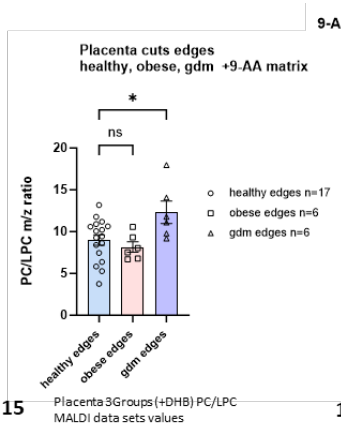

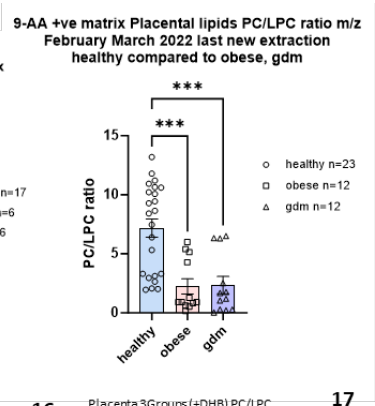

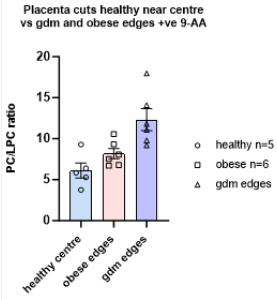

15

Placenta 3Groups (+DHB) PC/LPC MALDI data sets values

healthy edges n=17	obese edges n=6	gdm edges n=6
8.647	8.053	17.974
8.418	10.571	14.088
10.072	6.715	9.183
9.448	6.789	11.103
7.472	7.530	11.805
11.791	9.325	9.796
10.601		
10.928		
10.641		
11.205		
10.222		
13.199		
6.393		
3.753		
5.291		
9.284		
5.835		

16

Placenta 3Groups (+DHB) PC/LPC MALDI data sets values

healthy n=23	obese n-12	gdm n=12
2.074	4.277	2.525
3.302	0.156	1.686
5.317	0.623	1.045
1.954	1.276	0.034
2.025	0.821	1.763
3.302	0.530	1.200
3.120	0.900	0.217
2.649	0.900	0.282
2.959	0.900	0.298
10.601	5.139	6.505
10.928	5.995	6.331
8.647	5.389	6.305
8.418		
10.072		
6.393		
10.641		
11.205		
9.448		
10.222		
9.284		
7.472		
11.791		
13.199		

17

Placenta 3Groups (+DHB) PC/LPC MALDI data sets values

Healthy central n=5	obese edges n=6	gdm edges n=6
6.393	8.053	17.974
3.753	10.571	14.088
5.291	6.715	9.183
9.284	6.789	11.103
5.835	7.530	11.805
	9.325	9.796

Table:15	Placenta 3Groups (+DHB) PC/LPC Results				
Kruskal-Wallis test Anova Results					
F	4.856				
P value	0.0162				
P value summary	*				
Significant diff. among means (P < 0.05)?	Yes				
R squared	0.2719				
Kruskal-Wallis test Multiple comparisons					
Holm-Šídák's multiple comparisons test	Mean Diff.	Below threshold?	Summary	Adjusted P Value	A-?
healthy edges vs. obese edges	0.8478	No	ns	0.4883	B-obese edges
healthy edges vs. gdm edges	-3.313	Yes	*	0.0214	C-gdm edges
Mean	9.012	8.164	12.32		
Std. Deviation	2.538	1.52	3.257		
Std. Error of Mean	0.6156	0.6203	1.33		

Table:16	Placenta 3Groups (+DHB) PC/LPC Results				
Date: 01-04-22	Placenta aded more healthy				
ANOVA summary					
Kruskal-Wallis test Anova Results					
P value	<0.0001				
Exact or approximate P value?	Approximate				
P value summary	****				
Do the medians vary signif. (P < 0.05)?	Yes				
Number of groups	3				
Kruskal-Wallis statistic	20.18				
Kruskal-Wallis test Multiple comparisons					
Dunn's multiple comparisons test	Mean rank diff.	Significant?	Summary	Adjusted P Value	
healthy vs. obese	18.26	Yes	***	0.0006	A-B
healthy vs. gdm	17.67	Yes	***	0.0009	A-C
obese vs. gdm	-0.5833	No	ns	>0.9999	B-C

Placenta 9AA 02-02-22 01-04-22 New

Table:17	Placenta 3Groups (+DHB) PC/LPC Results				
Dates: 02-02-22 , 01-04-22 New	Placenta healthy near cordcentre vs edges gdm and edges obese				
ANOVA summary					
Kruskal-Wallis test Anova Results					
P value	0.001				
Exact or approximate P value?	Exact				
P value summary	**				
Do the medians vary signif. (P < 0.05)?	Yes				
Number of groups	3				
Kruskal-Wallis statistic	10.5				
Kruskal-Wallis test Multiple comparisons					
Dunn's multiple comparisons test	Mean rank diff.	Significant?	Summary	Adjusted P Value	
Healthy central vs. obese edges	-4.333	No	ns	0.4693	A-B
Healthy central vs. gdm edges	-9.833	Yes	**	0.0039	A-C
obese edges vs. gdm edges	-5.5	No	ns	0.1777	B-C

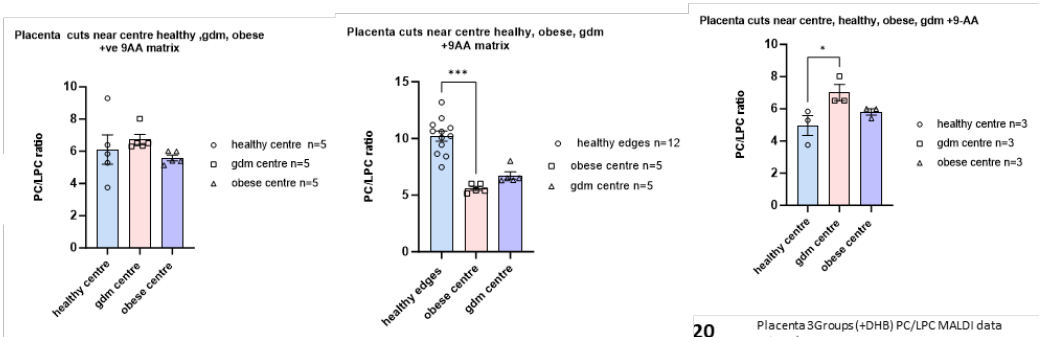

18 Placenta 3Groups (+DHB) PC/LPC MALDI data sets values

healthy centre n=5	obese centre n=5	gdm centre n=5
6.393	5.139	8.019
3.753	5.995	6.505
5.291	5.389	6.505
9.284	6.002	6.331
5.835	5.413	6.305

19 Placenta 3Groups (+DHB) PC/LPC MALDI data sets values

healthy centre n=12	obese centre n=5	gdm centre n=5
6.393	5.139	8.019
3.753	5.995	6.505
5.291	5.389	6.505
9.284	6.002	6.331
5.835	5.413	6.305

20 Placenta 3Groups (+DHB) PC/LPC MALDI data sets values

healthy centre n=3	obese centre n=3	gdm centre n=3
3.753	5.995	8.019
5.291	6.002	6.505
5.835	5.413	6.505

Table:18						**18**	Placenta 3Groups (+DHB) PC/LPC MALDI data sets values		
Table Analyzed	Placenta healthy edges centre vs gdm obese						healthy centre n=5	obese centre n=5	gdm centre n=5
ANOVA summary							6.393	5.139	8.019
Kruskal-Wallis test Anova Results							3.753	5.995	6.505
P value	0.065						5.291	5.389	6.505
Exact or approximate P value?	Exact						9.284	6.002	6.331
P value summary	ns						5.835	5.413	6.305
Do the medians vary signif. (P < 0.05)?	No								
Number of groups	3								
Kruskal-Wallis statistic	5.36								
Kruskal-Wallis test Multiple comparisons									
Dunn's multiple comparisons test	Mean rank diff.	Significant?	Summary	Adjusted P Value					
healthy centre vs. obese centre	2	No	ns	>0.9999	A-B				
healthy centre vs. gdm centre	-4.4	No	ns	0.3594	A-C				
obese centre vs. gdm centre	-6.4	No	ns	0.071	B-C				
Table:19									
Table Analyzed	Placenta healthy edges centre vs gdm obese								
ANOVA summary						**19**	Placenta 3Groups (+DHB) PC/LPC MALDI data sets values		
Kruskal-Wallis test Anova Results							healthy centre n=12	obese centre n=5	gdm centre n=5
P value	0.065						6.393	5.139	8.019
Exact or approximate P value?	Exact						3.753	5.995	6.505
P value summary	ns						5.291	5.389	6.505
Do the medians vary signif. (P < 0.05)?	No						9.284	6.002	6.331
Number of groups	3						5.835	5.413	6.305
Kruskal-Wallis statistic	5.36								
Dunn's multiple comparisons test	Mean rank diff.	Significant?	Summary	Adjusted P Value					
healthy centre vs. obese centre	2	No	ns	>0.9999	A-B				
healthy centre vs. gdm centre	-4.4	No	ns	0.3594	A-C				
obese centre vs. gdm centre	-6.4	No	ns	0.071	B-C				
Table:20									
Kruskal-Wallis test Anova Results									
P value	0.0107					**20**	Placenta 3Groups (+DHB) PC/LPC MALDI data sets values		
Exact or approximate P value?	Exact						healthy centre n=3	obese centre n=3	gdm centre n=3
P value summary	*						3.753	5.995	8.019
Do the medians vary signif. (P < 0.05)?	Yes						5.291	6.002	6.505
Number of groups	3						5.835	5.413	6.505
Kruskal-Wallis statistic	6.489								
Dunn's multiple comparisons test	Mean rank diff.	Significant?	Summary	Adjusted P Value					
healthy centre vs. obese centre	-2.333	No	ns	0.8902	A-B				
healthy centre vs. gdm centre	-5.667	Yes	*	0.0338	A-C				
obese centre vs. gdm centre	-3.333	No	ns	0.4081	B-C				

Table 4.8: GraphPad Plots No.15-to-No.20 MALDI-ToF MS analysis of PC/LPC ratios for a set of samples.

Plot 15 Placenta group samples (healthy n=17, obese n=6, GDM n=6) 1*star rating showing only significance healthy edges cut to the gestational diabetes edges cut and no importance to obese. Plot 16 Placenta group samples (healthy n=23, obese n=12, GDM n= 12) 3*star rating showing good significance in healthy and obese groups similarly observed in plots no.13 and no.14.Plot 17 Placenta group samples(healthy n=5, obese n=6, GDM n=6) showed no significance in placenta chunks cut from edges and central near cord. Plot 18 Placenta group samples (healthy n=5, obese n=5, GDM n=5) 2 no significance showing significance healthy and obese and 2*healthy

with gestational diabetes GDM group. Plot 19 Placenta group samples (healthy n=12, obese n=5, GDM n= 5) 3*star rating showing significance for healthy and obese, which suggests that twice the number of healthy samples needed to observe differences, which could be down to the quality of the sample, contamination during extraction or just biological heterogeneity. Plot 20 Placenta groups samples (healthy n=3, obese n=3, GDM n= 3) 1*star rating showing only significance 1*healthy with gestational diabetes GDM groupThe plot results show that TLC combined with MALDI can measure the relevant trends.

4.5 Collaboration with the University of Warwick

The MALDI results above show that using mass spectra analytical data processing knowledge can identify lipid classes and lipid chain lengths by comparing the measured masses to the known or expected structures from the literature. However, literature values have substantial ambiguity in the lengths of the acyl chains as well as acyl chain structural features such as double bond position, branching, hydroxyl positions, and cis/trans isomerism, although all are known to vary within the range of biologically relevant lipid structures. A straightforward approach to determining some of these detailed structural features is to use tandem mass spectrometry techniques (MS/MS or MSn) rather than just simple mass measurement (MS). As MSn is not possible on the instruments available at Swansea University, further work was done in collaboration with the Ion Cyclotron Resonance Facility at the University of Warwick.

Mr Basim Hussain, a PhD student in the facility, performed high mass resolution and mass accuracy analysis to confirm our lipid assignments. Then, he performed MS/MS experiments using a variety of fragmentation techniques, including collision-induced dissociation (CID), electron detachment dissociation (EDD), and ultraviolet photodissociation (UVPD) to generate fragment ions from the isolated, individual lipid species. He used these techniques in his experiments to determine the (sn-1) versus (sn-2) lipid positional assignments and the position of double bonds within the lipid chains.

Mr Hussain diluted the sample 10-fold to 1 mg/ml and used a micropipette to put 2 µl of sample into a glass capillary pulled under heat to make a 1 □m inner diameter nano-electrospray tip. The sample was placed in the nano-electrospray ion source and measured on the FTICR mass spectrometer. A phosphatidylcholine precursor ion's primary sodiated ion peak at m/z 758.6 was isolated and fragmented with CID in the collision cell. The resulting MS/MS spectrum showed the phosphate head group at 184.5 Da and two fatty acid chains from fragmentation at the sn-1 and sn-2 positions. The sample was run directly on the FTICR mass spectrometer with no additional sample preparation other than dilution, which means that the sample preparation methodologies used in chapters 2 and 3 effectively generated good, clean samples.

Figure 4:24: Photographs taken during experiments with PhD student Basim at the University of Warwick FTICR MS Centre.

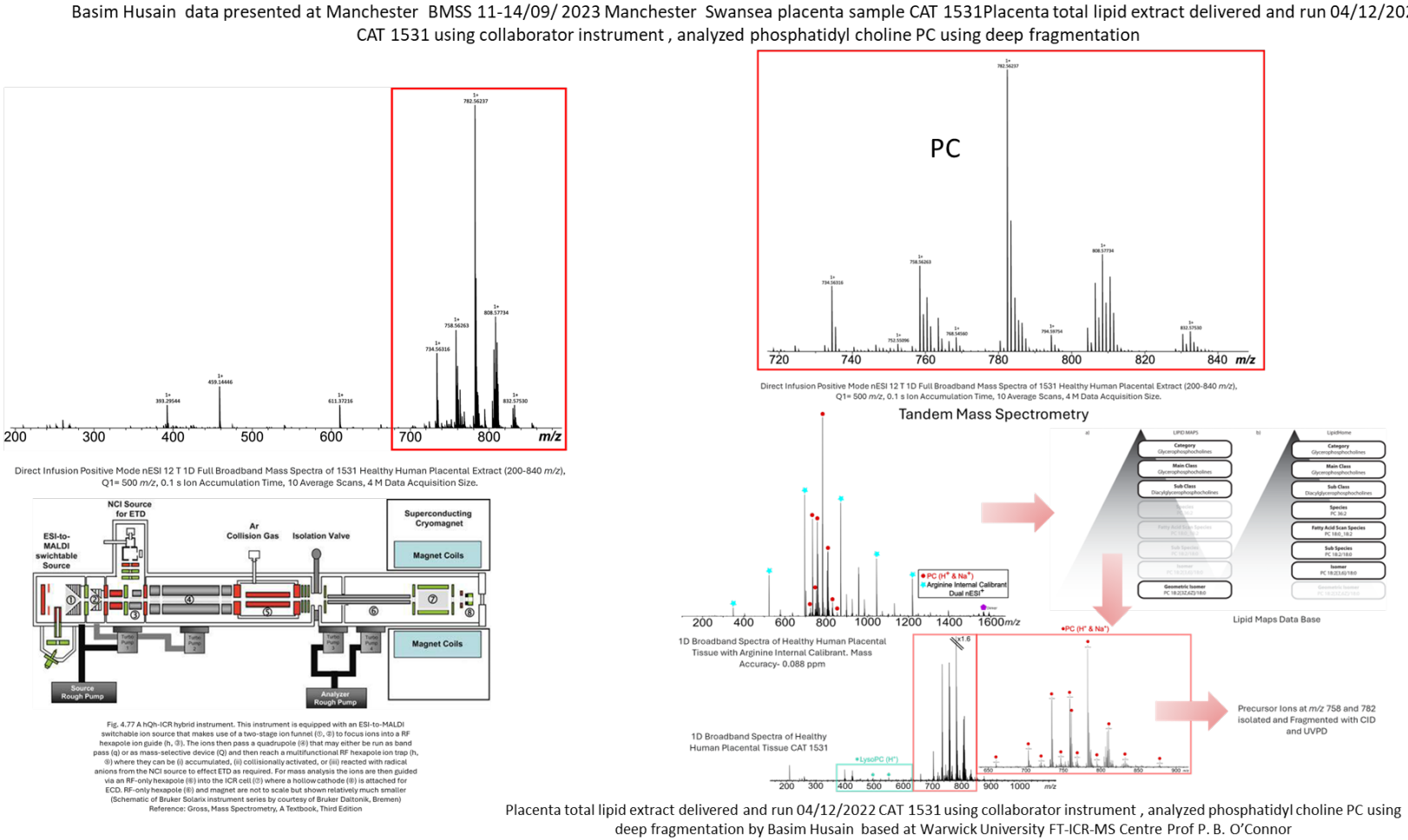

Figure 4:25: FTICR MS/MS analysis of Swansea total lipid extracts run by PhD student collaborator Mr Basim Hussain at the University of Warwick.

Basim Husain data presented at Manchester BMSS 11-14/09/ 2023 Manchester Swansea placenta sample CAT 1531

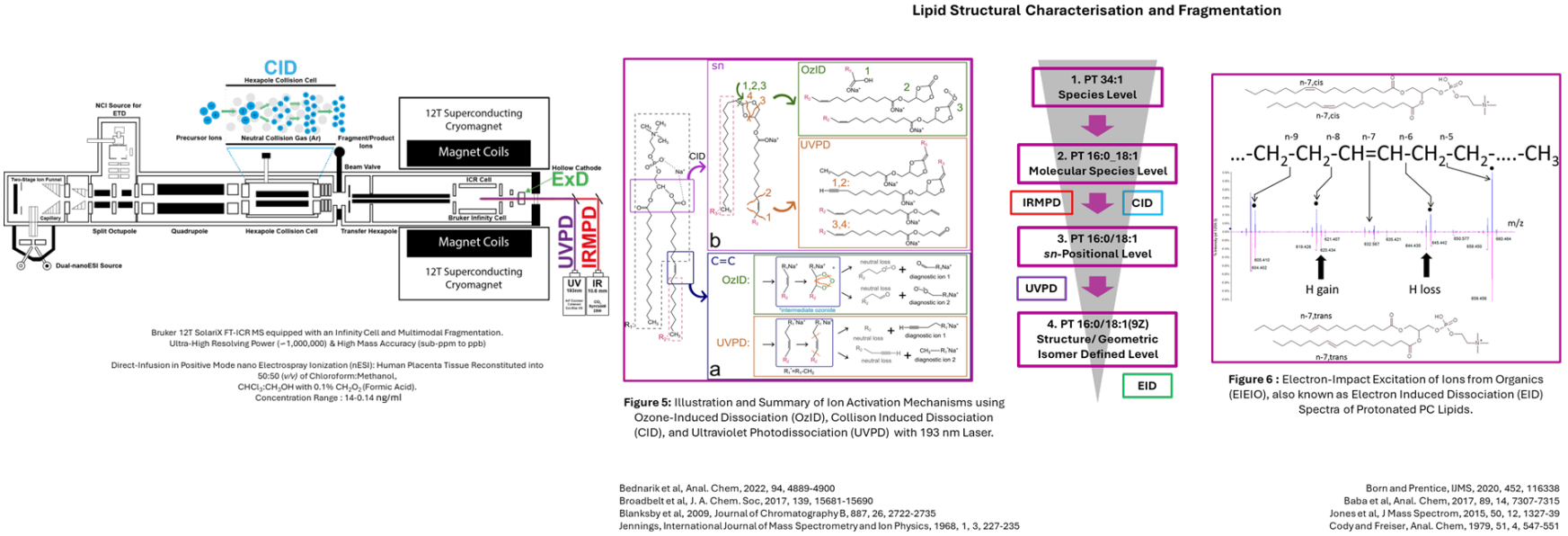

Figure 5: Illustration and Summary of Ion Activation Mechanisms using Ozone-Induced Dissociation (OzID), Collison Induced Dissociation (CID), and Ultraviolet Photodissociation (UVPD) with 193 nm Laser.

Figure 6 : Electron-Impact Excitation of Ions from Organics (EIEIO), also known as Electron Induced Dissociation (EID) Spectra of Protonated PC Lipids.

Bednarik et al, Anal. Chem, 2022, 94, 4889-4900
Broadbelt et al, J. A. Chem. Soc, 2017, 139, 15681-15690
Blanksby et al, 2009, Journal of Chromatography B, 887, 26, 2722-2735
Jennings, International Journal of Mass Spectrometry and Ion Physics, 1968, 1, 3, 227-235

Born and Prentice, IJMS, 2020, 452, 116338
Baba et al, Anal. Chem, 2017, 89, 14, 7307-7315
Jones et al, J Mass Spectrom, 2015, 50, 12, 1327-39
Cody and Freiser, Anal. Chem, 1979, 51, 4, 547-551

Placenta total lipid extract delivered and run 04/12/2022 CAT 1531 using collaborator instrument , analyzed phosphatidyl choline PC using deep fragmentation by Basim Husain based at Warwick University FT-ICR-MS Centre Prof P. B. O'Connor

Figure 4:26: Diagram of the FTICR MS/MS experiment analyses by PhD student Mr. Basim Husain based at the University of Warwick on total lipid extracts from the placenta of an obese placenta CAT 1531 patient. Basim utilised UVPD, IRMPD, and CID collision-induced dissociation MS/MS. Using CID, Mr. Hussain was able to identify the headgroup and the lipid sidechains, and using UVPD and EDD, he was able to determine the double bond position on those same lipids.

4.6 Discussion

Most lipids are readily observable by MALDI MS in the negative ion mode; the only lipid groups observable in the positive ion mode using 9AA or DHB are PC and LPC, sphingolipids, sphingomyelins, which are choline-based, also ceramides that belong to the same family with acidic groups which can help to stabilise protons. The negative mode is best for most phospholipids, inositol, serine, ethanolamine, glycerol, cardiolipin, as well as gangliosides and many more sulfatides and other molecules that are not identified as they are outside MALDI ToF MS limits of detection. Although we did not have access to the equipment for such studies, we expect that more sensitive mass spectrometry techniques using atmospheric pressure ionisation and tandem mass spectrometry for MRM and SRM studies would work very well for detection and potentially for quantitation of these lipids, provided sufficient effort was made to develop the methods and quantitative calibration curves. Furthermore, the MALDI results show a need to be able to observe ions at lower *m/z* ranges, where matrix peaks dominate MALDI signals. Also, many fragment ions, such as the phosphate headgroup of PC lipids at 182 m/z, would be difficult to detect in a MALDI experiment due to the dominance of matrix peak signals in the low m/z region.

There are many opportunities to further develop these studies with the right approach and collaborations with specific bioanalytical techniques to quantify all phospholipids, neutral lipids, sterols, cholesterol esters, cholesterol sulphates, and especially cardiolipin, which are overwhelmingly negative in the matrix 9AA, in negative ion mode and the negative ion DHB, especially in obese and placentas with GDM, but not in the healthy placenta—presence of glycolipid gangliosides in the obese placenta and GDM in negative ions. An example is the collaboration with the Warwick Mass Spectrometry Centre shown in the figures above work by PhD student Basim Hussain, who presented his work at an international mass spectrometry conference in the USA and UK twice, and the Warwick -Swansea collaborative publication is in due future to come.

The PC/LPS ratio was explored as a measure of global inflammation as per early literature indicators as a pro-inflammatory biomarker. The results in figures 4.16-

4.18 show a trend that PC/LPC ratios generally rise from healthy to obese to GDM patients and are much higher than the bulk PC/LPC ratios in the plasma of non-pregnant donors. Plots 4-6 in Figure 4.14 show a different trend, which we speculate is due to the tissue sampling being done close to the umbilical cord, which likely is impacted by the increased blood flow in that region.

The literature and all pathological studies of human placenta tissue have noted that the biological integrity of the placenta rapidly degrades and processes within 40 minutes from vaginal delivery. *(588)* Physiological and hormonal factors influence the levels of lyso-glycerol-phospholipids (LGPs) and lyso-sphingoid-phospholipids (LSPLs) during healthy, obese, and gestational diabetes mellitus (GDM) pregnancies. Alterations in lysoglycerophospholipids and also-sphingoid-phospholipids during healthy, obese, and GDM pregnancies indicate the complex interplay between lipid metabolism, hormonal changes, and metabolic disorders. GDM's impact on lysoglycerophospholipid levels underscores their potential as biomarkers for GDM. It highlights the need for further research to elucidate these alterations' underlying mechanisms.

LPC species levels are reduced in obesity and type 2 diabetes *(589)*. LPCs, which are lipids associated with pro-inflammatory and atherogenic conditions, are increased in obese individuals *(590)*. Studies have confirmed that obesity alters LPC species, especially LPC 16:1 *(591)*. LPCs decrease in obese individuals experiencing chronic pain *(592)*. LPCs in early pregnancy are also associated with GDM risk in Chinese women, suggesting that LPCs may mediate disease risk*(593)*. Obesity and changes in LPC levels have also been linked to inflammation and metabolic syndrome *(184, 594)*. A study showed a significant decrease in brain phosphatidylcholine after an ischemic stroke, indicating a potential role for LPCs in neurological disorders *(595)*. A possible biomarker for GDM risk assessment is LPCs in early pregnancy, which are differentially associated with GDM severity (Wang et al., 2022). Pregnant women with insufficient insulin production develop GDM *(596)*. There has also been evidence that serum levels of specific LPC species are lower in GDM patients than in normal pregnant women *(597)*. Pregnant women with GDM exhibit decreased levels of LGPs, particularly lysoglycerophospholipids, in their plasma *(598)*. Such an observation was also confirmed with studies on type

2 diabetes (T2D), indicating a potential link between altered LGP levels and cardiovascular disorders *(599)*. Additionally, metabolic profiling of women with GDM and their offspring has revealed decreased circulating glycerophospholipids, with lysoglycerophospholipids being the most prominently affected during pregnancy and postpartum *(599)*.

Further proof that LPC levels are associated with obesity comes from animal models that show reduced levels of unsaturated LPCs *(600)*. Besides metabolic control, LPCs are involved in immune response modulation and parasite transmission regulation *(601, 602)*. LPCs induce endothelial nitric oxide synthase downregulation and abnormal vascular reactivity, implicating them in cardiovascular health *(603)*. LPCs cause arrhythmias similar to ischemia-induced ones *(604)*. Therefore, analyses that study placenta tissue require coordination with the medical ward to prepare the placenta organ immediately after birth, keep it on ice, and wash it with PBS saline.

Future studies would also be useful in studying total lipid content in whole blood compared to the already isolated plasma. Full blood samples at the time of collection were limited by return after the COVID-19 lockdown, so the priority was researchers who investigated cell work. As this project's main focus was initially on the placenta, the separated and given plasma was only provided if there were enough blood samples to share. Using full blood instead of already separated plasma comparison would be beneficial in observing comparative total lipid extract from full blood, then from already separated plasma. For the total lipid extract as an initial groundwork discovery study, this work has provided a wide area of information on the total lipid composition in the human placenta. The placenta is almost like a sponge that absorbs and filters out all metabolic nutrients.

4.6.1 Conclusion

Part of this project involved testing the hypothesis that PC/LPC ratios are correlated with adverse pregnancy outcomes, but the samples were only provided noting the body-mass index of the mother and the gestational diabetes status of the mother. Therefore, the plots in figures 4.16-4.18 instead show that there is a general, but not a fully consistent, correlation between rising PC/LPC ratios from healthy to obese to GDM patients. Given that the trend is not fully consistent with healthy vs obese vs

GDM, much less the unknown parameter of adverse pregnancy outcomes, it is not clear that PC/LPC ratios are a true and diagnostic biomarker for such outcomes. More specific sample information must be provided to fully test that hypothesis, including the occurrence of said outcomes, blood analysis of cholesterol, LDL, and HDL, and, ideally, some information about the patient's diet. This research work confirms higher levels of PC/LPC in plasmas from obese GDM patients (GraphPad plot nr.10) indicative of metabolic disorders when compared with other literature findings as per study finding of the group co-colleague Rees et al. 2023 *(115)*. An example of collaboration with the Warwick Mass Spectrometry Centre FTICRMS is in the above figure by PhD student Basim Hussain, showing his work of detailed lipid characterisations that can be done on each lipid group species with fragmentation. It is necessary to confirm the structures by verifying the position of double bonds in fatty acids' chemical structure. Only then can it be said by confirming which PC it is, 18:1 or 18:2, seen in the placenta's or plasma's total lipids. Depending on the researcher's needs, this detailed structure can enhance confidence in identifying or discovering structurally lipid biomarkers.

The cost of performing such data analysis externally by an outsourced company is approximately 1200-1500 pounds sterling GB per sample, excluding a comprehensive study and explanation. Educational collaboration with lipidomics experts would be very helpful, and these goals are achievable. It takes much effort and dedication to ensure that the sample preparation for placenta extraction is clean, reproducible, and observable by thin-layer chromatography. The repeatability, consistency, and accuracy of MALDI peaks are compared to MALDI ToF MS data analysis. Intensities always vary, so they cannot be considered absolutes. This method is partially semi-quantitative, using relative percentage measurements to indicate the lipid groups present in the sample and mass spectrum, assuming the isobaric head group overlaps the glycerophospholipids such as PC, LPE, and PE.

Several liposome species contain NH4+ choline PC head groups in glycosphingolipids, sphingomyelin, and ceramides. This study identified lipids by analysing the literature, which is a helpful starting point for the next researcher. If they choose, they can promote LC-MS/MS or other hyphenated approaches to chromatography, including gas chromatography, CC-MS, atmospheric pressure

chemical ionisation (APCI) ion source hyphenated with mass spectrometry detector, for example, present at the Swansea cholesterol specialist research group Griffiths laboratory showing cholesterol-related analysis is of interest which would enhance value to the placenta lipidome since cholesterol related oxidised sterols 3-beta-hydroxysteroid dehydrogenase was learnt and discovered. *(605)* Its carriers, such as HDLP, LDLP, and blood, are abundant in the placenta and plasma. *(606, 607)* Many studies have compared full glycerophospholipid fractional analyses, for example, not just PC/LP, but all the phospholipids comparison bar chars as a graphical representation, a standard approach in the literature. To conclude, this work has achieved a reasonable quality of bioanalytical sample preparation and extraction, as confirmed by TLC and MALDI ToF MS and enhanced by the Warwick collaboration. It suggests the method is good enough and needs more analytical work to answer more actual biological questions. Future collaborations are needed and appreciated to expand this work further.

Chapter: 5 MALDI Imaging

5.1 Introduction

MALDI Imaging Mass Spectrometry (MALDI IMS) has provided several key insights into the role of lipids in placental function based on literature insights. The MALDI IMS visualizes lipid localization within placental tissue structures at high resolution (typically 10-50 μm). It is possible to map lipids to specific areas of the placenta and particular types of cells. It has been shown that dynamic changes in lipid distribution and composition during pregnancy can be revealed using MALDI IMS. Researchers found that the distribution of several phosphatidylserines PS, phosphatidylinositols PI, and phosphatidylglycerols PG varied from days 4-8 of pregnancy in mice. It has been demonstrated that specific lipid localization is related to significant biological processes. During embryo implantation, arachidonate-containing PE lipids correlate with prostaglandin signalling enzyme expression. It has been shown that the placenta's lipid composition varies across its various regions using MALDI IMS. Studies have found that 12 lipid groups (largely phosphatidylcholines and sphingomyelins) differ significantly between the chorionic plate and basal plate, with the basal plate showing higher abundances of most of these lipids. Apoptosis-response regions were localized to docosahexaenoate-containing PE lipids, while angiogenesis regions were localized to oleate- and arachidonate-based PE lipids. It has been possible to examine the distribution of Phosphatidylcholine PC species in placental tissue by MALDI IMS. Using MALDI IMS, lipid changes associated with pregnancy complications or placental pathologies could be detected, potentially identifying new biomarkers or therapeutic targets. The findings of this study provide evidence that MALDI IMS can be a powerful tool for understanding the complex roles of lipids in the structure, function, and development of the placenta during pregnancy, and it is an exciting prospect for future research in this field *(236, 237, 608, 609) (238, 610)*.

5.2 Rationale

To develop methods for placenta lipids density maps using MALDI Imaging.

5.3 Materials and Methods

5.3.1 Samples and ethics (as per Chapter 2, section 2.3.1)

See chapter 2, section 3.2.2. All reagents, materials and equipment used for the work described in this chapter are summarized in Table 3.1. All sample and ethical approval as described in Chapter 2, section 2.3.1

5.3.1.1 Sample collection

A critical limiting factor in these experiments is tissue integrity. The placenta from a caesarean birth should go immediately in a plastic bag and be stored on ice awaiting collection to avoid tissue lysis.

5.3.2 Sample preparation

The placenta is a soft tissue that must be frozen and sectioned before generating mass spectral images. Snap freezing, also known as flash freezing, is a rapid cooling process that lowers samples to temperatures below -70 °C and involves using dry ice or liquid nitrogen to achieve a rapid freezing rate. Snap freezing using a pre-cooled module flask, such as the one shown in Figure 5.1, ensures that the freezing process occurs efficiently and maintains the molecular integrity of the samples. The placental samples undergo proper cleaning, washing, cutting, and efficient freezing, ensuring the minimisation of contamination and preservation of the molecular integrity of the tissue. To avoid oxidation, strict handling procedures should be followed. Tissue frost burning is a risk, but rapid freezing minimises that risk, depending on the size and density of the tissue. A fast freezing process minimises ice crystal formation. The frozen sections can follow immunochemistry, enzyme detection, and in situ hybridisation.

Fresh placental tissue is first prepared and washed thoroughly with PBS for flash freezing, as described in Chapter 2. Section 3.2.2 to remove any blood. It is then dried gently on tissue paper before cutting into small chunks, approximately 1 cm^3.

A chunk of tissue is washed in PBS, a small globe chank, pad dry, the blood and weighed, wrapped in aluminium foil and with a silver tweezer placed on a thermo flask containing dry ice slurry with isopentane and the small aluminium parcel wrapped inside tissue placed gently on the white weighing bat and onto the dry ice slurry or if liquid nitrogen just put into fumes holding with long tongues. It is not compulsory to use liquid nitrogen for immunohistochemistry. For MALDI imaging, yes, but anything with dry ice is fine. Then, After freezing, wrap it tightly in aluminium foil to protect it from oxidation and place it in a plastic box inside a dry ice box (the foggy atmosphere generated by the sublimation of carbon dioxide ice is also helpful for reducing reaction with atmospheric oxygen). The labelled box with appropriate identifiers is promptly transferred to a freezer (-80 °C) until it is ready for cryostat cutting.

If using isopentane instead of dry ice, prepare a box full of crushed water ice and add 50-100 ml of isopentane to create a slurry. The tweezers place the wrapped tissue chunk on top of the slurry. It is crucial to ensure that the fresh placenta tissue is not wet but pad-dried and kept on an ice box protected with white weighing boats (top and bottom) to prevent air exposure and dust contamination of the surrounding tissue. Following these procedures, one will have frozen chunks of placenta tissue embedded in optimum cutting temperature polymer gel clear white gel to hold tissue onto the holder mounting (OCT), a clear white gel ready for cutting on the cryostat.

Dr Angelini was the overseeing supervisor, and we followed his suggestions as a learning point. Firstly, freezing tissue in gelatine, but getting out of the tube was difficult. One is frozen, so you must break the tube from -80C, which is difficult. I would not recommend that, and then gelatine interferes with the sample. It is probably best to freeze on dry ice slurry. I have recommended plenty of literature and Tissue Bank UK to search and read up more on tissue freezing, as it is very important from birth that it needs to be immediately placed on ice, not in the box waiting in warm. So the alternative was to learn and ask around how to flash freeze and learn by trial and error. I have learned that way. Dr Angelini explained to put a dry ice box in a silver dish and gently place dry ice and some isopentane on the button. I tried that approach until I learned how to do it by making mistakes and burning the tissue. Learning takes a few trials, but it is fast and easy once you practice

it. I did not know any other method, only through reading papers, and until you do it yourself by your hand, you get a feel for it. Reading papers does not give you that feeling. Nobody has advised or suggested how to freeze. I asked Dr Owain, and he explained to wrap it up in aluminium foil, use dry ice, and keep practising, similar to cryostat cutting.

I am unsure how to decide as I have only done one or twice, a few and then spent a week on cryostat cutting the same tissue 100 times. That is the hardest part. By imaging, academics may offer their learned help to guide new students. OCT tissue freezing medium aqueous based. Leica tissue freezing medium, cutting blades, brushes, and all specialist supplies for tissue imaging. Leica Biosystems Microsystems UK, Histopathology instrumentation , Berkland. The placenta tissue was prepared in 5% pork teleostean gelatine (G7765 and G7741 r Sigma Aldrich Merck Life Science UK) for freezing and cutting prior to chemical staining and for MALDI Imaging mass spectrometry. The representative images from A-T in the image figure are visual method steps for sample preparation, freezing and cutting. The placenta's left side in Image A is ideal for cutting and washing. Look for the striped patterns observed in images B and C—a 5% porcine gelatine solution on dry ice in the falcon tube sample hole. The sample is placed into the falcon tube filled with gelatine. Image E. Wait until the sample freezes, and move the sample to the -80 °C freezer for storage. The sample is removed from the freezer, cut from the frozen gelatine, and attached to the cryostat stage holder using dropwise amounts of OCT solution to freeze it into the holding stage sample holder. The sample holder can adjust the level and height to move the sample to the cryostat-cutting stage. With practice, the angle and speed control are adjusted by manually turning the nob (images I – J) to generate 10 μm tissue slices.

5.3.3 Sample cutting and slide selection

MALDI-ToF mass spectrometry requires a conductive substrate to prevent static charging during ionisation, causing potential drift and reducing mass resolution. Therefore, MALDI imaging used conductive indium tin oxide (ITO) slides (add supplier details). Carefully hold the slide, with gloves, on the sides to avoid contamination of the front surface, and mark the frosted side of the slide with a pencil

to label it with the sample reference information. The frozen placental tissue is retrieved, and the OCT can be removed with a scalpel before the bare tissue is attached to the cryostat. Using new, clean scalpels and tweezers is critical to avoid sample cross-contamination.

The tissue is then cut into slices 10 micrometres (μm) thick. Prepare the thermo flask with crushed ice and place the thermo conductive tray platform into the ice until water vapour collects on the surface. Allow it to cool until condensed. Note that adding isopentane causes it to become hot. Alternatively, use Liquid nitrogen; dry ice is much easier. If liquid nitrogen is used, the tissue should remain submerged in the liquid nitrogen for at least 30 seconds or until the liquid nitrogen boiling minimises. Before cutting the placenta chunks of tissue on the cryostat, the tissue should be allowed to equilibrate to the cryostat temperature (-18°C). The placenta tissue is ready for the cryostat for cutting *(303, 507, 611-613)*. Before freezing, cells and small tissues can be mixed in an inert support medium such as an optimal cutting temperature [OCT] compound. These references provide in-depth information on cryosection protocols *(611, 614-616)*. For mounting on the ITO glass slides, use a clean glass slide to touch the front surface to the tissue slice, using capillary action and freezing to attach the tissue to the slide, being sure to use gloves and hold the slide along the edges only to avoid contamination. The slide is lifted as in image L and placed into the dry ice box filled with dry ice so that it is under a carbon dioxide atmosphere to avoid reaction with atmospheric oxygen. Then, cut a slice of placement tissue on the stage and press it onto the slide.

5.3.4 Slide preparation for MALDI Imaging

Describing photographic images that were taken during the actual learning of experiments and kept specifically towards this thesis as a visual aid with the content, these include figures from (Figures 5.1 to Figure 5.6). Once the tissue is embedded on the ITO slide, preserved in the holder box, and kept at -80C till ready for instrumental analysis, the next steps are to prepare the slide for matrix spaying and imaging and be careful not to contaminate the slide. Firstly, take it out of the -80C freezer into the dry ice box and keep the temperature constant; it is a very important deep ice box. Place the slide into the plastic chamber and put it into a cassette slide

holder. The plastic bubble chamber is filled with silica granules as the drying agent. This step aims to remove all the humidity from the tissue with air suction on floor 3 in Professor William Griffiths' laboratory air vacuum pump. Set it to 180-220 air suction until it reaches the number and seals the chamber.

5.3.4.1 Preparing matrix for tissue spraying

Matrix solution: cyano-4-hydroxycinnamic acid Sigma Aldrich CAS number: 28166-41-8; code: 70990-1G-F 30mg of matrix powder into 6ml matrix delivery solvent (30% water; 40% IPA; 30% ACN) matrix solution concentration of [5mg/mL]. Before removing the matrix mix from the sonicate, completely dissolve the powder. The next day, MALDI MSI allowed the desiccator to reach room temperature. The slides were sprayed using an alpha-cyano-4-hydroxycinnamic acid (CHCA) MALDI matrix.

5.3.4.2 Prepare the sprayer

The HTXTM-Sprayer (HTX) was used to spray CHCA Technologies, NC, USA) at 5 mg/mL in water: propane-2-ol: acetonitrile (3:4:3, v:v:v) at a flow rate of 80L/min and a linear velocity of 1200mm/min, with a line spacing of 2 mm and with a crisscross deposition method that alternates vertical and horizontal passes. The matrix density is 1.3 mg/mm2. The sprayer nozzle was heated to 70 degrees Celsius for faster solvent evaporation.

5.3.4.3 Prepare the slides

Mark them with White Tippex, leaving around 2mm between them so the slides can be taped to the matrix sprayer without touching the tissue. Use the Epson scanner to scan each slide, one slide at a time, using white paper to border each slide. Save the scanned images to MALDI Imaging.

5.3.4.4 Spray the matrix.

To do this, turn on the computer, plug it in, and click on the desktop - do not open the software. Remove the attachment from the syringe, remove the air bubbles from the lines, and push the solvent through the waste tube. Make sure no air bubbles are

moved in. Set the air pressure at ten psi. Turn on the sprayer unit (press the start button on the left of the unit) and set the valve to LOAD. On the computer, launch TM-Sprayer. To use more than one slide, change the bottom margin (to 35 for two slides) and change the operating temperature to 70°C by selecting the load method previously used and saved as "Roberto-CHCA-07" and plate (Std. Glass Slide). Put sellotape over the slide, making sure it does not touch the Tipp-Ex crosses and does not move. The sprayer needle must be crystal-free; if so, use 100% methanol on a cotton bud to remove the crystals. Wait until 70°C, and check if it sprays a circle.

The matrix solution must be loaded into the machine in 5ml syringes. Keep the valve in the load position. Upon loading the matrix, the valve should be converted to the SPRAY position, waited 25 seconds, and then sprayed. White tissue under the sprayer should be held for 15-20 minutes. Put the slides in a desiccator under a vacuum, peel the Sellotape off the white sand, and prepare the stand for MALDI (clean stand with 100% MeOH). The machine should be shut down as instructed.

5.3.4.5 MALDI Flex Imagine Set the sequence

The lower the resolution, the better the Image, but the longer it takes. Create an original sequence with Flex Imaging software and save it as date_name.mis (2024-01-24-ECP-CAT1535). Place the three marks on the Tipp-Ex crosses using the scanned Image and the slide coordinates. Make sure the methods are correct before defining the first measurement region. Save the sequence (Imaging_name_region1.xml) and auto-execute it. Note how long it takes to image each region and record it in the facility logbook. Make a second measurement region and delete the first. Name the sequence name_region2.xml, and save the auto-execute sequence. Adapt the method if necessary for the remaining areas. Repeat the above steps if there are other slides. Lastly, start the batch runner with the auto-execute sequence.

5.3.4.6 Imaging by mass spectrometry

Before any analysis, the mass spectrometer must optimise several parameters driving ionisation and detection. MLDI-TOF vacuum parameters are set up, as well as laser and data acquisition. The experiments were conducted on an UltrafleXtreme MALDI

TOF MS and MS/TOF mass spectrometer operated in reflectron mode and positive polarity (Bruker Daltonics, Bremen, Germany). The mass spectrums were automatically acquired in the m/z 400–1000 range using Flex Control (Bruker Daltonics) software. Bruker Daltonics FlexImaging 4.1 software (small laser focus) set the spatial resolution to 50 nanometres (nm).

5.3.4.7 Laser power

Laser power was tuned to optimise the signal-to-noise (S/N) ratio without distortions of the baseline at 80% of maximum with Global Offset at 5%, Attenuator Offset at 40%, and Attenuator Range at 40%. The laser spot measures about 50mm in diameter, according to factory specifications and confirmed by visual inspection. Among the voltages used for the extraction were IS1 20.00 kV, IS2 17.90 kV, Lens 8.50 kV, Rfl 21.10 kV, and Rfl2 10.95 kV. A 3.0X reflector gain was set and timed at 160 ns, Pulsed Ion Extraction. Ion suppression was applied up to 375 m/z. A raster was sampled with 200 shots in 5 steps for 1000 shots. An average of 11.5 hours was spent acquiring 27000 positions and 24000 MB of data.

5.3.4.8 Calibration

MALDI was calibrated with phosphatidylcholine and lysophosphatidylcholine (Avanti Polar Lipids) of known compositions and with mass ranges in the target ranges. 20 ppm deviation is typical. Spectra were recalibrated using the batch process after measurement. The data were analysed and visualised using FlexImaging 3.0 (Bruker Daltonics) and SCiLS Lab 2014b (SCiLS, Bremen, Germany). [2H7]Cholesterol data were visualised with “window” (ISTD) normalisation at 525.4. The mass filter width was 0.5, typically resulting in a mass resolution of 20000 grains per unit width.

5.3.4.9 Laser Nd: YAG technology smart beam

Neodymium-doped Yttrium Aluminium Garnet (Nd:YAG). In laser technology, it is a solid-state laser crystal. Neodymium ions (Nd3+) are added as dopants to a synthetic crystal composed of yttrium, aluminium, and garnet to make YAG lasers. Near-infrared Nd: YAG lasers emit light with a 1064 nanometres (nm) wavelength.

The Nd: YAG laser is versatile and operates in pulsed and continuous modes. These lasers can produce high-energy laser pulses applied in laser surgery and therapy for skin conditions, eye disorders, kidney stones, vascular lesions, pigmented lesions, tattoo removal, and hair removal. These devices can deliver short, high-intensity laser pulses, making them ideal for precision and power applications. A Q-switched Nd-YAG laser produces extremely short, intense light pulses important for laser rangefinders and laser-induced breakdown spectroscopy (LIBS). Below (Figures 5.1 to 5.6) is a photographic collection of images from experimental work as learning points towards the future. They are included here to provide a visual representation of the narrative context. Literature reference on MALDI Imaging tissue biospecimen method challenges in clinical settings and direct analysis *(301, 304, 332, 611, 617-623)*

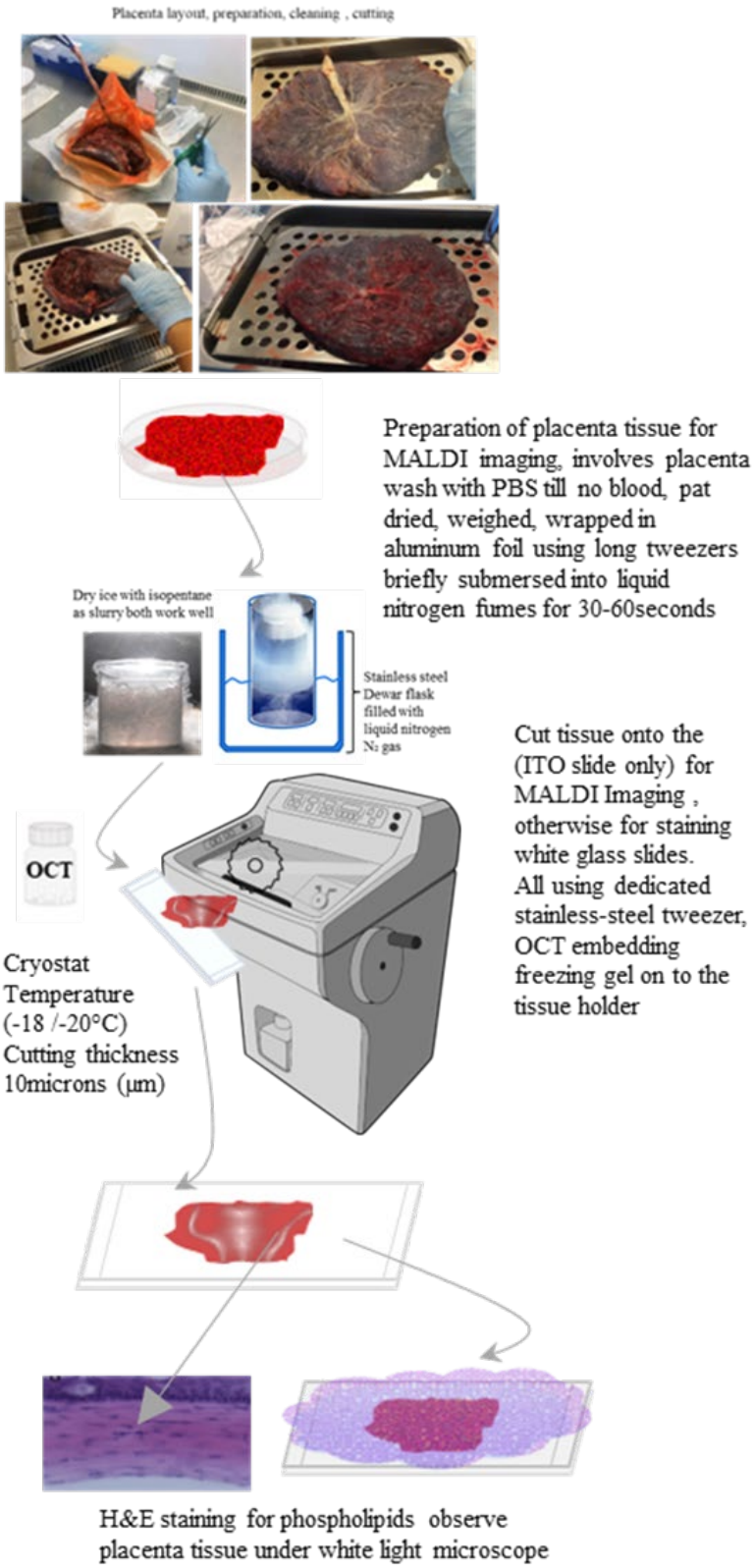

Figure 5:1: Flash freezing of placental tissue prior to cryostat cutting and embedding onto the slide for chemical staining and MALDI imaging.

5.3.5 Observations and results

5.3.5.1 Literature on tissue flash freezing

The study of placental biology and pathology can be enhanced with immunohistochemistry (IHC). IHC has been used in several studies to examine placenta cellular components and molecular markers. IHC studies certain proteins, such as Notch family proteins *(624)*, NADPH oxidase isoform 1 (Nox1), and TonEBP, has been studied by IHC in the placenta and pregnancy complications*(625)*. Furthermore, IHC uses specific antigens to obtain insight into cellular processes, apoptosis, and hypoxic conditions within the placenta, including granzyme B (GrzB) and caspase-3 *(624)*. In addition, IHC has been applied to examine infectious agents and their effect on the placenta. Studies have used IHC to detect bacterial antigens, such as Coxiella until *(625)*, and specific pathogens, such as Leptospira *(626)*, demonstrating how IHC can be used in placenta infection evaluation. In addition, IHC has proven useful in examining placental anatomy and molecular characteristics under various pathological conditions. As part of the study, collagen fibre architecture was assessed *(627)* and apoptosis in infected placentas and preeclampsia markers. IHC has also been used to study the impact of placental pathology on later health outcomes, such as white matter damage and cerebral palsy *(628)*. The literature shows how IHC can investigate protein expression, infectious diseases, structural characteristics, and maternal and fetal health outcomes due to pathology *(629-631)*.

5.3.5.2 What has been learnt?

Literature offers many different techniques, and prior expert knowledge is required to follow the appropriate protocols depending on what molecular species we want to learn. The student learning knowledge came from reading around literature and trying to ask questions of more experienced users in the lab but without any success. It was a self-exploratory learning journey, and the initial trial was freezing placenta tissue in the gelatine solution of 5% porcine gelatine in methanol prepared using the plastic tube 50ml, the same as for blood separation. The 5% gelatine was prepared by weighing the gelatine powder, dissolved in analytical grade LC-MS methanol, and placed in a dry ice box in the container until the solution was semi-permeable.

Gently use tweezers, submerse it into the gelatine, and let it sit naturally on the ice box. Place the lid and keep it at -80C till ready for cryostat cutting. Please keep it on ice and cut the tube carefully with a knife. Please do not destroy the sample inside; make it with a watertight marker or label it where the tissue sits in the tube. Do not destroy it when breaking the tube later. Dr Angelini showed and taught this process based on his past knowledge and experience. The second trial was preparing tissue by flash freezing per freezing protocol. Dried weighed tissue was wrapped in aluminium foil and gently placed on a dry ice slurry containing isopentane. These newly flashed froze on dry ice slurry placenta samples were conducted and embedded onto the ITO slides, and they only ran once on the instrument before the instrument breakdown. The results presented here are from this flashed-free sample, not gelatine, as there was too much interference in data acquisition, and the spectra were unresolved to identify anything.

5.3.5.3 Protocol setup to snap-frozen a biospecimen.

This work describes the method and development of standard operating procedures (SOPs) for flash-freezing human tissues, biospecimen organs, and the placenta. A representative collection of photographic and schematic diagrams and figures starting from (*Figure 5.2 to Figure 5.7)* is specifically used to help recreate the experimental time during this research. It is here as a visual aid for the reader and further research to continue and expand this methodical process.

The origins of this protocol came from medical and pathological literature relevant to human tissue processing, storage, and collection. Adapted and learned from the National Cancer Institute's Best Practices for Biospecimen Resources, this evidence-based method practice applies to all human tissues to be snap-frozen for preservation. These procedures preserve biospecimens for downstream DNA, RNA, protein, and morphology analyses. This document does not cover additional analytical endpoints, such as viability, cell sorting, drug sensitivity testing, or primary tissue culture donor specimens. A tissue-dedicated clean bench paper, plastic double bagging, sterile disposable containers and cutting instruments are needed to perform tissue cutting. It needs liquid nitrogen, a flask, and a cryogenic container (cryovial, cryomold) designed for temperatures of -190°C storage. Alternatively, freezing media include

pre-cooled isopentane with dry ice, dry ice alone, and a -80°C freezer. Record pre-acquisition data whenever possible.

The integrity of the biospecimen may be compromised. The data may include references and BMI. For each placenta tissue organ dissection, cryogenic containers are pre-labelled and arranged. Organization and labelling of specimen containers are essential. Segregate healthy and diseased tissue samples (tumour and normal tissues) according to BMI groups of patients. When cutting tissues, use disposable scalpels and forceps. Cutting and tissue dissection should be performed on wet ice in a sterile container immediately after placenta release from the hospital to minimize cold ischemia. Ideally, the hospital could place the placenta on an ice box until collection so it does not sit on the warm shelf. It should take less than 2 hours from tissue biopsy and be placed in cryogenic specimen storage if thicker than 1cm. Specimens can be prepared for morphological analysis before freezing, and an OCT medium is used; however, it is not required but is suitable for some molecular analysis methods.

An ideal cryogenic specimen storage container should be frozen in LN2 vapour. Stainless steel beakers can be suspended inside benchtop Dewar flasks pre-filled with LN2. Once the specimen storage container is inside the steel beaker, it should stay there for 2 minutes or less. Alternatives to freezing in liquid nitrogen vapour include immersion in liquid nitrogen or isopentane pre-cooled to -80°C. Alternatively, isopentane pre-cooled with dry ice or placed in a freezer at -80°C may be used. It is advisable to avoid freezing specimens directly on dry ice for morphological analysis. Biospecimen transfer and storage are recommended to store cryogenic specimens in a liquid nitrogen vapour freezer after freezing. Without liquid nitrogen, specimen storage containers can be stored at (-70°C). Alternatives include placing frozen specimens directly on liquid nitrogen shippers for immediate transport. It is recommended that specimens should stay in liquid nitrogen vapour before and during transfer to a repository or long-term storage. Without liquid nitrogen, specimen storage containers can be shipped on dry ice. Dry ice should be used before and during transporting specimen containers destined for storage at -80°C.

5.3.5.4 Tissue preservation and analysis

Ischemia, freezing methods, and storage conditions are discussed in the literature to give valuable insight into the preservation and analysis of tissue samples. The findings emphasize the importance of minimizing ischemia time, choosing appropriate freezing methods, and considering the impact of OCT embedding. Tissue specimens may also be affected by storage temperature and shipping conditions. These references support the key findings on tissue preservation. These include tissue preservation impact on microbiota, RNA integrity, cryopreservation methods, tissue procurement procedures, RNA integrity, gene expression, and morphology in breast cancer. They contribute to developing an evidence-based protocol for snap-freezing human placenta organ samples. Considering tissue integrity and downstream analysis should be part of the evidence-based protocol for snap-freezing human placenta organ tissues. Molecular components and tissue integrity are preserved by snap freezing (Fouhy et al., 2015). A study by Hatzis et al. (2011) demonstrated that samples preserved in RNA later had improved RNA integrity and greater RNA yield. The Leidenfrost effect can also adversely affect snap-frozen samples (Wieser et al., 2022). A genome-wide analysis of nucleic acids requires optimized collection procedures for the success of basic molecular research using biospecimens (Wolfe et al., 2014). Careful consideration of integrity in tissue management procedures is crucial for preserving RNA, gene expression, and morphology (Kap et al., 2015). The references complement each other in emphasizing the importance of maintaining tissue integrity and molecular components during snap-freezing. Gene expression and morphology are influenced by tissue procurement procedures and the effects of freezing on RNA integrity and yield.

5.3.5.5 OCT embedding effect:

It is not reported that OCT-embedded specimens immersed in isopentane pre-cooled with liquid nitrogen adversely affect PCR, RT-PCR, immunohistochemistry, or Western blot analyses. However, recent studies have found no harmful effects on PCR analysis of various amplicons with OCT embedding. Assays of receptor binding capability and other assays produce similar results between embedded and

unembedded controls. Several assays, such as the Lowry Protein and dextran-charcoal assays, interfere with OCT. Removing the OCT compound by ether-methanol precipitation or filter-aided sample preparation is possible.

5.3.5.6 The Freezing Method:

The morphology of specimens immersed in liquid nitrogen vapour within a double-walled vessel or in media is superior to that of specimens directly immersed in liquid nitrogen or on dry ice using a cooling device. Upon contact with substances hotter than the boiling point of liquid nitrogen, direct immersion in liquid nitrogen can lead to the Leidenfrost effect. The DNA, RNA, and protein yields in samples preserved in liquid nitrogen or isopentane pre-cooled to -80°C are comparable. RNA from frozen specimens can be used for cDNA library construction and other analyses after freezing at -70°C or immersing in liquid nitrogen. It is possible to compromise specimen morphology when frozen on dry ice or with carbon dioxide freeze. Tissue types may differ in their response to ice crystal formation.

5.3.6 MALDI MS image analysis

In mass spectrometry imaging (MSI), many molecules can be mapped with unmatched chemical specificity in a biological tissue slice. MSI can measure many ions simultaneously without tagging molecular targets in a single experiment. A camera creates three colour channels: red, green, and blue. Each channel corresponds to the intensity of a specific wavelength of light. MSI generates images with tens of thousands to millions of different “channels”, each representing the intensity of a particular m/z value. MSI enables the untargeted screening of thousands of biomolecules in a single tissue section. Data analysis is important because the technology generates large, complex datasets. Data from a single experiment, i.e., one tissue section, typically amounts to tens of gigabytes up to multiple terabytes. Therefore, high-throughput settings require efficient, streamlined workflows for bioinformatics to process resulting data and extract insights quickly.

5.3.7 Acquiring data from mass spectrometry imaging

Mass spectra are acquired at various points (pixels) in a tissue section in an MSI experiment. As a concept, MSI data sets are images with mass spectrums associated with each pixel. For example, how does the MALDI MSI experiment work? In brief, a tissue section is cut about 8-10 micrometres thick at a temperature of approximately (-18-20°C) and gently adjusted, making sure it does not roll, but it is flat cut directly deposited onto the stage so the blade level needs changing, and then gently pressed and mounted onto an ITO slide. Once cut and preserved, it is then covered with a chemical matrix, for example, 9AA, DHB or CHCH, which aids in the ionisation process, and placed in the slide holder marked with white crosses and inserted into the sample holder of the mass spectrometer. In each grid cell, a laser is fired after a virtual grid is laid out. By ionising molecules in that pixel, a mass spectrum is compiled for that pixel by sending those locally generated ions to the mass analyser. Each grid cell is processed separately. Ionisation methods differ slightly, but the general concept remains the same.

5.3.7.1 MALDI-MSI experiment.

First, the tissue is coated with a chemical matrix that aids ionisation. A laser is fired locally in each grid cell to ionise the tissue, resulting in localised ion mass spectra with chemical information. The grid is repeated in every cell. The stage moves quickly with MSI instruments, and the laser fires at a high rate, enabling spectra to be acquired at different locations on the section at a greater speed than with non-imaging MS instruments. It applies to instruments that acquire MSI data at a high spatial resolution, resulting in many pixels. It is often necessary to exchange between a low number of pixels measured at a high mass resolution (low spatial resolution, long measurement times per pixel) and a high number of pixels measured at a low mass resolution (high spatial resolution, short measurement times per pixel). While some non-imaging MS instruments can be made imaging-capable using custom sources, most MSI instruments operate the same way as non-imaging MS instruments. The advantages and challenges of MSI naturally map onto MS since it is based on mass spectrometry.

Nevertheless, some methods used in other types of MS cannot be used in imaging. Liquid chromatography, for instance, cannot be used to separate ingredients within a mixture. MSI usually analyses.

5.3.7.2 Mass spectrometry imagining (MSI) data.

MSI data sets are spectral images characterised by the mass spectra associated with each pixel. A standard MSI data set has three axes: spatial (x and y) and spectral (m/z). In some advanced approaches, such as ion mobility, additional axes can be added, but not covered here. The number of pixels can vary between a few thousand and several million per tissue section, while the number of m/z bins can also vary from several thousand to several million. The number of pixels can be numerically higher in SIMS, characterised by extremely high spatial resolution. In raw data, the size is determined by the pixels in the set and the number of m/z bins per spectrum. For example, consider MSI data sets with around 50,000 pixels per spectrum and 100,000 m/z bins. When stored as 32-bit floating point numbers, an intensity dataset of this size would require about 20 gigabytes (GB) of storage. Using a spatial resolution of 50 micrometres, 50,000 pixels correspond to an imaged area of 125 mm^2, i.e., a square with sides of 1.12 cm.

5.3.7.3 Background format (mathematical matrix)

Matrix representations of MSI data have rows denoting pixels and columns denoting m/z bins. Therefore, a single MSI data set is represented by the number of pixels (x) and the number of spectral bins (y), which is m/z, and each row of depth (d) is the mass spectrum of a pixel in the sample. Unlike a matrix representation, MSI data does not directly encode the spatial location of pixels (rows), but many types of data analysis do not require them. Spectral grid coordinates are also stored separately in a separate data structure. A high spatial resolution experiment usually produces a tall data matrix (many pixels, few m/z bins).

In contrast, a high-mass resolution experiment typically produces a wide data matrix (fewer pixels, many m/z bins). The shape of the data matrix can impact computer memory requirements, depending on the type of data analysis. Data analysis may require explicit realignment during MSI data analysis due to the matrix representation of m/z compartments (bins) used in the spectra columns of depths (d).

In MSI terminology, data sets with common m/z bins are called continuous data sets based on the nomenclature used in m/z.

5.3.7.4 An example of tissue obese BMI CAT 1351

The following section illustrates how MSI data can be analysed. Spatial analysis often uses complementary strategies to generate images from MSI data by slicing along the m/z axis. This research acquired MSI datasets using Bruker UltraFlex MALDI ToF MS with imaging cell instruments. In the Placenta tissue, two slides of the same CAT 1351 were deposited by spraying the 9AA matrix and DHB with a 2,5-DHB matrix. Around 500.000 pixels were collected with a sampling resolution of 10 microns. Six thousand ion images are obtained in the m/z range of 600-1000 Da.

5.3.7.5 A visualisation of biomolecule

MSI data provides an understanding of the spatial distribution of biomolecular ions by plotting the intensities for each m/z value across all pixels. In MSI terminology, this is called an ion image. An image is a heat map rendered in a colour map, so these false-colour images are sometimes called false-colour images. The below figures show three example ion images at different m/z values.

An example image of placenta tissue with obese BMI CAT 1351 shows a spectrum of the internal standard ions in Figure 5.6 in all photographic images and mass. Each m/z value in the spectrum corresponds to an ion image. With MSI technology, studying the localisation of thousands of biomolecular ions at once is possible. Other technologies, however, have a limited range of applications. There are many ways to multiplex biomolecular ion distributions on a single image. The easiest approach uses different m/z values for colour channels. As shown in *Figure 5.6,* each colour channel receives an image with multiple ion intensities.

5.3.7.6 A region of interest (ROI)

This study aims to use MALDI Imaging on placenta tissue to learn about lipids and create total lipid maps, which could be complemented with immunohistochemistry, chemical staining, and microscopy. It would allow us to correlate the lipids visually

and spatially to have better biological insights on placentas cell distribution and correlation of the placental maternal fetal sides cells to investigate the biomolecular composition of two regions of interest analysed by imaging spatial information, which is different from non-imaging MS technology. A region of biospecimen chemical interactions can be defined based on many properties, such as tumours versus healthy tissue, anatomical structures, cell types or even ions in the MSI data. It is common to pair MSI data with stained microscopy sections (usually H&E) to identify morphologically relevant regions. The regions are independent of MSI data acquisition during post-acquisition analyses, regardless of how they are defined. The Image in *Figure 5.5* shows regions of interest marked with white crosses, and a strip depth of 5mm of the whole tissue on the slide is isolated on the computer to investigate further. It is the area where the laser beam fires to acquire a signal of depth and intensity. *Figure 5.7* shows the 5mm region mean spectrum for each region. Literature includes identifying biomolecules in different regions based on chemical information given prior, and the mean spectrum of two areas is computed. The first step in non-imaging mass spectrometry analysis would have been to homogenise the tissue. As a result, the single mass spectrum would resemble a convoluted mixture of the spectra of all chemically distinct regions. That means that MSI technology enables us to select mass spectra from the homogeneous areas within tissues rather than whole organs. This method identifies molecular differences in small tissue regions for which non-imaging MS miss the signal.

5.3.7.7 Molecular isotopic detection

MSI data is a powerful tool for detecting isotopes in this final example. MS without imaging relies on assessing peaks with some statistical certainty if they correspond to an expected isotopic distribution. MSI allows one to look at ion images of all potentially relevant peaks to verify spatial consistency. Because these molecules have the same biochemical behaviour in the tissue, their spatial expression should be similar. An example of three isotopic peaks is shown in *Figure 5.7:* These peaks have 1 Da and are, therefore, likely to be isotopic. These peaks have similar spatial expressions on the ion images, confirming that they are isotopes. A higher mass resolution in the mass spectrometer allows a more confident assessment. Eventually, identification is needed to determine the analyte's nature, extending beyond this

introduction and student knowledge. The internal standard (IS) ion images in *Figure 5.7* (at 518.5 m/z and 525.4 m/z) represent the isotopic distribution of a single biomolecule lysophosphatidylcholine LPC. The mean spectrum shows the isotope distribution and each ion image has an intensity scale.

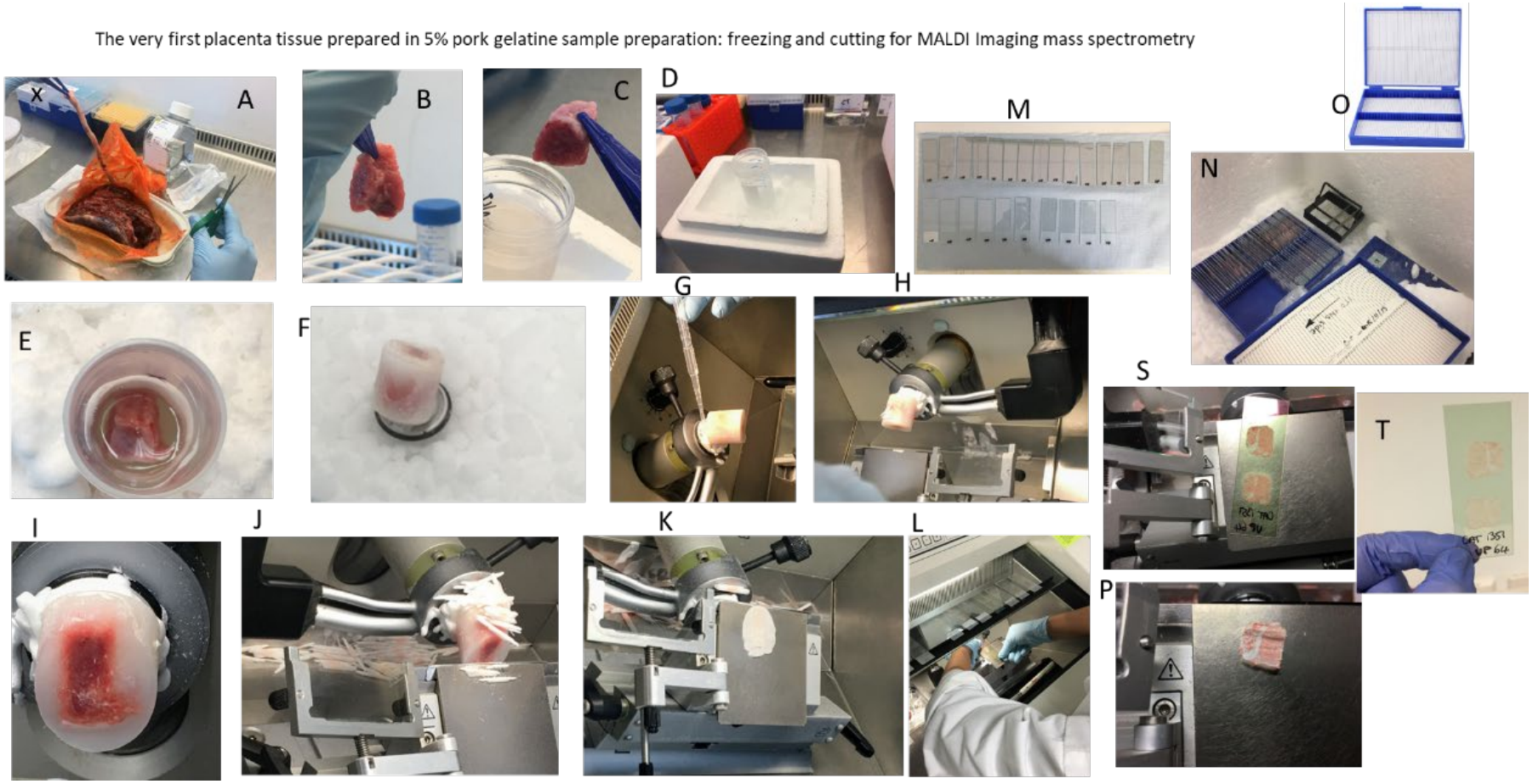

Figure 5:2: The cryotome tissue sectioning process was followed by mounting the tissue slices on ITO microscope slides for MALDI imaging.

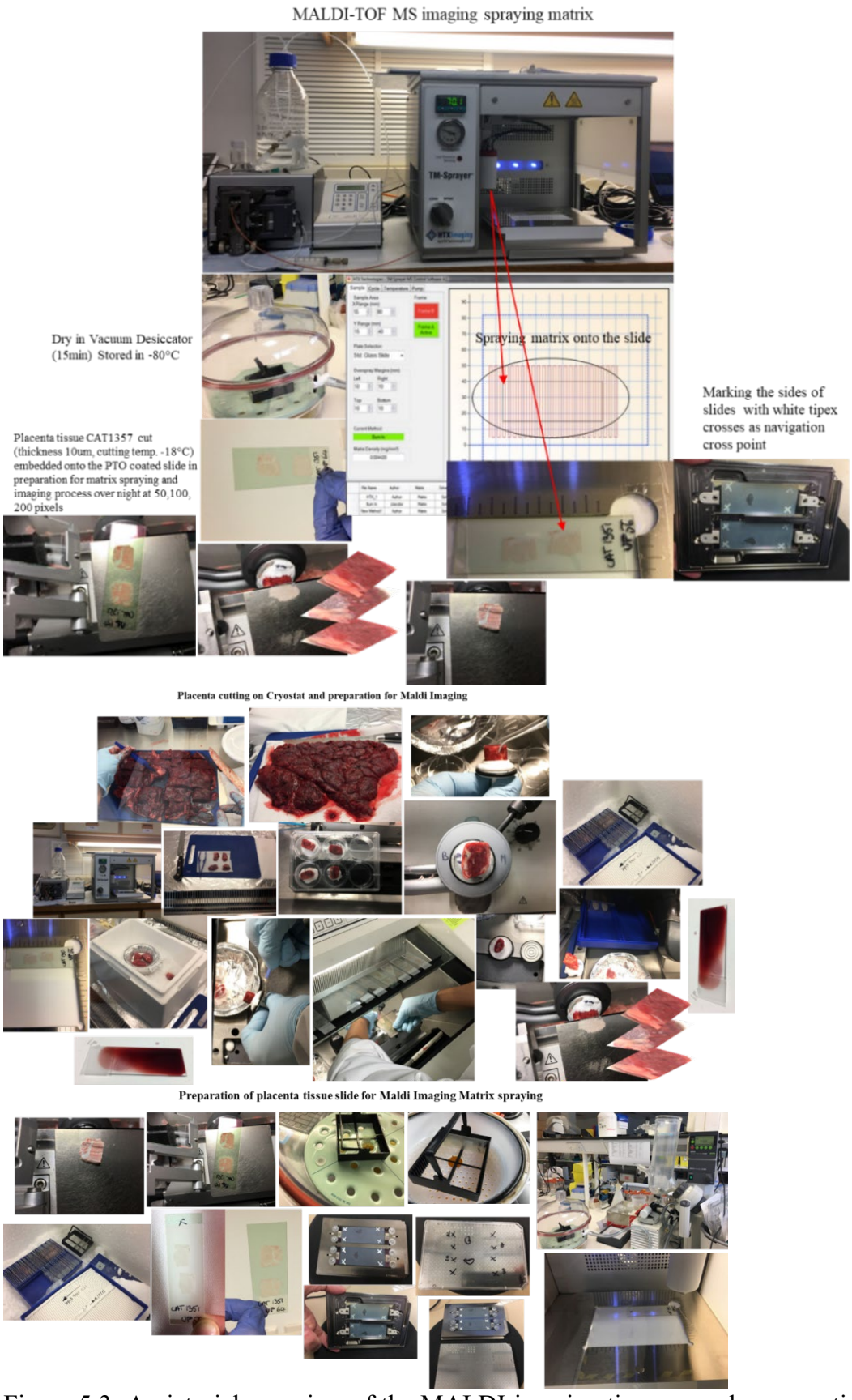

Figure 5:3: A pictorial overview of the MALDI-imaging tissue sample preparation procedure.

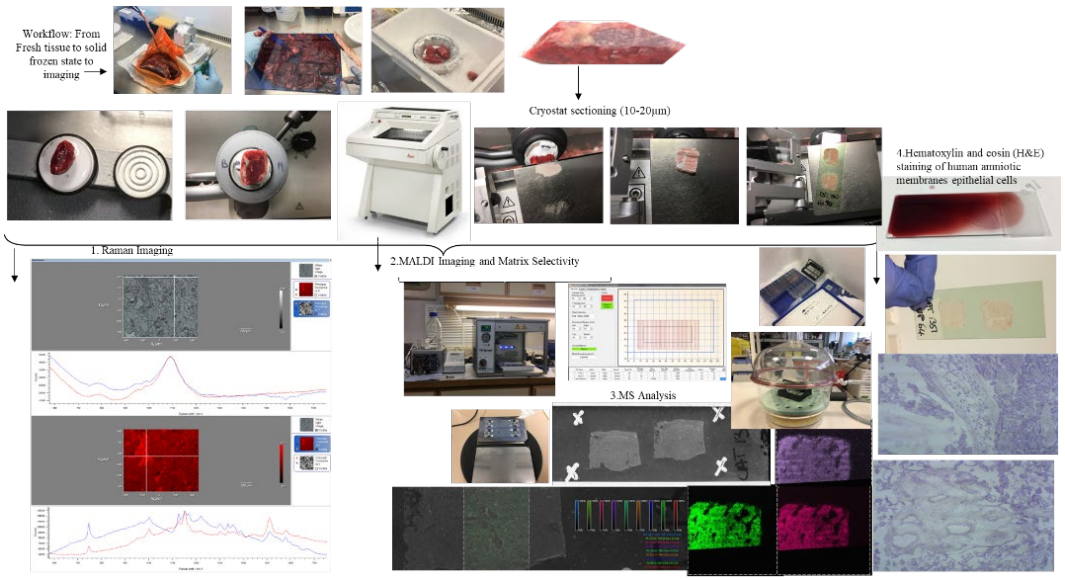

Figure 5:4: General images of the tissue sectioning and imaging procedures.

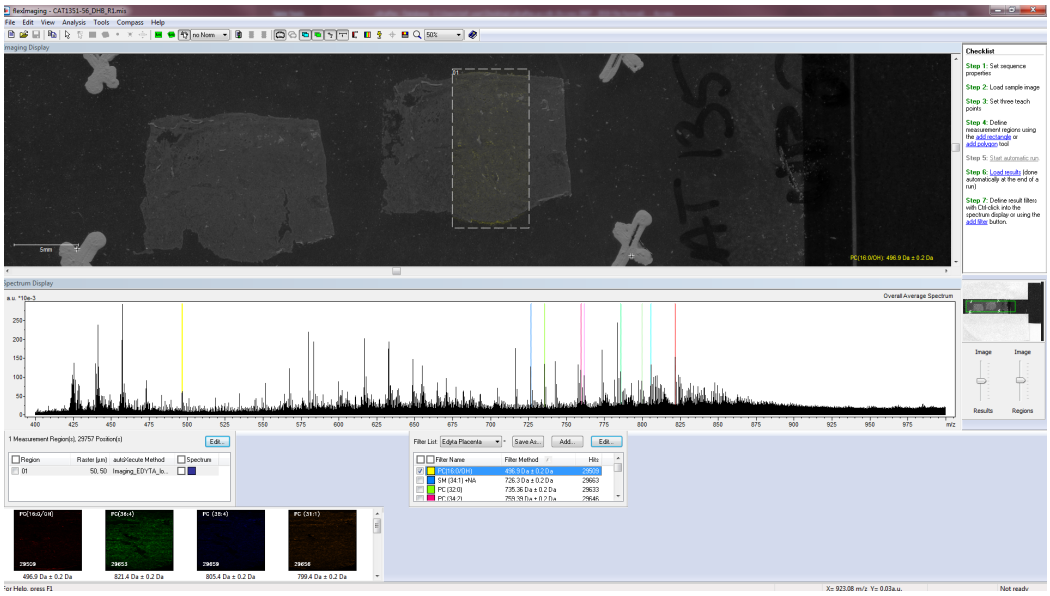

Figure 5:5: The MALDI-ToF imaging mode acquisition. A descriptive narrative is used in the text, explaining the process of the imaging experiment.

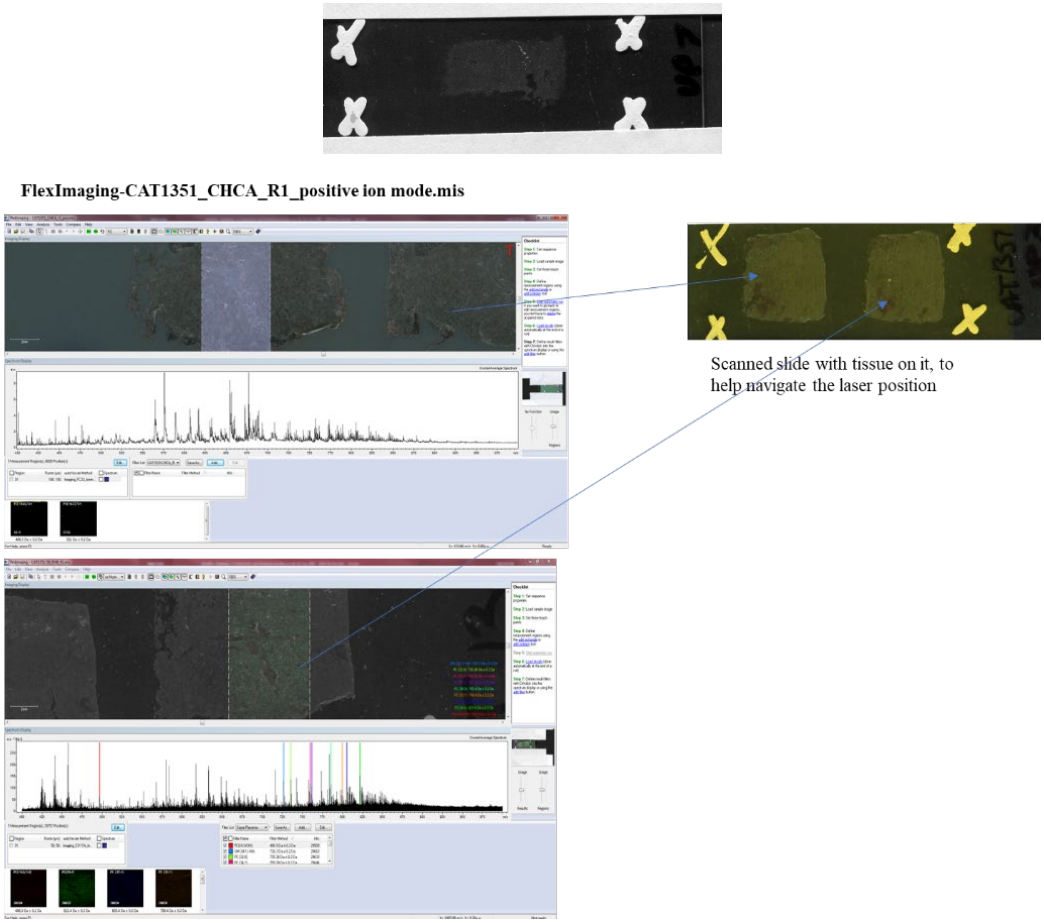

Figure 5.6: MALDI ToF MS imaging of a placental tissue sample at ‘low’ spatial resolution of 200 microns (top) and 50 microns (bottom). Below, the narrative in the text refers to the images with the explanation.

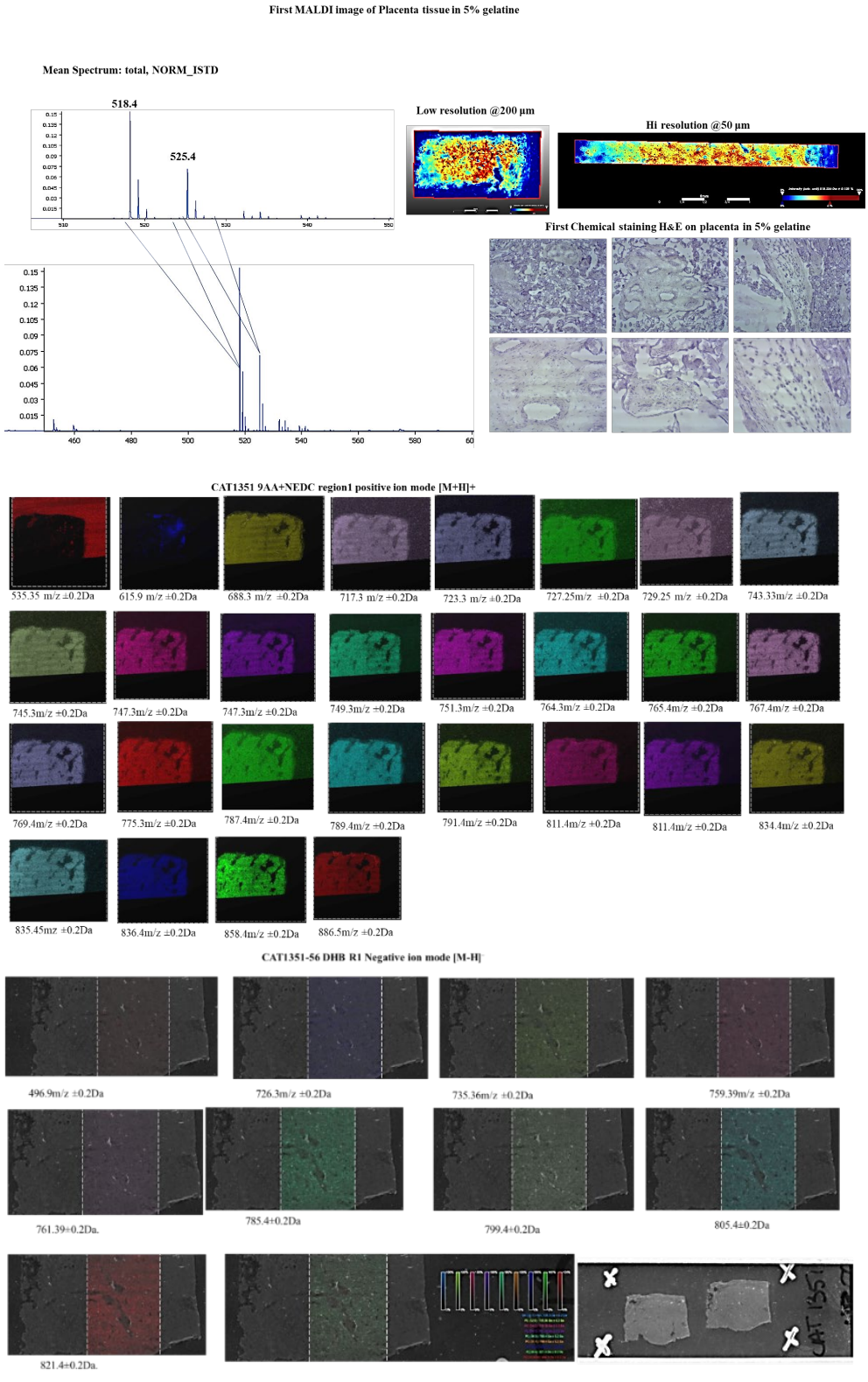

Figure 5.7: MALDI-ToF mass spectrometry tissue imaging of various lipid peaks in the mass spectra. Below is a narrative relating to the images in more detail

5.3.8 Discussing MALDI Imaging results

5.3.9 What has been achieved?

As shown in (*Figure 5.7)*, the top images compare the mean spectrum of a placenta sample frozen in 5% porcine gelatine solution compared to a 50-um and 200-um high-resolution first trail of placenta tissue. Here are photographs of the same placenta tissue stained with H&E for the first time and observed with a white light microscope. The internal standard IS phosphatidylcholine PC added to the matrix during sample spraying of the placenta tissue was to keep track of the section of interest, a 5mm section of placenta tissue subjected to laser imaging. These are initial first-time-go results. (*Figure 5.5 - Figure 5.6)* shows marked crosses on the sliding grid for the laser to navigate and select a strip of tissue sample size 5mm. The detector generates clusters of density signals for every ion hitting it. These signals are converted to intensities and produce a mass spectrum, which can be a colourful image as a density map encoded and processed by a supercomputer. The mass spectra of each peak are assigned a coloured line (Figure 5.6), and then the scanned area strip is assigned a colour for each spectral peak, starting with the mass-to-charge ratio.

Peak data were taken for obese placenta BMI CAT 1351 sample in gelatine peaks, positive ion mode [M+H]+ 9AA/NEDC matrix [5mg/ml] internal standard phosphatidylcholine PC and lysophosphatidylcholine LPC [1mg/ml] (535.35m/z, 615.9m/z, 688.3m/z, 717.3m/z,723.3 m/z, 727.25m/z, 729.25m/z, 743.33 m/z, 745.3 m/z, 747.3 m/z, 749.3 m/z, 751.3 m/z, 764.3 m/z,765.3 m/z, 757.3 m/z, 769.3m/z, 775.3m/z, 787.4m/z, 789.4 m/z, 791. 4m/z, 811.4 m/z, 834.4 m/z, 835.45 m/z, 836.4 m/z, 858.4 m/z, 886.5 m/z).

Peak data were taken for obese placenta BMI CAT 1351 sample in gelatine, negative ion mode [M-H]- DHB matrix [5mg/ml]- LPC internal standard [1mg/ml] (496.9 m/z, 726.3 m/z, 735.6 m/z, 759.39 m/z, 761.39 m/z, 785.4 m/z, 799.4 m/z, 805.4 m/z, 821.4 m/z), scanned with white crosses to navigate before entering MALDI. Since the supercomputer was unavailable due to a COVID-19 lockdown delivery delay, this acquired data has yet to be processed or further analysed. Nevertheless, it is hoped that it can be utilized as a guide to lay the foundation for future research. Insights from the literature suggest that variant analyses of differences should be

performed. Based on chemical information, it is possible to identify biomolecular variances between areas*(632)*.

In contrast to non-imaging MS, mass spectrometry imaging (MSI) allows the selection of MS spectra from homogeneous tissue areas, providing a more detailed and accurate analysis *(632)*. By verifying spatial consistency in ion images of potentially relevant peaks, data can be used to detect isotopes *(633)*. In the spatial expression of ion images as isotopic peaks, it is possible to identify molecules in a tissue according to their biochemical behaviour *(633)*. As shown in (*Figure 5.6), the* top graph, the mean total spectrum of two peaks (518.4m/z, 525.4m/z), corresponding to the isotopic distribution of biomolecule in the placenta, the Internal Standard (IS) phosphatidylcholine PC and hydrolyses lysophosphatidylcholine LPC biomolecule shows clear isotopic distribution inside the placenta. That confirms that mass spectrometry imaging on placenta samples is possible and capable of isotopic detection *(634)*. As a result, this initial groundwork can be explored further and even sent for detailed analysis using advanced imaging techniques or similar imaging techniques, such as high resolution, where the instrument's biomolecular accuracy allows the identification of elemental formulas and isotope patterns in the detection process *(635)*. High-resolution and accurate measurements of metabolites and biomolecules within biological samples can be achieved using MALDI imaging, which enables the identification of differences in biomolecular compositions within small tissue regions and the detection of isotopic distributions.

5.3.10 What has been learnt from it?

This chapter represents the initial attempts towards MALDI-ToF mass spectrometry imaging analysis of placental tissue. The results shown in (*Figures 5.5-5.7)* demonstrate that such analysis is possible, but further testing and refinement of the method are required. More spatial analysis of placental tissue was impossible due to significant instrument downtime, lockdown, and loss of key personnel and expertise from the former National Mass Spectrometry Facility.

Nevertheless, the methodology shows promise when combined with the MALDI lipid analysis in Chapter 4. The types of lipids that we observed in our MALDI ToF MS data analysis are molecules such as phosphatidylcholines, sphingomyelins,

phosphatidylethanolamine, and phosphatidylserines in positive mode. The primary identifier is the phosphatidylcholine species identified by the loss of choline phosphate with a monoisotopic mass of 182.05877 Da in the neutral state.

However, powerful signals from highly abundant charged quaternary nitrogen-containing phosphatidylcholines suppress the ion yields of other lipids in low abundance, i.e., some phospho- and glycolipids *(636)*, as the protonation event inside the evolution of the MALDI plume has a limited number of possible protons and molecules with very slightly higher proton affinity dominates the spectra by capturing a disproportionate number of the available protons. This so-called 'signal suppression effect' is a significant challenge in the quantitation of lipids from MALDI, except for ions of very similar proton affinities, so our approach in Chapter 4 of using PC/LPC ratios is inherently inaccurate but still provides an indication of relative changes. The suppression of ions is less evident in negative ion mode, allowing us to observe phosphatidylserines, phosphatidylinositols, phosphatidylethanolamines, phosphatidylglycerols, cardiolipins, and glycerolipids. Some lipid classes also show low ionisation efficiencies in negative ion mode or cannot be analyzed (e.g., phosphatidylcholines, diacyl, and triacylglycerols).

MALDI can also analyze oxidatively modified lipids since, during analysis, the samples are in a high vacuum to minimize oxidative artefacts *(619)*.To overcome the suppression of ions caused by phosphatidylcholines, a modification of the ion source called "MALDI-2" by Soltwisch, introduced in 2015 *(637)*, increased ion yields by further laser-based post-ionisation, initiated by a secondary MALDI-like ionisation in the gas phase with a second laser pulse fired nanoseconds after the first. Quantifying absolute concentrations of various lipid classes by MALDI-MSI is also possible by adding appropriate internal standards *(637-639) (640)*.

5.3.11 Conclusions about MALDI Imaging

This initial trial allowed for the running of planta samples and the identification of the internal standard run positive and negative ions, so it was a good start. It should continue as it has much potential with placenta tissue. To conclude, what was achieved was a brief, intense learning experience that lasted until the end of this research. The research began with Raman Imaging, and one experiment is shown in

Figure 5.4 under Raman Imaging. It shows a cluster of density areas and a Raman spectrum with wavelength absorbance bands underneath. By assigning vector distance values and algorithms to the differences, mathematical computing and coding programs, such as MATLAB and Machine Learning, are required to analyse the differences in multidimensional ways. It is beyond the scope of this thesis and has not been discussed. However, it may be an opportunity for a future researcher in mathematical coding and learning tissue density. Spectrometry imaging is an extremely fascinating technology. From the start to the end, sample preparation skills are required, which is the key to this analysis. Flash freezing, crayon cutting, matrix application, data acquisition, and data analysis are the most challenging parts of this experience. It would be nice to gain more knowledge, become an expert in tissue imaging, and learn more about it. It was a short period that gave me a good taste of the technique and a love for it.

Chapter: 6 Discussion

6.1 General Discussion

The findings of this thesis support MALDI-TOF MS as a powerful tool for screening the lipid composition of organic extracts of cells and tissues. The advantages of MALDI-TOF mass spectrometry toward lipid analysis are the excellent signal-to-noise ratio, the low extent of fragmentation, and good mass resolution. Additionally, the method is fast and has a low sensitivity toward impurities (e.g., buffer salts) compared to other mass spectrometric techniques. The matrix and the analyte mixture are highly homogeneous in contrast to proteins and carbohydrates because both are readily soluble in organic solvents. All these advantages of MALDI-TOF mass spectrometry make this method a very convenient tool for analysing samples of biological origin.

Different phospholipids suppressed by PC or LPC depend on their concentrations in the mixture. LPC may even prevent the detection of other lysophospholipids, especially acidic ones. Therefore, caution should apply when interpreting the spectra of total lipid mixtures dominated by peaks emerging from PC or LPC. These problems of the detectability of different phospholipid species are significant if organic biological extracts are analysed since PC is one of the most abundant species in cell membranes. In this case, the recording of spectra with varying concentrations of phospholipids is necessary. The second problem addressed in this paper is the potential quantification of one individual phospholipid in a lipid mixture.

MALDI-TOF mass spectrometry makes quantifying phospholipids in PC or LPC impossible. In the presence of PC, the peak intensity does not reflect the abundance of phospholipids within the mixture. Despite some advantages of MALDI-TOF mass spectrometry, at present, quantification of individual phospholipids in a mix is rather complex, and prior separation of phospholipids, e.g., by HPLC into separate classes, is required. MALDI-TOF mass spectrometry is suitable for investigating phospholipase A2 activity and detecting lysophospholipids. These findings are significant because routine lysophospholipid analysis by electrospray ionisation and

mass spectrometry (30) shows advantages in lipid analysis. Mass spectrometry provides immediate information on the fatty acid composition of the corresponding lysophospholipid and the lipid class simultaneously. That indicates MALDI-TOF mass spectrometry's capability for studying enzyme activities and kinetic studies. That is the first report on the different sensitivity of MALDI-TOF mass spectrometry toward detecting other phospholipids in a phospholipid mixture.

Further studies on the quantification of different phospholipids in placenta tissue and blood plasma would add an accurate and quantitative value given the total lipids in the placenta. Future studies may expand further toward quantitative method optimisation based on full lipid knowledge achieved by preparative TLC setup.

6.2 Lipid identification

There are specific and nonspecific regions of the biomolecule within lipids groups that separate or elute in the chromatograph of TLC with nonpolar species. These observations can be monitored directly by targeted lipidomics studies using mass spectrometry, where nonpolar lipids have similar fragmentation patterns in losses of molecular ion species in terms of head group, fatty acids chains, oxidative phosphorylation, methylation, hydrolysis, and many more. These fragments use the collision cell to induce the gas phase of the nitrogen line so that the molecules can collide and break up into smaller fragments. All separate carbons, hydrogens, oxygens, and nitrogen atoms with phosphorus ionic groups are calculated looking to where the cleavage occurs by adding all the numbers from the head group to the glycerol or sphingosine backbone, with acyl tails of sn1 and sn2 if searching for phospholipids like choline, ethanolamine, inositol, serine, sphingomyelin, glycerol, and hydrated version also. The difference in the monoisotopic group in a mass spectrum means that the mass of the isotopic peaks and their elemental composition include the most abundant isotopes of each element, and the average mass consists of the average isotopic abundance.

There are various mass spectrometry websites, but this one is used worldwide: https://www.jeolusa.com/ https://www.jeolusa.com/Application-List/Life Sciences.

Enter the box to determine the species of the lipid group and hundreds of lipids there to differentiate PC from SM. The lipid maps database only has computer-simulated predictors for data fragment ions. The Lipid Maps calculator predictor characterised the markers and the fragment values visible in [M+H]+. Due to the inability to use the collision cell within the MALDI ToF MS instrument, fragmentation was impossible. The fragmentation method is confirmed only by collision-induced dissociation, where applying higher energy to the precursor ion induces smashing it into smaller parts, known as fragments, that belong to the same parent ion. The insourced fragments during the ionisation process are known as in-source fragmentation, but this is not confirmed.

However, the spectrum can still be searched against the common precursor fragmentation ions via literature and see if moderate intensity, taking a minimum reading at the three-time signal-to-noise ratio of (3x S/N), which is the minimum requirement in data acquisition in mass spectrometry, can be observed. In the instrument method, parameters set up accounts to collect the signal at minimum the required rules of mass spectrometry requirements. The technique acquires intensity at a noise level noted as one thousand or arbitrary units on the y-axis [$1x10^{-3}$], considered noise, and the acquisition for intensity measurements was minimum [$1x10^{-4}$]. Therefore, it is possible to meet the (3x S/N) noise levels. Peak shapes are Gaussian shapes.

These studies run at Swansea Labs used collaborator help in using their external method validation of the samples prepared at Swansea and delivered to the collaborator. The Warwick student collaborator Basim Husain worked alongside the Swansea student (myself) and prepared further dilutions for the collaborator sample preparation to run the Swansea sample on high-resolution mass spectrometry with a 15-Tesla magnet interconnected to ion cyclotron mass spectrometry ICR-MS. The supervisory postdoctoral researcher ensured we were doing everything correctly and not disturbing the instrument. Basim has acquired the mass spectra of the healthy placenta sample reference, which was freshly homogenised, extracted, and run in TLC and MALDI a few days before transfer to Warwick to ensure that the samples were fresh and of acceptable quality for the high-resolution instrument at Warwick. At Warwick labs, fragmentation in the collision cell CID with the sodiated adducts

phosphatidylcholine precursor ion (758.6 m/z) ion and identified the phosphate head group at (184.5 m/z), and the two fatty acid chains referred to as acyl bonds (sn1) and (sn2) was performed. Via structural calculations of monoisotopic masses for each atom, the possible segments of predicted fragments were calculated, and spectra searched spectra to correlate them with the structure. The exact position of hit cleavage was calculated with an assigned double-bond work and accurately derived details of molecular structure elucidation and analytical chemistry knowledge.

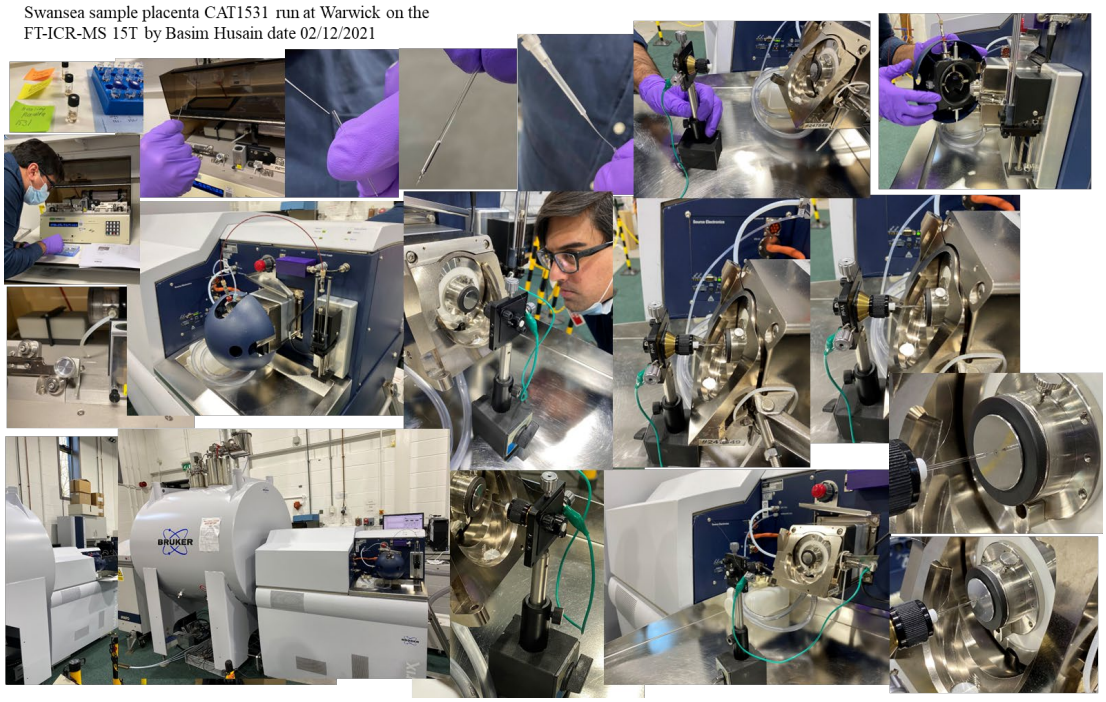

Figure 6:1 Images taken during the sample delivery and run with collaborative work student to student date 02/12/2021

Due to methodological differences, these molecules differ in experimental detection by other fields of proteomic, peptidome, or lipidomic approaches. Our research approach with placenta tissue molecules adds to biological tissue and plasma knowledge. It needs to be expanded through mass spectrometry assistance in collaborative work of analytical chemistry, specialising in structural chemistry. The reproducibility of the TLC was sufficient to allow qualitative comparisons of the total lipid extracts. Further purification by preparative TLC gave us better separation of individual band species, running on MALDI toward further observation and viable identification. Observed identification of the lipid species in TLC and MALDI was adequate for identification by lipid map search and via collaborative mass

spectrometry project with the Warwick student. Our instrument MALDI Flex at Swansea labs has instrument limitations to the level of sensitivity, where spectral noise came from 0 to 400m/z, so data was acquired from 396-2000 m/z. Any small organic molecules and their diagnostic ions are not showing in MALDI, but they could hopefully be observed and identified with Warwick collaborators on other instruments. If we were to approach from the lipoprotein point of view, we would need to perform complete protein sequencing for any lower abundance of smaller molecules.

Research on the human placenta is interesting clinically but challenging analytically and pathologically. Most placenta studies involve proteomics and investigate the most abundant proteins in the placenta. Preeclampsia, maternal death, and problems affecting pregnancies are not understood, and placental pathologies and the cause of abnormalities are still unanswered. The contributing factors to unsuccessful pregnancy are related to metabolism deregulation. Our TLC plates show total lipids in healthy and diseased human placental tissue and blood plasma. Comparisons among healthy and diseased groups have been highlighted with statistical significance to identify differences and create a visual map of phospholipids in placental tissue layers. The ambitious approach sounds complex and requires multidisciplinary collaboration.

The sample preparation method and lipid species observation confirm that the chromatographic separation extraction method by TLC is valid, followed by preparative TLC and MALDI. Validation of the sample preparation was provided through collaboration between Swansea and Warwick students and gave positive and encouraging outcomes of the initial setup with great potential for further development.

The placental lipidome, alongside the transcriptome, proteome and metabolome, can help to understand the physiology of the placenta and help medical diagnoses identify adverse pregnancies such as preterm birth, intrauterine growth restriction, hypertension, and preeclampsia, amongst others associated with fetal and maternal morbidity and mortality.

6.3 Future work

This project initially intended to use MALDI imaging to determine the spatial distribution of lipids within placental tissue. However, this part of the project was only partially successful due to the lockdown and substantial instrument downtime. There was some progress in developing MALDI imaging methodologies and generating some initial mass spectrometry images, but as MALDI imaging requires extensive instrument time, the issues noted above precluded further analysis. Nevertheless, the methods developed and the results shown herein demonstrate that MALDI imaging of placental tissue is feasible and likely to generate new knowledge about the spatial distribution of lipids, especially

concerning adverse pregnancy outcomes. Accompanying these with immunostaining and chemical staining would complement this imaging of placenta tissue. CID fragmentation is currently the best method for quantitative analysis, and it uses MRM analysis on a triple quadrupole. However, it is feasible to perform MRM analysis on other tandem mass spectrometry systems, such as a TOF-TOF mass spectrometer, so by combining these techniques, more efficient and more quantitatively accurate results can be obtained toward placenta lipids, including fuller evaluation of the PC/LPC ratio as a biomarker for adverse pregnancy. To further improve this research study on placenta tissue and the molecular identification of total lipids in blood plasma, robust instrumentation and the expertise to establish a bio map of placenta lipids are required if advances are to be made with cellular studies in obstetrics *(639)*. Many other combinations of complex mass analyses, such as linear ion traps, are equally capable systems and allow quantitative analysis and single or multiple reaction monitoring *(641-643)*and triple quadrupole *(642)*.

Furthermore, advanced mass spectrometry offers the highest mass resolution power and measurement accuracy, such as the fifteen tesla fourier transform ion cyclotron resonance (FTICR) systems. These instrumental techniques belong to the specialist areas of mass spectrometry and require expertise, knowledge, and understanding of the instrument and technique. They are best done by collaboration with the experts as initiated here.

Appendix A-T: includes calculation Excel Tables, BMI, Inventory

Appendix Table A: MALDI intensities for PC/LPC, GDM Placentas 9AA+

Appendix Table B: MALDI intensities for PC/LPC, GDM Placenta DHB+

Appendix Table A: Healthy Plasma PC-LPC, 4 groups Plasmas 9AA+ve

Appendix Table D: GDM Plasma PC-LPC, 4 groups Plasmas 9AA+ve

Appendix Table E: Obese Plasma PC-LPC, 4 groups Plasmas 9AA+ve

Appendix Table F: Non-Pregnant Plasma PC-LPC, 4 groups Plasmas 9AA+ve

Appendix Table G: Obese Placenta 9AA+

Appendix Table H: Obese placenta DHB DHB+

Appendix Table I: Placenta Healthy (+DHB) calculated Results PC-LPC redone

Appendix Table K: Healthy placentas (TLC smear) but good in DHB +ve

Appendix Table L: GDM placentas +ve DHB GDM

Appendix Table M: Health placentas +ve DHB Healthy

Appendix Table N: Obese placentas +ve DHB Obese

Appendix Table P: New placentas different cuts edges, centre after Hamilton syringe sterilisation deep cleaning due to previous smearing, Warwick trip 9AA+

Appendix Table Q: Placentas GDM PC-LPC 9AA+v

Appendix Table R: Placenta different cuts edges, centre groups healthy, obese, GDM results PC LPC all run in +9AA

Appendix Table S: Body Mass Index of all samples used in this study BMI

Appendix Table T: Inventory includes all equipment, standards, and solvents used in this research work.

GDM 9AA Placenta (10mg/ml)	LPC 16:0 (+H+)	LPC 16:0 (+Na+)	LPC 18:2 (+H+)	LPC 18:1 (+H+)	LPC 18:0 (+H+)	LPC 18:2 (+Na+)	LPC 18:1 (+Na+)	LPC 18:0 (+Na+)	PC 16:0/18:2 (+H+)	PC 16:0/18:1 (+H+)	PC 16:0/18:2 (+Na+)	PC 16:0/18:1 (+Na+) and PC 16:0/20:4 (+H+)	PC 18:0/18:3 (+H+)	PC 18:0/18:2 (+H+)	PC 16:0/20:4 (+Na+)	PC 18:0/18:3 (+Na+)	PC 18:0/18:2 (+Na+)	∑LPC	∑PC	∑PC/∑LPC	Average relative ratio of 3 repeats MaldI Intensities calculated m/z ∑PC / ∑LPC m/z
CAT No. rep	496.3398	518.3241	520.2905	522.1672	524.2854	542.3241	544.2672	546.355	758.5694	760.5851	780.5538	782.5694	784.5851	786.6454	804.5749	806.5694	808.5851				
blank-1	65471.000	0	17963.000	19133.000	19577.000	22397.000	18575.000	0.000	157500.000	161452.000	0.000	15887.000	155627.000	85434.000	0.000	51159.000	88869.000	163116.000	715928.000	4.389	3.8
blank-2	263577.000	25913.000	32364.000	33562.000	35926.000	51747.000	39815.000	0.000	281817.000	281472.000	34175.000	504980.000	268613.000	150127.000	22111.000	95514.000	159383.000	482904.000	1798192.000	3.724	
blank-3	17201.000	5620.000	0	25487.000	5145.000	5940.000	5131.000	0.000	36335.000	44265.000	56370.000	33561.000	18704.000	0.000	0.000	10910.000	17943.000	64524.000	218088.000	3.380	
1494-1	12483.000	0	0	0	0	0.000	0.000	0.000	8289.000	5419.000	5461.000	18430.000	9767.000	5692.000	6682.000	6871.000	7478.000	12483.000	74089.000	5.935	4.3
1494-2	16277.000	0	0	15288.000	4843.000	0.000	0.000	0.000	10920.000	9532.000	6857.000	20871.000	11369.000	7150.000	8757.000	7656.000	8972.000	36408.000	92084.000	2.529	
1494-3	29108.000	0	0	9734.000	9596.000	0.000	0.000	0.000	19941.000	19472.000	18933.000	44425.000	23648.000	20754.000	27416.000	25282.000	19877.000	48438.000	219748.000	4.537	
1496-1	100678.000	0	0	26560.000	28303.000	0.000	0.000	0.000	68913.000	65697.000	30146.000	121906.000	66586.000	39601.000	31725.000	43472.000	19449.000	155541.000	487495.000	3.134	3.2
1496-2	44973.000	0	0	11566.000	13758.000	0.000	0.000	0.000	30413.000	31503.000	12093.000	53139.000	31618.000	17300.000	13668.000	17573.000	21843.000	70297.000	229150.000	3.260	
1496-3	103391.000	0	0	17806.000	30942.000	30965.000	0.000	0.000	80514.000	79913.000	34230.000	146183.000	83683.000	47284.000	39450.000	48298.000	21337.000	183104.000	580892.000	3.172	
1512-1	91206.000	0	0	23528.000	24069.000	0.000	0.000	0.000	60678.000	61537.000	123691.000	58724.000	35856.000	43947.000	0.000	43001.000	19927.000	138803.000	447361.000	3.223	3.3
1512-2	57992.000	0	0	14939.000	14743.000	0.000	0.000	0.000	39091.000	35551.000	22815.000	71255.000	38327.000	21720.000	27417.000	27546.000	27026.000	87674.000	310748.000	3.544	
1512-3	129632.000	0	0	29842.000	31581.000	0.000	0.000	0.000	69982.000	70267.000	35995.572	143509.000	72266.000	43261.000	45032.000	47093.000	54841.000	191055.000	582246.572	3.048	
1513-1	20611.000	0	0	62250.000	0.000	0.000	0.000	0.000	14395.000	12365.000	26794.000	13650.000	0.000	8455.000	13680.000	10928.000	10210.000	82861.000	110477.000	1.333	2.8
1513-2	114688.000	0	0	30166.000	27511.000	0.000	0.000	0.000	72232.000	67999.000	46930.000	141350.000	67939.000	40874.000	56662.000	53970.000	55982.000	172365.000	603938.000	3.504	
1513-3	44158.000	0	0	11829.000	10921.000	0.000	0.000	0.000	31558.000	29305.000	16248.000	60844.000	29487.000	17935.000	21118.000	18428.000	21874.000	66908.000	246797.000	3.689	
1530-1	75906.000	0	11061.000	18429.000	18254.000	0.000	0.000	0.000	40356.000	42713.000	12574.000	68055.000	36453.000	20306.000	12806.000	18980.000	23146.000	123650.000	275389.000	2.227	2.1
1530-2	67893.000	0	9357.000	16668.000	16085.000	0.000	0.000	0.000	32282.000	32424.000	14445.000	55565.000	29278.000	15918.000	16265.000	18796.000	21940.000	110003.000	236913.000	2.154	
1530-3	44459.000	0	6274.000	11405.000	12771.000	0.000	0.000	0.000	21663.000	23221.000	7268.000	38632.000	18941.000	11676.000	0.000	9540.000	11680.000	74909.000	142621.000	1.904	
1545-1	145563.000	0	20016.000	34843.000	38883.000	16739.000	0.000	0.000	95675.000	97884.000	22602.000	173328.000	96074.000	56436.000	20768.000	43884.000	62853.000	256044.000	669504.000	2.615	2.6
1545-2	218338.000	0	28538.000	49249.000	54435.000	0.000	0.000	0.000	145407.000	149096.000	36681.000	254402.000	0.000	83722.000	34240.000	65994.000	91914.000	350560.000	861456.000	2.457	
1545-3	463862.000	0	63801.000	117580.000	124455.000	0.000	0.000	0.000	277667.000	276019.000	91787.000	491681.000	282222.000	162451.000	97334.000	146976.000	185513.000	769698.000	2011650.000	2.614	
1564-1	76105.000	0	8351.000	16904.000	0.000	7444.000	0.000	0.000	45647.000	46243.000	12518.000	88211.000	44668.000	24520.000	13028.000	20934.000	26831.000	108804.000	322600.000	2.965	2.3
1564-2	81873.000	0	8699.000	17999.000	17831.000	0.000	0.000	0.000	38836.000	9186.000	0.000	74256.000	36973.000	20206.000	8818.000	16146.000	23668.000	126402.000	228089.000	1.804	
1564-3	131388.000	0	15921.000	27332.000	28665.000	15426.000	0.000	0.000	82155.000	29216.000	0.000	156325.000	76641.000	43172.000	40337.000	43732.000	19445.000	218732.000	491023.000	2.245	
1568-1	52841.000	0		12682.000	14597.000	0.000	0.000	0.000	33890.000	32050.000	15044.000	62369.000	37430.000	18270.000	20260.000	22659.000	25931.000	80120.000	267903.000	3.344	2.9
1568-2	29968.000	0	5052.000	7091.000	7670.000	0.000	0.000	0.000	14756.000	16155.000	0.000	28185.000	15632.000	10357.000	6580.000	10290.000	10926.000	49781.000	112881.000	2.268	
1568-3	14561.000	0	0	3963.000	4160.000	0.000	0.000	0.000	10417.000	4417.000	0.000	20696.000	11328.000	6156.000	4957.000	6320.000	7419.000	22684.000	71710.000	3.161	
1574-1	10154.000	0	0	26927.000	0.000	0.000	0.000	0.000	9062.000	8073.000	5814.000	17134.000	9798.000	5396.000	7337.000	7485.000	6238.000	37081.000	76337.000	2.059	2.2
1574-2	14353.000	0	0	3730.000	0.000	0.000	0.000	0.000	7819.000	7836.000	5251.000	18304.000	9649.000	5633.000	8582.000	7263.000	7906.000	18083.000	78243.000	4.327	
1574-3	5584.000	0	0	3846.000	0.000	0.000	0.000	0.000	3871.000	3898.000	0.000	7354.000	4375.000	3135.000	0.000	3506.000	3800.000	9430.000	29939.000	3.175	
1577-1	145359.000	0	23471.000	38463.000	41230.000	0.000	0.000	0.000	106774.000	106866.000	29443.000	180947.000	99697.000	59677.000	32147.000	52184.000	58715.000	248523.000	736450.000	2.963	3.7
1577-2	76975.000	0		20048.000		0	0.000	0.000	55099.000	52515.000	20113.000	99854.000	57686.000	31452.000	22098.000	29000.000	36554.000	97023.000	404371.000	4.168	
1577-3	110499.000	0		28574.000	32540.000	0.000	0.000	0.000	88755.000	85128.000	32517.000	162336.000	93828.000	56623.000	38263.000	52057.000	65140.000	171613.000	674647.000	3.931	
1578-1	66191.000	0	12966.000	19800.000	21657.000	11290.000	0.000	0.000	48689.000	45236.000	12644.500	70566.000	46648.000	28733.000	13223.000	22556.000	29254.000	131904.000	317549.500	2.407	2.1
1578-2	40435.000	0	8648.000	31545.000	12899.000	0.000	0.000	0.000	24972.000	27677.000	0.000	42348.000	25630.000	17279.000	0.000	13769.000	17719.000	93527.000	169394.000	1.811	
1578-3	141879.000	0	25031.000	41480.000	43494.000	23956.000	0.000	0.000	84243.000	82661.000	26376.000	132322.000	80651.000	54160.000	28410.000	42795.000	56744.000	275840.000	588362.000	2.133	
1669-1	2368.000	3910.000	4072.000	26796.000	0.000	2312.000	0.000	0.000	18062.000	16467.000	0.000	27599.000	15029.000	8349.000	0.000	6750.000	9660.000	39458.000	100916.000	2.558	5.0
1669-2	4032.000	4802.000		11237.000	0.000	2670.000	0.000	0.000	23123.000	20686.000	0.000	31155.000	19847.000	12396.000	0.000	6975.000	10267.000	22741.000	124449.000	5.472	
1669-3	2361.000	8884.000		1406.000	0.000	1943.000	0.000	0.000	15799.000	17458.000	1877.000	26693.000	15218.000	9694.000	1439.000	5987.000	9652.000	14594.000	103817.000	7.114	
1677-1	28193.000	7230.000	0	0	8540.000	0.000	0.000	0.000	22919.000	18193.000	11666.000	34978.000	23362.000	14120.000	12273.000	16284.000	16077.000	43963.000	169872.000	3.864	3.6
1677-2	79917.000	21606.000	0	0	24375.000	0.000	0.000	0.000	54061.000	41990.000	35672.000	82980.000	49029.000	29240.000	32776.000	37974.000	38957.000	125898.000	402679.000	3.198	
1677-3	44850.000	12490.000	0	0	12380.000	0.000	0.000	0.000	34499.000	28485.000	21145.000	52575.000	32109.000	20032.000	21402.000	26521.000	25741.000	69720.000	262509.000	3.765	
1699-1	34962.000	10050.000	0	0	10320.000	0.000	0.000	0.000	21991.000	23089.000	6524.000	41194.000	23339.000	15218.000	6802.000	12299.000	15296.000	55332.000	165752.000	2.996	3.0
1699-2	36500.000	9912.000	0	0	10777.000	0.000	0.000	0.000	20528.000	18209.000	11183.000	35804.000	19200.000	13027.000	15474.000	17041.000	15725.000	57189.000	166191.000	2.906	
1699-3	23354.000	6055.000	0	0	6440.000	0.000	0.000	0.000	14520.000	13889.000	7814.000	26420.000	15407.000	9872.000	8580.000	9392.000	10014.000	35849.000	114908.000	3.205	
1719-1	108956.000	15531.000	0	25534.000	27127.000	14668.000	0.000	0.000	69845.000	68445.000	21650.000	134780.000	64404.000	37353.000	27831.000	35401.000	45418.000	191816.000	505127.000	2.633	2.8
1719-2	106528.000	24966.000	0	26232.000	0.000	0.000	0.000	0.000	60562.000	57487.000	22520.000	115662.000	55096.000	31430.000	31006.000	34581.000	41519.000	157726.000	449863.000	2.852	
1719-3	152408.000	23179.000	0	37954.000	37897.000	0.000	0.000	0.000	89513.000	90900.000	33384.000	183933.000	91158.000	49892.000	42216.000	52536.000	56114.000	251438.000	699646.000	2.783	

Appendix Table B: MALDI intensities for PC/LPC, 12-01-2022 GDM Placentas 9AA+, each sample is run in triplicate and last column value Average relative ratio of 3 repeats MALDI Intensities calculated m/z ∑PC / ∑LPC m/z is used to plot on GraphPad

GDM Placenta Matrix DHB	LPC 16:0 (+H+)	LPC 16:0 (+Na+)	LPC 18:2 (+H+)	LPC 18:1 (+H+)	LPC 18:0 (+H+)	LPC 18:2 (+Na+)	LPC 18:1 (+Na+)	LPC 18:0 (+Na+)	PC 16:0/18:2 (+H+)	PC 16:0/18:1 (+H+)	PC 16:0/18:2 (+Na+)	PC 16:0/18:1 (+Na+) and PC 16:0/20:4 (+H+)	PC 18:0/18:3 (+H+)	PC 18:0/18:2 (+H+)	PC 16:0/20:4 (+Na+)	PC 18:0/18:3 (+Na+)	PC 18:0/18:2 (+Na+)	∑LPC	∑PC	∑PC/∑LPC	Average relative ratio of 3 repeats Maldi Intensities calculated m/z ∑PC / ∑LPC m/z
	496.3398	518.3241	520.2905	522.1672	524.2854	542.3241	544.2672	546.3554	758.5694	760.5851	780.5538	782.5694	784.5851	786.6454	804.5749	806.5694	808.5851				
1578-1	68676	15081	0	17018	29621	0	31669	0	223955	444352	141073	839695	443061	248372	186370	271849	325483	162065	3124210	19.27751211	18.3
1578-1	80123	0	0	18557	28873	0	33700	0	579242	541010	154649	993271	533894	281515	207124	301873	371497	161253	3964075	24.5829535	
1578-1	77335	16661	11086	19210	42947	0	28288	16671	340747	336224	106141	563214	310732	176190	141408	171630	202220	212198	2348506	11.06752184	
1494-1	80824	14323	15515	16413	50747	0	30554	15457	507563	490887	147219	924656	497773	243266	224542	275260	318339	223833	3629505	16.21523636	34.3
1494-2	15817	0	0	0	8749	0	9138	8418	279825	250187	105427	607575	292675	133829	171590	193821	213191	42122	2248120	53.37163478	
1494-3	23687	7296	8492	0	11690	0	9138	8418	256771	220060	134104	543228	258367	112803	229464	211048	318339	68721	2284184	33.23851516	
1496-1	44754	0	11809	8477	22436	0	12979	9503	404467	307354	107613	561002	347960	183361	116886	199510	198386	109958	2426539	22.06787137	21.8
1496-2	39263	9923	9690	0	30111	0	11561	11668	382764	303140	130493	524237	325031	19343	145950	198673	203224	112216	2232855	19.89783097	
1496-3	39263	0	9690	0	30111	0	11561	11668	382764	303140	130493	524237	325031	174573	145950	198673	203224	102293	2388085	23.34553684	
1512-1	34026	9639	6834	0	15231	0	9560	0	233999	215009	84812	487856	212840	97144	142909	137718	151601	75290	1763888	23.42791871	23.8
1512-2	47696	11560	7502	8585	15002	0	12512	0	301089	279526	96109	613164	277713	122117	172391	176423	188528	102857	2227060	21.65200229	
1512-3	45527	8086	8861	7887	12033	0	11951	0	340672	314777	100154	711956	314716	128548	176070	190534	216782	94345	2494209	26.43710848	
1513-1	60267	10886	8298	9670	18696	0	15902	0	329156	291265	87520	674555	300017	127637	154447	175552	199570	123719	2339719	18.91155764	26.1
1513-2	61105	10374	7489	9911	29234	0	14908	9918	298370	281870	90588	594268	262823	117452	145220	148923	167238	142939	2106752	14.73881866	
1513-3	25170	0	0	0	9689	0	7194	0	247953	226973	84710	540763	230894	100971	136184	146647	167827	42053	1882922	44.77497444	
1530-1	50526	8654	10129	10165	18001	0	13588	0	332390	321995	90498	624214	282418	131199	120527	146780	183384	111063	2233405	20.10935235	20.3
1530-2	46081	8678	7053	8926	20211	0	10180	7655	243502	241638	70021	462895	210848	102549	104664	114100	124150	108784	1674367	15.39166605	
1530-3	39136	8661	0	8406	12706	0	9170	0	291597	279656	74452	576671	251570	115919	103753	128421	161777	78079	1983816	25.40780492	
1564-1	60716	10957	11271	9132	27029	0	18075	0	387138	359731	105998	776042	345393	144257	169545	201143	228913	137180	2718160	19.81455023	18.5
1564-2	38246	6924	7698	7980	21175	0	12712	5568	260925	244753	62855	528109	234716	103134	99775	131334	154504	100303	1820105	18.14606742	
1564-3	59759	13080	8699	10832	21762	0	15012	7983	327196	309804	103516	670668	290782	125864	176334	182780	198342	137127	2385286	17.39472168	
1568-1	54666	12350	14562	9587	40529	0	17412	14342	407819	377110	137958	797075	404113	189709	213010	244283	265978	163448	3037055	18.58116955	15.7
1568-2	61830	13018	8048	11382	47259	0	19446	13494	367448	344160	113729	682091	356062	163539	172529	195583	214441	174477	2609582	14.956596	
1568-3	59141	14767	7166	11525	44084	0	17292	13327	309894	298423	101767	586286	308046	144712	157358	169551	189494	167302	2265531	13.54156555	
1574-1	31745	0	13162	0	12886	0	9841	0	0	0	0	0	0	0	0	0	0	67634	0	0	23.2
1574-2	24480	0	8353	0	9996	0	9313	0	274424	247057	78319	542624	272231	129902	116403	156199	183869	52142	2001028	38.3765103	
1574-3	27380	0	11365	0	16747	0	9575	0	11883	288889	99187	617753	307641	143676	157384	186874	212177	65067	2025464	31.12889791	
1577-1	40173	6909	11797	9911	19142	0	15892	7621	348315	322302	94344	631299	341418	163849	135703	181122	214847	111445	2433199	21.83318229	19.5
1577-2	45784	10321	10010	0	39719	0	17611	11857	326764	298672	101277	578897	311979	153226	151176	174033	198767	135302	2294791	16.96051056	
1577-3	48326	10964	10156	11430	27194	0	17474	10097	369429	349719	118009	672626	355131	169551	183199	209148	228921	135641	2655733	19.57913168	
1677-1	32239	0	0	0	14461	0	11195	0	396137	312145	119702	589153	361893	182677	143739	216550	229161	57895	2551157	44.06523879	41.6
1677-2	23298	0	0	0	9152	0	8880	0	330811	267094	97747	502665	300582	156948	113486	175313	193269	41330	2137915	51.72792161	
1677-3	77054	15149	15716	0	36221	0	27225	0	795535	617303	236961	1147737	693894	364154	274656	410629	442347	171365	4983216	29.07954366	
1699-1	43456	0	0	0	9656	0	7770	0	277714	253073	116169	553165	272020	129167	192717	197457	195269	60882	2186751	35.91785749	38.7
1699-2	51531	11848	9517	10197	26914	0	19981	11090	375850	360162	126320	712827	377036	18590	200516	219857	235400	141078	2626558	18.61777173	
1699-3	39474	0	0	0	0	0	0	0	285957	262108	138967	619869	293378	141156	241746	220090	229272	39474	2432543	61.62392968	
1719-1	59383	9669	10511	10569	18914	0	19965	0	409750	363247	100845	800564	372450	156823	166923	221081	257316	129011	2848999	22.08338049	31.2
1719-2	48533	12132	11943	0	25484	0	9935	9757	323731	292398	113494	650775	288428	123904	197715	187857	201248	117784	2379550	20.2026591	
1719-3	30252	0	0	0	12866	0	0	0	273953	245649	115446	617864	249763	109254	218313	189575	189114	43118	2208931	51.22990398	

Appendix Table C: MALDI intensities for PC/LPC, 19-01-2022 GDM Placenta DHB+, each sample is run in triplicate and last column value Average relative ratio of 3 repeats MALDI Intensities calculated m/z ∑PC / ∑LPC m/z is used to plot on GraphPad

Healthy Plasma BMI ≤30 [10mg/ml]	LPC 16:0 (+H+)	LPC 16:0 (+Na+)	LPC 18:2 (+H+)	LPC 18:1 (+H+)	LPC 18:0 (+H+)	LPC 18:2 (+Na+)	LPC 18:1 (+Na+)	LPC 18:0 (+Na+)	PC 16:0/18:2 (+H+)	PC 16:0/18:1 (+H+)	PC 16:0/18:2 (+Na+)	PC 16:0/18:1 (+Na+) and PC 16:0/20:4 (+H+)	PC 18:0/18:3 (+H+)	PC 18:0/18:2 (+H+)	PC 16:0/20:4 (+Na+)	PC 18:0/18:3 (+Na+)	PC 18:0/18:2 (+Na+)	∑LPC	∑PC	∑PC/∑LPC	Average relative ratio of 3 repeats Maldi intensities calculated m/z ∑PC / ∑LPC m/z
CAT No.	496.3398	518.3241	520.2905	522.1672	524.2854	542.3241	544.2672	546.3554	758.5694	760.5851	780.5538	782.5694	784.5851	786.6454	804.5749	806.5694	808.5851				
1531	47740.000	0	0	0	0	0	0	0	130105.500	82546.500	30963.000	69928.000	47405.000	53737.000	11735.000	32039.000	24575.000	47740.000	483034.000	10.11801424	8.085486357
1531	59553.750	0	14551.500	12785.500	17452.500	0	0	0	146153.000	93301.000	33862.500	83791.500	56664.500	63722.500	12348.500	35217.500	30818.500	104343.250	555879.500	5.327412171	
1531	45063.000	0	11428.500	0	11488.500	0	0	0	171087.125	114054.125	27791.250	79896.250	66302.250	68847.250	9550.250	34166.250	27279.250	67980.000	598974.000	8.811032657	
1532	139963.818	0	31343.945	25279.454	33003.165	0.000	0.000	0.000	278917.285	144957.149	47115.248	122825.089	67844.681	88263.078	17504.457	58746.190	39713.964	229590.381	865887.140	3.771443453	3.720273676
1532	81044.152	0	16624.893	15842.089	20016.357	0.000	0.000	0.000	153312.504	73092.643	32023.351	79261.848	41604.315	55051.134	11776.365	40843.238	26787.891	133527.491	513753.289	3.847546942	
1532	108904.472	0	22998.911	18911.738	25664.183	0.000	8814.394	0.000	209890.353	101185.477	35732.374	101316.341	52306.560	67167.225	13321.785	45555.398	29803.383	185293.698	656278.896	3.541830632	
1543	79122.500	12993.500	18704.500	15440.500	20483.500	0.000	0.000	0.000	189128.125	118746.125	54756.000	111358.000	75353.000	76001.000	20712.000	50062.000	41625.000	146744.500	737741.250	5.027386035	5.039880129
1543	75418.000	9736.250	16615.250	14941.250	19256.250	0.000	0.000	0.000	203848.000	131308.000	59696.000	121591.000	76775.000	81704.000	18212.000	52444.000	45110.000	135967.000	790688.000	5.815293417	
1543	105603.000	20471.000	21524.000	19080.000	27770.000	0.000	0.000	0.000	216436.500	141465.500	57610.500	121645.500	82893.500	86978.500	24115.500	58940.500	41560.500	194448.000	831646.500	4.276960936	
1649	49901.793	0.000	11858.138	9099.268	11665.059	0.000	0.000	0.000	131576.891	68894.598	15339.381	57968.826	38558.909	45198.913	7024.113	27698.239	17646.535	82524.258	409906.405	4.96710198	3.9056232
1649	99844.271	0.000	20543.977	18986.850	23497.822	0.000	8610.151	0.000	189374.382	97533.019	34958.307	88976.063	43773.222	61962.542	13405.392	46837.838	27886.212	171483.072	604706.977	3.526336261	
1649	76230.737	0.000	15437.486	13157.774	18775.135	0.000	0.000	0.000	124326.088	60672.070	30497.648	55826.725	33145.517	33545.908	9242.313	30585.266	20578.234	123601.133	398419.769	3.223431359	
1639	185073.000	8954.000	38760.000	34317.000	46529.000	0.000	11502.500	11468.500	352716.000	222165.000	64500.500	172364.500	120347.500	138423.500	19434.500	77142.500	56697.500	336604.000	1223791.500	3.635701002	3.724514393
1639	150815.250	9539.250	30181.250	25134.250	36317.250	0.000	11294.375	10766.375	269060.125	177291.125	62374.500	142032.500	99019.500	27748.500	18297.500	67092.500	51355.500	274048.000	914271.750	3.336173772	
1639	109054.500	8708.500	24724.500	20170.500	27194.500	0.000	8313.750	7868.750	234199.500	147623.500	54840.250	125917.250	89654.250	92819.250	16607.250	58307.250	45722.250	206035.000	865690.750	4.201668406	
1642	63938.500	4451.000	15057.000	14148.000	18147.000	0.000	0.000	4270.000	178528.500	115645.500	25026.500	86130.500	66287.500	79477.500	8887.500	36487.500	27229.500	120011.500	623700.500	5.19700612	4.970079152
1642	124675.000	8013.000	28533.000	0.000	30824.000	0.000	8837.500	7647.500	251514.500	161086.500	50448.000	127304.000	95431.000	105919.000	15607.000	57729.000	48143.000	208530.000	913182.000	4.379139692	
1642	61645.750	5282.750	13516.750	13677.750	16429.750	0.000	0.000	0.000	156556.000	97006.000	34925.500	90263.500	63042.500	68307.500	9869.500	38919.500	30808.500	110552.750	589698.500	5.334091644	
1643	243694.250	11538.750	51965.750	42941.750	59789.750	0.000	15841.500	12629.500	407843.250	258966.250	75130.250	210433.250	148366.250	167688.250	22565.250	95436.250	72382.250	438401.250	1458811.250	3.327570918	3.98679906
1643	133312.625	0.000	28553.500	23383.500	33017.500	0.000	0.000	0.000	262118.000	161940.000	68104.000	151203.000	100397.000	109338.000	32764.000	73323.000	54888.000	218267.125	1014075.000	4.646027202	

Appendix Table D: Healthy Plasma PC-LPC, 12-10-2021 ALL 4 groups of Plasmas 9AA+ve

GDM Plasma BMI 20-50 [10mg/ml]	LPC 16:0 (+H+)	LPC 16:0 (+Na+)	LPC 18:2 (+H+)	LPC 18:1 (+H+)	LPC 18:0 (+H+)	LPC 18:2 (+Na+)	LPC 18:1 (+Na+)	LPC 18:0 (+Na+)	PC 16:0/18:2 (+H+)	PC 16:0/18:1 (+H+)	PC 16:0/18:2 (+Na+)	PC 16:0/18:1 (+Na+) and PC 16:0/20:4 (+H+)	PC 18:0/18:3 (+H+)	PC 18:0/18:2 (+H+)	PC 16:0/20:4 (+Na+)	PC 18:0/18:3 (+Na+)	PC 18:0/18:2 (+Na+)	∑LPC	∑PC	∑PC/∑LPC	Average relative ratio of 3 repeats Maldi Intensities calculated m/z ∑PC / ∑LPC m/z
CAT No.	496.3398	518.3241	520.2905	522.1672	524.2854	542.3241	544.2672	546.3554	758.5694	760.5851	780.5538	782.5694	784.5851	786.6454	804.5749	806.5694	808.5851				
1530	33939.500	0	7640.500	7170.500	8212.500	0.000	0.000	0.000	124864.434	77557.434	14795.563	52880.563	44087.563	55023.563	28219.563	17166.563	0.000	56963.000	414595.242	7.278325267	6.4
	35735.000	0	7371.500	7300.500	9563.500	0.000	0.000	0.000	130272.813	82835.813	19156.000	57018.000	46484.000	50590.000	5012.000	26744.000	0.000	59970.500	418112.625	6.971971636	
	51336.250	0	10568.750	8966.750	13040.750	0.000	0.000	0.000	154547.500	95311.500	25794.438	68837.438	0.000	7287.438	32730.438	23230.438	0.000	83912.500	407739.188	4.859099508	
1545	69769.250	6218.750	14276.750	14345.750	20317.750	0.000	0.000	0.000	176601.125	112754.125	49307.000	90235.000	62421.000	66930.000	14668.000	40669.000	0.000	124928.250	613585.250	4.911501202	5.7
	45575.000	0	9327.500	7470.500	12439.500	0.000	0.000	0.000	122428.875	78259.875	34606.000	63808.000	45930.000	48677.000	11302.000	28958.000	22615.000	74812.500	456584.750	6.103054302	
	53629.438	0	11065.938	11343.938	11426.938	0.000	0.000	0.000	145824.750	91761.750	43275.500	73175.500	54038.500	59233.500	11800.500	35418.500	30101.500	87466.250	544630.000	6.226744601	
1557*	25760.750	0	7092.250	5466.250	7664.250	0.000	0.000	0.000	107935.250	5713.250	11330.500	46537.500	39341.500	44572.500	0.000	20758.500	14444.500	45983.500	290633.500	6.32038666	7.4
	30511.188	0	8113.938	6368.938	9190.938	0.000	0.000	0.000	136684.500	91384.500	15922.250	56515.250	50241.250	54131.250	5050.250	27107.250	18287.250	54185.000	455323.750	8.403132786	
	36212.188	0	8256.188	7839.188	7612.188	0.000	0.000	0.000	134510.250	86673.250	19136.125	56488.125	48504.125	55066.125	4941.125	26056.125	17203.125	59919.750	448578.375	7.486319202	
1558	69769.250	6218.750	14276.750	14345.750	20317.750	0.000	0.000	0.000	176601.125	112754.125	49307.000	90235.000	62421.000	66930.000	14668.000	40669.000	0.000	124928.250	613585.250	4.911501202	1.9
	0.000	0	0.000	41209.500	0.000	0.000	0.000	0.000	8828.625	8059.625	0.000	786.723	3930.000	4735.000	0.000	0.000	0.000	41209.500	26339.973	0.639172361	
	0.000	0	0.000	61603.500	0.000	0.000	0.000	0.000	10426.125	7172.125	0.000	0.000	0.000	0.000	0.000	0.000	0.000	61603.500	17598.250	0.285669645	
1564	30675.250	0	5945.250	6855.250	7494.250	0.000	0.000	0.000	108870.938	71834.938	16074.781	48197.781	38541.781	6236.781	5249.781	22016.781	14084.781	50970.000	331108.344	6.496141726	5.9
	31019.000	0	0.000	25209.000	0.000	0.000	0.000	0.000	104182.500	65704.500	16411.500	46132.500	35840.500	40333.500	0.000	22589.500	14127.500	56228.000	345322.000	6.141459771	
	44507.500	0	0.000	24626.500	0.000	0.000	0.000	0.000	103566.125	66994.125	24280.500	48860.500	32140.500	39910.500	0.000	23681.500	18136.500	69134.000	357570.250	5.172133104	
1565	37370.750	0	8662.250	7755.250	9794.250	0.000	0.000	0.000	122343.000	79924.000	19653.000	55994.000	44861.000	47217.000	6219.000	27381.000	18230.000	63582.500	421822.000	6.634246845	5.6
	48571.750	0	9715.750	10491.750	12902.750	0.000	0.000	0.000	171092.313	109311.313	26031.000	78669.000	61804.000	68083.000	7326.000	37263.000	25270.000	81682.000	584849.625	7.160079638	
	128161.250	0	0.000	0.000	0.000	0.000	0.000	0.000	128161.250	9952.250	27780.000	61999.000	48246.000	54168.000	6914.000	28746.000	21308.000	128161.250	387274.500	3.021775303	
1568	27272.000	0	6271.500	5665.500	6909.500	0.000	0.000	0.000	102931.125	68508.125	15381.000	46305.000	36488.000	40881.000	4892.000	20725.000	13658.000	46118.500	349769.250	7.584141939	7.3
	43558.500	0	9165.500	8665.500	0.000	0.000	0.000	0.000	165379.250	111477.250	23374.500	73628.500	60208.500	67192.500	7055.500	31418.500	22959.500	61389.500	562694.000	9.165964864	
	48963.875	0	10665.500	0.000	11764.500	0.000	0.000	0.000	130289.750	83865.750	27744.500	0.000	45176.500	10003.500	8848.500	29289.500	22059.500	71393.875	357277.500	5.004315848	
1574	0.000	0	0.000	0.000	0.000	0.000	0.000	0.000	171092.313	10120.313	26031.000	78669.000	61804.000	68083.000	7326.000	37263.000	25270.000	0.000	485658.625		7.3
	29978.250	0	7022.750	7084.750	0.000	0.000	0.000	0.000	124787.375	78538.375	13001.875	52668.875	46222.875	48322.875	4390.875	24379.875	17325.875	44085.750	409638.875	9.291865852	
	28829.000	0	5990.500	6088.500	8106.500	0.000	0.000	0.000	122963.188	78014.188	13204.000	54149.000	44399.000	48160.000	26625.000	19473.000	20147.000	49014.500	427134.375	8.714449296	
1578	200978.375	9950.375	39324.375	34998.375	49583.375	0.000	12505.500	12262.500	352899.750	230897.750	75823.000	181633.000	128004.000	140641.000	22034.000	78543.000	59738.000	359602.875	1270213.500	3.532267366	7.3
	163093.500	9880.500	33867.500	28348.500	40413.500	0.000	10428.000	9915.000	323452.625	213413.625	67497.000	171223.000	120717.000	131764.000	18967.000	76114.000	59693.000	295946.500	1182841.250	3.9968077	
	163081.000	10214.750	33932.750	29906.750	38408.750	0.000	10574.500	10505.500	310949.000	201430.000	64015.500	156342.500	115272.500	126085.500	20007.500	68260.500	56302.500	296624.000	1118665.500	3.771324977	

Appendix Table E: GDM Plasma PC-LPC,12-10-2021 ALL 4 groups of Plasmas 9AA+ve

Plasma Obese BMI ≥30-60 [10mg/ml]	LPC 16:0 (+H+)	LPC 16:0 (+Na+)	LPC 18:2 (+H+)	LPC 18:1 (+H+)	LPC 18:0 (+H+)	LPC 18:2 (+Na+)	LPC 18:1 (+Na+)	LPC 18:0 (+Na+)	PC 16:0/18:2 (+H+)	PC 16:0/18:1 (+H+)	PC 16:0/18:2 (+Na+)	PC 16:0/18:1 (+Na+) and PC 16:0/20:4 (+H+)	PC 18:0/18:3 (+H+)	PC 18:0/18:2 (+H+)	PC 16:0/20:4 (+Na+)	PC 18:0/18:3 (+Na+)	PC 18:0/18:2 (+Na+)	∑LPC	∑PC	∑PC/∑LPC	Average relative ratio of 3 repeats Maldi Intensities calculated m/z ∑PC / ∑LPC m/z
CAT No. rep	496.3398	518.3241	520.2905	522.1672	524.2854	542.3241	544.2672	546.3554	758.5694	760.5851	780.5538	782.5694	784.5851	786.6454	804.5749	806.5694	808.5851				
CAT1544	143070.000	0	30890.000	28277.000	36384.000	0.000	0.000	0.000	340456.500	214353.500	75392.000	177447.000	127541.000	139330.000	25845.000	81984.000	63469.000	238621.000	1245818.000	5.220906794	5.1
	83384.500	7315.500	15497.500	15185.500	20681.500	0.000	6468.500	6484.500	188286.000	120934.000	43005.500	102055.500	70253.500	80196.500	14365.500	44778.500	35763.500	155017.500	699638.500	4.51328721	
	78176.000	8179.500	15530.500	15998.500	18766.500	0.000	0.000	0.000	207568.500	133371.500	45917.000	105064.000	78841.000	86097.000	15500.000	47527.000	39369.000	136651.000	759255.000	5.556161316	
CAT1557	99526.000	6575.500	19625.500	19008.500	26203.500	0.000	7328.500	5928.500	220869.500	146620.500	42816.500	115966.500	86455.500	93915.500	13821.500	50615.500	38441.500	184196.000	809522.500	4.394897283	3.5
	164258.151	9966.329	34415.729	30526.100	37943.842	0.000	0.000	0.000	290108.326	142833.016	46575.952	137439.345	73142.228	88089.810	17890.856	66479.518	38791.360	277110.151	901350.411	3.252679153	
	133416.882	0.000	28134.022	23965.041	33440.265	0.000	9959.862	0.000	217015.650	100980.517	40345.590	100115.729	55071.795	59436.013	12995.239	48767.883	31228.414	228916.072	665956.830	2.909174629	
CAT1593	234665.500	15913.000	46858.000	41495.000	57561.000	0.000	15564.500	14853.500	383398.000	257411.000	92148.000	201906.000	140529.000	150112.000	26979.000	91273.000	71494.000	426910.500	1415250.000	3.315097661	4.4
	77321.500	5613.500	16312.500	13949.500	17710.500	0.000	0.000	0.000	148256.500	97154.500	33687.000	82019.000	57130.000	62254.000	10552.000	34533.000	25311.000	130907.500	550897.000	4.208292115	
	52086.000	0.000	11929.500	10980.500	13399.500	0.000	0.000	0.000	131493.250	89019.250	29122.000	74473.000	51945.000	56227.000	8352.000	29882.000	25736.000	88395.500	496249.500	5.613967906	
CAT1606	43263.933	0.000	10264.123	8319.542	11240.133	0.000	0.000	0.000	104706.652	53008.450	0.000	52770.891	27734.818	35713.978	7535.658	26153.498	17377.354	73087.731	325001.299	4.446728523	4.1
	89812.627	0.000	19829.744	15321.163	22975.841	0.000	0.000	0.000	185991.789	89692.892	31945.423	81501.514	47902.369	59540.791	11075.830	42002.837	24439.103	147939.375	574092.548	3.880593305	
	61453.960	0.000	13124.260	10261.496	14676.614	0.000	0.000	0.000	120556.140	61952.040	24379.138	59989.728	33306.524	40523.854	7543.644	30788.406	20442.270	99516.329	399481.743	4.014233106	
CAT1613	44151.500	3901.000	10158.000	8429.000	10926.000	0.000	0.000	0.000	145889.000	95339.000	27613.000	74891.000	54609.000	61241.000	8104.000	34698.000	25750.000	77565.500	528134.000	6.808877658	5.7
	89036.000	5692.000	19591.000	17329.000	23266.000	6403.250	0.000	0.000	205943.000	13021.000	38382.000	104472.000	74378.000	84389.000	12172.000	45847.000	37208.000	161317.250	615812.000	3.817397086	
	47669.000	0.000	9760.000	8653.000	11455.000	0.000	0.000	0.000	144279.000	95268.000	23610.500	72157.500	55184.500	58323.500	7412.500	30690.500	21325.500	77537.000	508251.500	6.554954409	
CAT1614	99081.000	6795.500	20301.500	18254.500	23443.500	0.000	8202.000	0.000	206136.000	16102.000	43923.000	110312.000	14509.000	18700.000	14748.000	51126.000	38377.000	176078.000	513933.000	2.918780313	4.5
	50896.500	0.000	11387.500	10066.500	12375.500	0.000	4862.000	4532.000	152623.000	99948.000	27702.500	82024.500	57630.500	62634.500	8686.500	36303.500	28087.500	94120.000	555640.500	5.903532724	
	55759.500	0.000	12497.000	10039.000	12417.000	0.000	0.000	0.000	110115.500	69102.500	34329.000	63779.000	44617.000	46467.000	12105.000	31795.000	24069.000	90712.500	436379.000	4.810571862	
CAT1636	261206.000	12517.000	50486.000	45160.000	61893.000	0.000	16408.000	15314.000	421439.000	274617.000	74562.500	215836.500	145766.500	167181.500	23815.500	92676.500	68921.500	462984.000	1484816.500	3.207057911	3.4
	228612.250	11673.500	46932.500	40357.500	55495.500	0.000	15607.000	12216.000	380759.000	246597.000	73362.000	197281.000	140291.000	151046.000	23973.000	86660.000	67073.000	410894.250	1367042.000	3.326992286	
	164298.000	9589.000	30463.000	27766.000	39392.000	0.000	12684.500	10984.500	301370.500	192412.500	63234.500	160110.500	113133.500	120040.500	20163.500	71008.500	55704.500	295177.000	1097178.500	3.717018941	

Appendix Table F: Obese Plasma PC-LPC 12-10-2021 ALL 4 groups of Plasmas 9AA+ve

Non Pregnanta Plasma [10mg/ml]	LPC 16:0 (+H+)	LPC 16:0 (+Na+)	LPC 18:2 (+H+)	LPC 18:1 (+H+)	LPC 18:0 (+H+)	LPC 18:2 (+Na+)	LPC 18:1 (+Na+)	LPC 18:0 (+Na+)	PC 16:0/18:2 (+H+)	PC 16:0/18:1 (+H+)	PC 16:0/18:2 (+Na+)	PC 16:0/18:1 (+Na+) and PC 16:0/20:4 (+H+)	PC 18:0/18:3 (+H+)	PC 18:0/18:2 (+H+)	PC 16:0/20:4 (+Na+)	PC 18:0/18:3 (+Na+)	PC 18:0/18:2 (+Na+)	∑LPC	∑PC	∑PC/∑LPC	Average relative ratio of 3 repeats Maldi Intensities calculated m/z ∑PC / ∑LPC m/z
CAT No. rep	496.3398	518.3241	520.2905	522.1672	524.2854	542.3241	544.2672	546.3554	758.5694	760.5851	780.5538	782.5694	784.5851	786.6454	804.5749	806.5694	808.5851				
384	48386.500	5444.0	22221.000	15310.000	18167.000	0.0	6483.000	0.0	122588.500	77567.500	26541.500	63130.500	48457.500	63753.500	8543.500	28122.500	26843.500	116011.5	465548.5	4.0129513	2.7
384	47437.000	0.0	20656.000	15735.000	16299.000	0.0	5307.000	0.0	119131.500	76036.500	26085.000	59184.000	46364.000	64486.000	7378.000	23956.000	23403.000	105434	446024	4.23036212	
384	0	0.0	0	39966.000	0	0.0	0	0.0	0	0	0	0	0	0	0	0	0	39966	0	0	
424	48386.500	5444.0	22221.000	15310.000	18167.000	0.0	6483.000	0.0	122588.500	77567.500	26541.500	63130.500	48457.500	63753.500	8543.500	28122.500	26843.500	116011.5	465548.5	4.0129513	4.2
424	47437.000	0.0	20656.000	15735.000	16299.000	0.0	5307.000	0.0	119131.500	76036.500	26085.000	59184.000	46364.000	64486.000	7378.000	23956.000	23403.000	105434	446024	4.23036212	
424	62697.500	7194.0	30847.000	19953.000	21589.000	0.0	6590.500	0.0	173808.000	107956.000	32764.500	89971.500	64313.500	92413.500	10013.500	37483.500	36972.500	148871	645696.5	4.33728866	
453	59728.750	0	23627.500	20010.500	20252.500	0.0	0.000	0.0	102955.000	71212.000	25525.500	52206.500	37090.500	0.000	0.000	0.000	0.000	123619.25	288989.5	2.33773866	1.7
453	14373.000	0	0.000	60756.500	9862.000	0.0	0.000	0.0	19694.000	13709.000	0.000	10239.000	7049.000	55517.500	10037.500	21057.500	21511.500	84991.5	158815	1.86859862	
453	24072.500	0	0.000	46392.000	15396.832	0.0	0.000	0.0	18494.500	11005.500	0.000	8141.000	8675.000	10075.000	5843.000	10075.000	5843.000	85861.3316	78152	0.91021183	
458	0.000	0	23162.758	12222.725	15396.832	0.0	5455.270	0.0	157516.031	87264.478	15495.155	71035.276	45295.503	78850.716	0.000	28374.803	21322.887	56237.5845	505154.849	8.98251328	4.5
458	0.000	0	60992.523	27914.016	19850.806	19907.0	0.000	0.0	94783.788	41418.292	16964.052	45195.269	25791.955	46729.271	0.000	20070.397	15679.477	128664.327	306632.501	2.3831975	
458	0.000	0	68089.500	32314.000	22055.000	24138.0	0.000	0.0	89953.000	53597.000	17210.500	42807.500	31989.500	49458.500	0.000	17715.500	18006.500	146596.5	320738	2.18789671	
474	0.000	0.0	0.000	39199.500	0.000	0.0	0.000	0.0	0.000	0.000	0.000	0.000	0.000	0.000	0.000	0.000	0.000	39199.5	0	0	1.4
474	47437.000	0.0	20656.000	15735.000	16299.000	0.0	5307.000	0.0	119131.500	76036.500	26085.000	59184.000	46364.000	64486.000	7378.000	23956.000	23403.000	105434	446024	4.23036212	0.0
474	0.000	0.0	0.000	64765.000	0.000	0.0	0.000	0.0	0.000	0.000	0.000	0.000	0.000	0.000	0.000	0.000	0.000	64765	0	0	0.0
480	0.000	0.0	0.000	31567.000	0.000	0.0	0.000	0.0	0.000	0.000	0.000	0.000	0.000	0.000	0.000	0.000	0.000	31567	0	0	0.8
480	59728.750	0.0	23627.500	20010.500	20252.500	0.0	0.000	0.0	102955.000	71212.000	25525.500	52206.500	37090.500	0.000	0.000	0.000	0.000	123619.25	288989.5	2.33773866	0.0
480	0.000	0.0	0.000	62128.500	5924.500	0.0	0.000	0.0	0.000	0.000	0.000	0.000	0.000	0.000	0.000	0.000	0.000	68053	0	0	0.0
497	47437.000	0.0	20656.000	15735.000	16299.000	0.0	5307.000	0.0	119131.500	76036.500	26085.000	59184.000	46364.000	64486.000	7378.000	23956.000	23403.000	105434	446024	4.23036212	2.9
497	62697.500	7194.0	30847.000	19953.000	21589.000	0.0	6590.500	0.0	173808.000	107956.000	32764.500	89971.500	64313.500	92413.500	10013.500	37483.500	36972.500	148871	645696.5	4.33728866	0.0
497	0.000	0.0	0.000	35719.000	0.000	0.0	0.000	0.0	0.000	0.000	0.000	0.000	0.000	0.000	0.000	0.000	0.000	35719	0	0	0.0
513	47437.000	0.0	20656.000	15735.000	16299.000	0.0	5307.000	0.0	119131.500	76036.500	26085.000	59184.000	46364.000	64486.000	7378.000	23956.000	23403.000	105434	446024	4.23036212	2.0
513	14373.000	0.0	0.000	60756.500	9862.000	0.0	0.000	0.0	19694.000	13709.000	0.000	10239.000	7049.000	55517.500	10037.500	21057.500	21511.500	84991.5	158815	1.86859862	0.0
513	0	0.0	0	83139.500	7037.500	0.0	0	0.0	0	0	0	0	0	0	0	0	0	90177	0	0	0.0
515	8784.000	0.0	0	33012.000	0	0.0	0	0.0	14111.000	7020.000	0	8652.500	5824.500	7779.500	0.000	0.000	0.000	41796	43387.5	1.03807781	2.0
515	47437.000	0.0	20656.000	15735.000	16299.000	0.0	5307.000	0.0	119131.500	76036.500	26085.000	59184.000	46364.000	64486.000	7378.000	23956.000	23403.000	105434	446024	4.23036212	
515	9894.000			62655.000	0	0.0	0	0.0	17416.500	7370.500	0	7916.000	6480.000	8909.000	0.000	0.000	0.000	72549	48092	0.66288991	
518	0	6784.0	23831.000	14159.000	17529.000	0.0	5885.000	0.0	106245.000	10291.000	32857.000	59343.000	39141.000	52754.000	12441.000	24165.000	26280.000	68188	363517	5.33109931	5.6
518	0	0.0	22475.000	15544.000	15475.000	0.0	0	0.0	106016.000	60034.000	38376.500	62276.500	38212.500	53034.500	14600.500	26263.500	26940.500	53494	425754.5	7.95892063	
518	41277.000	5918.0	20945.000	13676.000	14239.000	5471.0	5471.000	0.0	100780.000	59680.000	24581.000	55636.000	36398.000	50994.000	8542.000	23140.000	24670.000	106997	384421	3.59282036	

Appendix Table G: Non-Pregnant Plasma PC-LPC, 12-10-2021 ALL 4 groups of Plasmas 9AA+ve

Obese 9-AA [10mg/ml]	LPC 16:0 (+H+)	LPC 16:0 (+Na+)	LPC 18:2 (+H+)	LPC 18:1 (+H+)	LPC 18:0 (+H+)	LPC 18:2 (+Na+)	LPC 18:1 (+Na+)	LPC 18:0 (+Na+)	PC 16:0/18:2 (+H+)	PC 16:0/18:1 (+H+)	PC 16:0/18:2 (+Na+)	PC 16:0/18:1 (+Na+) and PC 16:0/20:4 (+H+)	PC 18:0/18:3 (+H+)	PC 18:0/18:2 (+H+)	PC 16:0/20:4 (+Na+)	PC 18:0/18:3 (+Na+)	PC 18:0/18:2 (+Na+)	∑LPC	∑PC	∑PC/∑LPC	Average relative ratio of 3 repeats Maldi Intensities calculated m/z ∑PC / ∑LPC m/z
CAT No. rep	496.3398	518.324	520.29	522.1672	524.2854	542.32	544.27	546.3554	758.5694	760.5851	780.5538	782.5694	784.5851	786.6454	804.5749	806.5694	808.5851				
1487-1	29089.855	0	0	6167.997	7688.854	0	0	0	21965.165	15504.274	9810.762	46954.444	13201.690	6939.213	10934.434	11449.653	14529.862	42946.706	151289.496	3.522726	3.5
1487-2	28748.578	0	0	5489.128	6468.177	0	0	0	20488.146	12071.130	8895.002	48511.334	0.000	10235.895	13201.367	13035.424	13033.127	40705.884	139471.425	3.426321	
1487-3	28561.344	0	0	5580.271	7071.952	0	0	0	19166.072	14547.421	9861.114	43685.801	12869.573	0.000	13533.707	13512.462	14768.857	41213.566	141945.008	3.444133	
1489-1	21201.732	0	0	5320.647	5705.752	0	0	0	18737.366	14336.564	10137.048	45705.492	11439.448	0.000	13799.569	10790.271	13817.702	32228.131	138763.461	4.305663	4.3
1489-2	39679.60	0	0	40704.73	40773.23	0	0	0	48954.32	49018.77	49652.16	49726.14	49779.23	49851.94	50402.98	50465.68	50528.34	########	448379.568	3.700797	
1489-3	18981.776	0	0	7808.855		0	0	0	17950.053	12014.516	10366.671	46076.645	0.000	8355.492	16295.585	13487.996	10297.428	26790.630	134844.387	5.033267	
1492-1	26512.712	0	0	6491.814	8861.953	0	0	0	21571.779	15149.753	8946.928	43387.675	14073.617	9553.667	12463.157	13855.594	17404.221	41866.479	156406.390	3.735838	3.5
1492-2	27525.598	0	0	7822.024	8987.354	0	0	0	22902.693	15917.892	9339.160	48161.531	16528.972	12053.626	12174.100	15694.428	16969.873	44334.976	169742.275	3.828631	
1492-3	26877.531	0	0	7207.041	8826.549	0	0	0	20751.292	13636.556	39712.849	13665.542	9478.889	0.000	7212.786	9252.981	13574.082	42911.121	127284.977	2.966247	
1499-1	26183.456	0	0	6052.423	8505.315	0	0	0	21434.453	16339.557	7101.283	43212.051	14257.421	9702.364	8732.847	12984.573	7707.395	40741.194	141471.944	3.472455	3.4
1499-2	23401.408	0	0	6003.719	8057.616	0	0	0	18934.139	13881.766	0	37641.745	15445.400	26687.160	6656.577	10819.340	12155.016	37462.743	142221.141	3.796336	
1499-3	25188.219	0	0	6625.590	7856.264	0	0	0	19060.434	12727.460	0	38078.519	14614.337	8250.127	0.000	9403.638	12372.799	39670.073	114507.314	2.886491	
1500-1	28701.903	0	0	6714.692	7321.035	0	0	0	19226.100	15372.607	9266.968	52736.059	0.000	9530.391	13963.217	13044.107	9999.499	42737.630	143138.947	3.349249	3.3
1500-2	28677.429	0	0	6958.757	6729.693	0	0	0	17181.074	13553.507	8074.374	48244.577	0.000	8977.583	12079.282	13676.484	9684.875	42365.879	131471.756	3.103246	
1500-3	25016.952	0	0	5796.449	6963.344	0	0	0	17109.832	13580.278	7425.041	44868.626	0.000	8337.742	10937.325	10975.937	13753.362	37776.745	126988.144	3.361543	
1505-1	26805.434	0	0	5827.616	7002.627	0	0	0	20464.797	14263.372	8684.565	49958.906	0.000	0.000	11043.270	11589.938	8678.317	39635.676	124683.166	3.145731	3.5
1505-2	31301.289	0	0	6191.849	6469.549	0	0	0	9215.007	17645.620	9230.775	53399.845	14670.372	9735.827	11789.790	13278.639	14499.904	43962.688	153465.781	3.490819	
1505-3	25590.792	0	0	5316.937	6081.877	0	0	0	18826.380	14786.991	9256.655	46405.193	12172.052	8058.281	13450.961	12520.079	12311.671	36989.606	147788.263	3.9954	
1514-1	23973.578	0	0	6668.902	7180.765	0	0	0	16381.415	15361.673	10983.330	39548.626	10807.848	8019.223	15914.131	14762.501	14125.116	37823.246	145903.864	3.857518	3.9
1514-2	24663.493	0	0	6862.884	7154.401	0	0	0	20702.340	14118.470	10190.181	43407.420	16717.285	9164.484	15035.613	13982.004	16515.731	38680.779	159833.528	4.132118	
1514-3	29114.939	0	0	8200.465	8650.230	0	0	0	24388.376	15529.357	9147.145	47268.493	17299.693	9740.679	13329.444	16987.947	17581.761	45965.635	171272.894	3.726107	
1539-1	25654.679	0	0	5679.568	6768.199	0	0	0	21444.491	14020.263	8401.336	48497.462	13528.923	8310.187	10475.954	12893.760	13529.432	38102.446	151101.807	3.965672	4.1
1539-2	26124.507	0	0	5156.863	5758.501	0	0	0	19703.634	14624.456	8616.459	49528.507	0.000	6541.744	11638.837	12877.646	12929.291	37039.870	136460.575	3.684154	
1539-3	25724.238	0	0	5365.734	6714.816	0	0	0	19425.869	13637.271	7357.853	48526.495	13386.135	34601.705	10468.929	11856.248	13790.212	37804.788	173050.717	4.577482	
1606-1	31002.205	0	0	6995.953	7623.109	0	0	0	20057.345	14950.406	46902.041	0.000	11678.931	0.000	0.000	9723.047	12758.132	45621.268	116069.902	2.544206	2.9
1606-2	41050.070	0	0	8803.881	9791.603	0	0	0	22186.190	18476.994	11549.705	68317.618	0.000	0.000	20309.893	17371.802	20532.179	59645.553	178744.382	2.996776	
1606-3	37365.231	0	0	8641.592	8982.330	0	0	0	22103.114	18029.817	12441.556	64816.074	0.000	11296.111	19833.717	14210.038	11083.079	54989.153	173813.505	3.160869	
1622-1	10498.043	0	0	10381.394		0	0	0	10378.131	6565.420	17431.656	6666.797	0.000	13437.417	4926.276	5700.930	6397.283	20879.437	71503.909	3.424609	3.9
1622-2	14028.772	0	0	4856.814		0	0	0	12478.060	10777.482	21825.405	0.000	8744.282	0.000	0.000	0.000	8593.690	18885.586	62418.919	3.305109	
1622-3	14958.780	0	0	5259.717		0	0	0	14311.214	11980.634	26009.412	0.000	10175.845	19053.059	0.000	7342.194	8941.402	20218.497	97813.760	4.837835	
1655-1	30571.107	0	0	6723.088	8102.578	0	0	0	18019.468	16756.444	45512.181	0.000	0.000	8783.904	7591.771	11142.474	14331.658	45396.774	122137.898	2.690453	2.6
1655-2	39089.705	0	0	8381.373	9940.304	0	0	0	22340.427	18562.635	57050.037	0.000	0.000	9343.301	6720.103	12432.889	9250.975	57411.382	135700.367	2.363649	
1655-3	46283.068	0	0	9913.810	11268.827	0	0	0	26048.981	22081.850	7486.372	61523.064	15081.474	9993.011	9032.751	14597.375	19554.130	67465.704	185399.008	2.748048	
1656-1	31947.479	0	0	7112.388	8329.392	0	0	0	21566.392	19323.972	7549.410	53609.768	14606.117	0.000	10827.796	12358.692	15368.107	47389.259	155210.254	3.27522	3.4
1656-2	29463.431	0	0	6582.065	7059.992	0	0	0	18514.299	17263.972	8303.388	52661.323	0.000	0.000	13137.461	13355.542	15253.920	43105.489	138489.904	3.212814	
1656-3	25935.115	0	0	5610.556	7037.554	0	0	0	18145.200	14215.090	8267.021	46673.319	11852.346	7458.439	12827.295	12159.129	12307.680	38583.226	143905.518	3.729743	
1670-1	23293.795	0	0	8244.032	6108.878	0	0	0	16167.299	13214.073	10484.132	48177.470	0.000	9020.782	19634.960	13377.264	12959.795	37646.704	143035.775	3.799424	3.7
1670-2	22878.670	0	0	5728.911	6429.690	0	0	0	16437.355	14486.716	0	45306.826	0.000	9886.898	21853.847	15084.777	13397.822	35037.271	136454.241	3.894545	
1670-3	24660.524	0	0	5896.770	6948.223	0	0	0	15581.400	13830.603	10435.397	47738.775	0.000	0.000	15913.215	14435.286	14684.360	37505.518	132619.036	3.535987	
1686-1	24419.899	0	0	7638.382	6104.940	0	0	0	17634.699	14482.200	12237.358	49222.762	13380.696	0.000	21990.097	14429.279	13490.825	38163.222	156867.917	4.110447	4.0
1686-2	25811.533	0	0	8629.802	6021.122	0	0	0	17887.374	14111.356	11404.480	46436.015	12450.885	0.000	17970.461	14756.684	12480.013	40462.457	147497.268	3.645287	
1686-3	26820.636	0	0	9728.400	6605.443	0	0	0	18809.721	15559.431	13728.379	51449.031	13427.856	13494.155	22219.730	18038.697	15083.315	43154.479	181810.317	4.213011	
1759-1	13307.800	0	0	10517.821	4731.490	0	0	0	10911.005	7845.674	7045.214	26616.601	8738.667	7797.788	10401.247	8551.189	10203.654	28557.112	98111.039	3.435608	3.2
1759-2	16270.342	0	0	11193.767	5777.169	0	0	0	13216.197	7970.449	7537.596	27316.629	8866.538	0.000	10548.909	10203.978	9873.340	33241.278	95533.637	2.873946	
1759-3	16030.087	0	0	11357.386	6201.342	0	0	0	13662.120	10134.616	7993.569	29472.922	9177.232	6683.150	11623.086	11002.538	10663.138	32588.815	110412.372	3.388045	

Appendix Table H: 13-01-2022 Obese Placenta 9AA+

Reference DHB Matrix Obese Placenta	LPC 16:0 (+H+)	LPC 16:0 (+Na+)	LPC 18:2 (+H+)	LPC 18:1 (+H+)	LPC 18:0 (+H+)	LPC 18:2 (+Na+)	LPC 18:1 (+Na+)	LPC 18:0 (+Na+)	PC 16:0/18:2 (+H+)	PC 16:0/18:1 (+H+)	PC 16:0/18:2 (+Na+)	PC 16:0/18:1 (+Na+) and PC 16:0/20:4 (+H+)	PC 18:0/18:3 (+H+)	PC 18:0/18:2 (+H+)	PC 16:0/20:4 (+Na+)	PC 18:0/18:3 (+Na+)	PC 18:0/18:2 (+Na+)	∑LPC	∑PC	∑PC/∑LPC	Average relative ratio of 3 repeats Maldi Intensities calculated m/z ∑PC / ∑LPC m/z
	496.3398	518.3241	520.2905	522.1672	524.2854	542.3241	544.2672	546.3554	758.5694	760.5851	780.5538	782.5694	784.5851	786.6454	804.5749	806.5694	808.5851				
1492-1	10381.742	0	0	0	0	0	0	0	124813.975	103185.713	31215.391	264685.370	102268.216	53773.750	49742.914	67483.870	85237.254	10381.742	882406.453	84.99599041	
1492-2	12367.991	0	0	0	4451.376	0	0	0	95595.825	79426.421	28694.949	195058.871	79840.209	37398.235	47057.164	55653.980	61662.378	16819.367	680388.032	40.45265461	
1492-3	9039.338	0	0	0	0	0	0	0	90919.918	75673.320	24498.032	191806.481	74649.912	38558.352	39216.958	48450.589	61828.352	9039.338	645601.914	71.4213707	65.6
		0	0	0		0	0	0													
1499-1	8804.600	0	0	0	3237.455	0	0	0	87592.589	73060.189	21659.685	183421.421	72320.559	35944.582	33845.910	46121.263	55537.946	12042.056	609504.144	50.61462585	
1499-2	12382.721	0	0	0	4931.820	0	0	0	107325.117	91071.961	266501.434	105207.929	52954.477	48598.263	81891.519	0	0	17314.541	693550.700	40.05596803	
1499-3	8680.744	0	0	0	3742.501	0	0	0	87095.135	70256.322	23700.380	175458.062	68619.753	33592.244	42758.076	55782.181	0	12423.245	557262.153	44.85640784	18.8
		0	0	0		0	0	0													
1500-1	11900.038	0	0	0	3307.478	0	0	0	81269.288	76559.200	26847.430	224560.955	57416.674	31582.831	56469.989	47869.954	57205.024	15207.516	659781.346	43.38521414	
1500-2	10007.086	0	0	0	78579.220	0	0	0	75711.732	27337.797	229670.270	56219.457	31461.159	57693.640	48234.967	58018.039	0	88586.306	584347.061	6.596358815	
1500-3	9721.851	0	0	0	67238.958	0	0	0	64232.461	23215.442	184092.827	49499.128	23474.346	53378.079	40810.542	48054.693	0	76960.809	486757.518	6.32474532	18.8
						0	0	0													
1505-1	10362.783	2002.900	1560.057	1484.619	2657.141	0	1827.148	0	49676.623	42457.612	15427.861	111129.540	36807.425	14871.823	25477.299	23876.835	26593.959	19894.648	346318.977	17.40764508	
1505-2	10147.978	83351.282	69018.385	23555.202	195617.024	0	65617.252	0	23392.992	40066.244	40899.514	49776.201	0	0	0	0	0	447307.124	154134.951	0.344584163	
1505-3	10549.202	3379.747	80910.916	65780.378	27116.323	0	192746.682	0	61603.443	23590.590	47989.284	43840.599	46955.676	0	0	0	0	380483.248	223979.592	0.588671362	6.1
		0	0	0	0	0	0	0													
1514-1	13183.913	0	6100.585	0	0	0	0	0	140651.726	128366.090	32223.381	240902.394	103577.815	49553.187	42838.989	58850.725	69295.270	19284.498	866259.576	44.91999542	
1514-2	11544.568	0	4279.457	0	0	0	0	0	108155.640	102024.886	26863.466	186379.849	83289.286	36327.287	35901.690	45856.851	54372.632	15824.025	679171.588	42.92028151	
1514-3	10880.025	0	3900.238	0	0	0	0	0	95394.368	86061.623	20961.753	160392.081	69843.933	33924.381	26441.494	37275.938	47458.727	14780.263	577754.297	39.08958218	42.3
		0	0	0	0	0	0	0													
1539-1	10957.616	0	0	0	0	0	0	0	89898.083	73971.289	27021.307	223452.867	66985.289	26801.102	48263.319	48135.780	52781.653	10957.616	657310.690	59.9866492	
1539-2	9563.499	0	0	0	0	0	0	0	86302.198	71245.807	27579.893	208533.102	64164.558	26199.868	46436.270	46385.437	51539.836	9563.499	628386.968	65.70680369	
1539-3	10235.431	0	0	0	0	0	0	0	87970.027	71265.678	26427.296	221502.677	68784.285	25155.091	47677.855	47820.679	54344.249	10235.431	650947.836	63.59750259	63.1
		0	0	0	0	0	0	0													
1606-1	11250.198	0	0	0	2965.061	0	2913.045	0	67738.191	64122.742	23875.918	179832.828	47457.873	25189.701	53403.741	39426.323	47264.439	17128.304	548311.757	32.01202812	
1606-2	10467.644	0	0	0	3271.324	0	2581.660	0	60435.708	56755.860	21267.499	161122.962	42388.566	23321.132	42353.953	34601.997	41835.893	16320.629	484083.570	29.6608411	
1606-3	15811.153	0	0	0	4439.744	0	110992.052	0	105868.308	37953.294	303656.203	78332.827	39272.344	81667.683	62073.278	77555.946		131242.949	786379.884	5.991787664	22.6
		0	0	0	0	0		0													
1622-1	14205.367	0	0	0	0	0		0	108753.286	104120.331	35695.672	303609.073	78665.821	41702.380	73377.577	61891.882	76470.172	14205.367	884286.193	62.25014782	
1622-2	8287.508	0	0	0	0	0		0	70099.719	67924.915	21720.337	195163.537	50979.185	27525.842	43740.004	38689.660	48371.404	8287.508	564214.604	68.08012384	
1622-3	11165.697	0	0	0	0	0		0	86421.055	83648.296	27137.078	231474.932	60559.494	32671.394	55178.381	48827.433	63333.907	11165.697	689251.971	61.72942005	64.0
		0	0	0	0	0		0													
1655-1	10991.754	0	0	0	0	0		0	93449.780	86801.972	36072.535	274258.679	64946.952	36336.747	76348.684	57618.334	72643.892	10991.754	798477.575	72.64332606	
1655-2	10262.547	0	0	0	0	0		0	79985.365	72665.417	26237.838	231869.768	54315.302	29022.059	52514.332	47364.141	59260.151	10262.547	653234.373	63.65226785	
1655-3	10594.268	0	0	0	0	0		0	128381.774	123471.942	49437.671	371730.025	95418.938	48782.547	106241.431	81932.474	97636.111	10594.268	1103032.913	104.116013	80.1
		0	0	0	0	0		0													
1656-1	11702.516	0	0	0	0	0		0	99079.113	90592.670	32840.639	263957.554	74059.872	36554.868	74474.643	63266.770	72429.102	11702.516	807255.230	68.98133761	
1656-2	11816.901	0	0	0	0	0		0	88971.370	86070.691	25262.159	237042.803	65417.260	34374.621	52505.018	49745.772	64271.311	11816.901	703661.006	59.54699829	
1656-3	11663.934	0	0	0	0	0		0	84075.565	79723.193	29956.055	246066.733	59839.635	31926.082	60644.184	52322.393	61657.676	11663.934	706211.515	60.54659658	63.0
		0	0	0	0	0		0													
1670-1	7689.874	0	0	0	2387.001	0		0	51062.342	42948.888	17689.292	125226.996	37590.350	14983.312	30154.060	27028.714	30323.222	10076.875	377007.176	37.41310371	
1670-2	8977.899	0	0	0	2439.469	0		0	53356.032	43988.259	18887.970	125171.997	37418.217	15542.370	34683.032	27187.606	24493.648	11417.369	380729.132	33.34648717	
1670-3	11047.415	0	0	0	78754.473	0		0	66102.949	27745.058	195184.283	63729.093	24589.500	51042.117	43710.805	48371.822		89801.888	520475.629	5.795820581	25.5
		0	0	0	0	0		0													
1686-1	9193.174	0	0	0	0	0		0	65618.593	55623.702	21736.185	160457.115	52119.254	20298.980	35843.961	35781.538	40733.718	9193.174	488213.047	53.10604027	
1686-2	10032.500	0	0	0	0	0		0	3557.657	77684.551	63953.743	20982.452	187804.282	57865.928	23883.372	37189.575	38080.598	10032.500	511002.159	50.93468031	
1686-3	9896.630	0	0	0	0	0		0	2647.557	65354.122	53299.080	21918.340	160645.948	49590.421	18238.743	38832.596	35313.319	9896.630	445840.127	45.04969076	49.7
		0	0	0	0	0		0													
1759-1	6724.872	0	0	0	2841.641	0		0	62499.269	51911.769	22018.892	131290.365	47759.600	23981.993	35737.614	37174.587	45149.259	9566.513	457523.348	47.82550934	
1759-2	16657.325	0	0	0	8476.663	0		0	161685.149	134275.568	48304.830	347199.338	131486.272	68394.230	77282.623	90501.023	113809.182	23133.988	1172938.216	50.70194704	
1759-3	10800.801	0	0	0	4081.002	0		0	77704.655	67460.919	23256.101	165548.940	64622.917	31283.703	35699.294	43897.150	49699.432	14881.803	559173.112	37.5742854	45.4

Appendix Table I: Obese placenta DHB 14-01-22 DHB+

Healthy Placenta 20-01-2022 n DHB Matrix, 4ul sample 4ul Matrix	LPC 16:0 (+H+)	LPC 16:0 (+Na+)	LPC 18:2 (+H+)	LPC 18:1 (+H+)	LPC 18:0 (+H+)	LPC 18:2 (+Na+)	LPC 18:1 (+Na+)	LPC 18:0 (+Na+)	PC 16:0/18:2 (+H+)	PC 16:0/18:1 (+H+)	PC 16:0/18:2 (+Na+)	PC 16:0/18:1 (+Na+) and PC 16:0/20:4 (+H+)	PC 18:0/18:3 (+H+)	PC 18:0/18:2 (+H+)	PC 16:0/20:4 (+Na+)	PC 18:0/18:3 (+Na+)	PC 18:0/18:2 (+Na+)	ΣLPC	ΣPC	ΣPC/ΣLPC	Average relative ratio of traps Matdi intensities calculated m/z ΣPC / ΣLPC m/z
	496.3398	518.3241	520.2905	522.1672	524.2854	542.3241	544.2672	546.3554	758.5694	760.5851	780.5538	782.5694	784.5851	786.6454	804.5749	806.5694	808.5851				
1491-1	11374.63	2278.16	2516.36	0	3269.94	0	2761.13	0	87544.31	64850.07	29017.22	137059.59	60539.54	23006.07	36168.15	38458.55	37105.67	22200.22	513749.17	23.14162517	24.4
1491-2	11374.63	2278.16	2516.36	0	3269.94	0		0	87544.31	64850.07	29017.22	137059.59	60539.54	0	36168.15	38458.55	37105.67	19439.09	490743.1	25.24516837	
1491-3	13475.6	4014.62	0	0	0	0	2853.5	0	88796.71	64173.05	31116.88	132762.12	58440.99	21984.35	34587.99	35483.33	35513.86	20343.72	502859.28	24.71815774	
1495-1	15848.09	6250.79	2846.96	0	6652.8	0	4291.18	0	131395.31	86005.66	48912.99	199699.28	81238.54	40489.67	59505.14	55598.5	55951.07	31889.82	768796.16	24.10788647	49.4
1495-2	6300.07	0	0	0	0	0	0	0	66990.43	44230.51	32510.88	111970.38	47750.82	0	42299.09	35932.82	35530.33	6300.07	417215.26	66.22390862	
1495-3	8592.05	0	0	0	3437.6	0	0	0	109278.25	72789.86	47287.08	175198.92	76462.24	35341.32	52769.2	54930.81	61499.38	12029.65	695557.06	57.8202242	
1501-1	7317.57	0	0	0	0	0	0	0	84982.77	53848.73	30344.99	128978.99	52266.46	28093.28	39231.42	40505.39	48813.45	7317.57	507065.48	69.29424385	56.7
1501-2	4400.59	0	0	0	1585.23	0	0	0	62209.78	39085.99	21909.99	98520.24	40738.44	20057.53	25761.76	28340.73	31000.76	5985.82	369625.22	61.7501395	
1501-3	5884.77	0	0	0	2154.75	0	1863.51	0	65239.16	40795.15	22553.94	95805.59	42775.91	22285.29	27354.87	31867.26	36905.31	9903.03	385582.48	38.93580854	
1502-1	7732.22	0	0	0	0	0	0	0	80005.7	55225.98	40695.5	146470.67	56633.31		59686.29	46413.39	36397.12	7732.22	521527.96	67.44867063	42.7
1502-2	19137.87	0	0	0	6831.85	0	5638.99	0	162066.96	111658.49	54620.25	272799.31	96459.58	47794.93	69670.79	69701.88	73224.46	31608.71	957996.65	30.3079958	
1502-3	16103.31	0	0	0	5053.42	0	4535.78	0	133311.75	92293.48	44789.69	219751.14	79698.71	38935.43	57100.3	55496.52	61864.75	25692.51	783241.77	30.48521807	
1509-1	6644.83	0	0	0	2643.52	0	2417.12	0	48486.71	34349.6	17007.46	100324.56	30462.01	15644.55	31823.35	29337.76	35769.76	11705.47	343205.76	29.32011786	37.7
1509-2	13067.27	3105.08	0	0	6196.63	0	4093.28	0	87849.07	61225.37	32782.22	188504.16	58953.28	27313.56	58038.6	51273.6	56139.15	24462.26	622079.01	25.43015281	
1509-3	8038.38	0	0	0	2496.46	0	0	0	84404.72	61397.4	34721.38	185398.62	58962.42	25450.74	64854.03	51091.29	49218.56	10534.84	615499.16	58.42510755	
1514-1	11465	0	0	0	3994.85	0	0	0	71746.78	47518.54	23224.77	140966.33	70265.56	0	34513.22	35360.29	34704.84	15459.85	398300.33	25.76351134	26.8
1514-2	9836.63	0	0	0	3105.88	0	0	0	56587.07	36742.77	22677.34	96629.49	35816.02	17708.17	26107.77	21526.36	24905	12942.51	348699.99	26.94222295	
1514-3	13348.48	3020.57	0	0	4250.18	0	0	0	92416.86	72656.97	38560.11	166279.59	55773.23	27428.87	50604.21	33847.27	31405.52	20619.23	568972.63	27.59427146	
1515-1	19388.56	0	4536.42	0	6201.11	0	0	0	130001.8	104427.66	43988.37	198055.67	71427.65	35847.46	48760.28	36347.7	43974.26	30126.09	712830.85	23.66157872	19.4
1515-2	25965.06	4318.62	0	0	7082.83	0	0	0	127898.77	105204.82	43604.16	203830.05	75038.05	36833.97	51654.16	39370.29	41153.56	37366.51	724587.83	19.39137024	
1515-3	22763.91	0	0	0	8751.26	0	0	0	89425.91	76668.24	137648.66	51229.39	0	28359.73	34390.43	27208.27	31188.61	31515.17	476119.24	15.10762087	
1516-1	24685.27	5048.32	0	4343.21	8068.28	0	4932.86	0	116712.67	87070.5	38850.25	158466.88	76176	28435.11	41059.03	42398.91	41872.36	47077.94	631041.71	13.40419122	20.1
1516-2	16091.16	0	0	0	5780.61	0	0	0	98564.55	72477.71	36609.7	132793.73	61252.98	25154.13	35357.17	36645.73	34162.3	21871.77	532518	24.34727505	
1516-3	15862.14	3908.41	0	0	5365.89	0	0	0	89133.43	73859.55	39554.48	142480.49	66482	27216.31	40992.55	42940.28	36454.47	25136.44	569113.56	22.640977	
1518-1	8926.85	0	2978.93	0	3188.28	0	0	0	35172.34	36575.46	41913.68	179482.74	37594.92	25158.37	60357.09	46446.88	36292.99	15094.06	608994.47	40.34663106	33.7
1518-2	12323.93	0	0	0	6491.92	0	0	0	93156.85	66767.28	37367.57	170809.87	54789.17	29274.02	56399.89	41271.28	31698.3	16815.85	585736.43	34.83240098	
1518-3	17088.1	0	0	0	5843.41	0	3350.57	0	114721.13	83042.02	37832.13	205258.26	69993.43	33079.7	55462.77	42234.67	42221.93	26282.08	683846.04	26.01947943	
1531-1	8126.27	0	0	0	2843.5	0	0	0	56832.88	50605.66	32160.01	108995.86	36205.12	16318.84	18343.59	22992.39	31871.18	10969.77	354325.53	32.30017858	18.4
1531-2	21559.15	3607.81	3142.64	4478.83	5597.71	0	5124.92	0	70555.33	61572.84	38601.53	131730.6	41971.28	20244.17	25062.48	28562.04	36136.38	43511.06	434436.65	9.984510835	
1531-3	13875.49	2460.54	0	2792.92	3341.66	0	2658.03	0	51056.14	47628.16	14318.48	101671.01	30405.51	15530.18	16196.43	20423.56	29128.66	25128.64	326358.13	12.98749674	
1534-1	15488.63	2478.56	0	2830.2	3538.84	0	3447.16	0	75593.24	65788.34	18735.15	156799.11	49569.79	22995.73	24927.41	29725.82	44738.44	27783.39	488873.03	17.59587401	15.4
1534-2	13444.17	0	0	4965.54	2876.88	0	3249.95	0	69019.81	61082.78	15258.55	139812.05	42644.06	19346.7	20544.09	27975.72	36817.94	24536.54	432501.7	17.62684144	
1534-3	18650.24	2111.68	0	3991.33	3756.39	0	4368.48	0	58276.74	50163.26	15222.33	109129.59	38093.62	16115.24	18906.81	21565.16	32722.98	32878.12	360195.73	10.95548438	
1537-1	13998.52	0	0	0	4279.96	0	3265.36	0	54641.55	53174.69	17512.4	121310.55	47141.96	20577.13	24393.33	24137.76	29891.51	21543.84	392780.48	18.23168386	18.1
1537-2	12251.37	0	0	0	4706.04	0	0	0	50403.07	47521.21	16186.84	107627.61	40068.81	0	21604.5	23001.77	26758.08	16957.41	333171.89	19.64756941	
1537-3	13179.1	0	0	2606.34	4336.69	0	0	0	47677.93	45589.15	14982.12	99478.74	37513.31	16488.6	23741.24	20723.77	21893.01	20122.13	328087.87	16.30682807	
1541-1	10866.33	2309.1	0	0	2832.62	0	3635.53	0	107434.24	73814.38	34832.46	155237.87	72999.93	35091.82	42129.25	44624.1	58188.09	19643.58	624352.14	31.7840302	43.4
1541-2	7647.81	1921.59	1698.64	0	1849.85	0	2154.59	0	76647.11	51213.09	26875.99	109612.98	52822.66	24608.59	31121.09	33496.83	40053.27	15272.48	446451.61	29.23423394	
1541-3	6612.11	0	0	0	0	0	0	0	80151.98	51667.37	27024.78	118472.71	50037.78	24659.64	30557.22	34898.62	40717.81	6612.11	458187.91	69.2952643	
1542-1	15677.46	0	0	0	5259.27	0	0	0	72622.03	18751.53	30122.31	66230.34	39950.49	0	15170.78	18810.49	17113.12	20936.73	278771.09	13.31492979	14.3
1542-2	10893.36	0	0	0	3658.1	0	0	0	51189.27	55327.47	20017.12	47408.59	29135.79	16087.96	12060.27	11698.67	12771.08	14551.46	255696.22	17.57186014	
1542-3	14091.27	4899.21	0	0	4581.76	0	0	0	59497.56	56949.12	27917.13	60548.59	30539.84	16289.33	16077.86	14638.79	0	23572.24	282458.22	11.98266351	
1543-1	10738.83	0	0	0	3604.92	0	0	0	102659.03	71158.67	28051.77	157074.58	59899.79	28536.3	31664.8	36377.45	42940.6	14143.75	558362.99	39.47771913	32.8
1543-2	17930.18	2757.79	0	0	5585.47	0	3962.68	0	119884.44	82516.14	34101.4	181426.92	70129.42	33123.52	40871.56	37857.07	42954.74	30236.12	642865.21	21.26149817	
1543-3	11267.92	0	0	0	3629.15	0	0	0	98962.56	67860.97	30934.54	158279.52	58290.1	29031.07	37423.52	38027.56	42184.73	14897.07	560994.57	37.65804752	
1546-1	11852.47	0	0	0	3382.71	0	0	0	80656.85	59638.49	23445.89	93856.56	33635.06	25388.55	22987.31	22132.74	21827.99	15235.18	393768.84	25.84602479	30.1
1546-2	7163.75	0	0	0	0	0	0	0	55811.97	40628.53	20542.36	72913.04	31610.19	16370.32	20537.43	18883.45	20129.6	7163.75	297426.89	41.5183235	
1546-3	9551.62	0	0	0	2664.91	0	0	0	56855.29	43443.99	16653.83	67926.75	31693.91	16919.21	14822.32	14643.32	16581.1	12216.53	279539.72	22.88208845	
1547-1	7391.36	0	0	0	2724.42	0	0	0	62863.96	47836.79	22239.42	138541.97	43197.12	19728.85	41991.84	38442.06	31942.33	10115.78	446784.34	44.16706769	40.1
1547-2	11938.75	0	0	0	4449.11	0	3634.3	0	76386.88	56147.25	30966.3	165297.79	60074.51	24106.47	55488.01	44381.31	50157.53	20022.16	553006.05	27.61969987	
1547-3	6788.34	0	0	0	2450.45	0	0	0	60619.7	44726.03	26348.78	139059.08	39452.58	18457.36	44575.98	39957.91	35245.53	9238.79	448442.95	48.53914311	
1548-1	13294.01	0	0	0	4317.51	0	3567.43	0	107286.83	104127.71	45268.44	201283.58	75631.61	41486.15	56906.47	53597.17	64033.16	21178.95	749621.12	35.39463099	40.1
1548-2	15827.52	0	0	0	5081.41	0	0	0	138898.02	131270.42	56552.18	255592.09	94387.21	51610.16	72343.56	68989.14	91166.42	20908.93	960809.2	45.95209798	
1548-3	18208.6	0	5869.54	0	7149.35	0	0	0	173245.38	166705.27	75184.34	312703.25	117655.57	63893.46	89475.79	91670.19	114935.77	31227.49	1215469.02	38.92304569	
1549-1	8264.01	2664.08	0	0	4238.07	0	0	0	70123.55	47155.86	24713.96	109926.97	38552.17	21361.03	33351.33	36882.86	35347.48	15166.16	437415.21	28.84152679	35.4
1549-2	6034.78	0	0	2272.86	2190.75	0	0	0	65923.59	46832.33	21641.04	113497.14	38133.62	21712.44	28499.78	35058.58	40449.94	10498.39	431748.46	41.12520682	
1549-3	4209.26	0	0	5011.9	2553.95	0	0	0	65878.46	46628.54	23924.35	112350.52	33940.73	20243.61	29217.12	34306.97	38835.34	11775.11	425325.64	36.12073603	
1550-1	25430.98	0	0	0	7960.17	0	0	0	147649.71	117530.97	43286.99	171560.2	86339.57	39469.18	39540.87	37391.36	42581.75	33391.15	725350.6	21.72283973	20.0
1550-2	20457.71	0	0	0	5918.72	0	0	0	133185.19	106011.07	36265.7	154350.54	81944.57	35980.47	32959.86	32806.33	39899.11	26376.43	653402.84	24.77222429	
1550-3	39209.13	5853.3	5765.23	0	13100.74	0	6054.78	0	198708.75	166433.29	52533.36	224517.25	120712.11	53277.86	44128.87	45166.4	49892.35	69983.18	955370.24	13.65142653	
1551-1	16500.84	4839.54	0	0	6697.21	0	4392.38	0	117665.25	82839.01	51112.48	191222.84	72689.4	33794.94	68688.49	54325.56	44936.77	32429.97	717274.74	22.11765043	27.5
1551-2	15788.19	0	0	0	5992.54	0	4276.5	0	83603.74	59569.69	31193.03	143382.01	48101.9	25909.38	43066.52	34635.88	44358.19	26057.23	513820.34	19.7189164	
1551-3	14244.1	0	0	0	4877.53	0	0	0	120453.22	87298.13	64587.75	219637.72	77217.32	33458.01	73321.63	63268.89	50744.5	19121.63	779987.17	40.79083059	
1552-1	11266.29	0	0	0	0	0	0	0	52485.7	56682.34	21970.28	86381.43	31191.06	17719.98	27386.31	19199.75	22898.51	11266.29	335915.36	29.81596959	19.6
1552-2	28052.76	5642.75	0	0	8435.14	0	0	0	72196.65	91498.3	30224.22	126293.66	50098.65	0	35852.99	21819.9	30106.88	42130.65	458091.25	10.8731138	
1552-3	6440.21	0	6642.58	0	0	0	0	0	30860.64	35063.55	14358.79	56612.75	20847.76	0	16830.45	11862.69	14653.23	21082.79	201089.86	28.1443355	
Blank-1 9Aa	23859.09	0	387352.25	0	0	0	0	0	55684.68	44894.15	39842.57	111482.56	0	0	55741.34	38089.21	35037.87	411211.34	384772.38	0.935704691	1.1
Blank-2 9Aa	34752.07	0	281833.24	0	0	0	0	0	67801.89	60686.56	25368.02	120575.12	44891.54	30496.58	32713.74	32531.52	39933.34	316585.31	454998.31	1.437206009	
Blank-3 9Aa	21024.56	0	376885.25	0	0	0	0	0	51579.25	46864.23	39965.88	106253.96	34746.79	22423.03	50942.72	38501.52	34106.31	397909.81	425383.69	1.069045496	

Appendix Table J: 20-01-2022 Placenta Healthy (+DHB) calculated Results PC-LPC redone

Healthy placenta different areachunks	Healthy Placenta New Exctracs (9aa+ve) 31-03-2022 Random chunks of the same healthy placenta x10	LPC 16:0 (+H+)	LPC 16:0 (+Na+)	LPC 18:2 (+H+)	LPC 18:1 (+H+)	LPC 18:0 (+H+)	LPC 18:2 (+Na+)	LPC 18:1 (+Na+)	LPC 18:0 (+Na+)	PC 16:0/18:2 (+H+)	PC 16:0/18:1 (+H+)	PC 16:0/18:2 (+Na+)	PC 16:0/18:1 (+Na+) and PC 16:0/20:4 (+H+)	PC 18:0/18:3 (+H+)	PC 18:0/18:2 (+H+)	PC 16:0/20:4 (+Na+)	PC 18:0/18:3 (+Na+)	PC 18:0/18:2 (+Na+)	∑LPC	∑PC	∑PC/∑LPC	Average relative ratio of 3reps Maldi Intensities calculated m/z ∑PC / ∑LPC m/z
		496.3398	518.3241	520.2905	522.1672	524.2854	542.3241	544.2672	546.3554	758.5694	760.5851	780.5538	782.5694	784.5851	786.6454	804.5749	806.5694	808.5851				
chunk1 central cord	healthy 1706-1	29892	0	0	55418	0	0	0	0	89034	69485	34800	143509	80614	41095	39857	48850	50513	85310	597557	7.004536	
	healthy 1706-2	7294	0	0	18830	0	0	0	0	28496	19682	9561	43876	27883	19456	11603	13025	17775	26124	191357	7.32495	7.12
	healthy 1706-3	12453	0	0	24028	0	0	0	0	36013	52009	16336	61632	31326	19863	17994	18348	22484	36481	256005	7.017489	
chunk 2 edges left	healthy 1706-4	1131	0	0	8988	0	0	0	0	2993	2639	0	4941	12543	2041	9602	18348	1911	10119	55018	5.437099	
	healthy 1706-5	6175	0	0	4461	0	0	0	0	11165	8193	0	15230	12985	0	0	18348	6469	10636	72390	6.80613	6.92
	healthy 1706-6	13663	0	0	9823	0	0	0	0	26956	24611	9536.84	53152	27875	13694	13694	13918	16447	23486	199883.8	8.510766	
chunk 3 edges right	healthy 1706-7	10695	0	0	6988	0	0	0	0	36568	27041	10328	59918	32172	18149	8753	12905	17525	17683	223359	12.63128	
	healthy 1706-8	19722	0	0	54694	0	0	0	0	56596	39396	21067	93568	52036	28967	23991	29240	51633	74416	376494	5.059315	7.84
	healthy 1706-9	11640	0	0	17865	0	0	0	0	31015	23508	8720	52882	32741	14164	8968	14981	19831	29505	206810	7.00932	
	healthy 1706-10	7220	0	0	15871	0	0	0	0	24278	17989	6974	38416	22640	9878	8140	11625	14227	23091	154167	6.676497	
centre	healthy 1645-1	22350	0	0	29860	9596	0	0	0	93796	76530	13008	100311	78930	48552	12643	32708	42916	61806	499394	8.080025	7.21
	healthy 1645-2	16079	0	0	28641	7424	0	0	0	72211	55014	12311	79480	58925	39531	9785	24239	33923	52144	385419	7.391435	
	healthy 1645-3	10966	0	0	24094	6631	0	0	0	52155	38870	0	51555	43485	23755	8796	15180	23250	41691	257046	6.165503	7.27

Appendix Table K: placenta different area cuts edges/Centre 31-03-20220 Healthy 9AA +ve

Healthy Placenta in DHB	LPC 16:0 (+H+)	LPC 16:0 (+Na+)	LPC 18:2 (+H+)	LPC 18:1 (+H+)	LPC 18:0 (+H+)	LPC 18:2 (+Na+)	LPC 18:1 (+Na+)	LPC 18:0 (+Na+)	PC 16:0/18:2 (+H+)	PC 16:0/18:1 (+H+)	PC 16:0/18:2 (+Na+)	PC 16:0/18:1 (+Na+) and PC 16:0/20:4 (+H+)	PC 18:0/18:3 (+H+)	PC 18:0/18:2 (+H+)	PC 16:0/20:4 (+Na+)	PC 18:0/18:3 (+Na+)	PC 18:0/18:2 (+Na+)	∑LPC	∑PC	∑PC/∑LPC	Average relative ratio of 3reps Maldi Intensities calculated m/z ∑PC / ∑LPC m/z
CAT.NO.	496.3398	518.3241	520.2905	522.1672	524.2854	542.3241	544.2672	546.3554	758.5694	760.5851	780.5538	782.5694	784.5851	786.6454	804.5749	806.5694	808.5851				
1537-1	5963	883	1011	1338	2471	0	1855	1127	20267	21668	4877	40265	20314	9167	7717	9386	12049	14648	145710	9.947433	
1537-2	6602	1370	910	1151	3014	0	1997	990	23620	25220	5566	43939	24427	12581	6810	10639	14645	16034	167447	10.44325	
1537-3	4263	518	968	613	1995	0	1447	1144	16216	19526	4741	30137	14850	7381	7556	7887	9828	10948	118122	10.78937	10.4
1653-1	2193	0	0	782	1484	0	747	0	12615	10943	5489	23193	11984	7123	5515	7208	8990	5206	93060	17.87553	
1653-2	1605	608	585	543	1111	0	657	0	8791	5918	4078	12588	6172	3799	3477	4363	4835	5109	54021	10.57369	
1653-3	2389	564	719	2040	957	0	0	0	8017	6449	2974	14918	7458	3722	4052	4761	5190	6669	57541	8.62813	12.4
1676-1	2120	869	0	1581	1199	0	1189	0	12207	11625	2979	20509	9932	5737	5154	5238	8427	6958	81808	11.7574	
1676-2	5411	0	0	1307	1965	0	1668	0	29709	30983	7205.76	47355	24708	15318	8336	10987	17246	10351	191847.8	18.53422	
1676-3	3597	0	0	0	939	0	931	0	22233	20079	4795	30859	16609	10085	5647	8043	10639	5467	128989	23.59411	18.0
1678-1	1041	485	0	5534	615	0	0	570	6263	5544	2491	8014	5244	2833	2138	3445	3599	8245	39571	4.799394	
1678-2	541	0	0	12770	555	0	0	0	3377	3072	1900	4075	3345	2160	2247	1907	1631	13866	23714	1.710226	
1678-3	3000	0	0	13021	1740	0	0	0	19964	17837	7916	23958	19611	12312	6187	7399	9872	17761	125056	7.041045	4.5
1684-1	1547	606	457	978	1200	0	473	0	7646	8157	2278	656	6969	3140	3389	3582	6116	5261	41933	7.970538	
1684-2	3854	999	851	768	1967	0	0	899	21340	18046	5882	35976	16295	9973	7668	9332	10745	9338	135257	14.48458	
1684-3	2816	335	477	0	1673	0	484	440	14320	13683	2108	22830	13667	7476	912	4252	6432	6225	85680	13.76386	12.1
1760-1	3709	0	0	10370	1254	0	0	0	14672	15167	5496	23357	11719	6639	5828	7472	7294	15333	97644	6.368225	
1760-2	2159	0	0	0	1028	481	856	0	13479	12485	1959	18484	11420	7941	3363	4331	5473	4524	78935	17.44805	11.9

Appendix Table L: Healthy placentas 06-04-2022 showing (TLC smear) but good in MALDI DHB +ve

DHB +ve ion GDM PLACENTA 06-04-2022 +ve DHB 4ul +4ul	LPC 16:0 (+H+)	LPC 16:0 (+Na+)	LPC 18:2 (+H+)	LPC 18:1 (+H+)	LPC 18:0 (+H+)	LPC 18:2 (+Na+)	LPC 18:1 (+Na+)	LPC 18:0 (+Na+)	PC 16:0/18:2 (+H+)	PC 16:0/18:1 (+H+)	PC 16:0/18:2 (+Na+)	PC 16:0/18:1 (+Na+) and PC 16:0/20:4 (+H+)	PC 18:0/18:3 (+H+)	PC 18:0/18:2 (+H+)	PC 16:0/20:4 (+Na+)	PC 18:0/18:3 (+Na+)	PC 18:0/18:2 (+Na+)	∑LPC	∑PC	∑PC/∑LPC	Average relative ratio of 3reps Maldi Intensities calculated m/z ∑PC / ∑LPC m/z
CAT.NO.	496.3398	518.3241	520.2905	522.1672	524.2854	542.3241	544.2672	546.3554	758.5694	760.5851	780.5538	782.5694	784.5851	786.6454	804.5749	806.5694	808.5851				
1494-1	1246	591	0	484	985	0	653	462	8488	6365	2412	10715	6244	4273	2860	2820	3498	4421	47675	10.78376	14.8
1494-2	1346	0	422	0	1858	0	714	0	10242	6291	3758	13724	7103	3845	2915	4716	5677	4340	58271	13.4265	
1494-3	1221	611	573	0	1327	0	0	0	11040	9232	5124	17080	10374	5195	4227	5480	8122	3732	75874	20.33065	
Sm.1494-1	3023	0	814	5468	1759	0	1163	0	19602	18747	4962	866	20813	10098	1016	6571	9957	12227	92632	7.57602	16.3
Sm.1494-2	1824	0	1141		2419	0	1051	667	22525	20673	4481	37953	18441	8746	5014	8644	11716	7102	138193	19.45832	
Sm.1494-3	4402	0	1179	1028	3146	0	1493	1157	38448	38287	8865	72737	37501	19991	10334	18680	25360	12409	270203	21.78178	
1545-1	1478.17	462.47	0	0	506.11	0	642.53	0	16205.08	13491.3	4139.63	31966.66	13374.86	5054.55	4789.16	6471.17	9846.2	3089.28	105338.6	34.09811	31.4
1545-2	761.24	0	680.88	500.49	0	0	728.32	0	10627.76	9263.02	2423.18	19991.94	8296.22	3593.28	3589.88	3589.91	5968.14	2670.93	67343.33	25.21344	
1545-3	3083.12	0	923.74		1277.76	0	0	0	29506.96	24872.03	7572.27	51954.78	23819.22	8970.41	9290.29	12706.22	15615.44	5284.62	184307.6	34.87623	
1574-1	4445	1155	792	1054	2508	0	1195	739	19049	16449	5539	44609	16451	6415	9891	9331	11504	11888	139238	11.71248	16.4
1574-2	2620	1155	0	410	1471	0	0	0	14224	13799	5488	39670	11860	9046	8780	9639	13742	5656	126248	22.32107	
1574-3	1169	0	0	1108	856	0	453	0	5832	7334	2010	15865	7045	3007	4139	4690	4571	3586	54493	15.19604	
1577-1	893.81	324.29	0	0	355.94	0	0	0	13989.75	9445.23	3220.32	16079.43	7370.9	3592.37	3185.27	4695.65	5405.97	1574.04	66984.89	42.55603	33.3
1577-2	1623.57	373.98	0	620.21	0	0	823.65	0	21685.42	13831.2	4967.99	25733.85	17639.11	7218.42	5097.85	7089.71	7398	3441.41	110661.6	32.15588	
1577-3	368.03	358.65	0	620.63	279.26	0	0	0	8325.27	6241.76	9863.61	0	5641.46	2288.14	1691.82	2915.62	3777.58	1626.57	40745.26	25.0498	
1656-1	1765.1	0	0	0	1076.07	0	665.85	0	14512.29	14784.05	4443.63	30149.75	11495.38	5974.08	5121.42	9946.05	7274.9	3507.02	103701.6	29.56971	38.1
1656-2	1522.83	0	337.85	363.78	516.93	0	0	0	10043.38	11077.14	3934.41	23757.74	9150.62	3955.88	5279.85	5923.16	6730.35	2741.39	79852.53	29.12848	
1656-3	1780.65	0	0	0	914.12	0	0	0	22704.79	20661.96	5930.6	43694.24	16764.41	8130.95	7362.73	11007.58	13194.28	2694.77	149451	55.45966	
1699-1	1376.67	0	0	1028.03	0	0	0	946.54	21517.94	13139.61	5463.39	30539.83	14201.18	6643.02	5090.44	8004.44	8425.77	3351.24	113025.6	33.72651	33.7
1785-1	1028	0	364	0	889	0	0	387	5892	7039	1106	13757	5336	3171	2464	2430	3439	2668	44634	16.72939	20.0
1785-2	1953	0	0	0	1766	0	1203	0	16294	15918	4136	41480	11935	6222	6775	9401	10224	4922	122385	24.86489	
1785-3	994	0	0	0	356	0	528	0	5537	4834	1786	10918	3124	397	2383	2502	3190	1878	34671	18.46166	
1564-1	2475	636	578	1285	1745	0	544	642	17350	18974	3699	31146	16218	5759	6732	7593	8993	7905	116464	14.73295	14.5
1564-2	2503	0	435	2168	1233	0	512	451	13921	12615	3373	25913	10857	5840	4451	6988	7521	7302	91479	12.52794	
1564-3	3800	1017	0	1587	1566	0	1281	1028	23372	21167	5855	46751	19931	11765	8441	14100	14526	10279	165908	16.14048	
1578-1	2588	0	453	0	947	0	720	0	12040	11995	21351	9492	4113	3687	5961	5413	3056	4708	77108	16.37808	15.8
1578-2	1467	0	0	1865	0	0	0	0	6431	5905	1956	13151	6073	2558	2684	3438	3716	3332	45912	13.77911	
1578-3	2178	0	354	472	948	0	530	310	12444	14656	3426	23136	9490	4329	3745	4923	7068	4790	83217	17.37307	
1651-1 cebtre	523	513	457	0	1235	0	393	0	5672	5175	1968	11301	5553	2984	1783	497	3056	3121	37989	12.17206	28.3
1651-2 centre	2663	0	661	930	2665	0	0	0	23951	24292	5716	48436	22957	12616	8040	11156	14394	6919	171558	24.7952	
1651-3 centre	806	0	0	0	451	0	0	0	6411	7888	2622	16527	8534	3904	3852	4443	5919	1257	60100	47.81225	
1651-3 edges	3653	0	0	2027	2122	0	956	848	39261	27944	8066	59459	26809	14318	9023	15824	20602	9606	221306	23.03831	30.5
1651-2 edges	2042	0	0	0	891	0	697	0	27247	23198	5439	42990	20980	12919	7723	12900	15192	3630	168588	46.44298	
1651-1 edges	1669	0	0	2390	1563	0	0	0	17507	16254	6128	32241	14654	8724	7993	10237	10258	5622	123996	22.0555	
1661-1	1669	0	0	2390	1563	0	697	0	17507	16254	6128	32241	14654	8724	7993	10237	10258	6319	123996	19.62273	27.9
1661-2	2042	0	0	0	891	0	956	848	27247	23198	5439	42990	20980	12919	7723	12900	15192	4737	168588	35.58961	
1661-3	3653	0	0	2027	2122	0	0	0	39261	27944	8066	59459	26809	14318	9023	15824	20602	7802	221306	28.36529	
1677-1	679	0	414	0	592	0	505	0	9010	6906	2730	12372	5511	2597	2622	4414	4838	2190	51000	23.28767	34.3
1677-2	477	0	0	719	410	0	634	0	11677	7356	2063	18971	9069	4425	3711	4620	4678	2240	66570	29.71875	
1677-3	681	0	0	0	0	0	472	0	10180	8745	2317	14819	7437	3458	2565	3597	4305	1153	57423	49.80312	
1719-1	2075	694	0	1448	1566	0	712	752	11342	11087	4240	23330	9078	5337	4742	4855	6514	7247	80523	11.11122	11.4
1719-2	4223	804	778	602	2154	0	1200	670	16930	15090	4645	29036	13175	7053	5569	6347	9513	10431	107358	10.29221	
1719-3	2277	462	637	695	1462	0	750	858	13765	14546	4316	26252	10879	939	7721	5758	8196	7141	92372	12.93544	

Appendix Table M: GDM placentas +ve DHB GDM 06-04-22

	Healthy placenta in +ve DHB 4ul +4ul	LPC 16:0 (+H+)	LPC 16:0 (+Na+)	LPC 18:2 (+H+)	LPC 18:1 (+H+)	LPC 18:0 (+H+)	LPC 18:2 (+Na+)	LPC 18:1 (+Na+)	LPC 18:0 (+Na+)	PC 16:0/18:2 (+H+)	PC 16:0/18:1 (+H+)	PC 16:0/18:2 (+Na+)	PC 16:0/18:1 (+Na+) and PC 16:0/20:4 (+H+)	PC 18:0/18:3 (+H+)	PC 18:0/18:2 (+H+)	PC 16:0/20:4 (+Na+)	PC 18:0/18:3 (+Na+)	PC 18:0/18:2 (+Na+)	∑LPC	∑PC	∑PC/∑LPC	Average relative ratio of 3reps Maldi intensities calculated m/z ∑PC / ∑LPC m/z
	CAT.NO.	496.3398	518.3241	520.2905	522.1672	524.2854	542.3241	544.2672	546.3554	758.5694	760.5851	780.5538	782.5694	784.5851	786.6454	804.5749	806.5694	808.5851				
only one repeat	1621	2492.53	0	0	0	0	0	0	0	32537.71	19155.77	11443.5	48906.67	26303.51	12086.77	12277.78	15386.58	16248.48	2492.53	194346.8	77.97169	78.0
1	1679-1	2641	399	957	1975	1264	0	1068	393	16358	14961	4402	29235	17049	9951	5842	9006	13488	8697	120292	13.83144	12.6
1	1679-2	800			1355	791	0	498		6031	6047	2179	9289	4663	3564	1446	2722	3174	3444	38115	11.06707	
1	1679-3	2974	819	841	2500	2418	0	1691	686	21598	22873	6683	36916	18986	12041	7426	12340	14468	11929	153331	12.85363	
																			0	0		
2	1687-1	1391	0	0	0	0	0	516	374	6972	5958	1649	12318	6631	2909	2436	3424	4913	2281	47210	20.69706	14.8
2	1687-2	2920	761	616	871	1641	433	620	691	18763	16398	6057	30614	17770	9859	8965	10887	9439	8553	128752	15.05343	
2	1687-3	1975	1078	986	1975	1661	0	1021	883	12335	11619	3550	19976	10987	6481	4803	6472	7497	9579	83720	8.739952	
3	1701-1	2371	520	615	922	997	0	0	0	17146	15793	3222	31045	15702	7407	4022	4821	6974	5425	106132	19.5635	16.9
3	1701-2	1988	661	388	0	0	0	398	0	9048	8377	2183	19409	5573	3531	2270	4461	5661	3435	60513	17.61659	
3	1701-3	656.41	0	372.94	656.8	0	0	580.57	0	5179.5	4591.84	0	10271.56	3445.51	1263.47	1261.92	2228.59	2324.42	2266.72	30566.81	13.48504	
3	1701-4	2083	0	482	0	943	0	484	0	16088	12640	3301	22834	11279	5956	2958	5684	7795	3992	88535	22.17811	
4	1706-3	2521	0	1066	1164	0	0	2328	0	25325	19467	7934	46882	22991	8884	10193	12744	13617	7079	168037	23.73739	24.8
4	1706-2	2077	0	0	528	1358	0	791	628	20182	16453	5263	35961	18668	8818	8674	7947	10953	6382	133919	24.88276	
4	1706-1	4106	0	662	590	0	0	1762	0	28969	20695	7911	50228	26114	12155	10605	13384	13391	7120	183452	25.76573	
																			0	0		
5	1763-1	850.43	267.87	0	0	0	0	0	279.78	9660.74	6355.86	0	18057.74	9807.38	3082.6	4152.88	4606.5	5866.21	1398.08	61589.91	44.05321	40.6
5	1763-2	1013.27	0	0	0	260.97	0	531.96	0	8472.97	5843.32	0	19206.23	7347.03	2121.52	5029.24	5315.46	4822.59	1806.2	58158.36	32.19929	
5	1763-3	1101.17	0	274.96	0	614.08	0	0	0	15404.57	9391.55	4856.79	30105.6	10749.75	0	6391.01	7201.98	6750.96	1990.21	90852.21	45.64956	
6	1574-1	3210	0	0	1855	1853	0	1493	0	22627	20708	7528	41549	23066	11853	14020	11373	15217	8411	167941	19.96683	17.4
6	1574-2	2841	980	906	619	2034	0	1099	1137	16006	15001	9641	38248	16038	8590	13163	12268	14029	9616	142984	14.86938	
6	1574-3	1429	961	735	0	1381	0	805	0	10818	9597	5827	23264	11735	7020	7250	7615	8449	6311	91575	17.24252	
7	1645-1	778	0	0	483	440	0	0	0	10977	8379	5299	17449	10117	6998	3833	5845	6018	1701	74915	44.04174	28.4
7	1645-2	4878	0	0	5639	3744	0	2223	0	51112	35661	24894	64316	44386	24786	24843	29350	29717	16484	329065	19.96269	
7	1645-3	1248	541	607	770	732	0	433	0	15255	10786	4328	18148	13300	7294	5632	8844	8219	4331	91806	21.19741	
																			0	0		
8	1688-1	1419	451	545	1134	1284	0	0	0	10238	8849	3514	18284	8607	4505	4735	5725	6622	4833	71079	14.70701	11.6
8	1688-2	971	490	464	1985	758	0	474	967	8088	8890	3494	15425	7318	3539	4098	4161	5769	6109	60782	9.949583	
8	1688-3	1903	787	648	4142	1546	0	682	1166	13276	13741	6774	29889	14453	6216	7886	8464	10400	10874	111099	10.21694	
9	1702-1	1104	0	0	1428	615	0	603	0	4678	4799	2949	7491	3879	2649	2309	2776	2093	3750	33623	8.966133	9.5
9	1702-2	4323	1572	1336	3499	2192	0	1600	0	16844	16701	7035	28278	15814	8258	9922	9799	11064	14522	123715	8.519143	
9	1702-3	1124	0	0	1503	1502	0	1168	915	9303	9044	3428	16476	7327	3950	4162	6811	7354	6212	67855	10.92321	
10	1707-1	7747	1637	1793	6507	4626	0	3799	1902	51490	47645	17602	95974	46750	27866	19936	34654	35291	28011	377208	13.46642	12.5
10	1707-2	6415	1750	1525	5539	3748	0	3105	1834	43305	43173	15152	79114	39686	22855	17248	26684	29770	23916	316987	13.25418	
10	1707-3	6626	1978	1685	8630	5218	0	4448	2441	45832	46011	15240	79834	40503	21145	21518	31169	33203	31026	334455	10.77983	
11	1708-1	11607	0	2292	7623	5950	0	3296	2375	59052	59920	14392	86875	43572	22000	19057	20122	25179	33143	350169	10.5654	8.5
11	1708-2	9931	0	0	21201	5089	0	3661	0	46829	44536	11015	3352	37241	17435	15062	16349	22619	39882	214438	5.376812	
11	1708-3	7056	2235	1261	1562	2911	0	2051	0	21165	24076	8192	43531	21888	10263	9882	11230	12390	17076	162617	9.523132	
only one repeat	1702	9786	0	1724	1935	4872	0	0	2308	32990	33804	9663	58260	27486	16306	15713	17550	19327	20625	231099	11.2048	11.2

Appendix Table N: Health placentas +ve DHB Healthy 06-04-22

Obese placenta in +ve DHB 4ul +4ul	LPC 16:0 (+H+)	LPC 16:0 (+Na+)	LPC 18:2 (+H+)	LPC 18:1 (+H+)	LPC 18:0 (+H+)	LPC 18:2 (+Na+)	LPC 18:1 (+Na+)	LPC 18:0 (+Na+)	PC 16:0/18:2 (+H+)	PC 16:0/18:1 (+H+)	PC 16:0/18:2 (+Na+)	PC 16:0/18:1 (+Na+) and PC 16:0/20:4 (+H+)	PC 18:0/18:3 (+H+)	PC 18:0/18:2 (+H+)	PC 16:0/20:4 (+Na+)	PC 18:0/18:3 (+Na+)	PC 18:0/18:2 (+Na+)	∑LPC	∑PC	∑PC/∑LPC	Average relative ratio of 3reps Maldi Intensities calculated m/z ∑PC / ∑LPC m/z
CAT.NO.	496.3398	518.3241	520.2905	522.1672	524.2854	542.3241	544.2672	546.3554	758.5694	760.5851	780.5538	782.5694	784.5851	786.6454	804.5749	806.5694	808.5851				
1550-1	885	588	0	1029	605	0	0	0	4930	5480	2297	9406	5624	3943	2164	2502	3296	3107	39642	12.75893	
1550-2	2367	861	600	888	1200	0	1126	0	10071	9307	3284	17906	10497	6513	5392	6814	6305	7042	76089	10.80503	
1550-3	6207	1938	0	4685	3004	0	2160	1644	36178	38156	14950	57258	29501	19317	18179	19584	22315	19638	255438	13.00733	12.2
																		0	0		
1606-1	1034	456	0	0	727	0	0	0	8861	8260	1893	17428	6540	4108	4606	3823	5310	7217	60829	27.43753	
1606-2	1957	871	569	906	1058	0	1041	474	13875	11605	3872	25572	11850	7276	4994	7092	7747	6876	93883	13.65372	
1606-3	1704	0	360	867	935	0	744	346	11121	12835	3499	25300	12038	6869	7427	6867	6931	4956	91887	18.54056	19.9
																		0	0		
1622-1	763.78	319.96	0	980.53	320.87	0	527.23	0	4073.65	3915.68	12139.06	0	3646.21	1839.85	3273.18	2703.47	3541.3	2912.37	35132.4	12.06317	
1622-2	298.03	0	0	0	287.04	0	323.54	339.8	3895.05	3658.3	10717.49	0	2538.51	0	0	0	2607.79	1248.41	23417.14	18.75757	
1622-3	780.24	0	336.82	0	0	0	0	0	3694.05	3888.72	0	10361.48	3180.84	1481.51	2518.65	2091.63	2559.59	1117.06	29776.47	26.65611	19.2
																		0	0		
1655-1	3225	574	915	427	1500	0	1018	456	17401	18028	5419	43703	15755	9264	7636	10005	12634	8115	139845	17.2329	
1655-2	4244	1228	696	961	2372		1089	1211	23686	23110	7622	60457	22835	10710	9512	10673	16431	11801	185036	15.67969	
1655-3	4603	964	0	1380	2114	0	831	975	19780	21577	6132	48531	19613	11410	11985	11995	15887	10867	166910	15.35934	16.1
																		0	0		
1656-1	1173.69	549.53	0	0	0	0	0	0	10490.35	9107.76	0	25984.27	7471.19	2946.77	5339.92	4707.06	5046.83	1723.22	71094.15	41.25657	
1656-2	1089.19	442.25	559.87	1843.67	0	0	0	344.9	6359.28	5219.89	0	13305	4115.56	1807.03	3561.21	2597.32	3007.03	4279.88	39972.32	9.339589	
1656-3	462.28	392.99	0	0	236.73	0	0	0	3045.81	3035.41	1963.65	10385.05	2563.55	867.4	3177.92	2173.37	1834.52	1092	29046.68	26.59952	25.7
																		0	0		
centre 1680-1	868.16	0	334.43	444.4	590.82	0	325.69	415.94	9327.14	7019.94	0	17612.43	6205.06	3758.35	2801.78	5092.72	5646.18	2979.44	57463.6	19.28671	
centre 1680-2	1746.56	0	0	624.41	834.16	0	0	0	14092	11963.99	4601.44	40007.42	11023.55	0	9862.35	7379.55	8552.06	3205.13	107482.4	33.53448	
centre 1680-3	813.61	0	0	0	519.66	0	0	458.23	10635.36	9054.13	3249.7	23655.25	9423.75	5077.03	3288.62	4450.68	7333.59	1791.5	76168.11	42.51639	31.8
																		0	0		
edge 1680-1	2704.79	0	0	0	1812.45	0	0	1072.98	17930.54	17466.3	6392.64	49203.05	13676.59	5596.14	13016.85	9505.69	12387.77	5590.22	145175.6	25.96956	
edge 1680-2	962.14	0	0	0	0	0	0	0	9167.58	9694.75	0	19253.98	6830.75	3950.01	3521.91	5918.32	7685.76	962.14	66023.06	68.62105	
edge 1680-3	577.17	0	0	520.83	368.77	0	0	0	4069.91	3861.22	0	11865.36	2628.78	1363.71	3798.96	2572.21	0	1466.77	30160.15	20.56229	38.4
																		0	0		
1500-1	1232	506	0	1011	1061	0	575	841	6210	7196	3126	14587	5485	3659	4686	4151	5170	5226	54270	10.38462	
1500-2	2085	0	791	0	1949	0	773	1346	13797	15268	6510	30181	14727	6143	8901	7739	10937	6944	114203	16.44628	
1500-3	4788	1116	1174	1583	3904	0	1761	1878	29256	29178	7201	61934	26503	13030	14137	13814	18679	16204	213732	13.19008	13.3
																		0	0		
1614-1	2480	0	655	697	1206	0	456	879	18077	16416	5246	36962	18143	10777	6444	11695	12425	6373	136185	21.36906	
1614-2	2574	596	1243	1673	1373	0	730	0	21085	21719	4490	39232	19391	11497	7241	11676	13694	8189	190025	18.32031	
1614-3	1408	0	0	0	0	0	0	456	19464	18171	4467	39553	19599	12238	3961	8471	13025	1864	138949	74.54345	38.1
																		0	0		
1644-1	1494	0	590	592	949	0	0	0	12361	10326	3555	21942	13693	6378	5690	5968	7129	3625	87042	24.01159	
1644-2	2324	1180	0	0	819	0	0	769	9718	8631	2619	19648	11053	4863	5192	6769	6535	5092	75028	14.73449	
1644-3	5472	1117	0	0	2089	0	0	0	29830	34079	6086	62581	35571	18751	10375	19020	24110	6678	243403	36.44849	25.1
																		0	0		
1661-1	1996	0	0	628	697	0	569	0	8887	8107	2214	17731	8120	4801	4110	3988	6067	3890	64025	16.45887	
1661-2	1405	0	0	1154	518	482	0	643	8426	10706	3372	19651	11372	5514	5918	8025	7500	4002	80484	20.11094	
1661-3	2538	0	651	5744	1675	0	1013	0	19786	19356	7158	35767	17488	10447	8679	11007	15616	11621	145304	12.50357	16.4
																		0	0		
1670-1	2628	0	1607	1620	1142	0	1293	0	28878	27460	6802	67737	27790	13975	10164	14963	20283	8290	218032	26.3006	
1670-2	506	0	768	9539	1038	0	900	0	10029	9420	2550	27391	10643	5778	5806	6307	9153	12751	86077	6.750608	
1670-3	1256	543	0	1077	842	0	876	696	10528	10113	3511	25877	10448	6088	4686	7922	8782	5290	86955	16.43762	16.5
																		0	0		
1707-1	3489	0	729	0	2090		805	1212	25541	23297	6671	47762	24040	14521	10804	13738	17222	8325	183596	22.05357	
1707-2	2913	1075		1549	2749	0	1011	1266	20306	17074	7671	38163	17809	8735	8545	11340	14954	10563	144597	13.68901	17.9
																		0	0		
1759-1	2256	0	0	2129	3386	0	0	2768	12831	12373	7027	32069	13829	7374	11630	8958	11945	10539	118036	11.19992	
1759-2	1637	0	0	0	2574	0	0	1167	12445	13412	5578	30349	11396	7844	9356	8363	12299	5378	111042	20.64745	
1759-3	2752	1195	1236	781	2029	0	0	776	14240	13135	3944	29427	14123	7947	6610	8548	8350	8769	106324	12.12499	14.7
																		0	0		
1771-1	1381	1183	0	0	1218	0	711	1915	13488	8646	7626	33480	12312	4884	12988	8954	10264	6408	112642	17.57834	
1771-2	2913	1751	0	1307	1389	0	784	953	15313	13537	7890	35628	13939	8077	13360	10217	9600	9097	127561	14.02232	
1771-3	932	513	0	1213	1286	0	451	610	4984	5062	2583	15178	6769	3232	6245	4837	5796	5005	63686	10.72647	14.1

Appendix Table O: Obese placentas +ve DHB Obese 06-04-22

Placentwo different chunks ta	Healthy Placenta BMI	Number of repeats	Healthy Placenta Refernce number stock at [10mg/ml]	LPC 16:0 (+H+)	LPC 16:0 (+Na+)	LPC 18:2 (+H+)	LPC 18:1 (+H+)	LPC 18:0 (+H+)	LPC 18:2 (+Na+)	LPC 18:1 (+Na+)	LPC 18:0 (+Na+)	PC 16:0/18:2 (+H+)	PC 16:0/18:1 (+H+)	PC 16:0/18:2 (+Na+)	PC 16:0/18:1 (+Na+) and PC 16:0/20:4 (+H+)	PC 18:0/18:3 (+H+)	PC 18:0/18:2 (+H+)	PC 16:0/20:4 (+Na+)	PC 18:0/18:3 (+Na+)	PC 18:0/18:2 (+Na+)	∑LPC	∑PC	∑PC/∑LPC	Average relative ratio of 3reps Maldi Intensities calculated m/z ∑PC / ∑LPC m/z
			CAT No. rep	496.3398	518.3241	520.2905	522.1672	524.2854	542.3241	544.2672	546.3554	758.5694	760.5851	780.5538	782.5694	784.5851	786.6454	804.5749	806.5694	808.5851				
left side of cord chunk1	Healthy BMI ≤30	1	1531	20899.000	0	3571.000	8146.000	5392.000	0	4478.000	0	54733.000	51559.000	6357.000	115850.000	50280.000	26555.000	4545.000	23927.000	37143.000	42486.000	370949.000	8.731087888	
		2	1531	20363.000	0	3605.000	2269.000	4979.000	0	4841.000	0	56205.000	53235.000	6743.000	126272.000	51378.000	25470.000	3754.000	24573.000	41369.000	36057.000	388999.000	10.78844607	
		3	1531	36618.000	0	8106.000	12622.000	9342.000	0	8121.000	0	75651.000	66146.000	9985.250	171227.000	72028.000	34298.000	7450.000	35990.000	58498.000	74809.000	531273.250	7.10172907	8.9
																					0.000			
right side of cord chunk1	Healthy BMI ≤30	1	1534	18272.000	0	3531.000	5439.000	4528.000	0	4267.000	1723.000	47261.000	39733.000	4904.000	108104.000	43403.000	20976.000	3234.000	21054.000	32678.000	37760.000	321347.000	8.510248941	
		2	1534	39683.30	0	40621.62	40699.32	40776.99	0	41538.79	0	48958.72	49023.12	49656.99	49720.25	49783.61	49846.93	50407.91	50470.19	50532.73	203320.014	448400.463	2.205392646	
		3	1534	22466.000	0	4317.000	7443.000	5622.000	0	4949.000	0	54640.000	49752.000	7244.000	126186.000	54223.000	24036.000	5318.000	26628.000	39388.000	44797.000	387415.000	8.648235373	6.5
																					0.000			
centre left of colrd chunk2	Healthy BMI ≤30	1	1531	36618.000	0	8106.000	12622.000	9342.000	0	8121.000	0	75651.000	66146.000	9985.250	171227.000	72028.000	34298.000	7450.000	35990.000	58498.000	74809.000	531273.250	7.10172907	
		2	1531	24922.000	0	4612.000	3295.000	7327.000	0	6599.000	2859.000	50732.000	46609.000	6407.000	109125.000	47701.000	21826.000	5976.000	22218.000	36891.000	49614.000	347485.000	7.003769097	
		3	1531	6833.000	0	1606.000	3658.000	1646.000	0	2443.000	1166.000	21611.000	18290.000	2444.000	54549.000	22173.000	10448.000	0	11671.000	19718.000	17352.000	160904.000	9.272936837	7.8
																					0.000			
lower centre right of cord chunk2	Healthy BMI ≤30	1	1534	22466.000	0	4317.000	7443.000	5622.000	0	4949.000	0	54640.000	49752.000	7244.000	126186.000	54223.000	24036.000	5318.000	26628.000	39388.000	44797.000	387415.000	8.648235373	
		2	1534	39682.98	0	40621.44	40698.92	40776.79	0	41538.08	41614.01	48958.28	49022.77	49656.43	49719.84	49783.23	49846.52	50407.18	50469.78	50532.29	244932.221	448396.322	1.830695531	
		3	1534	20743.000	0	4847.000	7338.000	6142.000	0	5813.000	2618.000	57555.000	50821.000	5443.000	132557.000	55162.000	27005.000	3952.000	28739.000	43345.000	47501.000	404579.000	8.517273321	6.3

Appendix Table P: New placentas homogenization different cuts edges, centre after Hamilton Seringer sterilisation deep cleaning due to previous smearing, healthy, obese, GDM 6-12-2021 Warwick trip 9AA+

Obese Placenta	Obese Placenta [10mg/ml] 9AA	LPC 16:0 (+H+)	LPC 16:0 (+Na+)	LPC 18:2 (+H+)	LPC 18:1 (+H+)	LPC 18:0 (+H+)	LPC 18:2 (+Na+)	LPC 18:1 (+Na+)	LPC 18:0 (+Na+)	PC 16:0/18:2 (+H+)	PC 16:0/18:1 (+H+)	PC 16:0/18:2 (+Na+)	PC 16:0/18:1 (+Na+) and PC 16:0/20:4 (+H+)	PC 18:0/18:3 (+H+)	PC 18:0/18:2 (+H+)	PC 16:0/20:4 (+Na+)	PC 18:0/18:3 (+Na+)	PC 18:0/18:2 (+Na+)	∑LPC	∑PC	∑PC/∑LPC	Average relative ratio of 3reps Maldi Intensities calculated m/z ∑PC / ∑LPC m/z
	CAT No. rep	496.3398	518.3241	520.2905	522.1672	524.2854	542.3241	544.2672	546.3554	758.5694	760.5851	780.5538	782.5694	784.5851	786.6454	804.5749	806.5694	808.5851				
Maternal edge	1550-1	20350	0	5169	8990	6702	0	5498	0	60130	5340	0	113646	62632	5283	5075	26616	41523	46709	320245	6.856173328	
		31369	0	7340	11850	9208	0	7510	0	54889	50018	8099	103411	55764	30883	0	27113	40533	67277	370710	5.510204082	
		34022	0	7530	12870	10381	0	7600	0	57191	53687	10108.5	106490	57997	7547	8589	28362	41530	72403	371501.5	5.131023576	5.8
Maternal edge	1622-1	39827	0	8250	19551	10340	0	8605	0	52924	52218	10666.75	99765	53864	28136	12724	28733	36846	86573	375876.75	4.341731833	
		39241	0	8437	13823	12569	0	9196		55418	52692	11456	109711	60428	32110	11522	29474	40810	83266	403621	4.847368674	
		35613	0	8206	18558	10749	0	0	0	69440	64504	17151	134308	74595	38215	19255	38964	49249	73126	505681	6.91520116	5.4
Maternal near Cor	1622-2	31823	0	6153	10331	8014	0	6812	0	68508	65539	11783	125401	70035	37776	10781	30445	47089	63133	467357	7.402737079	
		30918		6554	11460	9530	0	6963	0	68659	66694	9913	132631	73745	40980	9446	31135	44634	65425	477837	7.303584257	
		31823		6153	10331	8014	0	6812	0	68508	65539	11783	125401	70035	37776	10781	30445	47089	63133	467357	7.402737079	7.4
Maternal near Cor	1550-2	25972	0	6139	10638	7559	0	6507	0	54226	48978	7236	106401	57136	32707	0	22768	42031	56815	371483	6.538466954	
		14527	0	3268	5602	3907	0	3492	0	26508	27365	3202	52968	29512	15776	0	12010	20223	30796	187564	6.090531238	
		20350	0	5169	8990	6702	0	5498	0	60130	5340	0	113646	62632	5283	5075	26616	41523	46709	320245	6.856173328	6.5
Centre Right	1622-3	31823.0	0.0	6153.0	10331.0	8014.0	0.0	6812.0	0.0	68508.0	65539.0	11783.0	125401.0	70035.0	37776.0	10781.0	30445.0	47089.0	63133	467357.0000	7.4027	
	1622-3	30918.0	0.0	6554.0	11460.0	9530.0	0.0	6963.0	0.0	68659.0	66694.0	9913.0	132631.0	73745.0	40980.0	9446.0	31135.0	44634.0	65425	477837.0000	7.3036	
	1622-3	31823.0	0.0	6153.0	10331.0	8014.0	0.0	6812.0	0.0	68508.0	65539.0	11783.0	125401.0	70035.0	37776.0	10781.0	30445.0	47089.0	63133	467357.0000	7.4027	7.4
Centre left	1550-3	31369.0	0.0	7340.0	11850.0	9208.0	0.0	7510.0	0.0	54889.0	50018.0	8099.0	103411.0	55764.0	30883.0		27113.0	40533.0	67277	370710.0000	5.5102	
	1550-3	34022.0	0.0	7530.0	12870.0	10381.0	0.0	7600.0	0.0	57191.0	53687.0	10108.5	106490.0	57997.0	7547.0	8589.0	28362.0	41530.0	72403	371501.5000	5.1310	
	1550-3	25972.0	0.0	6139.0	10638.0	7559.0	0.0	6507.0	0.0	54226.0	48978.0	7236.0	106401.0	57136.0	32707.0	6194.0	22768.0	42031.0	56815	377677.0000	6.6475	5.8

Appendix Table Q: New placentas different cuts edges, centre after Hamilton syringe sterilisation deep cleaning due to previous smearing, healthy, obese, GDM 6-12-2021 Warwick trip 9AA+

9AA Matrix GDM placenta sides	GDM Placenta Refernce CAT	LPC 16:0 (+H+)	LPC 16:0 (+Na+)	LPC 18:2 (+H+)	LPC 18:1 (+H+)	LPC 18:0 (+H+)	LPC 18:2 (+Na+)	LPC 18:1 (+Na+)	LPC 18:0 (+Na+)	PC 16:0/18:2 (+H+)	PC 16:0/18:1 (+H+)	PC 16:0/18:2 (+Na+)	PC 16:0/18:1 (+Na+) and PC 16:0/20:4 (+H+)	PC 18:0/18:3 (+H+)	PC 18:0/18:2 (+H+)	PC 16:0/20:4 (+Na+)	PC 18:0/18:3 (+Na+)	PC 18:0/18:2 (+Na+)	∑LPC	∑PC	∑PC/∑LPC	Average relative ratio of 3reps Maldi Intensities calculated m/z ∑PC / ∑LPC m/z
	CAT No.	496.3398	518.3241	520.2905	522.1672	524.2854	542.3241	544.2672	546.3554	758.5694	760.5851	780.5538	782.5694	784.5851	786.6454	804.5749	806.5694	808.5851				
Maternal edge	1545-1	45330.000	0	10307.000	15083.000	14042.000	0.000	10866.000	0.000	55988.000	52221.000	13352.414	107793.000	56502.000	51913.000	12335.000	30922.000	43790.000	95628.000	404816.414	4.233241457	
Maternal edge	1545-1	45002.000	0	9778.000	15263.000	12581.000	0.000	10611.000	7425.000	56837.000	53839.000	12368.742	111188.000	61366.000	52400.000	11609.000	31145.000	43627.000	100660.000	414379.742	4.116627677	
Maternal edge	1545-1	54072.000	0	14292.000	18294.000	15070.000	0.000	14132.000	0.000	63901.000	58313.000	14863.135	117995.000	63579.000	40947.000	16643.000	35145.000	45504.000	115860.000	456890.135	3.943467416	4.1
Maternal edge	1578-1	23247.000	0	8093.000	8793.000	6340.000	0.000	7119.000	3069.000	61810.000	50173.000	7150.694	129581.000	67576.000	36528.000	0.000	32827.000	52305.000	56661.000	437950.694	7.729314593	
Maternal edge	1578-1	21082.000	0	5177.000	8762.000	6896.000	0.000	5573.000	0.000	49660.000	41475.000	5457.000	102281.000	50935.000	25575.000	4884.000	25556.000	39327.000	47490.000	345150.000	7.267845862	
Maternal edge	1578-1	23740.000	0	7672.000	5499.000	5723.000	0.000	7252.000	3684.000	55291.000	48780.000	7560.000	118171.000	58845.000	32985.000	0.000	32499.000	46134.000	53570.000	400265.000	7.471812582	7.5
Maternal edge	1669-1	48825.000	0	10039.000	16467.000	14260.000	0.000	12281.000	0.000	56503.000	53919.000	14859.846	108317.000	58696.000	34056.000	15752.000	29818.000	44318.000	101872.000	416238.846	4.085900404	
Maternal edge	1669-1	43737.000	0	8500.000	14556.000	13118.000	0.000	11331.000	8110.000	58625.000	55795.000	10974.337	119216.000	63968.000	33307.000	11011.000	32289.000	45739.000	99352.000	430924.337	4.337349396	
Maternal edge	1669-1	50654	0	11686	17725	14330	0.000	11736	0.000	66372	64453	12156	131124	72089	37641	11452	35346	49837	106131.000	480470.000	4.527140986	4.3
Maternal Cord	1545-2	47028.000	0	10708.000	28170.000	14225.000	0.000	11947.000	0.000	56913.000	56061.000	13056.000	111657.000	59220.000	36142.000	13154.000	29875.000	42165.000	112078.000	418243.000	3.731713628	
Maternal Cord	1545-2	47918.000	0	10367.000	17713.000	15415.000	0.000	12719.000	0.000	49292.000	46651.000	11524.342	90794.000	50025.000	28241.000	12726.000	25882.000	35753.000	104132.000	350888.342	3.369649505	
Maternal Cord	1545-2	54103.000	0	11860.000	17268.000	16633.000	0.000	13520.000	0.000	59718.000	53984.000	12270.000	114419.000	65631.000	35832.000	12725.000	34641.000	45119.000	113384.000	434339.000	3.830690397	3.6
Maternal Cord	1578-2	35178.000	0	9600.000	12317.000	9507.000	0.000	10678.000	0.000	51704.000	46157.000	8353.000	102154.000	56565.000	29652.000	6507.000	28882.000	38905.000	77280.000	368879.000	4.773278986	
Maternal Cord	1578-2	38499.000	0	10990.000	16787.000	13575.000	0.000	11895.000	7001.000	64069.000	57199.000	10098.750	131753.000	69488.000	39296.000	0.000	35260.000	54074.000	98747.000	461237.750	4.670903926	
Maternal Cord	1578-2	40570.000	0	11945.000	15841.000	12756.000	0.000	11796.000	6245.000	69154.000	57596.000	10627.000	140757.000	70964.000	38677.000	10010.000	36664.000	55413.000	99153.000	489862.000	4.940465745	4.8
Maternal Cord	1669-2	48825.000	0	10039.000	16467.000	14260.000	0.000	12281.000	0.000	56503.000	53919.000	14859.846	108317.000	58696.000	34056.000	15752.000	29818.000	44318.000	101872.000	416238.846	4.085900404	
Maternal Cord	1669-2	43737.000	0	8500.000	14556.000	13118.000	0.000	11331.000	8110.000	58625.000	55795.000	10974.337	119216.000	63968.000	33307.000	11011.000	32289.000	45739.000	99352.000	430924.337	4.337349396	
Maternal Cord	1669-2	50654	0	11686	17725	14330	0.000	11736	0.000	66372	64453	12156	131124	72089	37641	11452	35346	49837	106131.000	480470.000	4.527140986	4.3

Appendix Table R: Placentas GDM PC-LPC 9AA+ve

9-AA Matrix	Number of repeats	Placenta Refernce number stock at [10mg/ml]	LPC 16:0 (+H+)	LPC 16:0 (+Na+)	LPC 18:2 (+H+)	LPC 18:1 (+H+)	LPC 18:0 (+H+)	LPC 18:2 (+Na+)	LPC 18:1 (+Na+)	LPC 18:0 (+Na+)	PC 16:0/18:2 (+H+)	PC 16:0/18:1 (+H+)	PC 16:0/18:2 (+Na+)	PC 16:0/18:1 (+Na+) and PC 16:0/20:4 (+H+)	PC 18:0/18:3 (+H+)	PC 18:0/18:2 (+H+)	PC 16:0/20:4 (+Na+)	PC 18:0/18:3 (+Na+)	PC 18:0/18:2 (+Na+)	∑LPC	∑PC	∑PC/∑LPC	Average relative ratio of 3reps Maldi Intensities calculated m/z ∑PC / ∑LPC m/z
		CAT No. rep	496.3398	518.3241	520.2905	522.1672	524.2854	542.3241	544.2672	546.3554	758.5694	760.5851	780.5538	782.5694	784.5851	786.6454	804.5749	806.5694	808.5851				
Healthy BMI ≤30	1	1531-1	20899.0	0.0	3571.0	8146.0	5392.0	0.0	4478.0	0.0	54733.0	51559.0	6357.0	115850.0	50280.0	26555.0	4545.0	23927.0	37143.0	42486.0000	370949.0000	8.7311	
	2	1531-1	20363.0	0.0	3605.0	2269.0	4979.0	0.0	4841.0	0.0	56205.0	53235.0	6743.0	126272.0	51378.0	25470.0	3754.0	24573.0	41369.0	36057.0000	388999.0000	10.7884	
	3	1531-1	36618.0	0.0	8106.0	12622.0	9342.0	0.0	8121.0	0.0	75651.0	66146.0	9985.3	171227.0	72028.0	34298.0	7450.0	35990.0	58498.0	74809.0000	531273.2500	7.1017	8.9
Healthy BMI ≤30	1	1534-1	18272.0	0.0	3531.0	5439.0	4528.0	0.0	4267.0	1723.0	47261.0	39733.0	4904.0	108104.0	43403.0	20976.0	3234.0	21054.0	32678.0	37760.0000	321347.0000	8.5102	
	2	1534-1	39683.3	0.0	40621.6	40699.3	40777.0	0.0	41538.8	0.0	48958.7	49023.1	49657.0	49720.3	49783.6	49846.9	50407.9	50470.2	50532.7	203320.0139	448400.4635	2.2054	
	3	1534-1	22466.0	0.0	4317.0	7443.0	5622.0	0.0	4949.0	0.0	54640.0	49752.0	7244.0	126186.0	54223.0	24036.0	5318.0	26628.0	39388.0	44797.0000	387415.0000	8.6482	6.5
Healthy BMI ≤30	1	1531-2	36618.0	0.0	8106.0	12622.0	9342.0	0.0	8121.0	0.0	75651.0	66146.0	9985.3	171227.0	72028.0	34298.0	7450.0	35990.0	58498.0	74809.0000	531273.2500	7.1017	
	2	1531-2	24922.0	0.0	4612.0	3295.0	7327.0	0.0	5599.0	2859.0	50732.0	46609.0	6407.0	109125.0	47701.0	21826.0	5976.0	22218.0	36891.0	49614.0000	347485.0000	7.0038	
	3	1531-2	6833.0	0.0	1606.0	3698.0	1646.0	0.0	2443.0	1166.0	21611.0	18290.0	2444.0	54549.0	22173.0	10448.0		11671.0	19718.0	17352.0000	160904.0000	9.2729	7.8
Healthy BMI ≤30	1	1534-2	22466.0	0.0	4317.0	7443.0	5622.0	0.0	4949.0		54640.0	49752.0	7244.0	126186.0	54223.0	24036.0	5318.0	26628.0	39388.0	44797.0000	387415.0000	8.6482	
	2	1534-2	39683.0	0.0	40621.4	40698.9	40776.8	0.0	41538.1	41614.0	48958.3	49022.8	49656.4	49719.8	49783.2	49846.5	50407.2	50469.8	50532.3	244932.2205	448396.3216	1.8307	
	3	1534-2	20743.0	0.0	4847.0	7338.0	6142.0	0.0	5813.0	2618.0	57555.0	50821.0	5443.0	132557.0	55162.0	27005.0	3952.0	28739.0	43345.0	47501.0000	404579.0000	8.5173	6.3
Healthy BMI ≤30	1	1534-2	20350.0	0.0	5169.0	11551.0	9342.0	0.0	9131.0	0.0	60130.0	55539.0	9985.3	113646.0	62632.0	5283.0	5075.0	26616.0	41523.0	55543.0000	390429.2500	7.0293	
	2	1534-2	31369.0	0.0	7340.0	13823.0	7327.0	0.0	9599.0	0.0	54889.0	50018.0	8099.0	103411.0	55764.0	30883.0	0.0	27113.0	40533.0	69458.0000	370710.0000	5.3372	
	3	1534-2	34022.0	0.0	7530.0	10558.0	1646.0	0.0	9443.0	0.0	57191.0	53687.0	10108.5	106490.0	57997.0	7547.0	8589.0	28362.0	41530.0	63199.0000	371501.5000	5.8783	6.1
Obese BMI ≥30-60	1	1622-1	39827.0	0.0	8250.0	12622.0	10340.0	0.0	8605.0	0.0	52924.0	52218.0	10666.8	99765.0	53864.0	28136.0	12724.0	28733.0	36846.0	79644.0000	375876.7500	4.7195	
	2	1622-1	39241.0	0.0	8437.0	3295.0	12569.0	0.0	9196.0	0.0	55418.0	52692.0	11456.0	109711.0	60428.0	32110.0	11522.0	29474.0	40810.0	72738.0000	403621.0000	5.5490	
	3	1622-1	35613.0	0.0	8206.0	3658.0	10749.0	0.0	0.0	0.0	69440.0	64504.0	17151.0	134308.0	74595.0	38215.0	19255.0	38964.0	49249.0	58226.0000	505681.0000	8.6848	6.3
Obese BMI ≥30-60	1	1622-2	31823.0	0.0	6153.0	11551.0	8014.0	0.0	6812.0	0.0	48508.0	55539.0	11783.0	125401.0	70035.0	37776.0	10781.0	30445.0	47089.0	64353.0000	447357.0000	6.9516	
	2	1622-2	30918.0	0.0	6554.0	13823.0	9530.0	0.0	6963.0	0.0	57659.0	66694.0	9913.0	132631.0	73745.0	40980.0	9446.0	31135.0	44634.0	67788.0000	446837.0000	6.5917	
	3	1622-2	31823.0	0.0	6153.0	10558.0	8014.0	0.0	6812.0	0.0	48308.0	55539.0	11783.0	125401.0	70035.0	37776.0	10781.0	30445.0	47089.0	63360.0000	447157.0000	7.0574	6.9
Obese BMI ≥30-60	1	1550-2	25972.0	0.0	6139.0	10638.0	7559.0	0.0	6507.0	0.0	54226.0	48978.0	7236.0	106401.0	57136.0	32707.0	0.0	22768.0	42031.0	56815.0000	371483.0000	6.5385	
	2	1550-2	14527.0	0.0	3268.0	5602.0	3907.0	0.0	3492.0	0.0	26508.0	27365.0	3202.0	52968.0	29512.0	15776.0	0.0	12010.0	20223.0	30796.0000	187564.0000	6.0905	
	3	1550-2	20350.0	0.0	5169.0	8990.0	6702.0	0.0	5498.0	0.0	60130.0	5340.0	0.0	113646.0	62632.0	5283.0	5075.0	26616.0	41523.0	46709.0000	320245.0000	6.8562	6.5
Obese BMI ≥30-60	1	1622-3	31823.0	0.0	6153.0	10331.0	8014.0	0.0	6812.0	0.0	38508.0	55539.0	11783.0	125401.0	70035.0	37776.0	10781.0	30445.0	47089.0	63133	417357.0000	6.6108	
	2	1622-3	30918.0	0.0	6554.0	11460.0	9530.0	0.0	6963.0	0.0	47659.0	36694.0	9913.0	132631.0	73745.0	40980.0	9446.0	31135.0	44634.0	65425	426837.0000	6.5241	
	3	1622-3	31823.0	0.0	6153.0	10331.0	8014.0	0.0	6812.0	0.0	46110.0	25539.0	11783.0	125401.0	70035.0	37776.0	10781.0	30445.0	47089.0	63133	404959.0000	6.4144	6.5
Obese BMI ≥30-60	1	1550-3	31369.0	0.0	7340.0	11850.0	9208.0	0.0	7510.0	0.0	54889.0	50018.0	8099.0	103411.0	55764.0	30883.0		27113.0	40533.0	67277	370710.0000	5.5102	
	2	1550-3	34022.0	0.0	7530.0	12870.0	10381.0	0.0	7600.0	0.0	57191.0	53687.0	10108.5	106490.0	57997.0	7547.0	8589.0	28362.0	41530.0	72403	371501.5000	5.1310	
	3	1550-3	25972.0	0.0	6139.0	10638.0	7559.0	0.0	6507.0	0.0	54226.0	48978.0	7236.0	106401.0	57136.0	32707.0	6194.0	22768.0	42031.0	56815	377677.0000	6.6475	5.8
GDM BMI varied	1	1545-1	45330.0	0.0	10307.0	15083.0	14042.0	0.0	10866.0	0.0	55988.0	52221.0	13352.4	107793.0	56502.0	31913.0	12335.0	30922.0	43790.0	95628.0000	404816.4140	4.2332	
	2	1545-1	45002.0	0.0	9778.0	15263.0	12581.0	0.0	10611.0	7425.0	56837.0	53839.0	12368.7	111188.0	61366.0	32400.0	11609.0	31145.0	43627.0	100660.0000	414379.7420	4.1166	
	3	1545-1	54072.0	0.0	14292.0	18294.0	15070.0	0.0	14132.0	0.0	63901.0	58313.0	14863.1	117995.0	63579.0	40947.0	16643.0	35145.0	45504.0	115860.0000	456890.1348	3.9435	4.1
GDM BMI varied	1	1578-1	23247.0	0.0	8093.0	8793.0	6340.0	0.0	7119.0	0.0	61810.0	50173.0	7150.7	99581.0	57576.0	36528.0	0.0	32827.0	37305.0	53592.0000	382950.6942	7.1457	
	2	1578-1	21082.0	0.0	5177.0	8762.0	6896.0	0.0	5573.0	0.0	49660.0	41475.0	5457.0	92281.0	50935.0	25575.0	0.0	25556.0	29327.0	47490.0000	320266.0000	6.7439	
	3	1578-1	23740.0	0.0	7672.0	5499.0	5723.0	0.0	7252.0	3684.0	55291.0	48780.0	7560.0	8171.0	58845.0	32985.0	0.0	32499.0	26134.0	53570.0000	270265.0000	5.0451	6.3
GDM BMI varied	1	1669-1	48825.0	0.0	10039.0	16467.0	14260.0	0.0	12281.0	0.0	56503.0	53919.0	7859.8	108317.0	58696.0	34056.0	15752.0	29818.0	44318.0	101872.0000	409238.8460	4.0172	
	2	1669-1	43737.0	0.0	8500.0	14556.0	13118.0	0.0	11331.0	0.0	58625.0	55795.0	10974.3	119216.0	63968.0	33307.0	11011.0	32289.0	45739.0	91242.0000	430924.3372	4.7229	
	3	1669-1	50654.0	0.0	11686.0	17725.0	14330.0	0.0	11736.0	0.0	66372.0	64453.0	12156.0	131124.0	72089.0	37641.0	11452.0	35346.0	49837.0	106131.0000	480470.0000	4.5271	4.4
GDM BMI varied	1	1545-2	47028.0	0.0	10708.0	28170.0	14225.0	0.0	11947.0	0.0	56913.0	56061.0	13056.0	111657.0	59220.0	36142.0	13154.0	29875.0	42165.0	112078.0000	418243.0000	3.7317	
	2	1545-2	47918.0	0.0	10367.0	17713.0	15415.0	0.0	12719.0	0.0	49292.0	46651.0	11524.3	90794.0	50025.0	28241.0	12726.0	25882.0	35753.0	104132.0000	350888.3422	3.3696	
	3	1545-2	54103.0	0.0	11860.0	17268.0	16633.0	0.0	13520.0	0.0	59718.0	53984.0	12270.0	114419.0	65631.0	35832.0	12725.0	34641.0	45119.0	113384.0000	434339.0000	3.8307	3.6
GDM BMI varied	1	1578-2	35178.0	0.0	9600.0	12317.0	9507.0	0.0	10678.0	0.0	51704.0	46157.0	8353.0	102154.0	56565.0	29652.0	6507.0	28882.0	38905.0	77280.0000	368879.0000	4.7733	
	2	1578-2	38499.0	0.0	10990.0	16787.0	13575.0	0.0	11895.0	7001.0	64069.0	57199.0	10098.8	131753.0	69488.0	39296.0	0.0	35260.0	54074.0	98747.0000	461237.7500	4.6709	
	3	1578-2	40570.0	0.0	11945.0	15841.0	12756.0	0.0	11796.0	6245.0	69154.0	57596.0	10627.0	140757.0	70964.0	38677.0	10010.0	36664.0	55413.0	99153.0000	489862.0000	4.9405	4.8
				0.0				0.0															
GDM BMI varied	1	1669-2	48825.0	0.0	10039.0	16467.0	14260.0	0.0	12281.0	0.0	56503.0	53919.0	14859.8	108317.0	58696.0	34056.0	15752.0	29818.0	44318.0	101872.0000	416238.8460	4.0859	
	2	1669-2	43737.0	0.0	8500.0	14556.0	13118.0	0.0	11331.0	8110.0	58625.0	55795.0	10974.3	119216.0	63968.0	33307.0	11011.0	32289.0	45739.0	99352.0000	430924.3372	4.3373	
	3	1669-2	50654.0	0.0	11686.0	17725.0	14330.0	0.0	11736.0	0.0	66372.0	64453.0	12156.0	131124.0	72089.0	37641.0	11452.0	35346.0	49837.0	106131.0000	480470.0000	4.5271	4.3

Appendix Table S: Placenta different cuts edges, centre groups healthy, obese, GDM results PC LPC all run in +9AA

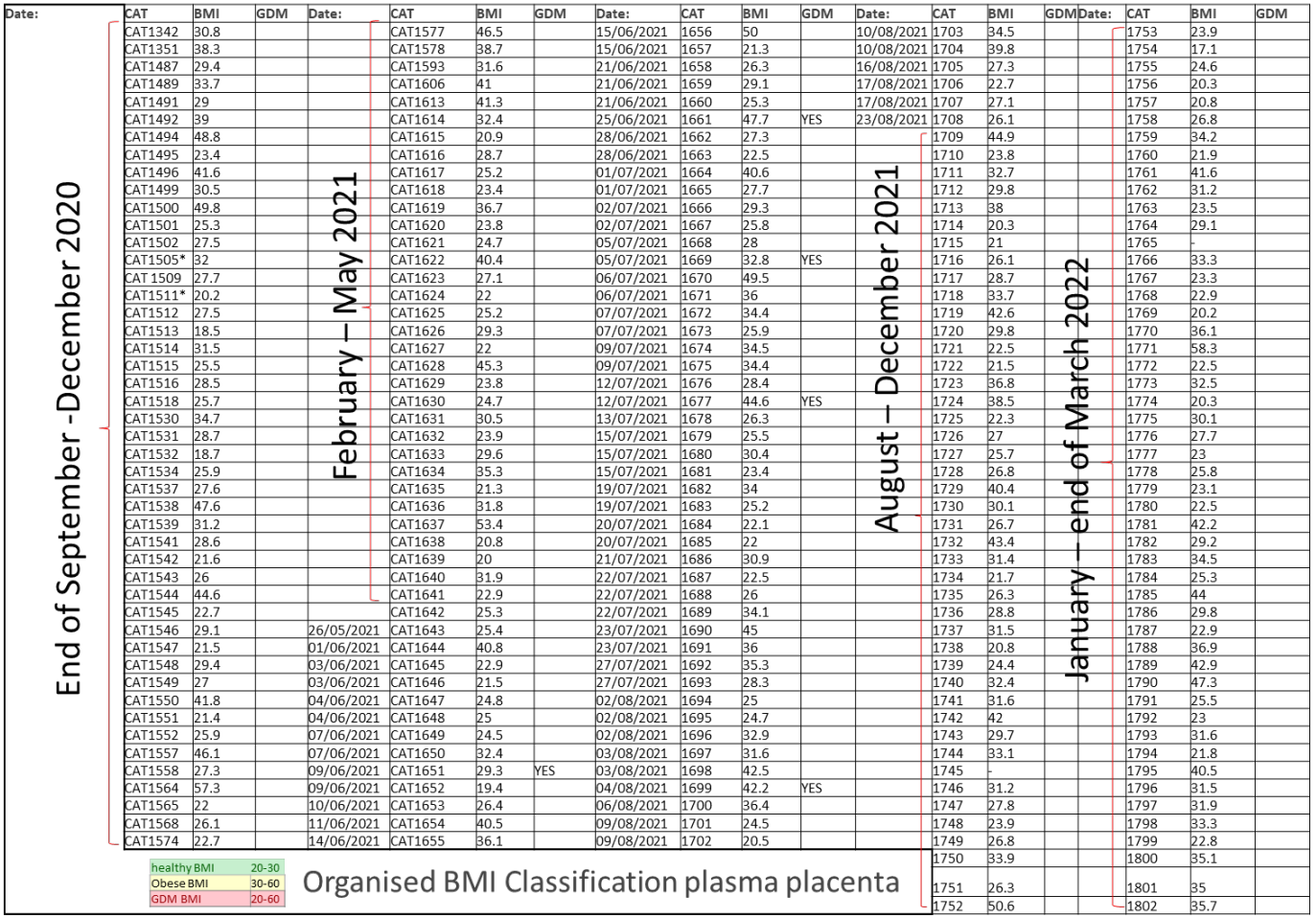

Date:	CAT	BMI	GDM	Date:	CAT	BMI	GDM	Date:	CAT	BMI	GDM	Date:	CAT	BMI	GDM	Date:	CAT	BMI	GDM
	CAT1342	30.8			CAT1577	46.5		15/06/2021	1656	50		10/08/2021	1703	34.5			1753	23.9	
	CAT1351	38.3			CAT1578	38.7		15/06/2021	1657	21.3		10/08/2021	1704	39.8			1754	17.1	
	CAT1487	29.4			CAT1593	31.6		21/06/2021	1658	26.3		16/08/2021	1705	27.3			1755	24.6	
	CAT1489	33.7			CAT1606	41		21/06/2021	1659	29.1		17/08/2021	1706	22.7			1756	20.3	
	CAT1491	29			CAT1613	41.3		21/06/2021	1660	25.3		17/08/2021	1707	27.1			1757	20.8	
	CAT1492	39			CAT1614	32.4		25/06/2021	1661	47.7	YES	23/08/2021	1708	26.1			1758	26.8	
	CAT1494	48.8			CAT1615	20.9		28/06/2021	1662	27.3			1709	44.9			1759	34.2	
	CAT1495	23.4			CAT1616	28.7		28/06/2021	1663	22.5			1710	23.8			1760	21.9	
	CAT1496	41.6			CAT1617	25.2		01/07/2021	1664	40.6			1711	32.7			1761	41.6	
	CAT1499	30.5			CAT1618	23.4		01/07/2021	1665	27.7			1712	29.8			1762	31.2	
	CAT1500	49.8			CAT1619	36.7		02/07/2021	1666	29.3			1713	38			1763	23.5	
	CAT1501	25.3			CAT1620	23.8		02/07/2021	1667	25.8			1714	20.3			1764	29.1	
	CAT1502	27.5			CAT1621	24.7		05/07/2021	1668	28			1715	21			1765	-	
	CAT1505*	32			CAT1622	40.4		05/07/2021	1669	32.8	YES		1716	26.1			1766	33.3	
	CAT 1509	27.7			CAT1623	27.1		06/07/2021	1670	49.5			1717	28.7			1767	23.3	
	CAT1511*	20.2			CAT1624	22		06/07/2021	1671	36			1718	33.7			1768	22.9	
	CAT1512	27.5			CAT1625	25.2		07/07/2021	1672	34.4			1719	42.6			1769	20.2	
	CAT1513	18.5			CAT1626	29.3		07/07/2021	1673	25.9			1720	29.8			1770	36.1	
	CAT1514	31.5			CAT1627	22		09/07/2021	1674	34.5			1721	22.5			1771	58.3	
	CAT1515	25.5			CAT1628	45.3		09/07/2021	1675	34.4			1722	21.5			1772	22.5	
	CAT1516	28.5			CAT1629	23.8		12/07/2021	1676	28.4			1723	36.8			1773	32.5	
	CAT1518	25.7			CAT1630	24.7		12/07/2021	1677	44.6	YES		1724	38.5			1774	20.3	
	CAT1530	34.7			CAT1631	30.5		13/07/2021	1678	26.3			1725	22.3			1775	30.1	
	CAT1531	28.7			CAT1632	23.9		15/07/2021	1679	25.5			1726	27			1776	27.7	
	CAT1532	18.7			CAT1633	29.6		15/07/2021	1680	30.4			1727	25.7			1777	23	
	CAT1534	25.9			CAT1634	35.3		15/07/2021	1681	23.4			1728	26.8			1778	25.8	
	CAT1537	27.6			CAT1635	21.3		19/07/2021	1682	34			1729	40.4			1779	23.1	
	CAT1538	47.6			CAT1636	31.8		19/07/2021	1683	25.2			1730	30.1			1780	22.5	
	CAT1539	31.2			CAT1637	53.4		20/07/2021	1684	22.1			1731	26.7			1781	42.2	
	CAT1541	28.6			CAT1638	20.8		20/07/2021	1685	22			1732	43.4			1782	29.2	
	CAT1542	21.6			CAT1639	20		21/07/2021	1686	30.9			1733	31.4			1783	34.5	
	CAT1543	26			CAT1640	31.9		22/07/2021	1687	22.5			1734	21.7			1784	25.3	
	CAT1544	44.6			CAT1641	22.9		22/07/2021	1688	26			1735	26.3			1785	44	
	CAT1545	22.7			CAT1642	25.3		22/07/2021	1689	34.1			1736	28.8			1786	29.8	
	CAT1546	29.1		26/05/2021	CAT1643	25.4		23/07/2021	1690	45			1737	31.5			1787	22.9	
	CAT1547	21.5		01/06/2021	CAT1644	40.8		23/07/2021	1691	36			1738	20.8			1788	36.9	
	CAT1548	29.4		03/06/2021	CAT1645	22.9		27/07/2021	1692	35.3			1739	24.4			1789	42.9	
	CAT1549	27		03/06/2021	CAT1646	21.5		27/07/2021	1693	28.3			1740	32.4			1790	47.3	
	CAT1550	41.8		04/06/2021	CAT1647	24.8		02/08/2021	1694	25			1741	31.6			1791	25.5	
	CAT1551	21.4		04/06/2021	CAT1648	25		02/08/2021	1695	24.7			1742	42			1792	23	
	CAT1552	25.9		07/06/2021	CAT1649	24.5		02/08/2021	1696	32.9			1743	29.7			1793	31.6	
	CAT1557	46.1		07/06/2021	CAT1650	32.4		03/08/2021	1697	31.6			1744	33.1			1794	21.8	
	CAT1558	27.3		09/06/2021	CAT1651	29.3	YES	03/08/2021	1698	42.5			1745	-			1795	40.5	
	CAT1564	57.3		09/06/2021	CAT1652	19.4		04/08/2021	1699	42.2	YES		1746	31.2			1796	31.5	
	CAT1565	22		10/06/2021	CAT1653	26.4		06/08/2021	1700	36.4			1747	27.8			1797	31.9	
	CAT1568	26.1		11/06/2021	CAT1654	40.5		09/08/2021	1701	24.5			1748	23.9			1798	33.3	
	CAT1574	22.7		14/06/2021	CAT1655	36.1		09/08/2021	1702	20.5			1749	26.8			1799	22.8	
													1750	33.9			1800	35.1	
													1751	26.3			1801	35	
													1752	50.6			1802	35.7	

Appendix Table T: Body Mass Index of all samples used in this study BMI

12 March 2020 First lipid extract Dr Lopalco CAT1351,	Edyta follws October 2020 method validation TLC quality control QC CAT 1342
Note: Covid -19 lockdown 20March 2020	Covid 19 lockdown closure
All Experimental items used:	Edyta PhD experimental items used:
MALDI Tof MS	Brucker Daltonics Flex Analysis 3.4 software
Path:	D:\ Brucker\MALDI ToF\FlexControl\FlexAnalysis\Data\Aacquisition\Methods\Lipids\Edyta
Flex Control / Flex Analysis:	version 3.4
Methods:	Reflectron +ve ion RP 400-2000Da-Lipids.par-ve ion RN 400-2000Da-Lipids.par
Laboratory:	NMSF Swansea University Swansea Wales
Operator:	Edyta Carrion Paczkowska
Dates:	from 03-06-2021 till last use 04/04/2022
Validation name:	Method development and optimisation placental blood plasma total lipids
Type of validation:	Biological assay
Reference standards	SKU:710335C-25mg
Name	18:1, 14:1 Cardilopin in chloroform
Chemichal product name:	1`,3`bis[1,2-dioleoyl-sn-glycerol-3phospho]-glycerol (sodium salt)
Molecular Weight:	1501.959 g/mol
Lot Number	5231CJB056
Standard purity:	0.998
Opening Date:	43897
Manufacture:	Avanti Polar Lipids,INC USA
CAS:	115404-77-8
Reference standards	SKU:700000-500mg
Name	Cholesterol (ovine wool)
Chemichal product name:	Cholesterol (ovine wool, 98%)
Molecular Weight:	386.654
Lot Number	700000-P-500mg-A-107
Standard purity:	0.998
Opening Date:	43897
Manufacture:	Avanti Polar Lipids,INC USA
CAS:	57-88-5
Reference standards	SKU:840032C-10mg
Name	Brain PS in chloroform
Chemichal product name:	L-α-phosphatydilserine (Brain, Porcine) (sodium salt)
Molecular Weight:	824.966 (average based on fatty acid contribution)
Lot Number	840032c-10mgG-B-827
Standard purity:	0.998
Opening Date:	43897
Manufacture:	Avanti Polar Lipids,INC USA
CAS:	383907-32-2
Reference standards	SKU:860512P-5mg
Name	C12 Cerammide (d18:1/12:0) powder
Chemichal product name:	N-lauroyl-D-erythro-sphingosine
Molecular Weight:	481.794
Lot Number	5966PHC010
Standard purity:	0.998
Opening Date:	43897
Manufacture:	Avanti Polar Lipids,INC USA
CAS:	74713-60-3
Reference standards	SKU:700144p-10mg
Name	15:0 cholesteryl-d7 ester
Chemichal product name:	cholesteryl-d7 pentadecanoate
Molecular Weight:	618.095
Lot Number	700144P-10MG-A-011 MLOT: 5209PIA011
Standard purity:	0.998
Opening Date:	43897
Manufacture:	Avanti Polar Lipids,INC USA
CAS:	Not avaialbe
Reference standards	SKU:70016p-25mg
Name	cholesterol sulfate powder
Chemichal product name:	cholesterol 3-sulfate (sodium salt)
Molecular Weight:	488.699
Lot Number	70016P-25MG-E-013, MLOT: 5103PJE013
Standard purity:	0.998
Opening Date:	43897
Manufacture:	Avanti Polar Lipids,INC USA
CAS:	2864-50-8
TLC plates for analytical Chromatography	Merk KGaA Damstad Germany , Milipore USA ,Sigma Aldrich
TLC Silica get 60	HX90656226
50 Glass plates 10 x 20cm	AZ292966, Lot:2009498, 1.05626.0001
TLC Silica gel 60	HX74397421
25 Glass plates 20 x 20 cm	lot: 2977498, Z292966
Analytical Balance Used:	A&D Instruments Ltd Japan,
ID:	GR-202
Weight accuracy:	Max 210g, min 1mg, e=1mg, d=0,01/0,1mg, accuracy 0,001
Calibration:	Build in automation check to weight accuracy 0,001
Calibation on arrival with 100 mg speacial weights	100.00mg date: 11/11/2020
Daily check:	intenal calibration adjustment correction
Performance Validation (PV)	Used 200 -100-50-10-1 mg l weights
Performance Monitoring (PM)	daily, weekly, yearly external contractor
Centrifuge Used:	Eppendorf AG, 22331 Hamburg, Germany
ID	Centrifuge 5811 No. 09814
Performance Validation (PV)	Avantor
Performance Monitoring (PM)	44236
Speed used rpm, g-force,	3500 rpm,
rpm= revolution per minute, g-force =gravity foce	maximu speed 140,000 g
time	15 min

Chemichal items recorder weight = (mg)	Borrowed from Dr .Angelini Lab
Ammonium acetate	155mM in pure water -HPLC grade Fisher Scientific UK
9-AA Matrix	9-Aminoacridine , 99,5% pure 92817-1G ,Sigma
DHB Matrix	9-Aminoacridine , 99,5% pure 92817-1G ,Sigma
Supelco Clear Glass,	USA , Lot:139032 , part 29391-U, Certified Screw Thread Cap, Bonded PTFE/Silicone
ninehydrin	Borrowed from Dr .Angelini Lab
azurea	Borrowed from Dr .Angelini Lab
5% sulphuric acid prepared from stoc 95% H2SO4	Borrowed from Dr .Angelini Lab
Ultrasonication batch	Fisherbrand Operation modes: sonicate, sweep, degass
ID	15051
Timer	automated setting, time upto 30 minutes
Deiones Milley Q water + ice	ICE cubes from internal building ils1 2nd floor labs
Volumetric Glassware	
100 ml volumetric cylinder class A	Cole-Parmer USA -UK
Glass pipetes 1ml, 5ml, 10ml class A	Cole-Parmer USA -UK
Rubber buld for glass pipettes	Cole-Parmer USA -UK
Glass solvents jars with glass tops 500 ml	Cole-Parmer USA -UK
Glass beackers	Shandon,
Glass volumetric flasks	Cole-Parmer USA -UK
Glass hend sprayer with glas diffuser	Cole-Parmer USA -UK
Glass Tubes 15 ml	Cole-Parmer USA -UK
Glass Pasteur Pitepptes long 15 ml	Cole-Parmer USA -UK
Pyrex Glass Tubes , black screw Caps disposable	GPI15-415, Product Code: 99502-15, Corning Life Sciences, Mexico,
Glass Pasteur Pitepptes SHORT 10 ml	Cole-Parmer USA -UK
Rubber tip for paster pipetter	Cole-Parmer USA -UK
Cole-Parmer USA : Hamilton seringes 2x boxes of 6	(12x 10ul) and individauls 1000ul, 500ul, 100ul, 50ul, 25 ul, 10ul, 5ul
Ependoft, Gibson , Fisherbrand Elite pipettes	1000ul, 100ul, 20ul, 10ul, 5ul, 1ul
MALDI	UltraFlex , Brucker Germany Bremen
Agilent glas 250ul, pulledd point inserts	Part Number: 5183-2085,
Brucker Target plate brushed steel	MTP 384 target plate polished steel BC # 8280781 Brucker Germany Bremen
Brucker Targer frame holder brushed steel	MTP target frame III # 8074115 Brucker Germany Bremen
IPN/CAN matrix solvent 3:2	Brucker Germany Bremen
Isopropanol/Acentonnitrile	Borrowed from Dr .Angelini Lab
Stiness steel spatula to weigh out 10mg	Cole-Parmer USA -UK
Methanol rinse solvent for plate wash	Cole-Parmer USA -UK
KimWipe tissue for target plate	Cole-Parmer USA -UK
CsI3 = Cesium Iodide mass calibrant Facility Manager Dr Ann Hunter	Lipid method set up by Dr.Angelini on Flex Analysis
Maldi Flex Analysis Method:	RP 400-2000Da-Edyta Lipids.par
Missolenious items needs oragnisation	
Cold Room Glass Rotator	MX-RD-Pro
Rotating plate with 20 clamps fitting	15ml tubes
Utomated temperature, with digital set rotation timer	Cold room freidge 4C with fanassisted air flow to maintain 4ctemp
Pyrex Glass Tubes , black screw Caps disposable	GPI15-415, Product Code: 99502-15, Corning Life Sciences, Mexico,
Pyrex Centrifuge glass tubes	Lot 06220009, cm 104402387 Corniing Life Sciences, Mexico,
Cryovials for blood plasma storage	storage at -80 C , volume 1,8ml
Dri-Block DB-3D	TECHNE brand
Ultra low temperature Freezers: Temperature -80C Chamber	New Brunswick Scientific
Part No.	U9440-001
Model:	U725-86
Serial:	1005-4033-05-07
Vortex:	JENCONS-PLS
Mill-Q water qgard00r1,	Q-grad1 lot : F8KA94393
Millipak Express 20 , filter 0.22um Merck, serial 8616,	lot no: F8DA49035
Thermostat Oven	Thermo Scinetific ,
Made in:	Termo Electron LED , Germany
Capacity:	Fisherbrand 65L Oven 230V
Maximum temperature:	250 Celsius
Serial	SN: 42680322, Cat. No.15805911
Freezer	Eppendorf CryoCube -80C automated digital dispaly control window F740hi
Disposable sterile sciecors	Rocialle,Wales
Disposable sterilee Gripprite Ble Forceps SW	Rocialle,Wales REF: RML 109-006 ,LOT: W479000
PBS ph7.4 Sterille A Phospate Buffered Saline 500ml	Gibco, Life Technologies, UK Ref: 10010-015, Lot: 2242218
Sulphuric Acid 95-97% Sigma Aldrich UK	07208-1L-M, Lot: STBG9176
Dieethyl Ether Sigma Aldich UK	296082-1L, Lot: STBJ1842
Acetone 99.6% Acrons Organics	Code: 423240010, Lot:A0414350
Hexane 95% HPLC Plus GC residue analysis, Sigma Aldrich UK	650552-1L, Lot:MKCH5832
Acetic Acid glacial 99% Fisher Scientific UK, Acros Organic Belgium	Code:A/036/PB17, Lot:1922268
Chlorofolrm 99.99% HPLC Plus,0.5-1.0% ethanol as stabiliser	1.06035.2500, 2.5L, Lot: I1102735033
ChemiDoc XRS + with Image Lab software	BioRad
DiamondCautter glass knife	Langlong LL20030
ZeroSta 3Milty	static charge emilinator for balance
Sodium cholesteryl Sulphate C9523-25mg for TLC staiing	lot: SLCD
Ninhydrin Sigma ALDRICH for tlc staiing amino acids detection	lot:BCBX4469 Sigma , N4876-100g
2,4 Lutidine 99% 2,4 dimethylpyridine, L3609-100 ml	Lot:MKCK5213
Homogeniser 150 Fisherbrand	Thermo Fisher Germany Darmastad,
Stainess steel probe for tissue cole palmer UK	cutting head 0.5mm specifit for hard fibroulus tissue colepalmer
TLC Chroma tank PANGLAS,	Shandon,
NH4OH 29% made from 100% NH4OH Mass Spec Rob	Borrowed from Dr .Angelini Lab
50ml Falcon tubes as holder inserts for glass centrifuge	ILS1 , 2ND Floor Lab stock

Appendix Table U: Inventory includes all equipment, standards, and solvents used in this research work.

Bibliography

Uncategorized References

([1.) Sahab, K. S. (**2019**) Alteration of Prolactin, Thyroid Hormones and Lipid Profiles During Three Stages of Pregnancy, *Earthline Journal of Chemical Sciences*.

([2.) Ochoa-Bernal, M. A., and Fazleabas, A. T. (**2020**) Physiologic Events of Embryo Implantation and Decidualization in Human and Non-Human Primates, *Int J Mol Sci 21*, 1973.

([3.) Chambers, M., Rees, A., Cronin, J. G., Nair, M., Jones, N., and Thornton, C. A. (**2020**) Macrophage Plasticity in Reproduction and Environmental Influences on Their Function, *Front Immunol 11*, 607328.

([4.) Muter, J., Kong, C., and Brosens, J. (**2021**) The Role of Decidual Subpopulations in Implantation, Menstruation and Miscarriage, *Frontiers in Reproductive Health 3*.

([5.) Llobat, L. (**2021**) Pluripotency and Growth Factors in Early Embryonic Development of Mammals: A Comparative Approach, *Veterinary Sciences*.

([6.) Sharpley, M. S., Chi, F., and Banerjee, U. (**2020**) Metabolic Plasticity Drives Development During Mammalian Embryogenesis.

([7.) Maltepe, E., Krampitz, G. W., Okazaki, K. M., Red-Horse, K., Mak, W., Simon, M. C., and Fisher, S. J. (**2005**) Hypoxia-Inducible Factor-Dependent Histone Deacetylase Activity Determines Stem Cell Fate in the Placenta, *Development*.

([8.) Mannully, C. T., Bruck-Haimson, R., Zacharia, A., Orih, P., Shehadeh, A., Saidemberg, D. M., Kogan, N. M., Alfandary, S., Serruya, R., Dagan, A., Petit, I., and Moussaieff, A. (**2022**) Lipid Desaturation Regulates the Balance Between Self-Renewal and Differentiation in Mouse Blastocyst-Derived Stem Cells, *Cell Death and Disease*.

([9.) Red-Horse, K., Zhou, Y., Genbačev, O., Prakobphol, A., Foulk, R. A., McMaster, M., and Fisher, S. J. (**2004**) Trophoblast Differentiation During Embryo Implantation and Formation of the Maternal-Fetal Interface, *Journal of Clinical Investigation*.

([10.) Frank, H.-G. (2017) Placental Development, In *Fetal and Neonatal Physiology*, pp 101-113.

([11.) Burton, G. J., and Fowden, A. L. (**2015**) The placenta: a multifaceted, transient organ, *Philosophical Transactions of the Royal Society B: Biological Sciences 370*, 20140066.

([12.) Gauster, M., Moser, G., Wernitznig, S., Kupper, N., and Huppertz, B. (**2022**) Early Human Trophoblast Development: From Morphology to Function, *Cellular and Molecular Life Sciences*.

([13.) Wamaitha, S. E., and Niakan, K. K. (**2018**) Human Pre-Gastrulation Development.

([14.) Burton, G. J., and Jauniaux, E. (**2015**) What Is the Placenta?, *American Journal of Obstetrics and Gynecology*.

([15.) Guttmacher, A. E., Maddox, Y. T., and Spong, C. Y. (**2014**) The Human Placenta Project: Placental Structure, Development, and Function in Real Time, *Placenta*.

([16.) Maître, J.-L. (**2017**) Mechanics of Blastocyst Morphogenesis, *Biology of the Cell*.

([17.) Solnica-Krezel, L., and Sepich, D. S. (**2012**) Gastrulation: Making and Shaping Germ Layers, *Annual Review of Cell and Developmental Biology*.

([18.) Favaron, P. O., Carvalho, R. R. D., Borghesi, J., Anunciação, A. R. A., and Moody, M. A. (**2015**) The Amniotic Membrane: Development and Potential Applications – A Review, *Reproduction in Domestic Animals*.

([19.) Labarrere, C. A., DiCarlo, H. L., Bammerlin, E., Hardin, J. W., Kim, Y. M., Chaemsaithong, P., Haas, D. M., Kassab, G. S., and Romero, R. (**2017**) Failure of Physiologic Transformation of Spiral Arteries, Endothelial and Trophoblast Cell Activation, and Acute Atherosis in the Basal Plate of The placenta, *American Journal of Obstetrics and Gynecology*.

([20.) Roberts, D., Brown, J., Medley, N., and Dalziel, S. R. (**2017**) Antenatal corticosteroids for accelerating fetal lung maturation for women at risk of preterm birth, *Cochrane Database Syst Rev 3*, CD004454.

([21.) Bolt, R. J., van Weissenbruch, M. M., Lafeber, H. N., and Delemarre-van de Waal, H. A. (**2001**) Glucocorticoids and lung development in the fetus and preterm infant, *Pediatr Pulmonol 32*, 76-91.

([22.) Grier, D. G. A. H., H. L. . (**2004**) Effects of glucocorticoids on fetal and neonatal lung development. *Treatments in Respiratory Medicine, 3(5), 295-306. 3*, 295-306.

([23.) McGoldrick, E., Stewart, F., Parker, R., & Dalziel, S. R. . (**2020**) Antenatal corticosteroids for accelerating fetal lung maturation for women at risk of preterm birth. , *Cochrane Database of Systematic Reviews, 2021 2*.

([24.) Sibiak, R., Ożegowska, K., Wender-Ozegowska, E., Gutaj, P., Mozdziak, P., and Kempisty, B. (**2022**) Fetomaternal Expression of Glucose Transporters (GLUTs)—Biochemical, Cellular and Clinical Aspects, *Nutrients*.

([25.) MS Sadik, H. F., K Jamil, C Patil. (**2012**) Study of TORCH profile in patients with bad obstetric history, *Biology and Medicine BMID: AR99-BM12 4*, 95-101.

([26.) Lynn, M. K., Aquino, M. S. R., Self, S., Kanyangarara, M., Campbell, B. A., and Nolan, M. S. (**2023**) TORCH Congenital Syndrome Infections in Central America's Northern Triangle, *Microorganisms*.

([27.) Christina J. Megli, C. B. C. (**2022**) Infections at the maternal-fetal interface: an overview of pathogenesis and defence, *Nature Reviews Microbiology 20*, 67-82.

([28.) Coyne, C. B., and Lazear, H. M. (**2016**) Zika virus - reigniting the TORCH, *Nat Rev Microbiol 14*, 707-715.

([29.) Macedo-da-Silva, J., Marinho, C. R. F., Palmisano, G., and Rosa-Fernandes, L. (**2020**) Lights and Shadows of TORCH Infection Proteomics, *Genes (Basel) 11*.

([30.) Fitzpatrick, D., Holmes, N. E., and Hui, L. (**2021**) A Systematic Review of Maternal TORCH Serology as a Screen for Suspected Fetal Infection, *Prenatal Diagnosis*.

([31.) Li, Z., Kurosawa, O., and Iwata, H. (**2020**) A Novel Human Placental Barrier Model Based on Trophoblast Stem Cells Derived From Human Induced Pluripotent Stem Cells, *Tissue Engineering Part A*.

([32.) J M Best, S. S. (**1990**) Diagnosis and prevention of congenital and perinatal infections, *BMJ 301 (6757)*, 888-889. .

([33.) SV, P. (**2015**) Epidemiological and serological profiles of TORCH infection in pregnancy, *Journal of Pathology of Nepal 5*, 705-708.

([34.) Noronha, L. d., Zanluca, C., Marina Luise Viola de, A., Luz, K. G., and Claudia Nunes Duarte dos, S. (**2016**) Zika Virus Damages the Human Placental Barrier and Presents Marked Fetal Neurotropism, *Memórias Do Instituto Oswaldo Cruz*.

([35.) Semmler-Behnke, M., Lipka, J., Wenk, A., Hirn, S., Schäffler, M., Tian, F., Schmid, G., Oberdörster, G., and Kreyling, W. G. (**2014**) Size Dependent Translocation and Fetal Accumulation of Gold Nanoparticles From Maternal Blood in the Rat, *Particle and Fibre Toxicology*.

([36.) Grafmueller, S., Manser, P., Diener, L., Diener, P.-A., Maeder-Althaus, X., Maurizi, L., Jochum, W., Krug, H. F., Buerki-Thurnherr, T., Mandach, U. v., and Wick, P. (**2015**) Bidirectional Transfer Study of Polystyrene Nanoparticles Across the Placental Barrier in An ex Vivo Human Placental Perfusion Model, *Environmental Health Perspectives*.

([37.) Sibley, C. P., Coan, P., Ferguson-Smith, A. C., Dean, W., Hughes, J., Smith, P. D., Reik, W., Burton, G. J., Fowden, A. L., and Constância, M. (**2004**) Placental-Specific Insulin-Like Growth Factor 2 (Igf2) Regulates the Diffusional Exchange Characteristics of the Mouse Placenta, *Proceedings of the National Academy of Sciences PNAS 101*, 8204 – 8208.

([38.) Rubinchik-Stern, M., and Eyal, S. (**2012**) Drug Interactions at the Human Placenta: What Is the Evidence?, *Frontiers in Pharmacology*.

([39.) Lee, J. S., Romero, R., Han, Y. M., Kim, H. C., Kim, C. J., Hong, J. S., and Huh, D. (**2015**) Placenta-on-a-Chip: A Novel Platform to Study the Biology of the Human Placenta, *The Journal of Maternal-Fetal & Neonatal Medicine*.

([40.) Mosavati, B., Oleinikov, A. V., and Du, E. (**2020**) Development of an Organ-on-a-Chip-Device for Study of Placental Pathologies, *International Journal of Molecular Sciences*.

([41.) Cao, R., Wang, Y., Liu, J., Rong, L., and Qin, J. (**2023**) Self-assembled Human Placental Model From Trophoblast Stem Cells in a Dynamic Organ-on-a-chip System, *Cell Proliferation*.

([42.) Burton, G. J., Watson, A. L., Hempstock, J., Skepper, J. N., and Jauniaux, E. (**2002**) Uterine glands provide histiotrophic nutrition for the human fetus during the first trimester of pregnancy, *J Clin Endocrinol Metab 87*, 2954-2959.

([43.) Hayward, C. E., Jones, R. L., and Sibley, C. P. (2017) Mechanisms of Transfer Across the Human Placenta, In *Fetal and Neonatal Physiology*, pp 121-133.e125.

([44.) Chatuphonprasert, W., Jarukamjorn, K., and Ellinger, I. (**2018**) Physiology and Pathophysiology of Steroid Biosynthesis, Transport and Metabolism in the Human Placenta, *Frontiers in Pharmacology*.

([45.) Frendo, J.-L., Olivier, D., Cheynet, V., Blond, J.-L., Bouton, O., Vidaud, M., Evain-Brion, D., and Mallet, F. (**2003**) Direct Involvement of HERV-W Env Glycoprotein in Human Trophoblast Cell Fusion and Differentiation, *Molecular and Cellular Biology*.

([46.) Chang, C.-W., Chang, G.-D., and Chen, H. (**2011**) A Novel Cyclic AMP/Epac1/CaMKI Signaling Cascade Promotes GCM1 Desumoylation and Placental Cell Fusion, *Molecular and Cellular Biology*.

([47.) Deng, D., Tan, X., Han, K., Ren, R., Jianhua, C., and Yu, M. (**2020**) Transcriptomic and ChIP-seq Integrative Analysis Reveals Important Roles of Epigenetically Regulated lncRNAs in Placental Development in Meishan Pigs, *Genes*.

([48.) Tian, F.-Y., Wang, X., Xie, C., Zhao, B., Niu, Z., Fan, L., Hivert, M.-F., and Chen, W.-Q. (**2018**) Placental Surface Area Mediates the Association

Between FGFR2 Methylation in Placenta and Full-Term Low Birth Weight in Girls, *Clinical Epigenetics*.

([49.) Handschuh, K., Gadrey, J., Tsatsaris, V., Guesnon, M., Laurendeau, I., Évain-Brion, D., and Fournier, T. (**2007**) Human Chorionic Gonadotropin Expression in Human Trophoblasts From Early Placenta: Comparative Study Between Villous and Extravillous Trophoblastic Cells, *Placenta*.

([50.) Mirbod, P. (**2018**) Analytical Model of the Feto-Placental Vascular System: Consideration of Placental Oxygen Transport, *Royal Society Open Science*.

([51.) Langhoff-Roos, J., Lindmark, G., Wibell, L., and Gebre-Medhin, M. (**1989**) Placental Hormones and Maternal Glucose Metabolism. A Study of Fetal Growth in Normal Pregnancy, *Bjog an International Journal of Obstetrics & Gynaecology*.

([52.) Ericsson, A., Hamark, B., Jansson, N., Johansson, B. R., Powell, T. L., and Jansson, T. (**2005**) Hormonal Regulation of Glucose and System and Amino Acid Transport in First Trimester Placental Villous Fragments, *Integrative and Comparative Physiology*.

([53.) Fowden, A. L., Valenzuela, O. A., Vaughan, O. R., Jellyman, J. K., and Forhead, A. J. (**2016**) Glucocorticoid programming of intrauterine development, *Domest Anim Endocrinol 56 Suppl*, S121-132.

([54.) Avagliano, L., Garò, C., and Marconi, A. M. (**2012**) Placental Amino Acids Transport in Intrauterine Growth Restriction, *Journal of Pregnancy*.

([55.) Dimasuay, K. G., Aitken, E. H., Rosario, F. J., Njie, M., Glazier, J. D., Rogerson, S. J., Fowkes, F. J. I., Beeson, J. G., Powell, T. L., Jansson, T., and Boeuf, P. (**2017**) Inhibition of Placental mTOR Signaling Provides a Link Between Placental Malaria and Reduced Birthweight, *BMC Medicine*.

([56.) Shibata, E., Hubel, C. A., Powers, R. W., Versen-Hoeynck, F. v., Gammill, H. S., Rajakumar, A., and Roberts, J. M. (**2008**) Placental System a Amino Acid Transport Is Reduced in Pregnancies With Small for Gestational Age (SGA) Infants but Not in Preeclampsia With SGA Infants, *Placenta*.

([57.) Roos, S., Powell, T. L., and Jansson, T. (**2009**) Placental mTOR Links Maternal Nutrient Availability to Fetal Growth, *Biochemical Society Transactions*.

([58.) Basak, S., Das, R. K., Banerjee, A., Paul, S., Pathak, S., and Duttaroy, A. K. (**2022**) Maternal Obesity and Gut Microbiota Are Associated With Fetal Brain Development, *Nutrients*.

([59.) M Carey Satterfield, A. K. E., Fuller W Bazer, Kathrin A Dunlap, Chelsie B Steinhauser and Guoyao Wu. (**2021**) Placental adaptation to maternal malnutrition, *Reproduction Reproduction 162* 73-83.

([60.) Veerkamp, J. H., Herman, T. B. v. M. A., and Zimmerman, A. W. (**2000**) Effect of Fatty Acid-Binding Proteins on Intermembrane Fatty Acid Transport, *European Journal of Biochemistry*.

([61.) Stern, C., Storre, J. H., Moser, G., Cvitic, S., Jantscher-Krenn, E., Gauster, M., and Hiden, U. (**2021**) Placental Endocrine Activity: Adaptation and Disruption of Maternal Glucose Metabolism in Pregnancy and the Influence of Fetal Sex, *International Journal of Molecular Sciences*.

([62.) Cetin, I., Parisi, F., Berti, C., Mandò, C., and Desoye, G. (**2012**) Placental Fatty Acid Transport in Maternal Obesity, *Journal of Developmental Origins of Health and Disease*.

([63.) Neville, M. C. (**1999**) Adaptation of Maternal Lipid Flux to Pregnancy: Research Needs, *European Journal of Clinical Nutrition*.

([64.) Carter, A. M. (**2022**) Evolution of Placental Hormones: Implications for Animal Models, *Frontiers in Endocrinology*.

([65.) Murphy, V. E., Smith, R., Giles, W. B., and Clifton, V. L. (**2006**) Endocrine Regulation of Human Fetal Growth: The Role of the Mother, Placenta, and Fetus, *Endocrine Reviews*.

([66.) Frost, M. S., Zehri, A. H., Limesand, S. W., Hay, W. W., and Rozance, P. J. (**2012**) Differential Effects of Chronic Pulsatile Versus Chronic Constant Maternal Hyperglycemia on Fetal Pancreatic Cells, *Journal of Pregnancy*.

([67.) Chan, K., and Lao, T. T. (**2006**) Fetal Haematocrit Is a Determinant of Placental Size in Term Pregnancies, *Acta Haematologica*.

([68.) Goodner, C. J., Conway, M. J., and Werrbach, J. H. (**1969**) Relation Between Plasma Glucose Levels of Mother and Fetus During Maternal Hyperglycemia, Hypoglycemia, and Fasting in the Rat, *Pediatric Research*.

([69.) Fahy, E., Subramaniam, S., Brown, H. A., Glass, C. K., Merrill, A. H., Murphy, R. C., Raetz, C. R. H., Russell, D. W., Seyama, Y., Shaw, W., Shimizu, T., Spener, F., Van Meer, G., VanNieuwenhze, M. S., White, S. H., Witztum, J. L., and Dennis, E. A. (**2005**) A comprehensive classification system for lipids, *Journal of Lipid Research 46*, 839-861.

([70.) Fahy, E., Subramaniam, S., Murphy, R. C., Nishijima, M., Raetz, C. R., Shimizu, T., Spener, F., van Meer, G., Wakelam, M. J., and Dennis, E. A. (**2009**) Update of the LIPID MAPS comprehensive classification system for lipids, *J Lipid Res 50 Suppl*, S9-14.

([71.) Calder, P. C. (**2015**) Functional Roles of Fatty Acids and Their Effects on Human Health, *Journal of Parenteral and Enteral Nutrition*.

([72.) Albi, E., Alessenko, A. V., and Grösch, S. (**2018**) Sphingolipids in Inflammation, *Mediators of Inflammation*.

([73.) Hait, N. C., and Maiti, A. (**2017**) The Role of Sphingosine-1-Phosphate and Ceramide-1-Phosphate in Inflammation and Cancer, *Mediators of Inflammation*.

([74.) Khanapure, S. P., Garvey, D. S., Janero, D. R., and Letts, L. G. (**2007**) Eicosanoids in Inflammation: Biosynthesis, Pharmacology, and Therapeutic Frontiers, *Current Topics in Medicinal Chemistry*.

([75.) Wei, J., and Gronert, K. (**2019**) Eicosanoid and Specialized Proresolving Mediator Regulation of Lymphoid Cells, *Trends in Biochemical Sciences*.

([76.) Simanshu, D. K., Kamlekar, R. K., Wijesinghe, D. S., Zou, X., Zhai, X., Mishra, S. K., Molotkovsky, J. G., Malinina, L., Hinchcliffe, E. H., Chalfant, C. E., Brown, R. E., and Patel, D. J. (**2013**) Non-Vesicular Trafficking by a Ceramide-1-Phosphate Transfer Protein Regulates Eicosanoids, *Nature*.

([77.) Arana, L., Gangoiti, P., Ouro, A., Trueba, M., and Gómez-Muñoz, A. (**2010**) Ceramide and Ceramide 1-Phosphate in Health and Disease, *Lipids in Health and Disease*.

([78.) Bozza, P. c. T., Yu, W., Penrose, J. F., Morgan, E. S., Dvorak, A. M., and Weller, P. F. (**1997**) Eosinophil Lipid Bodies: Specific, Inducible Intracellular Sites for Enhanced Eicosanoid Formation, *The Journal of Experimental Medicine*.

([79.) Watrous, J. D., Niiranen, T. J., Lagerborg, K. A., Henglin, M., Xu, Y. J., Rong, J., Sharma, S., Vasan, R. S., Larson, M. G., Armando, A. M., Mora, S., Quehenberger, O., Dennis, E. A., Cheng, S., and Jain, M. (**2019**) Directed Non-Targeted Mass Spectrometry and Chemical Networking for Discovery of Eicosanoids and Related Oxylipins, *Cell Chemical Biology*.

([80.) Shekhar, S., Varghese, K., Li, M., Fan, L., Booz, G. W., Roman, R. J., and Fan, F. (**2019**) Conflicting Roles of 20-Hete in Hypertension and Stroke, *International Journal of Molecular Sciences*.

([81.) Zhang, C., Booz, G. W., Yu, Q., He, X., Wang, S., and Fan, F. (**2018**) Conflicting Roles of 20-Hete in Hypertension and Renal End Organ Damage, *European Journal of Pharmacology*.

([82.) Napso, T., Yong, H. E. J., Lopez-Tello, J., and Sferruzzi-Perri, A. N. (**2018**) The Role of Placental Hormones in Mediating Maternal Adaptations to Support Pregnancy and Lactation, *Frontiers in Physiology*.

([83.) Marquardt, R. M., Kim, T. H., Shin, J. H., and Guo, S.-W. (**2019**) Progesterone and Estrogen Signaling in the Endometrium: What Goes Wrong in Endometriosis?, *International Journal of Molecular Sciences*.

([84.) Diao, H., Li, R., Zowalaty, A. E. E., Xiao, S., Zhao, F., Dudley, E., and Ye, X. (**2015**) Deletion of Lysophosphatidic Acid Receptor 3 (Lpar3) Disrupts Fine

Local Balance of Progesterone and Estrogen Signaling in Mouse Uterus During Implantation1, *Biology of Reproduction*.

([85.) Hewitt, S. C., Wu, S.-P., Wang, T., Young, S. L., Spencer, T. E., and DeMayo, F. J. (**2022**) Progesterone Signaling in Endometrial Epithelial Organoids, *Cells*.

([86.) Hao, R., Kong, S., Zhang, S., Cheng, J., Zhou, C., He, B., Xin, Q., Lydon, J. P., DeMayo, F. J., Feng, G. S., Xia, G., Lu, Z., Wang, C., and Wang, H. (**2017**) Nuclear Shp2 Directs Normal Embryo Implantation via Facilitating the ERα Tyrosine Phosphorylation by the SRC Kinase, *Proceedings of the National Academy of Sciences*.

([87.) Maekawa, R., Mihara, Y., Sato, S., Okada, M., Shinoda, M., Shirafuta, Y., Takagi, H., Tanaka, T., and Tamura, H. (**2019**) Aberrant DNA Methylation Suppresses Expression of Estrogen Receptor 1 (ESR1) in Ovarian Endometrioma, *Journal of Ovarian Research*.

([88.) Hertz, D. L., Henry, N. L., Kidwell, K. M., Thomas, D. G., Goddard, A. D., Azzouz, F., Speth, K., Li, L., Banerjee, M., Thibert, J. N., Kleer, C. G., Stearns, V., Hayes, D. F., Skaar, T. C., and Rae, J. M. (**2016**) ESR1 and PGR Polymorphisms Are Associated With Estrogen and Progesterone Receptor Expression in Breast Tumors, *Physiological Genomics*.

([89.) Pensler, J. M., Radosevich, J. A., Higbee, R. G., and Langman, C. B. (**2020**) Osteoclasts Isolated From Membranous Bone in Children Exhibit Nuclear Estrogen and Progesterone Receptors, *Journal of Bone and Mineral Research*.

([90.) Bairagi, S., Grazul-Bilska, A. T., Borowicz, P. P., Reyaz, A., Valkov, V., and Reynolds, L. P. (**2018**) Placental Development During Early Pregnancy in Sheep: Progesterone and Estrogen Receptor Protein Expression, *Theriogenology*.

([91.) Zhang, Y., Yan, L., Liu, J., Cui, S., and Qiu, J. (**2019**) cGMP-dependent Protein Kinase II Determines B-Catenin Accumulation That Is Essential for Uterine Decidualization in Mice, *Ajp Cell Physiology*.

([92.) Xie, Q., Qi, Q.-R., Chen, Y.-X., Xu, W., Liu, Q., and Yang, J. (**2013**) Uterine Micro-Environment and Estrogen-Dependent Regulation of Osteopontin Expression in Mouse Blastocyst, *International Journal of Molecular Sciences*.

([93.) Frendo, J. L. (**2000**) Defect of Villous Cytotrophoblast Differentiation Into Syncytiotrophoblast in Down's Syndrome, *The Journal of Clinical Endocrinology & Metabolism*.

([94.) Ghoshal, I., Suryakanth, V. B., Belle, V. S., and Prabhu, K. (**2018**) Role of Maternal Serum Human Placental Lactogen in First Trimester Screening, *Indian Journal of Clinical Biochemistry*.

([95.) Quehenberger, O., and Dennis, E. A. (**2011**) The Human Plasma Lipidome, *New England Journal of Medicine 365*, 1812-1823.

([96.) Hettema, E. H., Roermund, C. W. v., Distel, B., Berg, M. v. d., Vilela, C., Rodrigues-Pousada, C., Wanders, R. J. A., and Tabak, H. F. (**1996**) The ABC Transporter Proteins Pat1 and Pat2 Are Required for Import of Long-Chain Fatty Acids Into Peroxisomes of Saccharomyces Cerevisiae, *The Embo Journal*.

([97.) Wakil, S. J., and Abu-Elheiga, L. A. (**2009**) Fatty acid metabolism: a target for metabolic syndrome, *J Lipid Res 50 Suppl*, S138-143.

([98.) Sampaio, J. L., Gerl, M. J., Klose, C., Ejsing, C. S., Beug, H., Simons, K., and Shevchenko, A. (**2011**) Membrane lipidome of an epithelial cell line, *Proc Natl Acad Sci U S A 108*, 1903-1907.

([99.) Fagone, P., and Jackowski, S. (2009) Membrane phospholipid synthesis and endoplasmic reticulum function, In *Journal of Lipid Research*.

([100.) Pandit, S. A., Jakobsson, E., and Scott, H. L. (**2004**) Simulation of the Early Stages of Nano-Domain Formation in Mixed Bilayers of Sphingomyelin, Cholesterol, and Dioleylphosphatidylcholine, *Biophysical Journal*.

([101.) Mizuno, H., Abe, M., Dedecker, P., Makino, A., Rocha, S., Ohno-Iwashita, Y., Hofkens, J., Kobayashi, T., and Miyawaki, A. (**2011**) Fluorescent Probes for Superresolution Imaging of Lipid Domains on the Plasma Membrane, *Chemical Science*.

([102.) Feingold, K. R., and Grunfeld, C. (**2021**) Introduction to Lipids and Lipoproteins, *Endotext*.

([103.) Fuchs, B., Schiller, J., Süß, R., Zscharnack, M., Bader, A., Müller, P., Schürenberg, M., Becker, M., and Suckau, D. (**2008**) Analysis of stem cell lipids by offline HPTLC-MALDI-TOF MS, *Analytical and Bioanalytical Chemistry 392*, 849-860.

([104.) Fuchs, B., and Schiller, J. (**2009**) Lysophospholipids: their generation, physiological role and detection. Are they important disease markers? *Mini reviews in medicinal chemistry 9 3*, 368-378.

([105.) Rodriguez-Cuenca, S., Pellegrinelli, V., Campbell, M., Oresic, M., and Vidal-Puig, A. (**2017**) Sphingolipids and glycerophospholipids – The "ying and yang" of lipotoxicity in metabolic diseases, *Progress in Lipid Research 66*, 14-29.

([106.) Chroneos, Z. C., Sever-Chroneos, Z., and Shepherd, V. L. (**2010**) Pulmonary Surfactant: An Immunological Perspective, *Cellular Physiology and Biochemistry*.

([107.) Ahmadpour, S. T., Maheo, K., Servais, S., Brisson, L., and Dumas, J. F. (**2020**) Cardiolipin, the Mitochondrial Signature Lipid: Implication in Cancer, *Int J Mol Sci 21*.

([108.) Hoch, F. L. (**1992**) Cardiolipins and biomembrane function, *Biochimica Acta I I13*, 71 - 133.

([109.) Ahmadpour, S. T., Mahéo, K., Servais, S., Brisson, L., and Dumas, J.-F. (**2020**) Cardiolipin, the Mitochondrial Signature Lipid: Implication in Cancer, *International Journal of Molecular Sciences 21*, 8031.

([110.) Pomorski, T., Hrafnsdóttir, S., Devaux, P. F., and Van Meer, G. (**2001**) Lipid distribution and transport across cellular membranes, *Seminars in Cell and Developmental Biology 12*, 139-148.

([111.) Gerrit van Meer, D. R. V., and Gerald, W. F. (2008) Nature Reviews Molecular Cell Biology Membrane lipids: where they are and how they behave, pp 112-124.

([112.) Watson, H. (**2015**) Biological membranes, *Essays Biochem 59*, 43-69.

([113.) Serhan, C. N. (**2017**) Discovery of specialized pro-resolving mediators marks the dawn of resolution physiology and pharmacology, *Molecular Aspects of Medicine 58*, 1-11.

([114.) Lefkowitz, R. J. (**1998**) G Protein-Coupled Receptors, *Journal of Biological Chemistry*.

([115.) Rees, A., Edwards-I-Coll, Z., Richards, O., Raikes, M. E., Angelini, R., and Thornton, C. A. (**2023**). The dynamic inflammatory profile of pregnancy can be monitored using a novel lipid-based mass spectrometry technique, *Molecular Omics*.

([116.) Yetukuri, L., Ekroos, K., Vidal-Puig, A., and Oresic, M. (**2008**) Informatics and computational strategies for the study of lipids, *Mol Biosyst 4*, 121-127.

([117.) Kennedy, E. P., and Weiss, S. B. (**1956**) The function of cytidine coenzymes in the biosynthesis of phospholipides, *J Biol Chem 222*, 193-214.

([118.) Wang, B., and Tontonoz, P. (**2019**) Phospholipid Remodeling in Physiology and Disease, *Annual Review of Physiology*.

([119.) Herrera, E., and Ortega-Senovilla, H. (**2010**) Disturbances in lipid metabolism in diabetic pregnancy - Are these the cause of the problem? *Best Pract Res Clin Endocrinol Metab 24*, 515-525.

([120.) Homko, C. J., Sivan, E., Reece, E. A., and Boden, G. (**1999**) Fuel Metabolism During Pregnancy, *Seminars in Reproductive Medicine*.

([121.) Sattar, N., and Greer, I. A. (**2002**) Pregnancy Complications and Maternal Cardiovascular Risk: Opportunities for Intervention and Screening?, *BMJ*.

([122.) Vrijkotte, T. G. M., Krukziener, N., Hutten, B. A., Vollebregt, K. C., Eijsden, M. v., and Twickler, M. B. (**2012**) Maternal Lipid Profile During Early Pregnancy and Pregnancy Complications and Outcomes: The ABCD Study, *The Journal of Clinical Endocrinology & Metabolism*.

([123.) O'Tierney-Ginn, P., Presley, L., Myers, S. P., and Catalano, P. M. (**2015**) Placental Growth Response to Maternal Insulin in Early Pregnancy, *The Journal of Clinical Endocrinology & Metabolism*.

([124.) O'Tierney-Ginn, P., Roberts, V. A., Gillingham, M. B., Walker, J. E., Glazebrook, P. A., Thornburg, K. L., Grove, K. L., and Frias, A. E. (**2015**) Influence of High Fat Diet and Resveratrol Supplementation on Placental Fatty Acid Uptake in the Japanese Macaque, *Placenta*.

([125.) Biswas, T., Uddin, J., Mamun, A. A., Pervin, S., and Garnett, S. P. (**2017**) Increasing Prevalence of Overweight and Obesity in Bangladeshi Women of Reproductive Age: Findings From 2004 to 2014, *Plos One*.

([126.) Rusconi, F., and Popovic, M. (**2017**) Maternal Obesity and Childhood Wheezing and Asthma, *Paediatric Respiratory Reviews*.

([127.) Nam, J., Greenwald, E., Jack-Roberts, C., Ajeeb, T. T., Malysheva, O. V., Caudill, M. A., Axen, K., Saxena, D., Semernina, E., Nanobashvili, K., and Jiang, X. (**2017**) Choline Prevents Fetal Overgrowth and Normalizes Placental Fatty Acid and Glucose Metabolism in a Mouse Model of Maternal Obesity, *The Journal of Nutritional Biochemistry*.

([128.) Sebire, N. J., Jolly, M., Harris, J. P., Wadsworth, J., Joffe, M., Beard, R. W., Regan, L., and Robinson, S. T. (**2001**) Maternal Obesity and Pregnancy Outcome: A Study of 287 213 Pregnancies in London, *International Journal of Obesity*.

([129.) Bharathi, K. R., Vijayalakshmi, S., and Shrunga, R. P. (**2017**) A Study of Lipid Parameters Among GDM and Non-GDM Pregnant Women: A Hospital Based Study, *International Journal of Reproduction Contraception Obstetrics and Gynecology*.

([130.) Ivy, R., Jahan, R., and Ara, A. (**2016**) Severe Hypertriglyceridemia in Pregnancy a Case Report, *Bangladesh Journal of Obstetrics & Gynaecology*.

([131.) Lain, K., and Catalano, P. M. (**2007**) Metabolic Changes in Pregnancy, *Clinical Obstetrics & Gynecology*.

([132.) Zhang, L., Yu, X., Wu, Y., Fu, H., Xu, P., Zheng, Y., Li, W., Yang, X., Zhang, F., Hu, M., Wang, H., Liu, X., Qiao, J., Peng, C., Gao, R., Saffery, R., Fu, Y., Qi, H., Tong, C., Kilby, M. D., and Baker, P. N. (**2021**) Gestational

Diabetes Mellitus-Associated Hyperglycemia Impairs Glucose Transporter 3 Trafficking in Trophoblasts Through the Downregulation of AMP-Activated Protein Kinase, *Frontiers in Cell and Developmental Biology*.

([133.) Landau, D., Haghiac, M., Minium, J., Skomorovska-Prokvolit, Y., Calabuig-Navarro, V., and O'Tierney-Ginn, P. (**2019**) Activation of AMPK in Human Placental Explants Impairs Mitochondrial Function and Cellular Metabolism, *Reproductive Sciences*.

([134.) Hak, A. E., Stehouwer, C. D., Bots, M. L., Polderman, K. H., Schalkwijk, C. G., Westendorp, I. C. D., Hofman, A., and Witteman, J. C. M. (**1999**) Associations of C-Reactive Protein With Measures of Obesity, Insulin Resistance, and Subclinical Atherosclerosis in Healthy, Middle-Aged Women, *Arteriosclerosis Thrombosis and Vascular Biology*.

([135.) Lei, T., Ping, L., and Ling, L. (**2020**) Whole Transcriptome Expression Profiles in Placenta Samples From Women With Gestational Diabetes Mellitus, *Journal of Diabetes Investigation*.

([136.) Street, M. E., Viani, I., Ziveri, M., Volta, C., Smerieri, A., and Bernasconi, S. (**2011**) Impairment of Insulin Receptor Signal Transduction in Placentas of Intra-Uterine Growth-Restricted Newborns and Its Relationship With Fetal Growth, *Acta Endocrinologica*.

([137.) Radzicka, S., Pietryga, M., Iciek, R., and Brazert, J. (**2018**) The Role of Visfatin in Pathogenesis of Gestational Diabetes (GDM), *Ginekologia Polska*.

([138.) D'Ippolito, S., Tersigni, C., Scambia, G., and Simone, N. D. (**2012**) Adipokines, an Adipose Tissue and Placental Product With Biological Functions During Pregnancy, *Biofactors*.

([139.) Akerman F, L. Z., Rao CV. . (**2002**) Gynecological EndocrinologyHuman umbilical cord and fetal membranes co-express leptin and its receptor genes. , *Gynecol Endocrinol. 2002 Aug;16 4*, 299-306.

([140.) Masuzaki, H., Ogawa, Y., Sagawa, N., Hosoda, K., Matsumoto, T., Mise, H., Nishimura, H., Yoshimasa, Y., Tanaka, I., Mori, T., and Nakao, K. (**1997**) Nonadipose tissue production of leptin: Leptin as a novel placenta-derived hormone in humans, *Nature Medicine 3*, 1029-1033.

([141.) Lea, R. G., Howe, D., Hannah, L. T., Bonneau, O., Hunter, L., and Hoggard, N. (**2000**) Placental Leptin in Normal, Diabetic and Fetal Growth-Retarded Pregnancies, *Molecular Human Reproduction*.

([142.) Lepercq, J., Challier, J.-C., Guerre-Millo, M., Caüzac, M., Vidal, H., and Mouzon, S. H.-d. (**2001**) Prenatal Leptin Production: Evidence That Fetal Adipose Tissue Produces Leptin, *The Journal of Clinical Endocrinology & Metabolism*.

([143.) Ostafiichuk, S. O. (**2019**) The Role of Resistin in the Genesis of Metabolic Disorders in Pathological Pregnancy, *The Ukrainian Biochemical Journal*.

([144.) Marta, M., Ferraro, S., Aurora, D., and Ersilia, N. (**2021**) GDM-complicated Pregnancies: Focus on Adipokines, *Molecular Biology Reports*.

([145.) Faßhauer, M., Blüher, M., Stümvoll, M., Tönessen, P., Faber, R., and Stepan, H. (**2007**) Differential Regulation of Visfatin and Adiponectin in Pregnancies With Normal and Abnormal Placental Function, *Clinical Endocrinology*.

([146.) Faßhauer, M., and Paschke, R. (**2003**) Regulation of Adipocytokines and Insulin Resistance, *Diabetologia*.

([147.) Lappas, M., Yee, K., Permezel, M., and Rice, G. E. (**2005**) Release and Regulation of Leptin, Resistin and Adiponectin From Human Placenta, Fetal Membranes, and Maternal Adipose Tissue and Skeletal Muscle From Normal and Gestational Diabetes Mellitus-Complicated Pregnancies, *Journal of Endocrinology*.

([148.) Festa, A., Shnawa, N., Krugluger, W., Hopmeier, P., Schernthaner, G., and Haffner, S. M. (**1999**) Relative Hypoleptinaemia in Women With Mild Gestational Diabetes Mellitus, *Diabetic Medicine*.

([149.) Chan, T.-F., Su, J. H., Chung, Y.-F., Hsu, Y. H., Yeh, Y. T., Jong, S.-B., and Yuan, S. S. F. (**2003**) Amniotic Fluid and Maternal Serum Leptin Levels in Pregnant Women Who Subsequently Develop Preeclampsia, *European Journal of Obstetrics & Gynecology and Reproductive Biology*.

([150.) Pighetti, M., Tommaselli, G. A., D'Elia, A., Carlo, C. D., Mariano, A., Carlo, A. D., and Nappi, C. (**2003**) Maternal Serum and Umbilical Cord Blood Leptin Concentrations With Fetal Growth Restriction, *Obstetrics and Gynecology*.

([151.) Ranheim, T., Haugen, F., Staff, A. C., Brække, K., Harsem, N. K., and Drevon, C. A. (**2004**) Adiponectin Is Reduced in Gestational Diabetes Mellitus in Normal Weight Women, *Acta Obstetricia Et Gynecologica Scandinavica*.

([152.) Williams, M. A., Qiu, C., Muy-Rivera, M., Vadachkoria, S., Song, T., and Luthy, D. A. (**2004**) Plasma Adiponectin Concentrations in Early Pregnancy and Subsequent Risk of Gestational Diabetes Mellitus, *The Journal of Clinical Endocrinology & Metabolism*.

([153.) Simeonova-Krstevska, S., Krstevska, B., Velkoska-Nakova, V., Lega, M. H., Samardjiski, I., Serafimoski, V., Livrinova, V., Todorovska, I., and Sima, A. (**2014**) Effect of Lipid Parameters on Foetal Growth in Gestational Diabetes Mellitus Pregnancies, *Prilozi*.

([154.) Olmos, P., Rigotti, A., Busso, D., Berkowitz, L., Santos, J. L., Borzone, G., Poblete, J. A., Vera, C., Belmar, C., Goldenberg, D., Samith, B., Acosta, A.

M. a., Escalona, M., Niklitschek, I., Mandiola, J., and Mertens, N. (**2014**) Maternal Hypertriglyceridemia: A Link Between Maternal Overweight-Obesity and Macrosomia in Gestational Diabetes, *Obesity*.

([155.) Eppel, D., Feichtinger, M., Lindner, T., Kotzaeridi, G., Rosicky, I., Yerlikaya-Schatten, G., Eppel, W., Husslein, P., Tura, A., and Göbl, C. (**2021**) Association Between Maternal Triglycerides and Disturbed Glucose Metabolism in Pregnancy, *Acta Diabetologica*.

([156.) Schaefer-Graf, U. M., K, G., Kulbacka, I., Kjos, S. L., Dudenhausen, J., Vetter, K., and Herrera, E. (**2008**) Maternal Lipids as Strong Determinants of Fetal Environment and Growth in Pregnancies With Gestational Diabetes Mellitus, *Diabetes Care*.

([157.) Kim, S. Y., Sharma, A. J., and Callaghan, W. M. (**2012**) Gestational Diabetes and Childhood Obesity, *Current Opinion in Obstetrics & Gynecology*.

([158.) Schaefer-Graf, U. M., Meitzner, K., Ortega-Senovilla, H., K, G., Vetter, K., Abou-Dakn, M., and Herrera, E. (**2011**) Differences in the Implications of Maternal Lipids on Fetal Metabolism and Growth Between Gestational Diabetes Mellitus and Control Pregnancies, *Diabetic Medicine*.

([159.) Arbib, N., Shmueli, A., Salman, L., Krispin, E., Toledano, Y., and Hadar, E. (**2019**) First Trimester Glycosylated Hemoglobin as a Predictor of Gestational Diabetes Mellitus, *International Journal of Gynecology & Obstetrics*.

([160.) Luo, Z. C., Nuyt, A. M., Delvin, E., Audibert, F., Girard, I., Shatenstein, B., Cloutier, A., Cousineau, J.-M., Djemli, A., Deal, C., Lévy, É., Wu, Y., Julien, P., and Fraser, W. D. (**2012**) Maternal and Fetal IGF-I and IGF-II Levels, Fetal Growth, and Gestational Diabetes, *The Journal of Clinical Endocrinology & Metabolism*.

([161.) Kushtagi, P., and Arvapally, S. (**2009**) Maternal Mid-Pregnancy Serum Triglyceride Levels and Neonatal Birth Weight, *International Journal of Gynecology & Obstetrics*.

([162.) Kim, C. (**2014**) Maternal Outcomes and Follow-up After Gestational Diabetes Mellitus, *Diabetic Medicine 31*, 292-301.

([163.) Knopp, R. H., Warth, M. R., Charles, D., Childs, M. T., Li, J. R., Mabuchi, H., and Allen, M. L. (**1986**) Lipoprotein Metabolism in Pregnancy, Fat Transport to the Fetus, and the Effects of Diabetes, *Neonatology*.

([164.) Puhkala, J., Luoto, R., Ahotupa, M., Raitanen, J., and Vasankari, T. (**2013**) Postpartum Weight Retention Is Associated With Elevated Ratio of Oxidized LDL Lipids to HDL-Cholesterol, *Lipids*.

([165.) Wadsack, C., Tabano, S., Maier, A.-K. B., Hiden, U., Alvino, G., Cozzi, V., Hüttinger, M., Schneider, W. J., Lang, U., Cetin, I., and Desoye, G. (**2007**)

Intrauterine Growth Restriction Is Associated With Alterations in Placental Lipoprotein Receptors and Maternal Lipoprotein Composition, *Ajp Endocrinology and Metabolism*.

([166.) Muñoz, A. M. M., Uberos, J., Molina, A. R. d., Valenzuela, A., Cano, D. A., Ruiz, C., and Font, J. A. M. (**1995**) Relationship of Blood Rheology to Lipoprotein Profile During Normal Pregnancies and Those With Intrauterine Growth Retardation, *Journal of Clinical Pathology*.

([167.) Skryten, A., Johnson, P., and Gustafson, A. (**1980**) Studies in Normal Pregnancy — Serum Lipids, Lipoproteins, and Uric Acid (Ii), *Acta Obstetricia Et Gynecologica Scandinavica*.

([168.) Fuller, M., Priyadarshini, M., Gibbons, S. M., Angueira, A. R., Brodsky, M., Hayes, M. G., Kovatcheva-Datchary, P., Bäckhed, F., Gilbert, J. A., Lowe, W. L., and Layden, B. T. (**2015**) The Short-Chain Fatty Acid Receptor, FFA2, Contributes to Gestational Glucose Homeostasis, *Ajp Endocrinology and Metabolism*.

([169.) Martin, C. L., Siega-Riz, A. M., Robinson, W. R., Daniels, J. L., Perrin, E. M., and Stuebe, A. M. (**2016**) Maternal Dietary Patterns Are Associated With Lower Levels of Cardiometabolic Markers During Pregnancy, *Paediatric and Perinatal Epidemiology*.

([170.) Rhyu, H.-S., and Park, K.-S. (**2019**) Effects of Telephone Follow-Up Intervention on %Body Fat, Inflammatory Cytokines, and Oxidative Stress in Obese Hispanic Children, *International Journal of Environmental Research and Public Health*.

([171.) Livia, B., Carolina, A. F., Marcelle, A. S., Daniela de Barros, M., Antonio, M., Carla, L., Claire, V., Camille, O., Jean-Marie, G., Gabriela, D. A. P., Julian, L. G., Daniela, S. A., Thierry, D., Graham, J. B., Fátima Lúcia de Carvalho, S., and Tatiana, E.-B. (**2021**) Decreased Fatty Acid Transporter FABP1 and Increased Isoprostanes and Neuroprostanes in the Human Term Placenta: Implications for Inflammation and Birth Weight in Maternal Pre-Gestational Obesity.

([172.) Musa, E., Salazar-Petres, E., Arowolo, A., Levitt, N., Matjila, M., and Sferruzzi-Perri, A. N. (**2023**) Obesity and Gestational Diabetes Independently and Collectively Induce Specific Effects on Placental Structure, Inflammation and Endocrine Function in a Cohort of South African Women, *The Journal of Physiology*.

([173.) Hirschmugl, B., Desoyé, G., Catalano, P. M., Klymiuk, I., Scharnagl, H., Payr, S., Kitzinger, E., Schliefsteiner, C., Lang, U., Wadsack, C., and Mouzon, S. H. (**2016**) Maternal Obesity Modulates Intracellular Lipid Turnover in the Human Term Placenta, *International Journal of Obesity*.

([174.) Aye, I. L., Lager, S., Ramirez, V. I., Gaccioli, F., Dudley, D. J., Jansson, T., and Powell, T. L. (**2014**) Increasing Maternal Body Mass Index Is Associated

With Systemic Inflammation in the Mother and the Activation of Distinct Placental Inflammatory Pathways1, *Biology of Reproduction*.

([175.) Ye, K., Li, L., Zhang, D., Li, Y., Wang, H. Q., Lai, H., and Hu, C. L. (**2017**) Effect of Maternal Obesity on Fetal Growth and Expression of Placental Fatty Acid Transporters, *Journal of Clinical Research in Pediatric Endocrinology*.

([176.) Parisi, F., Milazzo, R., Savasi, V., and Cetin, I. (**2021**) Maternal Low-Grade Chronic Inflammation and Intrauterine Programming of Health and Disease, *International Journal of Molecular Sciences*.

([177.) Stuart, T., O'Neill, K., Condon, D. E., Sasson, I., Sen, P., Xia, Y., and Simmons, R. A. (**2018**) Diet-Induced Obesity Alters the Maternal Metabolome and Early Placenta Transcriptome and Decreases Placenta Vascularity in the Mouse†, *Biology of Reproduction*.

([178.) Herrera, E. (**2002**) Lipid Metabolism in Pregnancy and Its Consequences in the Fetus and Newborn, *Endocrine*.

([179.) Herrera, E., and Ortega-Senovilla, H. (**2014**) Lipid Metabolism During Pregnancy and Its Implications for Fetal Growth, *Current Pharmaceutical Biotechnology*.

([180.) Olmos-Ortiz, A., Flores-Espinosa, P., Díaz, L., Velázquez, P., Ramírez-Isarraraz, C., and Zaga-Clavellina, V. (**2021**) Immunoendocrine Dysregulation During Gestational Diabetes Mellitus: The Central Role of the Placenta, *International Journal of Molecular Sciences*.

([181.) Radaelli, T., Varastehpour, A., Catalano, P. M., and Mouzon, S. H.-d. (**2003**) Gestational Diabetes Induces Placental Genes for Chronic Stress and Inflammatory Pathways, *Diabetes*.

([182.) Saben, J., Zhong, Y., Gomez-Acevedo, H., Thakali, K. M., Borengasser, S. J., Andres, A., and Shankar, K. (**2013**) Early Growth Response Protein-1 Mediates Lipotoxicity-Associated Placental Inflammation: Role in Maternal Obesity, *Ajp Endocrinology and Metabolism*.

([183.) Saben, J., Lindsey, F., Zhang, Y., Thakali, K., Badger, T. M., Andres, A., Gomez-Acevedo, H., and Shankar, K. (**2014**) Maternal Obesity Is Associated With a Lipotoxic Placental Environment, *Placenta*.

([184.) Heimerl, S., Fischer, M., Baessler, A., Liebisch, G., Sigruener, A., Wallner, S., and Schmitz, G. (**2014**) Alterations of Plasma Lysophosphatidylcholine Species in Obesity and Weight Loss, *Plos One*.

([185.) Evemie, D., Maude, E.-C., and Julie, L. (**2013**) Modulation of Cholesterol Transport by Insulin-Treated Gestational Diabetes Mellitus in Human Full-Term Placenta1, *Biology of Reproduction*.

([186.) Delarue, J., and Magnan, C. (**2007**) Free Fatty Acids and Insulin Resistance, *Current Opinion in Clinical Nutrition & Metabolic Care*.

([187.) María, R.-P., Antonio, J. R.-A., María, S.-C., and Elvira, L. (**2017**) Role of Insulin in Placental Transport of Nutrients in Gestational Diabetes Mellitus, *Annals of Nutrition and Metabolism*.

([188.) María, R.-P., María, T. P.-S., Antonio, J. R.-A., José, E. B.-C., María, S.-C., Juan José, P., and Elvira, L. (**2017**) Insulin Treatment May Alter Fatty Acid Carriers in Placentas From Gestational Diabetes Subjects, *International Journal of Molecular Sciences*.

([189.) Justesen, S., Bilde, K., Olesen, R. H., Pedersen, L. H., and Ernst, E. (**2023**) ABCB1 Expression Is Increased in Human First Trimester Placenta From Pregnant Women Classified as Overweight or Obese, *Scientific Reports*.

([190.) Shrestha, D., Ouidir, M., Workalemahu, T., Zeng, X., and Tekola-Ayele, F. (**2020**) Placental DNA Methylation Changes Associated With Maternal Prepregnancy BMI and Gestational Weight Gain, *International Journal of Obesity*.

([191.) Shrestha, A., Prowak, M., Berlandi-Short, V.-M., Garay, J., and Ramalingam, L. (**2021**) Maternal Obesity: A Focus on Maternal Interventions to Improve Health of Offspring, *Frontiers in Cardiovascular Medicine 0*, 674-674.

([192.) Shrestha, N., Ezechukwu, H. C., Holland, O. J., and Hryciw, D. H. (**2020**) Developmental Programming of Peripheral Diseases in Offspring Exposed to Maternal Obesity During Pregnancy, *Ajp Regulatory Integrative and Comparative Physiology*.

([193.) Fisher, E. A., and McLeod, R. S. (2021) Assembly and secretion of triacylglycerol-rich lipoproteins, In *Biochemistry of Lipids, Lipoproteins and Membranes*, pp 515-546.

([194.) Cheng C. F., E. P., Michael L. Gross. (**1998**) Charge-Remote Fragmentations Are Energy-Dependent Processes, *J Am Soc Mass Spectrom 1998, 9, 840–844*.

([195.) M. Klingler, H. D., E. Larque, and B. Koletzko. (**2003**) Analysis of FA Contents in Individual Lipid Fractions from Human Placental Tissue, *Lipids 38*.

([196.) Strott, C. A., and Higashi, Y. (**2003**) Cholesterol sulfate in human physiology: what is it all about?, *Journal of Lipid Research 44*, 1268-1278.

([197.) Chen, L., Mir, S. A., Bendt, A. K., Esther, C. W. L., Narasimhan, K., Tan, K., Loy, S. L., Tan, K. H., Shek, L. P., Chan, J. K. Y., Yap, F., Meaney, M. J., Chan, S.-Y., Chong, Y. S., Gluckman, P. D., Eriksson, J. G., Karnani, N., and Wenk, M. R. (**2023**) Plasma Lipidomic Profiling Reveals Metabolic

Adaptations to Pregnancy and Signatures of Cardiometabolic Risk: A Preconception and Longitudinal Cohort Study, *BMC Medicine*.

([198.) Griffiths, W. J., Abdel-Khalik, J., Yutuc, E., Morgan, A. H., Gilmore, I., Hearn, T., and Wang, Y. (**2017**) Cholesterolomics: An update, *Anal Biochem 524*, 56-67.

([199.) Hsieh, H. Y., Li, L. H., Hsu, R. Y., Kao, W. F., Huang, Y. C., and Hsu, C. C. (**2017**) Quantification of Endogenous Cholesterol in Human Serum on Paper Using Direct Analysis in Real Time Mass Spectrometry, *Anal Chem 89*, 6146-6152.

([200.) Li, L. H., Dutkiewicz, E. P., Huang, Y. C., Zhou, H. B., and Hsu, C. C. (**2019**) Analytical methods for cholesterol quantification, *J Food Drug Anal 27*, 375-386.

([201.) Tarfeen, N., Nisa, K. U., and Nisa, Q. (**2022**) MALDI-TOF MS: application in diagnosis, dereplication, biomolecule profiling and microbial ecology, *Proceedings of the Indian National Science Academy 88*, 277-291.

([202.) Griesinger, H., Fuchs, B., Süss, R., Matheis, K., Schulz, M., and Schiller, J. (**2014**) Stationary phase thickness determines the quality of thin-layer chromatography/matrix-assisted laser desorption and ionization mass spectra of lipids, *Analytical biochemistry 451*, 45-47.

([203.) Armstrong, D. (2009) *Lipidomics Volume 1: Methods and Protocols*

([204.) Fuchs, B., Bischoff, A., Suss, R., Teuber, K., Schurenberg, M., Suckau, D., and Schiller, J. (**2009**) Phosphatidylcholines and -ethanolamines can be easily mistaken in phospholipid mixtures: a negative ion MALDI-TOF MS study with 9-aminoacridine as matrix and egg yolk as selected example, *Anal Bioanal Chem 395*, 2479-2487.

([205.) Leopold, J., Popkova, Y., Engel, K., and Schiller, J. (**2018**) Recent Developments of Useful MALDI Matrices for the Mass Spectrometric Characterization of Lipids, *Biomolecules 8*, 173.

([206.) Fuchs, B., Nimptsch, A., Süß, R., and Schiller, J. (2009) Capabilities and Drawbacks of Phospholipid Analysis by MALDI-TOF Mass Spectrometry, pp 103-125, Humana Press.

([207.) Fuchs, B., and Schiller, J. (**2009**) Application of MALDI-TOF Mass Spectrometry in Lipidomics, *European Journal of Lipid Science and Technology*.

([208.) Fuchs, B., Schiller, J., Süß, R., Nimptsch, A., Schürenberg, M., and Suckau, D. (**2009**) Capabilities and disadvantages of combined matrix-assisted laser-desorption/ionization time-of-flight mass spectrometry (MALDI-TOF MS) and high-performance thin-layer chromatography (HPTLC): Analysis of egg yolk lipids, *Journal of Planar Chromatography – Modern TLC 22*, 35-42.

([209.) Fuchs, B., Süß, R., Nimptsch, A., and Schiller, J. (**2009**) MALDI-TOF-MS Directly Combined with TLC: A Review of the Current State, *Chromatographia 69*.

([210.) Marijana Petkovic, J. S., Matthias Muller, Rosmarie Suß, Klaus Arnold, Jurgen Arnhold. (**2009**) Detection of Adducts with Matrix Clusters in the Positive and Negative Ion Mode MALDI-TOF Mass Spectra of Phospholipids.

([211.) Fuchs, B., Suss, R., and Schiller, J. (**2010**) An update of MALDI-TOF mass spectrometry in lipid research, *Progress in Lipid Research 49*, 450-475.

([212.) Kathrin Engel, J. S., Christina E. Galuska, Beate Fuch. (**2021**) Phospholipases and reactive oxygen species derived lipid biomarkers in healthy and diseased humans and animals, *Frontiers in Physiology Lipids and Fatty acids research*

([213.) Engel, K. M., Prabutzki, P., Leopold, J., Nimptsch, A., Lemmnitzer, K., Vos, D. R. N., Hopf, C., and Schiller, J. (**2022**) A new update of MALDI-TOF mass spectrometry in lipid research, *Progress in Lipid Research 86*.

([214.) Fuchs, B., Süss, R., and Schiller, J. (**2022**) A new update of MALDI-TOF mass spectrometry in lipid research, *Progress in Lipid Research 50*, 101145-101145.

([215.) Jakop, U., Muller, K., Muller, P., Neuhauser, S., Callealta Rodriguez, I., Grunewald, S., Schiller, J., and Engel, K. M. (**2022**) Seminal lipid profiling and antioxidant capacity: A species comparison, *PLoS One 17*, e0264675.

([216.) Teuber, K., Riemer, T., and Schiller, J. (**2010**) Thin-layer chromatography combined with MALDI-TOF-MS and 31P-NMR to study possible selective bindings of phospholipids to silica gel, *Analytical and Bioanalytical Chemistry 398*, 2833-2842.

([217.) Schiller, J., Fuchs, B., Teuber, K., Nimptsch, A., Nimptsch, K., and Süss, R. (2011) TLC/HPTLC with Direct Mass Spectrometric Detection: A Review of the Progress Achieved in the Last 5 Years.

([218.) Beate Fuchs, K. M. (**2015**) Combining TLC Separation with MS Detection - A Revival of TLC, *Journal of Glycomics & Lipidomics 05*.

([219.) Fuchs, B., Popkova, Y., Süß, R., and Schiller, J. (2015) Chapter 14 Separation of (Phospho)Lipids by Thin-Layer Chromatography, In *Instrumental Thin-Layer Chromatography*, pp 375-405.

([220.) Popkova, Y., Meusel, A., Breitfeld, J., Schleinitz, D., Hirrlinger, J., Dannenberger, D., Kovacs, P., and Schiller, J. (**2015**) Nutrition-dependent changes of mouse adipose tissue compositions monitored by NMR, MS, and chromatographic methods, *Anal Bioanal Chem 407*, 5113-5123.

([221.) Schröter, J., Popkova, Y., Süß, R., and Schiller, J. (2017) Combined Use of MALDI-TOF Mass Spectrometry and 31P NMR Spectroscopy for Analysis of Phospholipids, pp 107-122, Springer New York.

([222.) Eibisch, M., Fuchs, B., Schiller, J., Süss, R., and Teuber, K. (**2011**) Analysis of Phospholipid Mixtures from Biological Tissues by Matrix-Assisted Laser Desorption and Ionization Time-of-Flight Mass Spectrometry (MALDI-TOF MS): A Laboratory Experiment, *Journal of Chemical Education 88*, 503-507.

([223.) Eibisch, M., and Schiller, J. (**2011**) Sphingomyelin is more sensitively detectable as a negative ion than phosphatidylcholine: A matrix-assisted laser desorption/ionization time-of-flight mass spectrometric study using 9-aminoacridine (9-AA) as a matrix, *Rapid Communications in Mass Spectrometry 25*, 1100-1106.

([224.) Dinkla, S., van Eijk, L. T., Fuchs, B., Schiller, J., Joosten, I., Brock, R., Pickkers, P., and Bosman, G. J. (**2016**) Inflammation-associated changes in lipid composition and the organization of the erythrocyte membrane, *BBA Clin 5*, 186-192.

([225.) Bligh E G, D. W. J. (**1959**) A rapid method of total lipid extraction and purification., *Can. J. Biochem. Physiol. 37*, 911-1917.

([226.) Folch, J., Lees, M., and Stanley, G. H. S. (**1957**) A Simple Method for the Isolation and Purification of Total Lipides from Animal Tissues, *Journal of Biological Chemistry 226*, 497-509.

([227.) Yang, K., and Han, X. (**2016**) Lipidomics: Techniques, Applications, and Outcomes Related to Biomedical Sciences, *Trends Biochem Sci 41*, 954-969.

([228.) Ellis, S. R., Brown, S. H. J., Panhuis, M. i. h., Blanksby, S. J., and Mitchell, T. W. (**2013**) Surface Analysis of Lipids by Mass Spectrometry: More Than Just Imaging, *Progress in Lipid Research*.

([229.) Parchem, K., Sasson, S., Ferreri, C., and Bartoszek, A. (**2019**) Qualitative Analysis of Phospholipids and Their Oxidised Derivatives – Used Techniques and Examples of Their Applications Related to Lipidomic Research and Food Analysis, *Free Radical Research*.

([230.) Triebl, A., and Wenk, M. R. (**2018**) Analytical Considerations of Stable Isotope Labelling in Lipidomics, *Biomolecules*.

([231.) Lin, L., Han, J., Wang, Z., Liu, J., Wei, J., Xiong, S., and Zhao, Z. (**2014**) Mass Spectrometry Methodology in Lipid Analysis, *International Journal of Molecular Sciences*.

([232.) Yang, K., and Han, X. (**2016**) Lipidomics: Techniques, Applications, and Outcomes Related to Biomedical Sciences, *Trends in Biochemical Sciences*.

([233.) Han, X., Yang, J., Cheng, H., Ye, H., and Gross, R. W. (**2004**) Toward fingerprinting cellular lipidomes directly from biological samples by two-dimensional electrospray ionization mass spectrometry, *Anal Biochem 330*, 317-331.

([234.) Han, X., and Gross, R. W. (**2004**) Shotgun Lipidomics: Electrospray Ionization Mass Spectrometric Analysis and Quantitation of Cellular Lipidomes Directly From Crude Extracts of Biological Samples, *Mass Spectrometry Reviews*.

([235.) Creaser, C. S., and Ratcliffe, L. (**2006**) Atmospheric pressure matrix-assisted laser desorption/ionisation mass spectrometry: A review, *Current Analytical Chemistry 2*, 9-15.

([236.) Leopold, J., Prabutzki, P., Engel, K. M., and Schiller, J. (**2023**) A Five-Year Update on Matrix Compounds for MALDI-MS Analysis of Lipids, *Biomolecules 13*.

([237.) Tuzimski, T., and Sherma, J. (2016) Thin-Layer Chromatography and Mass Spectrometry for the Analysis of Lipids, In *Encyclopedia of Lipidomics*, pp 1-20.

([238.) Zemski Berry, K. A., Hankin, J. A., Barkley, R. M., Spraggins, J. M., Caprioli, R. M., and Murphy, R. C. (**2011**) MALDI imaging of lipid biochemistry in tissues by mass spectrometry, *Chemical Reviews 111*, 6491-6512.

([239.) J B Fenn, M. M., C K Meng, S F Wong, C M Whitehouse. (**1989**) Electrospray ionization for mass spectrometry of large biomolecules, *Science 246*, 64-71.

([240.) Fenn, J. B. (**2003**) Electrospray wings for molecular elephants (Nobel lecture), *Angew Chem Int Ed Engl 42*, 3871-3894.

([241.) Takats, Z., Wiseman, J. M., Gologan, B., and Cooks, R. G. (**2004**) Mass spectrometry sampling under ambient conditions with desorption electrospray ionization, *Science 306*, 471-473.

([242.) al., R. M. C. e. (**1997**) Selected Topics and Mass Spectrometry in the Biomolecular Sciences, 3-16.

([243.) Shaffer, S. A., Tang, K., Anderson, G. A., Prior, D. C., Udseth, H. R., and Smith, R. D. (**1997**) A novel ion funnel for focusing ions at elevated pressure using electrospray ionization mass spectrometry, *Rapid communications in mass spectrometry 11*, 1813-1817.

([244.) Kelly, R. T., Tolmachev, A. V., Page, J. S., Tang, K., and Smith, R. D. (**2010**) The ion funnel: theory, implementations, and applications, *Mass Spectrom Rev 29*, 294-312.

([245.) Grayson, M. A. (**2011**) John Bennett Fenn: a curious road to the prize, *J Am Soc Mass Spectrom 22*, 1301-1308.

([246.) Dellisanti, C. D. (**2015**) Electrospray makes molecular elephants fly, *Nature Methods 12*, 15-15.

([247.) Mann, M. (**2019**) The ever-expanding scope of electrospray mass spectrometry-a 30-year journey, *Nat Commun 10*, 3744.

([248.) Gross, X. H. a. R. W. (**1994**) Electrospray ionization mass spectroscopic analysis of human erythrocyte plasma membrane phospholipids, (plasma, red blood cell), *Proc. Natd. Acad. Sci. USA 91*, 10635-10639.

([249.) B. BRUGGER, G. E., R. SANDHOF, F. T. WIELAND, W. D. LEHMANN. (**1997**) Quantitative analysis of biological membrane lipids at the low picomole level by nano-electrospray ionization tandem mass spectrometry, *Cell Biology 94*, 2339–2344.

([250.) Harrison K.A, D. S. S., Marathe G.K, McIntyre T., Prescott S., Reddy K.M., Falck J.R., Murphy R.C. (**2000**) Analysis of oxidized glycerophosphocholine lipids using electrospray.pdf>, *J. Mass Spectrom. 35*, 224-236.

([251.) Kathleen A. Harrison, S. S. D., Gopal K. Marathe, Thomas McIntyre, Stephen Prescott, Komandla M. Reddy, J. R. Falck and Robert C. Murphy. (**2000**) Analysis of oxidized glycerophosphocholine lipids using electrospray ionization mass spectrometry and micro derivatization technique, *J. Mass Spectrom. 35*, 224–236

([252.) Han, X., and Gross, R. W. (**2003**) Global Analyses of Cellular Lipidomes Directly From Crude Extracts of Biological Samples by ESI Mass Spectrometry: A Bridge to Lipidomics, *The Journal of Lipid Research*.

([253.) Pulfer, M. K., and Murphy, R. C. (**2003**) Electrospray Mass Spectrometry of Phospholipids, *Mass Spectrometry Reviews*.

([254.) Byrdwell, W. C. (**2001**) Atmospheric Pressure Chemical Ionization Mass Spectrometry for Analysis of Lipids, *Lipids*.

([255.) Ivanova, P. T., Milne, S., Myers, D. S., and Brown, H. A. (**2009**) Lipidomics: A Mass Spectrometry-Based Systems Level Analysis of Cellular Lipids, *Current Opinion in Chemical Biology*.

([256.) Lee, S. H., Williams, M. L., DuBois, R. N., and Blair, I. A. (**2003**) Targeted Lipidomics Using Electron Capture Atmospheric Pressure Chemical Ionization Mass Spectrometry, *Rapid Communications in Mass Spectrometry*.

([257.) Saldanha, T., Alexandra Christine Helena Frankland, S., Eberlin, M. N., and Bragagnolo, N. (**2006**) HPLC Separation and Determination of 12

Cholesterol Oxidation Products in Fish: Comparative Study of RI, UV, and APCI-MS Detectors, *Journal of Agricultural and Food Chemistry*.

([258.) Tian, Q., Failla, M. L., Bohn, T., and Schwartz, S. J. (**2006**) High-performance Liquid Chromatography/Atmospheric Pressure Chemical Ionization Tandem Mass Spectrometry Determination of Cholesterol Uptake by Caco-2 Cells, *Rapid Communications in Mass Spectrometry*.

([259.) Stephens W, E. (**1946**) A Pulsed Mass Spectrometer with Time Dispersion, *Phys. Rev. 69*, 691.

([260.) Wiley, W. C., and Mclaren, I. (**1955**) Time of flight mass spectrometer with improved resolution, *Review of Scientific Instruments 26*, 1150-1157.

([261.) Michael Karas, F. H. (**1988**) Laser Desorption Ionization of Proteins with Molecular Masses Exceeding 10 000 Daltons, *Anal. Chem. 60*, 2301-2303.

([262.) Michael Karas, D. B., and Franz Hillenkamp. (**1985**) Influence of the Wavelength in High-Irradiance Ultraviolet Laser Desorption Mass Spectrometry of Organic Molecules, *Anal. Cham. 1985, 57, 2935-2939*.

([263.) Karas, M., Bachmann, D., Bahr, U., and Hillenkamp, F. (**1987**) Matrix-assisted ultraviolet laser desorption of non-volatile compounds, *International journal of mass spectrometry and ion processes 78*, 53-68.

([264.) Karas, M., Hillenkamp, F., Zhang, H., Caprioli, R. J., Vorm, O., Roepstorff, P., Mann, M., Axelsson, J., Dwyer, J., Botten, D., and Caprioli, R. M. (1987) Molecular Imaging of Biological Samples: Localization of Peptides and Proteins Using MALDI-TOF MS, In *Rapid Commun. Mass Spectrom*, pp 41-41, UTC.

([265.) Karas M, H. F. (**1998**) Laser Desorption Ionization of Proteins with Molecular Masses Exceeding 10 000 Daltons, *Analytical Chemistry 60*, 2299-2301.

([266.) Tanaka, K., Waki, H., Ido, Y., Akita, S., Yoshida, Y., Yoshida, T., and Matsuo, T. (**1988**) Protein and Polymer Analyses Up to m/z 100 000 by Laser Ionization Time-of-flight Mass Spectrometry, *Rapid Communications in Mass Spectrometry*.

([267.) Dass. C, K. J., and Keiderling T.A,. (2001) Principles and Practice of Biological Mass Spectrometry. Book review: The Anomalous Infrared Amide I Intensity Distribution in 13C Isotopically Labeled Peptide Sheets Comes from Extended, Multiple-Stranded Structures. , In *J. Am. Chem. Soc. 2001, 123, 6142-6150*

([268.) Tanaka, K. (**2003**) The origin of macromolecule ionization by laser irradiation (Nobel lecture), *Angew Chem Int Ed Engl 42*, 3860-3870.

([269.) Schiller, J., Suss, R., Fuchs, B., Muller, M., Zschornig, O., and Arnold, K. (**2007**) MALDI-TOF MS in lipidomics, *Front Biosci 12*, 2568-2579.

([270.) Schiller, J., Suss, R., Fuchs, B., Muller, M., Petkovic, M., Zschornig, O., and Waschipky, H. (**2007**) The suitability of different DHB isomers as matrices for the MALDI-TOF MS analysis of phospholipids: which isomer for what purpose? *Eur Biophys J 36*, 517-527.

([271.) Dass, C. (2000) Principles and Practice of Biological Mass Spectrometry.

([272.) Dass, C. (2007) *Fundamental of contemporary mass spectrometry*, Wiley, Canada, USA.

([273.) Strooband, H. (2007) *Mass Spectrometry Principles and Applications*, third.

([274.) Caro, J., Doudkowsky, M., Figueras, A., Fraxedas, J., Garcia, G., Santiso, J., Schamm, S., Ojeda, F., Vázquez, L., Albella, J. M., Cuerno, R., and Salvarezza, R. C. (2001) Chapter 4 – Morphological and Structural Aspects of Thin Films Prepared by Vapor Deposition.

([275.) Dong, H., Kemptner, J., Marchetti-Deschmann, M., Kubicek, C. P., and Allmaier, G. (**2009**) Development of a MALDI two-layer volume sample preparation technique for analysis of coloured conidia spores of Fusarium by MALDI linear TOF mass spectrometry, *Anal Bioanal Chem 395*, 1373-1383.

([276.) Dass, C. (2007) *Fundamentals of contemporary mass spectrometry* Published by John Wiley & Sons, Inc., Hoboken, New Jersey. Published simultaneously in Canada.

([277.) Hillenkamp, F., and Peter-Katalinic, J. (2013) MALDI MS: a practical guide to instrumentation, methods and applications.

([278.) B. A. Mamyrin, V. I. K., D. V. Shmikk, and V. A. Zagulin. (**1973**) The mass-reflectron, a new nonmagnetic time-of-flight mass spectrometer with high resolution, *Soviet. Phys. JETP, Vol. 37, No.1, July 1973 37*, 45-48.

([279.) Mamyrin, B. A. (**2001**) Time-of-Flight Mass Spectrometry (Concepts, Achievements, and Prospects), *International Journal of Mass Spectrometry*.

([280.) Jiang, D., He, J., Hua, S., Zhang, J., Liu, L., Shan, C., Cui, X., and Ji, C. (**2022**) A Comparative Lipidomic Study of the Human Placenta From Women With or Without Gestational Diabetes Mellitus, *Molecular Omics*.

([281.) Hu, C., Duan, Q., and Han, X. (**2019**) Strategies to Improve/Eliminate the Limitations in Shotgun Lipidomics, *Proteomics*.

([282.) Wang, M., Wang, C., Han, R. H., and Han, X. (**2016**) Novel Advances in Shotgun Lipidomics for Biology and Medicine, *Progress in Lipid Research*.

([283.) Yang, K., Cheng, H., Gross, R. W., and Han, X. (**2009**) Automated Lipid Identification and Quantification by Multidimensional Mass Spectrometry-Based Shotgun Lipidomics, *Analytical Chemistry*.

([284.) Lintonen, T., Baker, P. R. S., Suoniemi, M., Ubhi, B. K., Koistinen, K. M., Duchoslav, E., Campbell, J. L., and Ekroos, K. (**2014**) Differential Mobility Spectrometry-Driven Shotgun Lipidomics, *Analytical Chemistry*.

([285.) Chen, E., Kiebish, M. A., McDaniel, J., Gao, F., Narain, N. R., Sarangarajan, R., Kacso, G., Ravasz, D., Seyfried, T. N., Adam-Vizi, V., and Chinopoulos, C. (**2016**) The Total and Mitochondrial Lipidome of Artemia Franciscana Encysted Embryos, *Biochimica Et Biophysica Acta (Bba) - Molecular and Cell Biology of Lipids*.

([286.) Rampler, E., Schoeny, H., Mitic, B. M., El Abiead, Y., Schwaiger, M., and Koellensperger, G. (**2018**) Simultaneous non-polar and polar lipid analysis by on-line combination of HILIC, RP and high-resolution MS, *Analyst 143*, 1250-1258.

([287.) Rampler, E., Criscuolo, A., Zeller, M., Abiead, Y. E., Schoeny, H., Hermann, G., Sokol, E., Cook, K., Peake, D. A., Delanghe, B., and Koellensperger, G. (**2018**) A Novel Lipidomics Workflow for Improved Human Plasma Identification and Quantification Using RPLC-MSn Methods and Isotope Dilution Strategies, *Analytical Chemistry*.

([288.) Rampler, E., Abiead, Y. E., Rusz, M., Hildebrand, F., Fitz, V., and Koellensperger, G. (**2020**) Recurrent Topics in Mass Spectrometry-Based Metabolomics and Lipidomics—Standardization, Coverage, and Throughput, *Analytical Chemistry*.

([289.) Lam, S. M., Tong, L., Yong, S. S., Li, B., Chaurasia, S. S., Shui, G., and Wenk, M. R. (**2011**) Meibum Lipid Composition in Asians With Dry Eye Disease, *Plos One*.

([290.) Finnie, S., Jeannotte, R., and Faubion, J. M. (**2009**) Quantitative Characterization of Polar Lipids From Wheat Whole Meal, Flour, and Starch, *Cereal Chemistry*.

([291.) Furukawa, S., Tsuji, N., and Sugiyama, A. (**2019**) Morphology and Physiology of Rat Placenta for Toxicological Evaluation, *Journal of Toxicologic Pathology*.

([292.) Wildman, D. E. (**2011**) Review: Toward an Integrated Evolutionary Understanding of the Mammalian Placenta, *Placenta*.

([293.) Lange, M., and Fedorova, M. (**2020**) Evaluation of Lipid Quantification Accuracy Using HILIC and RPLC MS on the Example of NIST SRM 1950 Metabolites in Human Plasma, *Analytical and Bioanalytical Chemistry*.

([294.) Rampler, E., Coman, C., Hermann, G., Sickmann, A., Ahrends, R., and Koellensperger, G. (**2017**) LILY-lipidome isotope labelling of yeast: in vivo synthesis of¹³C labelled reference lipids for quantification by mass spectrometry, *The Analyst 142*, 1891-1899.

([295.) Kim, J.-H., Kang, D., 이성기, and Kim, T.-Y. (**2019**) Deuterium Oxide Labeling for Global Omics Relative Quantification: Application to Lipidomics, *Analytical Chemistry*.

([296.) Watkins, O. C., Islam, M. O., Selvam, P., Pillai, R. A., Cazenave-Gassiot, A., Bendt, A. K., Karnani, N., Godfrey, K. M., Lewis, R. M., Wenk, M. R., and Chan, S.-Y. (**2019**) Metabolism of 13c-Labeled Fatty Acids in Term Human Placental Explants by Liquid Chromatography–Mass Spectrometry, *Endocrinology*.

([297.) Watkins, O. C., Islam, M. T., Selvam, P., Pillai, R. A., Cazenave-Gassiot, A., Bendt, A. K., Karnani, N., Godfrey, K. M., Lewis, R. M., Wenk, M. R., and Chan, S.-Y. (**2019**) Metabolism of 13c-Labeled Fatty Acids in Term Human Placental Explants by Liquid Chromatography–Mass Spectrometry, *Endocrinology*.

([298.) Duttaroy, A. K. (**2009**) Transport of Fatty Acids Across the Human Placenta: A Review, *Progress in Lipid Research*.

([299.) Louwagie, E. J., Larsen, T. D., Wachal, A. L., and Baack, M. L. (**2018**) Placental lipid processing in response to a maternal high-fat diet and diabetes in rats, *Pediatric Research 83*, 712-722.

([300.) Dancy, B. C. R., Chen, S.-W., Drechsler, R., Gafken, P. R., and Olsen, C. P. (**2015**) 13c- And 15n-Labeling Strategies Combined With Mass Spectrometry Comprehensively Quantify Phospholipid Dynamics in C. Elegans, *Plos One*.

([301.) Stoeckli, M., Chaurand, P., Hallahan, D. E., and Caprioli, R. M. (**2001**) Imaging mass spectrometry: a new technology for the analysis of protein expression in mammalian tissues, *Nat Med 7*, 493-496.

([302.) Spengler, B. (**2015**) Mass Spectrometry Imaging of Biomolecular Information, *Analytical Chemistry 87*, 64-82.

([303.) Berry, K. A., Hankin, J. A., Barkley, R. M., Spraggins, J. M., Caprioli, R. M., and Murphy, R. C. (**2011**) MALDI imaging of lipid biochemistry in tissues by mass spectrometry, *Chem Rev 111*, 6491-6512.

([304.) Caprioli, R. M., Farmer, T. B., and Gile, J. (**1997**) Molecular Imaging of Biological Samples: Localization of Peptides and Proteins Using MALDI-TOF MS, *Analytical Chemistry 69*, 4751-4760.

([305.) MD., A. M. (**2020**) Mass spectrometry-based phospholipid imaging: methods and findings, *Expert Rev Proteomics 17*, 843-854.

([306.) Cornett, D. S., Reyzer, M. L., Chaurand, P., and Caprioli, R. M. (**2007**) MALDI Imaging Mass Spectrometry: Molecular Snapshots of Biochemical Systems, *Nature Chemical Biology*.

([307.) Cornett, D. S., Mobley, J. A., Dias, E. C., Andersson, M., Arteaga, C. L., Sanders, M. E., and Caprioli, R. M. (**2006**) A novel histology-directed strategy for MALDI-MS tissue profiling that improves throughput and cellular specificity in human breast cancer, *Molecular & Cellular Proteomics 5*, 1975-1983.

([308.) Cazares, L. H., Troyer, D. A., Wang, B., Drake, R., and Semmes, O. J. (**2011**) MALDI Tissue Imaging: From Biomarker Discovery to Clinical Applications, *Analytical and Bioanalytical Chemistry*.

([309.) Tuck, M., Grélard, F., Blanc, L., and Desbenoit, N. (**2022**) MALDI-MSI Towards Multimodal Imaging: Challenges and Perspectives, *Frontiers in Chemistry*.

([310.) Hannun, Y. A., and Obeid, L. M. (**2017**) Sphingolipids and Their Metabolism in Physiology and Disease, *Nature Reviews Molecular Cell Biology*.

([311.) Raphael, W., and Sordillo, L. M. (**2013**) Dietary Polyunsaturated Fatty Acids and Inflammation: The Role of Phospholipid Biosynthesis, *International Journal of Molecular Sciences*.

([312.) Yang, Y., Lee, M., and Fairn, G. D. (**2018**) Phospholipid Subcellular Localization and Dynamics, *Journal of Biological Chemistry*.

([313.) Chavan-Gautam, P., Rani, A., and Freeman, D. J. (2018) Distribution of Fatty Acids and Lipids During Pregnancy, In *Advances in Clinical Chemistry*, pp 209-239, Academic Press Inc.

([314.) Gitta, S., Márk, L., Szentpéteri, J., and Szabó, É. (**2023**) Lipid Changes in the Peri-Implantation Period With Mass Spectrometry Imaging: A Systematic Review, *Life*.

([315.) Lewis, R. M., Childs, C. E., and Calder, P. C. (**2018**) New perspectives on placental fatty acid transfer, *Prostaglandins Leukot Essent Fatty Acids 138*, 24-29.

([316.) Griffiths, W. J., and Wang, Y. (**2019**) Oxysterol research: a brief review, *Biochemical Society Transactions 47*, 517-526.

([317.) Griffiths, W. J., Yutuc, E., and Wang, Y. (**2023**) Mass Spectrometry Imaging of Cholesterol and Oxysterols.

([318.) Yutuc, E., Angelini, R., Baumert, M., Mast, N., Pikuleva, I., Newton, J., Clench, M. R., Skibinski, D. O. F., Howell, O. W., Wang, Y., and Griffiths, W. J. (**2019**) Imaging Oxysterols in Mouse Brain by On-Tissue

Derivatisation-Robotic Liquid Micro-Extraction Surface Analysis-Liquid Chromatography-Mass Spectrometry.

([319.) Yutuc, E., Angelini, R., Baumert, M., Mast, N., Pikuleva, I., Newton, J., Clench, M. R., Skibinski, D. O. F., Howell, O. W., Wang, Y., and Griffiths, W. J. (**2020**) Localization of sterols and oxysterols in mouse brain reveals distinct spatial cholesterol metabolism, *Proc Natl Acad Sci U S A 117*, 5749-5760.

([320.) Pól, J., Vidova, V., Hyötyläinen, T., Volný, M., Novák, P., Strohalm, M., Kostiainen, R., Havlíček, V., Wiedmer, S. K., and Holopainen, J. M. (**2011**) Spatial Distribution of Glycerophospholipids in the Ocular Lens, *Plos One*.

([321.) Zaima, N., Hayasaka, T., Goto-Inoue, N., and Setou, M. (**2010**) Matrix-Assisted Laser Desorption/Ionization Imaging Mass Spectrometry, *International Journal of Molecular Sciences 11*, 5040-5055.

([322.) Aisha, R., Fernanda, A., and Perrie, O. T.-G. (**2021**) Placental Impact of Dietary Supplements: More Than Micronutrients, *Clinical Therapeutics*.

([323.) Forest, S., Breault-Turcot, J., Chaurand, P., and Masson, J.-F. (**2016**) Surface Plasmon Resonance Imaging-Maldi-Tof Imaging Mass Spectrometry of Thin Tissue Sections, *Analytical Chemistry*.

([324.) Aisha, R., Taysir, M., Begum, M., Tomoko, K.-T., Danielle, R., Katharine, O. W., and Perrie, O. T.-G. (**2022**) Obesity Downregulates Lipid Metabolism Genes in First Trimester Placenta, *Scientific Reports*.

([325.) Rompp, A., and Spengler, B. (**2013**) Mass spectrometry imaging with high resolution in mass and space, *Histochem Cell Biol 139*, 759-783.

([326.) Xuan, Q., Hu, C., Yu, D.-Y., Wang, L., Yang, Z., Zhao, X., Li, Q., Hou, X., and Xu, G. (**2018**) Development of a High Coverage Pseudotargeted Lipidomics Method Based on Ultra-High Performance Liquid Chromatography–Mass Spectrometry, *Analytical Chemistry*.

([327.) Ellis, S. R., Wu, C., Deeley, J. M., Zhu, X. Y., Truscott, R. J., Panhuis, M. i. h., Cooks, R. G., Mitchell, T. W., and Blanksby, S. J. (**2010**) Imaging of Human Lens Lipids by Desorption Electrospray Ionization Mass Spectrometry, *Journal of the American Society for Mass Spectrometry*.

([328.) Vidová, V., Pól, J., Volný, M., Novák, P., Havlíček, V. r., Wiedmer, S. K., and Holopainen, J. M. (**2010**) Visualizing Spatial Lipid Distribution in Porcine Lens by MALDI Imaging High-Resolution Mass Spectrometry, *The Journal of Lipid Research*.

([329.) Wang, X., Han, J., Pan, J., and Borchers, C. H. (**2013**) Comprehensive Imaging of Porcine Adrenal Gland Lipids by MALDI-FTMS Using Quercetin as a Matrix, *Analytical Chemistry*.

([330.) Deeley, J. M., Hankin, J. A., Friedrich, M. G., Murphy, R. C., Truscott, R. J., Mitchell, T. W., and Blanksby, S. J. (**2010**) Sphingolipid Distribution Changes With Age in the Human Lens, *The Journal of Lipid Research*.

([331.) Na, C. H., Hong, J. H., Kim, W. S., Shanta, S. R., Bang, J. Y., Park, D., Kim, H. K., and Kim, K. P. (**2015**) Identification of Protein Markers Specific for Papillary Renal Cell Carcinoma Using Imaging Mass Spectrometry, *Molecules and Cells*.

([332.) Walch, A., Rauser, S., Deininger, S. O., and Höfler, H. (**2008**) MALDI Imaging Mass Spectrometry for Direct Tissue Analysis: A New Frontier for Molecular Histology, *Histochemistry and Cell Biology*.

([333.) Hu, C., Luo, W.-Q., Xu, J., and Han, X. (**2020**) Recognition and Avoidance of Ion Source-generated Artifacts in Lipidomics Analysis, *Mass Spectrometry Reviews*.

([334.) Zaima, N., Sasaki, T., Tanaka, H., Cheng, X. W., Onoue, K., Hayasaka, T., Goto-Inoue, N., Enomoto, H., Unno, N., Kuzuya, M., and Setou, M. (**2011**) Imaging mass spectrometry-based histopathologic examination of atherosclerotic lesions, *Atherosclerosis 217*, 427-432.

([335.) Zaima, N., Goto-Inoue, N., Adachi, K., and Setou, M. (**2011**) Selective analysis of lipids by thin-layer chromatography blot matrix-assisted laser desorption/ionization imaging mass spectrometry, *Journal of oleo science 60 2*, 93-98.

([336.) Denti, V., Mahajneh, A., Capitoli, G., Clerici, F., Piga, I., Pagani, L., Chinello, C., Bolognesi, M. M., Paglia, G., Galimberti, S., Magni, F., and Smith, A. (**2021**) Lipidomic Typing of Colorectal Cancer Tissue Containing Tumour-Infiltrating Lymphocytes by MALDI Mass Spectrometry Imaging, *Metabolites*.

([337.) Pinto, G. D. A., Murgia, A., Lai, C., Ferreira, C., Goes, V. A., Deborah de, A. B. G., Ranquine, L. G., Reis, D. L., Struchiner, C. J., Griffin, J. L., Burton, G. J., Torres, A. G., and El-Bacha, T. (**2022**) Sphingolipids and Acylcarnitines Are Altered in Placentas From Women With Gestational Diabetes Mellitus, *British Journal of Nutrition*.

([338.) Tressler, C. M., Ayyappan, V., Nakuchima, S., Yang, E. J., Sonkar, K., and Glunde, K. (**2022**) A Multimodal Pipeline Using NMR Spectroscopy and MALDI-TOF Mass Spectrometry Imaging From the Same Tissue Sample, *NMR in Biomedicine*.

([339.) Harvey, D. J. (**2023**) Analysis of carbohydrates and glycoconjugates by matrix-assisted laser desorption/ionization mass spectrometry: An update for 2019-2020, *Mass Spectrom Rev 42*, 1984-2206.

([340.) Kaya, I., Sämfors, S., Levin, M., Borén, J., and Fletcher, J. S. (**2020**) Multimodal MALDI Imaging Mass Spectrometry Reveals Spatially

Correlated Lipid and Protein Changes in Mouse Heart With Acute Myocardial Infarction, *Journal of the American Society for Mass Spectrometry*.

([341.) Blanc, L., Lenaerts, A. J., Dartois, V., and Prideaux, B. (**2018**) Visualization of Mycobacterial Biomarkers and Tuberculosis Drugs in Infected Tissue by MALDI-MS Imaging, *Analytical Chemistry*.

([342.) Schiller, J., Zschörnig, O., Petkovic´, M., Müller, M., Arnhold, J., and Arnold, K. (**2001**) Lipid analysis of human HDL and LDL by MALDI-TOF mass spectrometry and 31P-NMR, *Journal of Lipid Research 42*, 1501-1508.

([343.) Anschau, A., Caruso, C. S., Kuhn, R. C., and Franco, T. T. (**2017**) Validation of the Sulfo-Phospho-Vanillin (Spv) Method for the Determination of Lipid Content in Oleaginous Microorganisms, *Brazilian Journal of Chemical Engineering*.

([344.) Morita, S., Tsuji, T., and Takato, T. (**2020**) Protocols for Enzymatic Fluorometric Assays to Quantify Phospholipid Classes, *International Journal of Molecular Sciences*.

([345.) Tsuji, T., Morita, S., Ikeda, Y., and Takato, T. (**2019**) Enzymatic Fluorometric Assays for Quantifying All Major Phospholipid Classes in Cells and Intracellular Organelles, *Scientific Reports*.

([346.) Greenspan, P., Mayer, E. P., and Fowler, S. (**1985**) Nile Red: A Selective Fluorescent Stain for Intracellular Lipid Droplets, *The Journal of Cell Biology*.

([347.) Sitepu, I. R., Ignatia, L., Franz, A. K., Wong, D., Faulina, S. A., Tsui, M. K., Kanti, A., and Boundy-Mills, K. (**2012**) An Improved High-Throughput Nile Red Fluorescence Assay for Estimating Intracellular Lipids in a Variety of Yeast Species, *Journal of Microbiological Methods*.

([348.) Cao, Y., Wang, X., Shi, X., Clee, S. M., McGeer, P. L., Wolf, M. O., and Orvig, C. (**2017**) Biological Imaging With Medium-Sensitive Bichromatic Flexible Fluorescent Dyes, *Angewandte Chemie*.

([349.) Ritz, S. (2017) Histology and tissue staining, fluorescence labelling, In

Modern Techniques in Life Sciences.

([350.) Maira, C., Marcel, C., Kushal, G., Andrey, A. B., David, M., James, W. M., Gary, V., Guangchen, J., and Natalia, S.-L. (**2018**) Optical Tissue Clearing in Combination With Perfusion and Immunofluorescence for Placental Vascular Imaging, *Medicine*.

([351.) Furse, S., Fernandez-Twinn, D. S., Jenkins, B., Meek, C. L., Williams, H., Smith, G. C. S., Charnock-Jones, D. S., Ozanne, S. E., and Koulman, A. (**2020**) A High-Throughput Platform for Detailed Lipidomic Analysis of a

Range of Mouse and Human Tissues, *Analytical and Bioanalytical Chemistry*.

([352.) Samuel, F., Albert, K., Susan, E. O., Lucilla, P., Sara, J. W., and Claire, L. M. (**2022**) Altered Lipid Metabolism in Obese Women With Gestational Diabetes and Associations With Offspring Adiposity, *The Journal of Clinical Endocrinology &Amp; Metabolism*.

([353.) Furse, S., Fernandez-Twinn, D. S., Chiarugi, D., Koulman, A., and Ozanne, S. E. (**2021**) Lipid Metabolism Is Dysregulated Before, During and After Pregnancy in a Mouse Model of Gestational Diabetes, *International Journal of Molecular Sciences*.

([354.) Korkes, H. A., Sass, N., Moron, A. F., Câmara, N. O. S., Bonetti, T. C., Cerdeira, A. S., Ismael Dale Cotrim Guerreiro da, S., and Oliveira, L. D. (**2014**) Lipidomic Assessment of Plasma and Placenta of Women With Early-Onset Preeclampsia, *Plos One*.

([355.) Jayabalan, N., Nair, S., Nuzhat, Z., Rice, G. E., Zúñiga, F., Sobrevia, L., Leiva, A., Sanhueza, C., Gutiérrez, J., Lappas, M., Freeman, D. J., and Salomon, C. (**2017**) Cross Talk Between Adipose Tissue and Placenta in Obese and Gestational Diabetes Mellitus Pregnancies via Exosomes, *Frontiers in Endocrinology*.

([356.) Lu, Y., Zhao, J., Su, S., Han, L., Meng, L., Tang, G., Wang, J., Zhang, C., Xie, X., Zhang, Y., Zhang, Y., Zhai, Y., and Cao, Z. (**2021**) Establishment of Trimester-Specific Reference Intervals of Serum Lipids and the Associations With Pregnancy Complications and Adverse Perinatal Outcomes: A Population-Based Prospective Study, *Annals of Medicine*.

([357.) Geraghty, A. A., Alberdi, G., O'Sullivan, E., O'Brien, E., Crosbie, B., and Twomey, P. J. (**2017**) Maternal and Fetal Blood Lipid Concentrations During Pregnancy Differ by Maternal Body Mass Index: Findings From the ROLO Study, *BMC Pregnancy and Childbirth*.

([358.) Papacleovoulou, G., Abu-Hayyeh, S., Nikolopoulou, E., Briz, Ó., Owen, B. M., Nikolova, V., Ovadia, C., Huang, X., Vääräsmäki, M., Baumann, M., Jansen, E., Albrecht, C., Järvelin, M. R., Marin, J. J., Knisely, A. S., and Williamson, C. (**2013**) Maternal Cholestasis During Pregnancy Programs Metabolic Disease in Offspring, *Journal of Clinical Investigation*.

([359.) Visiedo, F., Bugatto, F., Sánchez, V., Cózar-Castellano, I., Bartha, J. L., and Perdomo, G. (**2013**) High Glucose Levels Reduce Fatty Acid Oxidation and Increase Triglyceride Accumulation in Human Placenta, *Ajp Endocrinology and Metabolism*.

([360.) Yang, Y.-Y., Yamaguchi, I., Kalo, Y., Weiler, E. W., Murofushi, N., and Takahashi, N. (**1993**) Qualitative and Semi-Quantitative Analyses of Cytokinins Using LC/APCI-MS in Combination With ELISA, *Journal of Plant Growth Regulation*.

([361.) Erin, B., and Metz, T. O. (**2017**) Characterizing the Lipid and Metabolite Changes Associated With Placental Function and Pregnancy Complications Using Ion Mobility Spectrometry-Mass Spectrometry and Mass Spectrometry Imaging, *Placenta*.

([362.) Mavrakis, E., Mavroudakis, L., Lydakis-Simantiris, N., and Pergantis, S. A. (**2019**) Investigating the Uptake of Arsenate by Chlamydomonas reinhardtii Cells and Its Effect on Their Lipid Profile Using Single Cell ICP–MS and Easy Ambient Sonic-Spray Ionization–MS, *Analytical Chemistry*.

([363.) Byrdwell, W. C. (**2002**) Dual Parallel Electrospray Ionization and Atmospheric Pressure Chemical Ionization Mass Spectrometry (MS), MS/MS and MS/MS/MS for the Analysis of Triacylglycerols and Triacylglycerol Oxidation Products, *Rapid Communications in Mass Spectrometry*.

([364.) Denison, F. C., Semple, S., Stock, S. J., Walker, J., Marshall, I., and Norman, J. E. (**2012**) Novel Use of Proton Magnetic Resonance Spectroscopy (1HMRS) to Non-Invasively Assess Placental Metabolism, *Plos One*.

([365.) Furse, S., Egmond, M. R., and Killian, J. A. (**2015**) Isolation of Lipids From Biological Samples, *Molecular Membrane Biology*.

([366.) Song, F. Z., Wu, W. B., Qian, Z. X., Zhang, G. F., and Cheng, Y. S. (**2017**) Assessment of the Placenta in Intrauterine Growth Restriction by Diffusion-Weighted Imaging and Proton Magnetic Resonance Spectroscopy: A Pilot Study, *Reproductive Sciences 24*, 575-581.

([367.) Barca, J. M. C. D. l., Chabrun, F., Lefebvre, T., Roche, O., Huetz, N., Blanchet, O., Legendre, G., Simard, G., Reynier, P., and Gascoin, G. (**2022**) A Metabolomic Profiling of Intra-Uterine Growth Restriction in Placenta and Cord Blood Points to an Impairment of Lipid and Energetic Metabolism, *Biomedicines*.

([368.) Pinto, J., Almeida, L., Martins, A. S., Duarte, D., Barros, A. S., Galhano, E., Pita, C., Almeida, M. d. C., Carreira, I. M., and Gil, A. M. (**2015**) Prediction of Gestational Diabetes Through NMR Metabolomics of Maternal Blood, *Journal of Proteome Research*.

([369.) Denison, F. C., Semple, S., Stock, S., Walker, J., Marshall, I., and Norman, J. E. (**2012**) Novel Use of Proton Magnetic Resonance Spectroscopy (1HMRS) to Non-Invasively Assess Placental Metabolism, *Plos One*.

([370.) Wang, C., Timári, I., Zhang, B., Li, D., Leggett, A., Amer, A. O., Bruschweiler-Li, L., Kopec, R., and Brüschweiler, R. (**2020**) COLMAR Lipids Web Server and Ultrahigh-Resolution Methods for Two-Dimensional Nuclear Magnetic Resonance- And Mass Spectrometry-Based Lipidomics, *Journal of Proteome Research*.

([371.) Oostendorp, M. v., Engelke, U. F. H., Willemsen, M. A. A. P., and Wevers, R. A. (**2006**) Diagnosing Inborn Errors of Lipid Metabolism With Proton Nuclear Magnetic Resonance Spectroscopy, *Clinical Chemistry*.

([372.) Himmelreich, U., Somorjai, R. L., Dolenko, B., Lee, O. C., Daniel, H.-M., Murray, R. J., Mountford, C. E., and Sorrell, T. C. (**2003**) Rapid Identification Of Candida Species by Using Nuclear Magnetic Resonance Spectroscopy and a Statistical Classification Strategy, *Applied and Environmental Microbiology*.

([373.) Medina, I., Sacchi, R., and Aubourg, S. P. (**1995**) A 13C-NMR Study of Lipid Alterations During Fish Canning: Effect of Filling Medium, *Journal of the Science of Food and Agriculture*.

([374.) Kostara, C., Ferrannini, E., Bairaktari, E., Papathanasiou, A., Elisaf, M., and Tsimihodimos, V. (**2020**) Early Signs of Atherogenic Features in the HDL Lipidomes of Normolipidemic Patients Newly Diagnosed With Type 2 Diabetes, *International Journal of Molecular Sciences*.

([375.) Walsh, S. W. (**1998**) Maternal-Placental Interactions of Oxidative Stress and Antioxidants in Preeclampsia, *Seminars in Reproductive Medicine*.

([376.) Walsh, S., Vaughan, J. E., Wang, Y., and Roberts, L. J. (**2000**) Placental isoprostane is significantly increased in preeclampsia, *The Faseb Journal Frontiers in Flow Cytometry 14*, 1289-1296.

([377.) Roos, S., Jansson, N., Palmberg, I., Säljö, K., Powell, T. L., and Jansson, T. (**2007**) Mammalian Target of Rapamycin in the Human Placenta Regulates Leucine Transport and Is Down-regulated in Restricted Fetal Growth, *The Journal of Physiology*.

([378.) Jarvie, E., Nelson, S. M., Sattar, N., Catalano, P. M., and Freeman, D. J. (**2010**) Lipotoxicity in Obese Pregnancy and Its Potential Role in Adverse Pregnancy Outcome and Obesity in the Offspring, *Clinical Science*.

([379.) Radaelli, T., Lepercq, J., Varastehpour, A., Basu, S., Catalano, P. M., and Mouzon, S. H.-d. (**2009**) Differential Regulation of Genes for Fetoplacental Lipid Pathways in Pregnancy With Gestational and Type 1 Diabetes Mellitus, *American Journal of Obstetrics and Gynecology*.

([380.) Lindegaard, M. R., Damm, P., Mathiesen, E. R., and Nielsen, L. K. (**2006**) Placental Triglyceride Accumulation in Maternal Type 1 Diabetes Is Associated With Increased Lipase Gene Expression, *The Journal of Lipid Research*.

([381.) Hulme, C. H., Nicolaou, A., Murphy, S. E., Heazell, A. E. P., Myers, J., and Westwood, M. (**2019**) The Effect of High Glucose on Lipid Metabolism in the Human Placenta, *Scientific Reports*.

([382.) Kevin, S. K. (**2016**) Cytotrophoblast Regulates Lipid Esterification and Metabolic Activity of the Human Term Placenta.

([383.) Elvira, L., Hans, D., and Berthold, K. (**2003**) Perinatal Supply and Metabolism of Long-Chain Polyunsaturated Fatty Acids.

([384.) Larque, E., Demmelmair, H., Klingler, M., De Jonge, S., Bondy, B., and Koletzko, B. (**2006**) Expression pattern of fatty acid transport protein-1 (FATP-1), FATP-4 and heart-fatty acid binding protein (H-FABP) genes in human term placenta, *Early Hum Dev 82*, 697-701.

([385.) Perry, S. G., Amos, R., and Brewer, P. I. (**1973**) The Technique of Thin-Layer Chromatography.

([386.) Ettre, L. S., and Sakodynskii, K. I. (**1993**) M. S. Tswett and the Discovery of Chromatography I: Early Work (1899–1903), *Chromatographia 35*.

([387.) Soffe, R., Nock, V., and Chase, J. G. (**2018**) Towards Point-of-Care Insulin Detection, *ACS Sensors*.

([388.) Shankar, U., Lenka, S. K., Ackland, M. L., and Callahan, D. L. (**2022**) Comparison of Different Solvent Extraction Compositions for the Analysis of Phytoplankton Pigments and Lipids Using a Rapid and Sensitive LC-MS Method.

([389.) Silva, M. R. D., Andrade, F. N., Fumes, B. H., and Lanças, F. M. (**2015**) Unified Chromatography: Fundamentals, Instrumentation and Applications†, *Journal of Separation Science*.

([390.) Strain, H. H. (**1942**) Chromatographic Adsorption Analysis, *Industrial & Engineering Chemistry Analytical Edition*.

([391.) Tswett, M. (1896) Etudes de physiologie cellulaire: Contribution à la connaissance des mouvements du protoplasme, des membranes plasmiques et des chloroplastes, Impr. Rey et Malavallon.

([392.) Ettre, L. S., and Sakodynskii, K. I. (**1993**) M. S. Tswett and the Discovery of Chromatography I: Early Work (1899–1903), *Chromatographia*.

([393.) Altova, E. P., and Hargittai, I. (**2021**) Mikhail S. Tsvet—pioneer of Chromatography—150 Years From His Birth, *Structural Chemistry*.

([394.) Nahar, A., Baker, A. L., Nichols, D. S., Bowman, J. P., and Britz, M. L. (**2020**) Application of Thin-Layer Chromatography-Flame Ionization Detection (TLC-FID) to Total Lipid Quantitation in Mycolic-Acid Synthesizing Rhodococcus and Williamsia Species, *Int J Mol Sci 21*.

([395.) Magny, R., Regazzetti, A., Kessel, K., Genta-Jouve, G., Baudouin, C., Parsadaniantz, S. M., Laprévote, O., and Auzeil, N. (**2020**) Lipid Annotation by Combination of UHPLC-HRMS (MS), Molecular Networking, and

Retention Time Prediction: Application to a Lipidomic Study of in Vitro Models of Dry Eye Disease, *Metabolites*.

([396.) Wang, Y., Gao, W., Wu, J., Liu, H.-J., Wang, Y., Wang, Y., and Jiang, G. (**2017**) Development of Matrix Solid-Phase Dispersion Method for the Extraction of Short-Chain Chlorinated Paraffins in Human Placenta, *Journal of Environmental Sciences*.

([397.) Hernández-Albaladejo, I., Ruiz-Palacios, M., Gázquez, A., Blanco, J. L., Parrilla, J. J., and Larqué, E. (**2014**) A Method for Lipid Droplet Isolation From Human Placenta for Further Analyses in Clinical Trials, *Acta Obstetricia Et Gynecologica Scandinavica*.

([398.) Klingler, M., Demmelmair, H., Larqué, E., and Koletzko, B. V. (**2003**) Analysis of FA contents in individual lipid fractions from human placental tissue, *Lipids 38*, 561-566.

([399.) Brown, S. H. J., Eather, S. R., Freeman, D. J., Meyer, B. J., and Mitchell, T. W. (**2016**) A lipidomic analysis of placenta in preeclampsia: Evidence for lipid storage, *PLoS ONE 11*.

([400.) Kumar, D., and Sharma, U. (**2018**) High-Performance Thin-Layer Chromatography: An Economical Alternative for the Quality Control of Medicinal Plants and Derived Products, *Separation Science Plus*.

([401.) Handloser, D., Widmer, V., and Reich, E. (**2008**) Separation of Phospholipids by HPTLC – An Investigation of Important Parameters, *Journal of Liquid Chromatography & Related Technologies 31*, 1857 - 1870.

([402.) Fuchs, B., Süß, R., Teuber, K., Eibisch, M., and Schiller, J. (**2011**) Lipid Analysis by Thin-Layer Chromatography—A Review of the Current State, *Journal of Chromatography A*.

([403.) Sparvero, L. J., Amoscato, A. A., Dixon, C. E., Long, J. B., Kochanek, P. M., Pitt, B. R., Bayır, H., and Kagan, V. E. (**2012**) Mapping of phospholipids by MALDI imaging (MALDI-MSI): realities and expectations, *Chemistry and Physics of Lipids 165*, 545-562.

([404.) Dynska-Kukulska, K., Ciesielski, W., and Zakrzewski, R. (**2013**) The use of a new, modified Dittmer-Lester spray reagent for phospholipid determination by the TLC image analysis technique, *Biomed Chromatogr 27*, 458-465.

([405.) Cebolla, V. L., Jarne, C., Vela, J., Garriga, R., Membrado, L., and Galbán, J. (**2021**) Scanning densitometry and mass spectrometry for HPTLC analysis of lipids: The last 10 years, *Journal of Liquid Chromatography & Related Technologies 44*, 148 - 170.

([406.) Lopes, R., Santana, M. S., Cruz, C. R. d., Fulindi, R. B., Gaspar, A. M. M., and Costa, P. I. d. (**2020**) Central cellular signalling pathways involved with

the regulation of lipid metabolism in the liver: a review, *Acta Scientiarum. Biological Sciences 42*.

([407.) Yamazaki, K., Masaki, N., Kohmura-Kobayashi, Y., Yaguchi, C., Hayasaka, T., Itoh, H., Setou, M., and Kanayama, N. (**2015**) Decrease in Sphingomyelin (d18:1/16:0) in Stem Villi and Phosphatidylcholine (16:0/ 20:4) in Terminal Villi of Human Term Placentas with Pathohistological Maternal Malperfusion.

([408.) Yamazaki, I., Kimura, F., Nakagawa, K., Nakai, K., Arima, T., Kawabata, T., Kagawa, Y., Saitoh, S., Mizuno, S., Yaegashi, N., and Miyazawa, T. (**2015**) Heterogeneity of the Fatty Acid Composition of Japanese Placentae for Determining the Perinatal Fatty Acid Status: A Methodological Study, *Journal of Oleo Science*.

([409.) Yamazaki, K., Nio, M., Kohmura-Kobayashi, Y., Yaguchi, C., Hayasaka, T., Itoh, H., Setou, M., and Kanayama, N. (**2015**) Decrease in Sphingomyelin (D18:1/16:0) in Stem Villi and Phosphatidylcholine (16:0/20:4) in Terminal Villi of Human Term Placentas With Pathohistological Maternal Malperfusion, *Plos One*.

([410.) Kim, S. Y., Lee, Y. J., An, S.-M., Kim, M. J., Jeong, J. S., Kim, D., Lim, Y., Jung, E.-M., Kim, S.-C., and An, B.-S. (**2022**) Dynamic Regulation of Lipid Metabolism in the Placenta of in Vitro and in Vivo Models of Gestational Diabetes Mellitus, *Biology of Reproduction*.

([411.) Djoussé, L., Arnett, D. K., Pankow, J. S., Hopkins, P. N., Province, M. A., and Ellison, R. C. (**2005**) Dietary Linolenic Acid Is Associated With a Lower Prevalence of Hypertension in the NHLBI Family Heart Study, *Hypertension*.

([412.) Noble, R. C., Shand, J. H., and Christie, W. W. (**1985**) Synthesis of C20 and C22 Polyunsaturated Fatty Acids by the Placenta of the Sheep, *Neonatology*.

([413.) Lindegaard, M. L. S., Olivecrona, G., Christoffersen, C., Kratky, D., Hannibal, J., Petersen, B. L., Zechner, R., Damm, P., and Nielsen, L. B. (**2005**) Endothelial and Lipoprotein Lipases in Human and Mouse Placenta, *The Journal of Lipid Research*.

([414.) Tan, L., Chen, Z., Sun, F.-Y., Guo, H., Wang, R., Mulder, M., Sun, Y., Lu, X., Zhang, J. V., Danser, A. H. J., Verdonk, K., Fan, X., and Yang, Q. (**2023**) Adipokine Chemerin Overexpression in Trophoblasts Leads to Dyslipidemia in Pregnant Mice: Implications for Preeclampsia, *Lipids in Health and Disease*.

([415.) Brown, L. D., Regnault, T. R. H., and Hay, W. W. (2017) Fetal Requirements and Placental Transfer of Nitrogenous Compounds, In *Fetal and Neonatal Physiology*, pp 444-458.e444.

([416.) Huang, Q.-t., Wang, S.-s., Chen, J.-h., Zhong, M., Tian, J.-w., Yu, Y.-h., Wang, Z.-j., Huang, L.-p., Fu, N., Hou, F.-f., and Zhang, M. (**2013**) Advanced oxidation protein products in the plasma and placenta of normal pregnant women and women with preeclampsia, *Placenta 34*.

([417.) Huang, Q.-t., Wang, S.-s., Zhong, M., Tian, J.-w., Yu, Y.-h., Wang, Z.-j., Huang, L.-p., Fu, N., Hou, F.-f., and Zhang, M. (**2013**) Increased plasma and placental advanced oxidation protein products levels in gestational diabetes mellitus with placental vascular complications, *Placenta 34*, A17-A18.

([418.) Lindegaard, M. L., Olivecrona, G., Christoffersen, C., Kratky, D., Hannibal, J., Petersen, B. L., Zechner, R., Damm, P., and Nielsen, L. B. (**2005**) Endothelial and lipoprotein lipases in human and mouse placenta, *J Lipid Res 46*, 2339-2346.

([419.) Kim, C., Ashrap, P., Watkins, D. J., Mukherjee, B., Rosario-Pabón, Z., Vélez-Vega, C. M., Cordero, J. F., and Meeker, J. D. (**2022**) Maternal Metals/Metalloid Blood Levels Are Associated With Lipidomic Profiles Among Pregnant Women in Puerto Rico, *Frontiers in Public Health*.

([420.) Huynh, J., Dawson, D. L., Roberts, D. J., and Bentley–Lewis, R. (**2015**) A Systematic Review of Placental Pathology in Maternal Diabetes Mellitus, *Placenta*.

([421.) Gauster, M., Desoyé, G., Tötsch, M., and Hiden, U. (**2011**) The Placenta and Gestational Diabetes Mellitus, *Current Diabetes Reports*.

([422.) Zhou, X., Zhang, H., Jiang, Y., Wei, L., Chen, Y., Zhang, J., Gao, P., Zhu, S., Fang, C., Du, Y., Su, R., He, M., Yu, J., Wang, S., Ding, W., and Li, F. (**2023**) The Role of Chemerin in the Regulation of cGAS-STING Pathway in Gestational Diabetes Mellitus Placenta, *The Faseb Journal*.

([423.) Fisher, J. J., Vanderpeet, C. L., Bartho, L. A., McKeating, D. R., Cuffe, J., Holland, O. J., and Perkins, A. V. (**2020**) Mitochondrial Dysfunction in Placental Trophoblast Cells Experiencing Gestational Diabetes Mellitus, *The Journal of Physiology*.

([424.) Herpen, N. A. v., and Schrauwen-Hinderling, V. B. (**2008**) Lipid Accumulation in Non-Adipose Tissue and Lipotoxicity, *Physiology & Behavior*.

([425.) Zhang, Y., Li, C., Yao, G.-F., Du, L.-J., Liu, Y., Zheng, X., Yan, S., Sun, J.-Y., Liu, Y., Liu, M., Zhang, X., Wei, G., Tong, W., Chen, X., Wu, Y., Sun, S., Liu, S., Ding, Q., Yu, Y., Yin, H., and Duan, S.-Z. (**2017**) Deletion of Macrophage Mineralocorticoid Receptor Protects Hepatic Steatosis and Insulin Resistance Through ERα/HGF/Met Pathway, *Diabetes*.

([426.) Kedziora, S., Obermayer, B., Sugulle, M., Herse, F., Kräker, K., Haase, N., Langmia, I. M., Müller, D. N., Staff, A. C., Beule, D., and Dechend, R. (**2022**) Placental Transcriptome Profiling in Subtypes of Diabetic Pregnancies Is

Strongly Confounded by Fetal Sex, *International Journal of Molecular Sciences*.

([427.) Tao, J., Mu, Y., Chen, P., Xie, Y., Liang, J., and Zhu, J. (**2022**) Pregnancy Complications and Risk of Uterine Rupture Among Women With Singleton Pregnancies in China, *BMC Pregnancy and Childbirth*.

([428.) Sun, S., Cao, C., Li, J., Meng, Q., Cheng, B., Shi, B., and Shan, A. (**2021**) Lycopene Modulates Placental Health and Fetal Development Under High-Fat Diet During Pregnancy of Rats, *Molecular Nutrition & Food Research*.

([429.) Itonori, S., Shirai, T., Kiso, Y., Ohashi, Y., Shiota, K., and Ogawa, T. (**1995**) Glycosphingolipid Composition of Rat Placenta: Changes Associated With Stage of Pregnancy, *Biochemical Journal*.

([430.) Izmailov, N., and Shraiber, M. (**1938**) A drop-chromatographic method of analysis and its applications to pharmacy, *Farmatsiya 3*, 1-7.

([431.) Berezkin, V. G., and Dzido, T. H. (**2008**) The Discovery of Thin-Layer Chromatography by N.A. Izmailov and M.S. Shraiber *JPC - Journal of Planar Chromatography - Modern TLC*.

([432.) Roberts, K., Riley, S. C., Reynolds, R. M., Barr, S. M., Evans, M. E., Statham, A., Hor, K., Jabbour, H. N., Norman, J. E., and Denison, F. C. (**2011**) Placental Structure and Inflammation in Pregnancies Associated With Obesity, *Placenta*.

([433.) Sibai, B. M., Dekker, G., and Kupferminc, M. J. (**2005**) Pre-Eclampsia, *The Lancet*.

([434.) Roberts, J. M., and Escudero, C. (**2012**) The Placenta in Preeclampsia, *Pregnancy Hypertension*.

([435.) Cecelia, M. O. B., Jennie, L., Andrea, R. D., and Jodie, M. D. (**2019**) Maternal Cardiometabolic Markers Are Associated With Fetal Growth: A Secondary Exploratory Analysis of the LIMIT Randomised Trial, *BMC Endocrine Disorders*.

([436.) Vora, N. L., and O'Brien, B. M. (2017) Prenatal Diagnosis, In *Fetal and Neonatal Physiology*, pp 14-23.e11.

([437.) Ramsay, T. G., Sheahan, J. A., and Martin, R. M. (**1984**) Comparison of Lactate and Glucose Metabolism in the Developing Porcine Placenta, *Ajp Regulatory Integrative and Comparative Physiology*.

([438.) Ramsay, J. E., Ferrell, W. R., Crawford, L., Wallace, A. M., Greer, I. A., and Sattar, N. (**2002**) Maternal obesity is associated with dysregulation of metabolic, vascular, and inflammatory pathways, *J Clin Endocrinol Metab 87*, 4231-4237.

([439.) Tim, R., Karousis, J., Martin, W., and Wolverton, C. K. (**1991**) Fatty Acid Metabolism by the Porcine Placenta, *Journal of Animal Science*.

([440.) Montelongo, A., Lasunción, M. A., Pallardo, L. F., and Herrera, E. (**1992**) Longitudinal Study of Plasma Lipoproteins and Hormones During Pregnancy in Normal and Diabetic Women, *Diabetes*.

([441.) Knopp, R. H., Magee, M., Walden, C. E., Bonet, B., and Benedetti, T. J. (**1992**) Prediction of Infant Birth Weight by GDM Screening Tests: Importance of Plasma Triglyceride, *Diabetes Care*.

([442.) Knopp, R. H., Bergelin, R. O., Wahl, P. W., Walden, C. E., Chapman, M. J., and Irvine, S. (**1982**) Population-Based Lipoprotein Lipid Reference Values for Pregnant Women Compared to Nonpregnant Women Classified by Sex Hormone Usage, *American Journal of Obstetrics and Gynecology*.

([443.) Robert, H. K., Warth, M. R., Charles, D., Marian, T. C., Job, R. L., Hideo, M., and Allen, M. I. V. (**1986**) Lipoprotein Metabolism in Pregnancy, Fat Transport to the Fetus, and the Effects of Diabetes, *Neonatology*.

([444.) Huda, S. S., Sattar, N., and Freeman, D. J. (**2009**) Lipoprotein Metabolism and Vascular Complications in Pregnancy, *Clinical Lipidology*.

([445.) Huda, S. S., Forrest, R., Paterson, N., Jordan, F., Sattar, N., and Freeman, D. J. (**2014**) In Preeclampsia, Maternal Third Trimester Subcutaneous Adipocyte Lipolysis Is More Resistant to Suppression by Insulin Than in Healthy Pregnancy, *Hypertension 63*, 1094-1101.

([446.) Naveed, S., Allan, G., Chris, J. P., and Ian, A. G. (**1996**) Potential Pathogenic Roles of Aberrant Lipoprotein and Fatty Acid Metabolism in Pre-Eclampsia, *Bjog an International Journal of Obstetrics &Amp; Gynaecology*.

([447.) Ramsay, J., Ferrell, W. R., Crawford, L., Wallace, A. M., Greer, I. A., and Sattar, N. (**2004**) Divergent Metabolic and Vascular Phenotypes in Pre-Eclampsia and Intrauterine Growth Restriction, *Journal of Hypertension*.

([448.) Stewart, F., Freeman, D. J., Ramsay, J., Greer, I. A., Caslake, M., and Ferrell, W. R. (**2007**) Longitudinal Assessment of Maternal Endothelial Function and Markers of Inflammation and Placental Function Throughout Pregnancy in Lean and Obese Mothers, *The Journal of Clinical Endocrinology & Metabolism*.

([449.) Kaaja, R., Laivuori, H., Laakso, M., Tikkanen, M. J., and Ylikorkala, O. (**1999**) Evidence of a State of Increased Insulin Resistance in Preeclampsia, *Metabolism*.

([450.) Liu, J., Ghaziani, T. T., and Wolf, J. L. (**2017**) Acute Fatty Liver Disease of Pregnancy: Updates in Pathogenesis, Diagnosis, and Management, *The American Journal of Gastroenterology*.

([451.) Ye, R., Mai, Z., Pan, X., Cai, S. Y., and Deng, L. (**2021**) Acute Fatty Liver of Pregnancy Causes Severe Acute Pancreatitis and Stillborn Fetus, *Medicine*.

([452.) Papafragkakis, H., Singhal, S., and Anand, S. (**2013**) Acute Fatty Liver of Pregnancy, *Southern Medical Journal*.

([453.) Costa, T. J., Oliveira, J. C. D., Giachini, F. R., Lima, V. V., Tostes, R. C., and Bomfim, G. F. (**2022**) Programming of Vascular Dysfunction by Maternal Stress: Immune System Implications, *Frontiers in Physiology*.

([454.) Lie, S., Morrison, J. L., Williams-Wyss, O., Suter, C. M., Humphreys, D. T., Ozanne, S. E., Zhang, S., MacLaughlin, S. M., Kleemann, D. O., Walker, S. K., Roberts, C. T., and McMillen, I. C. (**2016**) Impact of Maternal Undernutrition Around the Time of Conception on Factors Regulating Hepatic Lipid Metabolism and microRNAs in Singleton and Twin Fetuses, *Ajp Endocrinology and Metabolism*.

([455.) Larqué, E., Demmelmair, H., and Koletzko, B. (**2003**) Perinatal Supply and Metabolism of Long-Chain Polyunsaturated Fatty Acids.

([456.) Best, K., Gibson, R., Yelland, L. N., Leemaqz, S., Gomersall, J. S., Liu, G., and Makrides, M. (**2020**) Effect of Omega-3 LCPUFA Supplementation on Maternal Fatty Acid and Oxylipin Concentrations During Pregnancy.

([457.) Bryant, J., Hanson, M. A., Peebles, C., Davies, L., Inskip, H., Robinson, S., Calder, P. C., Cooper, C., and Godfrey, K. M. (**2015**) Higher Oily Fish Consumption in Late Pregnancy Is Associated With Reduced Aortic Stiffness in the Child at Age 9 Years, *Circulation Research*.

([458.) Scott, K., Morgan, H. L., Delles, C., Fisher, S., Graham, D., and McBride, M. W. (**2021**) Distinct Uterine Artery Gene Expression Profiles During Early Gestation in the Stroke-Prone Spontaneously Hypertensive Rat, *Physiological Genomics*.

([459.) Saito, T., Musha, Y., Miyakawa, M., Itoh, S., Ohtsuji, M., Hanson, M. A., and Takeda, S. (**2012**) Angiotensin II Receptor Antagonist Reduces Subsequent Uterine Arterial Dysfunction in Pregnant Offspring of Protein-restricted Rat Dams, *Journal of Obstetrics and Gynaecology Research*.

([460.) Sugden, M. C., and Holness, M. J. (**1994**) The Role of the Glucose/Fatty Acid Cycle in the Selective Modulation of Non-Oxidative and Oxidative Glucose Disposal by Oxidative Muscle in Late Pregnancy, *Biological Chemistry Hoppe-Seyler*.

([461.) Huang, X., Jain, A., Baumann, M., Körner, M., Surbek, D., Bütikofer, P., and Albrecht, C. (**2013**) Increased Placental Phospholipid Levels in Pre-Eclamptic Pregnancies, *International Journal of Molecular Sciences*.

([462.) Staff, A. C., Ranheim, T., Khoury, J., and Henriksen, T. (**1999**) Increased Contents of Phospholipids, Cholesterol, and Lipid Peroxides in Decidua Basalis in Women With Preeclampsia, *American Journal of Obstetrics and Gynecology*.

([463.) Korkes, H. A., Sass, N., Júnior, E. A., Câmara, N. O. S., Bonetti, T. C., Cerdeira, A. S., Ismael Dale Cotrim Guerreiro da, S., and Oliveira, L. L. d. (**2014**) Lipidomic Assessment of Plasma and Placenta of Women With Early-Onset Preeclampsia, *Plos One*.

([464.) He, B., Liu, Y., Maurya, M. R., Benny, P., Lassiter, C., Li, H., Subramaniam, S., and Garmire, L. X. (**2021**) The Maternal Blood Lipidome Is Indicative of the Pathogenesis of Severe Preeclampsia, *The Journal of Lipid Research*.

([465.) Hirschmugl, B., Desoye, G., Catalano, P. M., Klymiuk, I., Scharnagl, H., Payr, S., Kitzinger, E., Schliefsteiner, C., Lang, U., Wadsack, C., and Mouzon, S. H.-d. (**2016**) Maternal Obesity Modulates Intracellular Lipid Turnover in the Human Term Placenta, *International Journal of Obesity*.

([466.) Hirschmugl, B., Desoye, G., Catalano, P., Klymiuk, I., Scharnagl, H., Payr, S., Kitzinger, E., Schliefsteiner, C., Lang, U., Wadsack, C., and Hauguel-De Mouzon, S. (**2017**) Maternal obesity modulates intracellular lipid turnover in the human term placenta, *International Journal of Obesity 41*, 317-323.

([467.) Birgit, H., Sarah, C., Nina, M., Eva, K., Ingeborg, K., Hazel, I., Nicholas, C. H., Cyrus, C., Colin, P. S., Jocelyn, D. G., Christian, W., Keith, M. G., Gernot, D., and Rohan, M. L. (**2018**) Relation of Placental Alkaline Phosphatase Expression in Human Term Placenta With Maternal and Offspring Fat Mass, *International Journal of Obesity*.

([468.) Hirschmugl, B., Fawzy, N., Grill, M., Schicho, R., Lang, U., Zimmermann, R., and Wadsack, C. (**2019**) Monoacylglycerol lipase mobilises intracellular lipid stores in the human term placenta, *Placenta 83*.

([469.) Birgit, H., Simone, P., Bram, G. S., Rohan, M. L., Michael, G., Gernot, D., and Christian, W. (**2021**) Placental Mobilization of Free Fatty Acids Contributes to Altered Materno-Fetal Transfer in Obesity, *International Journal of Obesity*.

([470.) Navarro, A., Alonso, A., Garrido, P., Gonzalez, C., Rey, C. G. d., Ordóñez, C., and Tolivia, J. (**2010**) Increase in Placental Apolipoprotein D as an Adaptation to Human Gestational Diabetes, *Placenta*.

([471.) Virtu, C.-N., Michelle, P., Patricia, A. G., Maricela, H., Judi, M., Patrick, M. C., Sylvie Hauguel, d., and Perrie, O. T.-G. (**2016**) Effect of Ω-3 Supplementation on Placental Lipid Metabolism in Overweight and Obese Women, *American Journal of Clinical Nutrition*.

([472.) Liao, Y., Xu, G., Jiang, Y., Zhu, H., Sun, L., Peng, R., and Luo, Q. (**2018**) Comparative Proteomic Analysis of Maternal Peripheral Plasma and

Umbilical Venous Plasma From Normal and Gestational Diabetes Mellitus Pregnancies, *Medicine*.

([473.) Barrett, H. L., Gatford, K. L., Houda, C. M., Blasio, M. J. D., McIntyre, H. D., Callaway, L. K., Nitert, M. D., Coat, S., Owens, J. A., Hague, W. M., and Rowan, J. (**2013**) Maternal and Neonatal Circulating Markers of Metabolic and Cardiovascular Risk in the Metformin in Gestational Diabetes (MiG) Trial, *Diabetes Care*.

([474.) Vounzoulaki, E., Khunti, K., Abner, S., Tan, B. K., Davies, M. J., and Gillies, C. (**2020**) Progression to Type 2 Diabetes in Women With a Known History of Gestational Diabetes: Systematic Review and Meta-Analysis, *BMJ*.

([475.) Ryckman, K. K., Spracklen, C. N., Smith, C. Z. A., Robinson, J., and Af, S. (**2015**) Maternal Lipid Levels During Pregnancy and Gestational Diabetes: A Systematic Review and Meta-Analysis, *Bjog an International Journal of Obstetrics & Gynaecology*.

([476.) Son, G. H., Kwon, J. Y., Kim, Y. H., and Park, Y. W. (**2010**) Maternal Serum Triglycerides as Predictive Factors for Large-for-gestational Age Newborns in Women With Gestational Diabetes Mellitus, *Acta Obstetricia Et Gynecologica Scandinavica*.

([477.) Wang, J., Li, Z., and Li, L. (**2019**) Maternal Lipid Profiles in Women With and Without Gestational Diabetes Mellitus, *Medicine*.

([478.) Dubé, É., Éthier-Chiasson, M., and Lafond, J. (**2013**) Modulation of Cholesterol Transport by Insulin-Treated Gestational Diabetes Mellitus in Human Full-Term Placenta1, *Biology of Reproduction*.

([479.) Chen, H., Li, J., Cai, S., Tang, S., Zeng, S., Chu, C., Hocher, C.-F., Rösing, B., Krämer, B. K., Hu, L., Lin, G., Gong, F., and Hocher, B. (**2021**) Blastocyst Transfer: A Risk Factor for Gestational Diabetes Mellitus in Women Undergoing in Vitro Fertilization, *The Journal of Clinical Endocrinology & Metabolism*.

([480.) Cui, M., Li, X., Yang, C., Wang, L., Liu, L., Zhao, S., Guo, Q., and Liu, P. (**2022**) Effect of Carbohydrate-Restricted Dietary Pattern on Insulin Treatment Rate, Lipid Metabolism and Nutritional Status in Pregnant Women With Gestational Diabetes in Beijing, China, *Nutrients*.

([481.) Hossain, M. D., Rahman, A. K. M. S., Mahjabeen, S., Zaman, M., Abedin, M., Mahmood, T., Razzaque, M. A., and Alam, U. K. (**2020**) Comparison of Serum Lipid Profile Between Gestational Diabetes Mellitus and Pregnant Women With Normal Glucose Tolerance, *Journal of Biosciences and Medicines*.

([482.) Berkel, G. J. V., Sanchez, A. D., and Quirke, J. M. E. (**2002**) Thin-Layer Chromatography and Electrospray Mass Spectrometry Coupled Using a Surface Sampling Probe, *Analytical Chemistry*.

([483.) Burdge, G. C., Wright, P. S., Jones, A. E., and Wootton, S. (**2000**) A Method for Separation of Phosphatidylcholine, Triacylglycerol, Non-Esterified Fatty Acids and Cholesterol Esters From Plasma by Solid-Phase Extraction, *British Journal of Nutrition*.

([484.) Rejšek, J., Vrkoslav, V., Vaikkinen, A., Haapala, M., Kauppila, T. J., Kostiainen, R., and Cvačka, J. (**2016**) Thin-Layer Chromatography/Desorption Atmospheric Pressure Photoionization Orbitrap Mass Spectrometry of Lipids, *Analytical Chemistry*.

([485.) Chai, W., Leteux, C., Lawson, A., and Stoll, M. S. (**2002**) On-Line Overpressure Thin-Layer Chromatographic Separation and Electrospray Mass Spectrometric Detection of Glycolipids, *Analytical Chemistry*.

([486.) Pojjanapornpun, S. (**2021**) Effect of Mobile Phase Composition on the Separation of Neutral Lipids, Γ-Oryzanol and Its Saponified Compounds on a 100-Å Phenogel Column.

([487.) Dossou, K. S. S., Chiap, P., Chankvetadze, B., Servais, A.-C., Fillet, M., and Crommen, J. (**2010**) Optimization of the LC Enantioseparation of Chiral Pharmaceuticals Using Cellulose Tris(4-chloro-3-methylphenylcarbamate) as Chiral Selector and Polar Non-aqueous Mobile Phases, *Journal of Separation Science*.

([488.) Gogaladze, K., Chankvetadze, L., Tsintsadze, M. G., Farkas, T., and Chankvetadze, B. (**2015**) Effect of Basic and Acidic Additives on the Separation of Some Basic Drug Enantiomers on Polysaccharide-Based Chiral Columns With Acetonitrile as Mobile Phase, *Chirality*.

([489.) Jiskra, J., Claessens, H. A., and Cramers, C. A. M. G. (**2003**) Separation of Basic Central Nervous System Drugs by Capillary Electrochromatography, *Journal of Separation Science*.

([490.) Wan, H., Zhong, H., Xue, X., and Liang, X. (**2016**) Separation Behavior of Basic Compounds on Unbonded Silicon Oxynitride and Silica High-Performance Liquid Chromatography Stationary Phases With Reversed-Phase Eluents, *Journal of Separation Science*.

([491.) Sankaralingam, S., Xu, Y., Sawamura, T., and Davidge, S. T. (**2009**) Increased Lectin-Like Oxidized Low-Density Lipoprotein Receptor-1 Expression in the Maternal Vasculature of Women With Preeclampsia, *Hypertension*.

([492.) Yang, Y., Wang, Y., Lv, Y., and Ding, H. (**2022**) Dissecting the Roles of Lipids in Preeclampsia, *Metabolites 12*, 590.

([493.) Zhang, L., Bi, S., Liang, Y., Huang, L., Li, Y., Huang, M., Huang, B., Deng, W., Liang, J., Gu, S., Chen, J., Du, L., Chen, D., and Wang, Z. (**2022**) Integrated Metabolomic and Lipidomic Analysis in the Placenta of Preeclampsia, *Frontiers in Physiology*.

([494.) Vera B. Ivleva, Y. N. E., Bogdan A. Budnik, Susanne C. Moyer,† Peter B. O'Connor, and Catherine E. Costello. (**2004**) Coupling Thin-Layer Chromatography withVibrational Cooling Matrix-Assisted LaserDesorption/Ionization Fourier Transform MassSpectrometry for the Analysis of Ganglioside Mixtures, *Analytical Chemistry, American Chemical Society 76*, 6484-6491

([495.) Guittard, J., Hronowski, X. L., and Costello, C. E. (**1999**) Direct matrix-assisted laser desorption/ionization mass spectrometric analysis of glycosphingolipids on thin layer chromatographic plates and transfer membranes, *Rapid Communications in Mass Spectrometry 13*, 1838-1849.

([496.) Park, H., Zhou, Y., and Costello, C. E. (**2014**) Direct analysis of sialylated or sulfated glycosphingolipids and other polar and neutral lipids using TLC-MS interfaces, *J Lipid Res 55*, 773-781.

([497.) Batubara, A., Carolan, V. A., Loadman, P. M., Sutton, C., Shnyder, S. D., and Clench, M. R. (**2015**) Thin-layer chromatography/matrix-assisted laser desorption/ionisation mass spectrometry and matrix-assisted laser desorption/ionisation mass spectrometry imaging for the analysis of phospholipids in LS174T colorectal adenocarcinoma xenografts treated with the vascular disrupting agent DMXAA, *Rapid Communications in Mass Spectrometry 29*, 1288-1296.

([498.) Rabel, F., and Sherma, J. (**2017**) Review of the state of the art of preparative thin-layer chromatography, *Journal of Liquid Chromatography & Related Technologies 40*, 165-176.

([499.) Schiller, J., Süss, R., Fuchs, B., Müller, M., Zschörnig, O., and Arnold, K. (**2003**) Combined application of TLC and matrix-assisted laser desorption and ionisation time-of-flight mass spectrometry (MALDI-TOF MS) to phospholipid analysis of brain, *Chromatographia 57*, S297-S302.

([500.) Prošek, M., Milivojevic, L., Križman, M., and Fir, M. M. (**2004**) On-Line TLC-MS, *JPC – Journal of Planar Chromatography – Modern TLC 17*, 420 - 423.

([501.) Andreas Rohlfing, J. M., Gottfried Pohlentz, Ute Distler, Jasna Peter-Katalinic´, Stefan Berkenkamp, and Klaus Dreisewerd. (**2007**) IR-MALDI-MS Analysis of HPTLC-Separated Phospholipid Mixtures Directly from the TLC Plate, *Anal. Chem. 79*, 5793-5808.

([502.) Sherma, J. (**2008**) Modern Thin-Layer Chromatography, *Journal of AOAC INTERNATIONAL 91*, 1142-1144.

([503.) Fuchs, B., Süß, Rosemarie,Nimptsch, Ariane, Schiller, Jürgen. (**2008**) MALDI-TOF-MS Directly Combined with TLC: A Review of the Current State, *Chromatographia Supplement 69*.

([504.) Bischoff, A., Eibisch, M., Fuchs, B., Süss, R., Schürenberg, M., Suckau, D., and Schiller, J. (**2011**) A simple TLC-MALDI method to monitor oxidation products of phosphatidylcholines and -ethanolamines, *Acta Chromatographica 23*, 365-375.

([505.) Morlock, G. E. (**2014**) Background masssignals in TLC and HP-TLC-ESI-MS and practical advice for use of the TLC -MS interface, *Journal of Liquid Chromatography & Related Technologies 37*, 2892 - 2914.

([506.) Cheng, S. C., Huang, M. Z., and Shiea, J. (**2011**) Thin layer chromatography/mass spectrometry, *J Chromatogr A 1218*, 2700-2711.

([507.) Cole, L. M. (2017) *Methods in Molecular Biology -Imaging Mass Spectrometry* Vol. 1618, This Humana Press imprint is published by Springer Nature, The Center for Mass Spectrometry Imaging, Biomolecular Science Research Center, Sheffield Hallam University, Sheffield, South Yorkshire, UK.

([508.) Anna Crecelius, M. R. C. a. D. S. R. (**2004**) TLC–MALDI in Pharmaceutical Analysis, *Current Trends In Mass Spectrometry 19*.

([509.) Vera B. Ivleva, Y. N. E., Bogdan A. Budnik, Susanne C. Moyer, Peter B. O'Connor, Catherine E. Costello. (**2004**) Coupling Thin-Layer Chromatography with Vibrational Cooling Matrix-Assisted Laser Desorption/Ionization Fourier Transform Mass Spectrometry for the Analysis of Ganglioside Mixtures, *Analytical chemistry 76*, 6484–6491.

([510.) Ivleva, V. B., Sapp, L., O'Connor, P. B., and Costello, C. E. (**2005**) Ganglioside Analysis by Thin-Layer Chromatography Matrix-Assisted Laser Desorption/Ionization Orthogonal Time-of-Flight Mass Spectrometry, *Journal of the American Society for Mass Spectrometry*.

([511.) Klaus Dreisewerd, J. M. t., Andreas Rohlfing, Iris Meisen, Zeljka Vukelic´, Jasna Peter-Katalinic´, Franz Hillenkamp, and Stefan Berkenkamp. (**2005**) Analysis of Gangliosides Directly from Thin-Layer Chromatography Plates by Infrared Matrix-Assisted Laser Desorption/Ionization Orthogonal Time-of-Flight Mass Spectrometry with a Glycerol Matrix, *Anal. Chem. 77*, 4098-4107.

([512.) Joshua, A. R., Mirhan, K., Emily, F. H., Hao, C., Kenisha, A. P., Yan, Z., Katherine, O., Emily, P., Yunzhu, W., June-Soo, P., Joseph, F. C., and Susan, J. F. (**2018**) Genomic Profiling of BDE-47 Effects on Human Placental Cytotrophoblasts, *Toxicological Sciences*.

([513.) Gibson, D., Costello, Catherine E. (**2000**) Mass spectrometry of biomolecules, *Separation Science and Technology 2*, 299-327.

([514.) O'Connor, P. B., and Costello, C. E. (**2001**) A High-Pressure Matrix-assisted Laser Desorption/Ionization Fourier Transform Mass Spectrometry Ion

Source for Thermal Stabilization of Labile Biomolecules, *Rapid Communications in Mass Spectrometry*.

([515.) Muthing, J., and Distler, U. (**2010**) Advances on the compositional analysis of glycosphingolipids combining thin-layer chromatography with mass spectrometry, *Mass Spectrom Rev 29*, 425-479.

([516.) Ikeda, K., Shimizu, T., and Taguchi, R. (**2008**) Targeted Analysis of Ganglioside and Sulfatide Molecular Species by LC/ESI-MS/MS With Theoretically Expanded Multiple Reaction Monitoring, *The Journal of Lipid Research*.

([517.) Matyash, V., Liebisch, G., Kurzchalia, T. V., Shevchenko, A., and Schwudke, D. (**2008**) Lipid extraction by methyl-tert-butyl ether for high-throughput lipidomics, *Journal of Lipid Research 49*, 1137-1146.

([518.) Ulmer, C. Z., Jones, C. M., Yost, R. A., Garrett, T. J., and Bowden, J. A. (**2018**) Optimization of Folch, Bligh-Dyer, and Matyash sample-to-extraction solvent ratios for human plasma-based lipidomics studies, *Analytica Chimica Acta 1037*, 351-357.

([519.) Löfgren, L., Ståhlman, M., Forsberg, G. B., Saarinen, S., Nilsson, R. G., and Hansson, G. I. (**2012**) The BUME method: a novel automated chloroform-free 96-well total lipid extraction method for blood plasma[S], *Journal of Lipid Research 53*, 1690 - 1700.

([520.) Löfgren, L., Forsberg, G. B., and Ståhlman, M. (**2016**) The BUME method: A new rapid and simple chloroform-free method for total lipid extraction of animal tissue, *Scientific Reports 6*.

([521.) Jensen, O. E., and Chernyavsky, I. L. (**2019**) Blood Flow and Transport in the Human Placenta, *Annual Review of Fluid Mechanics 51*, 25-47.

([522.) Lagarde, M., Chen, P., Vericel, E., and Guichardant, M. (**2010**) Fatty acid-derived lipid mediators and blood platelet aggregation, *Prostaglandins Leukot Essent Fatty Acids 82*, 227-230.

([523.) Zhao, Z., and Xu, Y. (**2010**) An extremely simple method for extraction of lysophospholipids and phospholipids from blood samples, *J Lipid Res 51*, 652-659.

([524.) Maslanka, K., Smolenska-Sym, G., Michur, H., Wrobel, A., Lachert, E., and Brojer, E. (**2012**) Lysophosphatidylcholines: bioactive lipids generated during storage of blood components, *Arch Immunol Ther Exp (Warsz) 60*, 55-60.

([525.) Selkov, S. A., Selutin, A. V., Pavlova, O. M., Khromov-Borisov, N. N., and Pavlov, O. V. (**2013**) Comparative phenotypic characterization of human cord blood monocytes and placental macrophages at term, *Placenta 34*, 836-839.

([526.) Rose, H. G., and Oklander, M. (**1965**) IMPROVED PROCEDURE FOR THE EXTRACTION OF LIPIDS FROM HUMAN ERYTHROCYTES, *Journal of lipid research 6*, 428-431.

([527.) Connor, W. E., Lin, D. S., Thomas, G., Ey, F., DeLoughery, T., and Zhu, N. (**1997**) Abnormal phospholipid molecular species of erythrocytes in sickle cell anaemia, *Journal of Lipid Research 38*, 2516-2528.

([528.) Günther, G., Tiling, T., Uwe, H. B., and Werner, S. (**1972**) Fatty Acid Composition of Phospholipids in Erythrocytes of Adults, Normal Newborn Infants, and Neonates With Rh Erythroblastosis, *Pediatric Research*.

([529.) F. Babin, P. S., B. Limasset, B. Descomps, D. Rieu, F. Mendy, A. Crastes de Paulet (**1993**) Nervonic acid in red blood cell sphingomyelin in premature infants An index of myelin maturation., *Lipids*.

([530.) Sargent, I. L., Choo, Y. S., Redman, C. W. G. (1994) Isolating and analysing fetal leukocytes in maternal blood., In *Fetal Cells in Maternal Blood: Prospects for Noninvasive Prenatal Diagnosis* (Simpson, J. L., and Elias, S., Eds.), pp 147-153.

([531.) Leray, C., Pelletier, X., Hemmendinger, S., and Cazenave, J. P. (**1987**) Thin-Layer Chromatography of Human Platelet Phospholipids With Fatty Acid Analysis, *Journal of Chromatography B Biomedical Sciences and Applications*.

([532.) French, K. J., Zhuang, Y., Maines, L. W., Gao, P., Wang, W., Beljanski, V., Upson, J. J., Green, C. L., Keller, S. N., and Smith, C. D. (**2010**) Pharmacology and Antitumor Activity of ABC294640, a Selective Inhibitor of Sphingosine Kinase-2, *Journal of Pharmacology and Experimental Therapeutics*.

([533.) Doppler, C., Arnhard, K., Dumfarth, J., Heinz, K., Meßner, B., Stern, C., Koal, T., Klavins, K., Danzl, K., Pitterl, F., Grimm, M., Oberacher, H., and Bernhard, D. (**2017**) Metabolomic Profiling of Ascending Thoracic Aortic Aneurysms and Dissections - Implications for Pathophysiology and Biomarker Discovery, *Plos One*.

([534.) Mason, A. J., Martinez, A., Glaubitz, C., Danos, O., Kichler, A., and Bechinger, B. (**2005**) The Antibiotic and DNA-transfecting Peptide LAH4 Selectively Associates With, and Disorders, Anionic Lipids in Mixed Membranes, *The Faseb Journal*.

([535.) Chandra, A., and Datta, A. (**2022**) A Peptide-Based Fluorescent Sensor for Anionic Phospholipids, *ACS Omega*.

([536.) Schmidt, T., Suk, J.-E., Ye, F., Situ, A. J., Mazumder, P., Ginsberg, M. H., and Ulmer, T. S. (**2015**) Annular Anionic Lipids Stabilize the Integrin AIIbβ3 Transmembrane Complex, *Journal of Biological Chemistry*.

([537.) Kalli, A. C., Morgan, G., and Sansom, M. S. P. (**2013**) Interactions of the Auxilin-1 PTEN-like Domain With Model Membranes Result in Nanoclustering of Phosphatidyl Inositol Phosphates, *Biophysical Journal*.

([538.) Park, P., Franco, L. R., Chaimovich, H., Coutinho, K., Cuccovia, I. M., and Lima, F. d. S. (**2019**) Binding and Flip as Initial Steps for BP-100 Antimicrobial Actions, *Scientific Reports*.

([539.) Devrim, Y., Erkan, S., Baç, N., and Eroğlu, İ. (**2012**) Nafion/Titanium Silicon Oxide Nanocomposite Membranes for PEM Fuel Cells, *International Journal of Energy Research*.

([540.) Qin, H., Lin, L., Chu, W., Jiang, W., He, Y., Shi, Q., Deng, Y., Ji, Z., Liu, J., and Tao, S. (**2018**) Introducing Catalyst in Alkaline Membrane for Improved Performance Direct Borohydride Fuel Cells, *Journal of Power Sources*.

([541.) Ma, L., Xu, G., Li, S., Ma, J., Li, J., and Cai, W. (**2018**) Design and Optimization of a Hyper-Branched Polyimide Proton Exchange Membrane With Ultra-High Methanol-Permeation Resistivity for Direct Methanol Fuel Cells Applications, *Polymers*.

([542.) Shimokawa, N., Hishida, M., Seto, H., and Yoshikawa, K. (**2010**) Phase Separation of a Mixture of Charged and Neutral Lipids on a Giant Vesicle Induced by Small Cations, *Chemical Physics Letters*.

([543.) Khoomrung, S., Chumnanpuen, P., Jansa-Ard, S., Ståhlman, M., Nookaew, I., Borén, J., and Nielsen, J. (**2013**) Rapid Quantification of Yeast Lipid Using Microwave-Assisted Total Lipid Extraction and HPLC-CAD, *Analytical Chemistry*.

([544.) Sorensen, M. J., Miller, K. E., Jorgenson, J. W., and Kennedy, R. T. (**2020**) Ultrahigh-Performance Capillary Liquid Chromatography-Mass Spectrometry at 35 kpsi for Separation of Lipids, *Journal of Chromatography A*.

([545.) Vacher, M., Waks, M., and Nicot, C. (**1989**) Myelin Proteins in Reverse Micelles: Tight Lipid Association Required for Insertion of the Folch-Pi Proteolipid Into a Membrane-Mimetic System, *Journal of Neurochemistry*.

([546.) Byrdwell, W. C. (**2008**) Dual Parallel Liquid Chromatography With Dual Mass Spectrometry (LC2/MS2) for a Total Lipid Analysis, *Frontiers in Bioscience-Scholar*.

([547.) Reis, A., Rudnitskaya, A., Blackburn, G., Fauzi, N. M., Pitt, A. R., and Spickett, C. M. (**2013**) A Comparison of Five Lipid Extraction Solvent Systems for Lipidomic Studies of Human LDL, *The Journal of Lipid Research*.

([548.) Sugawara, T., and Miyazawa, T. (**1999**) Separation and Determination of Glycolipids From Edible Plant Sources by High-performance Liquid Chromatography and Evaporative Light-scattering Detection, *Lipids*.

([549.) Huang, Z., Wu, Q., Lü, H., Wang, Y., and Zhang, Z. (**2020**) Separation of Glycolipids/Sphingolipids From Glycerophospholipids on TiO₂ Coating in Aprotic Solvent for Rapid Comprehensive Lipidomic Analysis With Liquid Microjunction Surface Sampling-Mass Spectrometry, *Analytical Chemistry*.

([550.) Wojcik-Baszko, D., Charkiewicz, K., and Laudanski, P. (**2018**) Role of dyslipidemia in preeclampsia-A review of lipidomic analysis of blood, placenta, syncytiotrophoblast microvesicles and umbilical cord artery from women with preeclampsia, *Prostaglandins Other Lipid Mediat 139*, 19-23.

([551.) Green, J. R., and Northcote, D. H. (**1979**) Polyprenyl Phosphate Sugars Synthesized During Slime-Polysaccharide Production by Membranes of the Root-Cap Cells of Maize *Biochemical Journal*.

([552.) Guitaoui, M., Montet, A.-M., Takács, T., and Montet, J.-C. (**1995**) Contact Solvents for Common Bile Duct Stones. Study in an in Vitro System, *Liver International*.

([553.) Houde, A.-A., St-Pierre, J., Hivert, M. F., Baillargeon, J.-P., Perron, P., Gaudet, D., Brisson, D., and Bouchard, L. (**2014**) Placental Lipoprotein Lipase DNA Methylation Levels Are Associated With Gestational Diabetes Mellitus and Maternal and Cord Blood Lipid Profiles, *Journal of Developmental Origins of Health and Disease*.

([554.) Sultana, Z., Maiti, K., Aitken, R. J., Morris, J. M., Dedman, L., and Smith, R. (**2017**) Oxidative Stress, Placental Ageing-related Pathologies and Adverse Pregnancy Outcomes, *American Journal of Reproductive Immunology*.

([555.) Kuentzel, K. B., I, B., Mihalič, Z. N., Korbelius, M., Rainer, S., Pirchheim, A., Kargl, J., and Kratky, D. (**2022**) Dysregulation of Placental Lipid Hydrolysis by High-Fat/High-Cholesterol Feeding and Gestational Diabetes Mellitus in Mice, *International Journal of Molecular Sciences*.

([556.) Rasool, A., Mahmoud, T., and O'Tierney-Ginn, P. (**2023**) Lipid Aldehydes 4-Hydroxynonenal and 4-Hydroxyhexenal Exposure Differentially Impact Lipogenic Pathways in Human Placenta, *Biology*.

([557.) Gauster, M., Hiden, U., Mireille, N. M. v. P., Frank, S., Wadsack, C., Mouzon, S. H., and Desoye, G. (**2011**) Dysregulation of Placental Endothelial Lipase in Obese Women With Gestational Diabetes Mellitus, *Diabetes*.

([558.) Hirschmugl, B., Perazzolo, S., Sengers, B. G., Lewis, R. M., Gruber, M., Desoyé, G., and Wadsack, C. (**2021**) Placental Mobilization of Free Fatty

Acids Contributes to Altered Materno-Fetal Transfer in Obesity, *International Journal of Obesity*.

([559.) Moessinger, C., Klizaite, K., Steinhagen, A., Philippou-Massier, J., Shevchenko, A., Hoch, M., Ejsing, C. S., and Thiele, C. (**2014**) Two Different Pathways of Phosphatidylcholine Synthesis, the Kennedy Pathway and the Lands Cycle, Differentially Regulate Cellular Triacylglycerol Storage, *BMC Cell Biology*.

([560.) Chen, S., Jun, W., Wang, M., Lu, J., Cai, Y., and Li, B. (**2019**) In Vitro Fertilization Alters Phospholipid Profiles in Mouse Placenta, *Journal of Assisted Reproduction and Genetics*.

([561.) Mehlem, A., Hagberg, C. E., Muhl, L., Eriksson, U., and Falkevall, A. (**2013**) Imaging of Neutral Lipids by Oil Red O for Analyzing the Metabolic Status in Health and Disease, *Nature Protocols*.

([562.) Angelini, R. V., G., Corcelli, A., Fuchs, B. (**2014**) A fast method for the determination of the PC/LPC ratio in intact serum by MALDI-TOF MS: an easy-to-follow lipid biomarker of inflammation, *Chem Phys Lipids 183*, 169-175.

([563.) Angelini, R., Babudri, F., Lobasso, S., and Corcelli, A. (**2010**) MALDI-TOF/MS analysis of archaebacterial lipids in lyophilized membranes dry-mixed with 9-aminoacridine, *Journal of Lipid Research 51*, 2818-2825.

([564.) Angelini, R., Corral, P., Lopalco, P., Ventosa, A., and Corcelli, A. (**2012**) Novel ether lipid cardiolipins in archaeal membranes of extreme haloalkaliphiles, *Biochimica et Biophysica Acta - Biomembranes 1818*, 1365-1373.

([565.) Lopalco, P., Stahl, J., Annese, C., Averhoff, B., and Corcelli, A. (**2016**) Identification of unique cardiolipin and monolysocardiolipin species in Acinetobacter baumannii, *Nature Scientific Reports 7*.

([566.) Lopalco, P., Vitale, R., Cho, Y. S., Totaro, P., Corcelli, A., and Lobasso, S. (**2019**) Alteration of Cholesterol Sulfate/Seminolipid Ratio in Semen Lipid Profile of Men With Oligoasthenozoospermia, *Front Physiol 10*, 1344.

([567.) Lopalco, P., Lobasso, S., Lopes-Dos-Santos, R. M. A., Van Stappen, G., and Corcelli, A. (**2019**) Lipid profile changes during the development of Artemia franciscana, from cysts to the first two naupliar stages, *Frontiers in Physiology 10*.

([568.) Le Bon, A. M., Depretre, N., Sibille, E., Cabaret, S., Gregoire, S., Soubeyre, V., Masson, E., Acar, N., Bretillon, L., Grosmaitre, X., and Berdeaux, O. (**2018**) Comprehensive study of rodent olfactory tissue lipid composition, *Prostaglandins Leukot Essent Fatty Acids 131*, 32-43.

([569.) Han, X., Yang, K., and Gross, R. W. (**2012**) Multi-dimensional mass spectrometry-based shotgun lipidomics and novel strategies for lipidomic analyses, *Mass spectrometry reviews 31 1*, 134-178.

([570.) Rouser, G., Siakotos, A. N., and Fleischer, S. (**2007**) Quantitative analysis of phospholipids by thin-layer chromatography and phosphorus analysis of spots, *Lipids 1*, 85-86.

([571.) Gusev, A. I., Proctor, A., Rabinovich, Y. I., and Hercules, D. M. (**1995**) Thin-Layer Chromatography Combined with Matrix-Assisted Laser Desorption/Ionization Mass Spectrometry, *Analytical Chemistry 67*, 1805-1814.

([572.) Mcsavage, J., and Wall, P. E. (**1998**) Optimization of a mobile phase in reversed-phase HPTLC for the separation of unsaturated lipids in vegetable oils degraded during frying, *Jpc-journal of Planar Chromatography-modern Tlc 11*, 214-221.

([573.) Prošek, M., Medja, A., Kučan, E., and Katič, M. (**1980**) Quantitative Evaluation of Thin-Layer Chromatograms. 3. The Calculation of Fluorescence Using Multilayer Models, *Journal of High-Resolution Chromatography*.

([574.) Cebolla, V. L., Jarne, C., Domingo, P., Domínguez, A., Delgado-Camón, A., Garriga, R., Galbán, J., Membrado, L., Gálvez, E. M., and Cossío, F. P. (**2011**) Fluorescence detection by intensity changes for high-performance thin-layer chromatography separation of lipids using automated multiple development, *Journal of chromatography. 1218 19*, 2668-2675.

([575.) Rohlfing, A., Müthing, J., Pohlentz, G., Distler, U., Peter-Katalinić, J., Berkenkamp, S., and Dreisewerd, K. (**2007**) IR-MALDI-MS Analysis of HPTLC-Separated Phospholipid Mixtures Directly from the TLC Plate, *Analytical Chemistry 79*, 5793-5808.

([576.) Stübiger, G., and Belgacem, O. (**2007**) Analysis of lipids using 2,4,6-trihydroxyacetophenone as a matrix for MALDI mass spectrometry, *Analytical Chemistry 79*, 3206-3213.

([577.) Gadhvi, K. V., Modi, K. P., and Shah, M. B. (**2023**) Quantitative analysis of cystine in Thermopsis alterniflorae using high-performance thin layer chromatography HP-TLC *International Journal of Current Pharmaceutical Research*.

([578.) Teuber, K., Schiller, J., Jakop, U., Lupold, S., Orledge, J. M., Blount, J. D., Royle, N. J., Hoodless, A., and Muller, K. (**2011**) MALDI-TOF mass spectrometry as a simple tool to determine the phospholipid/glycolipid composition of sperm: pheasant spermatozoa as one selected example, *Anim Reprod Sci 123*, 270-278.

([579.) Liebisch, G., Ekroos, K., Hermansson, M., and Ejsing, C. S. (**2017**) Reporting of lipidomics data should be standardized, *Biochim Biophys Acta Mol Cell Biol Lipids 1862*, 747-751.

([580.) Satoh, T., Kubo, A., Shimma, S., and Toyoda, M. (**2012**) Mass Spectrometry Imaging and Structural Analysis of Lipids Directly on Tissue Specimens by Using a Spiral Orbit Type Tandem Time-of-Flight Mass Spectrometer, SpiralTOF-TOF, *Mass Spectrometry 1*, A0013-A0013.

([581.) Schröter, J., Fülöp, A., Hopf, C., and Schiller, J. (**2018**) The combination of 2,5-dihydroxybenzoic acid and 2,5-dihydroxyacetophenone matrices for unequivocal assignment of phosphatidylethanolamine species in complex mixtures, *Analytical and Bioanalytical Chemistry 410*, 2437-2447.

([582.) Vermillion-Salsbury, R. L., and Hercules, D. M. (**2002**) 9-Aminoacridine as a matrix for negative mode matrix-assisted laser desorption/ionization, *Rapid Communications in Mass Spectrometry 16*, 1575-1581.

([583.) Cerruti, C. D., Benabdellah, F., Laprevote, O., Touboul, D., and Brunelle, A. (**2012**) MALDI imaging and structural analysis of rat brain lipid negative ions with 9-aminoacridine matrix, *Anal Chem 84*, 2164-2171.

([584.) Eibisch, M., Zellmer, S., Gebhardt, R., Süß, R., Fuchs, B., and Schiller, J. (**2011**) Phosphatidylcholine dimers can be easily misinterpreted as cardiolipins in complex lipid mixtures: a matrix-assisted laser desorption/ionization time-of-flight mass spectrometric study of lipids from hepatocytes, *Rapid Communications in Mass Spectrometry 25*, 2619-2626.

([585.) Angelini, R., Vitale, R., Patil, V. A., Cocco, T., Ludwig, B., Greenberg, M. L., and Corcelli, A. (**2012**) Lipidomics of intact mitochondria by MALDI-TOF/MS, *Journal of Lipid Research 53*, 1417-1425.

([586.) Sârbu, M., Ica, R., and Zamfir, A. D. (**2022**) Gangliosides as Biomarkers of Human Brain Diseases: Trends in Discovery and Characterization by High-Performance Mass Spectrometry, *International Journal of Molecular Sciences*.

([587.) McMillen, J. C., Fincher, J. A., Klein, D. R., Spraggins, J. M., and Caprioli, R. M. (**2020**) Effect of MALDI matrices on lipid analyses of biological tissues using MALDI-2 postionization mass spectrometry.

([588.) Sjaarda, L. A., Ahrens, K. A., Kuhr, D. L., Holland, T. L., Omosigho, U. R., Steffen, B. T., Weir, N. L., Tollman, H. K., Silver, R. M., and Tsai, M. Y. (**2018**) Pilot Study of Placental Tissue Collection, Processing, and Measurement Procedures for Large Scale Assessment of Placental Inflammation, *Plos One*.

([589.) Barber, M., Risis, S., Yang, C., Meikle, P. J., Staples, M., Febbraio, M. A., and Bruce, C. R. (**2012**) Plasma Lysophosphatidylcholine Levels Are Reduced in Obesity and Type 2 Diabetes, *Plos One*.

([590.) Pietiläinen, K. H., Sysi-Aho, M., Rissanen, A., Seppänen-Laakso, T., Yki-Järvinen, H., Kaprio, J., and Orešič, M. (**2007**) Acquired Obesity Is Associated With Changes in the Serum Lipidomic Profile Independent of Genetic Effects – A Monozygotic Twin Study, *Plos One*.

([591.) Eisinger, K., Liebisch, G., Schmitz, G., Aslanidis, C., Krautbauer, S., and Buechler, C. (**2014**) Lipidomic Analysis of Serum From High Fat Diet-Induced Obese Mice, *International Journal of Molecular Sciences*.

([592.) Gonzalez, P., Simcox, J., Raff, H., Wade, G., Bank, H. V., Weisman, S. J., and Hainsworth, K. R. (**2022**) Lipid Signatures of Chronic Pain in Female Adolescents With and Without Obesity, *Lipids in Health and Disease*.

([593.) Liu, J., Li, J., Li, S., Leng, J., Li, W., Yang, W., Huo, X., Chen, L., Ma, R., Hu, G., Fang, Z. Z., and Yang, X. (**2020**) Circulating Lysophosphatidylcholines in Early Pregnancy and Risk of Gestational Diabetes in Chinese Women, *The Journal of Clinical Endocrinology & Metabolism*.

([594.) Chatterjee, B., and Thakur, S. (**2023**) Proteins and Metabolites Fingerprints of Gestational Diabetes Mellitus Forming Protein–metabolite Interactomes Are Its Potential Biomarkers, *Proteomics*.

([595.) Wang, H.-Y. J., Liu, C. B., Wu, H.-W., and Kuo, J. S. (**2010**) Direct Profiling of Phospholipids and Lysophospholipids in Rat Brain Sections After Ischemic Stroke, *Rapid Communications in Mass Spectrometry*.

([596.) Yuan, D., Wu, B. J., Henry, A., and Rye, K.-A. (**2018**) Role of Fibroblast Growth Factor 21 in Gestational Diabetes Mellitus: A Mini-review, *Clinical Endocrinology*.

([597.) Teng, B., Ma, Y., Zhang, L., Li, N., and Zhang, J. (**2020**) The Application of Metabolomics Analysis in the Research of Gestational Diabetes Mellitus and Preeclampsia, *Journal of Obstetrics and Gynaecology Research*.

([598.) Peng, S., Zhang, J., Liu, L., Zhang, X., Huang, Q., Alamdar, A., Tian, M., and Shen, H. (**2015**) Newborn Meconium and Urinary Metabolome Response to Maternal Gestational Diabetes Mellitus: A Preliminary Case-Control Study, *Journal of Proteome Research*.

([599.) Chen, Q., Francis, E. C., Hu, G., and Chen, L. (**2018**) Metabolomic Profiling of Women With Gestational Diabetes Mellitus and Their Offspring: Review of Metabolomics Studies, *Journal of Diabetes and Its Complications*.

([600.) Lu, Y., Reichetzeder, C., Prehn, C., Li, Y., Chen, Y., Zeng, S., Chu, C., Adamski, J., and Hocher, B. (**2018**) Cord Blood Lysophosphatidylcholine 16: 1 Is Positively Associated With Birth Weight, *Cellular Physiology and Biochemistry*.

([601.) Parra-Millán, R., Me, J.-M., Ayerbe-Algaba, R., Domínguez-Herrera, J., Díaz, C., Palacio, J. P. d., Pachón, J., and Smani, Y. (**2022**) Impact of the Immune Response Modification by Lysophosphatidylcholine in the Efficacy of Antibiotic Therapy of Experimental Models of Peritoneal Sepsis and Pneumonia by Pseudomonas Aeruginosa: LPC Therapeutic Effect in Combined Therapy, *Enfermedades Infecciosas Y Microbiología Clínica*.

([602.) Silva-Neto, M. A., Carneiro, A., Silva-Cardoso, L., and Atella, G. C. (**2012**) Lysophosphatidylcholine: A Novel Modulator of Trypanosoma CruziTransmission, *Journal of Parasitology Research*.

([603.) Choi, S. Z., Park, S., Liang, G. H., Kim, J. A., and Suh, S. H. (**2010**) Superoxide Generated by Lysophosphatidylcholine Induces Endothelial Nitric Oxide Synthase Downregulation in Human Endothelial Cells, *Cellular Physiology and Biochemistry*.

([604.) Daleau, P. (**2002**) Ethanol Protects Against Lysophosphatidylcholine-Induced Uncoupling of Cardiac Cell Pairs, *Pflügers Archiv - European Journal of Physiology*.

([605.) Dickson, A., Yutuc, E., Thornton, C. A., Dunford, J. E., Oppermann, U., Wang, Y., and Griffiths, W. J. (**2022**) HSD3B1 is an Oxysterol 3β-Hydroxysteroid Dehydrogenase in Human Placenta.

([606.) Yutuc, E., Dickson, A. L., Pacciarini, M., Griffiths, L., Baker, P. R. S., Connell, L., Ohman, A., Forsgren, L., Trupp, M., Vilarinho, S., Khalil, Y., Clayton, P. T., Sari, S., Dalgic, B., Hoflinger, P., Schols, L., Griffiths, W. J., and Wang, Y. (**2021**) Deep mining of oxysterols and cholestenoic acids in human plasma and cerebrospinal fluid: Quantification using isotope dilution mass spectrometry, *Anal Chim Acta 1154*, 338259.

([607.) Dickson, A. L., Yutuc, E., Thornton, C. A., Wang, Y., and Griffiths, W. J. (**2022**) Identification of unusual oxysterols biosynthesised in human pregnancy by charge-tagging and liquid chromatography-mass spectrometry, *Front Endocrinol (Lausanne) 13*, 1031013.

([608.) Goto-Inoue, N., Hayasaka, T., Zaima, N., and Setou, M. (**2011**) Imaging mass spectrometry for lipidomics, *Biochim Biophys Acta 1811*, 961-969.

([609.) Janusz, K. (**2014**) MALDI-IMS for spatial analysis of lipids and other small molecules-Metabolomics workshop.

([610.) Burnum-Johnson, K. E., Baker, E. S., and Metz, T. O. (**2017**) Characterizing the lipid and metabolite changes associated with placental function and pregnancy complications using ion mobility spectrometry-mass spectrometry and mass spectrometry imaging, *Placenta 60 Suppl 1*, S67-S72.

([611.) Seeley, E. H., and Caprioli, R. M. (2011) MALDI imaging mass spectrometry of human tissue: Method challenges and clinical perspectives, In *Trends in Biotechnology*, pp 136-143.

([612.) Wisztorski, M., Franck, J., Salzet, M., and Fournier, I. (**2010**) MALDI direct analysis and imaging of frozen versus FFPE tissues: what strategy for which sample?, *Methods Mol Biol 656*, 303-322.

([613.) Cornett, D. S., Reyzer, M. L., Chaurand, P., and Caprioli, R. M. (**2007**) MALDI imaging mass spectrometry: molecular snapshots of biochemical systems, *Nat Methods 4*, 828-833.

([614.) Caprioli R.M., T. B. F., Jocelyn Gile. (**1997**) Molecular Imaging of Biological Samples by MALDI TOF, *Anal. Chem. 69*, 4751-4760.

([615.) Caprioli, B. (**2009**) Supplement data

([616.) Yalcin, E. B., and de la Monte, S. M. (**2015**) Review of matrix-assisted laser desorption ionization-imaging mass spectrometry for lipid biochemical histopathology, *J Histochem Cytochem 63*, 762-771.

([617.) Aichler, M., and Walch, A. (**2015**) MALDI Imaging mass spectrometry: current frontiers and perspectives in pathology research and practice, *Lab Invest 95*, 422-431.

([618.) Chughtai, K., and Heeren, R. M. A. (**2010**) Mass Spectrometric Imaging for Biomedical Tissue Analysis, *Chemical Reviews 110*, 3237-3277.

([619.) Stutts, W. L., Menger, R. F., Kiss, A., Heeren, R. M. A., and Yost, R. A. (**2013**) Characterization of phosphatidylcholine oxidation products by MALDI MS n, *Analytical Chemistry 85*, 11410-11419.

([620.) McDonnell, L. A., and Heeren, R. M. A. (2007) Imaging mass spectrometry, In *Mass Spectrometry Reviews*, pp 606-643.

([621.) Marin, J. J., Macias, R. I., Briz, O., Perez, M. J., Blazquez, A. G., Arrese, M., and Serrano, M. A. (**2008**) Molecular bases of the fetal liver-placenta-maternal liver excretory pathway for cholephilic compounds, *Liver Int 28*, 435-454.

([622.) Goodwin, R. J. A., Pennington, S. R., and Pitt, A. R. (**2008**) Protein and peptides in pictures: Imaging with MALDI mass spectrometry, *Proteomics 8*, 3785-3800.

([623.) Rohner, T. C., Staab, D., and Stoeckli, M. (**2005**) MALDI mass spectrometric imaging of biological tissue sections, *Mechanisms of Ageing and Development 126*, 177-185.

([624.) Zhao, W., Huang, T., Jiang, M., Ran, F., and Lin, J. (**2014**) Expression of Notch Family Proteins in Placentas From Patients With Early-Onset Severe Preeclampsia, *Reproductive Sciences*.

([625.) Cui, X., Brockman, D. E., Campos, B., and Myatt, L. (**2006**) Expression of NADPH Oxidase Isoform 1 (Nox1) in Human Placenta: Involvement in Preeclampsia, *Placenta*.

([626.) Shin, J., Kwon, H. M., Han, K.-H., and Lee, H. Y. (**2012**) TonEBP and SMIT Expression in Human Placenta, *Anatomy & Cell Biology*.

([627.) El-Badawy, O., Abbas, A. M., Radwan, E., Makboul, R., Khamis, A. A., Ali, M., Elkabsh, M. M., Bakr, M. H., and Zahran, A. M. (**2023**) Cross-Talk Between Mucosal-Associated Invariant T, Natural Killer, and Natural Killer T Cell Populations Is Implicated in the Pathogenesis of Placenta Accreta Spectrum, *Inflammation*.

([628.) Myers, E. W., Ehrhart, E. J., Charles, B., Spraker, T. R., Gelatt, T., and Duncan, C. (**2012**) Apoptosis in Normal and Coxiella BurnetiiInfected Placentas From Alaskan Northern Fur Seals (Callorhinus Ursinus), *Veterinary Pathology*.

([629.) Wieser, M., Burger, S., Ertl, R., Kummer, S., Stargardt, M., and Walter, I. (**2022**) Example for Process Validation in Biobanking: Fit for Purpose Testing of a Cryopreservation Method Without Isopentane, *Frontiers in Molecular Biosciences*.

([630.) Wolfe, L., Thiagarajan, R. D., Boscolo, F. S., Taché, V., Coleman, R. L., Kim, J., Kwan, W., Loring, J. F., Parast, M. M., and Laurent, L. C. (**2014**) Banking Placental Tissue: An Optimized Collection Procedure for Genome-Wide Analysis of Nucleic Acids, *Placenta*.

([631.) Hatzis, C., Sun, H., Yao, H., Hubbard, R., Meric-Bernstam, F., Babiera, G., Wu, Y., Pusztai, L., and Symmans, W. F. (**2011**) Effects of Tissue Handling on RNA Integrity and Microarray Measurements From Resected Breast Cancers, *Jnci Journal of the National Cancer Institute*.

([632.) Prideaux, B., and Stoeckli, M. (**2012**) Mass Spectrometry Imaging for Drug Distribution Studies, *Journal of Proteomics*.

([633.) Claesen, J., Dittwald, P., Burzykowski, T., and Valkenborg, D. (**2012**) An Efficient Method to Calculate the Aggregated Isotopic Distribution and Exact Center-Masses, *Journal of the American Society for Mass Spectrometry*.

([634.) Pang, X., Gao, S., Ga, M., Zhang, J., Luo, Z., Chen, Y., Zhang, R., He, J., and Abliz, Z. (**2021**) Mapping Metabolic Networks in the Brain by Ambient Mass Spectrometry Imaging and Metabolomics, *Analytical Chemistry*.

([635.) Dilillo, M., Ait-Belkacem, R., Esteve, C., Pellegrini, D., Nicolardi, S., Costa, M., Vannini, E., Graaf, E. L. d., Caleo, M., and McDonnell, L. A. (**2017**) Ultra-High Mass Resolution MALDI Imaging Mass Spectrometry of Proteins and Metabolites in a Mouse Model of Glioblastoma, *Scientific Reports*.

([636.) Harkewicz, R., and Dennis, E. A. (**2011**) Applications of mass spectrometry to lipids and membranes, *Annu Rev Biochem 80*, 301-325.

([637.) Soltwisch, J., Kettling, H., Vens-Cappell, S., Wiegelmann, M., Müthing, J., and Dreisewerd, K. (**2015**) Mass spectrometry imaging with laser-induced postionization, *Science 348*, 211-215.

([638.) Souady, J., Soltwisch, J., Dreisewerd, K., Haier, J., Peter-Katalinić, J., and Müthing, J. (**2009**) Structural Profiling of Individual Glycosphingolipids in a Single Thin-Layer Chromatogram by Multiple Sequential Immunodetection Matched with Direct IR-MALDI-o-TOF Mass Spectrometry, *Analytical Chemistry 81*, 9481-9492.

([639.) Khan, S. A., R 2020. (**2020**) Lipidomics: Current and Emerging Techniques, *MASS SPECTROMETRY IMAGING OF LIPIDS*.

([640.) Bowman, A. P., Bogie, J. F. J., Hendriks, J. J. A., Haidar, M., Belov, M., Heeren, R. M. A., and Ellis, S. R. (**2020**) Evaluation of lipid coverage and high spatial resolution MALDI-imaging capabilities of oversampling combined with laser post-ionisation, *Analytical and Bioanalytical Chemistry 412*, 2277-2289.

([641.) Moreno-Gordaliza, E., Esteban-Fernández, D., Lázaro, A., Humanes, B., Aboulmagd, S., Tejedor, A., Linscheid, M. W., and Gómez-Gómez, M. M. (**2017**) MALDI-LTQ-Orbitrap mass spectrometry imaging for lipidomic analysis in kidney under cisplatin chemotherapy, *Talanta 164*, 16-26.

([642.) Franck, J., Arafah, K., Elayed, M., Bonnel, D., Vergara, D., Jacquet, A., Vinatier, D., Wisztorski, M., Day, R., Fournier, I., and Salzet, M. (**2009**) MALDI imaging mass spectrometry: state of the art technology in clinical proteomics, *Mol Cell Proteomics 8*, 2023-2033.

([643.) Landgraf, R. R., Garrett, T. J., Prieto Conaway, M. C., Calcutt, N. A., Stacpoole, P. W., and Yost, R. A. (**2011**) Considerations for quantification of lipids in nerve tissue using matrix-assisted laser desorption/ionization mass spectrometric imaging, *Rapid Communications in Mass Spectrometry 25*, 3178-3184.